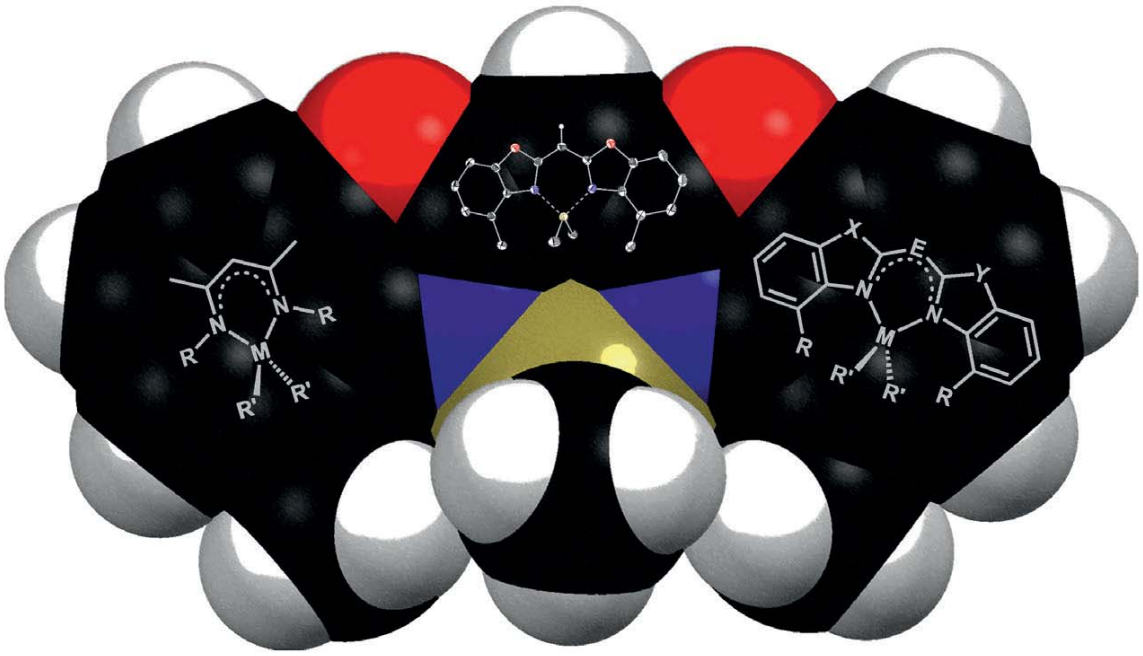

David-Raphael Dauer

STUDIES OF GROUP 13 METAL COMPLEXES BEARING NACNAC-MIMETIC BISHETEROCYCLO METHANIDES AND AMIDES

Cuvillier Verlag Göttingen
Internationaler wissenschaftlicher Fachverlag

Studies of Group 13 Metal Complexes Bearing nacnac-Mimetic Bisheterocyclo Methanides and Amides

STUDIES OF GROUP 13 METAL COMPLEXES BEARING NACNAC-MIMETIC BISHETERO-CYCLO METHANIDES AND AMIDES

Dissertation

zur Erlangung des mathematisch-naturwissenschaftlichen Doktorgrades
„Doctor rerum naturalium“
der Georg-August-Universität Göttingen

im Promotionsprogramm Chemie
der Georg-August University School of Science (GAUSS)

vorgelegt von
David-Raphael Dauer
aus Northeim

Göttingen, 2016

Bibliografische Information der Deutschen Nationalbibliothek
Die Deutsche Nationalbibliothek verzeichnet diese Publikation in der
Deutschen Nationalbibliografie; detaillierte bibliografische Daten sind im Internet
über http://dnb.d-nb.de abrufbar.
1. Aufl. - Göttingen: Cuvillier, 2016
Zugl.: Göttingen, Univ., Diss., 2016

Nonnenstieg 8, 37075 Göttingen
Telefon: 0551-54724-0
Telefax: 0551-54724-21
www.cuvillier.de

1. Auflage, 2016
Gedruckt auf umweltfreundlichem, säurefreiem Papier aus nachhaltiger Forstwirtschaft.

ISBN 978-3-7369-9376-1
eISBN 978-3-7369-8376-2

Betreuungsausschuss

Prof. Dr. Dietmar Stalke, Institut für Anorganische Chemie

Prof. Dr. Dr. h.c. mult. Herbert W. Roesky, Institut für Anorganische Chemie

Mitglieder der Prüfungskommission

Prof. Dr. Dietmar Stalke, Institut für Anorganische Chemie

Prof. Dr. Dr. h.c. mult. Herbert W. Roesky, Institut für Anorganische Chemie

Weitere Mitglieder der Prüfungskommission

Jun.-Prof. Dr. Selvan Demir, Institut für Anorganische Chemie

Dr. Michael John, Institut für Organische und Biomolekulare Chemie

Dr. Inke Siewert, Institut für Anorganische Chemie

Dr. Heidrun Sowa, GZG, Abteilung für Kristallographie

Tag der mündlichen Prüfung: 14.10.2016

Danksagung

Zuallererst möchte ich einen besonderen Dank meinem Doktorvater Herrn Prof. Dr. Dietmar Stalke dafür aussprechen, dass er mir ein sehr spannendes Themengebiet offeriert hat und mir während meines Promotionsvorhabens stets unterstützend zur Seite stand. Auch möchte ich ihm dafür danken, mir diverse Konferenzaufenthalte im Ausland ermöglicht zu haben.

Herrn Prof. Dr. Dr. h.c. mult. Herbert W. Roesky möchte ich ganz herzlich für die Übernahme des Korreferats und die zahlreichen Fachgespräche danken, durch welche ich neue vielversprechende Impulse für mein Dissertationsthema erhielt.

Mein Dank geht auch an die weiteren Mitglieder meiner Prüfungskommission, die sich die Zeit genommen haben, meine Arbeit zu bewerten.

Da sich der Hauptteil meiner Arbeit mit der Röntgenstrukturanalyse beschäftigt, möchte ich ebenfalls an dieser Stelle Frau Dr. Regine Herbst-Irmer ganz herzlich für kompetente Hilfe bei allen kristallographischen Fragestellungen danken. Ohne ihr Wissen wäre die eine oder andere Fehlordnung oder Verzwillingung übersehen worden.

Ebenso möchte ich Dr. Rajendra S. Ghadwal für seine fachlichen Anregungen im Bereich der Syntheseplanung und die zahlreichen Diskussionen über die Umstrukturierung des AC-0 Praktikums danken.

Neben der entspannten und angenehmen Arbeitsatmosphäre im Arbeitskreis, die durch die offene und hilfsbereite Art jedes einzelnen Mitglieds hervorgerufen wird, möchte ich noch besonders die langjährige Zusammenarbeit mit meinen beiden Laborkollegen Dr. Sebastian Wandtke und Dr. Arne Visscher hervorheben. Ich danke den beiden für die schöne gemeinsame Zeit inner- und außerhalb des Labors und Dr. Arne Visscher zudem für die Bereitstellung einer passenden Unterkunft für den Papierkrieg.

Meinen Freunden und Arbeitskollegen Dr. Ole M. Schütte, Dr. Matthias Heger und Dr. Andreas Jacob danke ich auch ganz herzlich dafür, dass sie sich in den letzten Zügen meiner Doktorarbeit zum Korrekturlesen bereit erklärten und konstruktive Verbesserungsvorschläge einbrachten. Auch möchte ich meinem Arbeitskollegen Dr. Julian Strohmeier für das entgegengebrachte Verständnis für die Mehrbelastung in den ersten paar Monaten im neuen Job danken.

Natürlich gilt ein besonderer Dank auch meinen Eltern, Geschwistern und der gesamten Familie, die mich immer unterstützen und an mich und meine Fähigkeiten glauben.

Zu guter Letzt möchte besonders meiner langjährigen Freundin Karina Joppe für ihre mir entgegengebrachte Liebe und Unterstützung in den letzten Jahren von ganzem Herzen danken. Ohne dich und deinen Rückhalt hätte ich die teils schwierigen Zeiten wohl kaum so gut meistern können. Ich bin sehr glücklich, dich an meiner Seite zu wissen.

Für meine Eltern und mein Patenkind

Auch aus Steinen, die einem in den Weg gelegt werden,
kann man Schönes bauen.
– Johann Wolfgang von Goethe

Table of Contents

List of Abbreviations

Å	Ångström
acac	acetylacetonate
aq.	aqueous
BASF	batch scale factor
box	bisoxazoline
bth	benzothiazole
conc.	concentrated
cps	counts per second
Cp*	pentamethyl cyclopentadienyl
δ	chemical shift
d_i / d_e	distance from Hirshfeld surface to the nearest atom interior / exterior surface
diox	1,4-dioxane
Dipp	2,6-diisopropylphenyl
dist.	distance
DMSO	dimethyl sulfoxide
EI	electron ionization
eq.	equivalent(s)
esd	estimated standard deviation
ESI	electrospray ionization
Et	ethyl
FLP	Frustrated Lewis Pairs
HSAB	hard and soft acids and bases
Hz	Hertz
*i*Bu	*iso*-butyl
*i*Pr	*iso*-propyl
KPG	sealed precision glass stirrer
M	molar
Me	methyl
MS	mass spectrometry
m/*z*	mass/charge relation
OMe	methoxy
NMR	nuclear magnetic resonance
nacnac	β-diketiminate
ppa	polyphosphoric acid
ppm	parts per million
p-Tol	*para*-toloyl
R_f	retention factor
rt	room temperature
sat.	saturated
SCXRD	single crystal X-ray diffraction
sof	site occupation factor
*t*Bu	*tert*-butyl
THF	tetrahydrofuran
Trip	2,4,6-triisopropylphenyl

Abbreviations concerning the ligands:

1-MeNCNC$_2$H$_2$

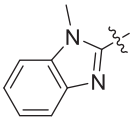

1-MeNCNC$_6$H$_4$

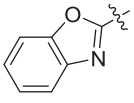

NCOC$_6$H$_4$

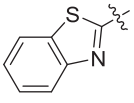

NCSC$_6$H$_4$

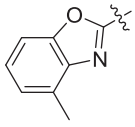

4-MeNCOC$_6$H$_3$

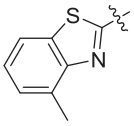

4-MeNCSC$_6$H$_3$

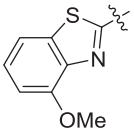

4-OMeNCSC$_6$H$_3$

Compound Index

Chapter 2.1

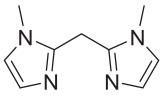
1

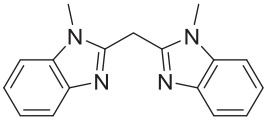
2

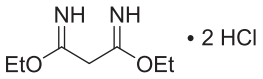

3

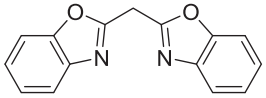
4

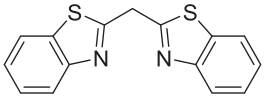
5

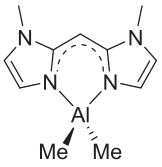

6

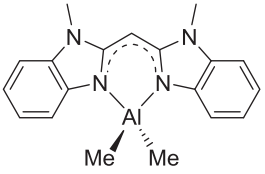

7

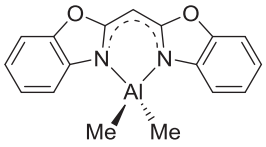

8

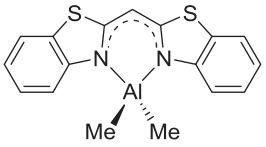

9

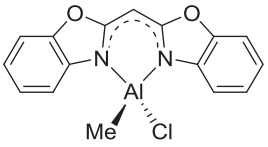

10

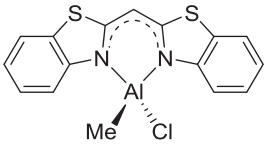

11

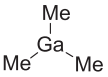

12

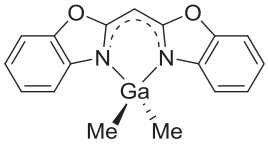

13

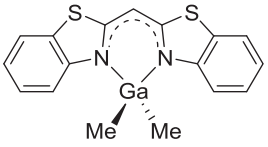

14

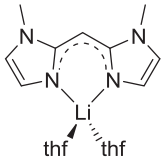

15

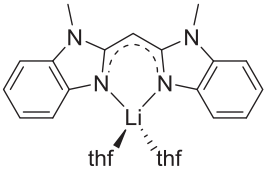

16

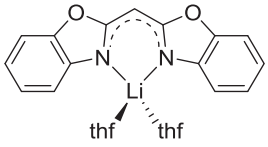

17

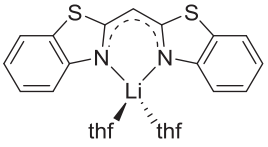

18

Chapter 2.2

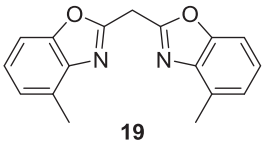
19

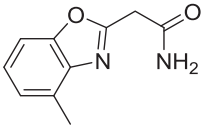

20

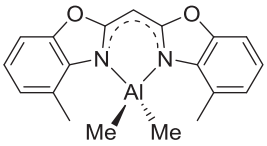

21

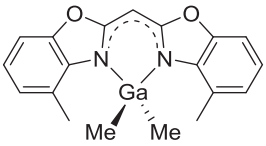

22

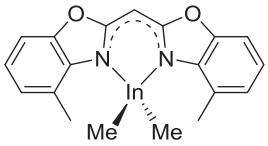

23

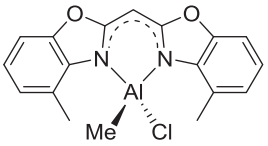

24

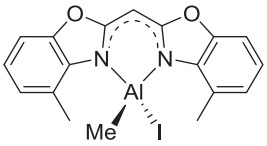

25

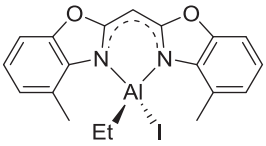

26

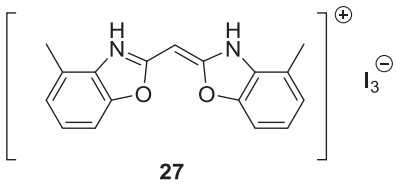

27

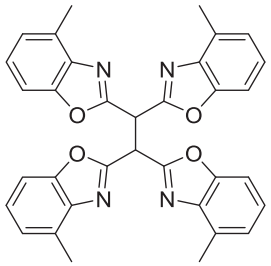
28

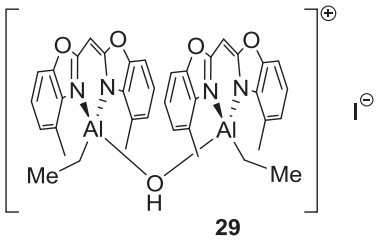

29

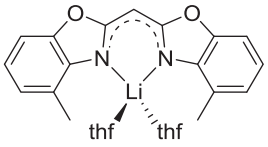

30

Chapter 2.3

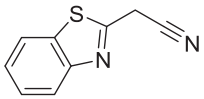

31

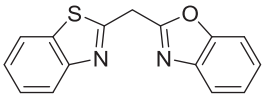

32

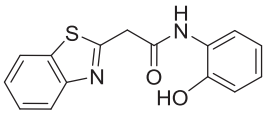

33

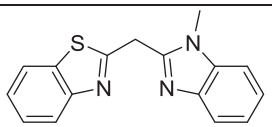

34

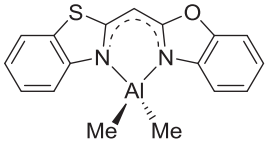

35

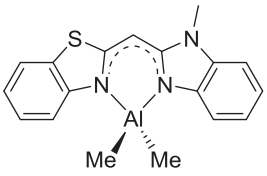

36

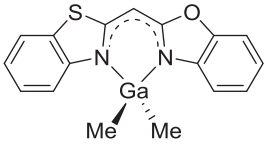

37

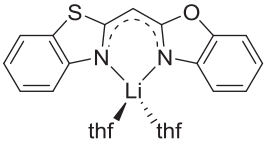

38

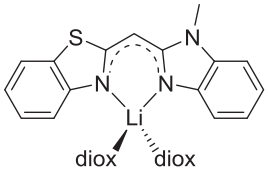

39

Chapter 2.5

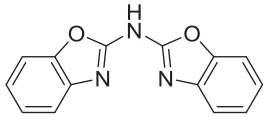

40

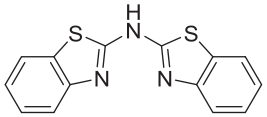

41

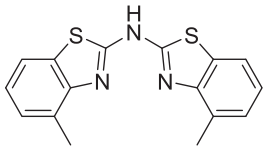

42

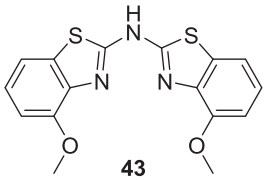

43

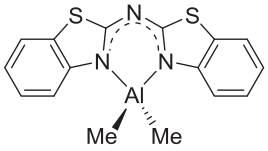

44

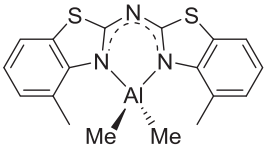

45

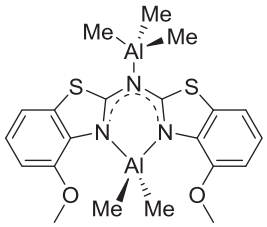

46

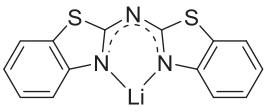

47

1/4

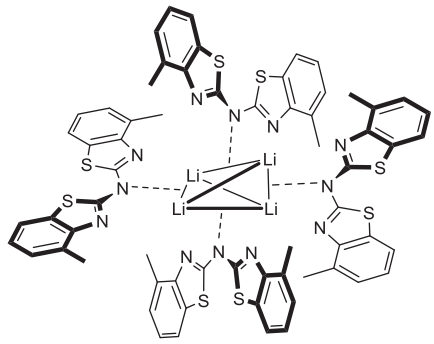

48

Chapter 2.7

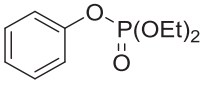

49

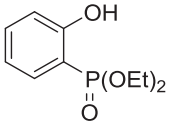

50

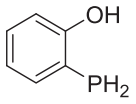

51

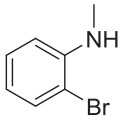

52

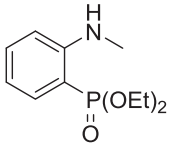

53

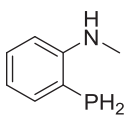

54

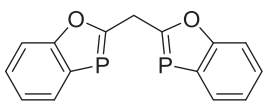

55

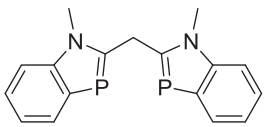

56

1 Introduction

1.1 History and Synthesis of the nacnac Ligand

Regarding the class of chelating ligand systems, the following three related monoanionic species **A** to **C** will be discussed in the context of this work (see Scheme 1-1), wherein all mentioned residues (R, R^1, R^2 and R^3) are mostly alkyl or aryl substituents. Starting with the *β*-diketonato or acetylacetonato ligand **A**,[1] also abbreviated as acac, it can be stated that this ligand system has widespread applications in coordination chemistry. Due to the keto-enol tautomerism in the parent diketone acacH depicted in Scheme 1-2, the remaining proton at the bridging methylene CHR^2 moiety is quite acidic and therefore prone to deprotonation reactions. The resulting negative charge can be easily stabilized by delocalization within the alternating double bonds of the C_3O_2 section, which is capable of chelating metal cations (*vide infra*).

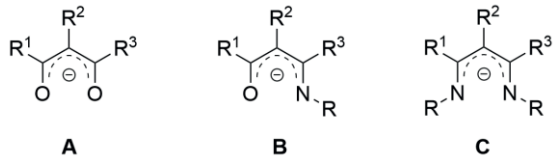

Scheme 1-1: Different monoanionic chelating ligands: acetylacetonato (**A**), *β*-enaminoketonato (**B**) and *β*-diketiminato (**C**).

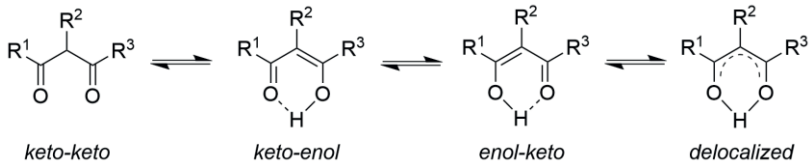

Scheme 1-2: Exemplary keto-enol tautomerism within the acacH ligand **A**.

The formal isoelectronic replacement of one oxygen atom of the diketone by an imine functionality NR leads to the formation of the *β*-enaminoketonato ligand system **B**.[2] By introducing this imine moiety, the delocalization of the negative charge is also taking place efficiently, but the additional substituent at the nitrogen atom can be varied to influence the electronic and steric properties of the ligand system **B**. Again, this class of ligands is well known in the literature because of its good coordination behaviour.

To complete the series, the *β*-diketiminato or *β*-dialdiminato ligand **C** – also called *N*-alkyl vinamidine or more concisely nacnac following from the nitrogen substitution of acac – has to be mentioned at this point. In contrast to ligand **B,** both keto or aldehyde functionalities are replaced by the same corresponding imine moiety, which improves the possibility of tuning the electronic and steric properties of the chelating ligand. In addition, more complex modifications of the nacnac ligand are known, where for example two

different substituents at the imine nitrogen atom are present, or these residues work as a linking moiety between two imines to form a macrocyclic compound.[3] This class of monoanionic, bidentate ligands has received increasing attention in the last two decades due to their ability to form stable metal complexes, which is visualized in Figure 1-1. Obviously, since 1996 the number of publications containing the keyword "diketiminate" is increased continuously until 2005 to reach afterwards a steady level of average 80 publications per year up to the present date. In 2010, a maximum number of 115 publications related to this topic were recorded. This statistic reflects the high degree of interest in this ligand system in current research and shows that the nacnac ligands are today one of the most popular ligand systems in coordination chemistry.[4]

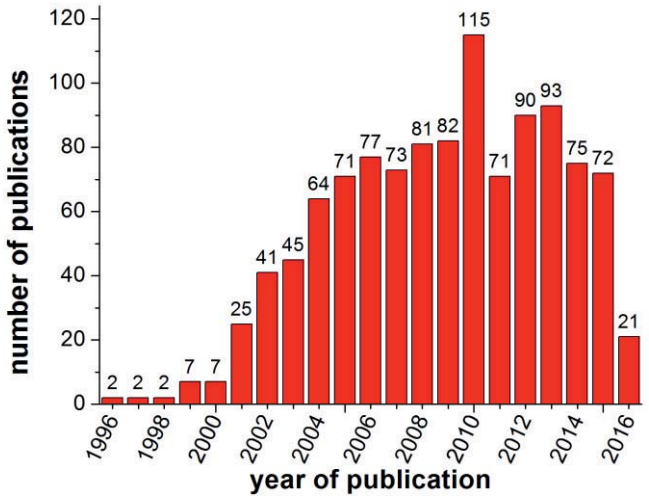

Figure 1-1: SciFinder search for the keyword "diketiminate" (executed at 13th may 2016).

The synthesis of the parent *β*-diketimine ligands can be accomplished mainly by using two different pathways shown in Scheme 1-3, which were developed over three decades ago. The upper pathway shows the condensation reaction starting from the corresponding *β*-diketone and the desired primary amine NH_2R. In order to avoid that the reaction stops at the stage of the single-condensation product (the *β*-enaminoketonato ligand **B**), the reaction procedure contains some additional steps like methylation of the remaining keto functionality by usage of a Meerwein salt,[5] before the second condensation of the imine can take place.[6] Another route for the formation of mainly aryl substituted imines is shown in the bottom pathway: in this route, one ketone reacts selectively with ethylene glycol to give the corresponding ketal, which can than undergo the condensation reaction with the primary amine.[7]

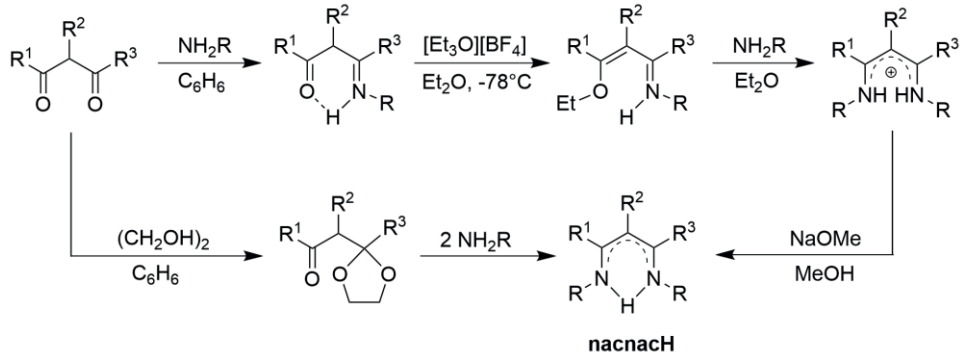

Scheme 1-3: Synthetic pathways to the formation of nacnacH starting from the corresponding *β*-diketone.

For the generation of nacnac ligands which do not contain any additional substituents in the backbone of the ligand, 1,1,3,3-tetraalkoxy propanes can also be used as a precursor. For this reaction, the hydrochlorides of the corresponding aromatic amines were added at 50 °C to the acetal propane derivative in an aqueous ethanol solution to obtain the *β*-diketimine hydrochloride, which is further treated with aqueous sodium hydroxide solution.[8]

Since the first described synthesis of the Dipp substituted ligand $[\{N(Dipp)C(Me)\}_2CH]^-$ in 1997,[9] this derivate probably developed to one of the most studied nacnac ligand systems in current research topics. Due to this fact, a more facile synthetic approach with good yields of about 80 % was developed, especially for ligands carrying aromatic imine substituents. In that case, the reaction was accomplished by imine formation of 2,4-pentadienone with the desired *ortho*-/*para*-substituted aniline derivative in an ethanolic solution over several days. After aqueous workup with sodium carbonate solution, the corresponding protonated nacnacH ligands could be isolated (see Scheme 1-4). [9, 10] For the implementation of further increased steric bulkiness at the backbone of the nacnac ligands, *t*Bu groups were introduced, starting from pivaloyl chloride and the corresponding primary amine and followed by lithiation reactions for coupling.[11] The *N*-terphenyl substituted nacnac ligand should also be mentioned in this series, because the super-sized imine residues are protecting the metal complexes from oligomerization,[12] which will be a part of the following chapter as well.

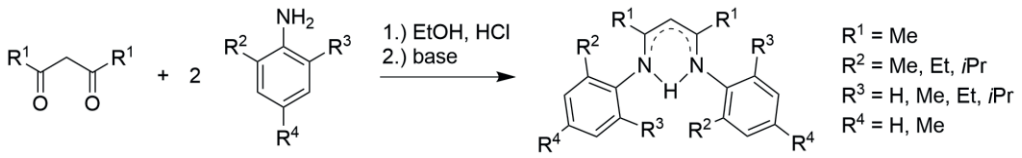

Scheme 1-4: Synthesis of the aryl substituted nacnacH ligands.

1.2 Group 13 Metal Diketiminato Complexes

Since the first transition metal complexes of the nacnac ligand were mentioned in 1968,[2b, 6, 13] in the past two decades also many *β*-diketiminate structures containing main group metals were synthesized and fully characterized.[14] These complexes embrace aluminium(III), gallium(III) and indium(III) compounds. The former range from the alkyl over the hydride to halide substituted metal centres. Furthermore, the dialkylaluminium *β*-diketiminates show catalytic activities towards ring-opening polymerisation.[15]

After deprotonation of the backbone of these nacnac ligands, a monoanionic *π*-system containing six electrons is generated, where a complete delocalization of the electrons is achieved. These ligands behave mostly as redox-inactive spectator ligands.[16] Usually these nacnac systems carry an aliphatic organic residue like Me or *t*Bu at the backbone imine carbon atom, as described earlier, and mostly some bulky moieties like Dipp, adamantyl or mesityl groups at the imine nitrogen atom (see Scheme 1-4).

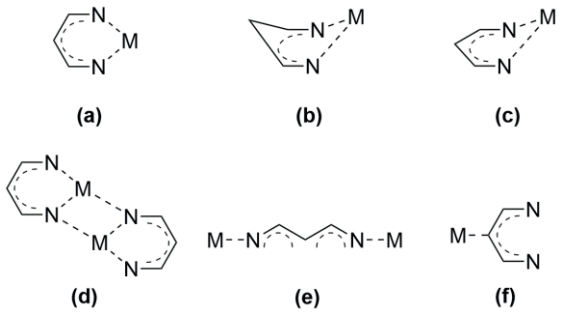

Scheme 1-5: Possible bonding motives observed for metal complexes of the nacnac ligand (the organic imine residues are omitted for clarity).

In Scheme 1-5, some different bonding modes of the deprotonated monoanionic nacnac ligand are shown, which have been structurally characterized and verified in the corresponding solid state structures. Mode **(a)** corresponds to the most common and also expected one, in which the six-membered metalla heterocycle is planar and the metal coordination is accomplished by the two imine nitrogen atoms in a terminal chelating fashion. In principle, the variants **(b)** and **(c)** show the same coordination motif as in **(a)**, but in these cases a boat-like conformation of the metalla heterocycle results.[17] Either the bridging methylene moiety as well as the coordinated metal fragment can bend out of plane **(b)** or just the metal cation is dislocated from the corresponding chelating plane, whereas the rest stays almost planar **(c)**. Motif **(d)** shows the presence of a dimeric species in which the metal cations are also coordinated in a chelating way similar to the previously mentioned binding modes, but two nitrogen atoms also operate as bridging donors to the neighbouring metal centre.[18]

Two further interesting binding motifs can be described by means of **(e)** and **(f)**: the coordination in **(e)** is still achieved by the nitrogen donors, but here the ligand itself does not act as a chelate. In contrast to the other binding modes, the ligand is arranged in an open chain, so that each terminal nitrogen atom can coordinate a metal centre. By this the

ligand acts as a bridge in between two metal centres.[19] Apart from the mostly nitrogen-centred coordination complexes obtained for the nacnac ligand, some examples for the coordination via the methylene bridge **(f)** are also observed.[20] In those quite rare cases, the metal cation is preferably coordinated in the solid state by the particular carbanionic centre instead of the more common nitrogen donors.

The first lithium containing nacnac complexes were reported in 1994 by reaction of bis-(trimethylsilyl)-methyl lithium and *tert*-butyl nitrile or benzonitrile in diethyl ether.[17a, 17c, 18b] In this kind of reaction, the first step covers the C–C coupling. Afterwards a 1,3-migration of an organic residue from a carbon to a nitrogen atom takes place. Besides this synthesis route, the most widespread preparation of lithium *β*-diketiminates is accomplished by simple deprotonation of the corresponding parent diketimine with alkyllithiums like *n*BuLi. In case of the Dipp-substituted nacnac ligand and in absence of donating solvents, two different crystal structures were observed for the resulting [Li{(N(Dipp)C(Me))$_2$CH}] and could be described as follows:[10b] one form appears as a dimeric species, in which the lithium cations are furthermore addressed by one aryl substituent of the second molecule. The other form is a dodecamer showing a slipped ladder structure also associated with the interactions of the Li^+ with one or two aryl carbon atoms. In the presence of diethyl ether or THF, monomeric complexes were observed, which exhibit a three coordinate lithium cation by means of the two imine nitrogen atoms and one additional oxygen donor from the Lewis-donating solvent.[10b] These lithiated compounds are commonly used as ligand transfer reagents for the synthesis of other metal complexes by simply adding different metal halides. Due to the resulting salt elimination reaction of the corresponding lithium halide, the desired transmetallated complex can be gained. For more practical reasons of separating the resulting salts, the sodium or potassium *β*-diketiminates were also used, because NaCl or KCl are less soluble in common organic solvents in comparison to LiCl, which facilitates the separation of this side product.[16b]

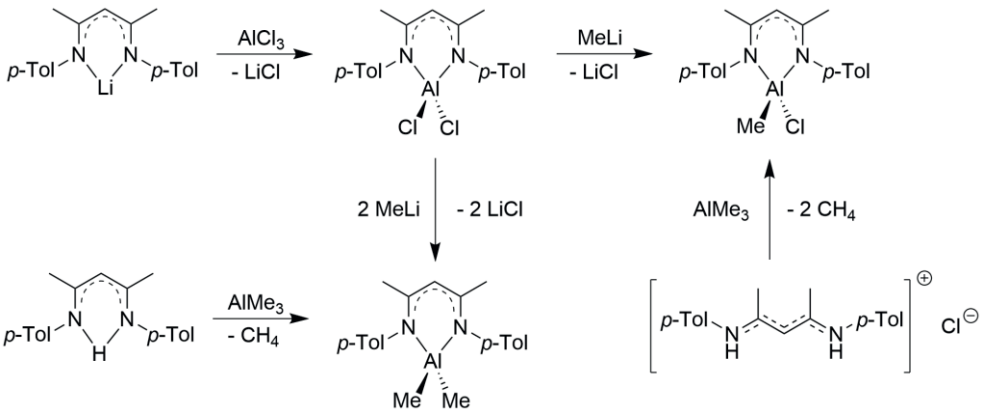

Scheme 1-6: Synthesis route for different exemplary Al(III) nacnac complexes.[14l]

Since the transition metal complexes of the nacnac ligand and the associated tuning of the ligand itself are playing a vital role in current research and catalytic applications,[4d, 4f, 9, 21]

the corresponding research area of main group metal complexes became more and more interesting. Continuing with the group 13 metal complexes of the nacnac ligand, at this point the focus of this section lies on the corresponding aluminium, gallium and indium compounds due to the better connection to the scope of this work. The first aluminium complex $[Cl_2Al\{(N(Me)C(Me))_2CH\}]$ was published in 1991 by preparation from the corresponding ligand, triethylamine as a base, and $AlCl_3$ for metallation.[22] In 1998, the reactivity of the *p*ara-toloyl substituted nacnac ligands was studied in detail and a series of Al(III) complexes could be characterized sufficiently in solution and in the solid state (see Scheme 1-6).[14l] The $AlCl_2$ containing complex was prepared by reaction of the lithiated ligand with $AlCl_3$ under formation of LiCl as the driving force. The remaining chlorido residues at the chelated aluminium atom can easily undergo nucleophilic substitution reactions: by adding methyllithium in different molar equivalents, it is possible to obtain the single or double methyl substituted AlMeCl or $AlMe_2$ bearing complexes, while salt elimination of LiCl is occurring. These two species can also be synthesized in another approach by just adding the alkylaluminium reagent $AlMe_3$ directly to the parent ligand or the corresponding hydrochloride adduct. The basicity of $AlMe_3$ is sufficient to deprotonate the bridging methylene moiety of the ligand's backbone under evolution of gaseous methane, and thus the aforementioned AlMeCl or $AlMe_2$ bearing complexes can be obtained. Furthermore, the synthesis of complexes which contain a MMeCl metal fragment can be achieved by two different approaches: either a transmetallation reaction can take place by using the lithiated species and adding $MMeCl_2$ as reagent, or by simply treating the parent nacnacH ligand with MMe_2Cl to generate methane as side product.[23]

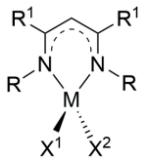

Scheme 1-7: General substitution pattern of the group 13 metal complexes of the nacnac ligand.

Table 1-1: Selected group 13 metal *β*-diketiminato complexes.

R	R^1	M	X^1	X^2	Ref.	R	R^1	M	X^1	X^2	Ref.
Me	Me	Al	H	H	[14h, 24]	Dipp	Me	Al	H	H	[25]
Me	Me	Al, Ga	Cl	Cl	[14j]	Dipp	Me	Al	Me	Me	[14k, 14l, 26]
Me	Me	Al	I	I	[14f]	Dipp	Me	Al	Et	Et	[26]
*i*Pr	Me	Al	H	H	[24]	Dipp	Me	Al	*i*Bu	*i*Bu	[26]
*i*Pr	Me	Al, Ga	Cl	Cl	[14j]	Dipp	Me	Al	Me	Cl	[14d, 27]
*i*Pr	Me	Al	I	I	[14f]	Dipp	Me	Ga, In	Me	Cl	[14d]
*t*Bu	Me	Al, Ga	Cl	Cl	[14j]	Dipp	Me	Ga	H	H	[14d]
Ph	Me	Al	H	H	[24]	Dipp	Me	Ga	Me	H	[14d]
p-Tol	Me	Al	Me	Me	[14l]	Dipp	Me	Al, Ga	F	F	[14d]
p-Tol	Me	Al	Me	Cl	[14l]	Dipp	Me	Al, Ga, In	Cl	Cl	[14i]
p-Tol	Me	Al	Cl	Cl	[14l]	Dipp	Me	Ga	Br	Br	[14d]
C_6F_5	Me	Al	Me	Me	[14e]	Dipp	Me	Al, Ga, In	I	I	[14i]
C_6F_5	Me	Al	Me	Cl	[14e]	Dipp	Me	Ga, In	Me	Me	[14i]
C_6F_5	Me	Al	Me	I	[14e]	Dipp	*t*Bu	Al	Et	Et	[28]
C_6F_5	Me	Al	Br	Br	[14e]	Dipp	*t*Bu	Al	I	I	[28]

Analogue to this synthetic approach, in the last two decades many nacnac metal complexes of aluminium, gallium and indium carrying either alkyl and/or halide substituents were described in the literature. For giving a short overview over these different compounds (see general substitution pattern depicted in Scheme 1-7), some examples for the group 13 metal *β*-diketiminato complexes are listed in Table 1-1.

In addition to the aforementioned ligand systems, which usually exhibit just a remaining hydrogen atom at the deprotonated methylene bridge in the backbone, there are also compounds available which are substituted at this position with aryl moieties[14c] or for example phosphino functionalities.[29] It is obvious from the examples given in Table 1-1 that the majority of the investigated nacnac ligands are carrying methyl groups at the imine carbon atoms and 2,6-diisopropylphenyl moieties at the imine nitrogen atoms. Even if there are also alkyl or other aryl substituted *β*-diketiminates present in ongoing research, the Dipp-substituted nacnac ligands are still the most wide-spread ones and of great interest because of their good shielding abilities. Upon metal coordination, a six-membered metalla heterocycle is formed and the phenyl entities are twisted nearly perpendicular with respect to this metalla heterocycle. By means of this, the *i*Pr groups of the Dipp residues can embrace the coordinated metal atom in an adequate manner, so that neither an oligomerization of the metal fragments in low oxidation state nor electrophilic attacks can occur (*vide infra* in the next chapter).[30] It is known that the scaffold tends to deviate from a planar arrangement within metal coordination by means of twisting or bending, and merely the backbone remains in plane. This deviation is caused by the flexible but bulky organic substituents at the imine moieties. They are twisted nearly perpendicular with respect to the chelating C_3N_2M-plane, which causes the metal atoms to be most protected. To visualize this bonding situation, the crystal structures of the corresponding $AlMe_2$[14l] and the higher congener $GaMe_2$[14i] Dipp substituted nacnac complex are shown in Figure 1-2.

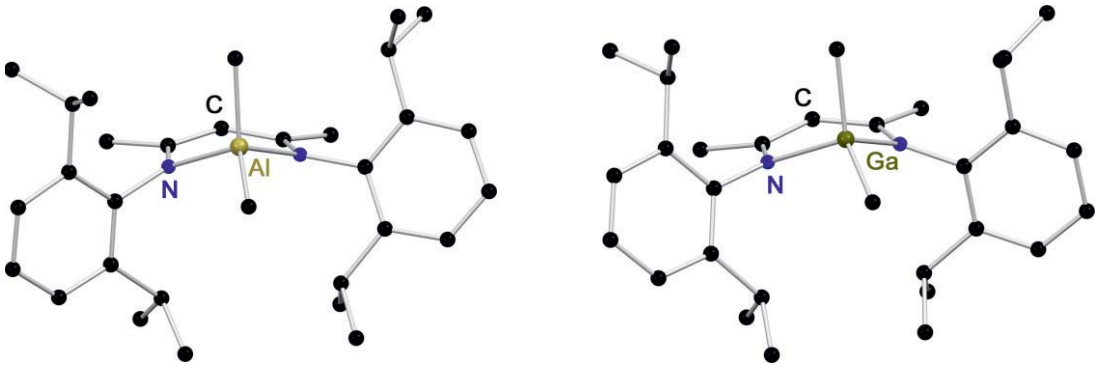

Figure 1-2: Crystal structures without anisotropic displacement parameters of some already known nacnac complexes: *left*: $[Me_2Al\{(N(Dipp)C(Me))_2CH\}]$;[14l] *right*: $[Me_2Ga\{(N(Dipp)C(Me))_2CH\}]$.[14i] Hydrogen atoms are omitted for clarity reasons.

Furthermore, partially hydrolyzed derivatives of the aluminium *β*-diketiminates are known, which exhibit terminal or bridging hydroxy functionalities or bridging oxides in the case of the corresponding alumoxanes.[4e, 23, 31] Referring to the popular methyl alum-

oxane (MAO), which is also generated by partial hydrolysis of trimethyl aluminium and a very potent cocatalyst in the Ziegler-Natta polymerization of ethylene and propylene,[32] and related partially hydrolyzed group 13 metalorganics,[33] the investigations on nacnac supported alumoxanes is of high interest in current research. For example, the formation of such a dialumoxane was achieved in 2012 by controlled NHC-assisted hydrolysis[14e, 31b] of the corresponding organoaluminium chloride [MeClAl{(N(2,6-$Me_2C_6H_4$)C(Me))$_2$CH}] and by an anhydrous approach using Ag_2O as an oxygen source (see Scheme 1-8).[23] Interestingly, the synthesis of the organoaluminium chloride precursor starting directly from the parent nacnacH ligand and dimethyl aluminium chloride yielded the Lewis acid-base-adduct at room temperature, where the aluminium is further coordinated by one imine nitrogen donor of the nacnacH ligand. The deprotonation of the ligand, the associated release of methane and thus the final formation of the AlMeCl complex were achieved in a second step, when the reaction mixture was heated up to the boiling point of toluene.

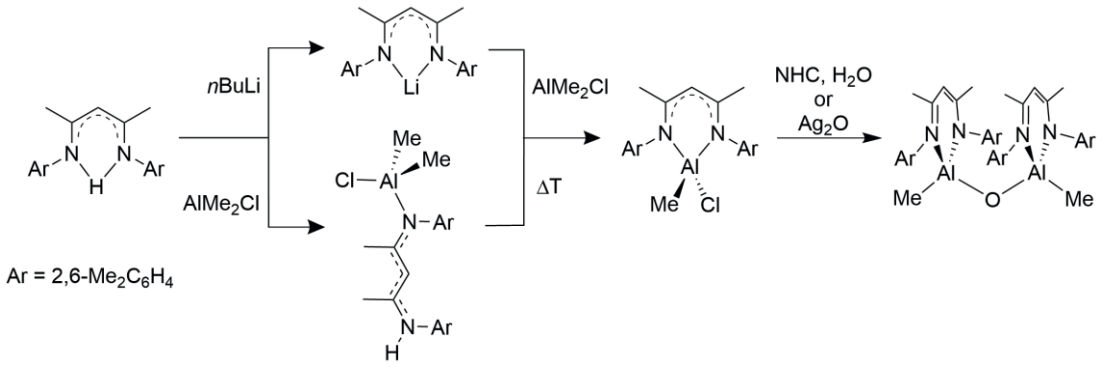

Scheme 1-8: Formation of a nacnac-supported dialumoxane.[23]

1.3 Low-Valent Group 13 Species – Metallylenes

As a further topic in the context of the omnipresent nacnac ligand, its low-valent group 13 metal complexes will be discussed in this section. Following the above-mentioned species in Table 1-1, in the cases of Al, Ga, In and Tl also the reduced species in the oxidation state +I are accessible by using the Dipp-substituted nacnac ligand system, which forms a six-membered metalla heterocycle.[28, 34] These so-called metallylenes, analogues of *N*-heterocyclic carbenes, are rare and offer interesting prospects as reagents in organic syntheses or as ligands in catalysis, where they might replace other commonly utilized *N*-heterocyclic carbenes or phosphanes.[35]

These low-valent group 13 metal centres combine two unifying properties: on the one hand, the low-valency leads to the presence of formally vacant π-orbitals, which causes the metal cation to also incorporate electrophilic reactivity behaviour. On the other hand, the coordinated metal cation carries an electron lone pair, which enables the metal centre to act as a nucleophile or simply as a Lewis donor like NHCs. This lone pair has a quasi-trigonal planar orientation in a *sp*-like hybrid orbital within the plane of the metalla het-

erocycle, which exhibits an increasing *s*-character for heavier metal atoms because of a lower affinity for hybridization.[34c, 35, 36] Due to those main features, the metallylenes are highly reactive species and their stabilization represents a challenging goal in current research.[35] Hence, the low-valent metal cation is stabilized by the mesomeric effect of the adjacent coordinating nitrogen donors. The electron density of their lone pairs, which are located in a *p*-orbital perpendicular to the chelating C_3N_2M plane within the π-system of the delocalized ligand system, is pushed towards the electrophilic metal centre and the electron deficiency of the low-valent group 13 element can be partially compensated (see Scheme 1-9 *left*).[35b]

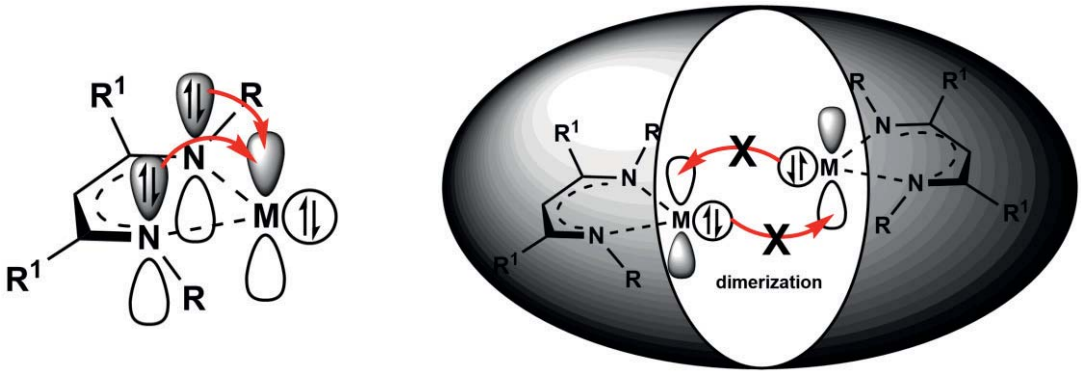

Scheme 1-9: *left:* Stabilization of the singlet ground state in six-membered metallylenes (M = Al, Ga, In, Tl; R^1 = Me, *t*Bu; R = Dipp); *right*: Suppression of self-dimerization due to the bulky nacnac ligand.[35b]

Theoretical calculations for the reactivity of neutral six-membered carbene analogues [M{(N(Ph)C(Me))$_2$CH}] (M = B, Al, Ga, In, Tl) revealed that the singlet-triplet splitting is increasing significantly from boron to the higher homologues.[30] Whereas the splitting for the boron carbenoid is just about 3.5 kcal/mol, the values for the aluminium and gallium derivatives are 45.7 kcal/mol and 54.5 kcal/mol, respectively. These values are highlighting that in the cases of Al and the higher congeners, a singlet ground state can be assumed, in which both electrons are paired in the *sp*-hybrid orbital. On the contrary, in the case of the boron carbenoid, which could not be synthesized successfully yet, a dimerization reaction is predicted to take place easily at room temperature, because also the triplet state (one electron in *p*-orbital and the second in the hybrid orbital) is populated. The dimerization of the heavier carbenoids is accordingly energetically unfavoured from a thermodynamic and kinetic point of view, so that the monomers can be isolated at room temperature. Hence, the reactivity of the group 13 metallylenes towards C–H bond insertion, cycloaddition and dimerization decreases with increasing atomic number of the incorporated metal cation in the order B > Al >> Ga > In > Tl.[30b]

Because of the high electrophilicity of the M(I) species, steric protection is essential to maintain the monomeric carbene-like structural motif and prevent dimerisation or nucleophilic attacks.[30] Therefore, the issue of steric shielding of metal centres within the group 13 complexes in the oxidation state +I is an important aspect for the further applications and reactions. As depicted at the right hand side of Scheme 1-9, the steric demand of the

Dipp-substituted nacnac ligand is sufficient for the suppression of self-dimerization, which is also supported by the theoretical findings in the previous paragraph.

The low-valent aluminium metallylene can be synthesized by converting the corresponding dialkyl aluminium complex into its AlI_2 derivative with the help of two equivalents of elementary iodine. By this procedure, the former methyl groups at the metal centre are replaced by iodide residues and two equivalents of methyl iodide were formed as side product. Afterwards, a reduction step takes place by using potassium or potassium graphite to obtain the carbene-like Al(I) species (see Scheme 1-10) in good overall yields.[28, 34c] The driving force in this reduction approach is the generation of potassium iodide.

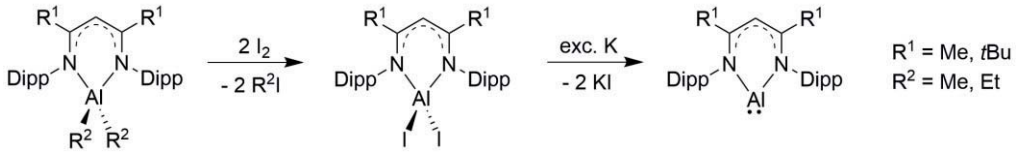

Scheme 1-10: Synthesis of the aluminium containing metallylenes.[28, 34c]

In contrast to the above-mentioned synthesis, the corresponding metallylenes encumbering the heavier congeners like Ga, In or Tl were gained easily by direct salt metathesis starting from the lithium or potassium nacnac complex and the stable low-valent metal iodide precursor. Because the higher congeners show an increasing stability of the metals in low oxidation states,[37] these metal halides are easily accessible in the oxidation state +I in contrast to the corresponding aluminium salt, which is not stable as Al(I) compound. For instance, the gallium metallylene is synthesized by using [Li{(N(Dipp)C(Me))$_2$CH}] and "GaI" and subsequent treatment with potassium to reduce the formed iodide species.[34d] The reactive starting material "GaI" represents a mixture of metalloid Ga and the low-valent species GaI, Ga_2I_3 and Ga_2I_4 and behaves like monovalent gallium iodide.[38] The corresponding In(I) and Tl(I) complexes were synthesized starting from the parent ligand, which is deprotonated by K[N(SiMe$_3$)$_2$] in a first step and undergoes salt elimination with InI[34a, 34b] or TlI[34a] in a one-pot-reaction.

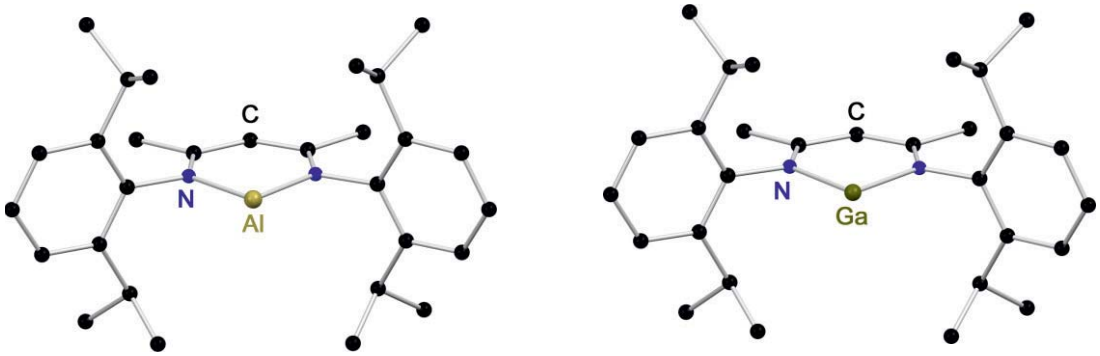

Figure 1-3: Crystal structures without anisotropic displacement parameters of some known nacnac assisted metallylenes: *left*: [Al{(N(Dipp)C(Me))$_2$CH}];[34c] *right*: [Ga{(N(Dipp)C(Me))$_2$CH}].[34d] Hydrogen atoms are omitted for clarity reasons.

In Figure 1-3, the crystal structures of the aluminium and gallium metallylenes, coordinated by the Dipp-substituted nacnac ligand, are depicted. In general, these two structures look quite identical: in both cases the imine substituents are twisted perpendicular with respect to the six-membered metalla heterocycle and the chelated Al(I) and Ga(I) cations are lying nearly ideally in the C_3N_2 plane. In contrast to the crystal structures of the dimethyl substituted M(III) fragments shown in Figure 1-2, it is obvious that there is a clear change in the bonding mode. While in the case of the M(I) species a planar coordination geometry is favoured (Scheme 1-5, case **(a)**), the corresponding M(III) compounds prefer a boat-like alignment in the solid state (Scheme 1-5, case **(b)**). Furthermore, all known group 13 metallylenes (Al, Ga, In and Tl), which are encumbered by the Dipp-substituted *β*-diketiminate ligand, are present as a monomeric species in the solid state. As a proof for the influence of the steric demand of the imine moieties on the aggregation, different indium compounds should be noted.[39] By decreasing the bulkiness of the moieties, changing from Dipp-residues in the monomers to mesityl or xylol substituents, dimeric species can be identified in the solid state.

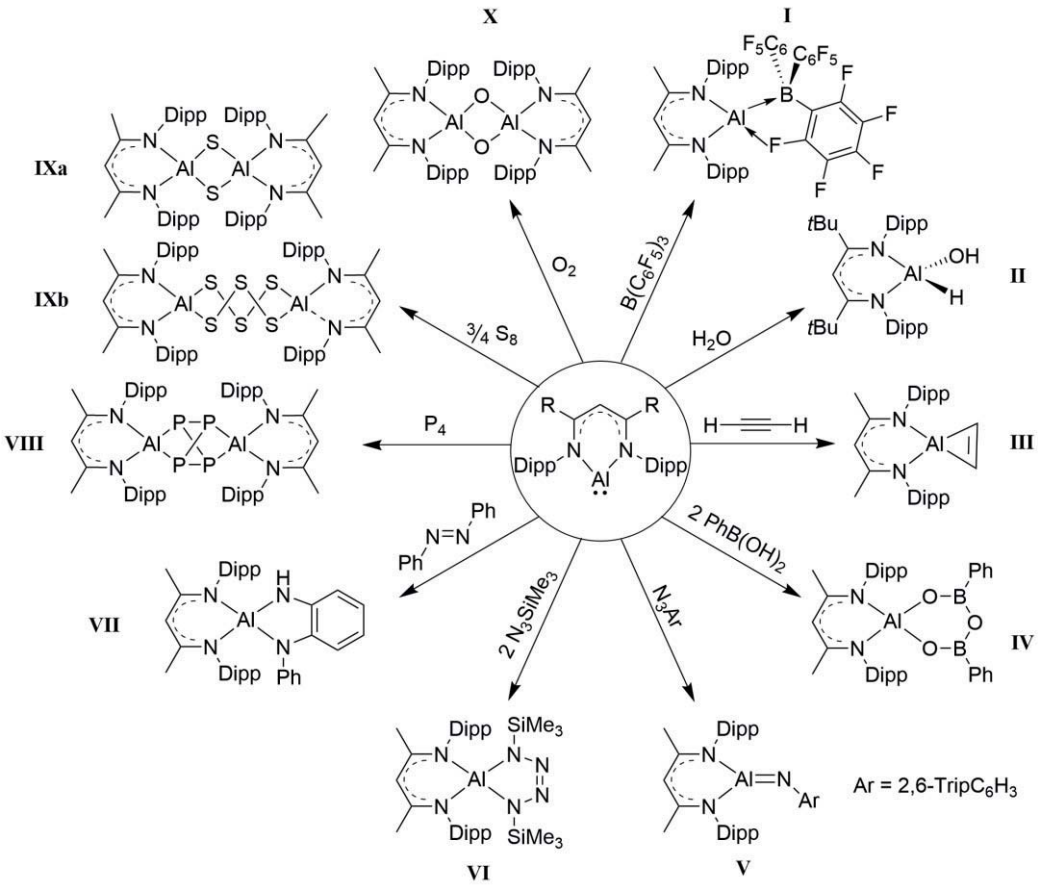

Scheme 1-11: Exemplary reaction behaviour of [Al{(N(Dipp)C(Me))$_2$CH}] with different organic and inorganic substrates.[14b, 16a, 35a, 36]

The different reactions displayed in Scheme 1-11 underline the versatility of the aluminium carbenoid for the transformation of unsaturated organic compounds or inorganic ma-

terial like P_4 or S_8. Starting clockwise with the top right structure, a very interesting Lewis acid-base adduct **I** of [Al{(N(Dipp)C(Me))$_2$CH}] and B(C_6F_5)$_3$ is shown. This compound highlights the electrophilic as well as nucleophilic character of the Al(I) centre: on the one hand, the lone pair at the aluminium is addressed to the boron atom (Al–B distance: 218.5 pm) and on the other hand, the aluminium cation is coordinated as Lewis acid (via its vacant *p*-orbital) by a fluoro substituent of one C_6F_5 moiety (Al···F distance: 215.6 pm).[40] The next molecule shows the hydrolysis product of [Al{(N(Dipp)C(*t*Bu))$_2$CH}], which is obtained upon oxidative addition of water to the low-valent aluminium centre. The resulting Al(III) complex **II** carries a hydroxido and a hydride substituent.[28] In analogy to NHCs, this carbenoid undergoes a [1+2]-cycloaddition reaction, when acetylene is added as reagent. The resulting metalla cyclopropene derivative **III** is shown at the right side of Scheme 1-11.[41] By adding two equivalents of phenylboronic acid to the metallylene, an unprecedented spirocyclic Al(III) complex **IV** with a six-membered B_2O_3Al ring is formed under dissociation of water and H_2.[42] The reaction with azides is dependent on the size of the covalently linked residue: while the reaction with bulky aryl substituted azides leads to the formation of a monomeric imide **V**,[43] the usage of two equivalents of N_3SiMe_3 promotes the formation of the corresponding metalla tetrazole derivative **VI**.[44] Furthermore, the reactivity towards *N*-unsaturated molecules like azobenzene should be mentioned in this context by means of **VII.** It is suggested, that after an intermediate [1+2]-cycloaddition reaction of the Al(I) centre and the N=N double bond, an *ortho*-C–H activation of one phenyl moiety takes place.[45] The compounds **VIII** and **IX** are prominent examples for representing the reducing properties of [Al{(N(Dipp)C(Me))$_2$CH}] in conjunction with inorganic substrates like P_4 or S_8. In compound **VIII**, an activated P_4^{4-} moiety is implemented in a bridging fashion between two Al(III) containing nacnac ligands. Formally, the aluminium centres are inserted into two opposing P–P edges of the white phosphorus to end up in the shown target molecule.[46] By adding elemental S_8 to the carbenoid species, two different (poly-)sulfide bridged molecules **IXa** and **IXb** could be isolated and structurally characterized. As the major product of that reaction, in the first case the two aluminium cations are linked by two μ-S entities,[47] whereas in the latter case as side product a S_3-bridged dimeric species was gained.[48] Finally, the reaction product with elemental O_2 is depicted as compound **X**. This compound shows the ability of the parent low-valent aluminium nacnac complex to activate small molecules by cleaving the O=O double bond under reducing conditions. This affords [(μ-O)Al{(N(Dipp)C(Me))$_2$CH}]$_2$ similar to the previously mentioned sulfide bridged dimer.[49]

As a consequence of the previously discussed reaction products, [Al{(N(Dipp)C(Me))$_2$CH}] seems to be a very promising reagent for small molecule activation or transformation of organic substrates. These features are induced by its ability to act as reducing agent in combination with electrophilic and nucleophilic reaction behaviour at the Al(I) centre. In summary, the aluminium metallylene shows similar reactivity like in the cases of singlet carbenes.[50] In the context of the ongoing increasing demand in the activation of small molecules like H_2, N_2, NH_3 or CO_2, the development of new synthetic approaches for generating catalytic active species is of high interest. Even though this research area of catalytic activation is mostly focused on the field of transition metal

complexes, the transfer to suitable main group metal complexes, which should adopt the same catalytic reactivity compared to the transition metals or even exceed them, plays a key role in current research.[51]

As figurehead for efficient small molecule activation, the FLP chemistry (frustrated Lewis pairs) developed to a promising research area over the last decade and is mentioned at this point for comparative reasons.[52] In this course, the usage of mainly phosphorus/boron, nitrogen/boron or carbon/boron FLP systems offers a simple access to the efficient splitting of dihydrogen[53] or ring opening of THF.[54] Aluminium-based FLP's were found to be advantageous for B–H or N–H bond activation,[55] polymerisation reactions of methyl methacrylate[56] and conversion of CO_2.[57] Furthermore, the nacnac ligand and the derived main group metal complexes, respectively, facilitate the stabilisation of metal ions in low oxidation states as mentioned previously. The synthesis of the first Mg(I) compound[58] and corresponding β-diketiminate Ca(II) complexes,[59] which were successfully applied for epoxide/CO_2 copolymerisation[60] or hydrogenation reactions of alkenes with H_2,[61] should be highlighted as alkaline earth metal complexes performing in catalysis.

As already mentioned above, the low-valent Al(I)[14b, 28, 34c, 36, 62] and Ga(I)[34d] species employing the Dipp-substituted nacnac ligand are accessible. More recently, the catalytic activity of the related alumoxanes was studied in detail.[31a, 23, 25a, 63] In this context also other common ligand types including substituted terphenyls should be mentioned briefly, which are used for stabilisation of dimeric low-valent group 13 species involving metal-metal multiple bonds and are prone for interaction with small molecules like H_2.[64]

The coordination chemistry as donor Lewis base of the first aluminium metallylene, whose reaction behaviour was briefly described in Scheme 1-11, towards other (transition) metals is presently just barely investigated. For example, there are three palladium complexes described in the literature, in which [Al{(N(Dipp)C(Me))$_2$CH}] acts as a σ-donor ligand in a terminal or bridging fashion at one or two Pd centres, respectively. In two cases, the palladium cations are further coordinated by dvds ligands (dvds = 1,1,3,3-tetramethyl-1,3-divinyldisiloxane), and in another case, those siloxane ligands are replaced by monovalent GaCp*.[65] Referring to the former mentioned palladium complexes bearing the dvds ligands, additionally a related complex was synthesized, which is terminally coordinated by a NHC instead of the Al(I) metallylene.[66] A structural comparison of those two complexes, one carrying a NHC and one a metallylene, reveals that the C–C bond lengths within the dvds ligands are nearly identical. This fact gives rise to the assumption that [Al{(N(Dipp)C(Me))$_2$CH}] has comparable σ-donor abilities like the NHC.

In contrast to the Al(I) species, the metal coordination abilities of the corresponding Ga(I) complex are much more developed, although its utilization in the transformation of organic substrates compared to the aluminium counterpart is less investigated due to its weaker reducing nature.[35a] In the same context as described in the former paragraph, the Pd(0) complex of [Ga{(N(Dipp)C(Me))$_2$CH}] and the dvds ligand was studied in detail. Additionally, different mono- and dinuclear Pt(0) complexes carrying two low-valent gallium ligands and carbonyl or isonitriles were synthesized and structurally characterized.[65a] To continue with further examples for derived transition metal complexes, the

following compounds should be mentioned at this point: an iron complex was accessible via facile reaction of $Fe(CO)_5$ with a gallium metallylene[67] and two rhodium chlorido complexes could be obtained by substitution of a PPh_3 or cyclooctene ligand in the starting material.[68] Furthermore, several homo- and multinuclear nickel olefin complexes are known in the literature, in which the [Ga{(N(Dipp)C(Me))$_2$CH}] acts as terminal or bridging Lewis donor ligand.[69]

1.4 Related Bridged Bisheterocycles

Because of the very high interest and the associated research activities in the broad field of nacnac metal complexes (see Figure 1-1), other promising ligand platforms have come into play which are closely related to the ubiquitous *β*-diketiminato ligand. Most of them are mimicking its chelating coordination behaviour, so that upon metallation a six-membered metalla heterocycle with six delocalized *π*-electrons is formed, in which two imine nitrogen atoms are working as Lewis donors for the metal centre. The two $R^1C{=}NR$ moieties of the prototype nacnac ligand are replaced by fused heterocycles, which each also possess an endocyclic C=N imine moiety to retain the same coordination abilities. Formally, the residues at the backbone of the parent nacnac ligand are fixed to the imine nitrogen atom, while formation of a mostly five- or six-membered heterocycle occurs. Examples for the derived bridged bisheterocyclic compounds, which were studied in the past two decades intensively, are depicted in Scheme 1-12.

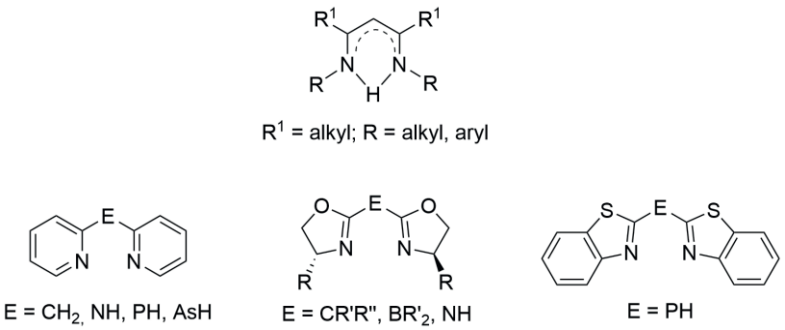

Scheme 1-12: Comparison of the nacnacH ligand (*top*) and related ligand systems carrying fused heterocyclic substituents (*bottom*).

Starting with the popular bis-(oxazolin-2-yl)-methanes, also abbreviated as BOX ligands, which is shown as the molecule in the middle of Scheme 1-12 (with E standing for a substituted methylene bridge), very fruitful ligand systems for asymmetric catalysis were developed in the beginning of the 1990s.[70] Those ligands consist of five-membered heterocycles, which are bearing a saturated C–C single bond in the backbone. This key feature is essential for the introduction of chiral centres at the ligand, mostly at the position adjacent to the nitrogen. Due to the coordination via the two imine nitrogen donors, the stereochemically active residues are in close proximity to the coordinated substrate, so that the chiral information can be transferred to that substrate, which enables efficient

asymmetric catalysis.[71] In the most metal complexes, the neutral BOX ligand is involved, where the bridging methylene moiety carries two alkyl substituents.[71b, 72] Although the neutral ligand is more prominent in coordination chemistry, the monoanionic form of the BOX ligands with at least one remaining hydrogen atom in the backbone (E = CH_2 or CHR) can be achieved by facile deprotonation. The related methanide complexes are established as well.[70c, 73] In addition to the common BOX ligands, asymmetrically substituted methane derivates are known, where e.g. one oxazoline heterocycle is substituted by a NHC[74] or bis-(*N*-arylamino)-phosphane residue.[75] The formal substitution of the methylene bridge by a nitrogen atom yields in bis-(oxazoline)-amines,[76] 5-aza-semicorrins[77] and chiral bis-(2-pyridylimino)-isoindoles[78] with interesting comparable organic scaffolds. Furthermore, it is possible to link two oxazoline moieties via a BR_2 bridge.[79] Other catalytically active species were synthesized in the work group of Kempe. For instance, two obtained iridium complexes containing each functionalized amine moieties can be used as efficient catalyst for pyrrole synthesis[80] or for *N*-alkylation of amino pyridines and anilines.[81]

Another ligand class is depicted at the left hand side of Scheme 1-12, where two 2-pyridyl moieties were introduced as side arms instead of the above-mentioned oxazolines. In the case, that the bridging moiety is a methylene bridge, the resulting dipyridyl methane[82] and the corresponding methanides were investigated in the 1990s. In former publications, our workgroup synthesized a series of lithium and group 13 metal complexes of the bis-(pyrid-2-yl)-methanide and an associated structure-reactivity study was performed based on the results of X-ray diffraction experiments.[83] Representing the group 1 complexes, $[([12]crown\text{-}4)_2Li][Li\{(2\text{-}NC_5H_4)_2CH\}]$ can be highlighted as a solvent separated ion pair, or $[(thf)_2Li\{(2\text{-}NC_5H_4)_2CH\}]$ as a monomeric lithiated compound, both solely yielding Li–N contacts.[83a, 83c] These two lithiated compounds were easily accessible via deprotonation reaction of the parent dipyridyl methane with equimolar amounts of *n*BuLi in either hexanes or THF as the solvent. As an intermediate of that deprotonation, it was moreover possible to isolate (at −80 °C) and characterize $[\{(2\text{-}NC_5H_4)_2CH_2\}Li\{(2\text{-}NC_5H_4)_2CH\}]$. In this complex, just one half of the starting material is deprotonated, whereas the other half equivalent remains untouched, so that a lithium complex with one monoanionic and one neutral ligand is formed.[83d] Additionally, some group 13 complexes like $[Me_2Al\{(2\text{-}NC_5H_4)_2CH\}]$ and $[Me_2Ga\{(2\text{-}NC_5H_4)_2CH\}]$, where the $(thf)_2Li$ unit is formally replaced by a Me_2Al or Me_2Ga moiety, were prepared by adding $AlMe_2Cl$ or $GaMe_2Cl$ to the lithiated compound, respectively.[83d, 84]

In further research on these ligand systems, the coordination abilities and electronic properties were affected by switching the bridging atom between the two heteroaromatic residues from a group 14 to a group 15 element. This means that the bridging CH_2 unit is isoelectronically replaced by NH,[85] PH[86] or AsH.[85c, 87] The corresponding investigated main group metal complexes of the derived monoanionic ligand systems will be described as follows: the dipyridyl amine, which contains a secondary amine functionality in the bridging position, reacts smoothly with the corresponding trimethyl organo metallic reagent MMe_3 (M = Al, Ga, In, Tl) to give the desired MMe_2 complex under formation of methane. In the case of the thallium complex, the reactive species $TlMe_3$ has to be gener-

ated *in situ* by usage of $TlMe_2I$ and MeLi, prior the parent amine ligand is added.[85c] The resulting crystal structures of those metal complexes are shown in Figure 1-4.

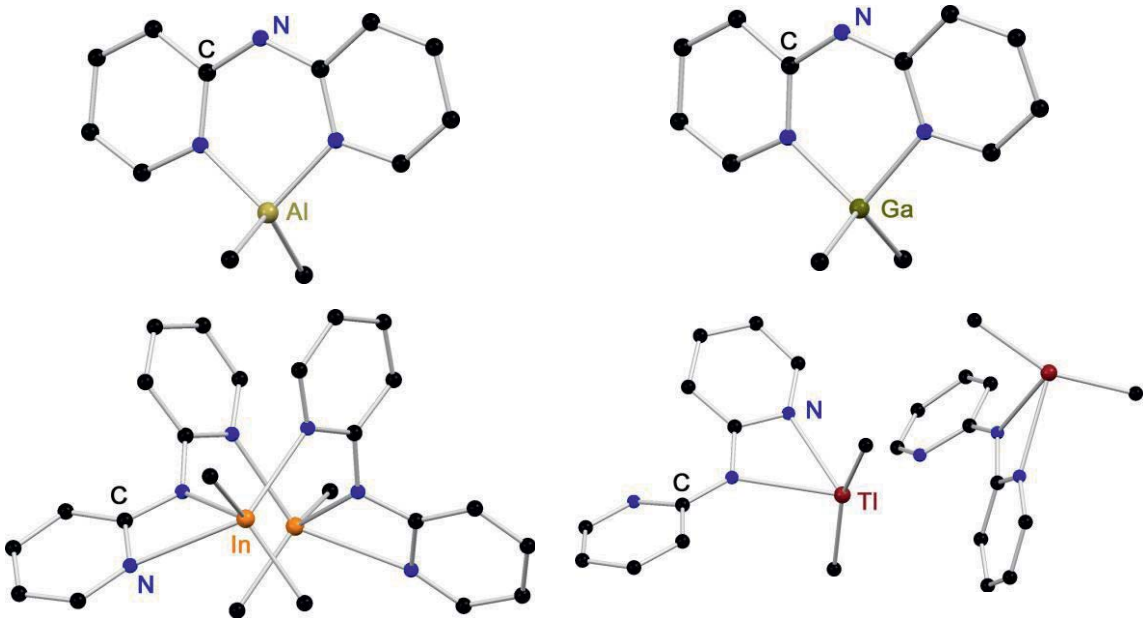

Figure 1-4: Crystal structures without anisotropic displacement parameters of the group 13 metal complexes $[Me_2M\{(2\text{-}NC_5H_4)_2N\}]$: *top left*: M = Al; *top right*: M = Ga; *bottom left:* M = In; *bottom right*: M = Tl.[85c] Hydrogen atoms are omitted for clarity reasons.

For the aluminium and gallium containing complexes, a monomeric species was elucidated in each case, where the metal fragment gets exclusively coordinated by the two endocyclic imine nitrogen donors of the pyridyl moieties in a *cis-cis* fashion (see Figure 1-4 *top*). The nomenclature of the binding mode by means of *cis* or *trans*, which the amide ligand can adopt, is described in Scheme 1-13. Due to the partially present C_{ipso}–N_{bridge} double bond,[83c, 85a, 85c, 87] the arrangement of the connected highest priority atoms distinguishes whether a *cis* or a *trans* (also called *Z* or *E*) conformation with respect to the considered C_{ipso}–N_{bridge} bond is present.[88] Both scenarios are highlighted with coloured bonds within Scheme 1-13.

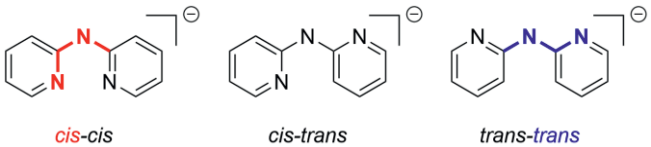

Scheme 1-13: Possible binding modes of the dipyridyl amide ligand.

For example, the *cis*-conformation of one pyridyl side arm is highlighted in red colour at the left hand side: in analogy to common C=C double bonds, the imine nitrogen atom N_{het} and C_{ipso} of the second heterocycle are aligned at the same side of the considered C_{ipso}–

N_{bridge} bond. Therefore, a *cis* conformation is postulated in this scenario. At this point it has to be mentioned, that this nomenclature is opposite to that one stated in the original publication because of the better plausibility.[85c]

In the cases of the higher group 13 homologues, the coordination behaviour looks quite different (see Figure 1-4 *bottom*). Presumably owed to the enhanced ionic radii of the indium and thallium fragments, the dipyridyl amide ligands are switching to other binding modes: whereas in the $InMe_2$ complex a nearly complete *trans-trans* conformation of the ligand is adopted to build up a dimeric structure, in the $TlMe_2$ derivative a *cis-trans* alignment is preferred to generate an infinite coordination chain. In both cases, the metals are addressed by three nitrogen donors (two originating from the same ligand and one from another), whereas the lighter congeners are just coordinated by two and the bridging amide functionality is not involved in any interactions.[85b, 85c]

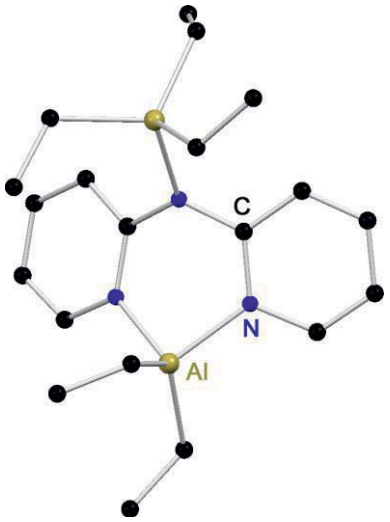

Figure 1-5: Crystal structure without anisotropic displacement parameters of $[Et_2Al\{(2\text{-}NC_5H_4)_2N\}]\cdot AlEt_3$.[85a, 85b] Hydrogen atoms are omitted for clarity reasons.

Especially for aluminium as metal centre, several additional complexes were synthesized and characterized. By addition of one equivalent of $AlEt_3$ to the neutral bis-(pyrid-2-yl)-amine ligand, the corresponding $AlEt_2$ complex could be isolated, which is coordinated by the *cis-cis* arranged ligand. Interestingly, the addition of a second equivalent of $AlEt_3$ leads to the formation of the butterfly-like shaped $AlEt_2$ complex additionally coordinated to a Lewis acidic $AlEt_3$ molecule (see Figure 1-5).[85a, 85b] This Lewis acid-base adduct reveals the fact, that the Lewis basicity of the bridging nitrogen atom is still high enough so that it can also participate actively in coordination, while both the endocyclic donors are chelating another metal centre. Analogue observations were made several years ago for Ni(II), Rh(I) and Ir(I) complexes of the dipyridyl amide ligand.[89] By changing the molecular stoichiometry of $(2\text{-}NC_5H_4)_2NH$: $AlEt_3$ from 1:1 to 3:1, the dissociation of three equivalents of ethane is triggered, so that three ligands are arranged around one Al(III) centre. In this six-coordinate aluminium complex, the dipyridyl amides are preferring a *cis-trans* conformation because this binding mode allows the accumulation of three

bulky ligands in close proximity of the coordinated Al(III) ion.[85a] A further six-coordinate aluminium compound was synthesized by addition of $AlCl_3$ to the lithiated ligand in pyridine. The resulting $[(NC_5H_4)_2Cl_2Al\{(2\text{-}NC_5H_4)_2N\}]$ complex carries two solvent pyridines as Lewis donors, and the ligand is again arranged in a *cis-trans* manner. It is assumed, that in a hypothetical *trans-trans* alignment, there would be steric repulsion between the chlorido substituents at the Al fragment and the hydrogen atoms of the ligand's pyridine rings.[85a]

The heavier analogues of the dipyridyl amine based ligands, in which the bridging moiety is a secondary phosphane or arsine, are also well-established and were thoroughly investigated especially by our workgroup. The synthesis of the related parent ligand system $(2\text{-}NC_5H_4)_2EH$ (E = P or As) is achieved by reductive cleavage of a E–aryl bond in the starting material $(2\text{-}NC_5H_4)_3E$ in the presence of elemental lithium and subsequent hydrolysis.[86e, 87] Referring to the above-mentioned amide metal complexes the treatment of $(2\text{-}NC_5H_4)_2PH$ with organometallic reagents like *n*BuLi or $AlMe_3$ leads to the formation of the desired metallated species $[(thf)_2Li\{(2\text{-}NC_5H_4)_2P\}]$ and $[Me_2Al\{(2\text{-}NC_5H_4)_2P\}]$ due to subsequent deprotonation of the ligand's backbone.[86b, 86e, 87] In the resulting compounds, each ligand adopts a *cis-cis* conformation to allow the chelation of the metal centre by the two pyridyl nitrogen donors, whereas the bridging sp^2-hybridized moiety is not involved in coordination to the hard metal cations Li^+ or Al^{3+}.[90] By switching to softer metal cations for coordination like Cs^+, with PMDETA as additional three dentate Lewis base, it was possible to observe the coordination via the bridging phosphorus atom and one pyridyl moiety of the *cis-trans* aligned ligand in the solid state.[86c]

The dimethyl aluminium containing compound is again available throughout transmetallation of the lithiated species with $AlMe_2Cl$. The same procedure was additionally successfully applied for the generation of the $GaMe_2$ phosphanide complex, but in this case no crystals suitable for SCXRD could be obtained, so that no structural comparison towards the $AlMe_2$ derivative can be made. Furthermore, the reaction of $(2\text{-}NC_5H_4)_2AsH$ leads to the corresponding $[Me_2Al\{(2\text{-}NC_5H_4)_2As\}]$ as expected.[87] A structural comparison of the lithium and aluminium containing phosphanide complexes revealed, that in the case of the lithiated species, the ligand is nearly ideally planar aligned. In contrast, the corresponding aluminium complex is folded like a butterfly (folding angle: 155 deg).[87] By adding $[CpFe(CO)_3][BF_4]$ to $[Me_2Al\{(2\text{-}NC_5H_4)_2P\}]$ it was attempted to generate a hetero bimetallic compound, in which the phosphanide is addressed to the Fe(II) centre, while the $AlMe_2$ fragment is still chelated. Unfortunately, the coordinated aluminium centre vanished in this reaction, presumably by the formation of AlF_3 as the driving force. Nevertheless, as a result the bridging phosphorus donor is involved in coordination as desired: two iron cations are coordinated by the linking unit and this time, the ligand framework prefers the *trans-trans* conformation in the solid state.[86c]

In the case of the secondary phosphanes, intensive studies were also carried out on derivatives containing larger heteroaromatic compounds like benzothiazole, which replace the former pyridyl residues. Within our work group, this phosphane $(NCSC_6H_4)_2PH$ was the main topic of several investigations since the last decade to claim the deprotonated phosphanide anion as a so called Janus head ligand.[84, 86b, 88, 91] This phrase is named after

the eponymous god of beginnings and endings of the ancient Roman mythology, which has two faces pointing in opposite directions (one into the future and the other one into the past) as depicted at the left side of Figure 1-6. Referring to his associated duality and ambivalence, these properties were assigned to ligand systems that include at least two different Lewis donor moieties. Depending on the introduced metal cation, different coordination behaviour of the same ligand can be obtained following the rules of the HSAB principle.[90, 92]

Figure 1-6: *left*: Coin representing the head of Janus,[93] *right*: possible binding sites of $[(NCSC_6H_4)_2P]^-$ towards either soft or hard metal cations.[90, 92]

These features can also be assigned to the previously mentioned bis-(benzothiazol-2-yl)-phosphane ligand, also abbreviated as $HP(bth)_2$, as it can be seen in Figure 1-6 right hand side. The deprotonated ligand itself contains three different potential donor atoms with varying degrees of hardness and metal site selectivities by means of the two endocyclic nitrogen and sulfur atoms as well as the bridging phosphorus. Theoretically, each of them can be addressed to a suitable metal centre in a corresponding metal complex: the nitrogen donors are classified as rather hard Lewis bases and therefore also the coordination of equally hard Lewis acids like Li^+ or Al^{3+} should be favoured. Due to the smaller charge-to-radius ratio and the comparatively facile polarizability of the phosphorus and even the sulfur atoms, these elements are designated as rather soft Lewis bases, which are forming stable adducts with also soft metal cations.

The ligand synthesis is similar to that one described for the pyridyl substituted phosphane, in this case starting from tris-(benzothiazol-2-yl)-phosphane.[88] Charge density studies and theoretical calculations on this particular ligand platform deal with its associated heteroaromaticity[94] and reveal that the NH tautomer is energetically most favourable in comparison to the according PH tautomeric form (see Scheme 1-14).[91e] Thus, a beneficial formation of N–H···N hydrogen bonds between the benzothiazole moieties is possible to support the stability of this rare example of a phosphane, where the phosphorus remains divalent and the hydrogen atom is located at the ligand periphery.

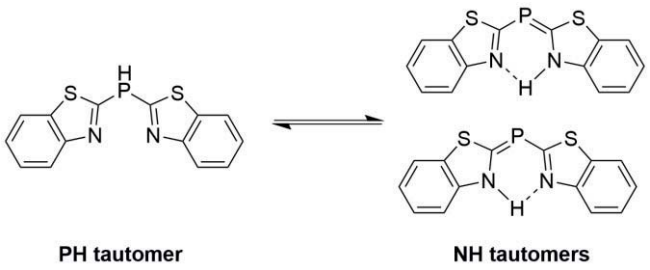

Scheme 1-14: Possible tautomeric forms of $HP(bth)_2$.

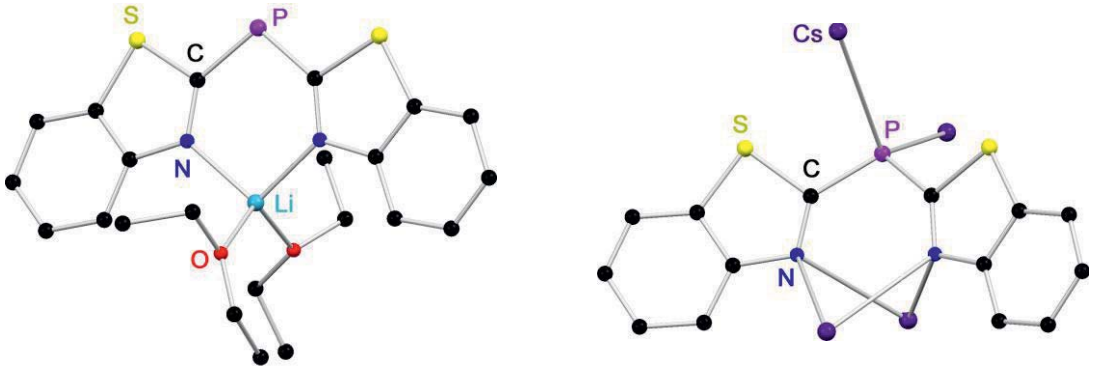

Figure 1-7: Crystal structures without anisotropic displacement parameters of metallated $P(bth)_2$ complexes: *left*: $[(Et_2O)_2Li\{(NCSC_6H_4)_2P\}]$;[88] *right*: $[Cs\{(NCSC_6H_4)_2P\}]_\infty$.[91e] Hydrogen atoms are omitted for clarity reasons.

Deprotonation of the neutral ligand via addition of *n*BuLi in diethylether yields in the *N*,*N*-chelating lithiated phosphanide monomer, which is stabilized by two Et_2O molecules (see Figure 1-7 *left*).[88] As expected, the hard lithium cation is coordinated exclusively by the imine nitrogen atoms of the benzothiazole side arms. To achieve a further coordination of the soft phosphorous backbone towards a second metal centre, $[CpMn(CO)_2(thf)]$ was added to the lithiated compound. As a result, the donating THF molecule was readily replaced by the phosphanide in the manner, that the phosphorus is bridging in between to two $CpMn(CO)_2$ moieties like in the case of $[\{Cp(CO)_2Fe\}_2\{(2\text{-}NC_5H_4)_2P\}]$ mentioned earlier.[86c] Moreover, the former diethylether molecules at the chelated Li^+ are replaced by two bridging carbon monoxide ligands, each one originating from the half-sandwich manganese fragments to give an overall coordination polymer.

Another main group metal complex of $P(bth)_2$ was also demonstrated in 2007 by means of $[Cs\{(NCSC_6H_4)_2P\}]_\infty$ (see Figure 1-7 *right*).[91e] This compound was synthesized by reaction of phosphane and elementary caesium under evolution of gaseous H_2, and the obtained crystal structure reveals a polymeric coordination motif. The monoanionic ligand is coordinated to four Cs^+ cations, each two at the phosphanide and two in a chelating fashion between the nitrogen donors. From another side of view, each caesium cation is coordinated by four ligands: two of them are donating via the P bridge and the remaining two are chelating via their imine functionalities to give a trigonal prismatic coordination geometry.[91e]

Finally, the phosphane's treatment with transition metal bis-(trimethylsilyl)-amides should be pointed out at this stage. Upon equimolar addition of zinc or cadmium bis-(trimethylsilyl)-amide, dimeric metal complexes were generated, in which the ligand system again adopts the *trans-trans* alignment for *N,N*-chelation of the $MN(SiMe_3)_2$ fragment.[91f] The resulting dimers are linked together via head-to-tail coordination, where the two metal complexes are stacked on top of each other with opposite orientation. This stacking allows the additional coordination of the metal cation by the phosphorus atom of the corresponding other ligand to gain five-fold coordination of the transition metal. In the case of metallation of $HP(bth)_2$ with iron bis-(trimethylsilyl)-amide, a molar ratio of 2:1 was chosen to give the iron centred complex carrying two monoanionic phosphanide ligands.[91a] The cation is distorted tetrahedrally coordinated by the four benzothiazole nitrogen atoms of the *trans-trans* aligned ligands and the backbone of the Janus head ligand shows no further intermolecular interactions. To invert this coordination motif and address the other face of the Janus head ligand, the following reaction procedure was executed: in a first step the parent ligand was deprotonated with dimethyl zinc for the synthesis of $[MeZn\{(NCSC_6H_4)_2P\}]$. In a second step, the half-sandwich complex $[CpFe(CO)_2I)]$ was added, and under elimination of ZnMeI and CO, the transmetallated dimeric product $[CpFe(CO)\{(NCSC_6H_4)_2P\}]_2$ was accessible. This molecule is an interesting example for this ligand, in which the coordination of the transition metal is exclusively accomplished by the Janus ligand's P-site, whereas the N-site is pointing loathly in the opposite direction. The two CpFe(CO) fragments behave as bridging moieties between the phosphanides in that dimer.[91a]

In conclusion, the bis-(benzothiazol-2-yl)-phosphanide ligand can be justifiably described as a promising Janus head ligand, which shows site selective coordination behaviour depending on the implemented metal cations. This coordination flexibility, the facile access and the possibility to build up hetero bimetallic complexes are underlining the importance and necessity to investigate the intrinsic properties of this class of ligands more detailed in future research.

1.5 Scope of This Thesis

The omnipresent monoanionic nacnac ligand enables the stabilisation of main group elements in low oxidation states and is used as supporting ligand in several catalytical applications. Referring to the nacnac ligand's advantages, in the context of this work new ligand systems should be exploited mimicking those electronic and steric properties.

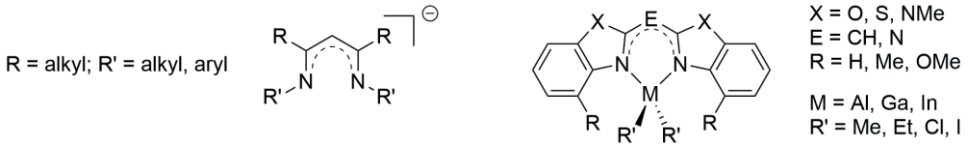

Scheme 1-15: Similarities between the monoanionic nacnac ligand (*left*) and the bisheterocyclo methanides or amides (*right*), respectively.

The desired parent bisheterocyclo methane and amine ligand platforms, shown in Scheme 1-15, are consisting of two benzannulated 1,3-azoles (mostly benzoxazole and benzothiazole), which are C2-connected via either a methylene or an amine spacer. In comparison to the paragon nacnac ligand, formally the imine substituents are fixed to the backbone of the ligand by building up an additional five-membered heterocycle, containing either oxygen or sulfur atoms as additional donor sites. In addition to the neutral ligands, also the syntheses and characterization of the derived group 1 and group 13 metal complexes thereof are a main goal of this thesis.

Due to the presence of four heteroatoms in the *β*-position, the bridge's protons can easily be abstracted by reaction with the corresponding metalorganic reagents to form the monoanionic species, carrying the remaining metal fragment. Hence, the resulting bisheterocyclo methanides or amides exhibit three possible donor sites for the metal coordination: the deprotonated bridging carbanionic/amidic centre, the endocyclic chalcogene atoms or the imine nitrogen donors. In analogy to the nacnac ligands, also a coordination motif for the metallated species is expected, wherein the metal centre is chelated by two endocyclic nitrogen donors of the *trans-trans* aligned ligand. Furthermore, an evaluation should take place, if depending on the size of the coordinated metal cation other binding modes can be identified due to the different Lewis-donor abilities of the implemented heteroatoms.

For future research on corresponding low-valent metallylenes based on these ligand systems, a screening for suitable derivatives and precursors will be approached, which considers the following criteria: **(1)** the planarity of the formed six-membered C_3N_2M metalla heterocycle and **(2)** the efficient shielding of the group 13 metal fragment. Therefore, the screening involves the variation of the heterocycles (including substitution at the annulated benzene moiety), the bridging moiety and the coordinated metal fragments.

With this in mind, in the field of main group transformations, ligand design in particular and the choice of suitable main group element has a significant influence on the stability and the catalytic abilities of the resulting compounds. Thus, the desired bisheterocyclo methanide and amide complexes should achieve the best from two worlds: the stabilisation abilities for future low-valent metal complexes and the reactivity of group 13 metals.

2 Results and Discussion

2.1 Symmetrically Substituted Bisheterocyclo Methanes

Major parts of this section were published in: David-Raphael Dauer, Dietmar Stalke, Heterocyclic substituted methanides as promising alternatives to the ubiquitous nacnac ligand, *Dalton Trans.* **2014**, *43*, 14432–14439.[95]

Since the past three decades, the bisheterocyclo methane ligand systems just received minor interest in coordination chemistry research. Although the synthesis of bis-(benzothiazol-2-yl)-methane is known many years ago,[96] just a few studies were undertaken for this interesting potential ligand concerning mostly NMR spectroscopic investigations.[97] In those investigations, the tautomerism of different alkyl substituted bis-(benzothiazol-2-yl)-methane derivatives is studied. Further NMR spectroscopic studies were also examined for the benzoxazole and (benz-)imidazole containing ligands and the derived deprotonated species to calculate the specific charge demands of the heteroaryl substituents.[98] This classification was accomplished by largely validated ^{13}C- and ^{15}N-NMR shift / charge ratios, which were determined for several heteroaromatic and primary organic substituents in related methylene bridged species.[99] Furthermore, it was shown that the bisheterocyclo methanes are appropriate ligands in transition metal complexation, because they can act either as neutral ligand LH or as monoanionic ligands L^-.[98a] In the first case, a salt complex $[M(LH)_2]^{2+}$ is achieved by adding divalent transition metal halides $M(II)X_2$. In contrast to that, the addition of corresponding metal acetates $M(II)(OAc)_2$ leads to the deprotonation of the ligand, which yields in the formation of neutral chelate complexes $[ML_2]$.

With this knowledge in mind and referring to the scope of the thesis, the following chapter deals with the syntheses and structural elucidation of the investigated bisheterocyclo methane and methanide derivatives, which are substituted twice with the same benzo-fused 1,3-azole moiety. In this context, mainly the bis-(benzoxazol-2-yl)- and bis-(benzothiazol-2-yl)-methanes and the derived group 13 metal complexes, bearing the monoanionic ligands, will be discussed in detail. To follow up with the previous results of the master thesis, additionally the *N*-methylimidazole and *N*-methylbenzimidazole containing ligand systems will contribute to some extent to the results of this section.

2.1.1 Ligand Syntheses

The herein discussed bisheterocyclo methanes **4** and **5** were synthesized with the intention to mimic the related *β*-diketiminate ligand, also known as nacnac ligand. As depicted in Scheme 2-2, both ligand systems **4** and **5** were synthesized in a cyclocondensation reaction of a suitable linker derived from a malonic acid derivative and two equivalents of the corresponding *ortho*-substituted anilines.

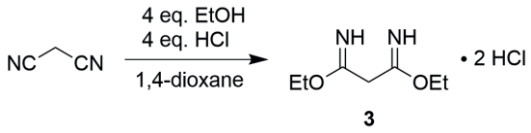

Scheme 2-1: Synthesis of the bisimidate linker **3**.

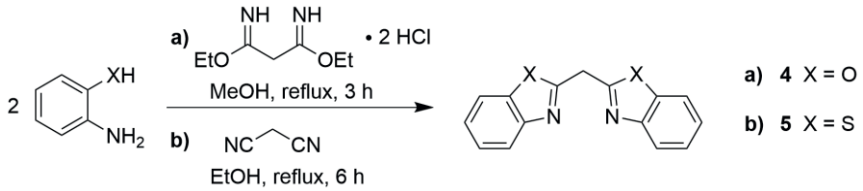

Scheme 2-2: Synthesis of the homo-disubstituted methylene ligand systems **4** and **5**.

In this cyclocondensation reaction, pathway **(a)** in Scheme 2-2 shows that the phenol derivatives are less reactive compared to the corresponding thiophenols **(b)**. Therefore, the former malononitrile has to be further activated before it undergoes a reaction with the phenolic nucleophile. This can be achieved by generating the derived ethylbisimidate dihydrochloride **3**, wherein ammonia as well as ethanol act as leaving groups. For the synthesis of **3**, malonic dinitrile was dissolved in 1,4-dioxane and afterwards four equivalents of ethanol and hydrogen chloride (also dissolved in 1,4-dioxane) were added to obtain **3** as a white solid (see Scheme 2-1).[100] In this reaction, the hydroxy group of the ethanol attacks the partially positively polarized nitrile carbon atom to form a primary imine as a nucleophile, which is protonated by hydrogen chloride. With this modification, the carbon atom is more positively polarized than in the nitrile group of the starting material and therefore a following nucleophilic attack of the aminophenol or aminothiophenol is facilitated. By performing the ligand syntheses as shown in Scheme 2-2 and storing the reaction solution over night in the refrigerator at −32 °C, compounds **4** and **5** can be isolated as solid precipitate in a moderate yield of 56 % and 74 %, respectively. Analogue to the procedure for the synthesis of the asymmetric substituted bisheterocyclo methanes, stated in the following Chapter 2.3, the synthesis of **4** was accomplished additionally by reaction of 2-aminophenol with malonic acid in polyphosphoric acid as solvent. Due to the lower yield (32 %) of **4**, this route was discarded.

In addition to the two ligand systems **4** and **5**, which are consisting of benzannulated oxazole or thiazole moieties, also the disubstituted imidazole methylene ligands **1** and **2** should be mentioned in this context, whose detailed syntheses were discussed within the results of my master thesis.[101] As depicted in Scheme 2-3 and Scheme 2-4, the synthesis route of those two imidazole based ligand systems differs from that of **4** and **5**, although the generation of **2** also involves a cyclocondensation reaction for building up the five-membered heterocycle. In the literature, also an alternative synthesis route for **1** is described, wherein ethylbisimidate dihydrochloride **3** was added to a solution of methylamino acetaldehyde dimethylacetal to give the desired ligand in a yield of 5 %.[98c] In

contrast to this, the overall yield of **1** could be significantly improved to a value of 46 % within my previous master thesis.[101a]

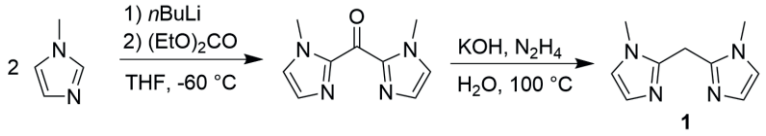

Scheme 2-3: Synthesis of (1-MeNCNC$_2$H$_2$)$_2$CH$_2$ (**1**).[101e, 101f]

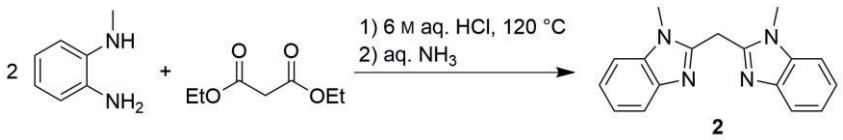

Scheme 2-4: Synthesis of (1-MeNCNC$_6$H$_4$)$_2$CH$_2$ (**2**).[101b, 101d]

The main difference between compound **1** and **2** is the absence of the annulated benzene perimeter in **1**, which offers the possibility to investigate the protective shielding abilities of the enhanced steric demand of the benzannulated derivatives. By means of this investigation, it is possible to achieve a comprehensive overview on the influence of the implemented heteroatom (either N, O or S) on the electronic properties and chelating abilities at the ligand of the resulting metal complexes.

2.1.2 Syntheses of the Group 13 Metal Complexes

The synthesis of the closely related nacnac complexes [Me$_2$Al{(N(Dipp)C(Me))$_2$CH}] and [Me$_2$Ga{(N(Dipp)C(Me))$_2$CH}] was reported in the literature by a facile reaction of nacnacH with AlMe$_3$ and GaMe$_3$, respectively.[14i, 14l, 15] Referring to this, the ligand platforms **1**, **2**, **4** and **5** can be deprotonated with the corresponding metalorganic reagent at the acidic methylene bridge by release of methane and coordinated by the group 13 metal fragment in a concerted way (see Scheme 2-6), because four heteroatoms are located in the *β*-position of those protons. For comparison reasons, the CH-acidity of the related 2-benzylbenzothiazole should be mentioned in this context, which yields in a pK_a value of 20.8 (measured in DMSO).[102] Due to the more pronounced electron-withdrawing properties of the second heteroaryl moiety compared to the phenyl ring in the reference, the expected carbon acidity is even higher (estimated pK_a: 10–20).[98c] Therefore, this ligand class exhibits great potential as activated carbon acids. For example, the corresponding active methylene behaviour could be shown in Knoevenagel-like condensation reactions with carbonyl reagents.[98a, 98c]

By using this reaction protocol, many different metallated compounds are accessible and can be compared structurally. In this context the effect of the diverging metal coordination (M = Al, Ga) and moreover the related substituents at these metal cations on the

bonding situation within the different ligand systems should be investigated. A typical synthetic procedure involves the parent ligand systems, dissolved in toluene, and the addition of either $AlMe_3$, $AlMe_2Cl$ or $GaMe_3$ at 0 °C to obtain the corresponding chelate complexes **6** – **9** (with a $AlMe_2$ moiety), **10** – **11** (with a AlMeCl moiety) and **13** – **14** (with a $GaMe_2$ moiety) (see Scheme 2-5 and Scheme 2-6).

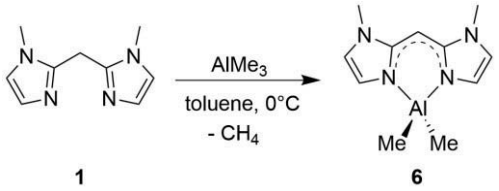

Scheme 2-5: Synthesis of the metallated homo-disubstituted bisheterocyclo methanide **6**.

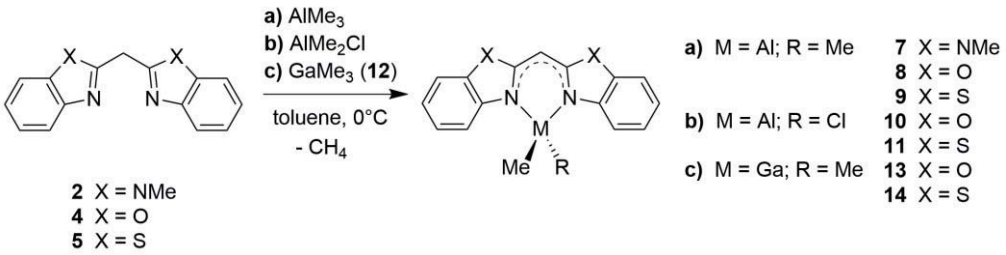

Scheme 2-6: Synthesis of the metallated benzannulated bisheterocyclo methanides **7** – **14**.

The aforementioned imidazole containing ligands **1** and **2** were treated with a slight excess of $AlMe_3$ to generate the monoanionic methanide derivatives **6** (see Scheme 2-5) and **7** (see Scheme 2-6). Further reactions concerning this kind of ligand systems were not accomplished due to the limited availability of the starting material, so that just the $AlMe_2$ derivatives of those ligands were synthesized and characterized.

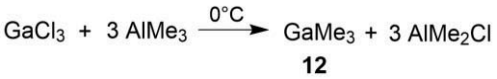

Scheme 2-7: Synthesis procedure of **12**.

Prior to the syntheses of the dimethyl gallium complexes **13** and **14**, the required pyrophoric $GaMe_3$ **12** has to be prepared starting from the commercially available $AlMe_3$. Therefore, three equivalents of the liquid $AlMe_3$ were added dropwisely to solid $GaCl_3$ under ice-cooling (see Scheme 2-7). After completed addition, the reaction mixture was allowed to warm up to room temperature and fractional distillation was applied to separate the two major products $GaMe_3$ and $AlMe_2Cl$.[103] **12** could be isolated in a good yield of 91 % as a colourless liquid (first fraction, collected at about 50 °C) of the distillation. It was used for the metallation reactions without further purification and spectroscopic

characterization due to its high pyrophoric reactivity. An alternate way to generate the corresponding dimethyl gallium etherate $GaMe_3 \cdot Et_2O$ (and the higher congener $InMe_3$)[104] in an etheral solution, is described elsewhere but was not performed due to the good yields of the first synthesis route to the pure metal organic reagent.

2.1.3 Structural Comparison of the Neutral Ligands

In the following part, a structural comparison of the parent ligand systems **1**, **2**, **4** and **5** and the metallated compounds **6** – **11** and **13** – **14**, which could be obtained by the earlier mentioned reaction protocols, will be discussed.

For a better commensurability, the molecular solid state structures of the parent ligand systems **4** and **5** were determined by applying single crystal X-ray diffraction and are shown in Figure 2-6 and Figure 2-7. Furthermore, the solid state structures of the ligands **1** and **2** are already known, so that the corresponding parameters for the bonding situation of those were adopted from previous work to complete the picture of the different used ligand types.[101a] The correlated molecular structures are displayed in Figure 2-2 and Figure 2-3.

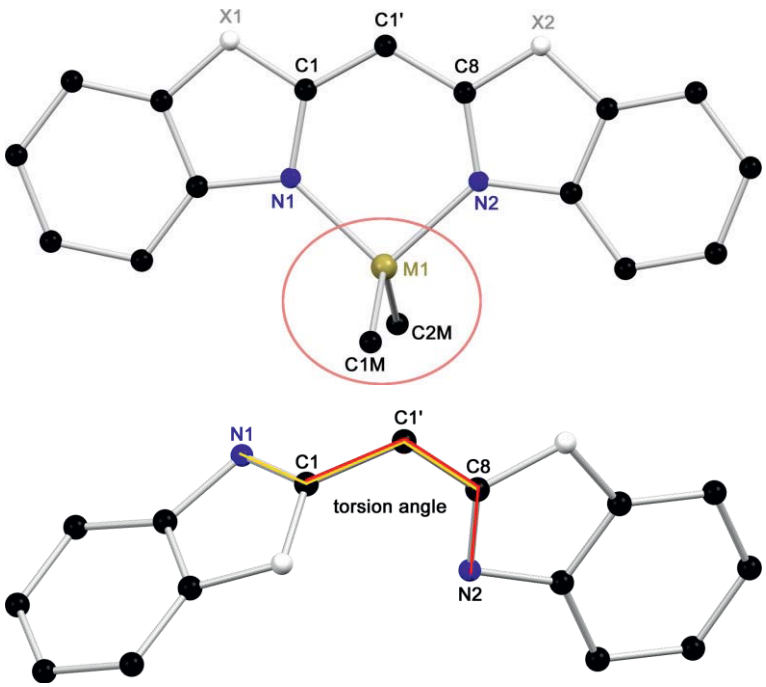

Figure 2-1: Important structural values deduced from the crystal structures.

For all crystal structures, which are presented in the following sections, the anisotropic displacement parameters are depicted at the 50 % probability level and C–H hydrogen atoms are omitted for clarity reasons, except the remaining ones at the bridging moiety unless stated otherwise. The bond lengths and angles for the annulated benzene perimeters were not discussed in detail for every compound, because those values are less im-

portant for the description of the resulting group 13 metal complexes. They also lie in a narrow range for typical delocalized C=C double bonds, as in the free benzene molecule. The numbering and labelling of the atoms in all upcoming discussed molecules is performed as depicted in the top picture of Figure 2-1. In this context, X1 or X2 represent the different heteroatoms (nitrogen, oxygen or sulfur) within each ligand system.

For these selected parts of the molecules, the bond lengths and angles are listed in the associated tables adjacent to the corresponding crystal structure. The encircled part should highlight, that this metal fragment including its two substituents is just present in the case of the metallated species. As a consequence thereof, the corresponding structural values are not present for the parent neutral ligand systems. Especially the twisting of the heteroaromatic substituents with respect to each other, which is displayed in Figure 2-1 at the bottom structure as the torsion angle, plays a key role for the comparison of the different synthesized ligand systems. In general, this overall torsion angle is defined as the sum of its underlying single torsion angles N1–C1–C1'–C8 and C1–C1'–C8–N2, which span from the first nitrogen atom via the bridging methylene moiety to the second nitrogen donor.

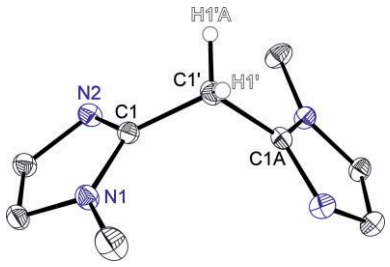

Figure 2-2: Solid state structure of ligand **1**.

Table 2-1: Distances [pm] and angles [deg] of **1**.

C1'–C1	150.20(14)	N1–C1–C1'	123.63(9)
C1–N1	136.17(14)	N2–C1–C1'	124.58(9)
C1–N2	132.47(14)	N1–C1–N2	111.74(10)
		C1–C1'–C1A	111.90(13)

Symmetry transformations used to generate equivalent atoms:

y, x, −z+1

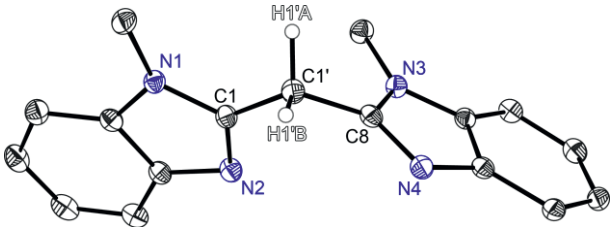

Figure 2-3: Solid state structure of ligand **2**.

Table 2-2: Distances [pm] and angles [deg] of **2**.

C1'–C1	149.89(16)	N2–C1–C1'	125.47(10)
C1'–C8	149.14(16)	N4–C8–C1'	123.99(10)
C1–N2	131.56(15)	N1–C1–C1'	120.66(10)
C8–N4	131.70(15)	N3–C8–C1'	122.04(10)
C1–N1	136.88(14)	N1–C1–N2	113.85(10)
C8–N3	137.18(14)	N3–C8–N4	113.93(10)
		C1–C1'–C8	113.52(9)

To conclude the results from the previous master thesis, the crystal structures of the already known imidazole based ligand systems **1** and **2** will be described briefly.[101a] The smallest investigated ligand system **1** (see Figure 2-2) which was applied for metallation reactions, crystallizes in the tetragonal space group $P4_32_12$ and half a molecule is present in the asymmetric unit. The whole molecule is generated by applying a 180 deg rotation

about the C_2-axis going through the bridging C1' atom. The benzannulated derivative **2** (see Figure 2-3) crystallizes in the triclinic space group $P\bar{1}$ and one molecule is located in the asymmetric unit. It is obvious, that these quite similar ligands adopt different alignments in the solid state. While in **1** the imidazole moieties are twisted about 171 deg against each other, so that the *N*-methyl groups are pointing in opposite directions to reduce the steric strain, in **2** the twisting is not that pronounced (96 deg) (see Table 2-6). For a better visualization of the differences among the above-mentioned compounds, an overlay of the crystal structures of **1** and **2** is depicted in Figure 2-4, in which the bridging CH_2 moieties of each compound are fixed at the same position.

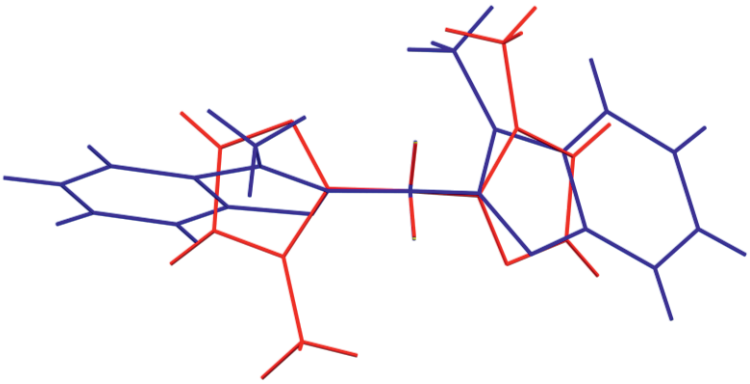

Figure 2-4: Overlay of the crystal structures for the ligand systems **1** (red) and **2** (blue).

The different torsion angles can be explained by the presence of well-pronounced hydrogen bonding properties in **1** resulting in a 3D network, which is based on the donor-acceptor interactions between the two imine nitrogen atoms and the hydrogen atoms at the backbone of the imidazole unit. This kind of interaction cannot take place in the case of **2**, because there are no hydrogen atoms available at the backbone due to the presence of the annulated perimeter. Furthermore, the remaining hydrogen atoms at the benzimidazole units are not prone for hydrogen bond formation due to the absence of adjacent, electron withdrawing heteroatoms, so that the electron density within the C–H bonds is less polarized as in the case of **1**.

In Figure 2-5, the Hirshfeld surfaces for compounds **1** and **2** are depicted to highlight the occurring interactions between the molecules in crystal packing. Therefore, the Hirshfeld surface for one whole molecule in the asymmetric unit was calculated each by using the computer program CrystalExplorer. The colour of the resulting surface deals as a criterion for the intermolecular distances towards the neighbouring molecules or atoms in the solid state. In 2004 McKinnon, Spackman and Mitchell coined following definition for the Hirshfeld surface:

> *"Molecular Hirshfeld surfaces are constructed by partitioning space in the crystal into regions where the electron distribution of a sum of spherical atoms for the molecule (the promolecule) dominates the corresponding sum*

over the crystal (the procrystal). Following Hirshfeld (1977), a weighting function w(r) for a particular molecule can be defined as

$$w(r) = \frac{\sum_{a\in\text{molecule}} \rho_a(r)}{\sum_{a\in\text{crystal}} \rho_a(r)} = \frac{\rho_{\text{promolecule}}(r)}{\rho_{\text{procrystal}}(r)} \cong \frac{\rho_{\text{molecule}}(r)}{\rho_{\text{crystal}}(r)}$$

from which it follows that the volume within which the promolecule dominates the procrystal electron density is that region where w(r) ≥ 0.5; we define the Hirshfeld surface by w(r) = 0.5. Here, $\rho_a(r)$ is a spherically averaged Hartree-Fock atomic electron density function (Clementi & Roetti, 1974) centred on nucleus a, and the ratio between promolecule and procrystal electron densities can be regarded as an approximation to the ratio between true molecule and crystal electron densities (...)"[105]

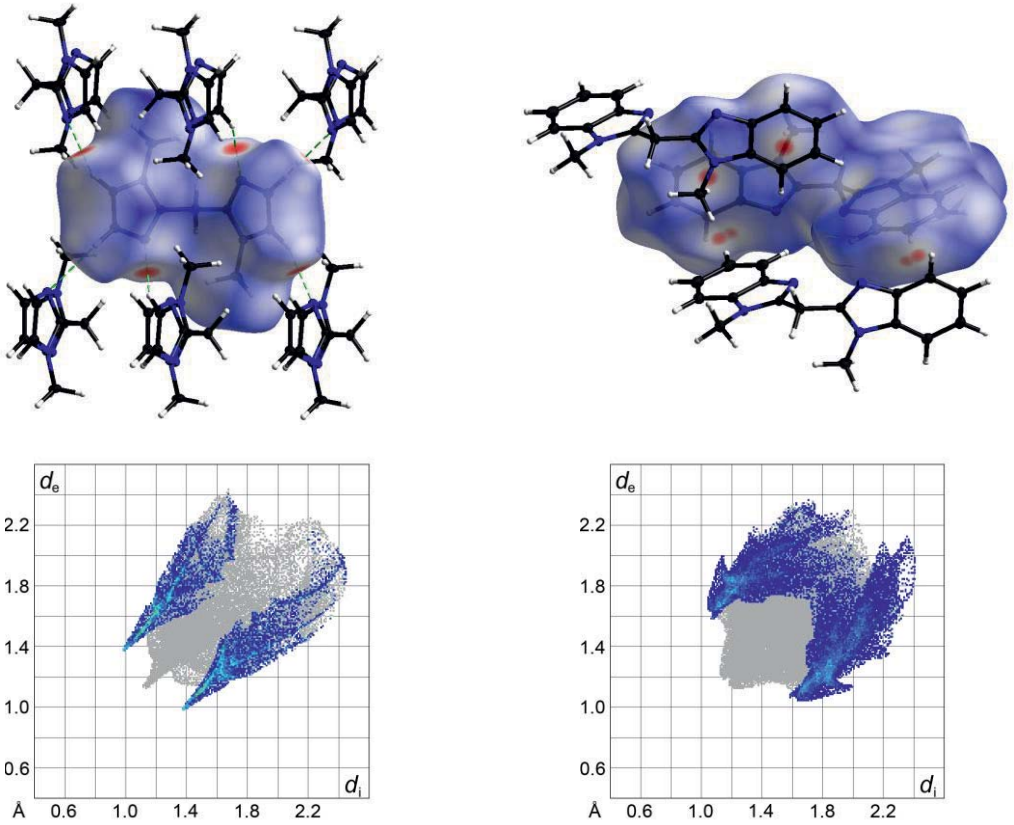

Figure 2-5: Hirshfeld surfaces[106] (*top*) and corresponding fingerprint plot[105, 106a, 107] for dominating N···H interactions (*bottom left*) and C···H interactions (*bottom right*) generated for **1** (*left*) and **2** (*right*), respectively.

In general, the colouration of this representation can be seen as a heat map, where the closest intermolecular interactions are shown in red and with increasing space between the considered moieties the colour turns to blue. The grey regions are ascribed to medium interactions. As an extension to the results noted in the master thesis,[101a] the Hirshfeld surface of **1** (see Figure 2-5, *top left*) shows six distinct red spots, which are illustrating the closest contacts towards neighbouring molecules. These contacts can be ascribed to

the corresponding C–H···N interactions, in which the carbon atoms of the ligand's backbone act as hydrogen donors and the imine nitrogen atom of each side arm as hydrogen acceptor, so that each molecule forms two hydrogen acceptor bonds and four hydrogen donor bonds. Interestingly, the protons at the acidic methylene bridge are not involved in any hydrogen bonding, seen from the absence of red spots at the Hirshfeld surface in the appropriate area.

At the bottom left side in Figure 2-5, the so-called two-dimensional fingerprint plot of **1** is depicted, which visually summarizes the obtained information of the intermolecular interactions in the crystal. The frequency of each combination of d_e (distance of the nearest exterior atom to the considered point at the Hirshfeld surface) and d_i (distance of the nearest interior atom to the same point at the Hirshfeld surface) across the molecule's surface is plotted again in a colour coded way: from blue for low frequency of occurrence of a special d_i-d_e combination, via green through to red, standing for an increasing frequency of occurrence of that pair. In this case, the fingerprint plot of **1** shows the presence of two significant peaks, which can be assigned to the dominating N···H interactions in the crystal. For clarity reasons, in the shown fingerprint plot just those interactions, which refer exclusively to the contacts between nitrogen and hydrogen atoms and vice versa, are highlighted in Figure 2-5 with the described colour code. All other observable interactions, e.g. C···C, C···H, C···N, are shaded in grey because they are not accountable for the closest intermolecular contacts. The corresponding d_i-d_e pairs for the coordinates of the maximum peaks, more precisely the sum of that values, yields the shortest observed N···H interactions regarding the distance of those nitrogen and hydrogen atoms inside and outside of the calculated Hirshfeld surface. The experimentally determined values for that hydrogen bonding pattern result in one rather short N2B···H3 distance of 246.9 pm (symmetry operation for generation of B: y+1/2, −x+1/2, z−1/4) and the corresponding N2B···H3–C3 angle of 151.58 deg. The other hydrogen bonds, formed via the other hydrogen atom H4 at the backbone, seem to be less stable due to the increased N2C···H4 distance of 264.8 pm (symmetry operation for generation of C: −x+3/2, y−1/2, −z+5/4), even though the corresponding N2C···H4–C4 angle (155.94 deg) is slightly closer to the favourable linearity.

In direct comparison to the crystal structure of **2** (see Figure 2-3) and its Hirshfeld surface (see Figure 2-5, *top right*), some striking differences compared to **1** can be detected. The calculated surface is mostly quite featureless, whereas the major part of that surface is coloured in white or blue representing rather distant contacts. Additionally, there are some red regions observable, which are standing for the closest intermolecular interactions within the crystal arrangement. Contrary to **1**, these spots are not located in the proximity to the nitrogen donor atoms. In the case of **2** no remarkable N···H interactions could be identified but rather C–H···π contacts are present, based on the evaluation of the corresponding Hirshfeld surface. One aromatic proton (H5) is pointing towards the annulated benzene ring of another molecule and one proton of the *N*-methyl group at C15 is also addressed to the π-system of another ligand. This fact is reflected by the fingerprint plot of **2** in Figure 2-5 (*bottom right*) by the blue and green highlighted outer areas, which cannot be identified as clear peaks as in the above-mentioned case of **1**. Referring to the dominating C···H interactions, no interactions like N···H were considered for frequency of

occurrence. This wing-like appearance is characteristic for C–H···π interactions and was also observed for benzene and other polycyclic aromatic hydrocarbons like naphthalene or anthracene.[107] In this case no hydrogen bonding interactions are observable, because in contrast to **1** no protons at the backbone of the imidazole unit are present due to the annulated benzene moiety.

Because of the composition of the symmetrically disubstituted bisheterocyclo methanes, each molecule consists of two similar parts, in which the bonding situation between the chemical equivalent environments should be almost comparable. To highlight this structural feature, it is underlined in the corresponding tables for each solid state structure, that the related, comparable bond lengths and angles are grouped and shaded in the same colour. Referring to this, averaged distances and angles are not presented to clarify the range of the experimentally determined values. If the second part of the molecule in the solid state is generated by a special symmetry operation, this grouping is not appropriate, because both residues are crystallographically identical. The corresponding symmetry operations for the generation of the counterpart will be mentioned at the bottom of each table.

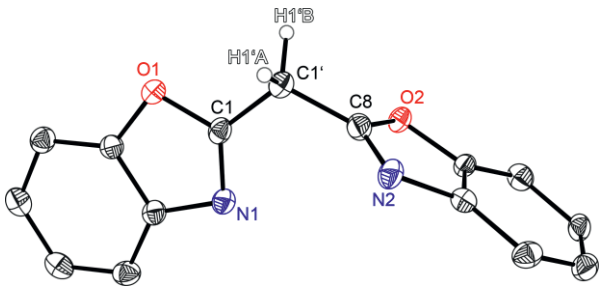

Figure 2-6: Solid state structure of ligand **4**.

Table 2-3: Distances [pm] and angles [deg] of **4**.

C1'–C1	149.17(15)	N1–C1–C1'	127.23(10)
C1'–C8	148.64(15)	N2–C8–C1'	124.9(2)
C1–N1	128.87(14)	O1–C1–C1'	116.07(9)
C8–N2	127.7(5)	O2–C8–C1'	118.80(19)
C1–O1	137.14(13)	O1–C1–N1	116.67(10)
C8–O2	137.6(3)	O2–C8–N2	116.3(3)
		C1–C1'–C8	111.23(9)

Starting with the crystal structure of **4**, the following crystallographic features can be stated: the ligand system bis-(benzoxazol-2-yl)-methane crystallizes, in the absence of any Lewis donating solvent, in the monoclinic space group $P2_1/c$ and the asymmetric unit consists of one molecule. Final refinement of one benzoxazole moiety shows the presence of a positional disorder with a site occupation factor of 0.790(10), in which mainly the position of the containing heteroatoms oxygen and nitrogen are exchanged. This disorder is achieved by a 180 deg rotation of the benzoxazole framework. The alignment of **4** shown in Figure 2-6 represents the preferred orientation in the solid state, whereas the minor fraction was omitted for clarity reasons. Due to this disorder, the obtained bond lengths and angles in that part of the molecule are not that reliable than the values of the other ordered part. This fact is displayed in the quite high estimated standard deviations. So, for further considerations of bonding situations within the molecule, the disordered moiety should be neglected, because the overlay of two different orientations with just slight differences, regarding the sequence of atoms, ensures that the bonding situation in that moiety is always detected as a mixture of both underlying parts.

Table 2-4: Selected averaged bond lengths (pm) and angles (deg) of the ligand backbone for the neutral ligands **1** – **5**.

compound	C_{ipso}–C1'	C_{ipso}–N1	C1–C1'–C8	Al–N1*	N1–Al–N2*
$(1\text{-MeNCNC}_2H_2)_2CH_2$ (**1**)	150.20(14)	136.17(14)	111.74(10)	–	–
$(1\text{-MeNCNC}_6H_4)_2CH_2$ (**2**)	149.52(16)	131.63(15)	113.52(9)	–	–
$(NCOC_6H_4)_2CH_2$ (**4**)	148.91(15)	128.87(14)	111.23(9)	–	–
$(NCSC_6H_4)_2CH_2$ (**5**)	151.06(15)	129.55(16)	109.59(14)	–	–

* parameter already mentioned for later comparison with the metallated species.

The coordination geometry of the central carbon atom C1' is distorted tetrahedral, whereby the C1–C1'–C8 angle is most widened to 111.2 deg due to the enhanced steric demand of the benzoxazole substituents. The observed C_{ipso}–C1' bond lengths with an average value of 148.91(15) pm are slightly shorter in comparison to a standard bond length of a C(sp^3)–C(sp^2) single bond (151.0 pm)[108] because of the high electron withdrawing properties of the neighbouring heteroatoms oxygen and nitrogen within the oxazole moiety. The C_{ipso}–N1 and C_{ipso}–O1 bond lengths are in good agreement with those ones of a typical C(sp^2)=N(sp^2) double bond (129.0 pm) and a C(sp^2)–O(sp^2) single bond (135.0 pm), respectively.[108]

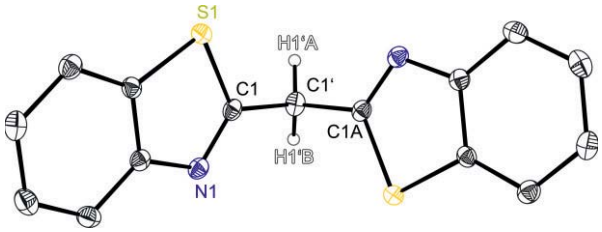

Table 2-5: Distances [pm] and angles [deg] of **5**.

C1'–C1	151.06(15)	C1–C1'–C1A	109.59(14)
C1–N1	129.55(16)	N1–C1–C1'	123.51(10)
C1–S1	174.98(12)	S1–C1–C1'	119.68(7)
		S1–C1–N1	116.67(9)

Symmetry transformations used to generate equivalent atoms: −x+1, y, −z+1/2

Figure 2-7: Solid state structure of ligand **5**.

The corresponding bis-(benzothiazol-2-yl)-methane **5**, which bears sulfur atoms instead of oxygen atoms in the former discussed ligand **4**, crystallizes in the monoclinic space group *C*2/*c* and half a molecule is present in the asymmetric unit. The second part of **5** is generated by a suitable symmetry operation stated in Table 2-5. As depicted in Figure 2-7, ligand system **5** prefers an orientation of the benzothiazole units, where the nitrogen donor atoms are pointing in opposite directions. This fact can be measured by the degree of torsion, which is present in each neutral parent ligand system referring to the alignment of the nitrogen atoms. In the case of **5** an overall torsion angle of about 188 deg can be experimentally determined, which indicates the nearly opposing orientation of both heterocycles. In contrast to this, the torsion angle obtained for **4** is just 81 deg (see Table 2-6). This vital difference can be explained by crystal packing effects, which cause the corresponding heterocycle to prefer the observed alignment.

Table 2-6: Selected folding parameters for compounds **1** – **5**.

compound	torsion angle [deg]	folding angle [deg]*	M···plane dist. [pm]*
$(1\text{-MeNCNC}_2\text{H}_2)_2\text{CH}_2$ (**1**)	171.82(11)	–	–
$(1\text{-MeNCNC}_6\text{H}_4)_2\text{CH}_2$ (**2**)	96.34(16)	–	–
$(\text{NCOC}_6\text{H}_4)_2\text{CH}_2$ (**4**)	81.3(9)	–	–
$(\text{NCSC}_6\text{H}_4)_2\text{CH}_2$ (**5**)	188.98(24)	–	–

* parameter is mentioned for later comparison with the metallated species.

From direct comparison of the imidazole based ligand systems **1** and **2** it is obvious, that the observed degree of torsion concerning the parent ligand system in the solid state is very dependent on the specific heteroatom within the five-membered heterocycle (see Table 2-6). Focussing on the determined bond lengths, it should be highlighted, that the distance between the *ipso*-carbon atom and the imine nitrogen atom is significantly longer for the imidazole derivatives (**1**: 136.17(14) pm; **2**: 131.63(15) pm) than for the chalcogen containing counterparts (**4**: 128.87(14) pm; **5**: 129.55(16) pm) (see Table 2-4). This bond elongation is caused by delocalization of the C=N double bond already occurring (see Scheme 2-8). The lone pair of the second nitrogen atom (by means of the NMe group) can be flipped into the ring system to form another, zwitterionic mesomeric resonance structure **(b)** for the imidazoles. This explains the elongation of the C_{ipso}–N distances within these species in contrast to **4** and **5** (see Scheme 2-8).

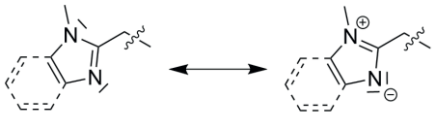

Scheme 2-8: Mesomeric resonance structures of the imidazole containing ligand systems.

After careful evaluation of the solid state structures of the parent methane ligand systems **1**, **2**, **4** and **5**, it is evident that in each case the CH tautomer was structurally determined, because the bridging carbon atom C1' carries two protons, whereas none could be detected at the endocyclic imine nitrogen atoms (see Scheme 2-9, case **(a)**). In contrast to this, it is known in the literature, that the implementation of methyl groups at the bridging moiety of bis-(benzothiazol-2-yl)-methane leads to the stabilization of the NH tautomeric form (see Scheme 2-9, case **(b)**).[97a] Based on the determined distorted tetrahedral coordination geometry of C1' and the identical C_{ipso}–C1' bond lengths (see Table 2-4), the bridging carbon atom is sp^3-hybridized.

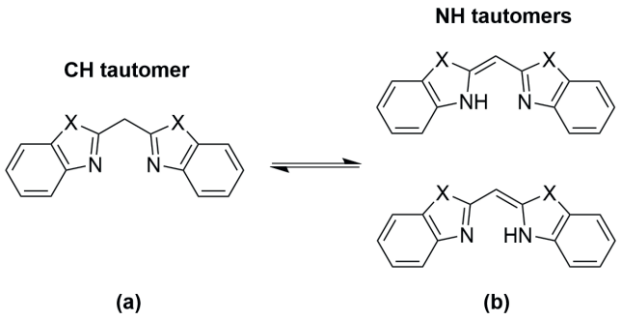

Scheme 2-9: Possible tautomeric forms of the parent ligands.

2.1.4 Structural Comparison of the Metal Complexes

In addition to the structural values stated in Figure 2-1, two further values have to be taken into account for the metal complexes. On the one hand, the folding angle should be mentioned, which replaces the former torsion angle observed in the protonated ligand systems (see Figure 2-8, *top*). Two planes can be fitted through each heteroaromatic substituent, which intersect at a characteristic angle, the so-called folding angle.

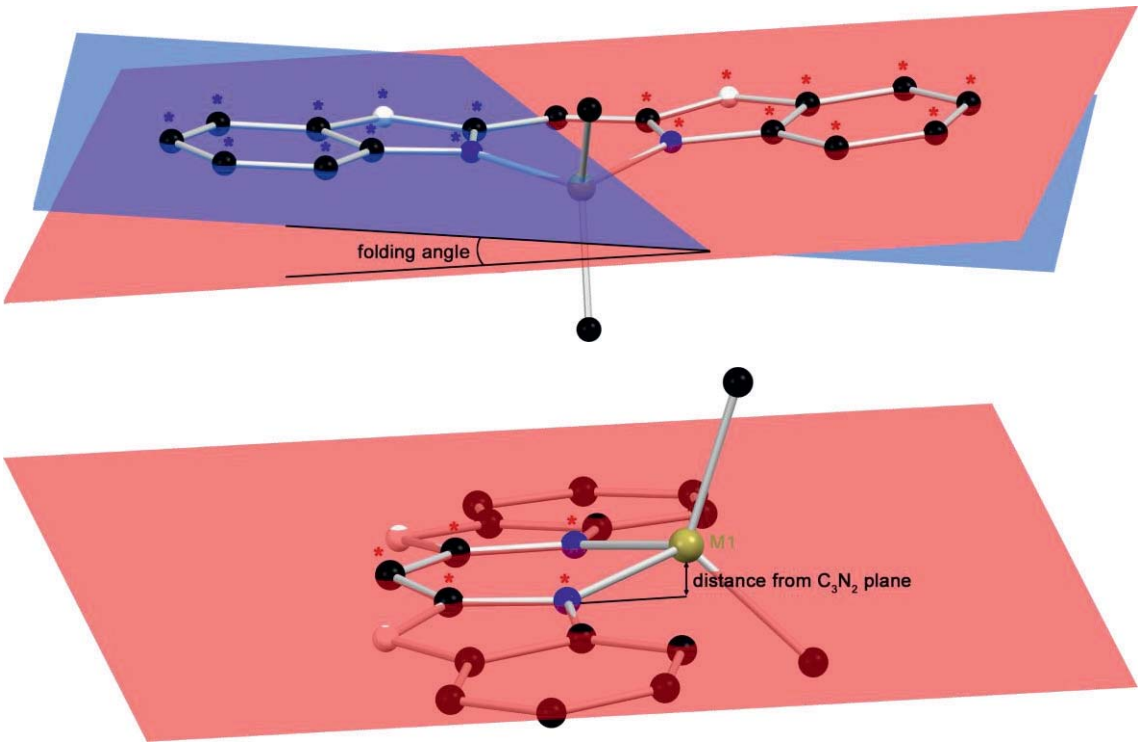

Figure 2-8: Important structural values deduced from the crystal structures of the metallated species.

In the top picture the red coloured plane was calculated based on the atoms highlighted with a red star and the blue plane with those marked with blue stars. The folding angle is a measure for how distinct the butterfly arrangement of the ligand system is pronounced

upon metallation. Because of the chelating abilities of the investigated ligand platforms, in the most cases the metal fragment gets coordinated by the two endocyclic imine nitrogen atoms N1 and N2. This leads to a nearly parallel alignment of the C1–N1 and C8–N2 bonds and the corresponding overall torsion angle tends to be about 0 deg in each metallated species.

On the other hand, the distance of the metal cation from the chelating C_3N_2 plane for the methanide derivatives (or C_2N_3 plane for the amide derivatives, *vide infra* in chapter 2.5) is the second additional value to be discussed (see Figure 2-8, *bottom*). Mostly a six-membered metalla heterocycle is formed upon deprotonation and subsequent coordination of the metal cation. Although the other involved atoms of this six-membered ring (N1, C1, C1', C8 and N2) are nearly arranged in plane, the metal atom can deviate significantly from that C_3N_2 plane. Therefore, a plane was fitted through the above-mentioned atoms, marked in Figure 2-8 *bottom* with red stars, and afterwards the distance of the corresponding metal ion from this plane can be determined.

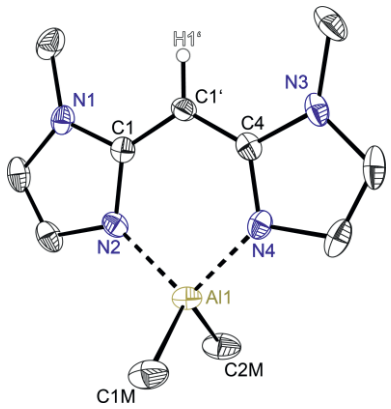

Figure 2-9: Solid state structure of complex **6**.

Table 2-7: Distances [pm] and angles [deg] of **6**.

C1'–C1	139.6(3) 139.6(3)	N2–C1–C1'	126.64(18) 126.68(18)
C1'–C4	139.7(3) 139.3(3)	N4–C4–C1'	126.93(18) 126.67(18)
C1–N2	136.5(3) 136.6(3)	N1–C1–C1'	125.34(18) 125.04(19)
C4–N4	136.1(3) 136.4(3)	N3–C4–C1'	125.06(19) 125.3(2)
C1–N1	136.5(3) 136.2(3)	N1–C1–N2	108.02(17) 108.27(17)
C4–N3	136.6(3) 136.4(3)	N3–C4–N4	108.01(17) 107.99(18)
N2–Al1	190.51(18) 190.09(18)	C1–C1'–C4	121.12(19) 121.09(19)
N4–Al1	190.35(19) 189.97(19)	N2–Al1–N4	93.79(8) 93.73(8)
Al1–C1M	196.6(2) 197.0(2)	C1M–Al1–C2M	112.86(11) 113.58(10)
Al1–C2M	196.9(2) 196.7(2)		

Due to the presence of two molecules in the asymmetric unit, for each parameter two values are given.

The crystal structure of the dimethyl aluminium containing complex **6** is representative for the metal complexes carrying the smallest ligand system due to the lack of a condensed benzene moiety: the compound crystallizes in the monoclinic space group $P2_1/c$ with two molecules in the asymmetric unit (Figure 2-9). The final structure refinement afforded the consideration of a small amount of pseudo-merohedral twinning with a BASF value of 0.04 to get the best solution. The twin law for the second domain, which transforms the cell into an equivalent one and belongs to a higher crystal system than the structure, was determined by the tool TwinRotMat to give TWIN −1 0 −1 0 −1 0 0 0 1.

The collected diffraction data barely display this kind of twinning, because the reflexes of both domains are located at the same position resulting in a nearly ideal overlap. The intensity differences between the two domains are not visible due to this overlap. This pseudo-merohedral twinning is quite common within the series of the structurally determined metal complexes, which are crystallizing in a monoclinic space group. The molecules themselves partially exhibit the higher symmetry of the orthorhombic system, and this twinning could also be detected for compounds **13**, **21**, **23** and **29**.[109]

The central carbon atom C1' adopts a nearly trigonal planar coordination environment upon deprotonation, which is indicated by the surrounding angles of about 120 deg. Additionally, the deprotonation of the former methylene bridge leads to a well-pronounced delocalization of the generated free electron pair, which can be seen in the determined bond lengths (see Table 2-7). The former C_{ipso}–C_{bridge} distance of 150.20(14) pm in the parent ligand system **1** is decreased to an average value of 139.6(3) pm in the corresponding metallated species **6**, indicating that the considered C(sp^2)–C(sp^2) bonds are half way between single and double bond character like a delocalized double bond in benzene with an ideal bond lengths of 139 pm.[108] Furthermore, the C_{ipso}–N2/N4 bonds are affected by the presence of the free electron pair of the monoanionic methanide ligand. In contrast to the bonding situation in **1**, where two values can be found indicating a single bond for C_{ipso}–N1/N3 (136.17(14) pm) and a double bond for C_{ipso}=N2/N4 (132.47(14) pm), in **6** an average value for these bond lengths is observed (136.4(3) pm). This elongation of the C_{ipso}–N2/N4 distances supports the presence of a delocalized C=N double bond character and is a consequence of the coordination of the Lewis acidic aluminium fragment. Because the lone pairs of the former imine nitrogen donors are involved in metal coordination, the electron density at N2/N4 is partially reduced, so that the other bond lengths are increased.

The collected data show almost no folding of the ligand, displayed by the observed folding parameters for this complex, which are listed in Table 2-10. The folding of the planes, spanned by the two imidazole moieties, results in an average value of 2.72(12) deg for both molecules in the asymmetric unit. Moreover, the aluminium atom is just slightly shifted out of the chelating C_3N_2 plane of the six-membered metalla heterocycle by 0.86(23) pm. The nearly flat arrangement of the ligand and the coordination manner of the Al^{3+} ion can be ascribed to the small steric hindrance of this ligand system. Due to the absence of an annulated benzene perimeter in **6**, the ligand backbone can be arranged in the solid state without adopting a butterfly-like alignment and the metal fragment can be coordinated in a perfect manner by the bidentate ligand. The transannular N1···N2 distance between the chelating donors results in 278.2(3) pm and the corresponding Al1···C1' distance, which is a measure for the penetration depth of the metal fragment, is about 333.9(2) pm.

Interestingly, a three-dimensional hydrogen bonding pattern is observed in the case of **6** as well as for the parent ligand system **1** (see Figure 2-10). The hydrogen bonds of both compounds have in common, that the C–H functionality of the backbone of the imidazole units acts as hydrogen donor and the protons of the methylene bridge are not involved in any significant interactions. The main difference between **1** and **6** is the fact, that in **1** the

imine nitrogen atom serves as hydrogen acceptor due to the following reasons: on the one hand, N2/N4 has less steric protection in contrast to the methylated amine moiety, which facilitates the coordination via the imine nitrogen atom. On the other hand, the sp^2-hybridized imine nitrogen atom carries the free electron pair in a sp^2-hybrid orbital, which lies in the plane of the aromatic system, resulting in a more pronounced Lewis basic character. In contrast to that, the tertiary amine moiety carries its lone pair in a *p*-orbital perpendicular to the heteroaromatic plane. The latter is delocalized over the whole π-system, while the lone pair of the imine is less affected. The nitrogen atom has therefore a more concentrated electron density, which allows the formation of energetically more favourable hydrogen bonds.

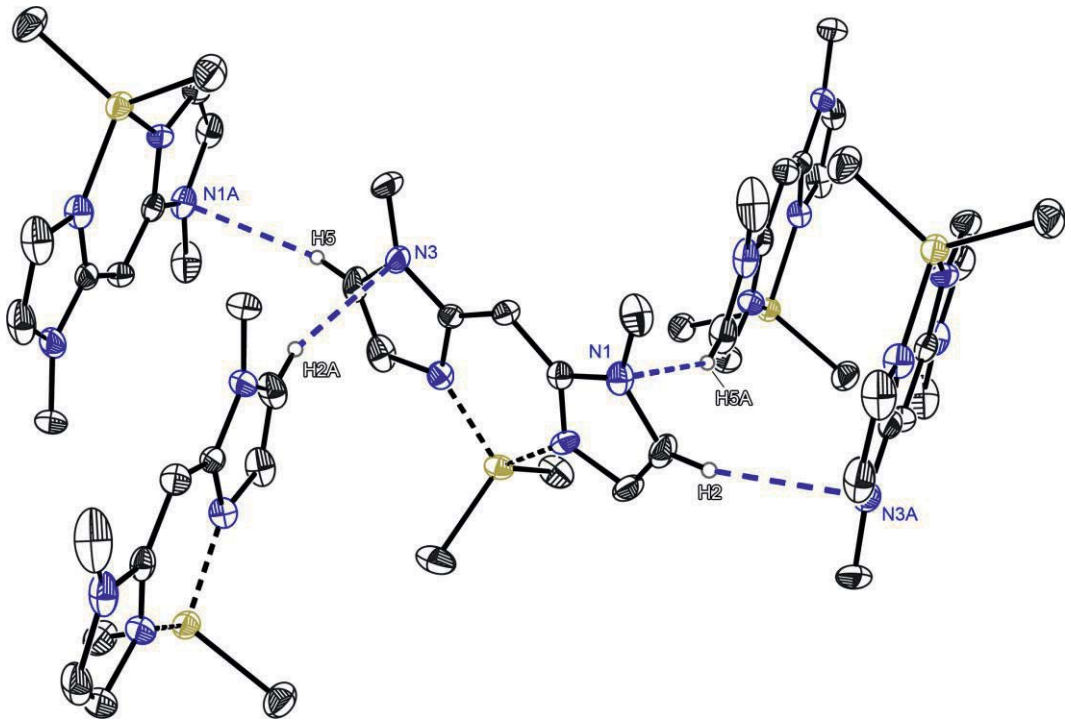

Figure 2-10: Hydrogen bonding pattern of **6**. C–H hydrogen atoms, which are not involved in any hydrogen bonding, are omitted for clarity reasons. (Symmetry transformations used to generate equivalent atoms: x−1, y, z for counterpart A, x−1,−y+1/2,z−1/2 for counterpart B and x,−y+1/2,z−1/2 for counterpart C)

In **6** the lone pair of imine nitrogen atom is already blocked by the coordination of the aluminium fragment and as a consequence thereof, only N1 is able to form hydrogen bonds with neighbouring molecules. In this case, three different hydrogen bonds could be determined: C2–H2···N3AA (H···A: 264 pm, angle: 162.5 deg), C5–H5···N1AB (H···A: 263 pm, angle: 159.4 deg) and C2A–H2A···N3 (H···A: 266 pm, angle: 162.2 deg).

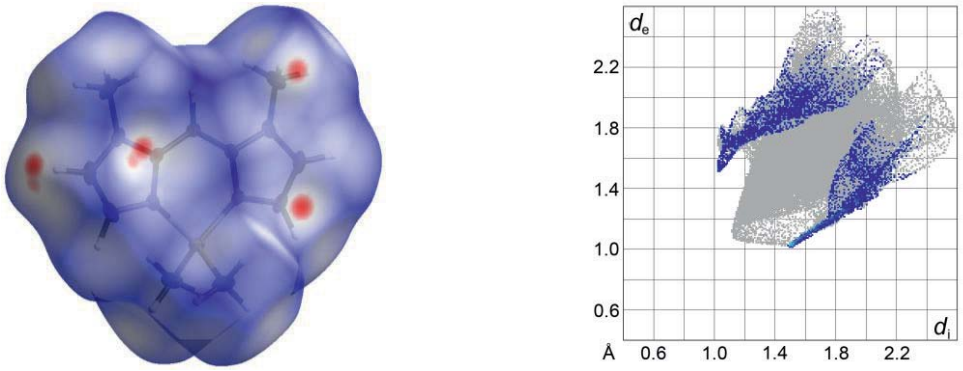

Figure 2-11: Hirshfeld surface[106] (*left*) and corresponding fingerprint plot[105, 106a, 107] for N···H interactions (*right*) generated for **6**.

The corresponding Hirshfeld surface for **6** is depicted in Figure 2-11. The calculated surface shows two distinct red areas at the left side of the molecule, which are caused by the closest intermolecular interactions regarding the above-mentioned C–H···N hydrogen bonding. These contacts are also present at the right rear side of the molecule, which is not visible in this representation. These kind of close contacts are highlighted in the corresponding fingerprint plot (see Figure 2-11, *right*). The comparison with the fingerprint plot of the parent neutral ligand **1** (see Figure 2-5, *left*) reveals, that those peaks concerning C–H···N interactions are not as pronounced as in the case of **1**. This fingerprint visualisation, in combination with the experimentally determined structural values for hydrogen bonding, indicates that the hydrogen bonding properties within **6** do not contribute to the observed arrangement in the solid state as much as it seems for **1**.

The two other red areas at the right front side of the surface can be assigned to weak C–H···π interactions based on one hydrogen atom of the *N*-methyl groups, which were also observed in the case of **2**. Due to symmetry operations, these interactions are also existent at the left rear side of the molecule's Hirshfeld surface.

It was not possible to determine a crystal structure of **7** by applying SCXRD because of the small isolated quantities and its sensitivity of the grown needle-like crystals. Hence, the NMR spectroscopic data of this dimethyl aluminium containing species were recorded as presented in Spectrum 2-1, which are verifying the successful synthesis of **7**. The top picture shows the ^{1}H-NMR spectrum of **7**, in which the presence of the two methyl groups H1M at the aluminium fragment is clearly observed with an integral of six protons (δ = −0.57 ppm). The resonance signal for the remaining proton H1' at the methylene bridge appears at 4.72 ppm with an integral of one proton, which equals the half of the parent ligand **2** due to successful deprotonation. The signals at 3.57 ppm can be assigned to the protons of the *N*-methyl groups, partially overlapping with the signal of the solvent. In the aromatic region of the spectrum, the four aromatic protons can be identified as three multiplets, where H6 is most downfield shifted (δ = 7.32 ppm).

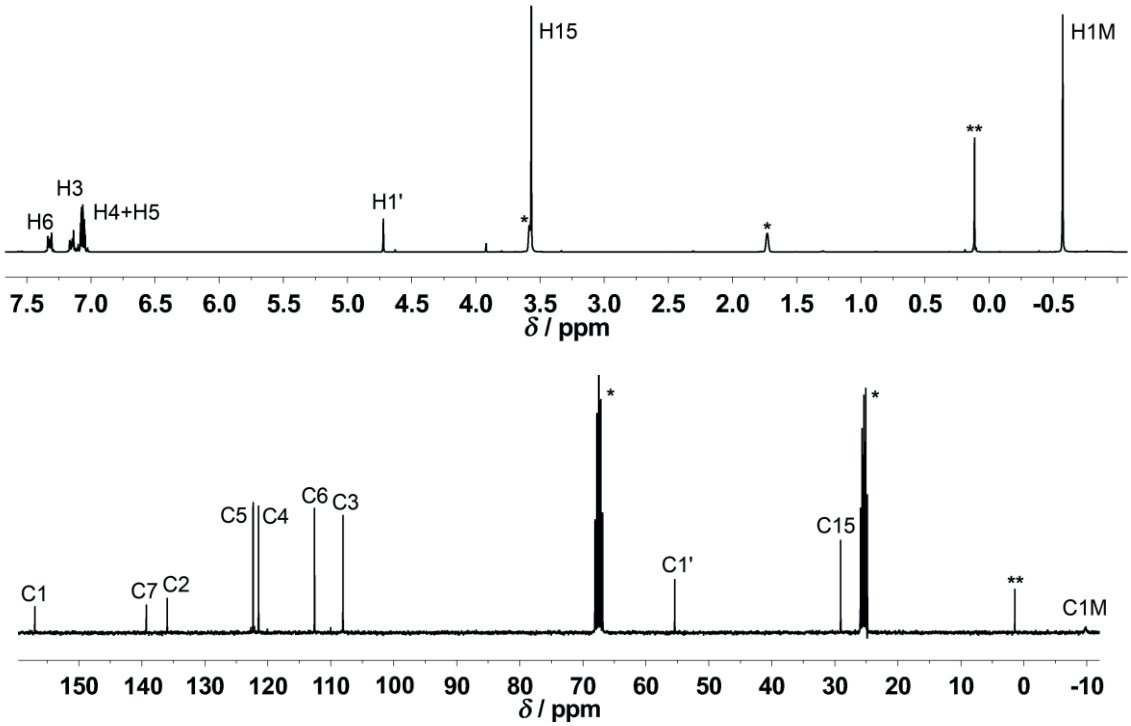

Spectrum 2-1: NMR spectroscopic data of **7** (THF-d_8, rt; solvent signals are highlighted with * and grease with **): *top*: ^{1}H-NMR (300 MHz), the spectrum contains minor contaminations of **2** due to decomposition; *bottom*: ^{13}C-NMR (75 MHz).

Additionally, the bottom trace in Spectrum 2-1 shows the fully assigned ^{13}C-NMR spectrum of **7**. The observed resonance signal for the $AlMe_2$ methyl groups C1M (δ = −9.85 ppm) is broadened leading to a quite weak peak intensity. Therefore and because of a low signal/noise ratio at a 300 MHz NMR spectrometer, this signal is hard to detect in each metallated species. Furthermore, the quaternary *ipso*-carbon atom C1 is most shifted towards downfield (δ = 156.98 ppm) due to the presence of two adjacent, electron-withdrawing heteroatoms. This observation was also made recurrently for all following metal complexes.

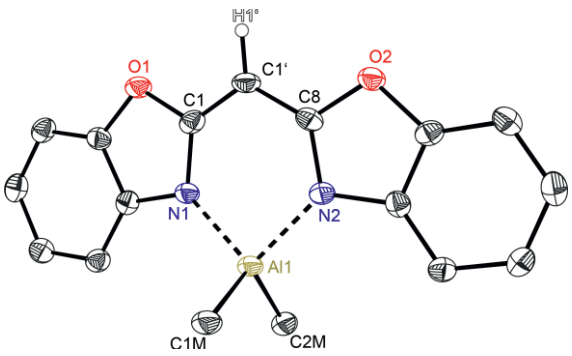

Figure 2-12: Solid state structure of complex **8**.

Table 2-8: Distances [pm] and angles [deg] of **8**.

C1'–C1	137.7(3)	N1–C1–C1'	128.2(2)
C1'–C8	138.3(3)	N2–C8–C1'	127.8(2)
C1–N1	134.8(3)	O1–C1–C1'	120.1(2)
C8–N2	134.4(3)	O2–C8–C1'	120.1(2)
C1–O1	136.8(3)	O1–C1–N1	111.75(19)
C8–O2	136.7(3)	O2–C8–N2	112.05(19)
N1–Al1	191.71(19)	C1–C1'–C8	119.5(2)
N2–Al1	191.8(2)	N1–Al1–N2	91.67(9)
Al1–C1M	195.9(2)	C1M–Al1–C2M	115.89(11)
Al1–C2M	195.1(2)		

Furthermore, the dimethyl aluminium containing complexes derived from bis-(benzoxazol-2-yl)- (**4**) and bis-(benzothiazol-2-yl)-methane (**5**) could be successfully synthesized by applying the aforementioned pathway (see Scheme 2-6). Complexes **8** and **9** could be characterized by SCXRD. The compounds **8** (see Figure 2-12) and **9** (see Figure 2-13) are isostructural, crystallize both in the triclinic space group $P\bar{1}$ and having each one molecule in the asymmetric unit. At this point, it is worth noting, that in the case of the thiazole derivative **9** non-merohedral twinning is present with a batch scale factor of 0.53. This means, that nearly the half of the domains in the lattice of the measured crystals is arranged with an arbitrary twin law. In contrast to pseudo-merohedral twinning, this twin law does not belong to a higher crystal system. This kind of twinning was recognized by careful inspection of the collected diffraction images due to difficulties in the cell refinement. At the images, some reflections were sharp and others split, so that the tool RLATT was used to separate the underlying domains in the reciprocal lattice view. After that, the separated domains were integrated and treated routinely to get a satisfying structure solution.[109] The same procedure was also applied for other crystal structures in the following context, where non-merohedral twinning was detected (**11** and **35**).

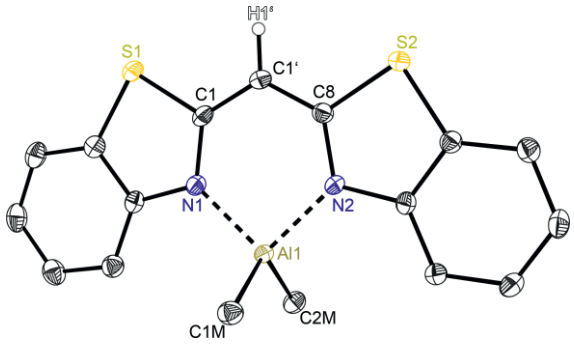

Figure 2-13: Solid state structure of complex **9**.

Table 2-9: Distances [pm] and angles [deg] of **9**.

C1'–C1	139.1(2)	N1–C1–C1'	126.50(14)
C1'–C8	138.9(2)	N2–C8–C1'	126.23(14)
C1–N1	135.02(19)	S1–C1–C1'	120.41(11)
C8–N2	135.28(19)	S2–C8–C1'	120.59(11)
C1–S1	174.74(16)	S1–C1–N1	113.09(11)
C8–S2	174.47(15)	S2–C8–N2	113.18(11)
N1–Al1	192.40(14)	C1–C1'–C8	123.54(14)
N2–Al1	192.36(13)	N1–Al1–N2	94.78(6)
Al1–C1M	196.25(16)	C1M–Al1–C2M	117.99(7)
Al1–C2M	196.00(16)		

The metallated, isostructural species **8** – **14** bearing either the bis-(benzoxazol-2-yl)- or the bis-(benzothiazol-2-yl)-methanide anion as ligand have several intrinsic features in common, which should be highlighted at this point:

(a) The deprotonated conjugated ligand system in the investigated metal complexes **8** – **14** shows a considerably smaller torsion angle concerning the C–N bonds within the heterocycles (see Table 2-10), when compared to the parent neutral ligands **4** and **5**.

(b) Upon deprotonation the whole ligand system becomes nearly planar in each molecule and the metal cations are coordinated exclusively by the two endocyclic imine nitrogen donor atoms to obtain isostructural crystal structures.

(c) Furthermore, the aluminium or gallium fragments are significantly dislocated from the ideal C_3N_2 planes, ranging from 10.93(27) pm in **11** to 29.57 (26) pm in **8**, depending on the heteroatom in the backbone of the ligand (see Table 2-10).

(d) The experimentally determined C–C and C–N distances for **8** – **14** span the narrow range of 138.0(3) to 1.394(9) pm and 132.3(9) to 136.5(3) pm, respectively. These

facts are an indicator of an apparent fully conjugated and delocalized ligand character, as far as the abovementioned bonds are concerned (see Table 2-11).

(e) In each considered metal complex, the observed N–M–N bite angle inside the formed six-membered C_3N_2M metalla heterocycle is the narrowest one (89.2(2) – 96.84(9) deg), whereas all other angles are mostly wider than 120 deg (see Table 2-11).

Table 2-10: Selected folding parameters for the neutral ligands **1**, **2**, **4**, **5** and the metal complexes **6** and **8** – **14**. (Addendum to Table 2-6)

compound	torsion angle [deg]	folding angle [deg]	M···plane dist. [pm]
$(1\text{-MeNCNC}_2H_2)_2CH_2$ (**1**)	171.82(11)	–	–
$(1\text{-MeNCNC}_6H_4)_2CH_2$ (**2**)	96.34(16)	–	–
$(NCOC_6H_4)_2CH_2$ (**4**)	81.3(9)	–	–
$(NCSC_6H_4)_2CH_2$ (**5**)	188.98(24)	–	–
$[Me_2Al\{(1\text{-MeNCNC}_2H_2)_2CH\}]$ (**6**)	–	1.500(124)* 3.938(33)	0.26(21)* 1.45(23)
$[Me_2Al\{(NCOC_6H_4)_2CH\}]$ (**8**)	–	9.12(8)	29.57(26)
$[Me_2Al\{(NCSC_6H_4)_2CH\}]$ (**9**)	–	1.36(2)	13.79(29)
$[ClMeAl\{(NCOC_6H_4)_2CH\}]$ (**10**)	–	3.69(40)	18.06(32)
$[ClMeAl\{(NCSC_6H_4)_2CH\}]$ (**11**)	–	1.21(2)	10.93(27)
$[Me_2Ga\{(NCOC_6H_4)_2CH\}]$ (**13**)	–	3.62(2)	14.34(3)
$[Me_2Ga\{(NCSC_6H_4)_2CH\}]$ (**14**)	–	8.90(6)	20.61(26)

* two values are given due to the discrepancy of the two molecules within the unit cell.

Table 2-11: Selected averaged bond lengths (pm) and angles (deg) of the ligand backbone for the neutral ligands **1**, **2**, **4**, **5** and the metal complexes **6** and **8** – **14**. (Addendum to Table 2-4)

compound	C_{ipso}–C1'	C_{ipso}–N1	C1–C1'–C8	M–N1	N1–M–N2
$(1\text{-MeNCNC}_2H_2)_2CH_2$ (**1**)	150.20(14)	136.17(14)	111.74(10)	–	–
$(1\text{-MeNCNC}_6H_4)_2CH_2$ (**2**)	149.52(16)	131.63(15)	113.52(9)	–	–
$(NCOC_6H_4)_2CH_2$ (**4**)	148.91(15)	128.87(14)	111.23(9)	–	–
$(NCSC_6H_4)_2CH_2$ (**5**)	151.06(15)	129.55(16)	109.59(14)	–	–
$[Me_2Al\{(1\text{-MeNCNC}_2H_2)_2CH\}]$ (**6**)	139.6(3)	136.4(3)	121.11(19)	190.23(19)	93.76(8)
$[Me_2Al\{(NCOC_6H_4)_2CH\}]$ (**8**)	138.0(3)	134.6(3)	119.5(2)	191.76(20)	91.67(9)
$[Me_2Al\{(NCSC_6H_4)_2CH\}]$ (**9**)	139.0(2)	135.15(19)	123.54(14)	192.38(14)	94.78(6)
$[MeClAl\{(NCOC_6H_4)_2CH\}]$ (**10**)	138.2(2)	134.8(3)	120.2(3)	189.30(17)	94.33(11)
$[MeClAl\{(NCSC_6H_4)_2CH\}]$ (**11**)	138.8(3)	136.5(3)	124.1(2)	189.4(2)	96.84(9)
$[Me_2Ga\{(NCOC_6H_4)_2CH\}]$ (**13**)	139.4(9)	132.3(9)	119.7(6)	199.6(6)	89.2(2)
$[Me_2Ga\{(NCSC_6H_4)_2CH\}]$ (**14**)	139.09(19)	134.36(19)	124.0(2)	199.45(13)	92.99(8)

The most interesting feature within the series of the obtained structures is the deviation of the metal atom from the extended plane, which is comprized from the N1–C1–C1'–C8–N2 array. The M···plane distance is associated with the folding angle between both heteroaromatic substituents, which can be seen as a reason for the different deviations. Various data concerning the M···plane distances, the torsion and the folding angles are listed in Table 2-10 and Table 2-11.

To highlight this special aspect, the molecular structures of **8** and **14** are shown in Figure 2-12 and Figure 2-17 (*vide infra*). Both species exhibit the greatest metal distance from the chelating C_3N_2 plane (29.57(26) pm in **8** and 20.61(26) pm in **14**) and also the greatest folding angle of the heteroaromates at 9.12(8) deg and 8.90(6) deg, respectively, for all synthesized complexes.

At this point, a comparison of some structural values concerning related groups 13 metal complexes, bearing either bis-(pyrid-2-yl)-methanide or nacnac ligand systems, will be presented.[14l, 83d] Starting with the $AlMe_2$ complex $[Me_2Al\{(2\text{-}NC_5H_4)_2CH\}]$, the coordinated aluminium cation just deviates 1.1 pm from the chelating C_3N_2 plane and the two pyridyl rings are slightly twisted by 0.8 deg. The averaged Al–N distance for this compound is 190.9 pm.[83d] These values are indicating, that this ligand system is appropriate for the coordination of a dimethyl aluminium fragment, because the resulting complex is nearly ideally planar arranged. The comparison to the herein discussed corresponding complexes **6**, **8** and **9** reveals that the benzofused derivatives (**8**, **9**) show significant variations referring to the former mentioned structural parameters, whereas the coordination geometry of the smallest ligand **6** is almost similar (see Table 2-10 and Table 2-11). In **6**, the deviation from the plane results in average 0.86 pm and the Al–N distance (190.2 pm) even shorter as in the compared complex. In contrast to this, the benzannulation causes an increase of the steric demand and therefore the observed parameters reflect the less favoured coordination of $AlMe_2$ when compared to $[Me_2Al\{(2\text{-}NC_5H_4)_2CH\}]$ (M···plane: 29.6 pm (**8**); 13.8 pm (**9**); Al–N distance: 191.8 pm (**8**); 192.4 pm (**9**)). The corresponding nacnac complex $[Me_2Al\{(N(Dipp)C(Me))_2CH\}]$ exhibits an even more pronounced puckering for the Al centre, which is displaced about 72 pm from the chelating plane. The observed Al–N bond length results in 193.3 pm and the N1–Al1–N2 bite angle is 96.2 deg.[14l] Regarding to these values, it can be stated that the bisheterocyclo methanides **8** and **9** have more in common with the nacnac species. The increased out-of-plane arrangement for the $AlMe_2$ nacnac complex is presumably contributed by the higher steric demand of the Dipp-substituents. Therefore, the steric demand of **8** and **9** lies in between $[Me_2Al\{(2\text{-}NC_5H_4)_2CH\}]$ and $[Me_2Al\{(N(Dipp)C(Me))_2CH\}]$, because the observed bonding situation exhibits intermediate values in the solid state.

Carrying on with the partially halogenated species **10** and **11**, which were obtained by reaction of the neutral ligands **4** and **5** with dimethyl aluminium chloride instead of trimethyl aluminium, two further interesting molecules could be synthesized and characterized in solution as well as in the solid state. Compound **10** (see Figure 2-14) crystallizes in the monoclinic space group *C*2/*m* and the asymmetric unit consists of three half molecules, of which one half molecule is disordered on a special position, and one toluene molecule as lattice solvent disordered on a special position. Another crystallographic

feature of these AlMeCl species is, that in the solid state the positions of both substituents at the aluminium fragment are not fixed to one specific side of the resulting metal complex. This means that a striking Cl-Me positional disorder occurs due to their quite similar size and bonding situation, with the consequence that there is no preferred alignment of the Cl or Me residue in the solid state. The resulting site occupation factors for the three molecules add up to values of 0.41, 0.40 and 0.20. Due to this occurring vital disorder and overlay of two differently oriented molecules, in the solid state no meaningful values regarding the Al1–C1M or Al1–Cl1 bond lengths can be stated. Nevertheless, in the adjacent Table 2-12 the above-mentioned angles and distances are listed for having a complete overview of the experimentally determined bonding situation within complex **10**. It should be mentioned, that the estimated standard deviation of those values are correspondingly higher than in the non-disordered parts of the molecule.

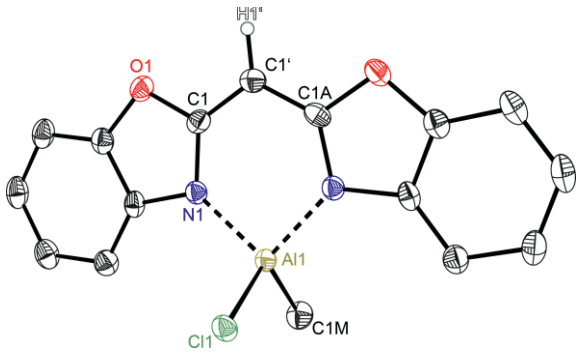

Figure 2-14: Solid state structure of complex **10**.

Table 2-12: Distances [pm] and angles [deg] of **10**.

C1'–C1	138.5(2) 137.8(2) 137.8(15)	N1–C1–C1'	128.21(19) 127.78(19) 128.3(6)
C1–N1	135.0(2) 134.6(3) 134.8(10)	O1–C1–C1'	119.71(18) 119.81(18) 119.7(6)
C1–O1	136.3(2) 136.3(2) 136.3(5)	O1–C1–N1	112.06(17) 112.40(17) 112.0(4)
N1–Al1	189.61(17) 188.99(17) 189.0(10)	C1–C1'–C8	119.6(3) 120.8(3)
Al1–C1M	194.2(12) 194.0(9) 193.5(12)	N1–Al1–N2	93.90(10) 94.75(11)
Al1–Cl1	213.0(3) 215.22(15) 212.9(3)	C1M–Al1–Cl1	113.3(6) 111.6(3)

Symmetry transformations used to generate equivalent atoms: x, −y+1, z
Due to the presence of three half molecules in the asymmetric unit, for each parameter three values are given.

In contrast to **10**, the benzothiazole derivative **11** (see Figure 2-15) crystallizes in the triclinic space group $P\bar{1}$ with one molecule in the asymmetric unit, although the observed coordination motif is the same like in **10**. Whereas the bonding situation is quite comparable within the triple estimated standard deviation (see Table 2-11), it is worth to mention, that the C1–C1'–C8 angle in the backbone of the ligand (120.0(3) deg in **10** vs. 124.1(2) deg in **11**) and the corresponding N1–Al1–N2 bite angle (94.33(11) deg in **10** vs. 96.84(9) deg in **11**) differ most upon comparison of their crystal structures. Furthermore, the folding parameters of both complexes show a significant discrepancy: the folding angle as well as the M···plane distance are much wider in **10** (3.69(40) deg and 18.06(32) pm) compared to **11** (1.21(4) deg and 10.93(27) pm) indicating, that the benzothiazole based ligand system is more suitable for the coordination of aluminium(III).

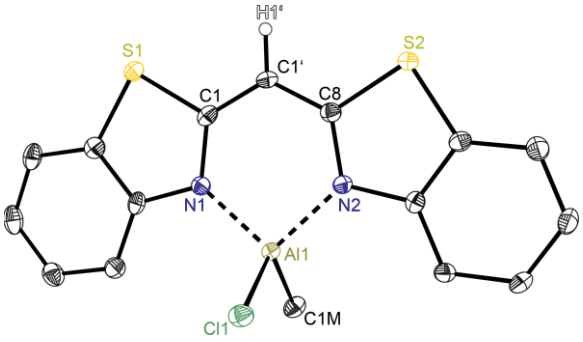

Figure 2-15: Solid state structure of complex **11**.

Table 2-13: Distances [pm] and angles [deg] of **11**.

C1'–C1	138.8(3)	N1–C1–C1'	126.1(2)
C1'–C8	138.7(3)	N2–C8–C1'	125.9(2)
C1–N1	136.4(3)	S1–C1–C1'	120.98(17)
C8–N2	136.5(3)	S2–C8–C1'	121.02(17)
C1–S1	174.7(2)	S1–C1–N1	112.96(17)
C8–S2	174.2(2)	S2–C8–N2	113.05(16)
N1–Al1	189.5(2)	C1–C1'–C8	124.1(2)
N2–Al1	189.3(2)	N1–Al1–N2	96.84(9)
Al1–C1M	197.6(14)	C1M–Al1–Cl1	113.2(5)
Al1–Cl1	212.0(2)		

By comparing the structural values of the parent ligands with those of the metallated species given in Table 2-11, it can be assumed that there is a change in hybridisation of the central bridging carbon atom from sp^3 to sp^2 upon metallation. As an evidence for this statement, the angular sum around the bridging carbon atom can be taken into account, ranging from 359.9(2) deg to 360.1(2) deg. These values display a nearly ideal trigonal planar coordination geometry for C1' as expected for a sp^2-hybridized carbon atom. In the benzothiazole as well as the benzoxazole containing ligand, a shortening of the C_{ipso}–C1' bond (starting from 151.06(15) pm and 148.91(15) pm to approx. 139 pm) and a widening of the C1–C1'–C8 angle (from 109.59(14) deg and 111.23(9) deg to approx. 120 deg) were observed. Including the corresponding elongated N–C_{ipso} distances for the deprotonated species **8** – **14**, an efficient delocalisation of the lone pair is anticipated. As shown in Scheme 2-10, there are different mesomeric resonance structures, which can be proposed: **(a)** a carbanionic, **(b)** an amidic and **(c)** a completely delocalized canonical form.

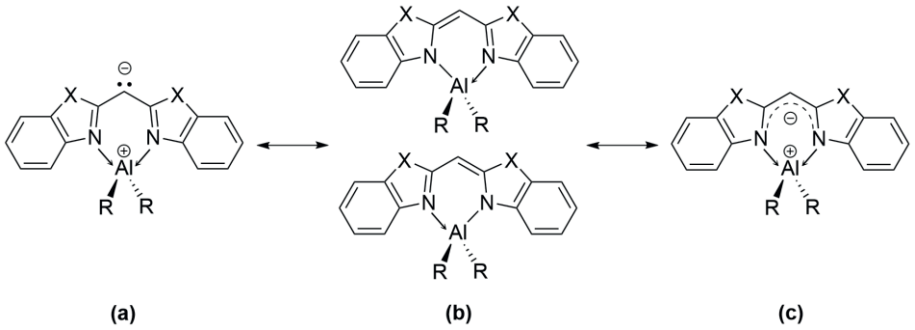

Scheme 2-10: Mesomeric resonance structures of the bisheterocyclo methanides.

In the carbanionic form **(a)**, formally the deprotonation of the acidic methylene bridge generates a lone pair, which is located directly at C1'. This lone pair is isolated from the adjacent π-systems of the heteroaromatics leading to a negative charge at C1' and the positively charged metal fragment is coordinated by the two imine nitrogen atoms via dative bonds. In contrast to that, the completely delocalized canonical form **(c)** displays the nacnac-like coordination motif, where the generated free electron pair is distributed

over both ring systems, especially by means of the former C_{ipso}=N double bonds. This leads to a delocalization of the double bonds within the six-membered metalla heterocycle. The amidic resonance structures **(b)** can be classified as a mixture of the former stated mesomeric forms **(a)** and **(c)**. In the upper case, the lone pair of the methanide was implemented into the former C1–C1' bond to give a distinct double bond. Therefore, the former C1=N1 double bond has tautomerized to a single bond with the nitrogen atom carrying a second lone pair, so that N1 is negatively charged (amidic). Again, the metal complexation is accomplished by the formation of one dative bond formed by the remaining imine nitrogen atom N2 and formally one covalent bond from the amidic nitrogen atom N1. Regarding to this, there is a distinct alternating sequence of single and double bonds present (N1–C1, C1=C1', C1'–C8, C8=N2), which should also be reflected by the determined bond distances obtained from X-ray diffraction experiments. The lower case, depicted in Scheme 2-10 as **(b)**, shows the counterpart for the last mentioned resonance structure. Here, just the double bonds have tautomerized to the other direction of the ligand by means of C8 and therefore the alternating sequence of single and double bonds is the other way around.

Regarding the abovementioned structural changes, species **(a)** has a certain eligibility as reported in previous studies of $[MeZn\{(2\text{-}NC_5H_4)_2CH\}]_2$. Here, the central methylene is deprotonated and the methanide carbon atom coordinates to the electropositive zinc fragment.[83a] But in the case of the investigated series of methanide complexes, this kind of coordination via the bridging moiety was not observed. Just for the amine derivatives, where the bridging moiety was isoelectronically replaced by an NH functionality, the coordination via the deprotonated bridge could be observed once (*vide infra*, see Chapter 2.5). Nevertheless, case **(c)** seems to explain the bonding situation best within the compounds **8** – **14**, because the C–C and C–N bond lengths lie in between a distinct single and double bond character (C(sp^2)–C(sp^3): 151.0 pm, C(sp^2)=C(sp^2): 133.5 pm, C(sp^2)–N(sp^3): 143 pm, C(sp^2)=N(sp^2): 129 pm).[108a] However, the presence of the mesomeric forms **(b)** is also feasible, because the analytical data obtained from SCXRD or NMR describe on a macroscopic scale only the averaged state of the investigated molecules in the solid state or solution. Therefore, it is also possible that both mesomeric forms depicted in **(b)** are equally present and due to the overlay of all molecules only a merged image can be received.

The crystal structures of the two synthesized dimethyl gallium species **13** and **14** are depicted in Figure 2-16 and Figure 2-17. As heavier homologues of the earlier discussed aluminium derivatives **8** and **9**, the observed crystallographic values and the bonding situations of these four species can be used in a comparative way to highlight the influence of the coordinated metal cation and the implemented ligand platform. Whereas the benzoxazole based metal complex **13** crystallizes in the monoclinic space group $P2_1$ and its asymmetric unit consists of two molecules, the corresponding bis-(benzothiazol-2-yl)-methanide **14** crystallizes in the orthorhombic space group *Pnma* with just half a molecule in the asymmetric unit. The aluminium species show a correlation between two important structural features: the narrower the N–M–N angle is, the greater the metal distance from the C_3N_2 plane and also the greater the folding angle of the heteroaromatic residues gets. However, in the case of the gallium complexes this tendency is inverted.

Having a closer look at the obtained crystal structure of **13**, it can be noted, that the average N1–Ga1–N2 angle is 89.2(2) deg accompanied with a folding angle of 3.62(2) deg and a M···plane distance of 14.34(3) pm (see Table 2-10 and Table 2-11). In contrast to this, the crystal structure of **14** exhibits a widened bite angle of 92.99(8) deg, which causes the ligand to adopt a more folded arrangement (folding angle: 8.90(6) deg; M···plane distance: 20.61(26) pm). These observations are reasons to believe, that the ligand derived from **4** coordinates gallium more properly than aluminium and the ligand derived from **5** vice versa.

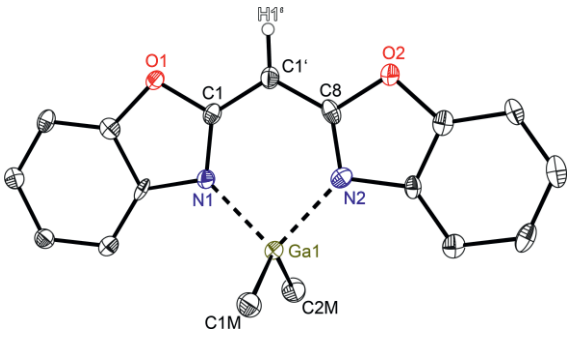

Figure 2-16: Solid state structure of complex **13**.

Table 2-14: Distances [pm] and angles [deg] of **13**.

C1'–C1	140.1(8) 138.7(9)	N1–C1–C1'	128.2(6) 129.6(6)
C1'–C8	139.2(8) 139.8(8)	N2–C8–C1'	127.7(5) 129.0(6)
C1–N1	132.9(8) 132.3(8)	O1–C1–C1'	119.3(6) 118.2(6)
C8–N2	131.1(7) 132.8(7)	O2–C8–C1'	119.2(5) 117.8(5)
C1–O1	136.9(7) 138.6(8)	O1–C1–N1	112.5(6) 112.2(6)
C8–O2	136.1(6) 136.2(7)	O2–C8–N2	113.1(5) 113.3(5)
N1–Ga1	200.0(5) 200.0(5)	C1–C1'–C8	120.0(6) 119.3(6)
N2–Ga1	199.3(5) 199.1(5)	N1–Ga1–N2	88.6(2) 89.9(2)
Ga1–C1M	197.2(6) 197.0(6)	C1M–Ga1–C2M	123.8(3) 121.3(3)
Ga1–C2M	196.4(6) 196.7(6)		

Due to the presence of two molecules in the asymmetric unit, for each parameter two values are given.

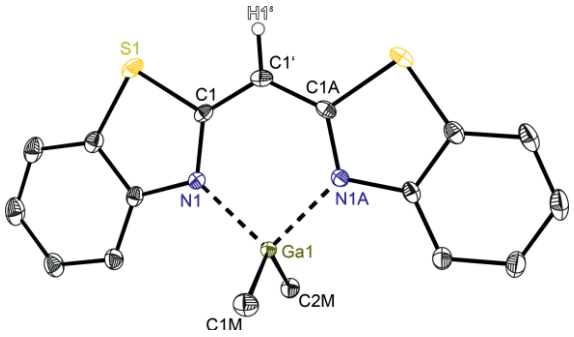

Figure 2-17: Solid state structure of complex **14**.

Table 2-15: Distances [pm] and angles [deg] of **14**.

C1'–C1	139.09(19)	N1–C1–C1'	127.20(15)
C1–N1	134.36(19)	S1–C1–C1'	119.78(12)
C1–S1	175.15(16)	S1–C1–N1	112.99(12)
N1–Ga1	199.45(13)	C1–C1'–C1A	124.0(2)
Ga1–C1M	196.4(2)	N1–Ga1–N1A	92.99(8)
Ga1–C2M	196.9(2)	C1M–Ga1–C2M	125.57(10)

Symmetry transformations used to generate equivalent atoms: x, −y+3/2, z

The C1–C1'–C8 angle in the backbone of the specific ligand system shows a slight widening in the $GaMe_2$ complexes compared to the $AlMe_2$ species. There is also a deviation in the bond lengths concerning the *ipso*-carbon atom: in the case of the benzoxazole de-

rivatives the C_{ipso}–N distance shrinks from 134.6(3) pm in **8** to 132.3(9) pm in **13**, whereas the C_{ipso}–C1' distance is elongated from 138.0(3) pm in **8** to 139.4(9) pm in **13**. In addition to this, the benzothiazole species show a less pronounced shortening of the C_{ipso}–N distance (**9**: 135.15(19) pm; **14**: 134.36(19) pm) and the C_{ipso}–C1' distance stays nearly the same in both metal complexes. Due to these findings, in **13** the C_{ipso}–N bond has more double bond character as in **8** and bonds concerning the bridging carbon atom C1' are rather single bonds. This fact indicates a weaker degree of delocalization of the lone pair in the gallium compounds (C(sp^2)–C(sp^2): 146.6 pm, C(sp^2)=C(sp^2): 133.5 pm, C(sp^2)–N(sp^3): 143 pm, C(sp^2)=N(sp^2): 129 pm).[108a] This aspect is also observed in solution (see Spectrum 2-4 and Spectrum 2-5), in which clearly can be seen, that the signal for the remaining proton at the methylene bridge is most upfield shifted for both deprotonated ligand platforms **4** and **5**. In contrast to the corresponding $AlMe_2$ species, this upfield shift is induced by an increased electron density at the methylene unit, because the lone pair is formally rather localized at this position.

The corresponding [$Me_2Ga\{(2\text{-}NC_5H_4)_2CH\}$] complex, bearing the bis-(pyrid-2-yl)-methanide ligand, shows twisting of 5.5 deg and the gallium fragment is located 29 pm above the C_3N_2 plane with an average Ga–N bond length of 198.1 pm.[83d] Similar folding parameters were found for the bisheterocyclo methanides (M···plane: 14.3 pm (**13**); 20.6 pm (**14**); folding angle: 3.6 deg (**13**); 8.9 deg (**14**)), whereas the Ga–N distances are elongated due to the enhanced steric demand (199.6 pm (**13**); 199.5 pm (**14**)) (see Table 2-10 and Table 2-11). Another interesting difference is the fact, that the deprotonated pyridyl substituted ligand system shows the presence of distinct, located double bonds, whereas the herein discussed monoanionic ligands show delocalized double bond pattern. Further comparison to the nacnac derivative [$Me_2Ga\{(N(Dipp)C(Me))_2CH\}$], which exhibits a Ga–N bond length of 199.9 pm and a bite angle of 93.9 deg, reveals again similar bonding situations upon metal coordination.[14i] But the metal distance from the chelating plane is also significantly closer to planarity (76 pm vs. 14.3 pm (**13**); 20.6 pm (**14**)) for the bisheterocyclo methanides **13** and **14**.

Taking all synthesized group 13 metal complexes of the bis-(benzothiazol-2-yl)- and bis-(benzoxazol-2-yl)-methanides into account, it should be emphasized, that the oxygen containing ligand has on average a significantly smaller bite angle than in the sulfur analogues (89.2(2) – 94.33(11) deg vs. 92.99(8) – 96.84(9) deg). Also the angle around the bridging carbon atom C1' in the backbone is also smaller (119.5(2) – 120.2(3) deg vs. 123.54(14) – 124.1(2) deg). For the sake of completeness, the imidazole based metal complex **6** should be mentioned in this context. Compared to the other $AlMe_2$ containing molecules **8** and **9**, the following concluding statements can be made: the bite angle (93.76(8) deg) and the backbone angle (121.11(19) deg) are placed in between the determined values of the corresponding species **8** and **9**. Due to the absence of the annulated benzene moiety the Al–N distance is the shortest one observed (190.23(19) pm) in all complexes (**6**, **8** and **9**) and the molecule's alignment in the solid state is nearly planar (folding angle: 2.72 deg; M···plane distance: 0.86 pm).

It is notable that in the series $AlMe_2$ > AlMeCl > $GaMe_2$ the N–M distances and the N–M–N angles in the solid state alter as expected. Comparison of **8** and **9** with **10** and **11**

shows a decrease of the N–M distance because of the more electronegative, electron withdrawing chlorido substituent in the latter cases. Concomitantly the N–M–N angles are widened. Furthermore, the dimethylgallium compounds **13** and **14** feature increasing N–M bond lengths and smaller bite angles due to the bigger covalent radius of the coordinated gallium cation (Al: 121 pm, Ga: 122 pm).[110]

2.1.5 NMR Spectroscopic Investigations

In addition to the former stated results, measurements of $^{1}H,^{15}N$-HMBC NMR data gave evidence that complexes **8**, **9**, **13** and **14** show the same structure in solution at room temperature (on the NMR time scale) and in the solid state. The coordination geometry concerning the nacnac-like chelating ability can be proven by the apparent cross peaks, which clearly display ^{3}J-coupling between the protons of the $AlMe_2$ or $GaMe_2$ unit and the nitrogen donor atoms N1 and N2. The recorded NMR data are shown in Spectrum 2-2 for the $AlMe_2$ compounds **8** – **9** and in Spectrum 2-3 for the $GaMe_2$ complexes **13** – **14**.

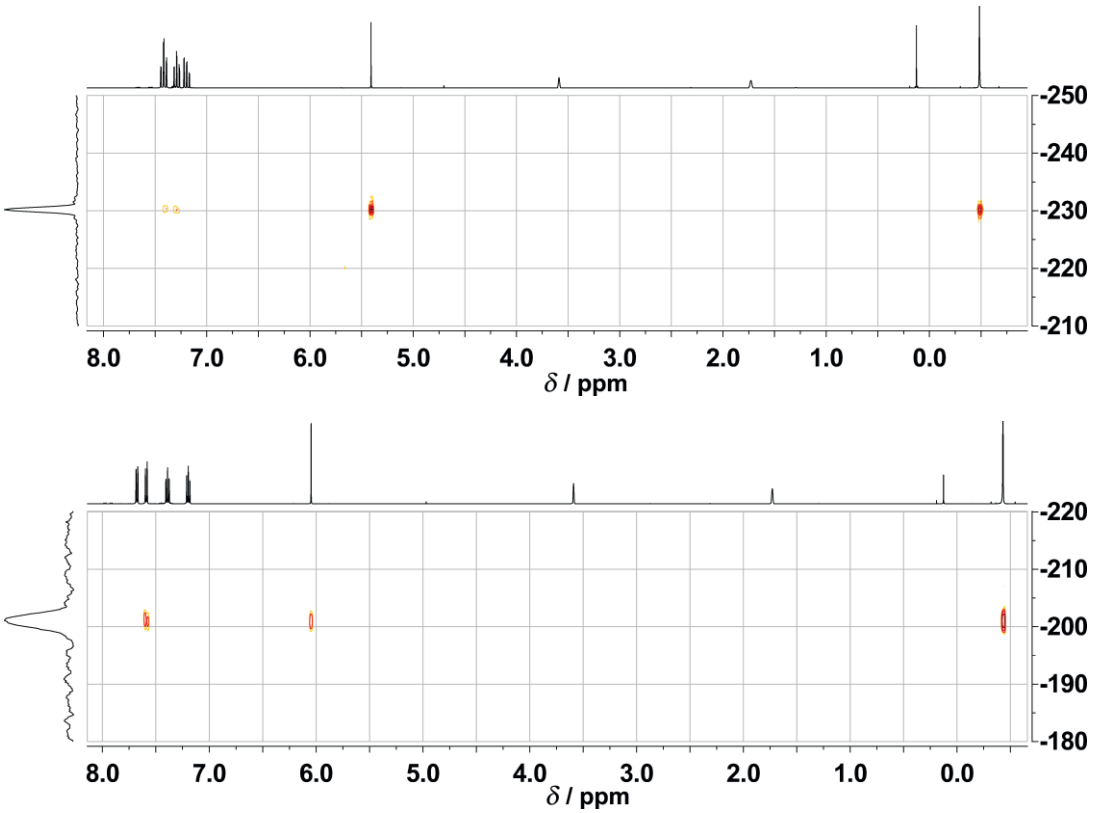

Spectrum 2-2: $^{1}H,^{15}N$-HMBC NMR spectra (THF-d_8, rt) for the compounds: *top:* **8** (300 MHz), *bottom:* **9** (300 MHz).

This is an evidence, that the metal fragment is still coordinated by both endocyclic nitrogen donors in solution. The upper part of Spectrum 2-2 clearly shows, that in the case of **8** the hydrogen atoms of the dimethyl aluminium unit ($\delta = -0.48$ ppm) as well as the remaining proton of the methylene bridge ($\delta = 5.41$ ppm) are coupling with the signal of the

endocyclic nitrogen atom (δ = −231.3 ppm). These ^{3}J-couplings are observed as cross peaks in the 2D-NMR experiment. Furthermore, there are two apparent cross peaks in the aromatic region of the ^{1}H-NMR spectrum at 7.42 ppm and 7.29 ppm. The first cross peak can be assigned to the proton H6, which is the aromatic proton in closest proximity to the chelating nitrogen donor, and represents also a ^{3}J-coupling towards N1. The second cross peak results from the ^{4}J-coupling between the aromatic proton H5 and the chelating imine donors. Other couplings of the remaining protons H3 or H4, located at the backside of the coordinating ligand, could not be observed. The ^{1}H-NMR spectrum shows three additional peaks not belonging to the investigated compound **8**: at 3.58 ppm and 1.73 ppm, the signals of the not completely deuterated solvent THF-d_8 can be observed and additionally at 0.13 ppm slight contaminations with silicon grease, originating from the flask, can be detected (see also Spectrum 2-4).

The same observations were made for the corresponding complex **9**, shown at the bottom of Spectrum 2-2, which carries sulfur atoms instead of oxygen in the ligand backbone. In this case just three cross peaks could be observed. Again, they could be assigned to the well-pronounced ^{3}J-couplings of the nitrogen atom (δ = −201.2 ppm) towards the protons of the $AlMe_2$ unit (δ = −0.43 ppm), the methylene bridge (δ = 6.05 ppm) and the aromatic proton H6 (δ = 7.59 ppm). No further cross peaks referring to long range couplings were detected in this ^{1}H,^{15}N-HMBC NMR spectrum. Comparing the ^{1}H-NMR spectra of **9** and **8**, it is obvious that the coupling pattern of the aromatic hydrogen atoms in **9** is better resolved than in **8**. This is caused by the nearly identical chemical shifts of H3 and H6, leading to a triplet-like peak with an integral of two protons. The chemical shifts of the aromatic protons have a wider range in **9** than in **8** (7.20 – 7.68 ppm vs. 7.19 – 7.42 ppm) and the signal of the remaining proton H1' at the central carbon atom shows a quite significant deviation in its observed chemical shift (6.05 ppm vs. 5.41 ppm). Also the detected shifts of the nitrogen atoms within the benzothiazole **9** or benzoxazole **8** unit show distinct differences (−201.2 ppm vs. −231.3 ppm).

The described discrepancies can be ascribed to the aromaticity of the particular underlying planar 1,3-azole heterocycle. For example, the aromaticity was found to be more pronounced for the thiazole moiety when compared to the electron rich oxazole counterpart.[111] Additionally, the delocalization of a negative charge, originating from the deprotonated methylene bridge, takes place most efficiently in thiazoles, whereas oxazoles and even more so imidazoles are more reluctant of accepting the negative charge. These findings were established by calculations of the charge demands of the different heterocycles based on NMR spectroscopic investigations, which were applied for the parent ligand systems **1**, **2**, **4** and **5** and the deprotonated monoanionic species.[98c] Those measurements were performed using DMSO as solvent and the corresponding carbanions were generated by treatment with dimsylsodium to afford solvent separated ion pairs or free ions.

Table 2-16: Selected NMR spectroscopic shifts of the metallated species **6** – **9** and their parent ligands.

compound	δ(H1') [ppm]	$\Delta\delta$* [ppm]	δ(C1') [ppm]	$\Delta\delta$* [ppm]	δ(N1) [ppm]	$\Delta\delta$* [ppm]
$[Me_2Al\{(1\text{-}MeNCNC_2H_2)_2CH\}]$ (**6**)	4.06	−0.06	50.46	23.40	−222.1	−102.5
$(1\text{-}MeNCNC_2H_2)_2CH_2$ (**1**)	4.12		27.06		−119.6	
$[Me_2Al\{(1\text{-}MeNCNC_6H_4)_2CH\}]$ (**7**)	4.72	0.09	55.41	27.09	−**	−**
$(1\text{-}MeNCNC_6H_4)_2CH_2$ (**2**)	4.63		28.32		−136.4	
$[Me_2Al\{(NCOC_6H_4)_2CH\}]$ (**8**)	5.41	0.71	60.48	30.90	−231.3	−97.7
$(NCOC_6H_4)_2CH_2$ (**4**)	4.70		29.58		−133.6	
$[Me_2Al\{(NCSC_6H_4)_2CH\}]$ (**9**)	6.05	1.08	82.56	43.37	−201.2	−132.2
$(NCSC_6H_4)_2CH_2$ (**5**)	4.97		39.19		−69.0	

* $\Delta\delta = \delta$(complex) − δ(ligand); positive values represent low-field shifts.
** value was not measured.

The results of the above-mentioned study reveal, that the charge demand is decreasing in the order benzothiazole > benzoxazole > benzimidazole > imidazole and that benzofusion of the 1,3-azoles increases their charge demand.[98a, 98c] The same trends can be observed for the chemical shifts of the compounds **6** – **9** in comparison to their parent ligand systems (see Table 2-16): having a closer look at the chemical shifts of H1' and C1' for the bridging moiety, it is evident that in the case of the metallated species, the corresponding signals for H1' and C1' arise at lower magnetic field than in the neutral starting material. The observed differences of their chemical shifts, which are an indicator for the electronic influence of the ligand's side arms, are increasing in the series **6** (smallest $\Delta\delta$) > **7** > **8** > **9** (biggest $\Delta\delta$). This observation shows that the electron density at the central methylene bridge decreases in the same order, which goes along with the above-stated increasing charge demand of the heterocycles. The higher grade of aromaticity in the thiazole facilitates the delocalization of negative charge and therefore causes the remaining electron density at the central carbon C1' atom to be decreased in comparison to the oxazole and even more so to the imidazole derivative.

As a result of the delocalization, the electron density within the different heterocycles is significantly increased when compared to the neutral ligands. Dependent on the particular heteroaromatic substituent and its according charge demand, the degree of additional accumulated density can be measured by the variation of the ^{15}N chemical shift for the imine nitrogen atom N1 upon metallation. In general, the chemical shifts of the nitrogen atoms are displaced to higher field upon deprotonation and metal coordination, because π-donation due to the delocalized negative charge takes place.[112] Although the imine donors are involved in σ-donation towards the metal centre, the resulting electronic shielding of the nitrogen atoms is enhanced for the metallated species and a high-field shift is detected. Indeed, analogue trends as for the methylene bridge can be detected: the determined $\Delta\delta$ value is significantly larger for the benzothiazole derivative **9** than it is for **8** (see Table 2-16). This observation reflects again, that the charge demand of the thiazole moiety is more pronounced.

Similar observations are found in the $^{1}H,^{15}N$-HMBC NMR spectra for the dimethyl gallium compounds **13** and **14**, shown in Spectrum 2-3. Both spectra indicate that in compound **13** (*top*) and **14** (*bottom*) three cross peaks can be identified: these belong to the earlier stated ^{3}J-couplings between the chelating nitrogen atom N1 and the protons of the methyl groups at the gallium fragment (δ = −0.06 ppm and −0.02 ppm), the proton H1' at the bridging moiety (δ = 5.25 ppm and 5.87 ppm) and the aromatic proton H6 in closest proximity to the coordinated metal cation (δ = 7.25 ppm and 7.40 ppm). Furthermore, there are slight differences in the recorded ^{1}H-NMR spectra: on the one hand, the signals of the aromatic protons in **14** are better resolved/separated and cover a broader range (7.64 – 7.14 ppm) in contrast to **13**, in which the signals of H5 and H6 are overlapping. On the other hand, the chemical shift of the remaining proton at the CH bridge is more high field shifted in **13** than in **14**. As a result, also the resonance signal of the coordinating nitrogen donor in the benzoxazole derivative **13** is more shifted to the higher field as observed for **14** (−229.9 ppm vs. −199.2 ppm). As mentioned in the previous paragraph, the same explanation for this behaviour, based on the different aromatic character of the heterocycles, can be applied.

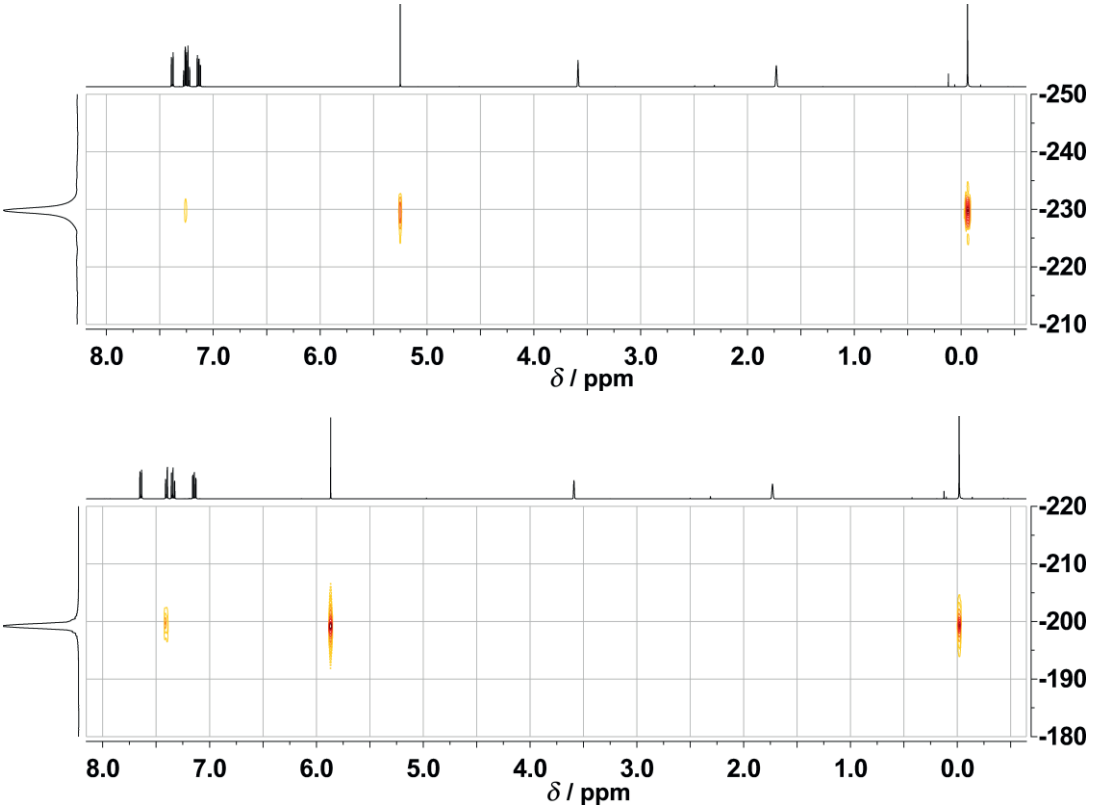

Spectrum 2-3: $^{1}H,^{15}N$-HMBC NMR spectra (THF-d_8, rt) for the compounds: *top:* **13** (500 MHz) and *bottom*: **14** (500 MHz).

In the next section, the NMR spectroscopic data of the different ligand systems and derived complexes will be discussed briefly. To gain a better understanding of the influence of the coordinated metal fragment on the chemical shift, overlays of the recorded ^{1}H-

NMR spectra are presented (see Spectrum 2-4 and Spectrum 2-5). Each overlay consists of a ^{1}H-NMR spectrum of the parent ligand (*top*), and the spectra of the derived methanide complexes containing a $AlMe_2$ (*2nd trace*), AlMeCl (*3rd trace*) or $GaMe_2$ unit (*bottom*), respectively.

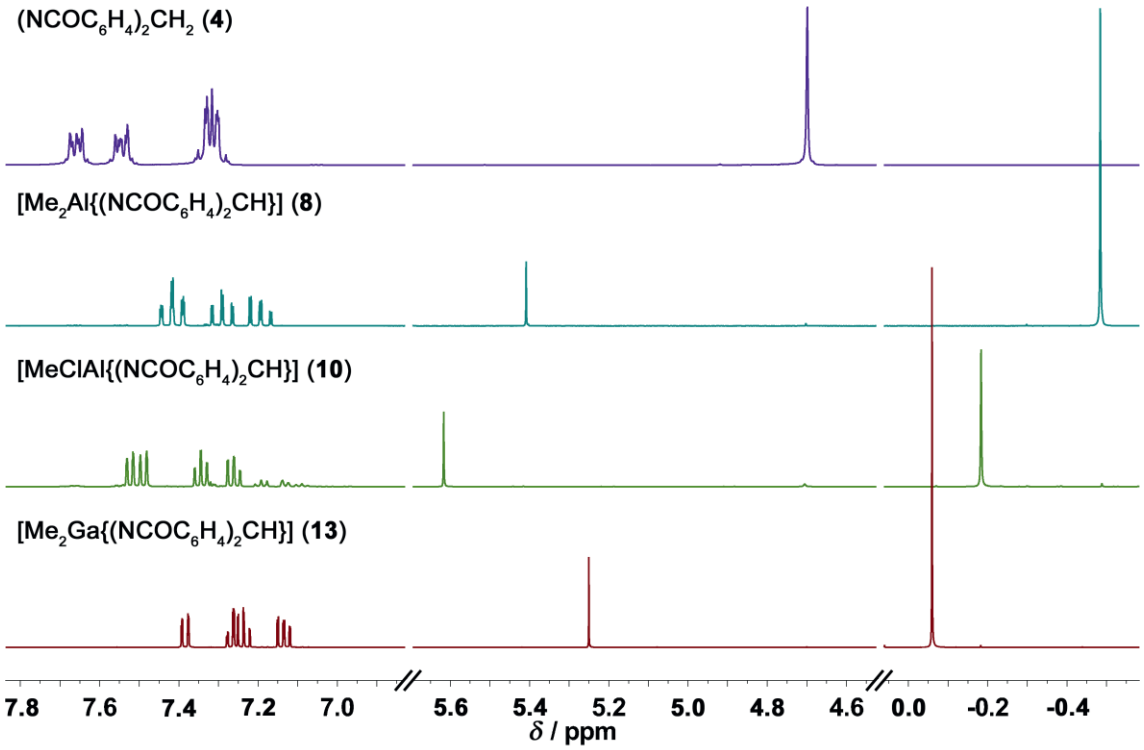

Spectrum 2-4: Overlay of the ^{1}H-NMR spectra (THF-d_8, rt) of the parent ligand system **4** and the corresponding metallated species **8**, **10** and **13**. The spectrum of **10** contains some minor contaminations of an unknown side product.

Having a closer look at the NMR overlay of the metallated species of **4** depicted in Spectrum 2-4, significant changes can be noticed upon metallation with the corresponding metal organic reagent. The ^{1}H-NMR spectrum of the free ligand **4** shows a quite unstructured signal pattern in the aromatic region. After coordination to a group 13 metal, the signals of the aromatic protons are split into distinct doublets or triplets, from which significant coupling constants can be deduced. This change in the multiplicity of the considered resonance signals can be explained by the flexibility of the organic framework in the free ligand as well as by the rigidity thereof in the metal complexes. In the parent ligand, the heterocyclic side arms can freely rotate around the C1–C1' or C8–C1' bond in solution, so that there is no preferred alignment of the ligand and its aromatic protons. As a consequence of the deprotonation of the methylene bridge, the C_{ipso}–C1' bonds adopt partial double bond character and due to the formation of the chelate complex, the ligand is fixed within certain limits to the metal fragment (see results of the ^{1}H,^{15}N-HMBC NMR experiments, Spectrum 2-2 and Spectrum 2-3). Both aspects prevent the ligand from unhindered rotation or free movement in solution, resulting in a rigid molecule, in which especially the aromatic protons underlie diverse chemical and magnetical environ-

ments. For example, complexation in **8** leads to a splitting of the former overlapped signal for the protons H4 and H5. Furthermore, the remaining aromatic protons H3 and H6 are influenced in a way, that the same chemical shift is observed and a triplet-like resonance signal is generated at δ = 7.42 ppm. The following general trends upon metallation can be identified: the ^{1}H-NMR signals referring to the benzoxazole moiety are electronically more shielded and therefore shifted to the higher magnetic field when compared to **4**. This can be explained by the higher accumulated electron density in the aromatic π-system due to the partially inclusion of the generated lone pair of the methanide. The other way around, the chemical shift of the methanide unit behaves upon deprotonation. It is evident that the signal arises at lower field, meaning that this proton is deshielded, because the delocalization of the methanide's electron pair leads to an extension of the π-system via the methylene bridge to the second heterocycle. Due to this extension, a ring current at the bridging CH functionality is induced, so that H1' is significantly shifted to lower field.

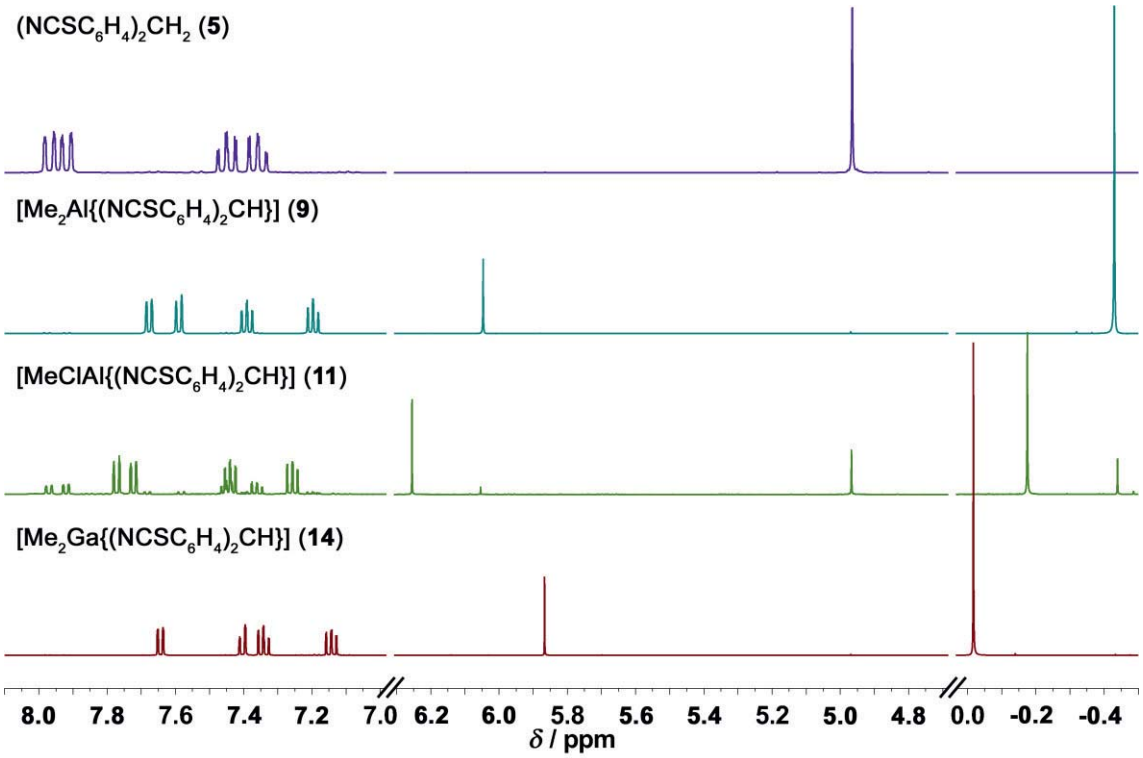

Spectrum 2-5: Overlay of the ^{1}H-NMR spectra (THF-d_8, rt) of the parent ligand system **5** and the corresponding metallated species **9**, **11** and **14**. The spectrum of **11** contains contaminations of **5** and **9**.

From a qualitative point of view, the same trends for ligand system **5** and its derived metallated species **9**, **11** and **14** are observed as already discussed for ligand **4** (see Spectrum 2-5). Again, the protons of the annulated benzene moiety are shifted towards higher field and the proton at the bridging position is shifted to lower field upon metallation in comparison to the neutral ligand **5**. In contrast to the benzoxazole derivative **4** (displayed in Spectrum 2-4), even the neutral ligand **5** shows a clearly defined doublet and triplet struc-

tures of the aromatic protons in the corresponding ^{1}H-NMR spectrum without any signal overlap. Another interesting feature shown in Spectrum 2-5 is, that the resonance signal of the methylene bridge is more downfield shifted in the bis-(benzothiazol-2-yl)-methanides than in the case of the corresponding bis-(benzoxazol-2-yl)-methanides. For example, that proton's signal arises for the $AlMe_2$ derivative **8** at 5.41 ppm (starting from 4.70 ppm in **4**), whereas the same signal for **9** occurs at 6.05 ppm (starting from 4.97 ppm in **5**). This increased downfield shift has to be assigned to the electronic properties of the thiazole containing ligand system, which allow a better delocalization due to the higher aromaticity compared to the oxazole ones. Furthermore, following descriptions in the series of the metallated species **8 – 11** and **13 – 14** for the recorded ^{1}H-NMR spectra should be mentioned: for each of the two ligand systems, as expected, the integral for the methylene bridge was divided in half after the metallation reaction due to the loss of one proton. It is obvious, that the chemical shift of the methanide bridge's proton is also dependent on the coordinated metal fragment. A comparison of the $AlMe_2$ and the AlMeCl derivatives reveals, that in the latter case the downfield shift is most pronounced. This difference is caused by the electronegative chlorido substituent at the metal fragment, which additionally decreases the electron density in the six-membered metalla heterocycle leading to a more deshielded methanide proton than in the $AlMe_2$ complexes. Focusing on the $GaMe_2$ derivatives, which are representing the higher homologues of the recently discussed species, the change in the chemical shift of H1' is for both ligand systems least pronounced (5.25 ppm in **13** and 5.87 ppm in **14**), indicating that the gallium complexes are less appropriate for an efficient electron delocalization.

For clarity reasons it should be mentioned, that in the recorded ^{1}H-NMR spectrum of **11** significant contaminations with the starting material **5** and the $AlMe_2$ derivative **9** can be detected. The resonance signals appearing at 6.05 ppm and −0.43 ppm in Spectrum 2-5 belong to the intermediate **9**, whereas the remaining singlet at 4.97 ppm can be assigned to the methylene proton of the free ligand **5**. The impurities of the partially halogenated metal complexes can be explained by the applied reaction procedure. The parent ligands show a good solubility in the used solvent toluene, whereas the AlMeCl complexes, formed during the reaction, have just a very limited solubility in a non-polar aprotic solvent. In contrast to the dimethyl aluminium or gallium species, which can easily be dissolved in toluene, the replacement of one methyl group at the aluminium centre by one chloride leads to a drastic decrease in the solubility of those species. This is caused by the enhanced polar character of the resulting AlMeCl complex. Due to the used non-polar solvent toluene, the resulting compounds **8** and **9** are immediately precipitating after addition of $AlMe_2Cl$ to the reaction solution. Because of the fast precipitation, it is also possible that to some extent the parent ligand was enclosed in the precipitate. In spite of filtering the microcrystalline solid and washing with pre-cooled toluene, a small amount of the starting material remained in the resulting powder after removal of the solvent. As an explanation for the occurrence of the $AlMe_2$ species, the equilibrium of the electron deficient $(AlMe_2Cl)_2$ dimer can be stated (see Scheme 2-11).

Group 13 compounds are prone to exist in dimeric rather than in monomeric forms because of their electron deficiency. This is also valid for the discussed Al(III) compounds $AlMe_3$ and $AlMe_2Cl$ at room temperature and ambient pressure.[113] This means, to com-

pensate the electron deficiency and fulfil the octet rule, two organo aluminium molecules aggregate to a dimeric species. Hence, one substituent of each molecule acts as a bridging moiety between the two aluminium centres to yield in a four-membered Al_2R_2 metalla heterocycle. The resulting bonds in such electron deficient systems are so-called 3-centre-2-electron bonds.[37] The same is valid for the higher congeners $GaMe_3$ and $InMe_3$ observed in the corresponding solid state structures.[114] In the case of $AlMe_3$, the methyl groups act as suitable linker unit, whose carbon atoms are formally five-coordinate. The monomeric form is also present in the monomer-dimer equilibrium. It serves as the reactive species and is responsible for the deprotonation of the ligand (Scheme 2-11, *top*). Because of the dimer formation and the present equilibrium, the methyl groups can interchange intermolecularly.

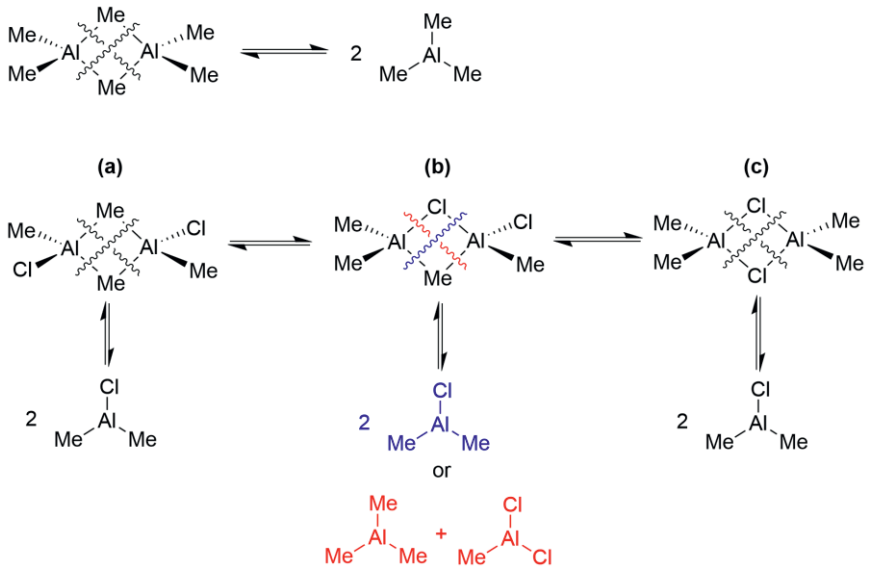

Scheme 2-11: Monomer-dimer equilibrium of the electron deficient organo aluminium compounds.

Transferring these considerations to $AlMe_2Cl$, some differences to $AlMe_3$ have to be taken into account. Due to the replacement of one methyl group by one chloride, there are three possibilities for the formation of the dimer, which just vary by the bridging moieties for the 3-centre-2-electron bonds. The first one is analogue to the previously mentioned Al_2Me_6, where two methyl groups are connecting the two metals centres (Scheme 2-11, **(a)**). This arrangement should also be the most common one for statistical reasons, because the number of methyl groups in the compound is twice as high as for chlorido residues. Contrary to this, the least feasible arrangement bears two bridging chlorides and is depicted in Scheme 2-11 as dimeric form **(c)**. Both species have in common, that two identical moieties are involved in the central Al_2R_2 unit and therefore the resulting active monomers are in each case the same: regardless how the Al_2R_2 heterocycle is bisected, every time two equivalents of $AlMe_2Cl$ are generated. The third arrangement, where a mixture of the both other forms is present, is shown as form **(b)** in Scheme 2-11. In this special case of the monomer-dimer equilibrium, one methyl group and one chloride are involved in the Al–R–Al 3-centre-2-electron bonds. However, the bisection of this dimer

leads to different monomers depending on the chosen Al–R bonds to be broken. If the bisection is performed as highlighted in blue colour, again two equivalents of $AlMe_2Cl$ are formed. In contrast to this, if the red coloured bond breaking is applied, two different monomers originate: $AlMe_3$ and $AlMeCl_2$. Due to the vital equilibrium within the $(AlMe_2Cl)_2$ dimer, a rapid interchange of whether the methyl groups or the chlorides is feasible as in the case of $AlMe_3$. Additionally, two other monomeric species, $AlMe_3$ and $AlMeCl_2$, can occur as a result of this equilibrium. Even if the fraction of those aforementioned monomeric species is quite small, the presence of $AlMe_3$ explains, that in the ^{1}H-NMR spectrum of the AlMeCl species **11** (see Spectrum 2-5) apart from the starting material also the $AlMe_2$ derivative **9** could be detected, although no $AlMe_3$ was added.

2.1.6 Conclusion

In summary, a variety of group 13 metal complexes containing bisheterocyclo methanides as ligand systems was successfully synthesized and structurally evaluated. In each case the metal cation is coordinated in a distorted tetrahedral fashion exclusively by the endocyclic imine nitrogen atoms acting as Lewis donors and the ligand became almost perfectly planar. Depending on the considered combination of the heterocycle (benzoxazole or benzothiazole) and the chelated metal (Al or Ga), some significant correlations between the folding angle of the scaffold and the metal distance from the chelating C_3N_2 plane were observed. The chalcogenes did not participate in coordination neither in the solid state nor in solution as proven in the appropriate crystal structures. The results of the ^{1}H,^{15}N-HMBC NMR experiments gave rise to the assumption that the metal fragments are also exclusively coordinated by the endocyclic nitrogen atoms in solution. These empirical results gave rise to the occurrence of preferred ligand-metal pairs derived from the obtained complexes: presumably, **4** seems to suit gallium more properly, whereas **5** fits aluminium the most.

Moreover, the negative charge arising upon deprotonation seems to be delocalized about the whole ligand backbone as it is indicated by the observed N–C_{ipso} and C_{ipso}–C_{bridge} bond lengths. In this context, the carbanionic canonical formula can be neglected, because the linking carbon atoms show clear sp^2-hybridisation and no involvement in any metal coordination. Referring to the results of this section, it can be concluded that the newly prepared ligands on basis of the bisheterocyclo methanides can definitely compete with the popular β-diketiminate ligand. They offer promising opportunities for investigating and exploring a new bright research area, which will be discussed in the following sections in a more detailed fashion.

2.2 Bis-(4-methylbenzoxazol-2-yl)-methane derivatives

Major parts of this section were published in: David-Raphael Dauer, Melchior Flügge, Regine Herbst-Irmer, Dietmar Stalke, Group 13 metal complexes containing the bis-(4-methyl-benzoxazol-2-yl)-methanide ligand, *Dalton Trans.* **2016**, *45*, 6149–6158.[115]

The previously introduced bisheterocyclo methanide ligands,[95] presented in Chapter 2.1, proofed to be effective chelating ligands for Al(III) and Ga(III) as metal centres. These ligands have shown upon deprotonation of the methylene bridge, that the coordination of the metal cation is preferentially accomplished by the endocyclic nitrogen donor atoms in a chelating fashion.[83c, 83d, 86b] A characteristic feature of the derived complexes is, that there is no further steric bulkiness attached to the ligands to influence the chelation behaviour of these molecules. Therefore, bis-(4-methylbenzoxazol-2-yl)-methane **19** should be introduced in this chapter as a new ligand, bearing two methyl groups next to the nitrogen donors. Those additional residues should enhance the protection of the coordinated metal and achieve a kinetic stabilisation in contrast to the former bis-(benzoxazol-2-yl)-methane ligand **4**. The corresponding group 13 metal complexes were synthesized to get the best of two worlds: the increased stabilisation abilities for low-valent metal complexes and the reactivity of the incorporated group 13 metals.

The issue of steric shielding of metal centres within the group 13 complexes is an important aspect for the further applications and reactions, because these Al(III) containing species should be converted into the low-valent Al(I) compounds like e.g. [Al{(N(Dipp)C(Me))$_2$CH}].[34c] Because of the high electrophilicity of the Al(I) species, steric protection is essential to maintain the monomeric carbene-like structural motif and prevent dimerisation or nucleophilic attacks.[30a] The challenge to synthesize a low-valent species, containing a bisheterocyclo methanide ligand backbone, is still the guiding idea of ongoing research and **19** seems to be a promising ligand system for subsequent reduction steps (*vide infra*, see Chapter 2.2.5).

2.2.1 Ligand Syntheses

The synthesis of the uncharged parent ligand system **19** is achieved as reported earlier for the corresponding unsubstituted bis-(benzoxazol-2-yl)-methane **4** and bis-(benzothiazol-2-yl)-methane **5**.[95, 100] A cyclocondensation reaction of two equivalents of 2-amino-3-methylphenol and one equivalent of a suitable C_3-linker unit, derived from malonic acid, yields the ligand. Two different synthesis routes were performed and optimized to give a moderate overall yield of 56 % (see Scheme 2-12).

The first route resembles the synthesis of the unsubstituted bis-(benzoxazol-2-yl)-methane **4**, where a bisimidate linker was used for the coupling of the two phenol derivatives. This pathway, however, leads to a smaller yield of the desired product **19** and also promotes the formation of a specific intermediate **20**. The side product could be identified as 4-methylbenzoxazol-2-yl-carboxamide, which occurs, if just one equivalent of the

starting material has cyclized and the remaining imidate unit was hydrolysed in the course of further purification.

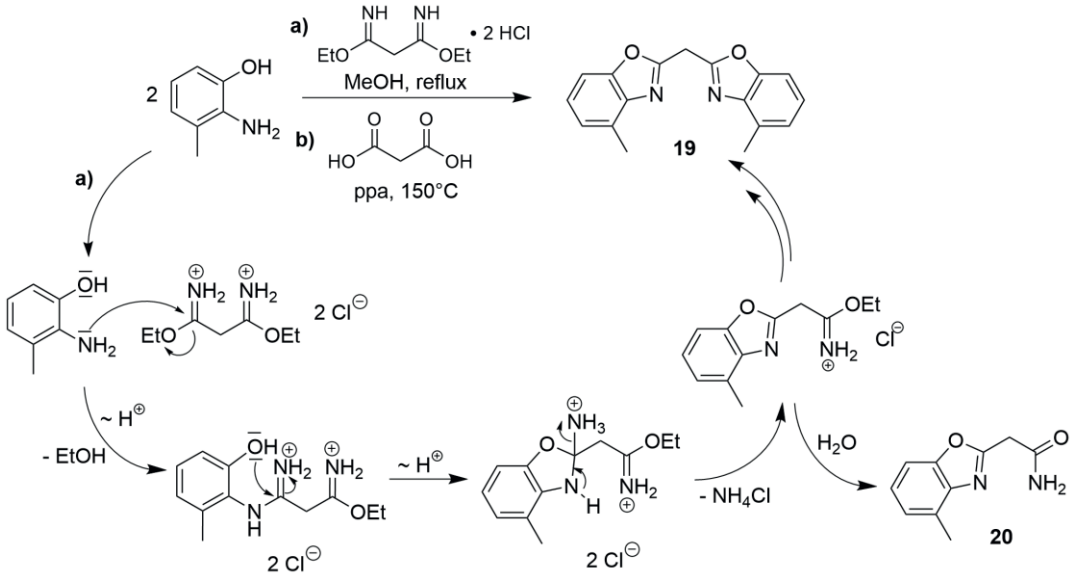

Scheme 2-12: Synthesis route and proposed formation mechanism of **19** and its side product **20**.

For improvement reasons, in the second synthesis route malonic acid was added to the phenolic starting material. In that case, polyphosphoric acid (ppa) was used as solvent and it additionally catalytically facilitates the cyclization reaction to give the parent ligand system **19**.

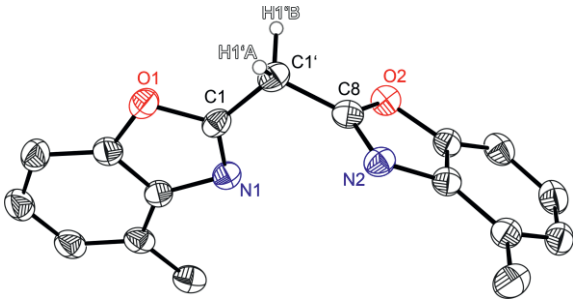

Table 2-17: Distances [pm] and angles [deg] of **19**.

C1'–C1	148.9(2)	N1–C1–C1'	128.23(13)
C1'–C8	148.4(2)	N2–C8–C1'	126.95(13)
C1–N1	128.96(19)	O1–C1–C1'	115.93(12)
C8–N2	129.24(18)	O2–C8–C1'	117.30(12)
C1–O1	137.40(17)	O1–C1–N1	115.82(12)
C8–O2	137.09(17)	O2–C8–N2	115.73(12)
		C1–C1'–C8	110.79(12)

Figure 2-18: Solid state structure of ligand **19**.

Compound **19** crystallizes in the triclinic space group $P\bar{1}$ and the asymmetric unit contains one molecule. Like the other symmetrically substituted bisheterocyclo methanes,[95] the central carbon atom C1' is also coordinated in a distorted tetrahedral fashion and the benzoxazole moieties are twisted nearly perpendicular (81.53(4) deg) relative to each other. Due to the higher steric demand of the heterocycles in **19**, the C1–C1'–C8 angle is widened to 110.8(1) deg, whereas all other angles around C1' are slightly compressed in

comparison to an ideal tetrahedral angle. Interestingly, in the solid state **19** forms a 3D-network of quite remarkable C–H···N hydrogen bonds: the two acidic hydrogen atoms of the methylene bridge are coordinated by imine nitrogen atoms of two adjacent molecules (see Figure 2-21). The experimentally determined values for intermolecular N···H interactions reveal two hydrogen bonds each, which are energetically favoured (H1'B···N2: 239 pm; C1'–H1'B···N2: 171.1 deg), and two further ones, which are less pronounced (H1'A···N1: 262 pm; C1'–H1'A···N1: 150.9 deg).

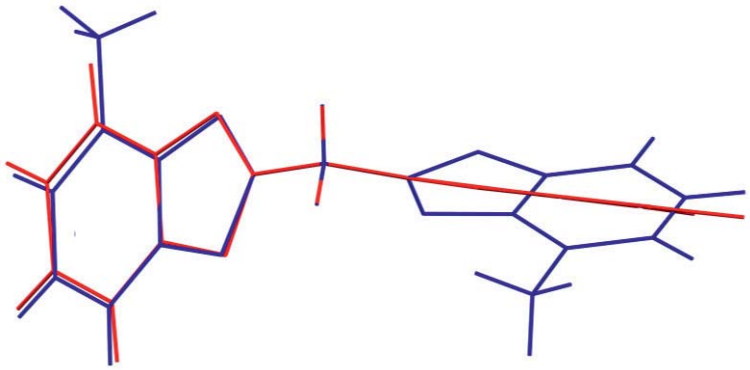

Figure 2-19: Overlay of the crystal structures for the unsubstituted ligand systems **4** (red) and its methylated derivative **19** (blue).

As depicted in Figure 2-19, the overlay of the observed crystal structures of the unsubstituted ligand **4** and the corresponding ligand **19** carrying two additional methyl groups at the annulated benzene perimeter shows, that there are visible differences in the observed alignment in the solid state. The experimentally determined torsion angle of the two imine nitrogen atoms N1 and N2 is in the case of the methylated derivative **19** increased by about 20 deg **(4**: 81.3(9) deg; **19**: 105.6(2) deg). This can be ascribed to the additional sterical hindrance of the methyl groups and is a result of the present hydrogen bonding.

To highlight these C–H···N hydrogen bonding properties, Figure 2-20 displays the calculated Hirshfeld surface for **19**. It is necessary to show the molecule's surface from the front (*left side*) and the rear view (*right side*) due to the tetrahedral bonding geometry of the central carbon atom C1', because both methylene protons are involved in hydrogen bonding. In the front view picture two intense red areas can be observed in close proximity to the imine nitrogen atom N2 and the methylene proton H1'B, which clearly displays the formation of the stronger, structure determining H1'B···N2 hydrogen bonds representing the closest intermolecular interactions. As opposed to this, also the less pronounced H1'A···N1 hydrogen bonds can be identified in Figure 2-20: because the H···A distance is about 20 pm longer than in the case of the first mentioned ones, the detected spots on the Hirshfeld surface are much less intense. In the top left picture, a pale red spot in vicinity to the other imine nitrogen donor N1 is detected. Furthermore, in the top right representation (rear view) the second pale red spot nearby the other acidic methylene proton H1'A can be observed as expected for those weak interactions. The additional fingerprint plot for this molecule (see Figure 2-20, *bottom*) confirms the formation of distinct

hydrogen bonds in the solid state shown as sharp signals observed for the N···H interactions. For a better comparability and evaluation of the present hydrogen bonding in **19**, the fingerprint plot of the unsubstituted derivative **4** is opposed at the bottom right picture of Figure 2-20. In that case, no sharp peaks appear and obviously, the C···H interactions contribute most.

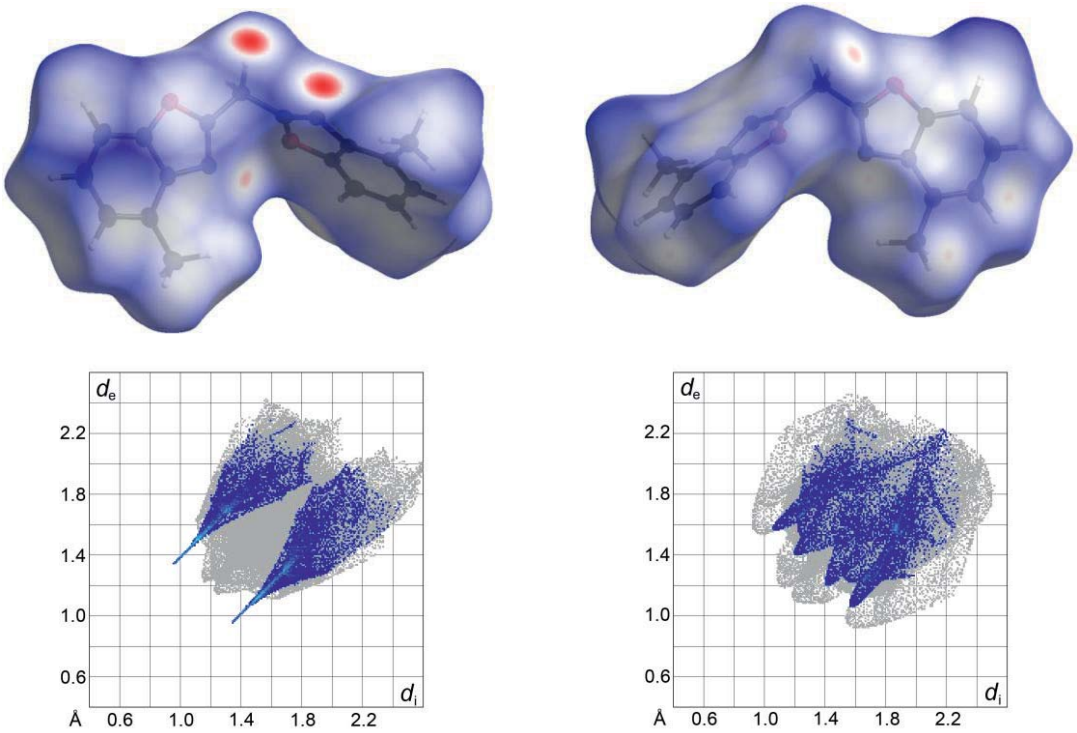

Figure 2-20: Hirshfeld surfaces from different points of view[106] (*top*) and corresponding fingerprint plot[105, 106a, 107] for N···H interactions generated for **19** (*bottom, left*) and **4** (*bottom, right*).

The crystal packing of the ligand system **19** reveals the 3D hydrogen bonding network in the solid state (see Figure 2-21), in which each molecule serves as a hydrogen donor twice and also twice as hydrogen acceptor. In this context, the differences in the strength of the different observed hydrogen bonds can be explained as follows: as previously mentioned, the H1'B···N2 distance (239 pm) is significantly shorter in comparison to the H1'A···N1 distance (262 pm). This fact is due to the formation of a dimeric aggregate regarding these C1'–H1'B···N2 interactions displayed in Figure 2-21, which is just possible because of the same orientation of H1'B and N2 in the solid state. Two neighbouring molecules are generating these reciprocal interactions leading to a more pronounced hydrogen bonding situation. The both other hydrogen bonds are less distinct, because H1'A and N1 are pointing into opposite directions. This arrangement forces the formation of hydrogen bonds between two different molecules, which are located above and beneath the considered central molecule.

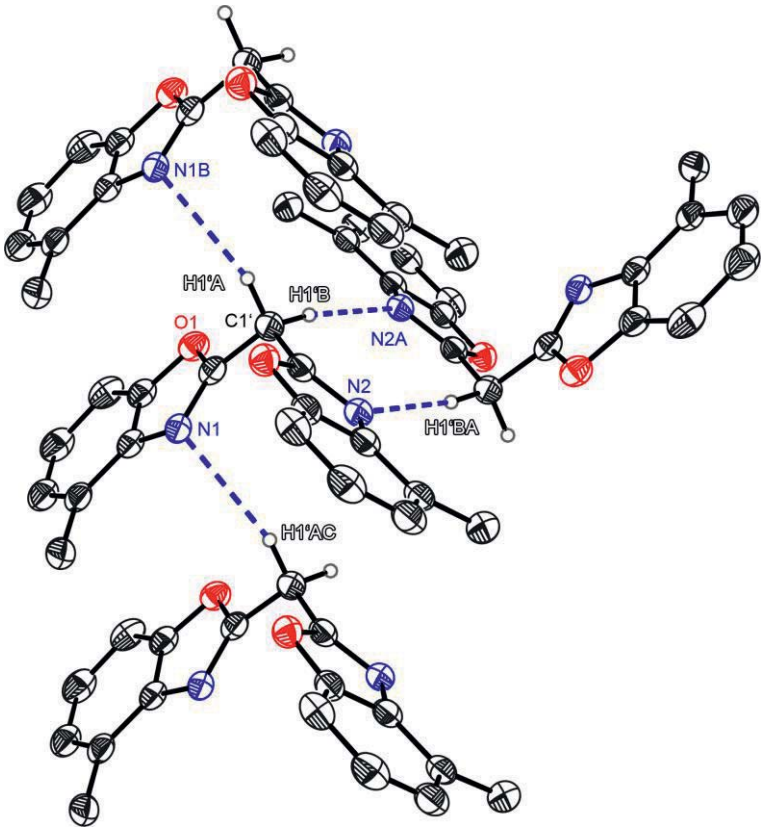

Figure 2-21: Hydrogen bonding pattern of **19**. (Symmetry transformations used to generate equivalent atoms: x−1, y, z for counterpart A, −x, −y+2, −z for counterpart B and x+1, y, z for counterpart C).

Based on NMR spectroscopic investigations on the crude reaction product of **19**, the not neglectable presence of a specific contamination was detected. After column chromatographic separation, the second fraction could be isolated in a yield of 8 % with respect to the starting material's equivalents and identified by NMR and SCXRD experiments as the carboxamide **20**, shown in Figure 2-22.

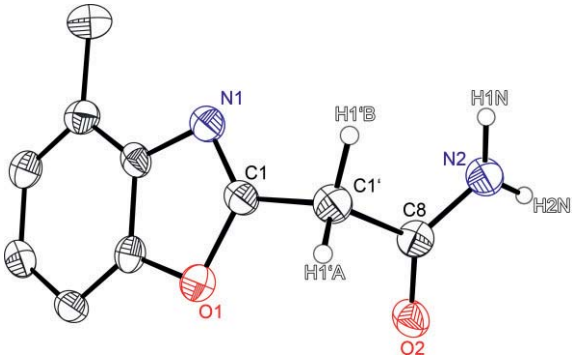

Figure 2-22: Solid state structure of side product **20**.

Table 2-18: Distances [pm] and angles [deg] of **20**.

C1'–C1	148.9(2)	N1–C1–C1'	128.23(13)
C1'–C8	148.4(2)	N2–C8–C1'	126.95(13)
C1–N1	128.96(19)	O1–C1–C1'	115.93(12)
C8–N2	129.24(18)	O2–C8–C1'	117.30(12)
C1–O1	137.40(17)	O1–C1–N1	115.82(12)
C8–O2	137.09(17)	O2–C8–N2	115.73(12)
		C1–C1'–C8	110.79(12)

The formation of such a species is explained in Scheme 2-12, where the proposed mechanism is shown in detail. In the first step of the synthesis for **19**, a nucleophilic attack of

the amine nitrogen atom of the 2-amino-3-methylphenol at one partially positively polarized imidate carbon atom of the C_3-linker takes place. After release of one equivalent ethanol, the phenol oxygen atom attacks at the same carbon atom again to form a NH_3^+ substituent as the leaving group. By elimination of one equivalent NH_4Cl, the cyclocondensation of the half target molecule is readily accomplished. The second remaining imidate moiety of the malonic acid linker can undergo in the further reaction process the same cyclocondensation reaction to give the aimed methyl substituted bis-(benzoxazol-2-yl)-methane ligand **19**.

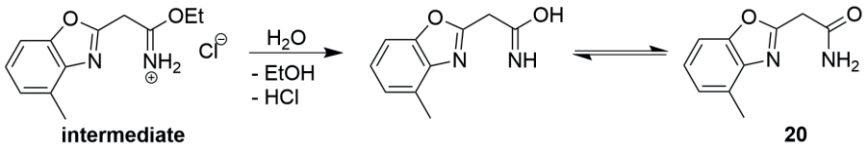

Scheme 2-13: Hydrolysis reaction of the intermediate species during the formation of **19**.

In this compound **20** the second cyclocondensation reaction for building up another benzoxazole moiety did not take place successfully, so that just one heterocycle is attached to the methylene bridge. The isolation of this species proves, that the reaction mechanism for the synthesis of the desired ligand **19** seems to follow a stepwise reaction pathway, in which initially only one benzoxazole is formed and then in a next step the second heterocycle is generated. If the reaction would proceed in a concerted manner, no intermediate species carrying one benzoxazole and one imidate function (see Scheme 2-13) would be observed as by-product. Indeed, this imidate species could not be isolated and characterized, because an aqueous workup was applied to the crude product (including the intermediate). This hydrolysis leads to the generation of an imidic acid species (Scheme 2-13, *middle*), which readily tautomerizes to the more stable primary amide **20**. This form was also found by applying X-ray diffraction studies (see Figure 2-22).

The benzoxazole-substituted carboxamide **20** crystallizes in the triclinic space group $P\bar{1}$ and the asymmetric unit consists of one molecule. As depicted in Figure 2-23, the side product **20** forms interesting hydrogen bonded networks in the solid state. In this case the NH_2-moiety twice acts as hydrogen donor and the amide oxygen as well as the endocyclic imine nitrogen atoms are hydrogen acceptors. It is worth noting, that the oxygen atom of the benzoxazole moiety is not involved in any hydrogen bonding due to the less pronounced Lewis basicity compared to the opposing nitrogen atoms.

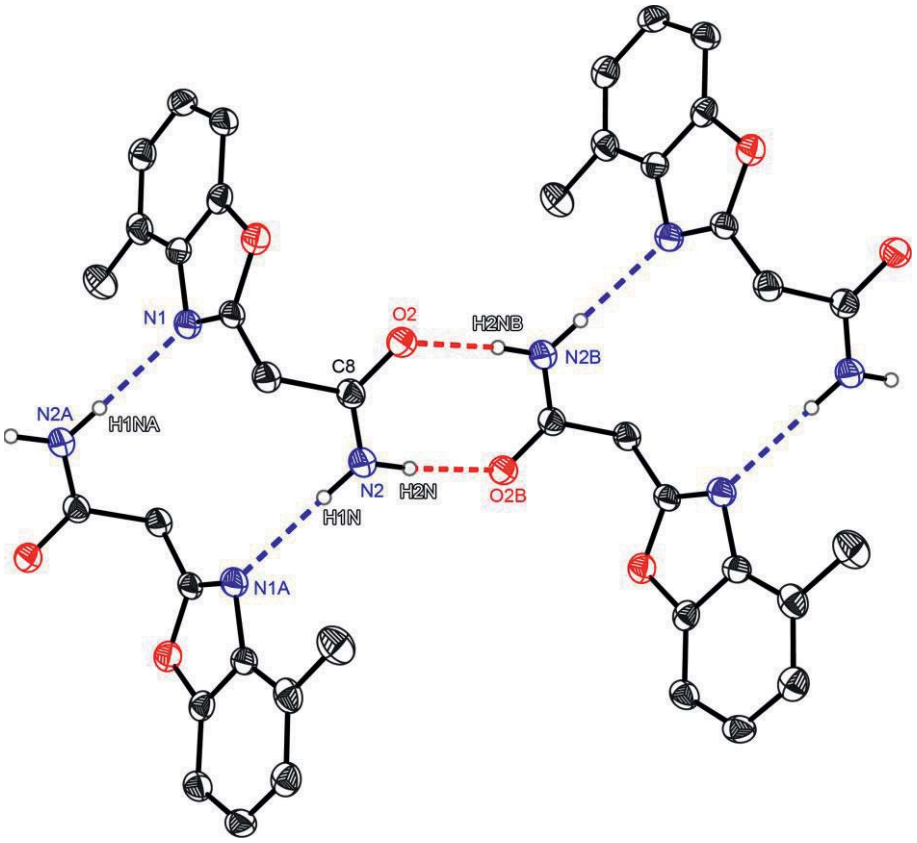

Figure 2-23: Hydrogen bonding pattern of **20**. (Symmetry transformations used to generate equivalent atoms: −x+1, −y+1, −z for counterpart A and −x+2, −y+1, −z+1 for counterpart B).

A closer look at the hydrogen bonding pattern in the crystal packing section (see Figure 2-23) shows, that the amide functionalities $RC(O)NH_2$ are forming a dimeric hydrogen bonded species, which is arranged in an eight-membered ring including the two hydrogen atoms similar to the case observed in **19** (see Figure 2-21). The hydrogen bonds for this dimer, which is also a well-known structural motif for carboxylic acids, result in following characteristic values: 199(3) pm for the H2N···O2B distance and a N2–H2N···O2B angle of 173(2) deg. Due to the short bond length and the beneficial angle, which is close to linearity, these hydrogen bonding interactions contribute significantly to the molecule's arrangement in the solid state. A two-dimensional network is accomplished by the other hydrogen bonds, which are formed on the backside of the ligand. At that side, the second hydrogen atom H1N of the NH_2 fragment generates reciprocal hydrogen bonds with the imine nitrogen atom N1 of another neighbouring molecule (H1N···N1A distance: 215(3) pm; N2–H1N···N1A angle: 177(2) deg). In the solid state, each molecule forms two hydrogen bonds (in a dimeric fashion) towards two adjacent molecules resulting in a nearly planar network.

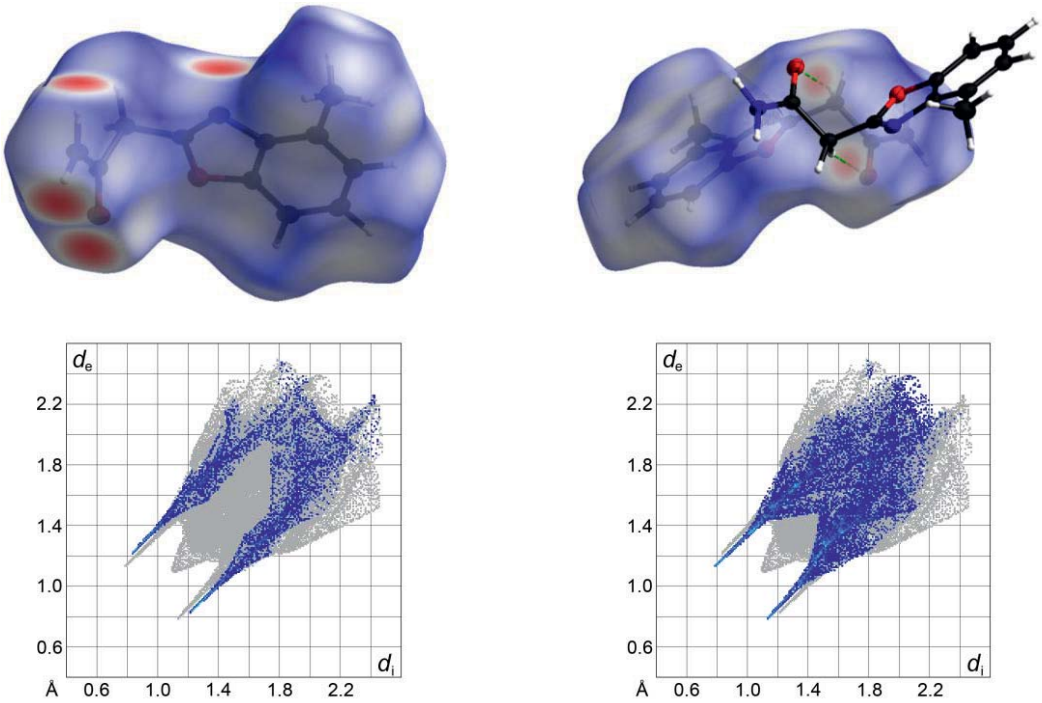

Figure 2-24: Hirshfeld surfaces[106] (*top*) and corresponding fingerprint plots[105, 106a, 107] for N···H (*bottom left*) and O···H interactions (*bottom right*) generated for **20**.

The hydrogen bonding properties are visualized in the derived Hirshfeld surfaces for compound **20** (see Figure 2-24). The top left picture clearly shows defined regions for the closest intermolecular interactions, concerning the amide functionality and the endocyclic imine nitrogen atom. The resulting fingerprint plot for this species looks quite different in comparison to the earlier described ones (see Figure 2-24, *bottom*): again sharp and well-defined peaks for the closest intermolecular interactions can be identified, but in this special case four peaks were found instead of just two. Those different kind of signals can be explained by the presence of two different heteroatoms, which are involved in hydrogen bonding (O and N). Using a filter to limit the observed interactions to just N···H (*bottom left*) or O···H interactions (*bottom right*), the particular different contributions can be clearly highlighted. At the top right picture can be seen, that the Hirshfeld surface at the rear side also shows two red spots, which are less pronounced compared to the other ones at the front perspective (Figure 2-24, *top left*). These areas display the hydrogen bonding abilities of the protons of the acidic methylene bridge towards the amide oxygen atom. Because these C–H···O interactions are less attractive, the determined bond values give elongated bond lengths (H1'A···O2: 243(3) pm) and a disadvantageous observed angle (C1'–H1'A···O2: 159(2) deg) compared to the described N–H···O or N–H···N interactions.

2.2.2 Syntheses of the Group 13 Metal Complexes

The reaction of **19**, dissolved in toluene, with the trimethyls of aluminium, gallium or indium lead to the formation of the monoanionic methanides containing the corresponding MMe_2 fragment (see Scheme 2-14). By addition of these organometallic reagents, the acidic methylene bridge gets deprotonated under evolution of gaseous methane and in a concerted manner the remaining dimethyl group 13 metal cation gets chelated by the two endocyclic nitrogen donor atoms. Among the nacnac derivatives and the bisheterocyclo methanides, the efficient metal shielding is almost comparable. In the case of the complexes derived from **19**, the methyl groups exert a shielding function as well, but due to less steric congestion, the metal centres are slightly more accessible to allow some specific substitution reactions. The new metal complexes containing a central six-membered metalla heterocycle are reminiscent of the analogue metal complexes bearing the omnipresent nacnac ligand.

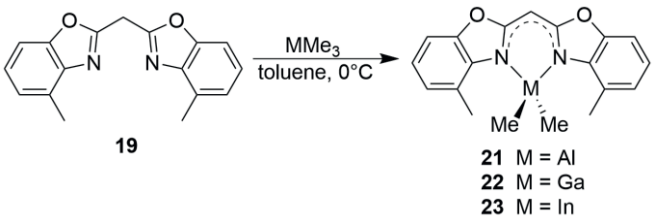

Scheme 2-14: Synthesis route for the dimethyl substituted group 13 metal complexes **21** – **23**.

Upon deprotonation, the C_{ipso}–C_{bridge} bond lengths found in the complexes **21** – **23** are shortened in comparison to **19** and the C_{ipso}–N distances are slightly elongated (see Table 2-19). This is caused by two facts, which are important for the structural features. On the one hand, the deprotonation of the central methylene moiety generates a free electron pair. Because of the adjacent conjugated π-systems of the two benzoxazole units, this free electron pair tends to be delocalized over the whole ligand framework resulting in different feasible resonance structures: carbanionic, amidic or completely delocalized. On the other hand, the hybridisation of the central carbon atom changes from sp^3 in the starting material **19** to sp^2 in the metallated species **21**, **22** and **23** based on the trigonal planar coordination geometry of C1'.

2.2.3 Structural Comparison of 21, 22 and 23

A closer look at the experimentally determined arrangement of the parent ligand **19** shows that the C_{ipso}–C_{bridge} distance is slightly shorter than it is to be expected for a typical C(sp^2)–C(sp^3) single bond (151 pm). This deviation can be explained by the presence of the four electronegative adjacent heteroatoms, which cause the C_{ipso}–C_{bridge} bonds to decrease due to their electron withdrawing ability.

In comparison to compounds **21**, **22** and **23**, the observed C_{ipso}–C_{bridge} distances (138.4 pm to 139.0 pm) are half way between a typical C(sp^2)–C(sp^2) single bond (147 pm) and a C(sp^2)=C(sp^2) double bond (134 pm), which is a result of the efficient delocalisation of the double bonds and the free electron pair. The same explanation is valid for the C_{ipso}–N bond lengths, which are in a narrow range from 133.7 pm to 135.1 pm. These values for the C_{ipso}–N bond lengths can also be seen as the average of a typical C(sp^2)–N(sp^2) single bond (140 pm) and a C(sp^2)=N(sp^2) double bond (129 pm).[108] In the light of previous results for the methanides $[Me_2Al\{(NCOC_6H_4)_2CH\}]$ and $[Me_2Al\{(NCSC_6H_4)_2CH\}]$[95] and the amide bridged species $[Me_2Al\{(NCSC_6H_4)_2N\}]$ and $[Me_2Al\{(4\text{-}MeNCSC_6H_3)_2N\}]$[116] (*vide infra* in Chapter 2.5), the discussed structural values are matching well (see Table 2-19).

Table 2-19: Selected averaged bond lengths (pm) and angles (deg) of the ligand backbone for compounds **19**, **21**, **22** and **23** in comparison to related species.

compound	C_{ipso}–C1'	C_{ipso}–N	C1–C1'–C8
$(4\text{-}MeNCOC_6H_3)_2CH_2$ (**19**)	148.7(2)	129.1(2)	110.79(12)
$[Me_2Al\{(4\text{-}MeNCOC_6H_3)_2CH\}]$ (**21**)	138.4(2)	135.1(2)	121.13(14)
$[Me_2Ga\{(4\text{-}MeNCOC_6H_3)_2CH\}]$ (**22**)	138.8(3)	134.1(2)	121.62(18)
$[Me_2In\{(4\text{-}MeNCOC_6H_3)_2CH\}]$ (**23**)	139.0(13)	133.7(12)	123.6(6)
$[Me_2Al\{(NCOC_6H_4)_2CH\}]$ (**8**)	138.0(3)	134.6(3)	119.5(2)
$[Me_2Al\{(NCSC_6H_4)_2CH\}]$ (**9**)	139.0(2)	135.2(2)	123.54(14)
$[Me_2Al\{(NCSC_6H_4)_2N\}]$ (**44**)	–*	133.1(3)	–*
$[Me_2Al\{(4\text{-}MeNCSC_6H_3)_2N\}]$ (**45**)	–*	134.3(2)	–*

* no values given due to insufficient comparability (nitrogen as bridging moiety).

Compounds **21** (see Figure 2-25) and **22** (see Figure 2-27) are isomorphous, each crystallize in the monoclinic space group $P2_1/c$ and the asymmetric unit contains one molecule. **23** (see Figure 2-28) crystallizes in the monoclinic space group *Pn* and contains two metallated molecules in the asymmetric unit.

The structural comparison of the MMe_2 derivatives shows that in each case the metal coordination is accomplished by the two nitrogen atoms of the benzoxazole moieties and the oxygen atoms are pointing away from the metal. This leads in all three cases to a distorted tetrahedral coordination geometry at the particular metal ion. As expected, the ligand framework in **21**, **22** and **23** exhibits nearly no folding of the heterocyclic residues. Additionally, the metal ion is placed within the C_3N_2 plane of the central six-membered metalla heterocycle without any significant deviation (see Table 2-20). Solely, this arrangement facilitates total conjugation of the whole anionic ligand. Due to the fourfold coordination of the metal ion, the methyl residues at that metal centre are aligned perpendicularly with respect to the N1–M–N2 plane. This V-shaped arrangement of the MMe_2 fragments allows the organometallic fragment to slot in between the methyl groups of the

ligand. The four methyl groups embrace the group 13 metal, which thus stays in plane (see Figure 2-26).

Table 2-20: Selected folding parameters for compounds **19**, **21**, **22**, **23**, **24**, **25** and **26**.

compound	folding angle [deg]	M···plane dist. [pm]
$(4\text{-MeNCOC}_6H_3)_2CH_2$ (**19**)	–	–
$[Me_2Al\{(4\text{-MeNCOC}_6H_3)_2CH\}]$ (**21**)	3.721(20)	0.54(22)
$[Me_2Ga\{(4\text{-MeNCOC}_6H_3)_2CH\}]$ (**22**)	3.803(20)	0.68(23)
$[Me_2In\{(4\text{-MeNCOC}_6H_3)_2CH\}]$ (**23**)	4.925(122)* 6.225(263)	5.72(287)* 15.45(269)
$[ClMeAl\{(4\text{-MeNCOC}_6H_3)_2CH\}]$ (**24**)	3.394(20)	0.90(19)
$[IMeAl\{(4\text{-MeNCOC}_6H_3)_2CH\}]$ (**25**)	3.042(16)	2.26(37)
$[IEtAl\{(4\text{-MeNCOC}_6H_3)_2CH\}]$ (**26**)	4.425(71)	4.83(20)

* two values are given due to the discrepancy of the two molecules within the unit cell.

In the row of the investigated group 13 metal complexes **21** – **23** of the bis-(4-methylbenzoxazol-2-yl)-methanide ligand, some clear trends obtained from structural data could be deduced (see Table 2-22):

- The transannular N1···N2 distance, which is indicative for the size of the chelated metal atom, increases in the series of **21** < **22** < **23** as expected. This is caused by the increasing covalent radii of the coordinated metal cations, which force the N1···N2 distance of the chelating ligand to be widened.
- Accordingly, also the observed N–M distances are increasing correlated to the increasing ionic radii of the group 13 ions Al^{3+}, Ga^{3+} or In^{3+}, respectively.
- As a further consequence of this bond elongation and due to the fact, that the metal stays in the ligand plane, the resulting N1–M–N2 bite angles are decreasing in the row of **21** > **22** > **23**.

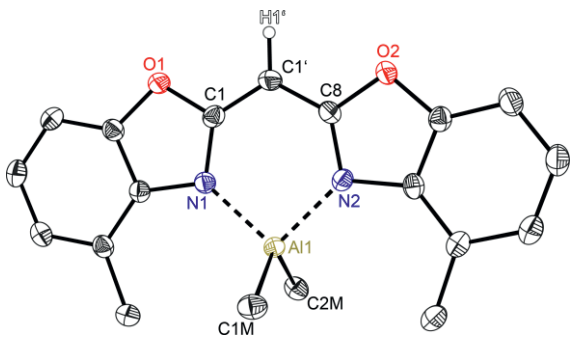

Figure 2-25: Solid state structure of complex **21**.

Table 2-21: Distances [pm] and angles [deg] of **21**.

C1'–C1	138.3(2)	N1–C1–C1'	128.88(15)
C1'–C8	138.4(2)	N2–C8–C1'	128.91(14)
C1–N1	135.0(2)	O1–C1–C1'	118.67(14)
C8–N2	135.1(2)	O2–C8–C1'	118.50(13)
C1–O1	135.78(19)	O1–C1–N1	112.45(14)
C8–O2	136.24(19)	O2–C8–N2	112.59(13)
N1–Al1	194.05(14)	C1–C1'–C8	121.13(14)
N2–Al1	193.95(14)	N1–Al1–N2	94.68(6)
Al1–C1M	196.01(19)	C1M–Al1–C2M	119.26(7)
Al1–C2M	197.0(2)		

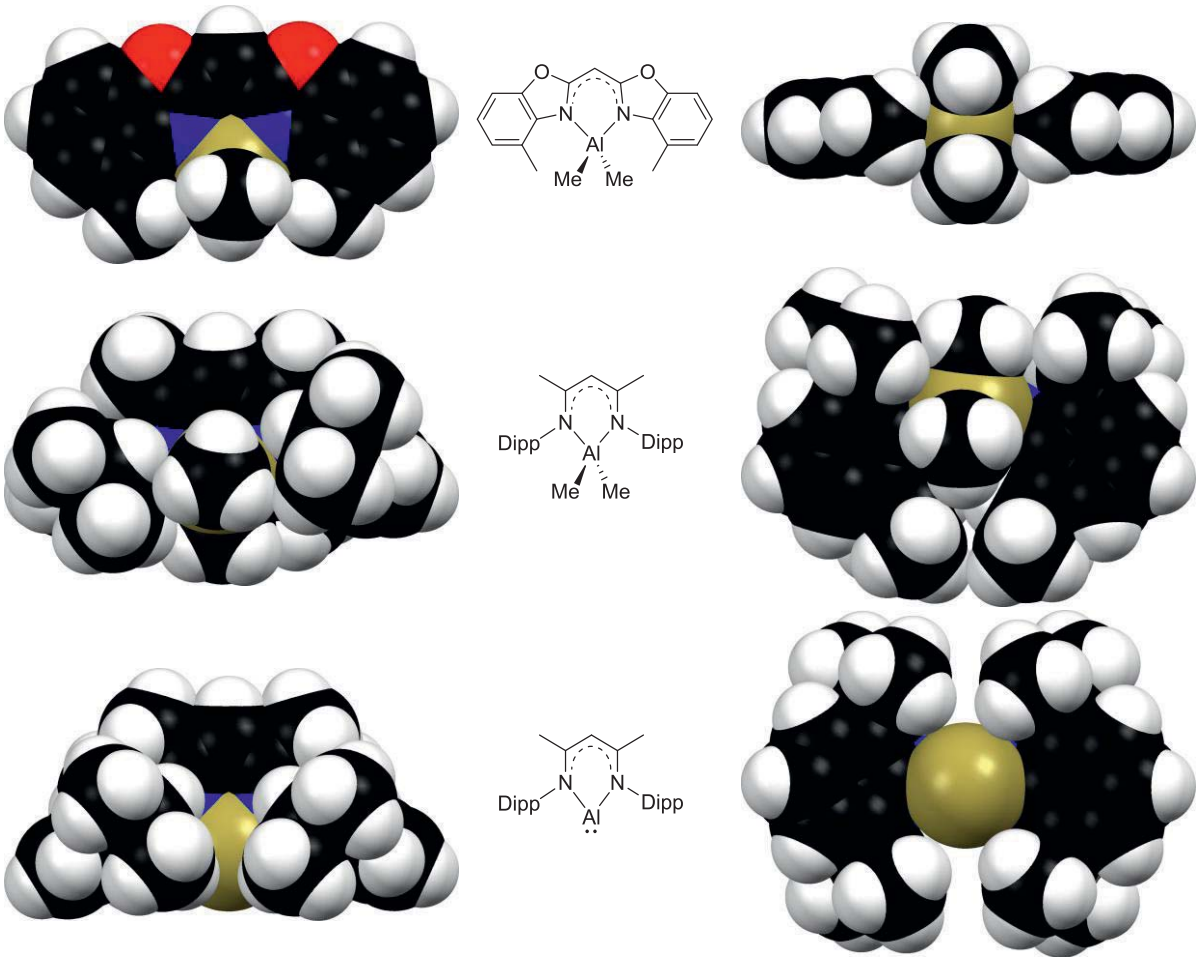

Figure 2-26: Space filling models from different perspectives (*left column*: front view; *right column*: bottom view) of the compared aluminium complexes **21** (*top*), $[Me_2Al\{(N(Dipp)C(Me))_2CH\}]$[14l] (**A**) (*middle*) and $[Al\{(N(Dipp)C(Me))_2CH\}]$[34c] (**B**) (*bottom*).

In Figure 2-26 compound **21** is compared to the literature known nacnac derivatives $[Me_2Al\{(N(Dipp)C(Me))_2CH\}]$[14l] (**A**) and $[Al\{(N(Dipp)C(Me))_2CH\}]$[34c] (**B**), which contain the Al(III)Me_2 or Al(I) moiety, respectively. From the space filling model the steric demand of each ligand can be visualized and provides a fair estimation of the shielding abilities around the metal atom.

Starting with the crystal structure of the Al(I) species **B**, it is evident that the metal atom is located almost ideally within the chelating C_3N_2 plane (see Figure 2-26, *bottom*). The *N*,*N*'-coordinated metal atom fits well into the pocket, made up from the four *i*Pr groups of the Dipp substituents and the carbon atoms in *ortho*-position of the associated phenyl rings. Furthermore, these phenyl rings are nearly perpendicularly aligned with respect to the C_3N_2 plane (89 deg and 91 deg). The *ortho*-carbon atoms provide the closest contact to the aluminium atom (averaged 360.6 pm) and presumably are equally important for the shielding of the low-valent Al(I) species (listed in column C15/16···M in Table 2-22). These distances are classified between the nacnac species and the complexes derived from **19**. The bottom view also reveals that the aluminium atom is not entirely embraced, so that the Lewis acidic metal centre is presumably accessible for further coordination.

The side view highlights the good shielding abilities of the *i*Pr groups, preventing the molecules from aggregation.

Table 2-22: Selected bond lengths (pm) and angles (deg) for compounds **19** and **21** – **26**.

compound	N1···N2	N1/2–M	C15/16···M	N1–M–N2
$(4\text{-MeNCOC}_6\text{H}_3)_2\text{CH}_2$ (**19**)	354.48(18)	–	–	–
$[\text{Me}_2\text{Al}\{(4\text{-MeNCOC}_6\text{H}_3)_2\text{CH}\}]$ (**21**)	285.34(19)	194.00(14)	344.78(19)	94.68(6)
$[\text{Me}_2\text{Ga}\{(4\text{-MeNCOC}_6\text{H}_3)_2\text{CH}\}]$ (**22**)	290.10(23)	200.43(15)	344.74(22)	92.73(6)
$[\text{Me}_2\text{In}\{(4\text{-MeNCOC}_6\text{H}_3)_2\text{CH}\}]$ (**23**)	304.85(55)	221.7(9)	348.05(167)	86.89(14)
$[\text{ClMeAl}\{(4\text{-MeNCOC}_6\text{H}_3)_2\text{CH}\}]$ (**24**)	285.00(20)	190.97(14)	347.36(19)	96.52(6)
$[\text{IMeAl}\{(4\text{-MeNCOC}_6\text{H}_3)_2\text{CH}\}]$ (**25**)	287.75(37)	190.9(2)	353.80(25)	97.84(12)
$[\text{IEtAl}\{(4\text{-MeNCOC}_6\text{H}_3)_2\text{CH}\}]$ (**26**)	287.53(21)	191.40(16)	353.41(22)	97.38(7)
$[\text{Me}_2\text{Al}\{(\text{N(Dipp)C(Me)})_2\text{CH}\}]$ (**A**)	287.0(4)	192.9(2)	378.9(3)	96.18(9)
$[\text{Al}\{(\text{N(Dipp)C(Me)})_2\text{CH}\}]$ (**B**)	276.4(3)	195.8(2)	360.6(3)	89.86(8)

The crystal structure of the dimethyl aluminium species **A** clearly deviates from the reduced species **B**. The central six-membered metalla heterocycle is less planar compared to **B**, which finds expression in the fact, that the $AlMe_2$ unit is located out of the chelating C_3N_2 plane. Furthermore, one of the two phenyl rings of the Dipp-substituents is considerably twisted away from orthogonality with respect to the C_3N_2 plane (112 deg). This deviation is caused by the additional methyl groups coordinated to the aluminium cation, which increases the steric demand compared to **B**, where no substituents are present at the Al(I) centre. The pocket formed in **A** is not appropriate in size to accommodate the additional methyl groups. As a result of the coordination, one of the Dipp-substituents is pushed away instead of retaining the perpendicular alignment.

As mentioned earlier, the methyl substituents at the C_6-moiety of the chelating ligand in **21** mimic the shielding role of the Dipp residues of the comparable nacnac complexes. These efficient shielding abilities are visualized in the space filling model at the bottom view of **21** in Figure 2-26: by chelation of the two nitrogen donor atoms of the ligand the $AlMe_2$ fragment is aligned in the C_3N_2 plane without any significant deviation. This planarity is also supported by the ligand's methyl groups, which fit nearly perfectly in between the pocket made up by the V-shaped coordinated $AlMe_2$ cation. So, in comparison to **A** and **B**, the kinetic shielding considered from the bottom view is even more pronounced. As opposed to this, the side view of **21** shows that the planar arrangement of the complex leads to less steric congestion from this point of view. The shielding abilities in **21** are not as pronounced as in the case of **A** and **B**, so that still beneficial, specific substitution reactions at the metal centre can take place. This advantageous property is exploited by the synthesis of **25**, described in the following paragraph.

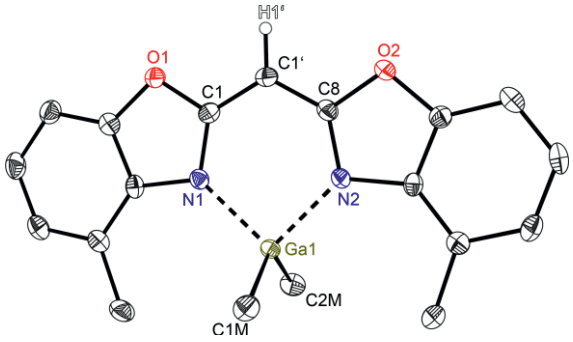

Figure 2-27: Solid state structure of complex **22**.

Table 2-23: Distances [pm] and angles [deg] of **22**.

C1'–C1	138.7(3)	N1–C1–C1'	129.28(17)
C1'–C8	138.9(3)	N2–C8–C1'	129.58(18)
C1–N1	134.0(2)	O1–C1–C1'	118.17(17)
C8–N2	134.2(2)	O2–C8–C1'	117.83(16)
C1–O1	136.0(2)	O1–C1–N1	112.55(16)
C8–O2	136.1(2)	O2–C8–N2	112.58(16)
N1–Ga1	200.55(15)	C1–C1'–C8	121.62(18)
N2–Ga1	200.30(15)	N1–Ga1–N2	92.73(6)
Ga1–C1M	196.6(2)	C1M–Ga1–C2M	123.95(9)
Ga1–C2M	196.3(2)		

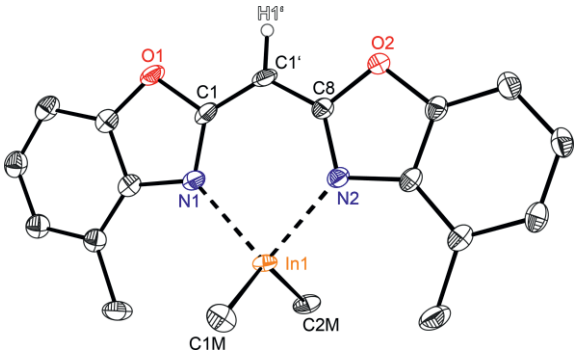

Figure 2-28: Solid state structure of complex **23**.

Table 2-24: Distances [pm] and angles [deg] of **23**.

C1'–C1	137.5(13) 137.0(13)	N1–C1–C1'	131.0(9) 129.4(10)
C1'–C8	139.6(12) 141.7(13)	N2–C8–C1'	130.5(10) 131.5(10)
C1–N1	133.8(11) 133.7(12)	O1–C1–C1'	116.8(10) 117.2(10)
C8–N2	133.8(11) 133.3(12)	O2–C8–C1'	117.1(10) 116.9(10)
C1–O1	138.6(12) 136.0(12)	O1–C1–N1	112.0(9) 113.4(10)
C8–O2	136.7(12) 139.2(12)	O2–C8–N2	112.2(9) 111.5(9)
N1–In1	221.1(9) 221.5(9)	C1–C1'–C8	123.3(5) 123.8(6)
N2–In1	221.5(9) 222.5(9)	N1–In1–N2	86.77(13) 87.01(14)
In1–C1M	215.4(10) 214.7(9)	C1M–In1–C2M	130.10(19) 126.85(18)
In1–C2M	215.2(10) 216.1(11)		

Due to the presence of two molecules in the asymmetric unit, for each parameter two values are given.

2.2.4 Structural Comparison of 24 – 26

In addition to the dimethyl substituted group 13 metal complexes three Al(III) derivatives **24** – **26**, in which one of the methyl groups is replaced by a halide, were successfully synthesized. This substitution is necessary to improve the reactivity of those species compared to the quite stable dimethyl aluminium complexes. These reaction products should facilitate the access to low-valent Al(I) or Al(II) species upon reductive dehalogenation reactions.

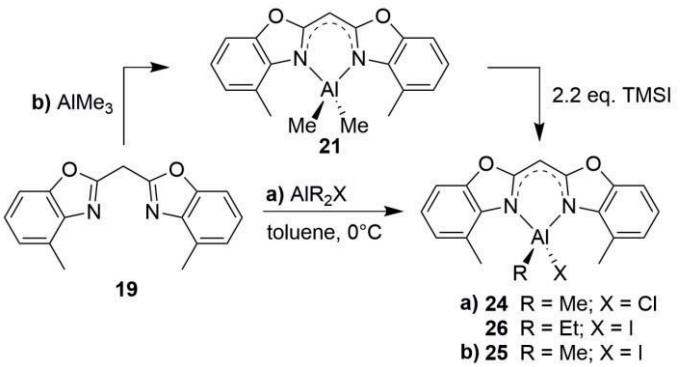

Scheme 2-15: Synthesis route for the mono halide substituted aluminium complexes **24** – **26**.

The synthesis of compounds **24** and **26** parallels the procedures to the abovementioned dimethyl derivatives. To a solution of the parent ligand **19**, dissolved in toluene, the organometallic reagent $AlMe_2Cl$ or $AlEt_2I$ was added in a slight excess at 0 °C (see Scheme 2-15, pathway **a**), respectively. This method was not applied for **25**. Instead of this, **25** was prepared starting from the metallated species **21** by reaction with an excess of trimethylsilyl iodide to prompt a methyl to iodide exchange at the metal atom (see Scheme 2-15, pathway **b**).

Having a closer look at the geometrical data of those halide substituted species **24** – **26**, following conclusions can be made: the derivatives **24** (see Figure 2-29) and **26** (see Figure 2-31) crystallize in the monoclinic space group $P2_1/c$ each and the asymmetric unit consists in both cases of one target molecule. Compound **25** (see Figure 2-30) crystallizes in the orthorhombic space group *Pbcm* and the asymmetric unit contains half a molecule.

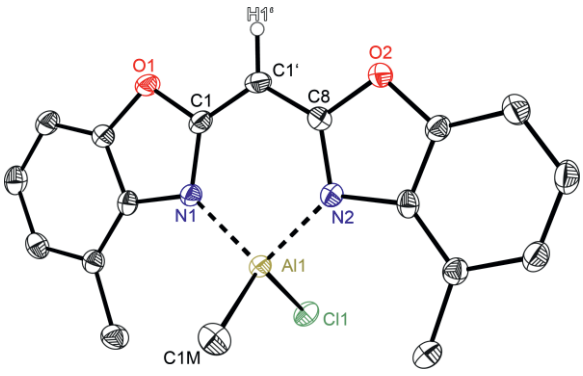

Figure 2-29: Solid state structure of complex **24**.

Table 2-25: Distances [pm] and angles [deg] of **24**.

C1'–C1	137.9(2)	N1–C1–C1'	128.86(15)
C1'–C8	138.0(2)	N2–C8–C1'	128.65(15)
C1–N1	134.9(2)	O1–C1–C1'	118.73(15)
C8–N2	135.0(2)	O2–C8–C1'	118.98(15)
C1–O1	135.60(19)	O1–C1–N1	112.40(14)
C8–O2	135.48(19)	O2–C8–N2	112.37(14)
N1–Al1	191.07(14)	C1–C1'–C8	121.39(16)
N2–Al1	190.86(14)	N1–Al1–N2	96.52(6)
Al1–C1M	198.4(11)	C1M–Al1–Cl1	116.2(5)
Al1–Cl1	209.2(4)		

In the halogenated complexes, the aluminium atom also adopts a distorted tetrahedral coordination by means of the two nitrogen donors and the remaining substituents at the metal atom. In direct comparison to the $AlMe_2$ derivative **21**, the N–Al distances in **24** – **26** are decreased and consequentially the corresponding N–Al–N bite angle is widened (see Table 2-22). Those observed changes are caused by the electron withdrawing halide

ligands Cl or I. These substituents increase the partial positive charge at the metal atom due to the negative inductive effect and their enhanced electronegativity compared to a carbon substituent. Hence, the substituted aluminium atom demands more electron density from the donating nitrogen ring atoms and the interactions towards the nitrogen Lewis donors are more attractive.

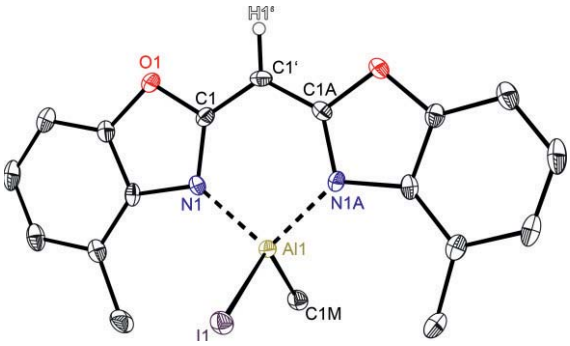

Figure 2-30: Solid state structure of complex **25**.

Table 2-26: Distances [pm] and angles [deg] of **25**.

C1'–C1	138.4(3)	N1–C1–C1'	129.2(2)
C1–N1	134.8(3)	O1–C1–C1'	118.2(2)
C1–O1	136.1(3)	O1–C1–N1	112.58(19)
N1–Al1	190.9(2)	C1–C1'–C1A	121.4(3)
Al1–C1M	191.2(4)	N1–Al1–N1A	97.84(12)
Al1–I1	254.58(11)	C1M–Al1–I1	116.63(14)

Symmetry transformations used to generate equivalent atoms: x, y, −z+1/2

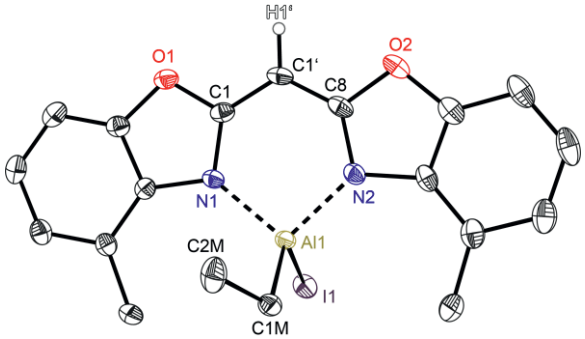

Figure 2-31: Solid state structure of complex **26**.

Table 2-27: Distances [pm] and angles [deg] of **26**.

C1'–C1	138.1(2)	N1–C1–C1'	129.08(16)
C1'–C8	138.0(3)	N2–C8–C1'	129.16(15)
C1–N1	135.2(2)	O1–C1–C1'	118.60(15)
C8–N2	135.0(2)	O2–C8–C1'	118.07(15)
C1–O1	135.5(2)	O1–C1–N1	112.30(14)
C8–O2	135.7(2)	O2–C8–N2	112.77(15)
N1–Al1	191.15(16)	C1–C1'–C8	121.56(15)
N2–Al1	191.64(15)	N1–Al1–N2	97.38(7)
Al1–C1M	194.0(2)	C1M–Al1–I1	118.28(7)
Al1–I1	256.74(8)		

The influence of the present halide atom on specific binding properties is displayed in Table 2-22. **24** shows, compared to **25**, that the bigger halide iodide causes the transannular N1···N2 distance to increase by about 3.0 pm (285.0 pm in **24** vs. 287.7 pm in **25**). This widening of the coordination pocket is also displayed in the bite angle, which also is enlarged from 96.52 deg to 97.84 deg. Predominantly, the higher steric demand of the iodide compared to the chloride accounts for the structural changes in the ligand. The observed differences among the two iodide derivatives **25** and **26** concerning those values are negligible. Within the triple estimated standard deviations, the values for both species are the same, indicating that the slightly enhanced steric demand in **26**, due to the ethyl group instead of a methyl group, has no significant effect on those structural features. Furthermore, it should be mentioned at this point, that in all mono halogenated species positional disorder of the substituents at the metal centre occurs as previously stated in Chapter 2.1.2 for the AlMeCl derivatives.

2.2.5 Reduction Attempts

Based on the results of Chapter 2.2, ligand system **19** seems to be most promising for the generation of a low-valent Al(I) species analogue to that one known for the omnipresent nacnac ligand.[28, 34c] After this intense evaluation, the next steps for the synthesis of a corresponding metallylene compound based on ligand system **19** should follow up. For the synthesis of a Al(I) compound, it is necessary to have an intermediate halogenated AlI_2 containing species in hand, which can be reduced afterwards to obtain the desired metallylene by reductive salt elimination as depicted in Scheme 2-16.

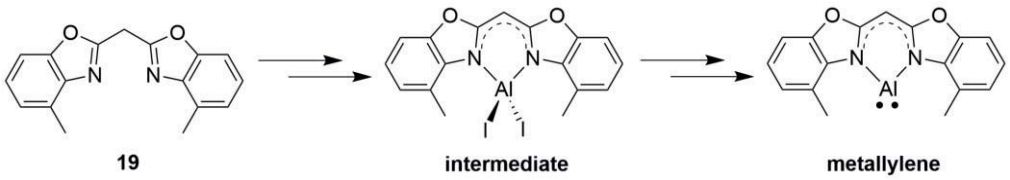

Scheme 2-16: Proposed reaction scheme for the generation of a metallylene species based on **19**.

The following Scheme 2-17 visualizes the three performed attempts to create the AlI_2 containing metal complex, because the synthesis of this desired intermediate can be accomplished on different ways.

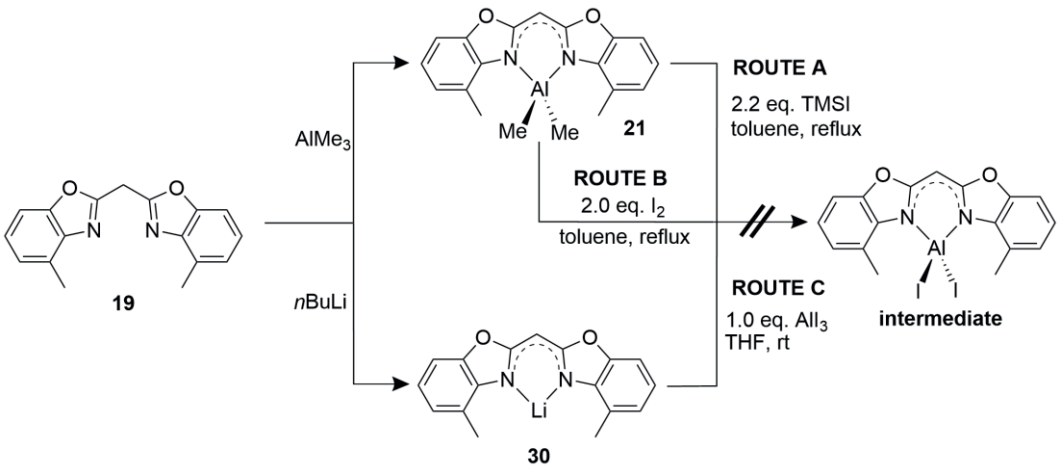

Scheme 2-17: Failed synthesis attempts of intermediate $[I_2Al\{(4\text{-}MeNCOC_6H_3)_2CH\}]$.

The upper route starts with the parent ligand **19**, which is treated with a slight excess of $AlMe_3$ to generate the $AlMe_2$ complex **21** like reported in Chapter 2.2.2. The next step is to replace the two methyl groups at the Al(III) fragment and to introduce subsequently two iodo substituents at the aluminium cation, whereby two different routes should be suitable. By applying route **A**, the already mentioned mono halogenated species **25** could be yielded, because even the usage of an excess of trimethylsilyl iodide results exclusively in the substitution of one methyl group against one iodide at the aluminium centre

(see in Scheme 2-18). Therefore, it can be supposed, that the driving force of the formation of tetramethyl silane is not sufficient to overcome the barrier for substituting the aluminium fragment a second time.

In analogy to the synthesis of $[I_2Al\{(N(Dipp)C(Me))_2CH\}]$,[28, 34c] route **B** in the middle of Scheme 2-17 was tried by adding elemental iodine to the dimethyl aluminium compound **21**, which was dissolved in toluene before. In this attempt, the reaction mixture was heated to reflux for three days. Increasing the concentration of the crude reaction mixture by removing solvent in vacuo, the resulting crystals were suitable for SCXRD experiments. The obtained crystal structure of the formed product is shown in Figure 2-32 and reveals, that the desired reaction did not take place under these conditions. Instead of getting the AlI_2 intermediate, the ionic species **27** could be isolated and structurally characterized in the solid state by means of X-ray diffraction (see Scheme 2-18).

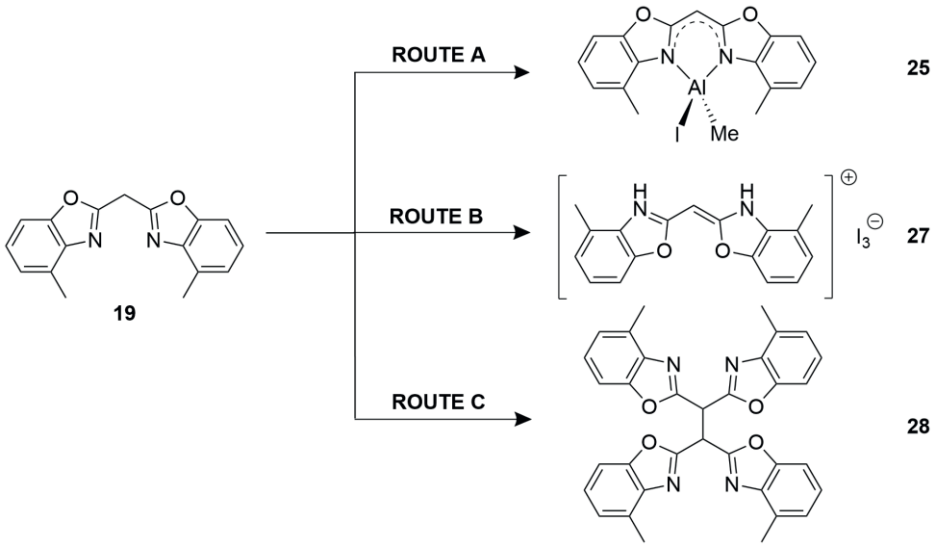

Scheme 2-18: Unexpected reaction products observed during the different synthesis routes towards the desired AlI_2 derivative.

Compound **27** crystallizes in the triclinic space group $P\bar{1}$ and contains one positively charged, protonated ligand system and a negatively charged triiodide as counter ion in the asymmetric unit. For the sake of clarity, Figure 2-32 shows only the organic residue of **27** and the triiodide is omitted, because just the bonding situations of the protonated ligand system will be discussed in comparison to the already explained derivatives of ligand **19**. A very striking feature of this molecule is, that upon protonation the parent ligand system bears two endocyclic NH moieties and the methylene bridge resembles the CH functionality of the metallated species. The amine hydrogen atoms and the remaining CH at the bridge were each freely refined by taking their positions from the difference Fourier map.

The bonding situation of the central carbon atom C1' is similar to that one of **21**, because the C_{ipso}–C1' and C_{ipso}–N distances are nearly the same (**19**: 148.7 pm and 129.1 pm; **21**: 138.4 pm and 135.1 pm) and their values are lying in between a defined corresponding single and double bond as mentioned in previous chapters. Due to the different arrange-

ment of the heteroaromatics in **27** (*cis-cis*) in comparison to **21** (*trans-trans*), the observed angles are differing significantly: the N–C_{ipso}–C1' and O–C_{ipso}–N angles are decreased to 126.0 deg / 109.5 deg (**21**: 128.9 deg / 112.5 deg), whereas the O–C_{ipso}–C1' and C1–C1'–C8 angles are widened to 124.5 deg / 125.7 deg (**21**: 118.6 deg / 121.1 deg).

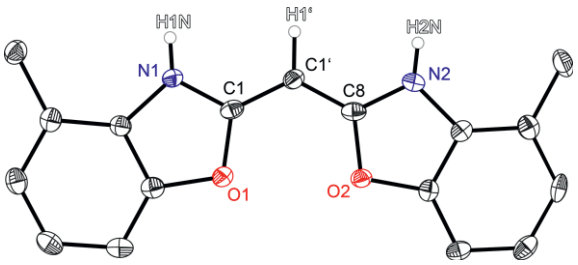

Table 2-28: Distances [pm] and angles [deg] of **27**.

C1'–C1	138.1(5)	N1–C1–C1'	126.0(3)
C1'–C8	137.4(5)	N2–C8–C1'	126.0(3)
C1–N1	133.9(5)	O1–C1–C1'	124.2(3)
C8–N2	134.9(5)	O2–C8–C1'	124.7(3)
C1–O1	135.5(4)	O1–C1–N1	109.8(3)
C8–O2	135.4(4)	O2–C8–N2	109.2(3)
N1–H1N	82(4)	C1–C1'–C8	125.7(3)
N2–H2N	80(4)		

Figure 2-32: Solid state structure of **27**.

The protonation of the parent ligand offers two possible tautomeric forms (see Scheme 2-19). In the tautomeric forms **(a)**, the additional proton is located at one specific nitrogen atom and the central methylene bridge remains as CH_2 unit. Therefore, the double bonds are located within the five-membered heterocycles and the bonds of the bridging C1' atom behave as single bonds. A pattern of N=C–CH_2–C=NH^+ is observed in these cases. In contrast to that, the tautomeric forms **(b)** show a behaviour of the complexed monoanionic ligand as found for compounds **21** – **26**, in which the methylene bridge carries just one hydrogen atom. Therefore, two hydrogen atoms are located at both nitrogen atoms N1 and N2 to give a NH–C=CH–C=NH^+ pattern at the backbone of the ligand. Unexpectedly, this arrangement seems to be most stable in the solid state, because the positive charge can be stabilized better by delocalisation over the alternating double bonds. This delocalisation is also proven by the fact, that the whole ligand framework is nearly planar arranged and the heteroaromatic residues show no twisting against each other (folding angle: 1.55(14) deg).

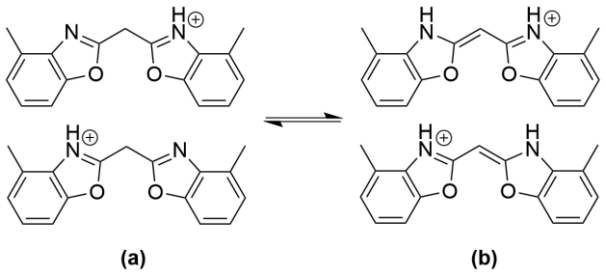

Scheme 2-19: Tautomeric forms of the protonated *cis-cis* conformer of **27**.

Interestingly, molecule **27** adopts the so called *cis-cis* conformation, in which both protonated nitrogen atoms N1 and N2 are pointing to the same side as the bridging carbon atom C1'. This is the first time for the investigated methanide ligands, that this conformation was observed within this work. In all other cases, where metal complexes were concerned, every time the *trans-trans* conformation was observed due to the chelating coordination abilities of the two imine nitrogen atoms. In Scheme 2-20 all possible configurational isomers for **27** are depicted, assuming that the arrangement remains ideally planar and the bonds towards the bridging methylene moiety exhibit partially double bond character. A detailed description of the applied *cis-trans* nomenclature will be given in Chapter 2.5, which refers to the investigated bisheterocyclo amines.

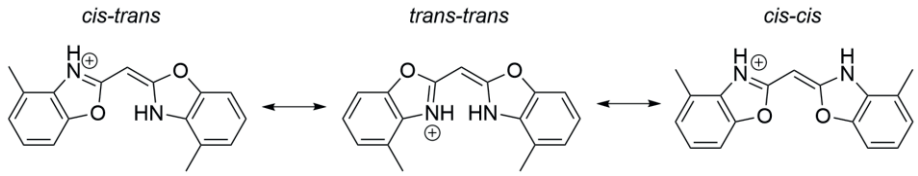

Scheme 2-20: Possible configurational isomers for the protonated ligand **27**.

The decomplexation of the former $AlMe_2$ complex **21**, which is a crucial step in generating **27**, is probably caused by intermediate formation of HI. Hydrogen iodide serves as a proton source for the ligand and the remaining iodide can react with the excess of elemental iodine to give triiodide as the stabilized polyhalogen adduct. As shown above in the crystal structure of **27**, the positive charge of the protonated ligand system is compensated by the formed I_3^- as counter ions. The presence of HI in solution can be explained by contamination with water supported by elevated temperature and long reaction time. The proposed redox equations displayed in Scheme 2-21 underline this hypothesis.[110]

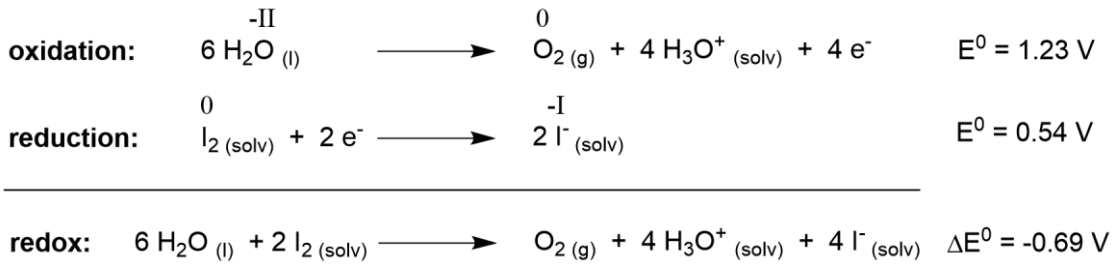

Scheme 2-21: Proposed redox reaction as explanation for the formation of **27**.

The necessary hydrogen iodide is formed by the proposed redox reaction in Scheme 2-21. Therefore, the small amount of water available in the reaction mixture is oxidized to gaseous dioxygen and hydronium ions with a standard potential of E^0(ox) = 1.23 V.[110] The corresponding reduction step consists of the electron acceptance of iodine to yield in iodide anions with a standard potential of E^0(ox) = 0.54 V.[110] This formal redox reaction

results in the difference of the standard potentials of $\Delta E^0 = E^0(\text{red}) - E^0(\text{ox}) = -0.69$ V. Due to the correlation with the free Gibbs energy $\Delta G^0 = -z \cdot F \cdot \Delta E^0$, in which z is the number of electrons transferred and F as Faraday constant, a positive value for ΔG^0 will be obtained for this redox reaction. This means, that this kind of reaction will not take place spontaneously under standard conditions. But the elongated reaction time at elevated temperature seems to support the overcoming of this barrier, so that this reaction works if only in small scale. By the presence of the resulting H_3O^+ and I^- ions in solution, the formation of **27** is feasible.

Regarding to route **C** in Scheme 2-17 and Scheme 2-18, also another route via a salt elimination reaction was attempted to synthesize the AlI_2 derivative. For this, the first step involves the *in situ* lithiation of the parent ligand system **19**, dissolved in THF, to obtain the lithiated species **30**, whose NMR spectroscopic characterisation is discussed in Chapter 2.4 in detail. Afterwards, aluminium triiodide, dissolved in THF, was added to the lithiated compound **30** and the reaction mixture was stirred for additional three days at room temperature. After removing residual solvent, crystals suitable for SCXRD could be obtained. The results of the diffraction experiment show, that the expected AlI_2 containing intermediate could not be synthesized by applying this pathway. Instead, the dimerized ligand **28** could be identified and structurally characterized in the solid state (see Figure 2-33).

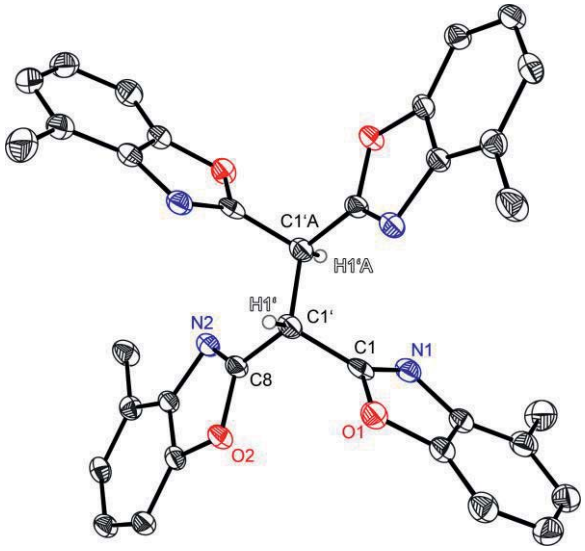

Figure 2-33: Solid state structure of dimer **28**.

Table 2-29: Distances [pm] and angles [deg] of **28**.

C1'–C1	149.9(3)	N1–C1–C1'	127.07(18)
C1'–C8	149.8(3)	N2–C8–C1'	128.03(17)
C1–N1	129.3(2)	O1–C1–C1'	116.15(16)
C8–N2	128.6(2)	O2–C8–C1'	115.73(16)
C1–O1	136.4(2)	O1–C1–N1	116.72(17)
C8–O2	137.4(2)	O2–C8–N2	116.20(16)
C1'–C1'A	154.1(4)	C1–C1'–C8	108.97(16)
		C1'A–C1'–C8	110.0(2)
		C1'A–C1'–C1	111.34(19)

Symmetry transformations used to generate equivalent atoms: −x+2, −y+1, −z+1

Unexpectedly, neither a lithium nor an aluminium containing complex or fragment were present in the crystal structure, but instead a C–C coupling reaction of two ligands has taken place at the central methylene bridge. However, the presence of AlI_3 in the reaction mixture catalytically promotes the C–C bond formation between two monoanionic ligand backbones and leads to the interesting new ligand system **28**. This kind of Lewis-acid catalyzed coupling reaction was also reported earlier in the literature for related bisheterocyclo methane derivatives in the presence of Mn(II), Fe(II) or Pb(II) acetate.[98a] It was

found out, that those metal ions promote the ligand's oxidation or dimerization (via either a single or a double bond) in solution. Presumably, this dimerization process is also supported by the presence of deprotonating reagents like acetate, *tert* butanolate or simply the already deprotonated ligand.[117] Interestingly, the coupling product **28** offers the possibility to act as a double chelating ligand. Due to the remaining two acidic protons at the two central bridging carbon atoms C1' and C1'A, a double deprotonation seems to be feasible to gain a dianionic ligand system, which can coordinate two metal fragments in a chelating fashion as in the case of the uncoupled methanides discussed so far. This kind of ligand should be able to form hetero as well as homo bimetallic complexes, which has to be investigated in further future studies.

The coupling product **28** crystallizes in the monoclinic space group $P2_1/n$ and the asymmetric unit consists of half a molecule. The bonding situation of the bridged central atoms C1' and C1'A is distorted tetrahedral, because the steric demand of the heteroaromatic substituents forces the corresponding angles to widen up. Therefore, the angles concerning the remaining hydrogen atom are smaller than the ideal tetrahedral angle of 109.5 deg. Even the C1–C1'–C8 angle is decreased to 109.0 deg, because the steric hindrance of the connected C1'A unit with its two benzoxazoles is higher than the demand of the two benzoxazoles directly bonded to C1'. The single bonds originating from C1' to the neighbouring carbon atoms are in good agreement with a typical C(sp^3)–C(sp^2) single bond (151 pm) and a C(sp^3)–C(sp^3) single bond (154 pm) (C_{ipso}–C1': 149.9 pm; C1'–C1'A: 154.1 pm).[108] The marginal decrease of the C_{ipso}–C1' distances in comparison to the literature values is caused by the adjacent heteroatoms, which have a higher electronegativity and shorten the bond lengths. All other structure specific values are comparable to those of the parent ligand **19** (C_{ipso}–C1': 148.7 pm; C_{ipso}–N: 129.1 pm; C_{ipso}–O: 137.3 pm).

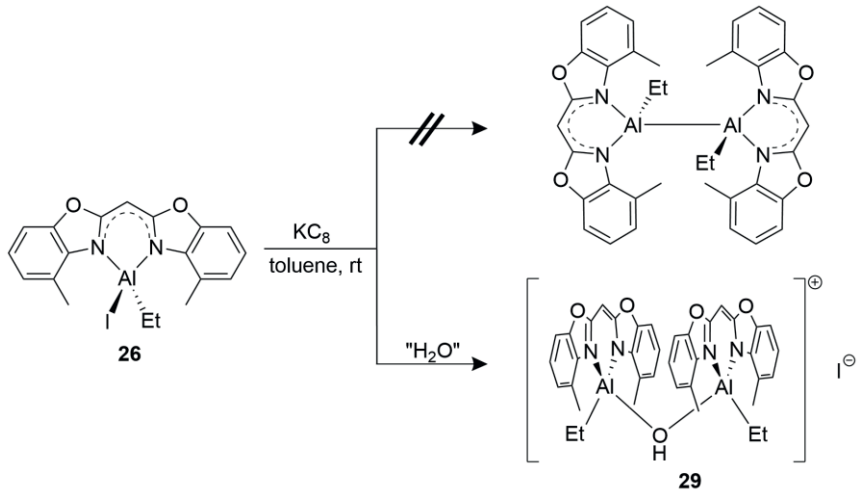

Scheme 2-22: Failed synthesis attempt of the desired Al(II) species $[EtAl\{(4\text{-}MeNCOC_6H_3)_2CH\}]_2$.

As a final attempt to achieve a low-valent aluminium species containing the designed deprotonated bis-(4-methylbenzoxazol-2-yl)-methanide as ligand, the readily accessible

AlIEt complex **26** was chosen for further investigations. Because the synthesis of this complex is straight forward as described in Chapter 2.2.2 (good yields of 50 %) due to the utilisation of $AlEt_2I$ as deprotonation reagent, **26** was treated at room temperature with KC_8 as a reducing agent. By application of this procedure, an interesting Al(II) species, shown in the upper right corner of Scheme 2-22, with an expected Al–Al bond should be synthesized. At this point it is worth to mention, that **26** was preferred instead of the analogue AlMeCl species **24**, because the intended reduction should work much better with iodide than with chloride due to the weaker bonding of Al^{3+} and I^-. This can be explained by the HSAB principle.[90, 92]

After purification, a small amount of single crystals was obtained upon crystallisation in a freezer over night, which were used for the structural elucidation of the formed compound. The results of the SCXRD experiment exhibit, that the intended reduction of **26** to the desired Al(II) complex was not successful. But instead of this compound, another fascinating molecule could be isolated and structurally characterized in the solid state: due to some contaminations with water, the former mono halogenated aluminium complex undergoes a nucleophilic substitution reaction to obtain the hydroxido bridged aluminium complex **29** shown in Figure 2-34.

The proposed reaction mechanism for the formation of this side product starts with one molecule of **26**, which is nucleophilicly attacked by one water molecule to end up in a hydroxy functionalized aluminium complex [(OH)EtAl{(4-$MeNCOC_6H_3)_2CH$}] under release of one equivalent of HI. In comparison to the starting material, the reactivity of this hydroxy derivative is enhanced featuring the consequence, that the lone pair of the hydroxy group undergoes a second nucleophilic attack at another molecule of **26**. Because of this, the second iodide gets substituted and a monocationic complex [(μ-OH){EtAl((4-$MeNCOC_6H_3)_2CH$)}$_2$]I is formed, consisting of two ligands and two coordinated AlEt fragments, each bridged by the same μ-OH moiety. The substituted iodide anion serves as counter ion for reaching charge neutrality of **29**. Surprisingly, the presence of water does not lead to the re-protonation of the ligand backbone, what is always accompanied with the decomposition of the complex, precipitation of the corresponding alumoxanes/Al_2O_3 and back formation of the parent ligand. In this case, the hydrolysis of the halogenated metal complex leads to a compound, where the aluminium coordination stayed intact and which can be seen as an intermediate species on the way to the following decomposition. This observation suggests the assumption, that the Al–I bond is the most labile one within the metal complex, because the chelating N–Al coordination and the covalent C1M–Al bonds were left untouched upon hydrolysis.

Comparable neutral dialumoxanes (μ-O)[RAl{N(2,6-$Me_2C_6H_3$)C(Me)}]$_2$ (R = H, Me), in which the metal centres are chelated by nacnac ligands and the bridging oxygen is not protonated, show a slightly different arrangement in the solid state.[23] Due to the twisting of the substituted phenyl entities in the corresponding nacnac species, the distance and the torsion between the two ligand frameworks is much more pronounced as in **29**. Therefore, the resulting coordination behaviour regarding to the $(RAl)_2$(μ-O) fragment changed, because the ligands are not as parallel aligned as in **29**. For example, in (μ-O)[MeAl{N(2,6-$Me_2C_6H_3$)C(Me)}]$_2$ the Al–O distances are decreased to 170.0(2) pm, whereas the Al1–

O–Al2 angle is closer to linearity (152.91(15) deg). It should be mentioned in this context, that the bending of the $(MeAl)_2(\mu\text{-}O)$ fragment in the nacnac assisted compex is inverted compared to the bisheterocyclo methanide **29**.

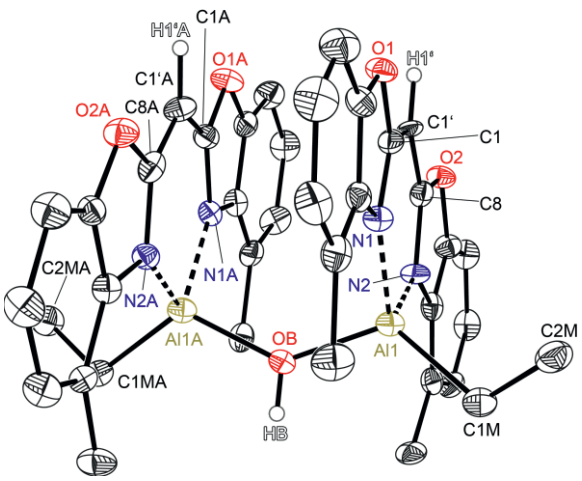

Figure 2-34: Solid state structure of alumoxane **29**.

Table 2-30: Distances [pm] and angles [deg] of **29**.

C1'–C1	137.8(6) 137.9(6)	N1–C1–C1'	128.9(5) 128.8(5)
C1'–C8	138.0(6) 136.9(7)	N2–C8–C1'	129.8(5) 129.1(5)
C1–N1	135.9(5) 135.1(5)	O1–C1–C1'	119.4(5) 118.9(5)
C8–N2	134.8(5) 135.3(5)	O2–C8–C1'	118.0(4) 117.6(5)
C1–O1	136.0(5) 136.4(5)	O1–C1–N1	111.8(4) 112.3(4)
C8–O2	136.4(5) 136.8(5)	O2–C8–N2	112.2(4) 113.3(4)
N1–Al1	190.1(4) 189.9(4)	C1–C1'–C8	120.4(6) 121.5(6)
N2–Al1	190.4(4) 190.8(4)	N1–Al1–N2	96.75(17) 97.06(17)
Al1–C1M	194.8(5) 195.2(5)	C1M–Al1–OB	119.07(19) 117.11(19)
Al1–OB	182.0(5) 181.0(5)	Al1–OB–Al1A	133.93(13)
OB–HB	82.2		

The ionic μ-OH bridged species **29** crystallizes in the monoclinic space group $P2_1/c$ and its asymmetric unit contains the cationic metal complex, one iodide anion and a disordered toluene molecule as lattice solvent. In direct comparison to the starting material **26**, the following structural statements can be made: the N–Al–N bite angle stayed nearly the same upon hydrolysis (97.4 deg in **26** vs. 96.6 deg in **29**). The C_{ipso}–C1', C_{ipso}–N and C_{ipso}–O distances are also almost the same (**26**: 138.1 pm, 135.1 pm and 135.6 pm). The arrangement of the both organic ligands is nearly ideally planar (folding angle: 2.93(15) deg and 1.59(15) deg) and the aluminium fragments are aligned in the chelating C_3N_2 plane of the metalla heterocycle (Al···plane deviation: 1.16(61) pm and 4.78(60) pm) as previously observed in the other metal complexes derived from **19**. Both ligands are also aligned almost parallel to each other, but they are not arranged in an ecliptic manner. Due to the steric demand of each part of the molecule, the ligand frameworks are slightly inclined against each other to occupy a staggered position. The N–Al distances result in 190.3 pm and the distorted tetrahedral bonding situation of Al1 exhibits merged Al–C1M and Al–OB distances of 195.0 pm and 181.5 pm, respectively. The bridging oxygen atom OB shows a Al1–OB–Al1A angle of 133.9 deg and the corresponding OB–HB distance to the freely refined hydrogen atom is about 82 pm. Additionally, hydrogen bonding for HB of the hydroxy group and the iodide is visible in the solid state structure. The hydrogen atom is pointing towards the iodide, which serves as hydrogen acceptor, with a measured HB···I distance of 247(4) pm and a corresponding OB–HB···I angle of 174(8) deg.

2.2.6 Conclusion

In this chapter the successful syntheses and solid state structure determinations of six metallated bis-(4-methylbenzoxazol-2-yl)-methanides **21** – **26** as well as the parent uncharged methane derivative **19** were presented. The previously reported bisheterocyclo methanes were chemically tuned by introducing methyl groups to the benzannulated heterocycles (in this case benzoxazole), giving a promising ligand system for metal complexation (see Scheme 2-23).

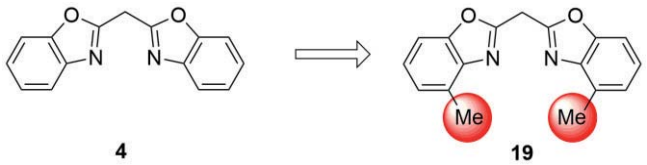

4 19

Scheme 2-23: Switch to the chemically tuned ligand system **19**.

19 exhibits a nearly perfect planar coordination geometry concerning the ligand side arms in all discussed solid state structures. This fact is displayed by the small values in the folding angles between both heteroaromatic planes and only slight deviations of the metal cations from the chelating C_3N_2 plane in each complex. This is outstanding in the row of the previously investigated methanide and the following amide complexes (*vide infra* in Chapter 2.5). The observed arrangement in the solid state can be explained by the steric strain induced by the additional methyl groups, which fit inside the properly shaped pocket made up from the particular V-shaped MR_2 fragments. Correspondingly, an intramolecular interlocking is responsible for the overall planar arrangement.

Due to the relatively pronounced inertness of the dimethyl group 13 metal complexes, the switch to the mono halide substituted compounds **24** – **26** presumably offers the access to low-valent group 13 complexes, which should be obtained by reductive salt elimination analogue to the synthesis route of [Al{(N(Dipp)C(Me))$_2$CH}] or [Ga{(N(Dipp)C(Me))$_2$CH}]. In theory, the planar arrangement of the ligand system and the metal cation within the precursors **21**, **24** – **26** should even facilitate the generation of new Al(I) species. The planar coordination geometry enables optimal orbital overlapping between the endocyclic nitrogen donors and the chelated future low-valent metal atom to obtain a more efficient delocalisation.

Unfortunately, already the formation of the necessary AlI_2 derivative failed in several attempts, although similar synthetic procedures were performed, which were known in the literature for the analogue nacnac complexes. The steric shielding around the metal centre, resulting from the planar organic ligand framework, is quite efficient for kinetic stabilisation. But in the case of **21** the reaction with an excess of trimethylsilyl iodide showed, that specific substitution reactions can still take place, which is beneficial in contrast to the comparable nacnac derivatives. Nevertheless, it is worth to mention, that even an excess of TMSI does not lead to a double halide substituted derivative. Furthermore, the protonated species **27** could be isolated as unexpected product of the reaction of **21**

with iodine, and the C–C coupled ligand system **28**, which originates from the lithiated species **30** in presence of AlI_3. Even the performed reduction attempts on the AlEtI derivative **26** with KC_8 as strong reducing agent does not lead to the desired Al(II) species. Instead, only the hydroxido bridged dinuclear aluminium complex **29** could be obtained, where the presence of water caused the exchange of the iodide substituents at the metal fragments.

2.3 Asymmetrically Substituted Bisheterocyclo Methanes

Apart from the symmetrically or homo disubstituted bisheterocyclo methane derivates **1**, **2**, **4**, **5** and **19**, which were presented in the previous Chapters 2.1 and 2.2, also the related ligand systems containing two different methylene bridged heteroaromatic side arms were part of intense investigations within this thesis. Correspondingly, this kind of ligand systems is tagged as asymmetric or hetero disubstituted in the following context. The advantage of these bisheterocyclo methanes finds expression in the fact, that the intrinsic properties of two different benzofused heteroaryls are combined. Presumably, these hybrid species exhibit new synergistic features in contrast to the comparable symmetrically substituted ligands, which can be displayed e.g. in the metal coordination. In the following section, the syntheses of **32** and **34** as well as their derived group 1 and 13 metal complexes are described in a comparative approach. In principal, the structural characterization was accomplished by applying SCXRD experiments and exhaustive NMR spectroscopic investigations.

2.3.1 Ligand Syntheses

The synthesis of the parent ligand systems **32** and **34** is depicted in Scheme 2-25. A two-step procedure was employed to connect two different benzannulated heterocycles via a bridging methylene moiety. One equivalent of malonic dinitrile is reacted with one equivalent of *ortho*-aminothiophenol to give the mono-benzothiazole-substituted methane derivative **31** as precursor. The remaining nitrile group is prone for the introduction of a second heterocycle (see Scheme 2-24).

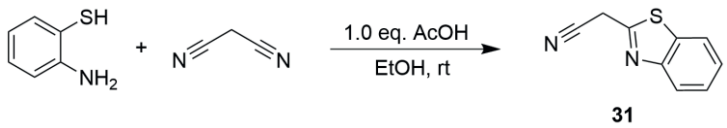

31

Scheme 2-24: Synthesis of the coupling reagent **31**.

In the second step, the corresponding *ortho*-substituted aniline derivative (*ortho*-aminophenol or *N*-methylphenylenediamine) was added, which under quite harsh conditions undergoes a cyclocondensation reaction with 2-(benzothiazol-2-yl)-acetonitrile **31** to build up the second heterocycle. This reaction takes places at elevated temperatures of 180 °C in the presence of polyphosphoric acid (ppa) as solvent under vigorous stirring with a KPG stirrer for several hours (see Scheme 2-25). After aqueous work up and purification the two different ligand systems **32** and **34**, which differ just by the benzoxazole or benzimidazole unit, could be obtained in appreciable yields of 89 % and 48 %, respectively. Referring to ligand system **34**, the yield reported earlier in the literature (6 %; with ethyl cyanoacetate as used linker unit) could be increased significantly by applying the aforementioned procedure.[98a]

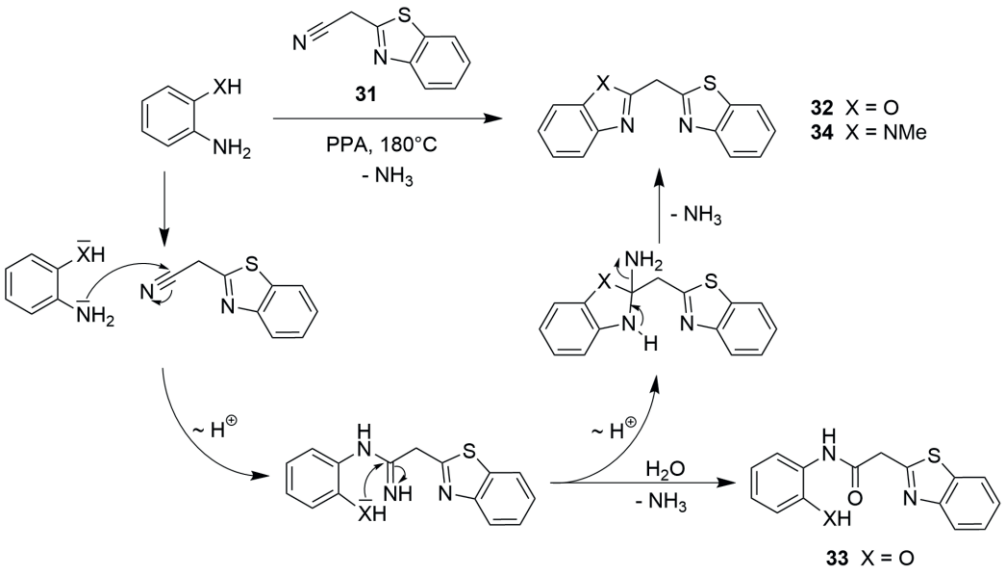

Scheme 2-25: Synthesis of the hetero-disubstituted ligand systems **32** – **34**.

As a side product in the synthesis of **32**, the amide 2-(benzothiazol-2-yl)-*N*-(2-hydroxyphenyl)-acetamide **33** could be isolated by applying column chromatography. It was characterized by NMR spectroscopy and single crystal X-ray determination. **33** can be regarded as an intermediate species, which occurs while generating the benzoxazole moiety in **32**. After the first nucleophilic attack of the amine nitrogen atom at the positive polarized nitrile carbon atom, a primary imine is formed temporarily. This imine is attacked afterwards by the hydroxy group to give a five-membered heterocycle for obtaining the desired products **32** and **34**. Because of insufficient reaction time, the cyclization reaction was not fully completed, so that some amount of the primary imine remained, which was hydrolysed by the aqueous work up (see bottom reaction of Scheme 2-25). Similar observations were made in former publications for the synthesis of related asymmetric bisheterocyclo methanes like $(NCOC_6H_4)CH_2(2\text{-}NC_5H_4)$.[98a] In that case, *ortho*-aminothiophenol and *ortho*-aminophenol were reacted with methyl 2-pyridyl acetate, respectively, to give the aimed asymmetrically substituted methylene bridged ligands via a cyclocondensation reaction. Whereas the reaction with the thiophenol derivative directly yields the bisheterocyclo methane, the analogue reaction with *ortho*-aminophenol stopped at the stage of the amide as observed for **33**. This different reaction behaviour can be ascribed to the better nucleophilicity of the sulfur atom when compared to oxygen.

2.3.2 Structural Comparison of the Neutral Ligands

After performing the above-mentioned synthesis route and recrystallisation from toluene or ethanol, single crystals of compounds **32**, **33** and **34** suitable for SCXRD experiments were obtained. The resulting crystal structures and hydrogen bonding properties will be discussed in the following sections.

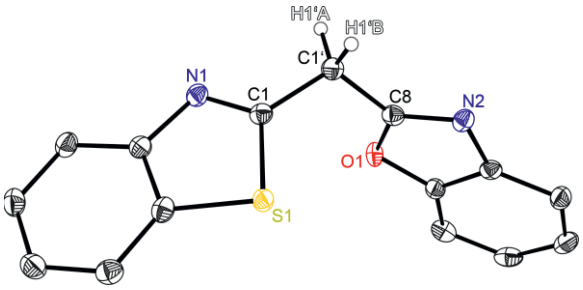

Table 2-31: Distances [pm] and angles [deg] of **32**.

C1'–C1	150.35(18)	N1–C1–C1'	123.37(12)
C1'–C8	149.15(18)	N2–C8–C1'	127.23(12)
C1–N1	129.30(17)	S1–C1–C1'	119.61(10)
C8–N2	129.97(17)	O1–C8–C1'	117.28(13)
C1–S1	175.63(14)	S1–C1–N1	117.00(10)
C8–O1	136.3(2)	O1–C8–N2	115.49(13)
		C1–C1'–C8	112.87(11)

Figure 2-35: Solid state structure of ligand **32**.

Starting with the asymmetric substituted methane derivative **32**, which consists of one benzothiazole and one benzoxazole substituent, it can be stated that the ligand crystallizes in the triclinic space group $P\bar{1}$ having one molecule in the asymmetric unit (see Figure 2-35). Due to the slight differences of the benzoxazole and benzothiazole moiety, there is not a preferred alignment of those residues in the solid state resulting in a positional disorder, in which the oxygen and sulfur atoms are interchanged (*sof*: 0.95). However, this positional disorder could be deconvoluted and the structure was refined satisfactorily but is omitted in Figure 2-35 for clarity reasons. The central carbon atom C1' is coordinated in a distorted tetrahedral geometry and both heteroaromatic residues are twisted against each other. The torsion angle of the moieties results in 254.30(27) deg referring to the position of the imine nitrogen atoms. At this point a short reminder for the calculation of the torsion angle should be given: if the ligand system is assumed to be planar and both nitrogen atoms are oriented to the opposite side of the bridging carbon atom C1', the torsion angle becomes zero (see Scheme 2-26). Therefore, the orientation of the heteroaromatics is quite different compared to the crystal structures of **4** and **5**, because the torsion is in this case most pronounced.

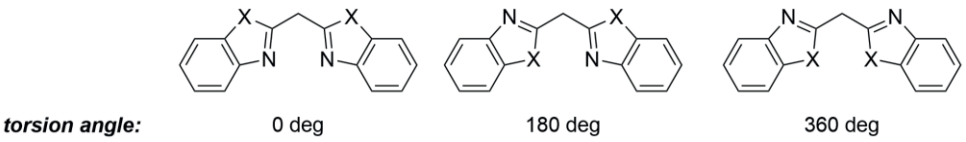

Scheme 2-26: Exemplary torsion angles within the bisheterocyclo methane derivatives.

The determined C_{ipso}–C1' bond lengths are comparable to that of the homo disubstituted methane derivatives **4** and **5** (148.91 pm and 151.06 pm) and for those ligand **32** represents a crossover. The observed C_{ipso}–N distances are also in good accordance with literature known C(sp^2)=N(sp^2) double bond distances of 129.0 pm. [108] The according C1–C1'–C8 angle in the backbone of the parent ligand is slightly widened to a value of 112.9 deg in comparison to **4** and **5** (111.2 deg and 109.6 deg), presumably accompanied with the enhanced torsion angle within the ligand.

As mentioned above, the intermediate compound **33** could be isolated in a quite reasonable yield of 13 % in the first up-scaling attempt of the synthesis of the completely coupled product **32** due to the insufficient reaction time. In this compound, the cyclocondensation reaction was not completely accomplished and therefore the reaction stopped after the first nucleophilic attack of the aniline. The resulting intermediate imine cannot be isolated, because under aqueous work-up conditions it readily hydrolyses to the carboxamide carrying a carbonyl functionality shown in Figure 2-36.

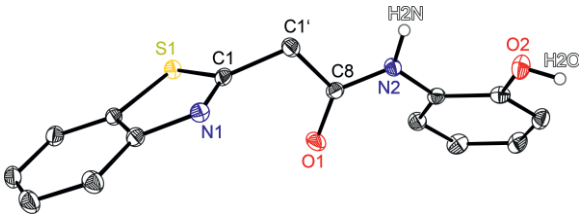

Figure 2-36: Solid state structure of side product **33**.

Table 2-32: Distances [pm] and angles [deg] of **33**.

C1'–C1	149.5(3)	N1–C1–C1'	123.8(2)
C1'–C8	153.5(3)	N2–C8–C1'	115.04(19)
C1–N1	128.7(4)	S1–C1–C1'	120.83(18)
C8–N2	133.4(3)	O1–C8–C1'	120.6(2)
C1–S1	174.8(2)	S1–C1–N1	115.31(18)
C8–O1	123.3(3)	O1–C8–N2	124.3(2)
N2–H2N	85(3)	C1–C1'–C8	111.1(2)
O2–H2O	83(3)		

From a structural point of view, the benzothiazole moiety is comparable to the other discussed ligand systems that contain also benzothiazole side arms. The hydrogen atoms at the C(O)NH functionality and the remaining hydroxy group of the phenyl perimeter were refined freely using the density Fourier map. Due to the very polar carboxamide and hydroxy groups, this molecule is prone for building up a hydrogen bonded network in the solid state, which is displayed in Figure 2-37. From the labelled molecule in the middle of the image it is obvious, that each molecule serves as double proton acceptor by means of the endocyclic imine nitrogen N1 and the carbonyl oxygen O1. Furthermore, also two atoms are acting as hydrogen donors (the amidic N2 and the phenolic O2) to result in the shown crystal packing behaviour. In this context, a one-dimensional N2–H2N···O1 chain (H2N···O1distance: 213(3) pm; N2–H2N···O1 angle: 152(3) deg) is formed by hydrogen bonding between the carboxamide moieties of neighbouring molecules in the unit cell, so that each molecule is linked to two other molecules. One of the two acidic hydrogen atoms at the methylene bridge (H1'B) also seems to stabilize to a certain amount this hydrogen bonding situation by formation of the comparatively weak C1'–H1'B···O1 interaction (H1'B···O1distance: 254 pm; N2–H2N···O1 angle: 115 deg).

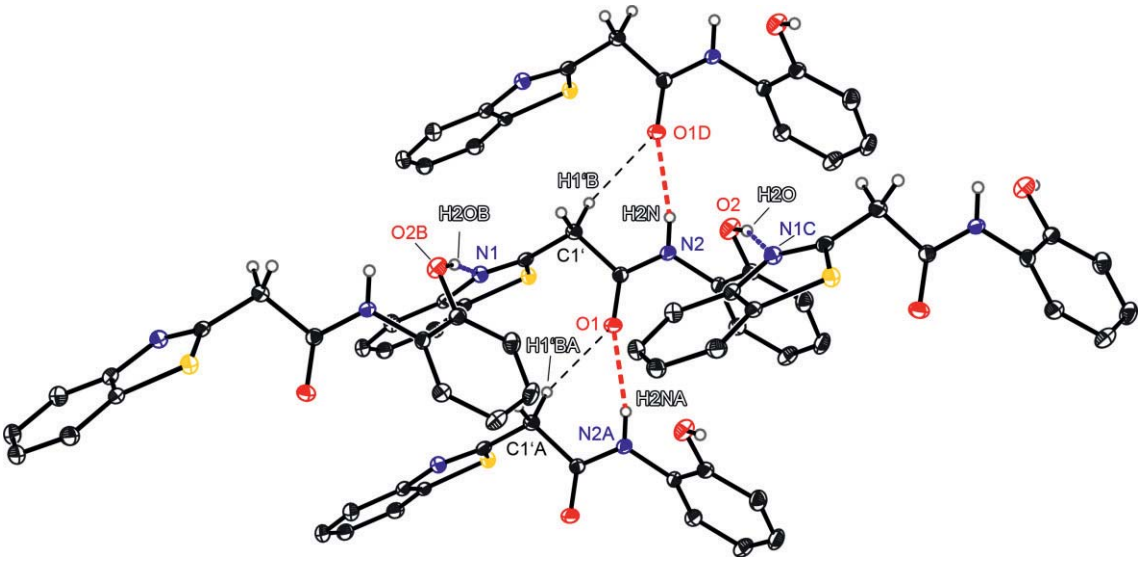

Figure 2-37: Hydrogen bonding pattern of **33**. (Symmetry transformations used to generate equivalent atoms: x, y−1, z for counterpart A, −x+1/2, y−1/2, z−1/2 for counterpart B, −x+1/2, y+1/2, z+1/2 for counterpart C and x, y+1, z for counterpart D).

The other hydrogen acceptor-donor interaction is found between the imine nitrogen atom N1 of the benzothiazole moiety as acceptor and the hydroxy group O2–H2O of the phenolic residue as donor. The observed H2O···N1distance results in 198(4) pm and the corresponding O2–H2O···N1 angle is 164(3) pm, indicating that this intermolecular interaction is energetically even more preferred as the first-mentioned one because of the decreased distance and a more linear D–H···A coordination angle. This hydrogen bonding is addressed to another two adjacent molecules, which results in a three-dimensional network of hydrogen bonded molecules of **33** in the solid state.

For further visualization of the hydrogen bonding situation within this interesting side product, in the top pictures of Figure 2-38 the corresponding Hirshfeld surface from different viewing perspectives is displayed. As already stated, the closest observed contacts in crystal packing are visualized as intense red spots at the calculated surface nearby the nitrogen atoms N1 and N2 and the two oxygen atoms O1 and O2. These atoms are mostly contributing to the formation of the hydrogen bonds in the network. Furthermore, it can be seen (upper left picture), that there is a small contribution from the acidic methylene bridge resulting in a small pale red area in close proximity to the red spot belonging to O1.

At the bottom part of Figure 2-38, the derived fingerprint plots for the intermolecular interactions are depicted, in which four very sharp peaks can be identified. In the left graph only the N···H interactions are shown and highlighted in the blue colour code. This picture reflects the above-mentioned fact, that the nitrogen atom is a more favourable hydrogen acceptor, shown as the two outer, more intense peaks. These are representative for the shorter intermolecular interactions. Additionally, the bottom right graph is limited to the weaker O···H interactions, highlighted as the two smaller, inlying peaks.

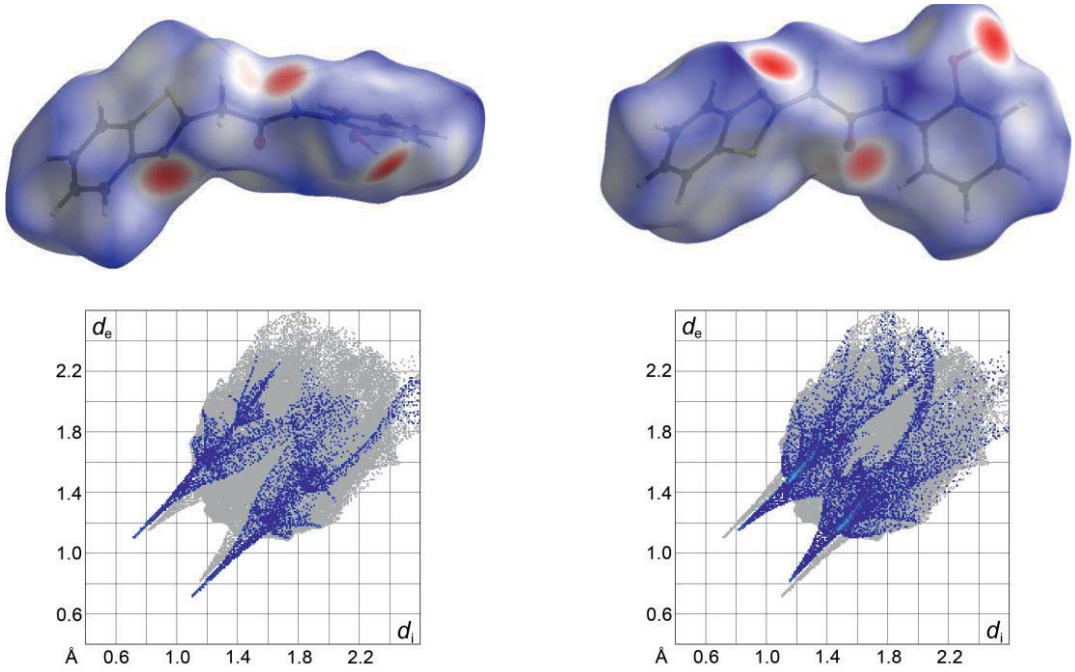

Figure 2-38: Hirshfeld surfaces[106] (*top*) and corresponding fingerprint plots[105, 106a, 107] for N···H (*bottom left*) and O···H interactions (*bottom right*) generated for **33**.

Compound **34** crystallizes in the monoclinic space group $P2_1$ and two target molecules as well as two water molecules can be found in the asymmetric unit (see Figure 2-39). Positional disorder occurs for one molecule in the asymmetric unit as observed for **32**. In this case the imidazole and thiazole moiety are disordered to a low fraction (*sof*: 0.94) in the crystal structure of the related ligand **34**, that carries a *N*-methylbenzimidazole instead of the benzoxazole substituent in **32**. In Figure 2-39, the not disordered molecule is displayed, whereas the second one and lattice solvent were omitted for clarity reasons.

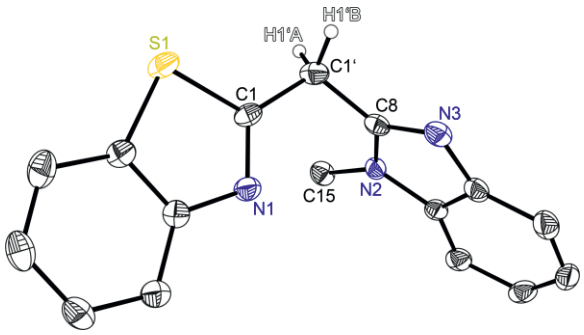

Figure 2-39: Solid state structure of ligand **34**.

Table 2-33: Distances [pm] and angles [deg] of **34**.

C1'–C1	150.3(4) 151.6(4)	N1–C1–C1'	123.4(2) 124.0(2)
C1'–C8	149.4(4) 149.4(4)	N3–C8–C1'	124.2(2) 125.0(2)
C1–N1	130.4(3) 129.5(3)	S1–C1–C1'	120.81(19) 119.34(19)
C8–N3	132.2(4) 131.1(4)	N2–C8–C1'	122.2(2) 122.8(3)
C1–S1	174.1(3) 174.7(3)	S1–C1–N1	115.8(2) 116.6(2)
C8–N2	136.3(3) 135.6(4)	N2–C8–N3	113.5(2) 112.2(3)
N2–C15	145.1(3) 147.6(4)	C1–C1'–C8	111.0(2) 110.2(2)

Due to the presence of two molecules in the asymmetric unit, for each parameter two values are given.

The observed torsion of both heteroaromatic planes (torsion angle: 101.2(7) deg) is not as pronounced as in the case of **5** or **32** and is almost comparable to that one determined in ligand system **2** (96 deg), which consists of two benzimidazole units. The values for the selected bond lengths and angles are in good agreement with the earlier found values for ligand systems **2** and **5** (see Table 2-33). The asymmetric substituted ligand **34** represents a hybrid of the latter mentioned ligands in equal shares, because it consists of one benzothiazole and one benzimidazole moiety. The C_{ipso}–C1' and C_{ipso}–N_{imine} distances are slightly different depending on, which side of the molecule is considered: the thiazole containing side shows a slightly longer C_{ipso}–C1' distance compared to the imidazole counterpart (151.0 pm vs. 149.4 pm). These values were also found in the corresponding homo disubstituted derivatives **2** and **5** (151.1 pm vs. 149.5 pm). In the case of the C_{ipso}–N_{imine} distances, the trend is inverted, because the determined value for the benzothiazole side arm is smaller than for the benzimidazole moiety (130.0 pm vs. 131.7 pm). Again, this fits well to the derivatives **2** and **5** (129.6 pm vs. 131.6 pm). In direct comparison, the value for the C1–C1'–C8 angle in the ligand's backbone (110.6 deg) in **34** lies in between those of **2** and **5** (109.6 deg vs. 113.5 pm), as expected. This seems to be a logical consequence, because **34** is a derived mixture from those ligands.

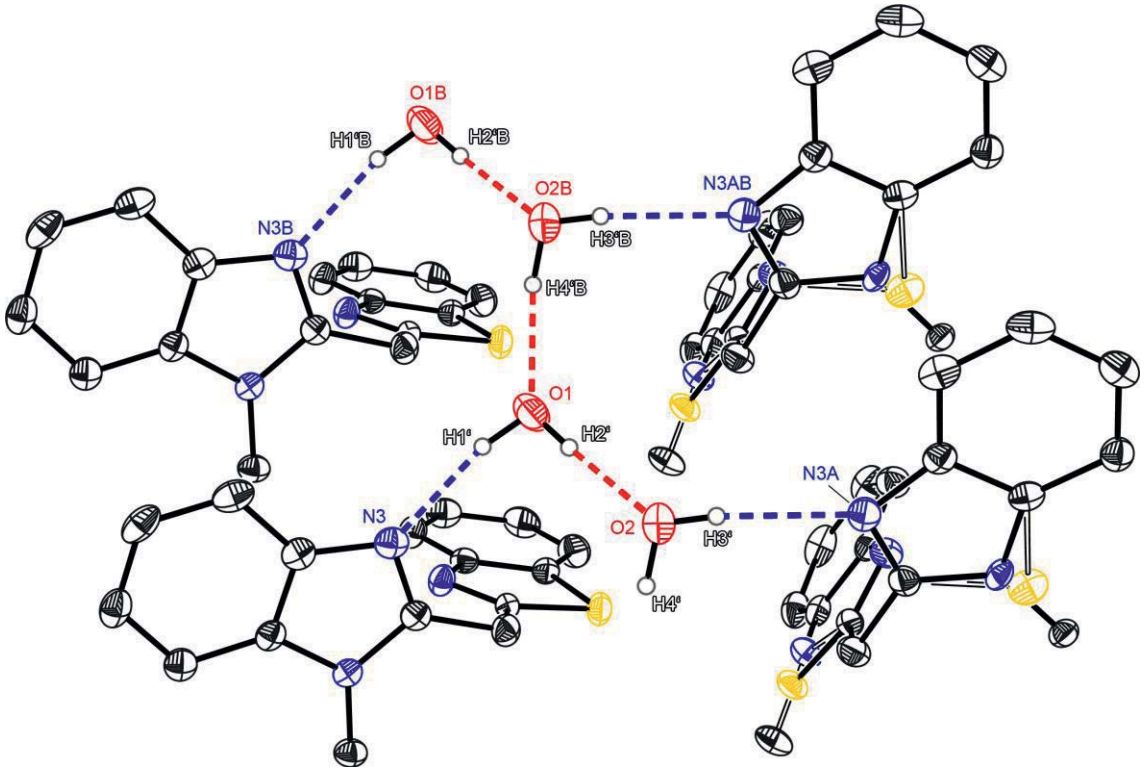

Figure 2-40: Hydrogen bonding pattern of **34**. (Symmetry transformations used to generate equivalent atoms: 1+x, y, z for counterpart B).

The water molecules in the unit cell originate from the aqueous ethanol solution used for recrystallisation of this ligand and are incorporated in an interesting hydrogen bonding network (see Figure 2-40). The water molecules form a hydrogen bonded chain in the

solid state. Every second water molecule is further linked to two neighbouring parent ligands via the endocyclic imine nitrogen atoms. Each oxygen atom acts as double hydrogen donor (O–H···O and O–H···N) and once as hydrogen acceptor from the adjacent water molecule (O···H–O).

The corresponding determined values for the hydrogen bonding properties are listed in Table 2-34. It is obvious, that the imine nitrogen atoms act as hydrogen bond acceptor and the associated bonding properties are less pronounced, if compared to the aforementioned H_2O molecules. This is expressed by the elongated distance between the hydrogen atom and the acceptor (approximately 17 pm longer than in the case of the H···N interactions). Because oxygen has a higher electronegativity than nitrogen, the resulting hydrogen bonds are contracted.[110]

Table 2-34: Hydrogen bonding properties of **34**.

H···A dist. [pm]		D–H···A angle [deg]	
H1'···N3	202(5)	O1–H1'···N3	168(3)
H3'···N3A	210(5)	O2–H3'···N3A	173(4)
H2'···O2	190(4)	O1–H2'···O2	178(3)
H4'B···O1	187(6)	O2B–H4'B···O1	163(5)

2.3.3 Syntheses of the Group 13 Metal Complexes

After successful preparation, the two different hetero disubstituted methane derivatives **32** and **34** were used for further transformations and reactions.

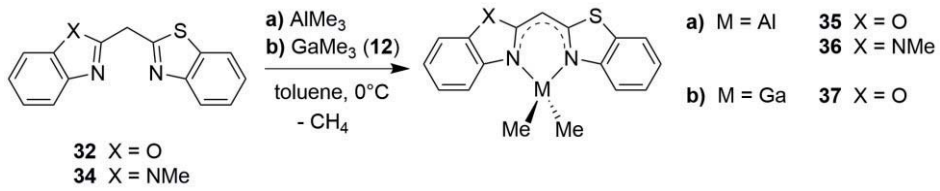

Scheme 2-27: Synthesis of the metallated asymmetric bisheterocyclo methanides **35** – **37**.

In this context, the next synthetic step covers the various metallation reactions, which were applied to the two asymmetric substituted bisheterocyclo methanes. As depicted in Scheme 2-27, the synthesis of the metallated species was accomplished by adding 1.1 equivalents of the organometallic reagent ($AlMe_3$ or $GaMe_3$) to **32** and **34**, dissolved in toluene as apolar solvent. After complete addition, the reaction mixture was stirred over night to achieve an optimized conversion. In analogy to the metallation reactions for the symmetric methanides described in Chapter 2.1.2, after completion of the reaction, the reaction mixture was concentrated to a few millilitres and was stored in the fridge for growing single crystals for X-ray diffraction experiments.

The reaction of **32** and $AlMe_3$ yielded in the corresponding methanide derivative **35**. By recrystallisation from toluene, crystals suitable for SCXRD could be obtained, which afforded the corresponding molecular structure shown in Figure 2-41. A nacnac-like coordination motif was observed, in which the two imine nitrogen atoms act as electron donors to chelate the implemented metal fragment after deprotonation. Regarding to Chapters 2.1, 2.2 and 2.5 (*vide infra*), also the corresponding methanide and amide derivatives could be formed and structurally characterized, though those mentioned complexes consist of a ligand backbone, which is substituted twice with the same benzannulated heterocycle.[95, 115, 116]

2.3.4 Structural Comparison of the Metal Complexes

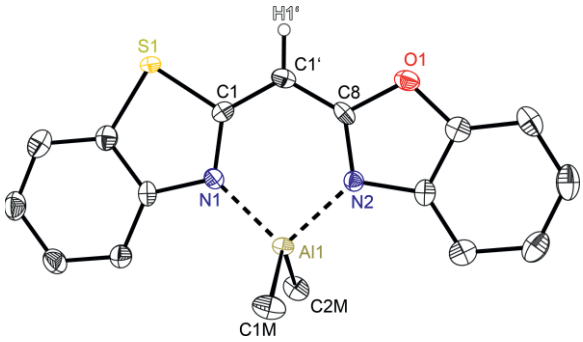

Figure 2-41: Solid state structure of complex **35**.

Table 2-35: Distances [pm] and angles [deg] of **35**.

C1'–C1	138.7(4)	N1–C1–C1'	126.7(3)
C1'–C8	138.5(4)	N2–C8–C1'	127.8(2)
C1–N1	134.7(4)	S1–C1–C1'	118.8(2)
C8–N2	134.3(4)	O1–C8–C1'	122.7(3)
C1–S1	174.1(3)	S1–C1–N1	114.5(2)
C8–O1	138.0(5)	O1–C8–N2	109.5(3)
N1–Al1	193.2(2)	C1–C1'–C8	121.7(3)
N2–Al1	191.6(2)	N1–Al1–N2	93.44(11)
Al1–C1M	195.4(3)	C1M–Al1–C2M	117.86(12)
Al1–C2M	195.2(3)		

The dimethyl aluminium compound **35** crystallizes in the monoclinic space group $P2_1/c$ and the asymmetric unit contains one target molecule (see Figure 2-41). Like in the parent ligand system **32**, in the case of **35** positional disorder (*sof*: 0.84) occurs due to the fact, that in the solid state no preferred alignment of either the benzoxazole or benzothiazole moiety is existent. Again, this disorder leads to an unreliability of the determined bond lengths and angles, because two different oriented molecules, which are rotated about 180 deg against each other, are superimposed in the solid state. The partially superposition of both alignments generates a merged bonding situation.

Table 2-36: Selected parameters for compounds **35** – **37** and **39**.

compound	M–N1 [pm]	N1–M–N2 [deg]	M···plane dist. [pm]	folding angle [deg]
$[Me_2Al\{(NCSC_6H_4)CH(NCOC_6H_4)\}]$ (**35**)	192.4(2)	93.44(11)	5.64(38)	0.78(1)
$[Me_2Al\{(NCSC_6H_4)CH(1\text{-}MeNCNC_6H_4)\}]$ (**36**)	191.1(6)	94.4(3)	28.96(63)	9.61(85)
$[Me_2Ga\{(NCSC_6H_4)CH(NCOC_6H_4)\}]$ (**37**)	199.3(8)	91.3(3)	24.06(50)	3.34(11)
$[(diox)_2Li\{(NCSC_6H_4)CH(1\text{-}MeNCNC_6H_4)\}]$ (**39**)	195.6(8)	96.8(3)	1.92(12)	1.93(13)

Therefore, no meaningful statements concerning the bond lengths and angles within the heterocycles will be expressed. Just the values for the bite angle, the N–M distances and

the deviation of the metal fragment from the chelating C_3N_2 plane are discussed in the following context for all metallated species due to the reasonable reliability of these values (see Table 2-36).

For **35**, Al1 is coordinated in a distorted tetrahedral fashion resulting in an averaged N–Al distance of 192.4 pm and a bite angle of 93.44 deg. In comparison to previous results for related bisheterocyclo methanide ligand systems like $[(NCSC_6H_4)_2CH]^-$ or $[(NCOC_6H_4)_2CH]^-$, which bear two identical benzoxazole or benzothiazole substituents respectively, the obtained values for the dimethyl aluminium species lie in between those values for the correlated complexes **8** (N–Al: 191.76(20) pm; N–Al–N: 91.76(9) deg) and **9** (N–Al: 192.38(14) pm; N–Al–N: 94.78(6) deg). However, it has to be noticed that the structure of **35** is closer related to the bis-(benzothiazol-2-yl)-methanide derivative **9**.

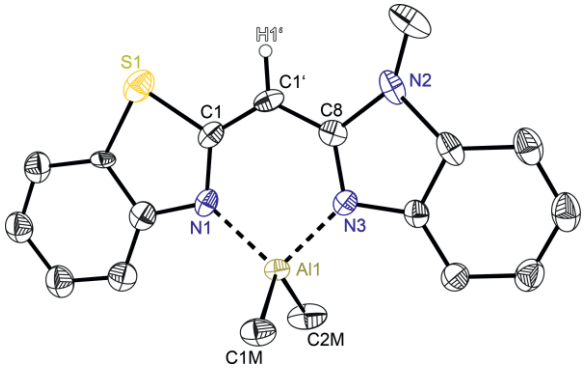

Figure 2-42: Solid state structure of complex **36**.

Table 2-37: Distances [pm] and angles [deg] of **36**.

C1'–C1	137.5(9)	N1–C1–C1'	126.2(5)
C1'–C8	138.5(7)	N3–C8–C1'	125.6(5)
C1–N1	136.1(8)	S1–C1–C1'	117.2(4)
C8–N3	135.5(7)	N2–C8–C1'	116.4(5)
C1–S1	173.5(5)	S1–C1–N1	116.6(5)
C8–N2	144.2(7)	N2–C8–N3	118.1(6)
N1–Al1	193.8(5)	C1–C1'–C8	123.8(5)
N3–Al1	188.3(6)	N1–Al1–N3	94.4(3)
Al1–C1M	196.4(4)	C1M–Al1–C2M	114.98(17)
Al1–C2M	195.5(4)		

The crystal structure of the second dimethyl aluminium containing complex **36** (see Figure 2-42), shows also a high amount of positional disorder on a special position, wherein the benzimidazole and benzothiazole residues are interchanging. The metal cation is coordinated exclusively by the endocyclic imine nitrogen donors in a distorted tetrahedral fashion. Again, the results of the previous chapters dealing with the homo disubstituted bisheterocyclo methane derivatives can be applied for a structural comparison. This comparison reveals, which influence the used heterocycles exert on the resulting structural motifs/binding situations in the solid state. In this case, the parent ligand system **34** is a hybrid of bis-(benzothiazol-2-yl)-methane **5** and its bis-(*N*-methylbenzimidazol-2-yl)-methane analogue **2**. Therefore, the derived $AlMe_2$ complexes of the ligand systems **2** and **5** are suitable for a reasonable structural comparison. Unfortunately, the solid state structure of the according dimethyl aluminium complex $[Me_2Al\{(1\text{-}MeNCNC_6H_4)_2CH\}]$ **7** could not be obtained, so that just spectroscopic data of this complex are available as shown in Chapter 2.1.2. Only the corresponding metal complex **9** is sufficiently characterized in the solid state, so that a structural comparison with the bonding situation of **36** can be accomplished (see Table 2-36). The observed N–M distances and bite angles are very similar to that one of **9** (192.4 pm and 94.8 deg). Nevertheless, it is striking that the observed folding angle and the cation's deviation from the chelating C_3N_2 plane is much more pronounced in the case of **36** (**9**: 1.36 deg and 13.8 pm). Due to the butterfly-like

conformation and the resulting large M···plane distance in **36**, it is assumed that this ligand type is not appropriate for coordination of the $AlMe_2$ fragment. Regarding to this, in direct comparison to the other metallated species **35**, **37** and **39** it is also visible, that the latter mentioned parameters exhibit the highest values determined in the case of **36**.

Additionally, the higher homologue $GaMe_2$ derivative **37** and the lithium complex **39** could be investigated by applying X-ray diffraction experiments to obtain their crystal structures. The detailed characterization of the dioxane coordinated lithiated compound **39** is reported in the next Chapter 2.4, because this content is more suitable for the therein-discussed topic of lithiated bisheterocyclo methanides. Nevertheless, also in the present chapter some connections regarding the NMR spectroscopic data of **39** were drawn to complete the overall comparison of the related compounds.

The dimethyl gallium complex **37** crystallizes in the orthorhombic space group *Pnma* and the asymmetric unit contains one molecule, which is disordered on a special position (see Figure 2-43). Again, this disorder is caused by the positional exchanging of the benzoxazole and the benzothiazole moiety against each other. For clarity reasons, not both disordered parts are shown in Figure 2-43. For comparison reasons the corresponding gallium compounds $[Me_2Ga\{(NCOC_6H_4)_2CH\}]$ **13** (N–Ga: 199.6(20) pm; N–Ga–N: 89.2(2) deg) and $[Me_2Ga\{(NCSC_6H_4)_2CH\}]$ **14** (N–Ga: 199.45(13) pm; N–Ga–N: 92.99(8) deg) are appropriate. As expected, the experimentally determined values for **37** represent a mixture in terms of the structural features of the related complexes **13** and **14**. Although the observed N–Ga distance in **37** (199.3(8) pm) fits well to the corresponding values of **13** and **14**, the bite angle in **37** (91.3(3) deg) lies in between those of the symmetrically substituted derivatives.

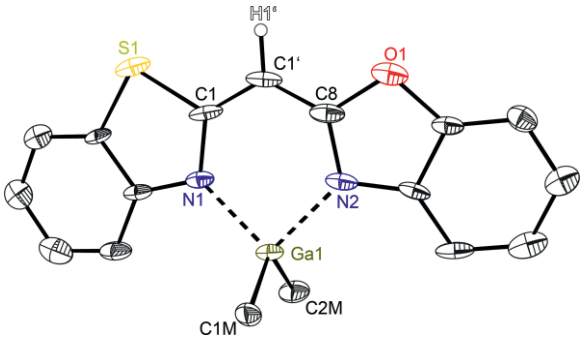

Figure 2-43: Solid state structure of complex **37**.

Table 2-38: Distances [pm] and angles [deg] of **37**.

C1'–C1	138.2(11)	N1–C1–C1'	127.4(9)
C1'–C8	136.7(10)	N2–C8–C1'	129.5(10)
C1–N1	135.6(10)	S1–C1–C1'	120.8(7)
C8–N2	134.3(10)	O1–C8–C1'	119.6(8)
C1–S1	173.7(11)	S1–C1–N1	111.8(7)
C8–O1	140.3(13)	O1–C8–N2	110.9(8)
N1–Ga1	199.2(8)	C1–C1'–C8	121.9(5)
N2–Ga1	199.4(8)	N1–Ga1–N2	91.3(3)
Ga1–C1M	196.0(4)	C1M–Ga1–C2M	120.4(2)
Ga1–C2M	196.8(5)		

Regarding the folding angle and the deviation of metal fragment from the C_3N_2 plane, it can be noticed, that the gallium fragment in **37** is coordinated less good as observed in the case of the $AlMe_2$ complex. This is supported by significantly increased values for these two parameters compared to **35**. The out-of-plane location of the metal cation and the butterfly-like arrangement of the ligand side arms are less pronounced as in **8** or **36**, but the determined values are indicating that this ligand system is not appropriate for coordination of $GaMe_2$. In comparison to **13** and **14** it can be stated, that the M···plane distance

in **37** even exceeds the values of the related complexes (**13**: 14.3 pm; **14**: 20.6 pm), whereas the folding angle is decreased when compared to the corresponding values (**13**: 3.6 deg; **14**: 8.9 deg).

2.3.5 NMR Spectroscopic Investigations

In the following section, NMR spectroscopic investigations confirm and support the previously discussed results obtained from SCXRD.

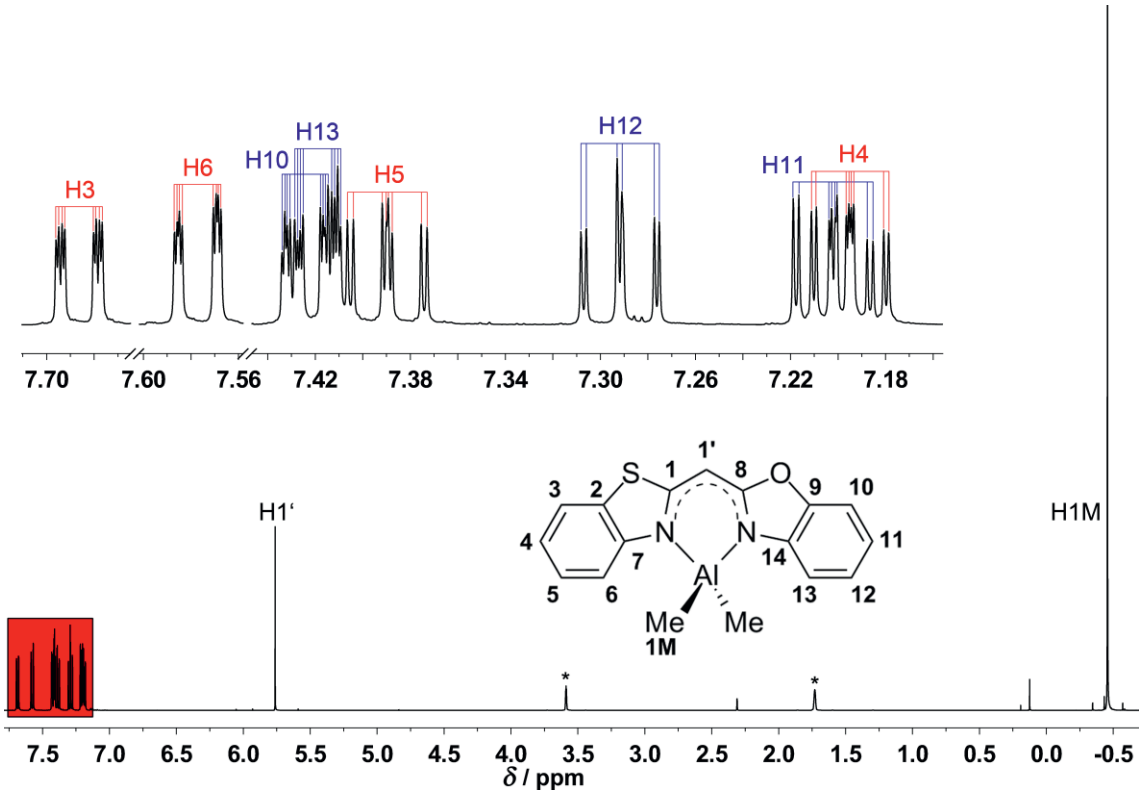

Spectrum 2-6: ^{1}H-NMR spectrum of **35** (500 MHz, THF-d_8, rt; solvent signals are highlighted with *).

The ^{1}H-NMR spectrum of the dimethyl aluminium containing complex **35** is shown in Spectrum 2-6. Besides the two singlets at −0.45 ppm and 5.76 ppm corresponding to the methyl groups bond to the aluminium fragment and the remaining proton at the bridging carbon atom, respectively, the multiplets in the aromatic region of the spectrum show a distinct, well-pronounced coupling pattern. Due to the fact, that the both side arms just differ by the dissimilar chalcogen atom at the five-membered ring (oxazole or thiazole), the hydrogen atoms at the annulated benzene parameters exhibit slightly different chemical shifts. The reasonable resolution of the recorded spectrum allows the determination of the underlying coupling constants, which can be derived from the observed multiplets. Each aromatic proton couples with three other protons of the corresponding heterocycle, so that in each case a *ddd* coupling pattern is observed. In the case of the terminal hydrogen atoms H3, H6 or H10, H13, the relatively large ^{3}J-coupling constant towards the *ortho*-protons as well as the smaller ^{4}J-coupling constants of the *meta*- and ^{5}J-coupling con-

stants of the *para*-protons can be identified. The other protons H4, H5 or H11, H12 show two large ^{3}J-couplings to the both neighbouring protons in *ortho*-position and a smaller ^{4}J-coupling towards the remaining proton in *meta*-position. By application of these values and with the assistance of 2D-NMR experiments like HSQC and HMBC, it was possible to assign the observed signals in the aromatic region to the related protons properly (see Scheme 2-28). The exact assignment of these, sometimes partially or completely superimposed, signals is depicted in the upper part of Spectrum 2-6 as magnification. It can be noticed, that the resonance signal of the terminal hydrogen atom H3 is most downfield shifted (7.69 ppm), whereas the neighbouring H4 is most upfield shifted (7.19 ppm) with respect to the considered aromatic area. This fact could also be observed in the recorded ^{1}H-NMR spectra of the metallated species **36**, **37** and **39** (*vide infra*).

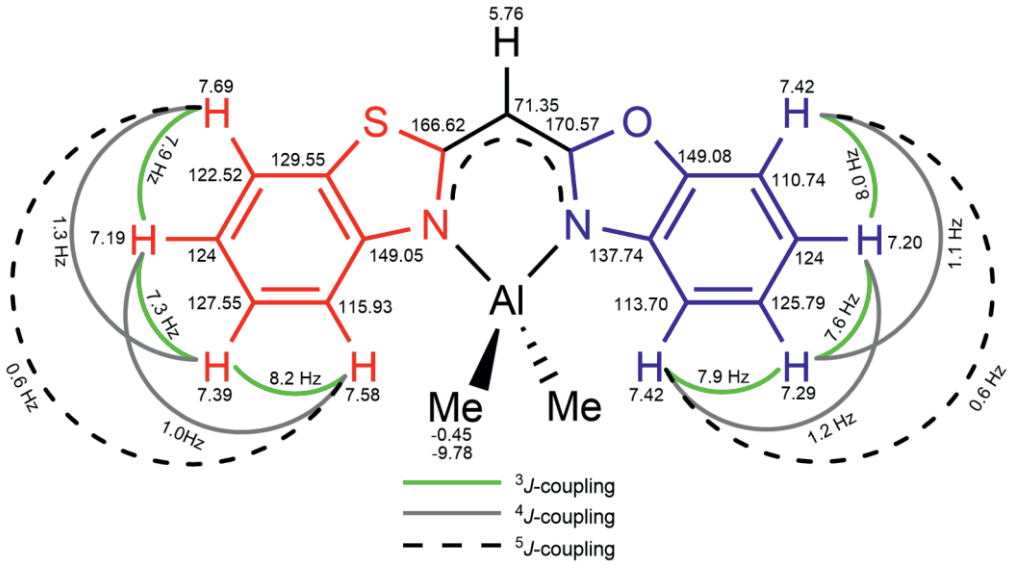

Scheme 2-28: Observed NMR coupling constants and assigned chemical shifts (^{1}H / ^{13}C) for **35**.

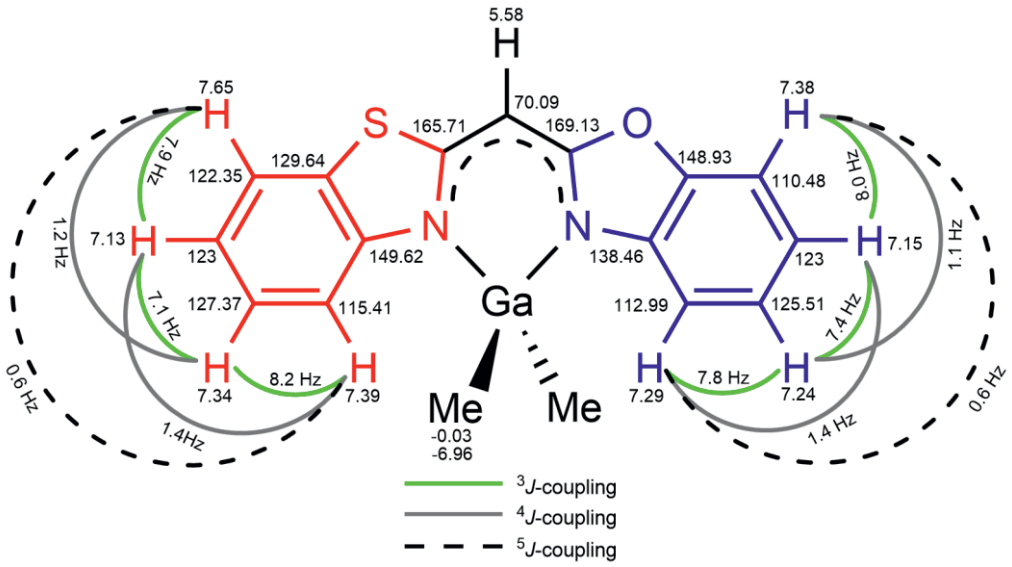

Scheme 2-29: Observed NMR coupling constants and assigned chemical shifts (^{1}H / ^{13}C) for **37**.

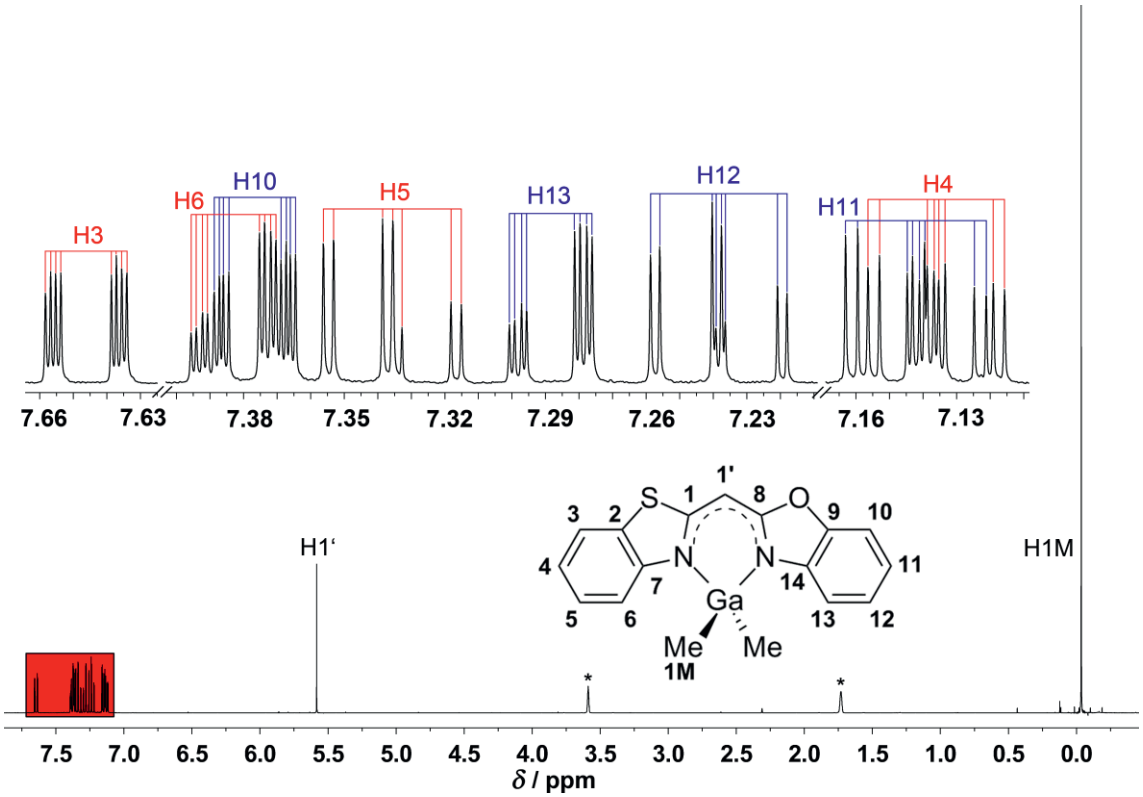

Spectrum 2-7: ^{1}H-NMR spectrum of **37** (400 MHz, THF-d_8, rt; solvent signals are highlighted with *).

The resulting ^{1}H-NMR spectrum of **37** is displayed in Spectrum 2-7. In **37** the aluminium cation of **35** is just replaced by its higher congener gallium, so that the recorded spectra of **35** and **37** are very similar. There is a singlet at −0.03 ppm for the dimethyl gallium moiety, another one for the deprotonated methylene bridge at 5.58 ppm and the region of the aromatic protons covers a similar range as in **35** (7.65 – 7.13 ppm), which is again determined by the chemical shifts of the protons H3 and H4. Analogue to the assignment procedure in **35**, the observed signals could be matched to their correct positions (see magnification in Spectrum 2-7). Here, the resolution and splitting of the signals is even better to gain proper coupling constants and as a consequence thereof, the related peaks of each multiplet could be assembled (see Scheme 2-29).

For a better comparison of the parent ligand **32** and the two derived group 13 metal complexes **35** and **37**, a superposition of the ^{1}H-NMR spectra is depicted in Spectrum 2-8 (focussed on the signals in the aromatic region). Obviously, upon deprotonation and subsequent metallation of **32**, the resonance signals of the aromatic protons are shifted significantly towards higher field. This is as a consequence of the generated electron pair and the negative charge is delocalized over the ligand backbone, which causes a higher electronic shielding of the protons. This effect is more pronounced for the gallium species **37**, where all signals are shifted most to a higher magnetic field.

From the spectra can be seen that after deprotonation the signal in the ^{1}H- and ^{13}C-NMR spectrum for the methylene bridge are significantly shifted downfield. More precisely, the former chemical shifts of H1’ and C1’ in **32** were located at 4.85 ppm / 34.38 ppm and

after successful conversion they result in chemical shifts of 5.76 ppm / 71.35 ppm in **35** and 5.58 ppm / 70.09 ppm in **37**.

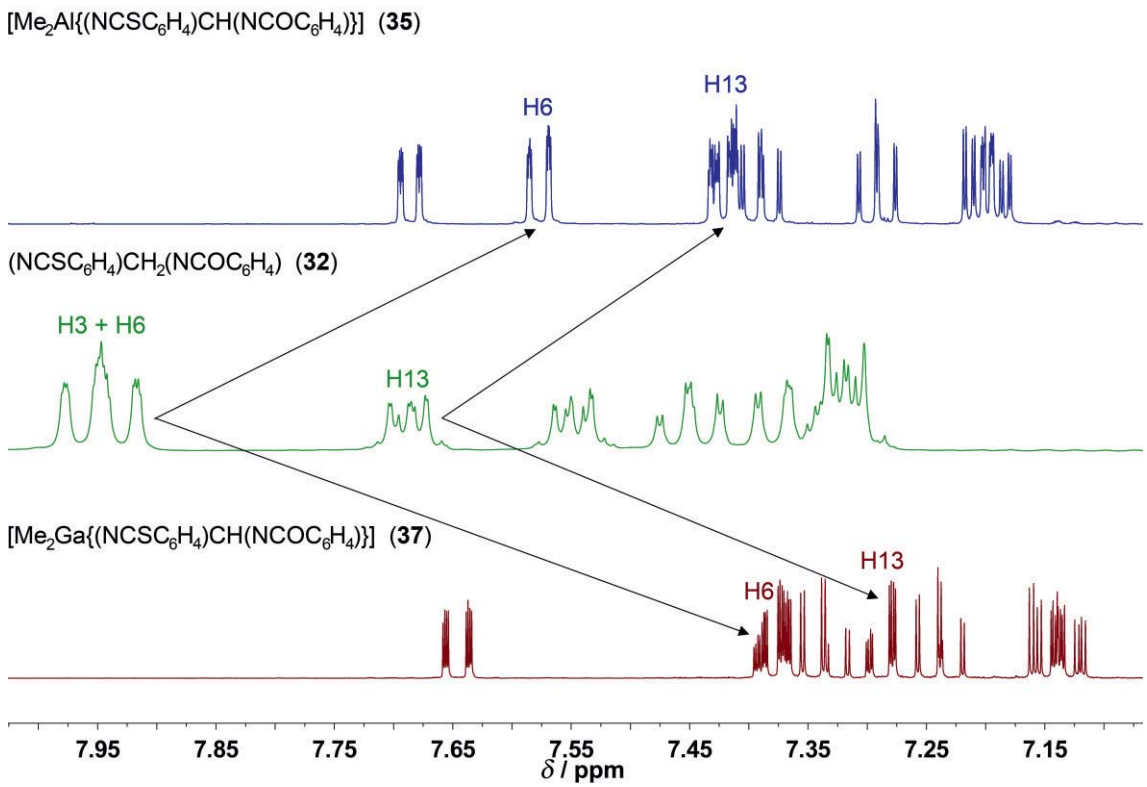

Spectrum 2-8: Overlay of the ^{1}H-NMR spectra (THF-d_8, rt) of the parent ligand system **32** and the metallated species **35** and **37**, for clarity reasons just the aromatic section is displayed.

To emphasize the differences in the spectra of the aluminium compound **35** and the gallium compound **37**, the signals of the terminal protons H3, H6 and H13 are highlighted (see Spectrum 2-8). The protons H6 and H13 seem to be most sensitive for the change of the size of the coordinated metal cation, because they are pointing directly to the side of the chelated metal centre. In contrast, H3 and H10 are pointing in the opposite direction and are therefore less affected by the metal. In the parent ligand **32**, the protons H3 and H6 show a quite similar chemical shift, but after metal coordination the signals of those protons are influenced in a different manner. In **35** and **37**, the change of the chemical shifts referring to the neutral ligand is more pronounced for the inwardly pointing protons H6 (**35**: $\Delta\delta$ = 0.37 ppm; **37**: $\Delta\delta$ = 0.56 ppm) and H13 (**35**: $\Delta\delta$ = 0.27 ppm; **37**: $\Delta\delta$ = 0.40 ppm) than for the outwardly arranged ones H3 (**35**: $\Delta\delta$ = 0.26 ppm; **37**: $\Delta\delta$ = 0.30 ppm) and H10 (**35**: $\Delta\delta$ = 0.13 ppm; **37**: $\Delta\delta$ = 0.17 ppm). Due to these findings, it can be assumed, that the size of the coordinated metal ion has a quite significant impact on the chemical shifts of the protons H6 and H13. In contrast to the Al^{3+} ion, Ga^{3+} owns a bigger ionic radius and more closed electron shells. Therefore, H6 and H13 are influenced more by higher electronic shielding in the case of **37** compared to **35**. This causes the corresponding resonance signals to be more upfield shifted.

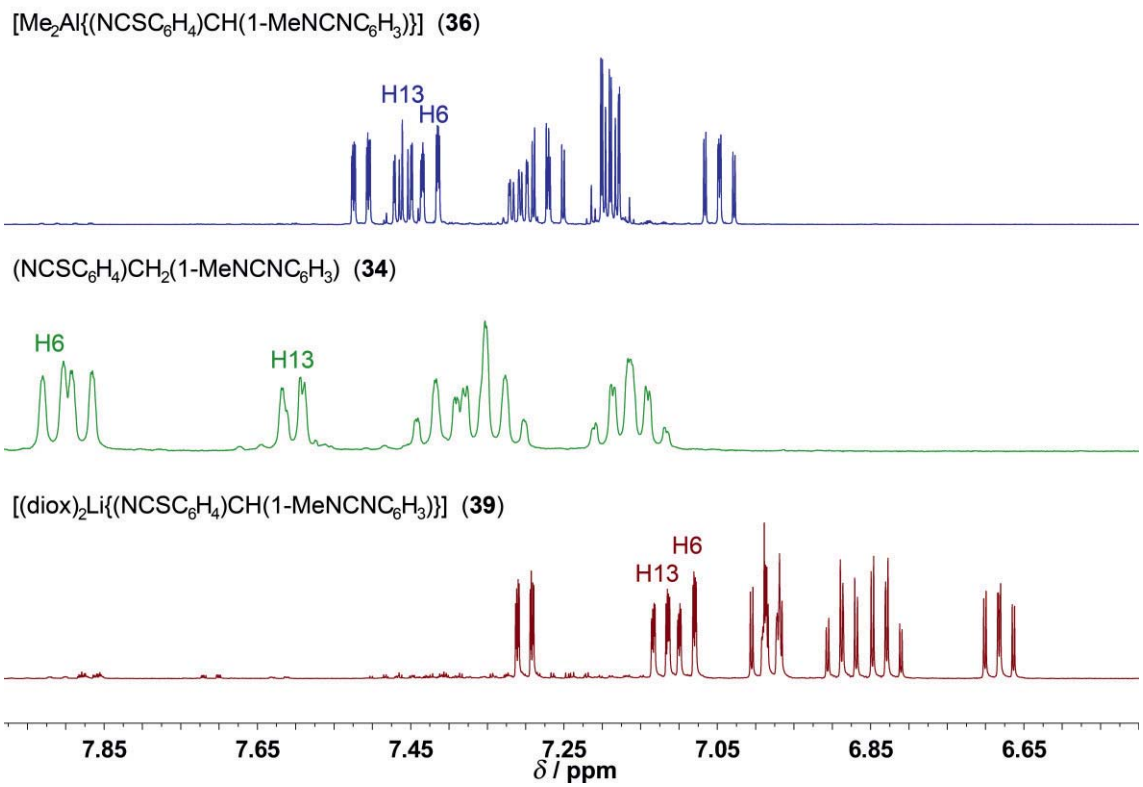

Spectrum 2-9: Overlay of the ^{1}H-NMR spectra (THF-d_8, rt) of the parent ligand system **34** and the metallated species **36** and **39**, for clarity reasons just the aromatic section is displayed.

Similar observations can be found for the changes of the chemical shifts upon metallation of the second ligand system **34**, where the benzoxazole moiety of **32** is formally replaced by a *N*-methyl benzimidazole residue. Concerning this kind of ligand, two metallated species could be synthesized in a moderate yield. In contrast to the first mentioned ligand system, here a dimethyl aluminium containing complex **36** and a lithiated compound **39** carrying 1,4-dioxane as Lewis donors were achieved. The recorded ^{1}H-NMR spectra of those three compounds are displayed in Spectrum 2-9 as an overlay. Following changes in the chemical shifts were noticed: the resonance signals of H6 (**36**: $\Delta\delta$ = 0.49 ppm; **39**: $\Delta\delta$ = 0.83 ppm) and H13 (**36**: $\Delta\delta$ = 0.13 ppm; **39**: $\Delta\delta$ = 0.48 ppm) are significantly larger than for that ones of H3 (**36**: $\Delta\delta$ = 0.36 ppm; **39**: $\Delta\delta$ = 0.58 ppm) and H10 (**36**: $\Delta\delta$ = 0.05 ppm; **39**: $\Delta\delta$ = 0.39 ppm). This result is in line with the observations made before, meaning that the protons at the side of the coordinated metal ion are interacting more with the coordinated fragment. Furthermore, it is evident that the changes of the chemical shift are higher in the case of the lithiated species **39**. This observation was expected due to the increasing ionic radii of the involved metal cations, which result in 0.39 Å for Al^{3+}, 0.47 Å for Ga^{3+} and 0.59 Å for Li^{+} each in fourfold coordination.[110] Like in **7**, the ionic radius of Li^{+} is bigger than that of Al^{3+} and therefore the inner protons H6 and H13 are more upfield shifted in the lithium containing species **39** than in **36**. Also analogue to the gallium complex, the chemical shifts of the lithium complex are in general most upfield shifted because of the bigger coordinated metal cation.

In contrast to **35**, the observed coupling pattern of **36** is partially more complex, because the protons of the benzimidazole moiety do not show clearly explainable *ddd* multiplet structures but rather signals of higher order, so that the coupling constants are not easy accessible. However, the spectrum of the lithiated compound **39** at the bottom of Spectrum 2-9 shows for both moieties (benzothiazole and benzimidazole) first order splitting pattern. This is due to the fact, that the difference of the chemical shift between the coupled protons is much larger than the coupling constant.

2.4 Lithiated Bisheterocyclo Methanides

In the course of the investigation of metallated bisheterocyclo methanides the lithium containing complexes of such ligand systems were synthesized as well. In addition to the dioxane stabilized asymmetric compound **39**, which was already partially discussed in the previous Chapter 2.3, further lithiated compounds were synthesized and structurally examined for following reasons: on the one hand, to fill the gap for the still pending group 1 metal complexes of this ligand type and on the other hand, to get precursor molecules for potential salt elimination reactions. The latter case was already partially discussed in Chapter 2.2.5 by means of the lithiated bis-(4-methylbenzoxazol-2-yl)-methanide **30**. Due to the subordinate role of this topic, just a short summary of the underlying syntheses and analytical data are given in the next subsection.

2.4.1 Syntheses of the Lithium Compounds

As depicted in Scheme 2-30, the synthesis of the lithium complexes is as straight forward as in the case of the earlier described group 13 metal complexes: to a toluene solution of the corresponding parent ligand, 1.1 equivalents of *n*BuLi in hexanes were slowly added at 0 °C. After deprotonation of the acidic methylene bridge, *n*butane is released and as a result thereof again the nacnac-like coordination motif is gained.

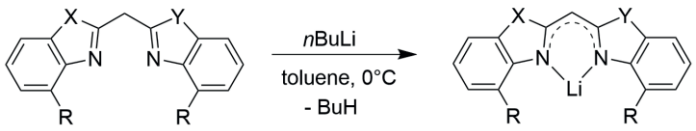

4 X = Y = O; R = H
5 X = Y = S; R = H
19 X = Y = O; R = Me
32 X = O; Y = S; R = H

17 X = Y = O; R = H
18 X = Y = S; R = H
30 X = Y = O; R = Me
38 X = O; Y = S; R = H

Scheme 2-30: Synthesis route for the lithiated benzannulated bisheterocyclo methanides **17**, **18**, **30** and **38**.

In addition to the above-mentioned synthesis route, a second lithiation route was carried out using 1,4-dioxane as polar solvent (see Scheme 2-31). This solvent was chosen to prevent precipitation of the lithium compounds during preparation, which readily occurs when toluene is applied. Therefore, 1,4-dioxane appeared to be a better solvent for crystallization than toluene, because the enhanced polarity presumably leads to the formation of well-soluble monomeric complexes instead of higher aggregates in solution.

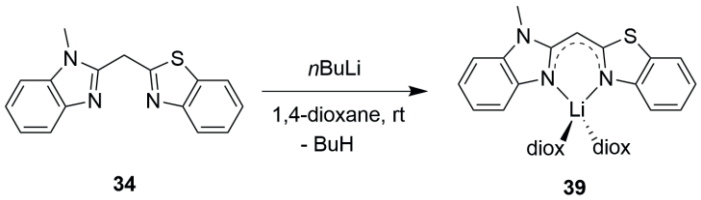

34 39

Scheme 2-31: Synthesis of the lithiated asymmetric bisheterocyclo methanide **39**.

This assumption was verified by using the asymmetrically substituted methane derivative **34**, which was dissolved in dioxane at room temperature, and *n*BuLi was added dropwisely to the resulting solution. After stirring over night, filtration and concentration of the mother liquor, the lithiated compound **39** could be isolated in a good yield of 78 % in the form of thin yellow needles, for which SCXRD was applied successfully.

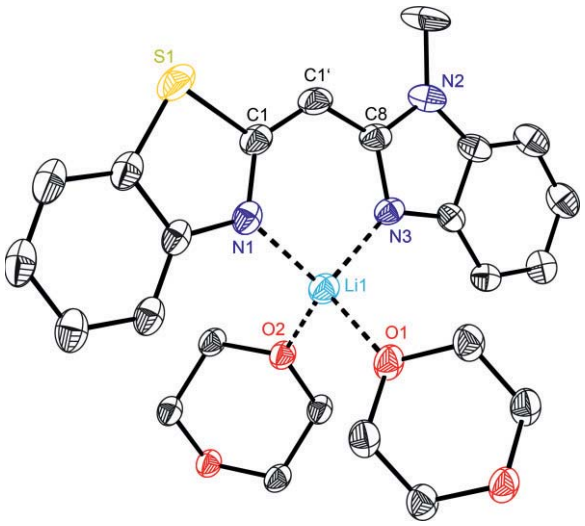

Table 2-39: Distances [pm] and angles [deg] of **39**.

C1'–C1	138.7(8)	N1–C1–C1'	128.3(5)
C1'–C8	141.1(7)	N3–C8–C1'	126.3(5)
C1–N1	134.3(7)	S1–C1–C1'	118.9(4)
C8–N3	139.1(7)	N2–C8–C1'	122.5(5)
C1–S1	178.4(5)	S1–C1–N1	112.8(5)
C8–N2	134.4(7)	N2–C8–N3	111.2(5)
N1–Li1	195.6(8)	C1–C1'–C8	124.5(4)
N3–Li1	195.5(8)	N1–Li1–N3	96.8(3)
Li1–O1	193.5(6)	O1–Li1–O2	99.7(3)
Li1–O2	194.1(6)		

Figure 2-44: Solid state structure of complex **39**.

Compound **39** crystallizes in the monoclinic space group $P2_1/c$ and the asymmetric unit consists of one lithiated ligand, two half dioxane molecules coordinating to the lithium cation and three additional dioxane molecules as remaining lattice solvent (see Figure 2-44). Lattice solvent and positional disorder are not depicted in the shown crystal structure. Analogue to the previously discussed crystal structures of the asymmetric methane derivatives (see Chapter 2.3), the whole ligand framework is positionally disordered (*sof*: 0.76). However, this time the disordered ligands are not covering completely the same positions, because both parts, which are 180 deg rotated against each other, are slightly displaced. In addition, the dioxane molecules, which are incorporated as lattice solvent, are disordered to a high degree due to the flexibility of the molecule's framework. Similar observations were previously made in the case of $[(thf)_2Li\{(1\text{-}MeNCNC_6H_4)_2CH\}]$, where THF molecules as lattice solvent show a comparable disorder phenomenon.[101a] The quality of the investigated crystal structure of **39** is just barely for performing struc-

tural comparisons because of the high degree of disorder. Both coordinated dioxane molecules are shared by lithium complexes in a bridging manner to give a chain-like coordination motif in the solid state.

Owing to the hybrid nature of the asymmetric ligand system in **39**, which consists of the bis-(*N*-methylbenzimidazol-2-yl)-methane ligand **2** and the bis-(benzothiazol-2-yl)-methane ligand **5**, the crystal structures of the corresponding lithium complexes are similar. Due to the lack of the crystal structure of [Li{(NCSC$_6$H$_4$)$_2$CH}] **18**, the almost closely related lithiated species [(thf)$_2$Li{(1-MeNCNC$_6$H$_4$)$_2$CH}], carrying two benzimidazole moieties, is taken into account for discussion of the crystal structures.[101a] The main difference between those structures is the donating solvent (THF instead of dioxane). In both cases the ligand framework is nearly planar (averaged 3.2 deg vs. 1.9 deg in **39**), but the deviation of the Li^+ from the chelating C_3N_2 plane differs much (averaged 15.0 pm vs. 1.9 pm in **39**). The determined N1–Li1–N3 bite angle of 96.8 deg and the C1–C1'–C8 backbone angle of 124.5 deg in **39** are quite similar to the obtained values in [(thf)$_2$Li{(1-MeNCNC$_6$H$_4$)$_2$CH}] (96.1 deg and 124.0 deg). The O1–Li1–O2 angle results in 99.7 deg in **39**, whereas that angle is much wider in the homo disubstituted imidazole compound (105.5 deg). The observed decreased O1–Li1–O2 angle and Li···plane distance in **39** are presumably accompanied with the higher steric demand of the dioxane molecules and the resulting coordination chain, which compresses that angle and forces the lithium cation more into the plane of the metalla heterocycle.

In comparison to the literature known lithiated bis-(pyrid-2-yl)-methanide species [(thf)$_2$Li{(2-NC$_5$H$_4$)$_2$CH}], also some similarities can be observed. The average N–Li distance was determined to a value of 197.0 pm and the bite angle results in 96.4 deg, while the O1–Li1–O2 angle involving the donating THF molecules is 98.9 deg.[83a, 83c, 118] Furthermore, the lithium cation is nearly placed within the plane of the metalla heterocycle also seen for the asymmetrical substituted methanide **39**. Regarding to these parameters, the observed coordination geometry in **39** is almost comparable to that one of the corresponding bis-(pyrid-2-yl)-methanide.

2.4.2 NMR Spectroscopic Investigations

It was not possible to obtain single crystals of those compounds suitable for SCXRD experiments except of **39**, so that the recorded analytical data are mainly limited to NMR spectroscopy in solution. Spectrum 2-10 shows an overlay of the recorded ^{1}H-NMR spectra for the above-mentioned lithiated species **17**, **18**, **30** and **38**. The following observations can be stated: all aromatic signals are shifted towards a higher magnetic field in comparison to their parent ligand system due to the enhanced electron density caused by the lone pair's delocalization. In the cases of compounds **17**, **18**, **30** and **38** the resolution of the signal sets is enhanced and their chemical shift changed quite significantly in comparison to the parent ligand systems. After deprotonation and lithiation of **17**, clearly two triplets for the protons H4/H5 and two doublets for the terminal protons H3/H6 were observable in the ^{1}H-NMR spectrum. In contrast to the ^{1}H-NMR spectrum of **4**, the resonance signals are much more defined and separated due to the complexation, which re-

stricts the motion of the heteroaromatics by fixed Li coordination of the endocyclic nitrogen donors. The same observation is valid for **18**, in which the distances in between the two doublets and triplets is increased compared to **5**, indicating again that the chemical environment of each proton is more diverse due to the complex formation. Especially, the ^{1}H-NMR spectrum of **38** should be highlighted at this point, because it can be seen as a mixture of **17** and **18** due to the presence of one benzoxazole and one benzothiazole unit. This leads to a merged chemical shift of the remaining bridge proton H1' of 5.11 ppm (**17**: 4.80 ppm; **18**: 5.38 ppm). In analogy to the related $AlMe_2$ and $GaMe_2$ complexes **35** and **37** (see Chapter 2.3), a distinct assignment of the underlying coupling constants to the particular protons is feasible due to the well resolved signal structure.

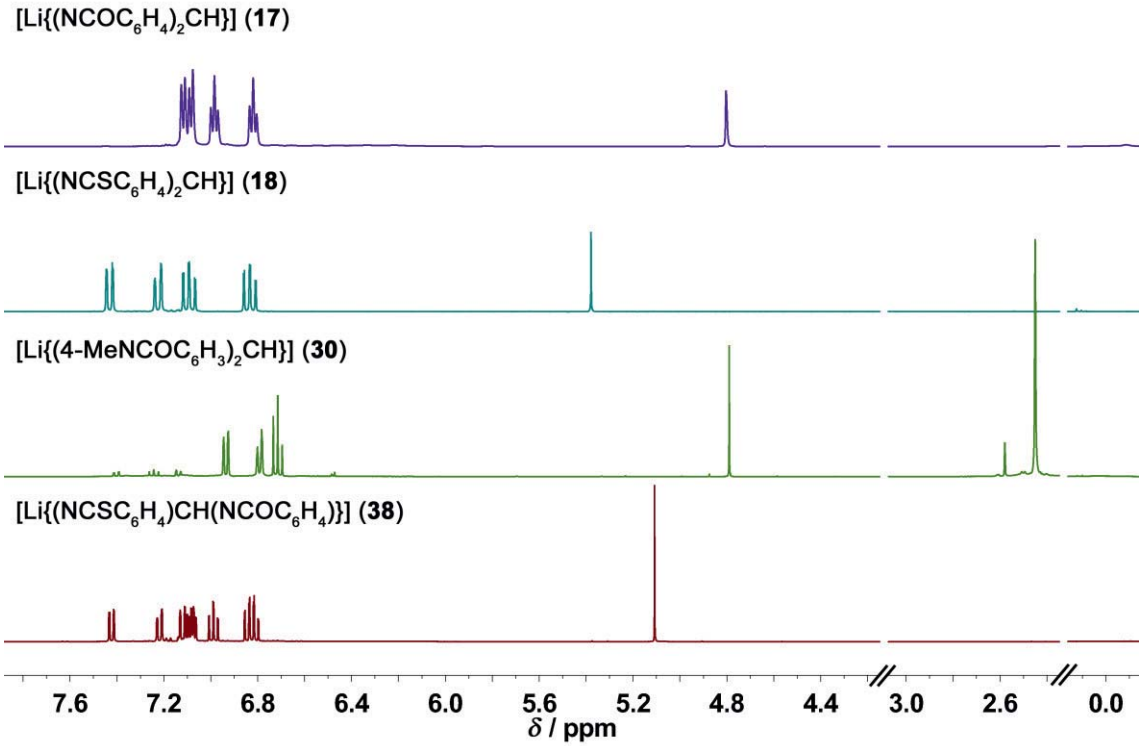

Spectrum 2-10: Overlay of the ^{1}H-NMR spectra (THF-d_8, rt) of the lithiated ligand systems **17**, **18**, **30** and **38**, for clarity reasons the solvent signals are not displayed. The spectra of **30** and **38** contain minor contaminations of the starting material.

To complete the NMR investigations of the lithiated compounds, Spectrum 2-11 shows the overlay of the corresponding ^{13}C-NMR spectra of the four discussed species. First of all, the signals of each spectrum match well to the estimated structure of the molecules. Therefore, just a short description of two characteristic resonance signals within the recorded ^{13}C-NMR spectra will be discussed afterwards: the bridging carbon atom C1' and the neighbouring quaternary ones C1/C8, which each exhibit the highest observed low-field shift.

Table 2-40: Selected ^{7}Li, ^{13}C and ^{15}N-NMR chemical shifts of **17**, **18**, **30**, **38** and **39** and their parent ligands.

compound	δ(C1/C8) [ppm]	δ(C1') [ppm]	δ(N1/N2) [ppm]	δ(Li1) [ppm]
[Li{$(NCOC_6H_4)_2CH$}] (**17**)	171.2	57.4	−201.4	1.89
$(NCOC_6H_4)_2CH_2$ (**4**)	161.5	29.6	−133.6	–
[Li{$(NCSC_6H_4)_2CH$}] (**18**)	167.1	80.1	−157.1	2.26
$(NCSC_6H_4)_2CH_2$ (**5**)	166.7	39.2	−65.0	–
[Li{$(4\text{-}MeNCOC_6H_3)_2CH$}] (**30**)	170.6	57.2	−203.7	2.03
$(4\text{-}MeNCOC_6H_3)_2CH_2$ (**19**)	160.6	29.7	−135.9	–
[Li{$(NCSC_6H_4)CH(NCOC_6H_4)$}] (**38**)	169.0 / 169.3	68.7	−160.0 / −198.7	0.35
$(NCSC_6H_4)CH_2(NCOC_6H_4)$ (**32**)	164.6 / 163.0	34.4	−64.4 / −132.4	–
[Li{$(NCSC_6H_4)CH(1\text{-}MeNCNC_6H_4)$}] (**39**)	167.4 / 157.8	68.5	−168.4 / −190.4	2.37
$(NCSC_6H_4)CH_2(1\text{-}MeNCNC_6H_4)$ (**34**)	167.4 / 151.2	33.8	−67.7 / −132.5	–

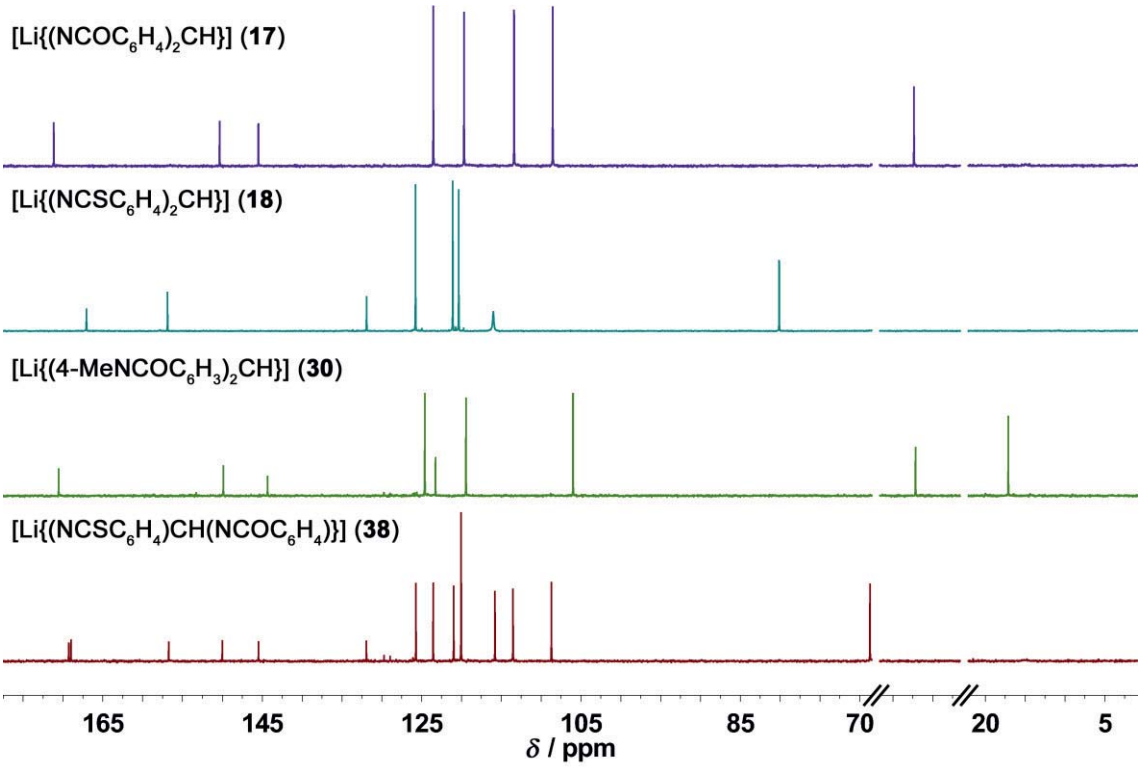

Spectrum 2-11: Overlay of the ^{13}C-NMR spectra (THF-d_8, rt) of the lithiated ligand systems **17**, **18**, **30** and **38**, for clarity reasons the solvent signals are not displayed. The spectra of **30** and **38** contain minor contaminations of the starting material.

The influence of the lithiation on the corresponding chemical shifts is listed in Table 2-40 as an overview with direct comparison to the parent ligand systems. The carbon atoms C1/C8, which are connected to two heteroatoms within the heterocycle, are shifted most towards low magnetic field. In the case of the resonance signal of C1/C8 and C1', the lithiation leads in each case to a significant low field shift compared to the neutral starting

material. The change of the chemical shift of the deprotonated methylene bridge is remarkably more effected. Furthermore, Table 2-40 involves also the ^{15}N-NMR spectroscopic shifts of the endocyclic imine nitrogen donor atoms N1/N2. The deprotonation and subsequent coordination of the lithium cation causes a significant shift of the resonance signal to higher magnetic field, because the electron density of those coordinating nitrogen atoms is increased due to delocalization of the negative charge. The observed chemical shifts for the coordinated lithium cations are shown in the last column of Table 2-40 as a proof for the fact, that the investigated lithium complexes stayed intact while measuring the spectra.

2.5 Bisheterocyclo Amines

Major parts of this section were published in: David-Raphael Dauer, Melchior Flügge, Regine Herbst-Irmer, Dietmar Stalke, Bis-(benzothiazol-2-yl)-amines and their metal amides: a structural comparison in the solid state, *Dalton Trans.* **2016**, *45*, 6136–6148.[116]

Catching up the discussion of bisheterocyclo methanes and methanides in previous chapters, at this point a switch to the corresponding amines is processed. By replacing the central CH_2 bridge by the isovalent NH building block,[119] a new class of bisheterocyclo amines will be developed. These new amine species presented in this chapter are comparable to the secondary phosphane $(NCSC_6H_4)_2PH$,[88, 91a, 91e, 91f, 94] because the linker unit is just replaced by the lighter congener of phosphorus. Despite of this, they offer also the possibility of making structural comparisons with dipyridyl amine,[82, 85b, 85c] because in this case the linker unit stays the same whereas the heterocyclic compounds are changed. Thus, the bis-(benzothiazol-2-yl)-methane derivatives (see Chapter 2.1) offer the chance to study appropriately the influence of either the bridging moiety or the different heteroaromates on the alignment in the solid state and especially the metal chelating abilities upon deprotonation.

2.5.1 Ligand Syntheses

As depicted in Scheme 2-32, the synthesis of the parent ligand systems **40** – **43**, which are homo-disubstituted with either benzoxazole or benzothiazole moieties, obviously differs from that one of the related equi-structural methane derivatives (see Scheme 2-2). In contrast to the synthesis of the corresponding symmetrically substituted bisheterocyclo methanes, where a cyclocondensation of two aniline derivatives and a C_3-linker takes place to generate the fused heterocycles,[95] the synthesis route shown in Scheme 2-32 has to be followed to obtain the symmetrically substituted amines.

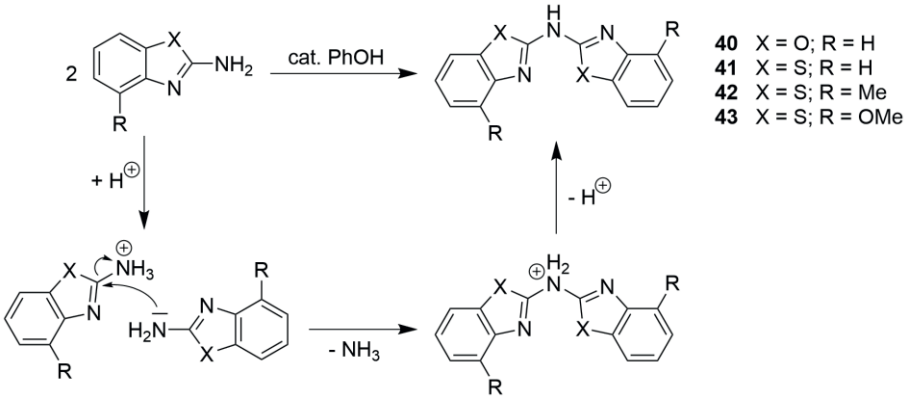

Scheme 2-32: Synthesis route of the parent amine ligand systems **40** – **43**.

For the synthesis of the parent ligand systems **40** – **43**, two equivalents of the appropriate substituted 2-aminobenzoxazole or 2-aminobenzothiazole and substoichiometric amounts

of phenol (1.4 eq.) were heated to reflux for several hours and afterwards ethanol was poured into the reaction mixture to trigger the precipitation of the products and remove phenol. A proposed mechanism for this reaction is described in the lower part of Scheme 2-32: by heating up the reaction mixture to the boiling point of phenol (182 °C), it becomes liquid and serves in this reaction as a solvent under refluxing conditions. Furthermore, the phenol serves as mild acid and ensures catalytical protonation of the starting material. Hence, a nucleophilic attack of a second unprotonated amine at the 2-position is feasible, because ammonia is released as a good leaving group at the elevated temperatures. After back formation of the catalytic amounts of protons, the amines **40** – **43** were generated.

2.5.2 Structural Comparison of the Neutral Ligands

It was possible to synthesize and characterize the four different ligands **40** – **43** (see Scheme 2-32), which should be further investigated in the following part especially in terms of the molecular structures in the solid state. The benzothiazole containing amines **41** – **43** could be collected in quite moderate yields and crystals suitable for X-ray crystallographic studies were grown from toluene. Due to the poor yields and bad solubility in common organic solvents, no crystalline material for further SCXRD investigations of bis-(benzoxazol-2-yl)-amine **40** was obtained. The structural comparison of this class of ligand systems is limited to the crystal structures of the three bis-(benzothiazol-2-yl)-amine derivatives, which enables to study the ligand's arrangement in the solid state in more detail.

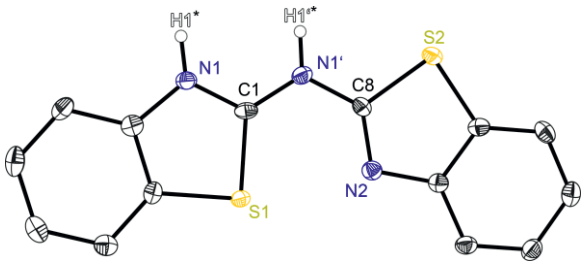

Figure 2-45: Solid state structure of ligand **41**.

Table 2-41: Distances [pm] and angles [deg] of **41**.

N1'–C1	133.6(4)	N1–C1–N1'	121.2(2)
N1'–C8	136.7(4)	N2–C8–N1'	126.8(3)
C1–N1	133.1(4)	S1–C1–N1'	125.8(2)
C8–N2	130.1(4)	S2–C8–N1'	117.0(2)
C1–S1	176.0(3)	S1–C1–N1	113.0(2)
C8–S2	176.8(3)	S2–C8–N2	116.2(2)
N1'–H1'	77(5)	C1–N1'–C8	120.3(2)
N1–H1	76(5)		

Starting with compound **41** (see Figure 2-45), the following crystallographic facts can be mentioned: it crystallizes in the monoclinic space group $P2_1$ and the asymmetric unit contains one single molecule. In contrast to this, the amine **42** carrying additional methyl groups at the C_6-perimeter (see Figure 2-46) crystallizes in the triclinic space group $P\bar{1}$, wherein two molecules and half a toluene molecule on an inversion centre are located in the asymmetric unit, and the methoxy functionalized ligand **43** (see Figure 2-47) crystal-

lizes in the monoclinic space group *C*2/*c*. In the last case two molecules and one co-crystallized toluene molecule belong to the content of the asymmetric unit.

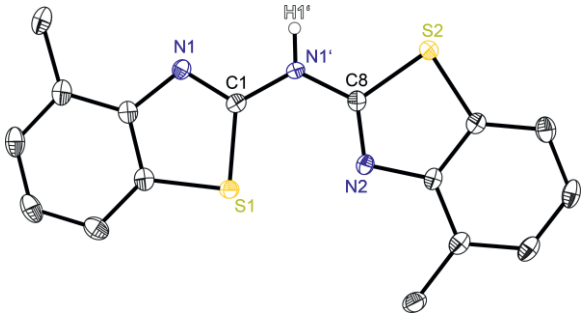

Figure 2-46: Solid state structure of ligand **42**.

Table 2-42: Distances [pm] and angles [deg] of **42**.

N1'–C1	137.0(2) 137.0(2)	N1–C1–N1'	120.31(14) 119.98(14)
N1'–C8	137.2(2) 137.6(2)	N2–C8–N1'	123.74(16) 124.02(15)
C1–N1	130.4(2) 131.0(2)	S1–C1–N1'	122.84(12) 123.13(11)
C8–N2	129.3(2) 129.3(2)	S2–C8–N1'	118.99(12) 118.45(12)
C1–S1	175.34(17) 174.69(16)	S1–C1–N1	116.85(12) 116.88(12)
C8–S2	175.95(18) 175.38(17)	S2–C8–N2	117.27(13) 117.52(12)
N1'–H1'	84.6(16) 84.3(16)	C1–N1'–C8	124.82(14) 124.96(14)

Due to the presence of two molecules in the asymmetric unit, for each parameter two values are given.

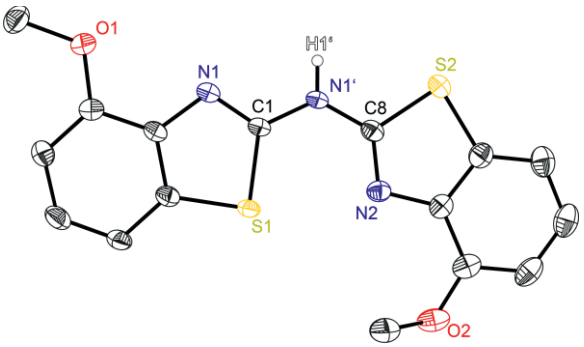

Figure 2-47: Solid state structure of ligand **43**.

Table 2-43: Distances [pm] and angles [deg] of **43**.

N1'–C1	136.5(2) 136.5(2)	N1–C1–N1'	120.97(17) 120.78(16)
N1'–C8	136.0(3) 136.6(2)	N2–C8–N1'	124.96(18) 124.84(17)
C1–N1	129.7(2) 130.5(2)	S1–C1–N1'	122.21(14) 122.52(13)
C8–N2	129.7(2) 128.6(2)	S2–C8–N1'	117.76(14) 118.20(14)
C1–S1	175.51(19) 174.68(19)	S1–C1–N1	116.78(14) 116.70(13)
C8–S2	174.8(2) 175.12(19)	S2–C8–N2	117.28(15) 116.95(14)
N1'–H1'	84.2(19) 84.4(19)	C1–N1'–C8	125.80(17) 125.37(16)

Due to the presence of two molecules in the asymmetric unit, for each parameter two values are given.

On closer examination it is obvious, that all parent amine based ligand systems **41** – **43** adopt a nearly planar arrangement in the solid state (see Figure 2-45 to Figure 2-47), in which the heteroaromatic residues are pointing in the opposite direction. This arrangement in the solid state is quite different from the ones of the corresponding methane derivatives, especially the benzothiazole substituted methane **5**, because the bisheterocyclo methanes showed in each case a distorted tetrahedral environment around the bridging sp^3-hybridized carbon atom. In theory, the isovalence-electronic replacement[119] of the methylene bridge by a secondary amine should also retain the sp^3-hybridization of that linking nitrogen atom, which is bonded to the two quaternary *ipso*-carbon atoms of the benzothiazole units and to one hydrogen atom. This trivalent nitrogen atom is expected to

be sp^3-hybridized considering the lone pair, but contrary to the expectations all amines show a planar alignment usually appearing in the case of a sp^2-hybridization. The angular sum around the bridging nitrogen atom with respect to the *ipso*-carbon atoms and the amine hydrogen atoms, which were each freely refined by taking their positions from the difference Fourier map, gives 360(2) deg for **42** and **43**, also supporting the sp^2-hybridization of the central nitrogen atom. This interesting aspect of the correct hybridization's elucidation is continued later on. At this point another remarkable feature of the solid state structures should be noticed. All ligands **41** – **43** display a clear preference for generating opposite disposed heteroaromatic residues as mentioned before. To establish an appropriate nomenclature for the arrangement of those moieties a *cis-trans* classification was used, which is depicted in Scheme 2-33 (in analogy to Scheme 1-13).

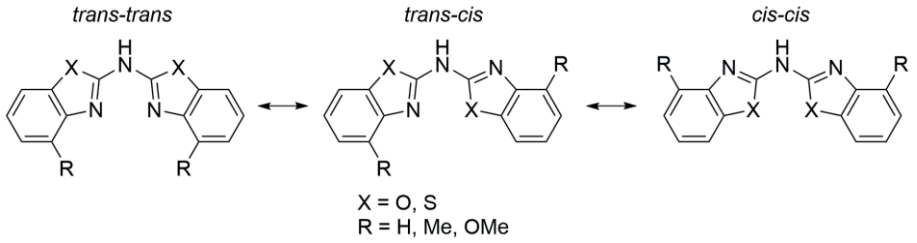

Scheme 2-33: Elucidation of the three possible configuration isomers of the twice heterocyclic substituted amines **40** – **43**.

As depicted in Scheme 2-33, there are three different configuration isomers conceivable, because each benzothiazole moiety can adopt in such a planar setting either the *cis* or the *trans* aligned orientation. This nomenclature is based on the earlier structural investigations of related ligand systems like bis-(pyrid-2-yl)-phosphanides[85c] as well as -amides[85a] and is distinguished by the arrangement of the highest priority atom, with respect to the partially existent C_{ipso}=N_{bridge} double bond and the other heterocycle. By means of this, a *trans-trans* alignment (see Scheme 2-33, *left*) as in the case of the metallated bisheterocyclo methanides can be achieved, where the nitrogen atoms are preorganized for building up a suitable coordination in a chelating manner and the residues at the C4-position are pointing inwards to the same direction. At the right side of Scheme 2-33, the counterpart to this motif, the *cis-cis* isomer, is depicted. In this case, both heteroaromatic nitrogen atoms and the bridging one are aligned to one single side and the substituents at the benzannulated perimeter are facing outwards. In the middle of Scheme 2-33, the *trans-cis* configuration isomer shows a hybrid species of the earlier mentioned ones, where one endocyclic nitrogen atom is pointing upwards and the other one downwards. By comparing these possible alignments to the experimentally determined solid state structures from **41** – **43**, the *trans-cis* conformation is apparently the most stable one, because each ligand system preferred this kind of orientation.

To continue the discussion about the reasons for the planarity of those amine ligand platforms, there is the possibility for the presence of an imine-enamine tautomerism depicted in Scheme 2-34 as well. Each conformer is able to form in this context three tautomeric

resonance structures, which differ from each other just by the position of the amine hydrogen atom. Assuming the *cis-trans* conformation as starting point, the hydrogen atom can be located either at the central bridging nitrogen atom N_{bridge} or at one of the heteroaromatic ones N_{het}. Depending on where the hydrogen atom is placed, the tautomerisation of the corresponding C_{ipso}=N double bonds is accompanied.

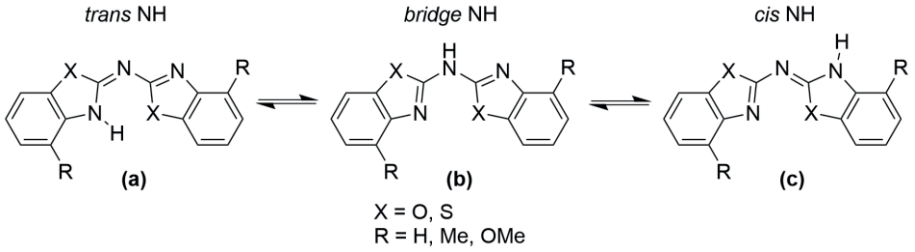

Scheme 2-34: Imine-enamine tautomerism within the parent ligand systems **40** – **43** in the case of the *trans-cis* configuration isomer.

A formal description of the three different imine-enamine tautomers in Scheme 2-34 results in following binding situations: starting from form **(b)** a bridging NH functionality and two C_{ipso}=N_{het} double bonds are present. Due to the linking sp^3-hybridized nitrogen atom and the interruption of the conjugation, a clear electronic separation of the two heteroaromatic residues is achieved. In both other cases **(a)** and **(c)**, one C_{ipso}=N_{het} and one C_{ipso}=N_{bridge} double bond are available, while the amine hydrogen atom is located at one heterocycle. In contrast to from **(b)**, formally one former endocyclic C_{ipso}=N_{het} double bond is tautomerized to an exocyclic C_{ipso}=N_{bridge} double bond of the linker unit. In these tautomeric resonance structures **(a)** and **(c)**, the bridging moiety is sp^2-hybridized and the ring-internal amine group becomes sp^3-hybridized. Such kind of tautomerism was also discussed in the context of heterocyclic substituted secondary phosphanes[94] and the well-known bis-(oxazoline)s.[120]

The evidence for this tautomerism is empirically confirmed by the crystal structure of **41** (see Figure 2-45), because upon refinement accumulated electron density at the nitrogen atoms N1 and N1' could be observed (see Figure 2-48). This remaining electron density at those positions suggests the assumption that a bridging or endocyclic secondary amine functionality is feasible and therefore the tautomeric forms **(b)** and **(c)** contribute in equal shares to explain the experimental findings. Apart from this, there is remaining electron density found directly on the bonds arising from the used refinement model, which does not consider bonding electrons. The treatment of the resulting positional disorder of the hydrogen atoms H1 and H1' gives a ratio of approximately 2 : 1, so that a slight dominance of form **(c)** can be estimated. However, these values are not that reliable, because the disorder refers to the position of an electron-poor hydrogen atom, which causes the estimated standard deviation of the site occupation factors to be increased.

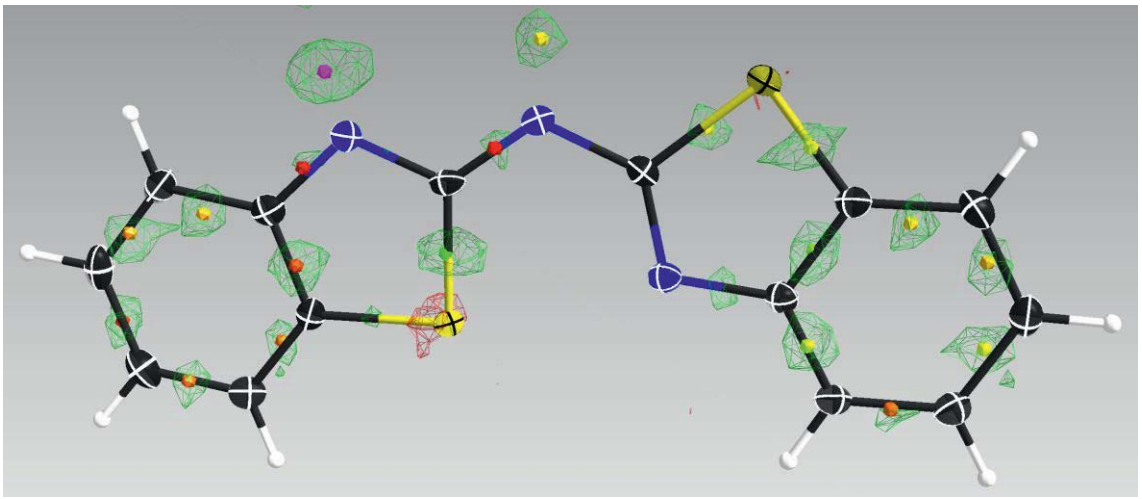

Figure 2-48: Fourier-density-difference map for **41** for the NH disorder (isolevel F_o–F_c = 0.17 e Å^{-3}).

Going on with the detailed discussion of the molecular structure of **41**, it is obvious, that C_{ipso}–N_{bridge} and C_{ipso}–N_{het} bond lengths show significant differences (see Table 2-41). In the case of the bonds concerning the bridging nitrogen atom N1', the determined C8–N1' distance is about 3 pm elongated in comparison to the C1–N1' distance (136.7(4) pm vs. 133.6(4) pm) and the ring-internal C1–N1 and C8–N2 distances differ by almost the same value (133.1(4) pm vs. 130.1(4) pm). Hence, an alternating pattern of quite reasonable C–N single (C1–N1, C8–N1') and C=N double bonds (C8–N2, C1–N1') can be estimated accompanied with the predominant influence of form **(c)** in Scheme 2-34. The experimentally obtained values for the C_{ipso}–N bond lengths deviate slightly from literature-known C(sp^2)–N(sp^3) single (143 pm) and C(sp^2)=N(sp^2) double bonds (129 pm), which also confirms the partially contribution of the resonance structure **(b)**.

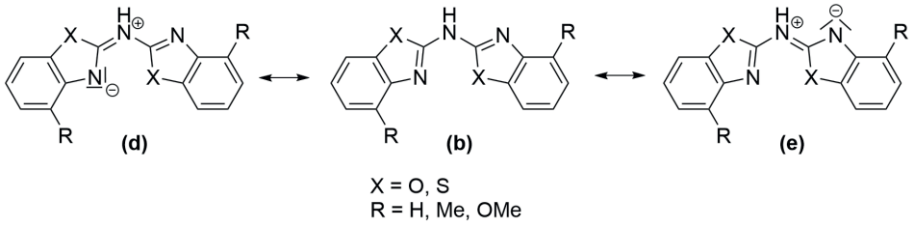

(d) (b) (e)

Scheme 2-35: Mesomeric resonance structures of the parent ligand systems **40** – **43** in the case of the *trans-cis* configuration isomer of the bridge NH tautomer.

Because the presence of a second, disordered hydrogen atom could be verified by SCXRD in the case of **41**, the planarity in the ligand systems **42** and **43** maybe has some other contributing mesomeric resonance structures shown in Scheme 2-35. These mesomeric structures **(d)** and **(e)** represent two zwitter-ionic species, which could give a hint for the partial sp^2-hybridization of the central nitrogen atom and the associated planarity of the whole ligand framework. Having a closer look at the C_{ipso}–N bond lengths within the

structures of **42** and **43**, no significant variation could be observed: C1–N1' 137.0(2) pm, C8–N1' 137.4(2) pm and C1–N1 130.7(2) pm, C8–N2 129.3(2) pm for **42**; C1–N1' 136.5(2) pm, C8–N1' 136.3(3) pm and C1–N1 130.1(2) pm, C8–N2 129.2(2) pm for **43**. In contrast to the quite convincing difference in bond lengths observed for **41**, it can be concluded that the bonds concerning the central nitrogen atom are more pronounced as single bonds, whereas the ring-internal nitrogen atoms are rather doubly bonded due to the decreased bond lengths. Moreover, these pairs of bonds are almost comparable, so that the C_{ipso}–N_{bridge} or C_{ipso}–N_{het} distances in each compound are in good accordance within their standard deviation. Nevertheless, the observed bond lengths and planarity of the ligand framework support the evidence of other tautomeric or mesomeric resonance forms. Due to the superposition of several possible resonance structures, the formal C=N double bonds are slightly elongated, whereas the C–N single bonds are slightly contracted and N1' shows partial sp^2-character.

2.5.3 Hydrogen Bonding Properties of 41 – 43

Regarding to Scheme 2-34, the amine hydrogen atom can form distinct hydrogen bonds depending on its tautomeric position. As in form **(a)** the hydrogen atom is bonded to the nitrogen atom of the *trans*-aligned benzothiazole moiety, intramolecular hydrogen bonds towards the opposing chalcogen acceptor can occur. The other tautomeric forms **(b)** and **(c)**, where the amine hydrogen atom is located either at the bridging nitrogen atom or at that one in the *cis*-aligned heteroaromatic residue, should favour the formation of intermolecular hydrogen bonds to other neighbouring ligands in the solid state.

Because of the preferred *trans*-*cis* conformation of the parent ligand systems **41** – **43**, different stable intermolecular N–H···N bonded aggregates can be identified in their solid state structures.[121] Again, this property of generating stable hydrogen bridged donor-acceptor pairs is a special feature of the bisheterocyclo amines, which leads to a vital difference compared to the bisheterocyclo methanes. Furthermore, the possibility to form energetically advantageous hydrogen bonds with neighbouring molecules can be claimed as another reason for the planarity of the amine derivatives in contrast to the distorted tetrahedral bonding environment within the methylene bridged compounds **1**, **2**, **4**, **5**, **19**, **32** and **34**.

Table 2-44: Hydrogen bonding properties of **41** – **43**.

	aggregation	H1'···N1 [pm]	H1···N1' [pm]	N1···N1' [pm]	N1'–H1'···N1 [deg]	N1–H1···N1' [deg]
41	chain	215(5)	215(5)	291.0(4)	167(5)	177(6)
42	dimer	208.2(17) 203.3(17) 213.1(16)	–	292.0(2) 287.1(2) 296.9(2)	171.5(18) 170.4(18) 172.6(18)	–
43	tetramer	212(2) 210(2) 214(2)	–	292.6(2) 290.1(2) 295.1(2)	161(2) 159(2) 162(2)	–

The hydrogen bonding pattern of compound **41** is depicted in Figure 2-49 and the corresponding determined values for the resulting hydrogen bonds are given above in Table 2-44. In the solid state the free ligand bis-(benzothiazol-2-yl)-amine is organized in a way, that each molecule in crystal packing can develop two hydrogen bonding interactions. Therefore, **41** acts in equal shares as hydrogen donor as well as hydrogen acceptor, limited to the nitrogen atoms N1' and N1, which are pointing to the same side of the ligand system.

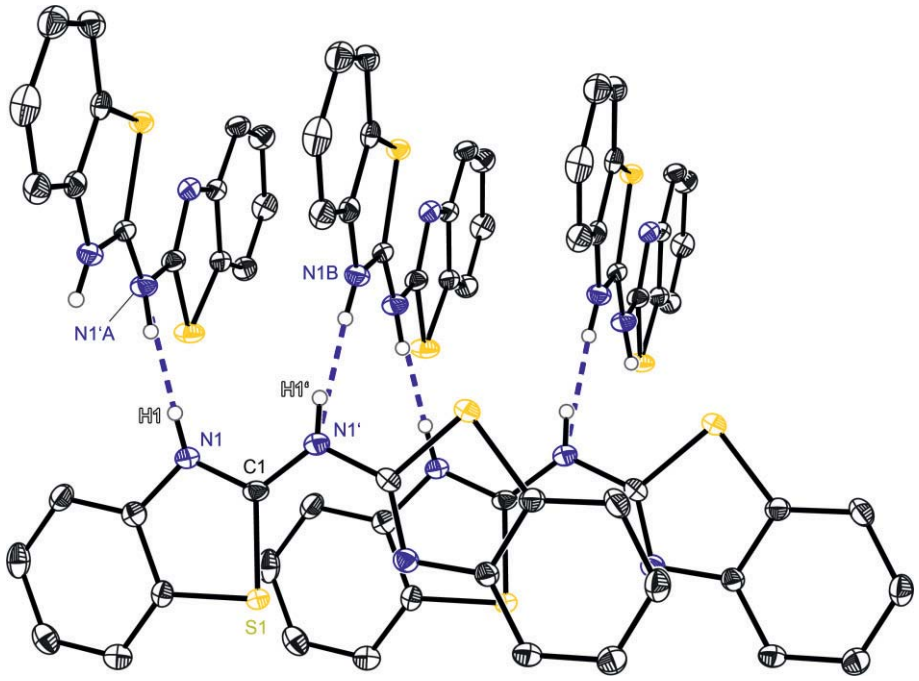

Figure 2-49: Hydrogen bonding pattern of **41**. (Symmetry transformations used to generate equivalent atoms: −x+1, y−1/2, −z+1 for counterpart B and −x+1, y+1/2, −z+1 for counterpart A).

As a result of this attractive, structure determining interaction, a two-dimensional chain of hydrogen bridged amines is formed, where each molecule serves as bridge for two other hydrogen bonded amines. The observed positional disorder of the amine hydrogen atom, which can either be located at N1' or N1 upon final crystallographic refinement, can originate from these strong intermolecular correlations, because the transannular distance between the hydrogen donor and acceptor is rather short (A···D: 291.0(4) pm) and the D–H···A angle results in a nearly linear coordination (D–H···A: 172(7) deg). Triggered by this advantageous arrangement in the solid state, the amine hydrogen atom can easily switch the position in between the donor-acceptor pair of N1' and N1, so that both tautomeric forms **(b)** and **(c)**, seen in Scheme 2-34, can be transferred into each other and no special preference is evident. Because the disordered hydrogen has two possible locations, it also can be refined as H1 bonded to the heteroaromatic N1 or H1', which belongs to the bridging N1'.

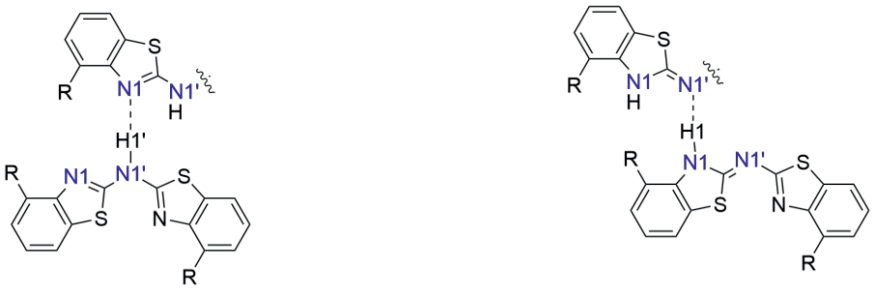

Scheme 2-36: Possible hydrogen donor and acceptor pairs: bridging nitrogen atom N1' as donor (*left*); endocyclic nitrogen atom N1 as donor (*right*).

As depicted in Scheme 2-36, two different hydrogen donor-acceptor pairs are feasible: on the one hand, N1 acts as a hydrogen donor, if the amine hydrogen atom is present as H1, and N1' of an adjacent molecule is the corresponding acceptor site. On the other hand, this relation is exactly inverted, if the hydrogen atom is present as H1', because in that case N1' is the donor functionality and N1 of another molecule acts as hydrogen acceptor. In summary, two different bonding situations are displayed in Table 2-44. Due to the positional disorder of that hydrogen atom, the estimated standard deviation is quite high and the freely refined positions of this insufficient scattering atom lead to a discrepancy of 10 deg in the both determined D–H···A angles (N1'–H1'···N1: 167(5) deg; N1–H1···N1': 177(5) deg).

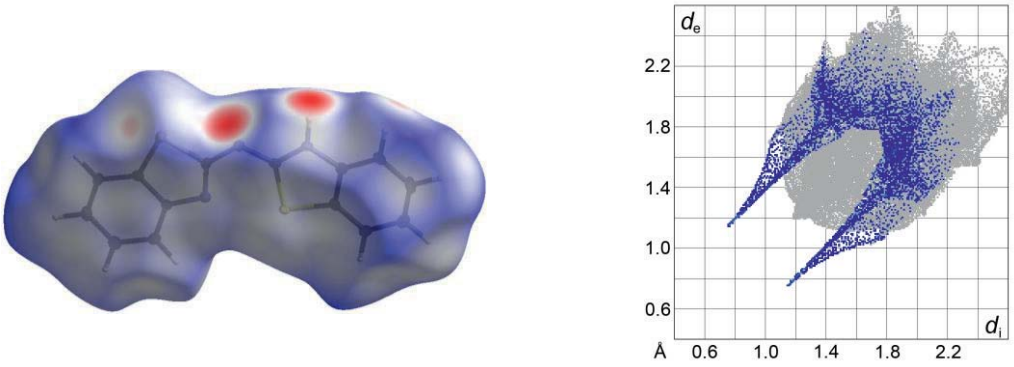

Figure 2-50: Hirshfeld surface[106] (*left*) and corresponding fingerprint plot[105, 106a, 107] for N···H interactions (*right*) generated for **41**, without taking the disorder of the amine hydrogen atom into account (just located at N1).

The corresponding Hirshfeld surface for **41** is shown in Figure 2-50 at left hand side. Due to the above-mentioned disorder of the NH proton either at N1 or N1', the surface was calculated for the species with the highest site occupation factor (at N1 as *cis*-NH like stated in Scheme 2-34). The resulting Hirshfeld surface indicates two very distinct closest intermolecular interactions highlighted as bright red spots. These spots represent the formation of the N1–H1···N1' hydrogen bonds, where the central nitrogen atom N1' acts as hydrogen acceptor and the endocyclic N1 as hydrogen donor. At the right side of Figure 2-50, the obtained fingerprint plot shows the presence of two clearly defined peaks, which

are ascribed to the occurring N···H interactions from the inside and the outside to the calculated surface. Once again, the positions of the peaks are an indicator for the observed N···H hydrogen bond distances.

In contrast to the hydrogen bonding situations of **1** and **2** discussed earlier (see Figure 2-5), the fingerprint plot in the case of the amine **41** shows very sharp peaks, which are clearly separated from the other occurring interactions of the molecule. In the case of **1** these peaks are slightly more pronounced compared to other C···H interactions.

Also in the other ligand system **42**, which carries additional methyl groups, the formation of hydrogen bonds plays a vital role as structure-determinating factor. This amine differs from the former mentioned ligand **41** just by the additional electron donating and sterical encumbering methyl groups at the C4-position of each heteroaromatic residue. The resulting hydrogen bonded aggregate in the solid state is smaller compared to that one of **41**. The amine proton is in this case exclusively bonded as H1' to the linking nitrogen atom N1'. Upon final crystallographic refinement, no evidence for a disorder of this atom at neither N1 of the *cis*-aligned benzothiazole nor N2 of the *trans*-aligned part was found. Having a closer look at the intermolecular interactions in the solid state, it is obvious that no chain-like hydrogen bonded amines can be detected, but rather discrete hydrogen bonded dimers are formed (see Figure 2-51).

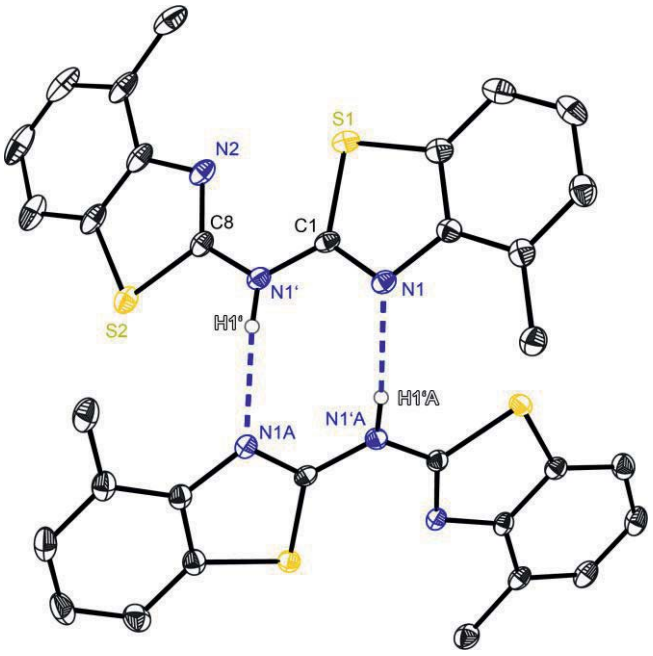

Figure 2-51: Hydrogen bonding pattern of **42**. (Symmetry transformations used to generate equivalent atoms: x, y−1, z for counterpart of H1'and x, y+1, z for counterpart of H1'A).

In that dimer N1' represents the hydrogen donor, while N1 of an adjacent amine molecule receives H1' as hydrogen acceptor. This interaction occurs twice at each dimeric species. As a consequence of having two different parent molecules as content of the asymmetric unit, also two corresponding D–H···A interactions are observed: the H1'···N1 distance

yields in 203.3(17) pm and 213.1(16) pm, respectively, and the generated N1'–H1'···N1 angle gives 170.4(18) deg and 172.6(18) deg, respectively (see Table 2-44).

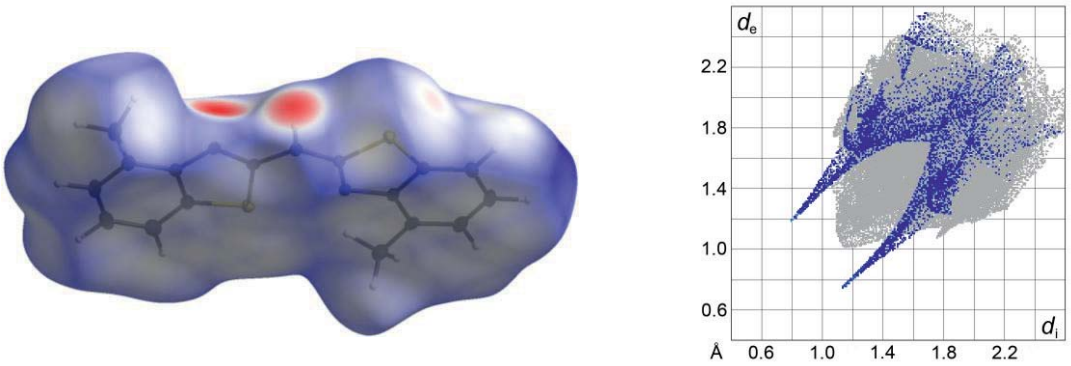

Figure 2-52: Hirshfeld surface[106] (*left*) and corresponding fingerprint plot[106a, 105, 107] for N···H interactions (*right*) generated for **42**.

The Hirshfeld surface representation of the amine ligand system **42** shows, as expected, again two red highlighted areas in the vicinity of the nitrogen atom N1 at the *cis*-aligned benzothiazole moiety and the bridging NH functionality (see Figure 2-52, *left*). As shown in the crystal packing pattern in Figure 2-51, that red areas reflect the closest intermolecular contacts by means of the observed N1'–H1'···N1 hydrogen bonds. The well-pronounced peaks in the fingerprint plot at the right hand side of Figure 2-52 emphasize the ligand's ability of forming beneficial hydrogen bonded dimers.

Contrary to the first impression of the dimer, displayed in Figure 2-51, both amine ligands are not aligned in a joint plane, which would be most beneficial for hydrogen bonding. However, both planes, consisting of one whole ligand framework, are twisted about 63.3 deg against each other. This twisting is presumably caused by the steric demand of the additional methyl groups at the annulated benzene perimeter. If both ligands would be arranged in one plane, the methyl group of the *cis*-aligned benzothiazole moiety of one molecule und the sulfur atom of the *trans*-aligned residue of the second molecule would gain an inauspicious close intermolecular distance (see Scheme 2-37).

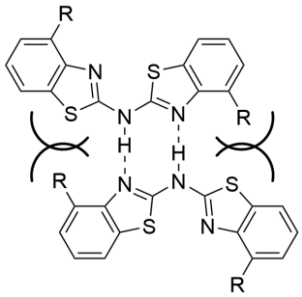

Scheme 2-37: Repulsive interactions within the formation of a hydrogen bonded dimeric species of **42**.

Similar to the earlier discussed bisheterocyclo amines **41** and **42**, the methoxy substituted amine derivative **43** exhibits interesting hydrogen bonding properties. In comparison to the both other observed aggregates in the solid state, this compound shows again another aggregation behaviour, whereas a tetrameric, cyclic arranged, hydrogen bonded species is formed (see Figure 2-54). As in the case of the methyl substituted derivative **42**, here the hydrogen atom is just present as H1' at the bridging position N1' as well. No other hint for the both other tautomeric forms is evident. Each ligand serves as hydrogen donor by means of N1' as well as hydrogen acceptor via N1. The four ligands in the tetrameric aggregate are arranged in a way, that each ligand splits up its hydrogen bonds towards two different neighbouring molecules like in **41**, one as acceptor and the other one as donor. The main difference between **41** and **43** is in their nature, that no infinite two dimensional chains are generated via hydrogen bonding, but rather discrete tetramers are formed by a grid-like stacking of a pair of two molecules. This means, two nearly parallel aligned ligands are capped with another two parallel aligned amines to give an almost perpendicular grid, in which the angles between the stacked ligand frameworks is 85.1 deg and 87.9 deg, respectively. The transannular N1···N1' distance results in 290.1(2) pm and 295.1(2) pm and is hence comparable to those observed in the molecular structures of the other amines. Having a determined averaged N1'–H1'···N1 angle of 161(2) deg, this structure features the most bent hydrogen bonds within this series of amines, which is an indicator for the higher strain induced by the formation of a tetrameric aggregate. Again, every time two pairs of values are given due to the presence of two molecules in the asymmetric unit.

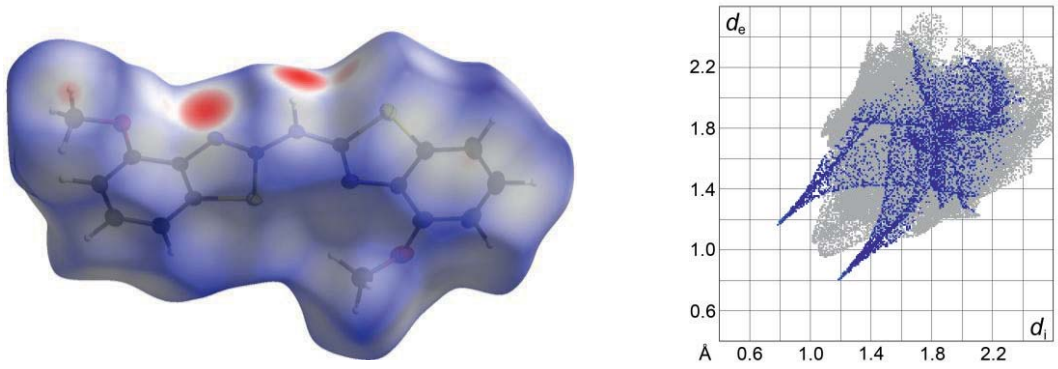

Figure 2-53: Hirshfeld surface[106] (*left*) and corresponding fingerprint plot[105, 106a, 107] for N···H interactions (*right*) generated for **43**.

On closer examination of the generated Hirshfeld surface for molecule **43** and the derived fingerprint plot, the same observations as in the previous cases of **41** and **42** can be made. The experimentally determined N1'–H1'···N1 hydrogen bonds are located at the Hirshfeld surface at the left side of Figure 2-53, highlighted as the closest interactions. Apart from the two corresponding sharp signals, which are nearly mirrored, a cumulated occurency frequency of quite short H···H distances can be detected in the space between those distinct signals. This fact is caused by the additional methoxy groups at the annulated benzene perimeter, which increase the steric demand of that ligand system. There-

fore, the protons attached to the OMe-moieties get in closer contact with the aromatic ring systems.

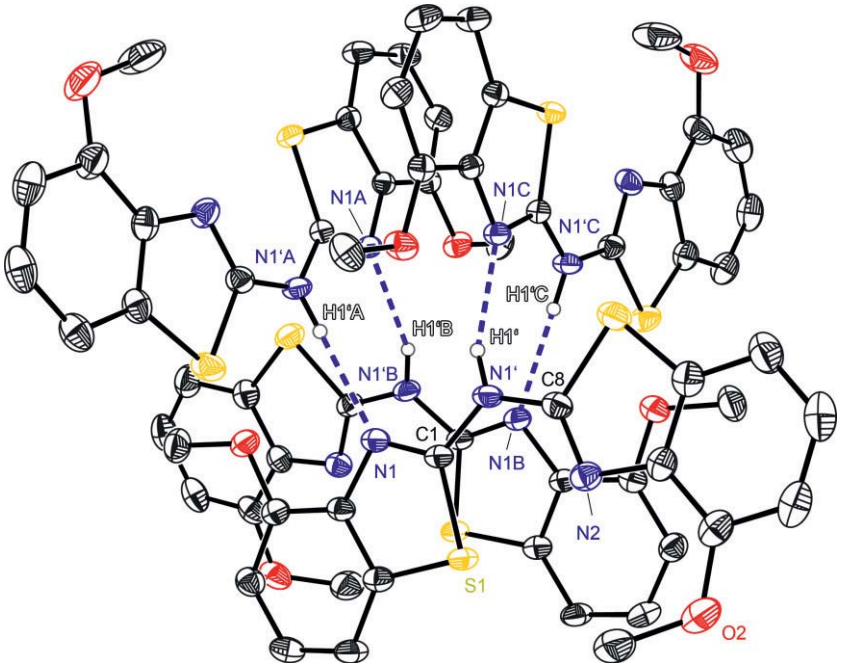

Figure 2-54: Hydrogen bonding pattern of **43**. (Symmetry transformations used to generate equivalent atoms: −x+1, y, −z+1/2 for counterparts B and C).

This broad peak arises within the series **41** < **42** < **43** of the different bisheterocyclo amines. In the case of the unsubstituted system **41**, the N···H interactions are dominating, whereas in the opposite case of **43** the difference in occurrence and spacing of N···H and C···H interactions is significantly smaller. These observations are in line with the increasing bulkiness of the considered ligand platforms (H < Me < OMe).

Although compound **42** has an increased steric demand compared to **41** and adopts a dimeric aggregation, for **43** it would be assumed to form a dimer as well. Presumably, the higher steric demand and the electron withdrawing properties of the methoxy moieties in comparison to **41** and **42** causes this molecule to achieve this rather disadvantageous arrangement in the solid state. Furthermore, the oxygen atoms of the methoxy groups could be suggested to be at least partially involved in hydrogen bonding, which could also be a further reason for this aggregation of higher order (see Figure 2-55). Referring to this, the methoxy groups of the *cis*-aligned part of the ligand own smaller thermal ellipsoids than those of the *trans*-aligned moiety, which shows the more pronounced rigidity of the first-mentioned ones. As a reason for this rigidity, a quite weak interaction of those oxygen atoms O1 towards the amine hydrogen atom H1’ can be postulated to form a five-membered ring, consisting of H1’ of one ligand and O1 as well as N1 of another ligand as acceptors. However, the experimentally obtained values for the oxygen involved hydrogen bridges show, that this kind of interaction can just be weak because of an averaged H1’···O1 distance of 263(2) pm and an averaged N1’–H1’···O1 angle of 116.6(19) deg. In

contrast to N1, acting as hydrogen acceptor, these values are significantly unfavourable due to an about 51 pm increased distance towards the hydrogen atom and a 44 deg acuter angle, but to some degree this interaction will contribute to the observed structure as depicted in Figure 2-55.

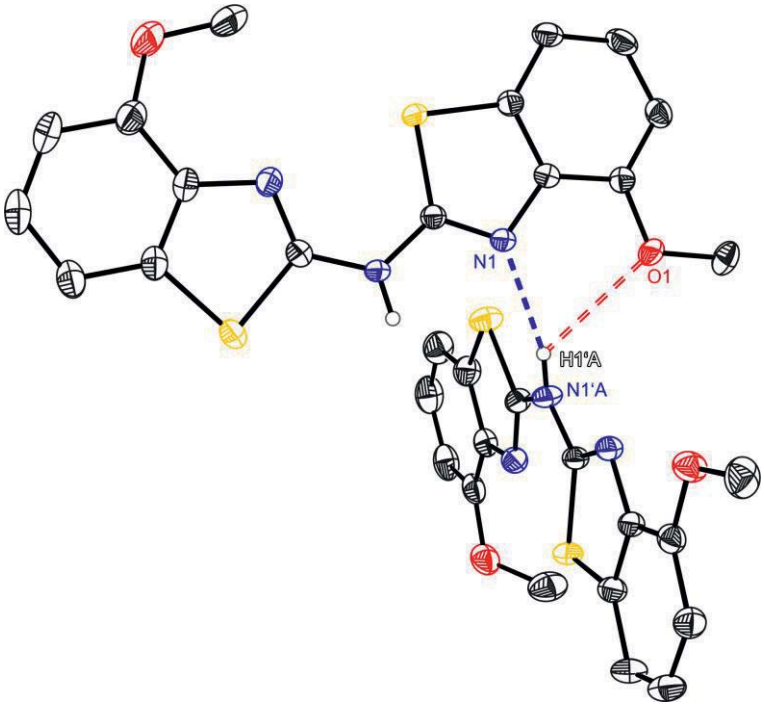

Figure 2-55: Hydrogen bonding pattern of **43** involving the methoxy groups as potential donor sites.

2.5.4 Syntheses of the Aluminium Complexes

To continue with the structural features of this kind of amine ligand systems, the corresponding amide metal complexes are investigated in detail. Therefore, a synthesis route analogue to the case of the related bisheterocyclo methanides,[95] shown in Chapter 2.1 or e.g. for the popular nacnac derivative $[Me_2Al\{(N(Dipp)C(Me))_2CH\}]$,[14i, 14l, 15] was applied. Deprotonation of the amine hydrogen atom is achieved by treating the parent ligands **41** – **43** with a slight excess of trimethyl aluminium and subsequently the amidic dimethyl aluminium complex is formed. Again, these reactions were carried out under Schlenk conditions at 0 °C with toluene as appropriate organic solvent and upon evolution of gaseous methane the Al(III) containing complexes could be synthesized (see Scheme 2-38).

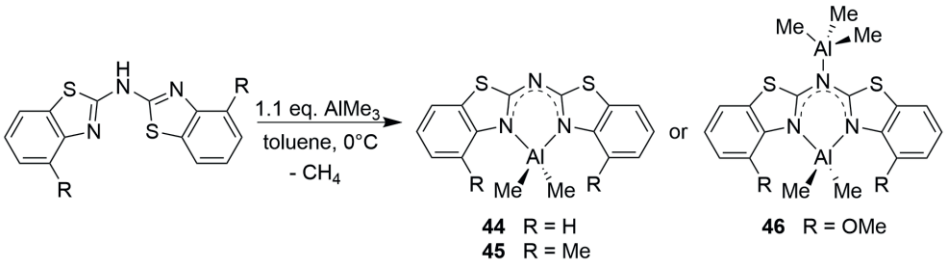

Scheme 2-38: Synthesis of the dimethyl aluminium containing compounds **44** – **46**.

Three different metallated species were isolated depending on the used parent ligand: compounds **44** and **45**, which differ just by the additional methyl groups at the heterocyclic side arms, show an isostructural arrangement in the solid state. In both cases, the dimethyl aluminium fragment is coordinated in a chelating fashion by the two endocyclic nitrogen atoms to form a nacnac-like six-membered metalla heterocycle. Surprisingly, in the case of the methoxy functionalized amide a different coordination behaviour could be observed. Presumably, impurities of the starting material led to a decreased amount of the ligand and caused the formation of **46**, where also the chelating abilities for the dimethyl aluminium fragment are present. But furthermore, a second Lewis acid by means of an additional $AlMe_3$ is coordinated by the bridging nitrogen atom in the backbone of the monoanionic ligand.

2.5.5 Structural Comparison of the Metal Complexes

For the parent bisheterocyclo amines and for the corresponding amides **44** – **46**, crystals suitable for application of X-ray diffraction could be obtained by crystallization from toluene solution. Starting with the metallated bis-(benzothiazol-2-yl)-amide **44**, the following facts of the determined solid state structure should be mentioned: **44** crystallizes in the triclinic space group $P\bar{1}$ containing two molecules in the asymmetric unit. Each molecule shows the presence of a slight fraction of a disordered counterpart (*sof*: 0.97), which is not neglectable due to the electron rich aluminium and sulfur atoms within the structure.

In comparison to the bisheterocyclo methanides,[95] where formally just the bridging nitrogen atom is iso-valence-electronically replaced by a CH-group,[119] a similar chelating coordination behaviour via the ring-internal nitrogen donor atoms N1 and N2, while adopting the *trans-trans* (*vide infra* in Scheme 2-41) arrangement, occurs (see Figure 2-56). It is evident, that upon deprotonation a delocalized six π-electrons containing monoanionic ligand system is generated as in the case of the mimicked nacnac species. Thus, the former distinct C_{ipso}–N_{bridge} and the C_{ipso}–N_{het} bond lengths are converging to nearly the same value, because due to the delocalization each C_{ipso}–N bond has partial single as well as double bond character in **44**. As a result, the C1–N1' distance provides 133.4(2) pm (**41**: 133.6(4) pm), C8–N1' 133.2(3) pm (**41**: 136.7(4) pm) and the averaged C1–N1 distance is 133.9(2) pm (**41**: 133.1(4) pm), C8–N2 134.7(3) pm (**41**:

130.1(4) pm). This experimentally observed bond lengths can be classified as half way between C(sp^2)–N(sp^2) single (140 pm) and C(sp^2)=N(sp^2) double bonds (129 pm)[108a] to give an overall average C–N bond length of about 133.8(3) pm.

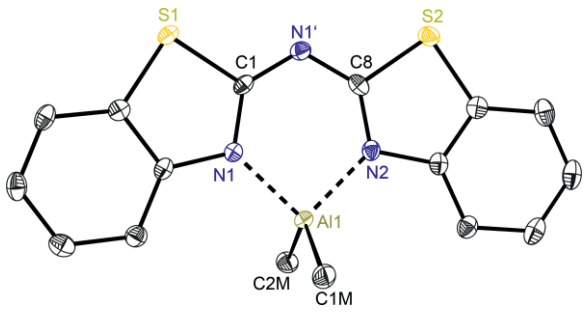

Figure 2-56: Solid state structure of complex **44**.

Table 2-45: Distances [pm] and angles [deg] of **44**.

N1'–C1	133.7(2) 133.1(2)	N1–C1–N1'	129.87(16) 129.84(17)
N1'–C8	133.0(3) 133.4(3)	N2–C8–N1'	129.83(18) 129.72(19)
C1–N1	133.7(2) 134.1(2)	S1–C1–N1'	116.70(13) 116.72(14)
C8–N2	134.5(3) 134.8(3)	S2–C8–N1'	116.88(15) 116.63(16)
C1–S1	175.27(18) 175.23(18)	S1–C1–N1	113.42(13) 113.44(14)
C8–S2	174.5(2) 174.4(2)	S2–C8–N2	113.27(15) 113.61(15)
N1–Al1	192.79(17) 193.03(17)	C1–N1'–C8	119.73(16) 119.85(17)
N2–Al1	192.86(17) 192.5(2)	N1–Al1–N2	91.48(7) 91.61(8)
Al1–C1M	195.8(2) 195.9(2)	C1M–Al1–C2M	120.54(10) 119.11(11)
Al1–C2M	196.0(2) 195.4(3)		

Due to the presence of two molecules in the asymmetric unit, for each parameter two values are given.

For further structural comparisons, especially the formed six-membered metalla heterocycle and the arrangement of the benzothiazole units, is paid most attention, because the derived values offer the possibility to estimate the chelating properties of each ligand system. Based on the metalla heterocycle, the following two values are considered: the C1–N1'–C8 angle at the backbone of the ligand and N1–Al1–N2 bite angle of the coordinated group 13 metal with respect to the nitrogen donor atoms of the benzothiazole moieties. In the case of compound **44**, the backbone angle slightly changed from 120.3(2) deg in the parent ligand **41** to 119.79(17) deg with an associated bite angle of 91.55(8) deg and an averaged N–Al distance of 192.80(20) pm.

As depicted in Table 2-46, the folding angle has increased to 7.61(9) deg (**41**: 1.18(10) deg) and the torsion between the two benzothiazole units was switched by almost 170 deg to give a torsion angle of 7.61(9) deg. The metal fragment is located 9.87(25) pm above the chelating C_2N_3 plane, which is built up from the atoms N1, C1, N1', C8 and N2.

Table 2-46: Folding parameters for **41** – **46**.

	M···plane dist. [pm]	torsion angle [deg]	folding angle [deg]	N1···N2 dist. [pm]	N1'···Al1 dist. [pm]
41	–	175.1(8)	1.184(103)	451.39(37)	–
42	–	171.96(44)	3.111(58)	418.18(23)	–
43	–	174.99(48)	5.763(68)	419.26(28)	–
44	9.87(25)	7.1(6)	7.608(89)	276.29(25)	333.34(19)
45	4.31(16)	0.9(4)	6.344(43)	292.68(17)	324.97(13)
46	15.77(32)	0.56(67)	25.457(53)	276.58(26)	341.08(20)

Next, the $AlMe_2$ complex **45** is described, whose ligand differs from **44** in two additional methyl groups in *ortho*-position to the chelating nitrogen atoms. **45** crystallizes in the orthorhombic space group *Pccn* and one molecule is present in the asymmetric unit. The observed C–N distances within the metalla heterocycle cover a narrow range of 133.05(19) pm to 134.35(18) pm as in the case of **44**, indicating again the well pronounced delocalization, which is achieved upon deprotonation. The ligand system has changed to its *trans-trans* conformer (see Figure 2-57). In contrast to that, the angle in the backbone as well as the bite angle of the chelating nitrogen atoms are widened (**44**: 119.79(17) deg; 91.55(8) deg; **45**: 122.97(12) deg; 96.52(5) deg) (see Table 2-47). Furthermore, the transannular distance between N1 and N2 shows a significantly larger value for the methyl substituted derivative **45** (292.68(17) pm vs. 276.29(25) pm in **44**; see Table 2-46). These findings can be explained by the additional steric demand induced by the methyl groups at the benzothiazole moieties, which causes the sidearms to bent away from each other and forces a widening of the aforementioned parameters.

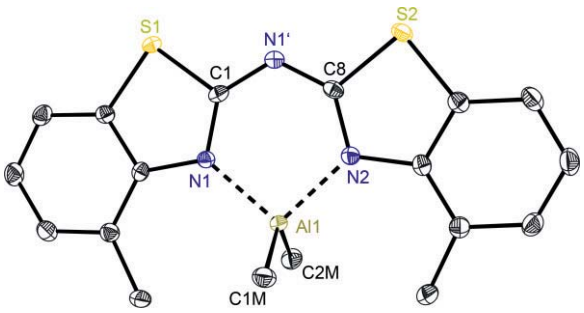

Figure 2-57: Solid state structure of complex **45**.

Table 2-47: Distances [pm] and angles [deg] of **45**.

N1'–C1	133.20(18)	N1–C1–N1'	131.20(13)
N1'–C8	133.05(19)	N2–C8–N1'	131.00(13)
C1–N1	134.05(17)	S1–C1–N1'	114.38(10)
C8–N2	134.35(18)	S2–C8–N1'	114.57(10)
C1–S1	174.19(14)	S1–C1–N1	114.42(10)
C8–S2	174.45(14)	S2–C8–N2	114.42(10)
N1–Al1	195.56(13)	C1–N1'–C8	122.97(12)
N2–Al1	196.70(12)	N1–Al1–N2	96.52(5)
Al1–C1M	196.02(15)	C1M–Al1–C2M	126.65(7)
Al1–C2M	196.25(15)		

As a consequence of this widening, the dimethyl aluminium fragment is allowed to penetrate the monoanionic ligand system more deeply to achieve a better embracement and shielding. Therefore, the distance between the bridging nitrogen atom N1' and the metal cation Al1 can be regarded as an appropriate value for the specific uptake properties of each ligand system, resulting in this case in 324.97(13) pm. This distance is the shortest

one observed in the series of the synthesized group 13 metal amide complexes **44** – **46**, illustrating that the methyl substituted ligand platform fits best for the coordination of an Al(III) cation. Confirming this assumption, also the deviation from the C_2N_3 plane mirrors the good chelation abilities, because the experimentally determined distance in **45** (4.31(16) pm) represents again the shortest one within this row, yielding in the most planar coordination geometry (torsion angle: 0.9 deg; see Table 2-46).

In an analogue amide bridged $AlMe_2$ complex, namely $[Me_2Al\{(2\text{-}NC_5H_4)_2N\}]$, following structural parameters were reported: the coordinated aluminium fragment is located 28.3 pm out of the plane and the corresponding N1–Al1–N2 bite angle results in 93.5 deg with a transannular N1···N2 distance of 279.1 pm. The observed Al–N distance is 191.5 pm and the pyridyl substituents are twisted by 10.4 deg against each other.[85c] By comparing those values with that one obtained for **44** and **45**, it can be stated that the latter mentioned complexes show a more planar coordination geometry within the six-membered metalla heterocycle. These findings are based on the decreased Al···plane distance and smaller folding and torsion angles, respectively (see Table 2-46). However, the transannular N1···N2 distance in **44** is almost the same as in $[Me_2Al\{(2\text{-}NC_5H_4)_2N\}]$. This distance is increased by about 16 pm in **45** presumably due to the enhanced steric demand of the additional methyl groups at the annulated benzene moieties. This widening enables the metal fragment to be coordinated in a more beneficial way, so that the ligand adopts a more planar arrangement compared to **44**.

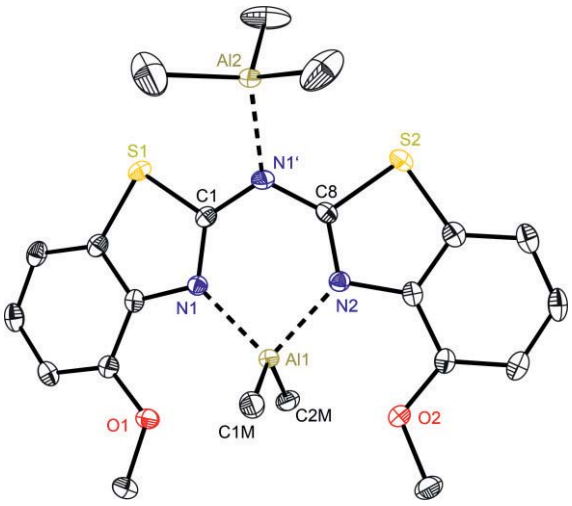

Figure 2-58: Solid state structure of complex **46**.

Table 2-48: Distances [pm] and angles [deg] of **46**.

N1'–C1	136.6(3)	N1–C1–N1'	128.17(19)
N1'–C8	136.5(3)	N2–C8–N1'	128.03(19)
C1–N1	133.4(3)	S1–C1–N1'	117.41(16)
C8–N2	132.8(3)	S2–C8–N1'	117.36(15)
C1–S1	174.7(2)	S1–C1–N1	114.35(16)
C8–S2	175.0(2)	S2–C8–N2	114.53(16)
N1–Al1	199.48(18)	C1–N1'–C8	118.44(18)
N2–Al1	199.57(19)	N1–Al1–N2	87.75(8)
Al1–C1M	196.0(2)	C1M–Al1–C2M	129.57(11)
Al1–C2M	196.7(2)	C1–N1'–Al2	120.34(14)
N1'–Al2	206.60(19)	C8–N1'–Al2	120.40(14)

To complete this chapter of Al(III) containing bisheterocyclo amides, the corresponding complex derived from the methoxy functionalized bis-(benzothiazol-2-yl)-amine is considered hereafter. Having a closer look at the solid state structure of **46** in Figure 2-58, several different features can be identified in contrast to the other amides and bisheterocyclo methanides: this ligand offers an additional binding site for a second metal fragment. A second equivalent of $AlMe_3$ as Lewis acid is coordinated by the central, bridging

nitrogen atom N1' to form a homo bimetallic complex. This binding motif is quite rare and was not observed, neither in the herein discussed bis-(benzoxazol-2-yl)- / bis-(benzothiazol-2-yl)-methanides nor –amides. Because **46** has two different donor sites for metal coordination, this ligand system is maybe also capable of creating hetero bimetallic complexes like Janus head ligands or scorpionates, which also have two different donor sites for metal coordination.[84, 88, 91a, 91e, 91f]

Additionally, it was found that the central six-membered metalla heterocycle of **46** differs most from planarity when compared to **44** and **45**. The bridging nitrogen atom N1' is no longer located within the plane made up from N1, C1, C8 and N2 as observed in the other structures. N1' and Al1 are displaced from the C_2N_2 plane to the same side, whereby even the deviation from that plane is more pronounced for N1' than for Al1 (21.1(3) vs. 15.8(3) pm) to result in a pronounced boat-like arrangement (see Scheme 1-5, case **(b)**). The C1–N1 and C8–N2 bonds are almost aligned parallel, resulting in a torsion angle of only 0.5 deg, but the folding of the whole framework, which is also indicated by the large displacement of the bridging amide functionality, is very distinct (about 25.5 deg, Table 2-46).

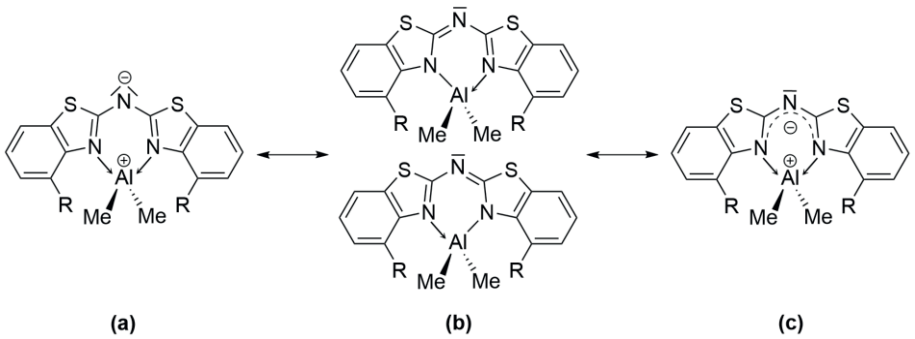

Scheme 2-39: Mesomeric resonance structures of the group 13 bisheterocyclo amides **44** – **46**.

These findings confirm the assumption, that the lone pair generated by the deprotonation of the parent ligand is not fully delocalized among the other C–N bonds, but rather predominantly localized at the central nitrogen atom N1'. This amidic resonance structure **(a)** in Scheme 2-39 seems to suit best this binding situation, because the amide anion is similar to the sp^3-hybridized carbanion.[122] Furthermore, there is an obvious difference between the bond lengths concerning the endocyclic and exocyclic C–N bonds, whereas the latter are significantly elongated.

The ^{1}H-NMR data of **46** (THF-d_8 solution at rt) show the presence of the $AlMe_2$ fragment and the additional $AlMe_3$ group. The apparent cross peak for the ^3J-coupling between the protons of the $AlMe_2$ unit and N1 observed in a ^{1}H,^{15}N-HMBC NMR experiment proves, that the $AlMe_2$ unit is still coordinated by the chelating endocyclic nitrogen donors in solution. The same is valid for the observed ^4J-coupling between the aromatic H5 and the same nitrogen donor. Those cross peaks were also detected in the case of the corresponding methanide derivatives.[95] However, no interaction of the $AlMe_3$ moiety with the

bridging N1' was detected, suggesting that the Lewis acid base adduct **46** is not maintained in solution.

Nevertheless, this kind of an additional Lewis acid base adduct formation was earlier recognized in previous works by means of $[Et_2Al\{(2\text{-}NC_5H_4)_2N\} \cdot AlEt_3]$ as representative for the amidic ligand systems, which is quite comparable to **46** although the residues at the aluminium centres are replaced by ethyl moieties.[85b] For this structure, an average Al1–N1 distance of 192.2 pm for the chelating metal coordination site and a Al2–N1' distance of 201.0 pm could be structurally determined. Consequently, the bonding situation in the six-membered metalla heterocycle can be regarded rather as covalent bonding, whereas the coordination in the backbone can be seen as a donor bond within a Lewis acid-base adduct. Analogue to the crystal structure of **46**, the complex adopts a highly pronounced butterfly or boat-like conformation and both aluminium centres are located at the same side of the chelating plane. The accompanied folding angle of the pyridyl rings (24.3 deg) is almost similar to the observed folding of 25.5 deg within **46**. In the case of the methylene bridged heteroaromates, one example based on the iso-electronic $[(2\text{-}NC_5H_4)_2CH]^-$ ligand was published in 2000 by our work group, where the bridging CH functionality is involved in coordination of a metal cation. Upon transmetallation of bis-(pyrid-2-yl)-methyl lithium using $ZnMe_2$, the dimeric species $[MeZn\{(2\text{-}NC_5H_4)_2CH\}]_2$ was obtained, in which the organozinc fragment is coordinated in a chelating fashion by the two ring-internal nitrogen atoms of one molecule as well as the bridging carbanion of the other ligand.[83a]

2.5.6 Syntheses and Bonding Properties of Lithiated Species

In addition to the above-mentioned metallation reactions employing mainly alkyl aluminium reagents, lithiation reactions of the bisheterocyclo amines **41** and **42** were carried out in the absence of donating Lewis-bases. Therefore, a slight excess of *n*BuLi was added at 0 °C to the corresponding amine ligand dissolved in toluene (see Scheme 2-40). In the case of the amine **42**, which carries methyl groups at the annulated benzene moieties, concentration of the reaction mixture to a few millilitres afforded crystals of **48** suitable for X-ray diffraction. For compound **47**, unfortunately, no suitable crystals for SCXRD could be grown under the same conditions as used for **48**. However, this species could also be sufficiently characterized in solution by applying several NMR spectroscopic techniques. The lithiated reaction product, illustrated as a tetrameric species, shown in Scheme 2-40, is based on the knowledge of the obtained crystal structure of **48**. Due to the fact that no crystal structure of **47** could be determined, its anticipated structure is assumed to be similar, because those compounds just differ in the presence of the methyl groups and accordingly the steric demand is even less.

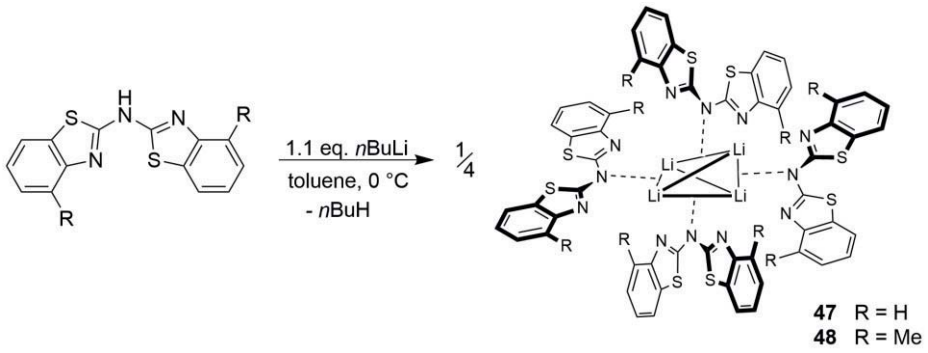

Scheme 2-40: Synthesis of the lithiated compounds **47** and **48**.

Starting with the experimentally determined solid state structure of **48** (see Figure 2-59), it has to be mentioned, that due to the insufficient quality of the measured crystal the observed binding motif can just be described in a qualitative way. The quantitative discussion of bond lengths and angles should be handled with care for the same reason.

The lithiated species **48** crystallizes in the triclinic space group $P\bar{1}$ and the asymmetric unit contains four deprotonated ligands, four lithium cations for charge neutrality and one disordered toluene solvent molecule. The right side of Figure 2-59 shows the tetrameric aggregation motif of the lithiated bis-(4-methylbenzothiazol-2-yl)-amide as ball and stick model without thermal ellipsoids. For clarity reasons, the annulated C_7-perimeters are depicted in faded colour, all remaining hydrogen atoms and the co-crystallized toluene molecule are omitted. The central distorted Li_4-tetrahedron is highlighted with blue surfaces and its edges as well as corners are coordinated by the four bis-(4-methylbenzothiazol-2-yl)-amide ligands, in which all three nitrogen atoms are acting as a donor site. These ligands are labelled from **L1** – **L4** in the following context and the six edges of the Li_4-tetrahedron are marked as **a** – **f** to gain a better overview about the coordination geometry. The central, bridging nitrogen atoms of each ligand **L1** – **L4** are pointing towards the centre of a Li···Li edge, so that in sum four of the six tetrahedral edges (**a** – **d**) are coordinated (indicated in Figure 2-59 (*right*) as turquoise dashed lines) by one bridging nitrogen donor atom. The remaining two opposite long edges **e** and **f** are occupied by the nitrogen atoms in the periphery of the ligands **L3** and **L4**. As noted earlier, the other considered methanide and amide metal complexes show no coordination via the sulfur atoms in the backbone, which can be explained by the better pronounced Lewis-donor abilities of the nitrogen atoms.

Apart from the coordination of the Li···Li edges, the apical lithium cations (corners) are addressed by the *cis*-arranged nitrogen donors of the endocyclic benzothiazole moieties to gain fourfold coordination (grey dashed lines) by the ligands **L1** – **L4**.

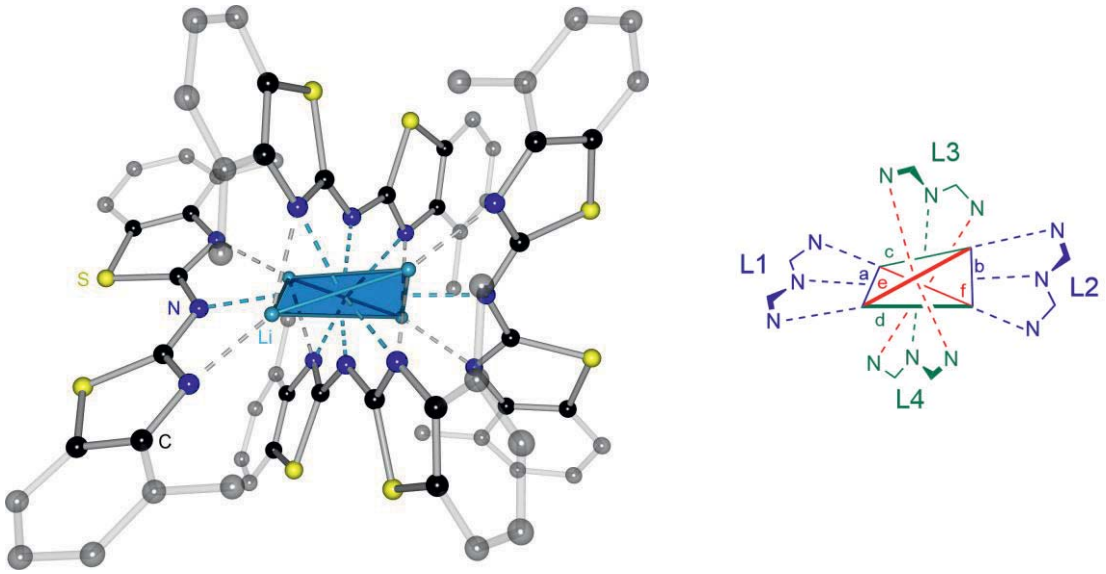

Figure 2-59: *left*: Molecular structure of $[Li\{(4\text{-}MeNCSC_6H_3)_2N\}]_4$ (**48**). For clarity reasons the co-crystallized solvent molecules and hydrogen atoms are omitted and the annulated moieties are represented in faded colour. *right:* simplified model of the coordination environment.

The ligands **L1** and **L2** show the same coordination behaviour, whereas the central nitrogen atoms are pointing towards the edges **a** and **b**, respectively. The neighbouring nitrogen atoms in the heterocycle are pointing to the lithium corners of the same edge. **L3** and **L4**, however, show a different binding motif. Each central amide moiety also points to the edges **c** and **d**, respectively, but the geminal bonded nitrogen donors are oriented to the centres of the other edges **e** and **f**. In these cases, the thiazole units equally bridge between the edges as well as one of those corners. Each edge is coordinated by at least one bridging amide (**a** – **d**) or two endocyclic thiazole nitrogen atoms (**e** and **f**). The corners are addressed each by two of the last mentioned ones (one from **L1** or **L2** and the other one from **L3** or **L4**).

A short comparison of other wide-spread Li_4-tetrahedra containing organolithiums[123] like $[EtLi]_4$,[124] $[MeLi]_4$[125] or $[t\text{BuLi}]_4$[126] or to lithium amide rings and ladders[127] shows, that in **48** a highly distorted Li_4-tetrahedron instead of the expected ring stack or ladder is formed. In contrast to the abovementioned tetrahedra with quite regular Li···Li edges (averaged values: $[EtLi]_4$: 253 pm; $[MeLi]_4$: 259 pm; $[t\text{BuLi}]_4$: 241 pm), **48** exhibits four shorter Li···Li (271(1) to 300(1) pm) and two elongated (348(1) to 413(1) pm) edges, because in the discussed complex the four ligands are divided into two different groups, which show an equivalent coordination pattern.

The binding motif is quite interesting and unique, because the ligand system adopts the *cis-cis* configuration in contrast to all other metallated species of bisheterocyclo methanes or amines, where the *trans-trans* configuration was preferred in the solid state (see Scheme 2-34 and Scheme 2-41). The $AlMe_2$ unit was coordinated by the endocyclic nitrogen donor atoms of the heterocycles. As depicted in Scheme 2-41, in total three different binding motifs can occur in the case of the metallated species **44** – **48**. The *cis-trans* conformation, shown at the left hand side, could not be observed yet in any bis-

(benzothiazol-2-yl)-amide and corresponding methanide.[95] Instead the *trans-trans* conformation facilitates the formation of a six-membered metalla heterocycle in contrast to the *cis-cis* arrangement, where a higher strained four-membered ring results. However, this *cis-trans* arrangement was present in the molecular structure of $[Me_2Tl\{(2\text{-}NC_5H_4)_2N\}]_\infty$ due to the larger and easier to polarize cation.[85b, 85c] In that case, the Tl^{3+} cation is addressed by three nitrogen donors (two from the same ligand and one from another) and therefore an infinite coordination chain is formed in the solid state.

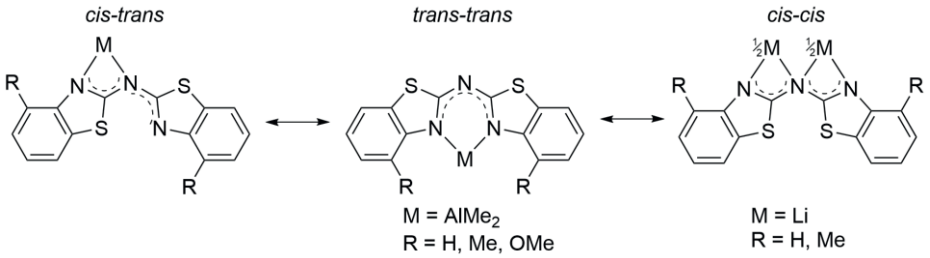

Scheme 2-41: Possible binding motifs upon metallation within **44** – **48**.

2.5.7 NMR Spectroscopic Investigations

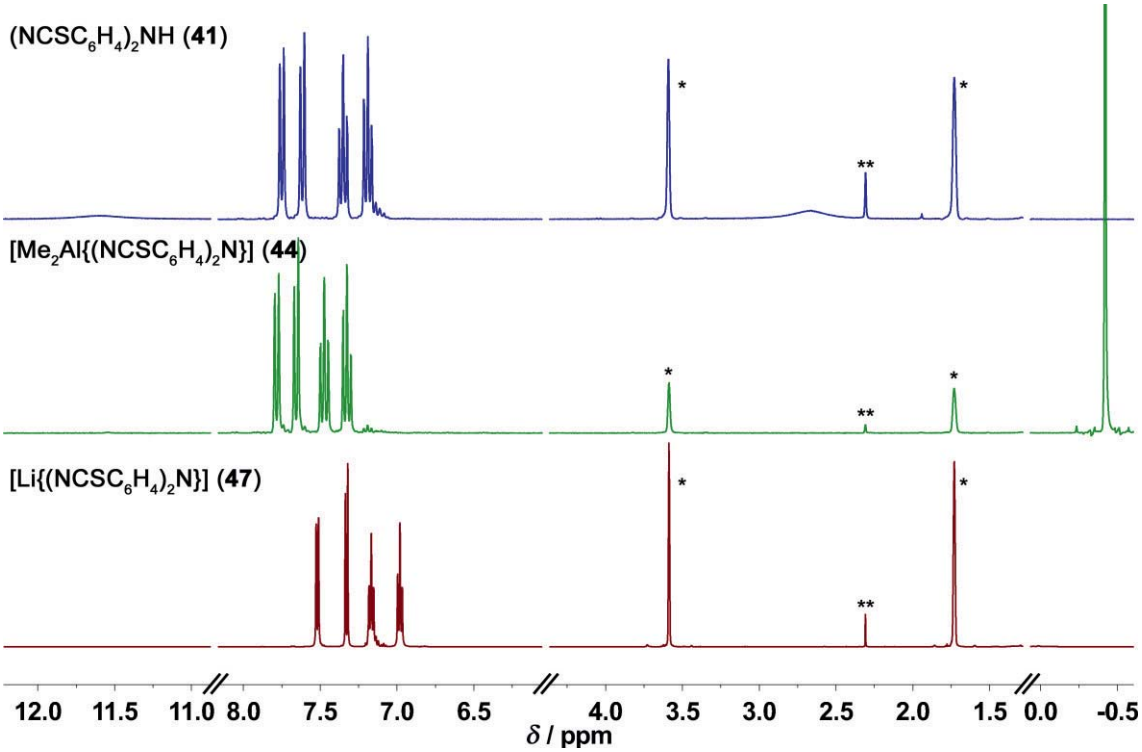

Spectrum 2-12: Overlay of the ^{1}H-NMR spectra (THF-d_8, rt) of the parent ligand system **41** and the corresponding metallated species **44** and **47**. Solvent signals are highlighted with * and residual toluene with **.

Detailed NMR spectroscopic investigations of the different amine ligand systems are presented as overlay in Spectrum 2-12 and Spectrum 2-13. Starting with the unsubstituted

bis-(benzothiazol-2-yl)-amine **41**, a spectroscopic comparison to the derived metallated species, containing either a $AlMe_2$ fragment (**44**) or a lithium cation (**47**), was applied in Spectrum 2-12. The top trace of Spectrum 2-12 shows the ^{1}H-NMR spectrum of the parent neutral amine ligand **41**, measured in THF-d_8 as solvent. In the spectrum four clearly separated and well-resolved signals for the aromatic protons of the benzothiazole moieties are observed. At a chemical shift of 7.75 ppm and 7.62 ppm two doublets for the terminal protons H3 and H6 arise, whereas at 7.35 ppm and 7.19 ppm two distinct triplets for the remaining aromatic protons H5 and H4 can be assigned. Due to the recrystallisation from toluene, in all spectra minor contaminations of residual toluene were observed (highlighted with ** in Spectrum 2-12) besides the signals for the not completely deuterated solvent THF (marked with *). Furthermore, a very broad singlet at 11.60 ppm was found to be correlated to the acidic proton H1' at the amine bridge N1'. In accordance to this, at about 2.7 ppm a broadened singlet for residual water traces was found due to the fast exchange with the amine proton.

Upon deprotonation and subsequent metallation with trimethyl aluminium, the signal of the former NH proton at about 11 ppm vanishes in the case of the $AlMe_2$ complex **44**, shown in the middle trace of Spectrum 2-12. The ^{1}H-NMR spectrum of **44** is slightly different compared to the parent amine: the signal sets (again two doublets and two triplets) for the aromatic protons are slightly shifted to lower field and the range of the observed chemical shifts is compressed (7.78 – 7.32 ppm in **44** vs. 7.75 – 7.19 ppm in **41**). The signal of the two methyl groups at Al1 appears as singlet with an integral of six protons at −0.42 ppm.

Even though no crystal structure for the lithiated species **47** could be experimentally determined, this compound could be characterized satisfactorily by application of NMR studies in solution. The bottom trace in Spectrum 2-12 shows the ^{1}H-NMR spectrum of **47**, where in similarity to **44** no peak for the former NH proton can be detected at the low-field side. It is obvious, that the resonance signals of the aromatic protons are significantly shifted to higher field (7.52 – 6.98 ppm). The chemical shift of the coordinated lithium cation in **47** in the corresponding ^{7}Li-NMR spectrum was observed as a singlet at 2.09 ppm.

Next, the overlay of ^{1}H-NMR spectra for the amine ligand **42** and the derived complexes is depicted in Spectrum 2-13. This ligand has two additional methyl groups implemented in *ortho*-position to the chelating nitrogen atoms, when compared to **41**. Again, the top trace represents the recorded spectrum for the parent compound **42**, which shows a quite broad singlet at 11.51 ppm standing for the apparent NH bridge. In this case the broadening is much less pronounced compared to **41**, because in this sample less water was present.[128] Due to this water content, the acidic proton of the NH functionality can exchange rapidly on the NMR time scale with the protons of the residual water, so that a line broadening of the NH and the H_2O signal occurs. As expected, three signals for the remaining three aromatic protons were detected in the region of 7.59 ppm to 7.10 ppm and one singlet of the six protons at the methyl group C15 was found at 2.64 ppm.

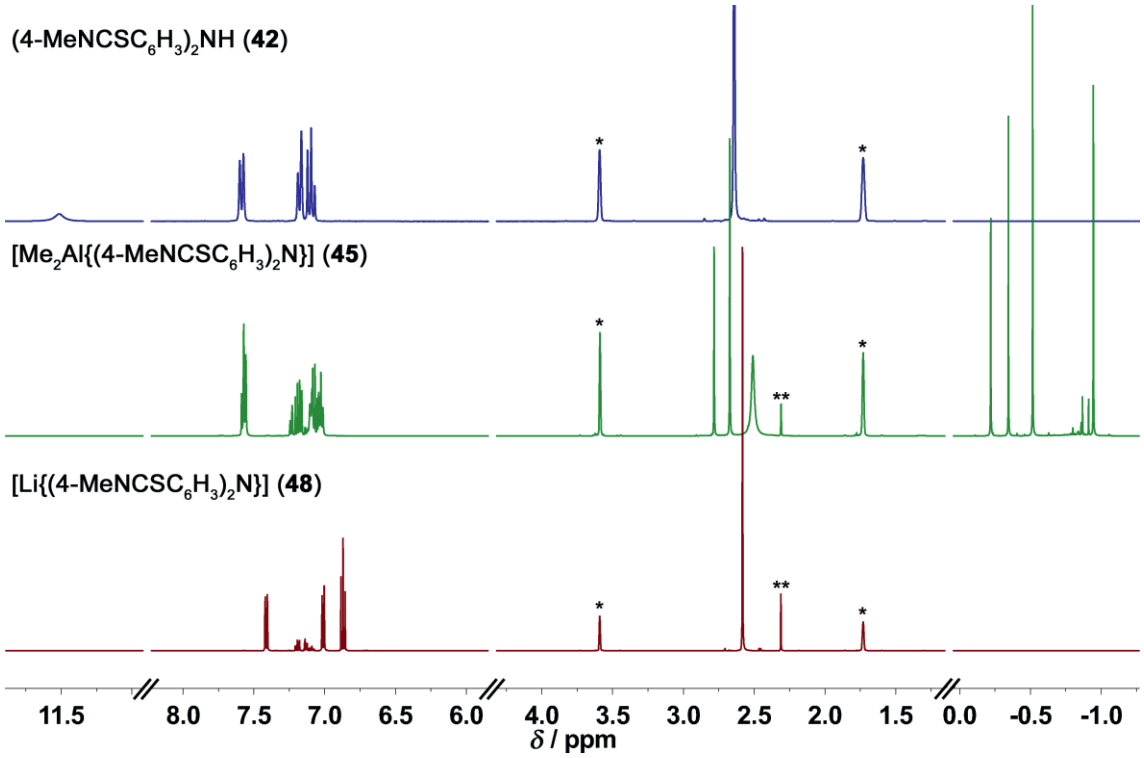

Spectrum 2-13: Overlay of the ^{1}H-NMR spectra (THF-d_8, rt) of the parent ligand system **42** and the corresponding metallated species **45** and **48**. Solvent signals are highlighted with * and residual toluene with **.

The intermediate spectrum in Spectrum 2-13 shows the recorded ^{1}H-NMR spectrum of the dimethyl aluminium complex **45**. In analogy to the previously discussed metallation reaction of **41**, the broad signal at 11.51 ppm vanishes upon metallation, which indicates a successful conversion to the desired metal complex **45**. Obviously, the recorded spectrum, which was directly measured from the isolated crystals also used for SCXRD and elemental analysis (found: C: 58.40, H: 5.26, N: 11.30, S: 17.41; calcd.: C: 58.51, H: 5.46, N: 11.37, S: 17.36), looks more complex as in the other considered cases. In theory, just one singlet for the ligand's methyl groups H15 and another singlet for the protons H1M of the $AlMe_2$ unit would be expected. But this spectrum clearly reveals that at least three different compounds, containing the ligand and the metal fragment, are existent in solution due to the presence of three characteristic singlets for H15 (δ = 2.78 ppm, 2.67 ppm and 2.51 ppm) and another three signals for H1M (δ = −0.22 ppm, −0.34 ppm and −0.52 ppm). Because of the slight differences in the observed chemical shifts, it is assumed that the species, which are responsible for those signals, just differ in the coordination fashion of the metal fragment. Therefore, the different coordination modes, already shown in Scheme 2-41, can be taken into account for this argumentation. Due to the possibility to involve the nitrogen donor at the backbone for metal coordination, the NMR spectrum recorded at room temperature shows, that **45** has a dynamic equilibrium between those three coordination modes in solution, which is resolved at the NMR time scale. However, this special feature was just observed in the case of **45**. The remaining singlet at −0.94 ppm can be assigned to the presence of residual $AlMe_3$, which shows nearly the same chemical shift as the additional Lewis acid in **46**.

The bottom trace of Spectrum 2-13 corresponds to the ^{1}H-NMR spectrum of the lithiated complex **48**. The reaction of **42**, dissolved in toluene, with *n*BuLi leads to the formation of the tetrameric lithiated species **48** (see Figure 2-59). The deprotonation of the former ligand led to a loss of the bridge's signal at low-field and all signals were slightly shifted to higher field. The resulting chemical shifts for the aromatic protons can be found as doublet at 7.41 ppm for H5, at 7.01 ppm for H5 and as triplet at 6.86 ppm for H4. The protons of the methyl groups appear at δ = 2.58 ppm. However, the recorded spectrum contains some minor contaminations of starting material **42**, clearly seen in the aromatic region around 7.2 ppm. The chemical shift for the coordinated lithium cation of **48** in the corresponding ^{7}Li-NMR spectrum was observed as a singlet at −0.68 ppm.

In Spectrum 2-14 the recorded ^{1}H,^{15}N-HMBC NMR spectra for the $AlMe_2$ amides **44**, **45** and **46** are depicted for a better comparison. In analogy to the results for the metallated species derived from the symmetrically substituted bisheterocyclo methanides (see Spectrum 2-2 and Spectrum 2-3), also for the corresponding amides couplings between the nitrogen donors and protons can be observed. Beginning with the upper spectrum, which belongs to compound **44**, just one signal in the ^{15}N-NMR spectrum at −196.3 ppm is present. The two occurring cross peaks can be assigned to the ^{3}J-coupling with the hydrogen atoms H6 and H1M, which are in closest proximity to the coordinating nitrogen donor N1.

The same observation was noticed for the bottom HMBC spectrum concerning molecule **46**. In this case one signal at the ^{15}N-NMR spectrum at −193.3 ppm can be detected, which causes two cross peaks with the protons H1M and H5 standing for ^{3}J- and ^{4}J-coupling with the endocyclic nitrogen atoms N1. In both cases no second signal and cross peaks for the bridging N1' in the backbone were observed, indicating that this nitrogen donor is presumably not involved in coordination in solution. The assumption, that the chelating coordination motif stays intact in solution, can be supported by the quite similar chemical shift of the coordinating nitrogen donors in the comparable benzothiazole containing methanide structures (**9**: δ = −201.2 ppm; **14**: δ = −199.2 ppm).

In contrast to the 2D-NMR spectra discussed above, the ^{1}H,^{15}N-HMBC NMR spectrum of **45** exhibits two main differences: on the one hand, no cross peak between the ^{1}H- and ^{15}N-NMR spectrum can be found in the aromatic region, so that no ^{4}J-and ^{5}J-coupling could be observed within this experiment. On the other hand, two different signals in the ^{15}N-NMR spectrum (δ = −135.7 ppm and −194.7 ppm) were detected for the first time in the context of the amide ligands. As mentioned earlier, the ^{1}H-NMR spectrum gave rise for the assumption, that different coordination species were present in solution. This thesis can be supported by the occurrence of the two cross peaks in the high field region, in which the signals for the $AlMe_2$ protons are located. The singlet at −0.34 ppm shows a clear ^{3}J-coupling with the ^{15}N-NMR resonance signal at −194.7 ppm, which can be assigned consequently to the chelating nitrogen donors. Interestingly, the major product, which is present in solution, is the singlet at −0.52 ppm. It has the largest integral and shows ^{3}J-coupling to the ^{15}N-NMR resonance signal at −135.7 ppm. Because this chemical shift of the nitrogen atom was not determined earlier for the methanides (e.g. **9** or **14**), this signal has to be assigned to the nitrogen donor N1', which is placed in the bridging

position of the backbone. This fact leads to the conclusion, that **45** exists in solution predominantly as a coordination complex, in which the bridging N1' is mainly involved in coordination of the metal fragment (see Scheme 2-41). However, this is a vital contrast to the determined arrangement in the solid state (see Figure 2-57) with the observed chelating ability of just the endocyclic imine donor sites.

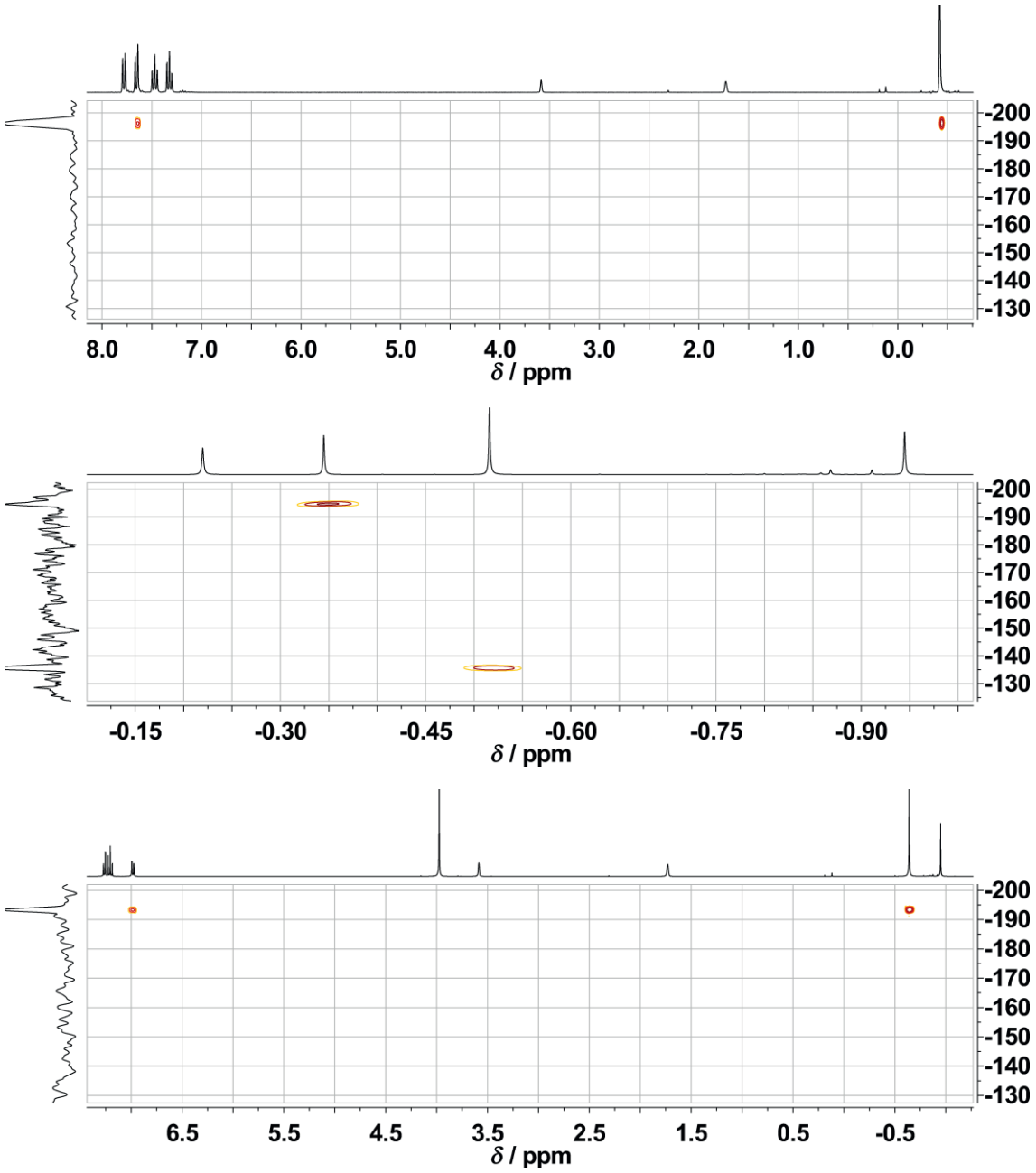

Spectrum 2-14: $^{1}H,^{15}N$-HMBC NMR spectra (THF-d_8, rt) for compounds: *top:* **44** (500 MHz), *middle:* **45** (400 MHz), *bottom:* **46** (400 MHz).

2.5.8 Conclusion

In summary, four neutral bisheterocyclo amines **40** – **43** and the corresponding metal amides **44** – **46** were synthesized and characterized by single crystal X-ray diffraction and via NMR spectroscopy in solution.

In contrast to the corresponding methane derivatives, the amines **41** – **43** always form a co-planar arrangement of the heteroaromatic substituents, preferentially in the *cis-trans* conformer with a torsion angle of almost 180 deg. Especially, the formation of different hydrogen bonded aggregates helps to maintain this planarity. An overall comparison of the hydrogen bonding abilities of the investigated systems shows, that the steric demand of the substituent at the C_6-perimeter has an increasing influence on the aggregation and the strength of the formed hydrogen bonds. While **41** has the smallest steric demand, it forms the most linear but also longest hydrogen bonds in a 2D chain-like aggregation motif. The implementation of methyl groups augments the steric demand of the ligand **42** compared to **41**. This leads to the formation of a dimeric species, causing an almost linear D–H···A angle and the shortest distances between the acceptor and the bridging hydrogen. Further increase of the steric congestion in **43**, the methoxy groups force the molecule to divide its hydrogen bonding pattern up to two neighbouring molecules instead of just saturating one in **42**.

The metallated species **44** – **45** are comparable to the related methanides having nitrogen atoms in the benzothiazole units chelating in a *trans-trans* fashion to the $AlMe_2$ moiety (Scheme 2-41). The experimentally determined values for the C–N bond lengths suggest a delocalized six electron π-system, indicated by C–N bond lengths, which are half way between a C(sp^2)–N(sp^2) single (140 pm) and C(sp^2)=N(sp^2) double bond (129 pm). The widening of the backbone and the bite angle of **44** – **45** can be attributed to the additional strain introduced by the methyl groups in **45**, which causes the benzothiazole units to bent away from each other. This evidence is mirrored by the transannular N1···N2 distance of 276.4(3) pm for **44** and 292.7(2) pm for **45** and by the N1'···Al1 distance (**44**: 333.4(2) pm; **45**: 325.0(2) pm), illustrating the deeper inserted organometallic moiety in **45** compared to **44**.

The coordination of the bridging amide to an additional Lewis acid in terms of Al2 in **46** causes the whole ligand framework to fold and, hence, lowers the orbital overlap of the concerned π-system. This folding can be explained, since N1' is slightly inclined towards Al2. This distortion leads to an environment of N1', which is indicating a partially stereochemically active lone-pair at the nitrogen atom. The angular sum around N1' of about 359 deg is marginally smaller than for an expected ideal sp^2-hybridized nitrogen atom. For further applications of such metal complexes to generate low valent metal fragments, the criterion of maximum orbital overlap is vital, because the tentative lone pair at Al(I) as a result of the reduction of the Al(III) can best be stabilized by planar arranged ligand systems.

The lithiated compounds **47** and **48** are different in comparison to the group 13 complexes: by means of the crystal structure of **48**, it was possible to determine the ligand arrangement in the presence of a non-polar, aprotic solvent like toluene. A tetrameric metal complex is formed upon lithiation of **42** in the absence of any Lewis donor base,

which shows a clear preference to promote a *cis-cis* configuration of the amide ligand, never observed in similar systems before. Due to the lack of other donors, the active ligand periphery has to suite a lithium tetrahedron in the centre of the molecular structure of **48**. Consequently, each available nitrogen donor site of the bisheterocyclo amides is involved in coordination to donate the required electron density to Li^+.

Moreover in each molecular structure, the metal coordination only involves the nitrogen atoms, no metal-sulfur interaction could be observed so far. Referring to the HSAB principle[90, 92] this fact was expected, because Al^{3+} and Li^+ cations are regarded as hard cations and therefore, preferentially coordinate the harder nitrogen rather than the soft sulfur atom.

2.6 Excursus: Fluorescence Studies on Bisheterocyclo Methanides

As a further characterization method of the synthesized group 13 metal complexes bearing the different methanide ligand systems, fluorescence spectroscopy was utilized, because the metal complexes of the anionic chelate ligands show interesting luminescence behaviour. This fluorescence phenomenon is caused by the deprotonation in the backbone of the ligand at the methylene bridge. Due to the deprotonation, a free electron pair is generated at C1', which can tautomerize between the three possible mesomeric resonance structures (see Scheme 2-10): **(a)** a carbanionic (negative charge located at the methylene bridge), **(b)** an amidic (negative charge located at the endocyclic nitrogen donor) and **(c)** a completely delocalized canonical form (see Scheme 2-10). The nearly planar arrangement of the whole ligand framework and the delocalization of the lone pair connects the both heteroaromatic moieties electronically, resulting in an expanded UV-light sensitive π-system. Regarding to this fact and to qualify these effects, some fluorescence spectroscopic investigations were run on three exemplary bisheterocyclo methanes **4**, **5**, **19** and the corresponding $AlMe_2$ derivatives **8**, **9**, **21**.

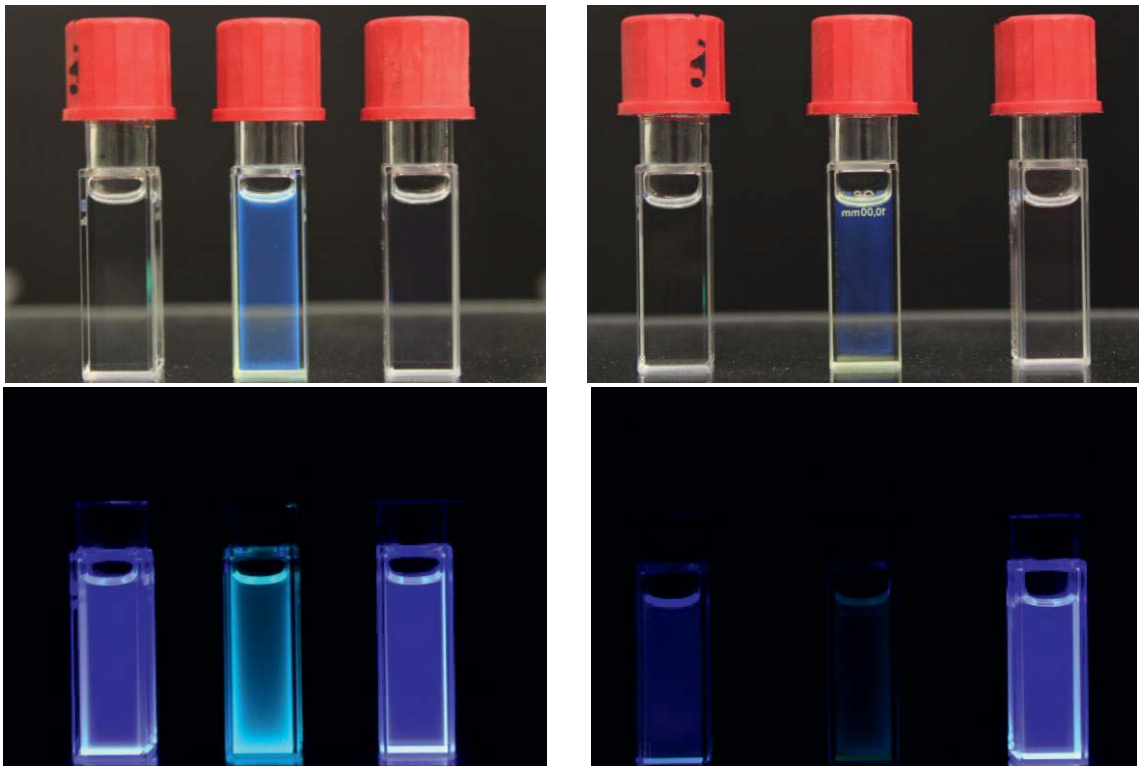

Figure 2-60: Pictures of cuvettes containing fluorescent solutions of the metallated species **8** (*left cuvette*), **9** (*middle cuvette*) and **21** (*right cuvette*). The pictures were taken at the following conditions: day light, t = 0 h (*top left*); day light, t = 24 h (*top right*); UV light 254 nm, t = 0 h (*bottom left*); UV light 254 nm, t = 24 h (*bottom right*).

The first step for this investigation was to set up 10^{-3} M solutions in toluene of the above-mentioned species for having comparable measuring conditions. The following fluorescence spectra were recorded with a slit width of 1 nm / 1 nm. In Figure 2-60 the filled

fluorescence cuvettes of the metallated compounds **8**, **9** and **21** are shown at different conditions: the pictures in the left column display the fluorescence properties of the three complexes at daylight (*top*) and under UV light irradiation of 254 nm (*bottom*), directly after transfer into the cuvettes. In addition to this, the pictures in the right column show the same cuvettes at daylight (*top*) and under UV light irradiation (*bottom*) after 24 h of aging at ambient air and without inert gas atmosphere (the caps are just loosely screwed onto the cuvettes, which explains the loss of solvent over the time).

In the case of the benzothiazole substituted ligand **9** (see middle cuvette of top left picture in Figure 2-60), daylight is sufficient to cause an intense emission of turquoise light. Only when the samples are irradiated by UV light with a wavelength of 254 nm, the oxazole containing metal complexes **8** and **21** show fluorescence phenomena by means of emitting blue light. When the samples are stored for 24 h without any inert gas atmosphere at ambient conditions, loss of emission intensity is observed under daylight as well as under UV light irradiation. In both cases the former fluorescence intensity under UV light irradiation of **9** has nearly vanished and the corresponding intensity of **8** is also much less after one day. The only exception is the solution of the methyl substituted bis-(benzoxazol-2-yl)-methanide ligand, which shows almost no change in the observed fluorescence behaviour. The observed differences in the kinetic stability of those investigated dimethyl aluminium complexes is discussed afterwards in a separate subsection (*vide infra*).

Following these qualitative observations, the next part deals with the measured fluorescence spectra of the corresponding species. Therefore, for each compound an emission and excitation spectrum was recorded. In each spectrum the detected intensity, measured in arbitrary units (counts per second), is plotted against the wavelength. The values in the brackets of the figure legend correspond to the wavelength, which is fixed for detection: e.g. "ex.(403 nm)" means, that an excitation spectrum was recorded, where only emitted light with a wavelength of 403 nm is detected, while the wavelength of the incoming irradiation for excitation is screened. In analogy to that, "em.(360 nm)" means, that an emission spectrum was recorded, where the wavelength of incoming irradiating light is fixed to 360 nm, while the wavelength dependent intensities of the emitted light are monitored.

Starting with the bis-(benzoxazol-2-yl)-methane ligand **4** and the derived $AlMe_2$ complex **8**, the recorded spectra are depicted in Spectrum 2-15. The excitation spectrum of the parent ligand **4** shows a shoulder at 360 nm and a maximum at 377 nm for detection of a fixed emission wavelength of 403 nm. The corresponding emission spectrum is almost mirror-like constructed in comparison to the excitation spectrum and exhibits two maxima at 385 nm and 403 nm for detection of a fixed excitation wavelength of 360 nm. Thus, the resulting Stokes shift between the closest maxima of the excitation and the emission adds up to 8 nm. Coming to the results of the fluorescence spectroscopic investigations of the derived group 13 complex **8**, the recorded excitation spectrum looks quite different in direct comparison to that one of **4**, because in this case two widely spaced maxima are observed (313 nm and 398 nm) with a detection wavelength of 415 nm. The emission spectrum bears a single maximum at 411 nm with a detection wavelength of 395 nm, so that the Stokes Shift results in 13 nm.

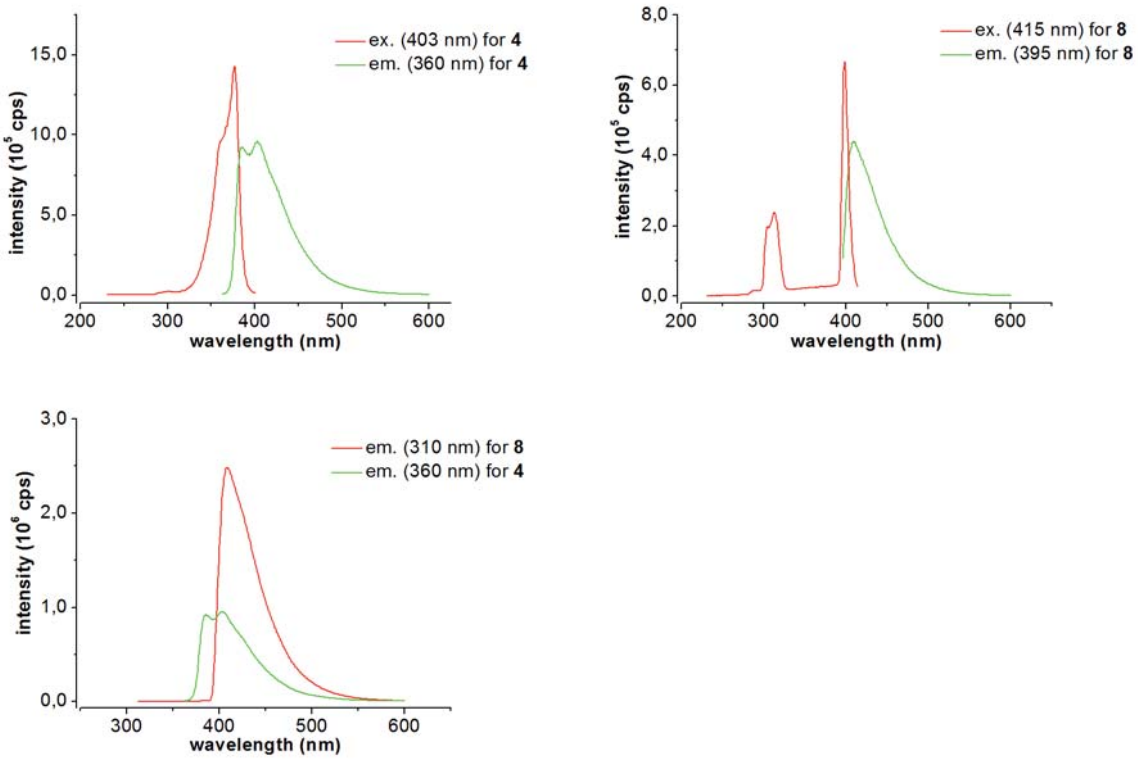

Spectrum 2-15: Fluorescence spectra for the dimethyl aluminium complex **8** compared to the parent ligand **4**: overlay of the recorded excitation and emission spectra of **4** (*top left*); overlay of the recorded excitation and emission spectra of **8** (*top right*); overlay of the emission spectra of **4** and **8** (*bottom left*).

The bottom left spectrum in Spectrum 2-15 shows an overlay of the both measured emission spectra to visualize the differences in the fluorescence intensity. In this overlay the emission spectrum of **8** was recorded at an excitation wavelength of 310 nm, because the observed emission intensity at that wavelength is five times higher as seen in the top right picture, measured with at an excitation irradiation of 395 nm. This direct comparison under same conditions reveals that the detected intensity of the metallated species **8** is about a factor of 2.7 higher than in **4**.

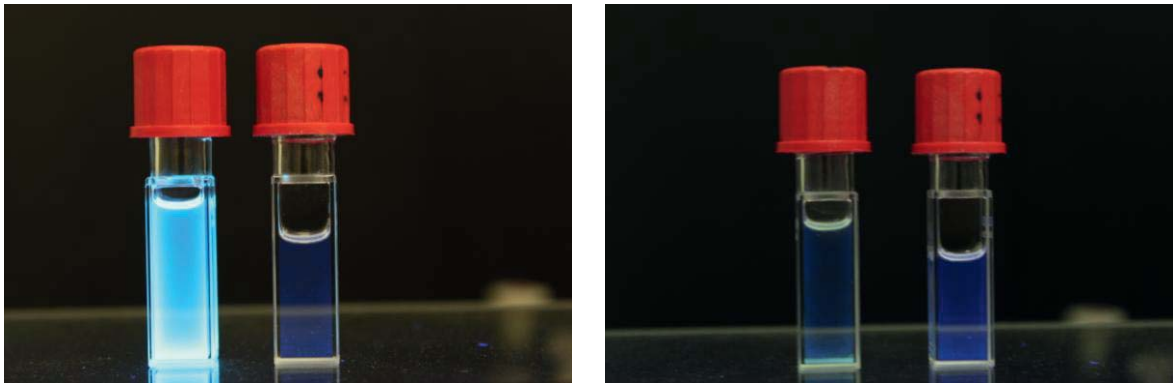

Figure 2-61: Time dependent fluorescence properties of **9** (*left cuvette*) compared to the parent ligand **5** (*right cuvette*) under UV light irradiation of 254 nm: t = 0 h (*left picture*); t = 24 h (*right picture*).

Figure 2-61 shows the time dependent fluorescence properties of the benzothiazole containing aluminium complex **9** in comparison to its starting material **5** under UV light irradiation of 254 nm. As mentioned earlier in this section, it is visible, that the former fluorescence intensity of the aluminium complex **9** is drastically decreased over a period of 24 h under ambient conditions. The observed intensity reaches nearly the same level as in the parent ligand, displayed at the right side of each picture. This decrease is supposed to be caused by the triggered decomposition of the metallated species in solution.

The corresponding fluorescence spectra of **5** and **9** are shown in Spectrum 2-16 to get a detailed impression of the different processes. Starting with the parent neutral ligand **5**, the excitation at an emission wavelength of 463 nm shows a clear defined maximum at 434 nm. The emission spectrum, recorded with an excitation wavelength of 426 nm, exhibits two maxima at 442 nm and 463 nm and shows a mirror-like shape in comparison to the excitation spectrum. Again in the case of the metallated species **9**, the recorded excitation spectrum at 480 nm consists of two well separated signal bands with in total four maxima at 333 nm, 357 nm, 463 nm and 467 nm. The emission spectrum at 357 nm consists of one small band with a maximum at 473 nm and a shoulder at 500 nm. In this case, the fluorescence spectra were measured with a slit width of 0.5 nm / 0.5 nm due to the high fluorescence intensity observed for this species.

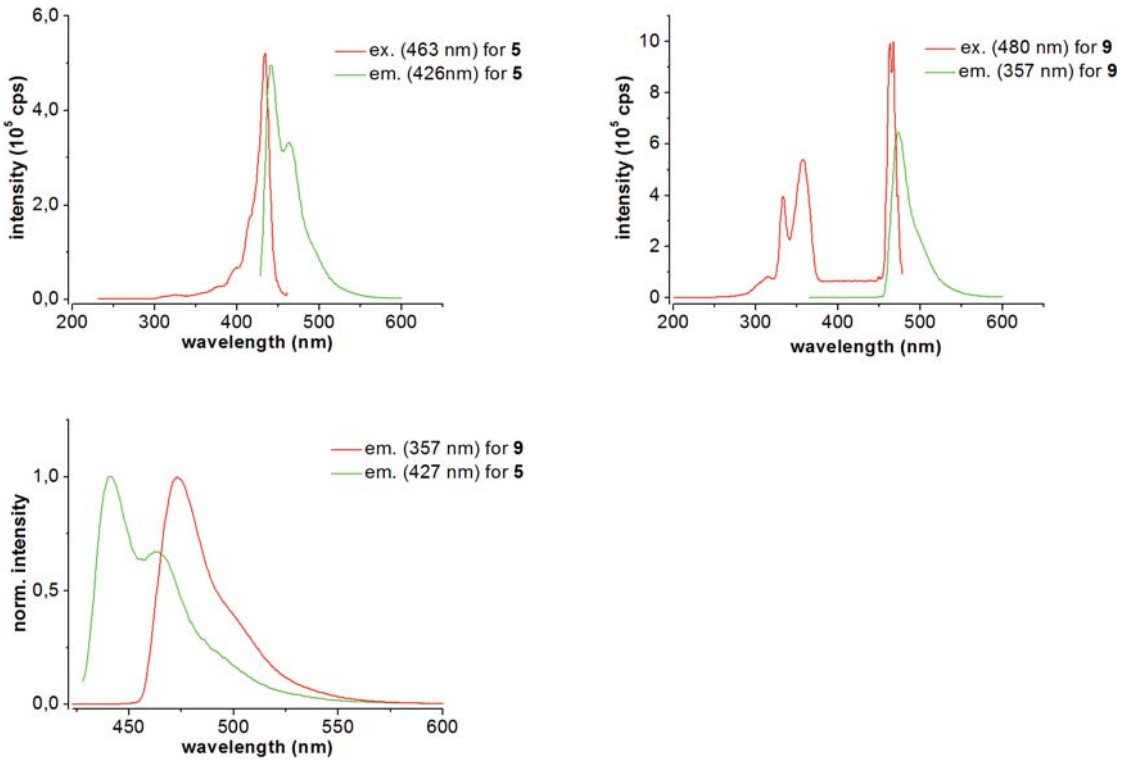

Spectrum 2-16: Fluorescence spectra for the dimethyl aluminium complex **9** compared to the parent ligand **5**: overlay of the recorded excitation and emission spectra of **5** (*top left*); overlay of the recorded excitation and emission spectra of **9** (*top right*); overlay of the normalized emission spectra of **5** and **9** (*bottom left*).

The Stokes Shift in **5** is 8 nm and in **9** about 6 nm. In the bottom left spectrum in Spectrum 2-16 a superposition plot of the emission spectra for **5** and **9** is depicted, in which the normalized intensities are plotted due to the big discrepancy in the intensities of both species. The underlying normalization was accomplished by division of each recorded intensity value by the intensity observed at the maximum. The fluorescence intensity of the metallated species is about a factor of 12.9 times higher as in the case of the neutral ligand under the same measuring conditions (slit width: 1 nm / 1 nm). The shape of both emission bands is quite similar, but due to the deprotonation the fluorescence band of **9** is shifted about 31 nm towards higher wavelength, because the expansion of the π-system leads to a red shift in emission.[129]

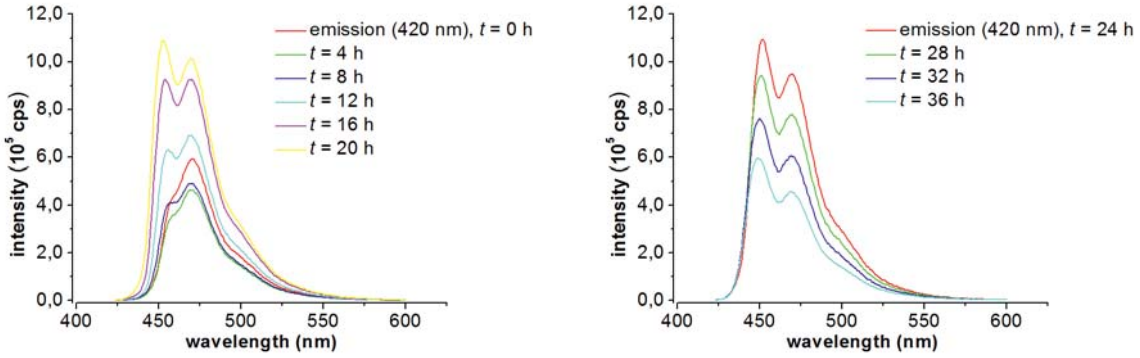

Spectrum 2-17: Fluorescence spectra for the time dependent decomposition of the dimethyl aluminium complex **9** into its parent ligand **5**: overlay of the recorded emission spectra for **9** from t = 0 h until t = 20 h (*left*); overlay of the recorded emission spectra for **9** from t = 24 h until t = 36 h (*right*).

Due to the observations, which were mentioned in the beginning of this chapter, that especially the metallated species **9** shows a strong time dependence of its fluorescence properties, time resolved emission spectra for this compound were recorded. Therefore, a freshly prepared sample solution was poured into one cuvette and the cap was just screwed loosely on it, so that the ambient air and the containing water vapour can slowly diffuse into the investigated solution of **9**. Afterwards, the emission spectra of the fluorescent solution were measured in time periods of four hours up to a total time of 36 hours to underline the changes of the fluorescence properties, which are shown in Spectrum 2-17.

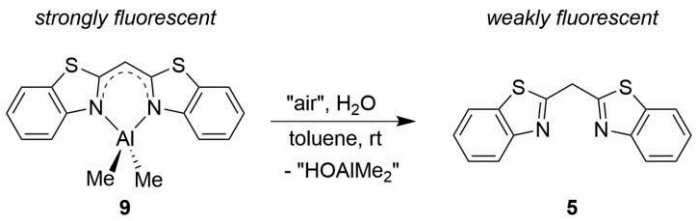

Scheme 2-42: Proposed decomposition of **9** in solution without inert gas atmosphere.

Before performing this kinetic study, it was suggested that the $AlMe_2$ complex **9** decomposes in solution preferentially into its parent neutral ligand system **5** (see Scheme 2-42) indicated by the significant loss of fluorescence intensity. Because of this assumption, the set up of the experiment has to be adjusted in that way that the emission spectra of both species should be monitored in an appropriate manner at the same time. To achieve this, the already measured excitation spectra of **5** and **9** have to be taken into account. In general, the wavelength corresponding to the maximum in the excitation spectrum should be irradiated to the sample to gain the best amplitude in intensity for the resulting emission spectrum. Therefore, the most effective excitation of both molecules would take place at the same wavelength, so that the observed emission spectrum shows maximum fluorescence intensity. In this case there is unfortunately not such an overlap in the corresponding excitation spectra of **5** and **9**, which causes to choose a wavelength of 420 nm for excitation as a kind of trade-off. For the parent ligand, this value is nearby the observed maximum and for the metallated species 420 nm is on a plateau in between the two maxima of the excitation spectra. By choosing this wavelength, it is possible to detect quite high emission intensity of **5** and still a significant emission amplitude for **9** at the same time, because the fluorescence properties of this deprotonated compound are much more intense as discussed earlier (see Spectrum 2-16), so that an excitation at the plateau level is even sufficient.

Having a closer look at the emission spectra depicted in Spectrum 2-17 left hand side, it is obvious, that the fluorescence is clearly originated by **9** at t = 0 h, referred to the observed band shape and its maximum at 473 nm. Over the next eight hours, the intensity of this band decreases slightly and a second peak at about 450 nm is fading in. After 20 hours, the emission intensity of the band increases and is nearly twice as high as in the beginning. The band shape drastically changed and is similar to that one observed for the starting material **5** itself, indicating that a large amount of the metallated species is already decomposed. Afterwards in the time frame up to 36 hours, the band shape does not change anymore, but the intensity decreases to almost half of the value monitored at t = 20 h. The interim increase of the emission intensity can maybe caused by the superposition of the both emission spectra of **5** and **9** or an adduct formation of the remaining metallated species with the proceeding amount of the free ligand, which exhibits different fluorescence behaviour.[129] The subsequent decrease can be ascribed to the proceeding decomposition of **9**, so that in the end no superposition or adduct formation is present and the observed emission originates only from the generated protonated ligand **5**.

To summarize the results of the decomposition study, it can be stated, that the bis-(benzothiazol-2-yl)-methanide complex **9** decomposes completely in solution into its parent system **5** within a period of 36 hours.

Figure 2-62: Time dependent fluorescence properties of **21** (*left cuvette*) compared to the parent ligand **19** (*right cuvette*) under UV light irradiation of 254 nm: t = 0 h (*left picture*); t = 24 h (*right picture*).

Finally, in this fluorescence study the results of the methyl substituted benzoxazole containing ligand **19** and the corresponding metal complex **21** will be presented. As it can be seen in Figure 2-62, the fluorescence intensity of the metallated compound **21** is much more intense than in the case of the parent ligand **19**. Regarding to the pictures in Figure 2-60 the utilisation of the sterically more crowded ligand system **19** enhances the kinetic stability of the derived metal complexes in solution, because the subjectively determined fluorescence intensity of **21** stayed almost the same after 24 hours. In contrast to this, the former fluorescence emission of **8** and **9** has nearly vanished after one day at ambient conditions. This result supports the hypothesis in Chapter 2.2.3, that the implementation of the additional methyl groups at the bis-(benzoxazol-2-yl)-methane scaffold causes the metal cation to be better shielded and protects it from nucleophilic attacks.

Spectrum 2-18 displays the measured fluorescence spectra of these compounds **19** and **21** in the same manner as for the previously discussed ligand systems. Starting with the neutral ligand system **19**, the upper left spectrum shows the overlay of the recorded excitation spectrum, with a fixed detected emission of 421 nm, and the corresponding emission spectrum, using irradiation with a wavelength of 357 nm. In the excitation spectrum there is a local maximum at 332 nm and a global maximum at 379 nm, whereas in the emission spectrum is just one maximum at 403 nm. The metallated species **21** shows two different bands in the excitation spectrum measured at 420 nm with peaks at 300 nm, 313 nm and 399 nm. The emission spectrum recorded at 396 nm has a maximum intensity at a wavelength of 410 nm.

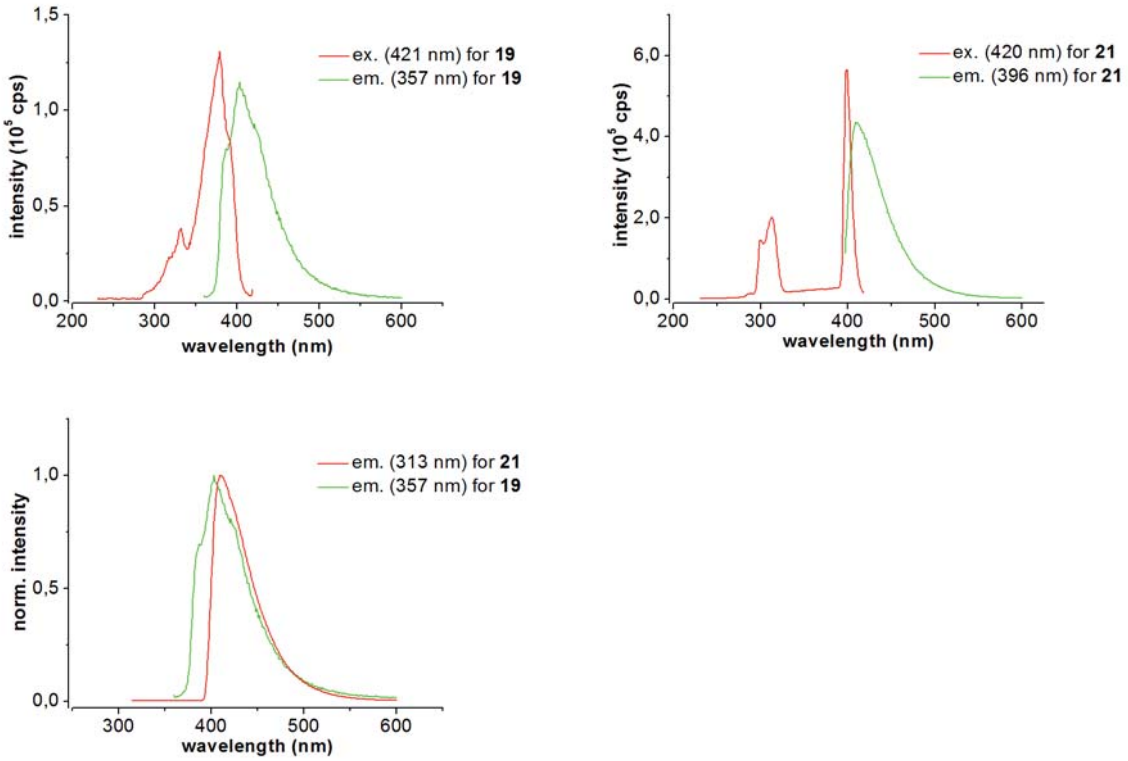

Spectrum 2-18: Fluorescence spectra for the dimethyl aluminium complex **21** compared to the parent ligand **19**: overlay of the recorded excitation and emission spectra of **19** (*top left*); overlay of the recorded excitation and emission spectra of **21** (*top right*); overlay of the normalized emission spectra of **19** and **21** (*bottom left*).

The bottom left picture displays in analogy to the other species mentioned before a superposition plot of the both normalized emission spectra of **19** and **21**, showing that the emission spectra of the starting material and the metal complex exhibit a quite similar band shape. The significant difference between those two species is the observed fluorescence intensity under same conditions, which is about 21 fold higher for the metallated species in comparison to the parent ligand.

In Spectrum 2-19, a comprehensive overview of the investigated metal complexes **8**, **9** and **21** is given to enable a quick comparison of their recorded fluorescence properties. From a qualitative point of view, the emission and excitation spectra of **8** and **21** are very similar, concluding that the additional methyl groups do not effect much the electronic properties of the ligand or the metal complex, respectively. Even the intensities of the observed maxima for each compound are nearly the same, but due to solvent and concentration effects[129] no quantitative statements regarding the absolute fluorescence emission intensities will be stated at this point. The most striking difference can be seen by having a look at the spectra of the benzothiazole compound **21**, which are noticeably red shifted compared to the oxygen containing ligand systems.

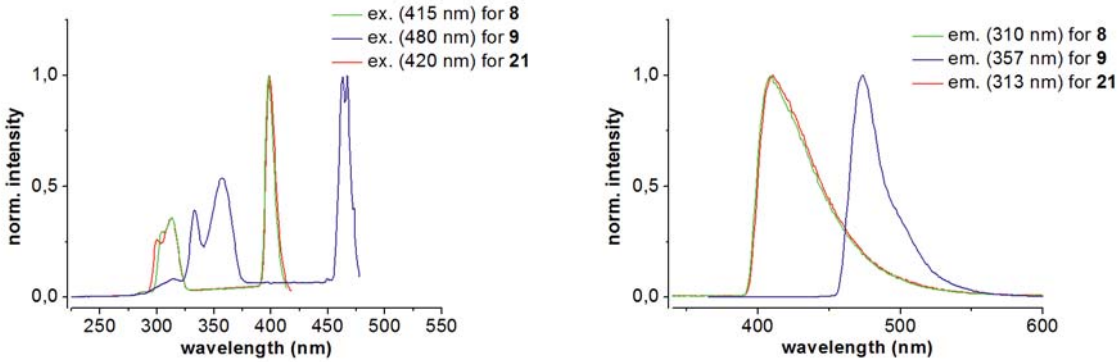

Spectrum 2-19: Overlay of the fluorescence spectra for the dimethyl aluminium complexes **8**, **9** and **21**: excitation (*left*) and emission spectra (*right*).

2.7 Excursus: Phosphorus Containing Bisheterocyclo Methanes

Following the synthetic approaches presented in Chapter 2.1 by means of the symmetrically substituted bisheterocyclo methane derivatives and the derived main group metal complexes, this section presents the synthesis attempts of phosphorus containing ligand systems. Formally, the idea behind this is that the imine nitrogen donor atoms within the five-membered heterocycles are replaced by their higher congener phosphorus to generate benzaza- and benzoxaphosphole substituents at the central methylene bridge (see Scheme 2-43). Due to this change, the differences in their reaction behaviour and the observed coordination motifs of the desired ligand systems **55** and **56** should be investigated.

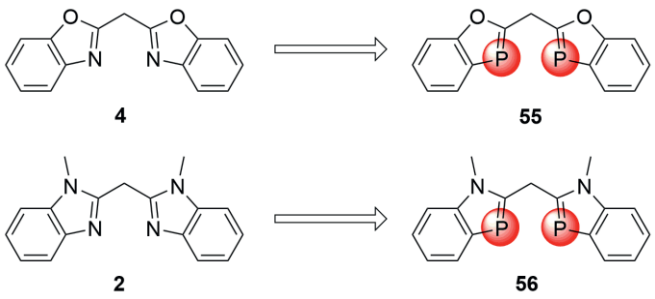

Scheme 2-43: Desired change to the phosphole derivatives **55** – **56**.

2.7.1 Outline of Phospholes

The class of benzazaphospholes, the phosphorous analogues of benzimidazoles, is already known since the end of the 1970s and several synthetic approaches were developed and improved since that time. The first described synthesis for the divalent phosphorus compound 1,3-benzazaphosphole, which could be further substituted at the 2-position, was based on the cyclization reaction of *ortho*-phosphino aniline with formimidoester hydrochlorides.[130] Further cyclization attempts were successfully performed by using acyl chlorides, esters, triethyl orthoformate or *N*,*N*-dimethyl formamide dimethyl acetal derivatives to obtain the desired phosphole in moderate yields (see Scheme 2-44).[131] Unexpectedly, these heteroaromatics are thermally stable and relatively inert towards hydrolysis and air oxidation in the solid state.[130, 131, 132] Even in solution, no hydrolysis products were monitored, while treating the reaction mixture with degassed water or aqueous H_2SO_4 or NaOH solutions for extraction of basic impurities, whereas the air oxidation is somehow triggered in solution to form oxidized compounds.[132a]

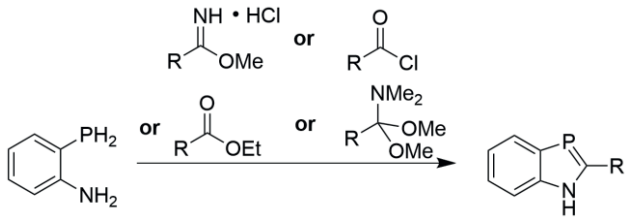

Scheme 2-44: Cyclocondensation reactions for the synthesis of benzazaphospholes starting from *ortho*-phosphino aniline.[131]

Other synthetic approaches are employing the reductive cyclocondensation of *N*-acetylated derivatives, which carry a phosphonic acid ester functionality in the *ortho*-position instead of the PH_2 moiety, with an excess of $LiAlH_4$.[132, 133] This conversion can be attributed to the slower reduction of the amide functionality in comparison to phosphonic acid. This means, that the primary phosphane is generated *in situ*, which performs a nucleophilic attack at the intermediate imidate carbon atom to give the fused heterocycle after aqueous workup at 0 °C (see Scheme 2-45). For example, the molecular structure of a C2 *t*Bu-substituted phosphole, which could be obtained in a sufficient yield of 46 % by Heinecke *et al.* executing the described procedure, is depicted at the left side of Figure 2-63.[132b] Moreover, the pyrido-annulated 1,3-azaphospholes, which differ from the benzazaphospholes by the annulated pyridine instead of a benzene moiety, are easily accessible both via reductive cyclization and by treatment of the 2-amino-3-phosphinopyridine with dimethylformamide dimethyl acetal or dimethyl acetamide dimethyl acetal.[134]

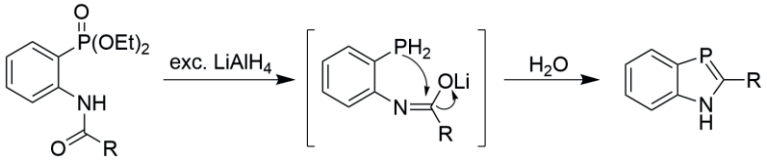

Scheme 2-45: Cyclocondensation reactions for the synthesis of benzazaphospholes starting from 2-acylamido phosphonates.[132b, 133]

Despite the functionalization of the C2-position of benzazaphosphole, bulky substituents can also be easily attached to the endocyclic nitrogen atom in a four-step synthesis by performing Pd-catalyzed C–N crosscoupling.[135] In this case, *ortho*-dibromobenzene is selectively monoaminated with bulky primary amines or anilines to give the *N*-secondary 2-bromoanilines. After phosphonylation, the reduction to the 2-phosphino derivatives and a cyclocondensation using dimethylformamide dimethyl acetal lead to the formation of the target molecules. The neopentyl substituted derivative is shown in Figure 2-63 *right*.[135]

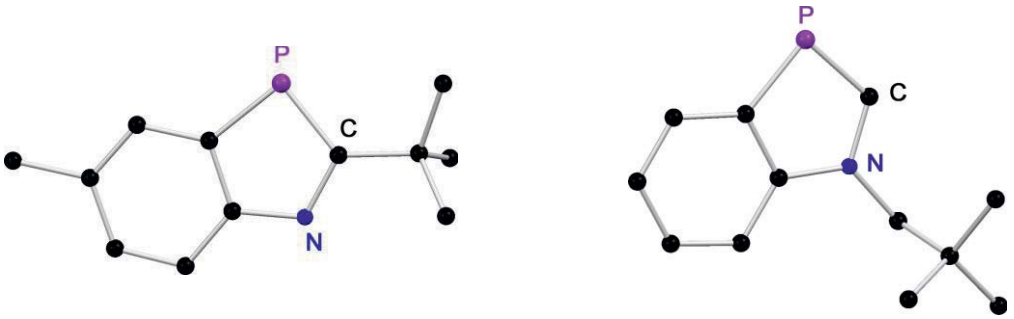

Figure 2-63: Exemplary crystal structures without anisotropic displacement parameters for a C2-substituted benzazaphosphole[132b] (*left*) and a *N*-substituted derivative[135] (*right*).

The reactivity of *N*-substituted phospholes towards *t*BuLi is shown in Scheme 2-46. For comparison reasons it should be noted in this context, that a structural investigation of the lithiated species of related benzannulated 1,3-heteroazoles like benzimidazole, benzoxazole and benzothiazole is known in the literature:[136] it was found out, that the lithiation in C2-position in the case of benzoxazole leads to the opening of the five-membered heterocycle to give the *ortho*-isonitrile substituted lithium phenolates. In contrast to this, the lithiation of the analogue imidazole or thiazole derivatives or 2-methylbenzoxazole does not lead to ring opening reactions and they remain as a fused heterocycle.[136a, 136b, 137] Switching to the benzazaphospholes, two different reactions can generally occur upon lithiation with *t*BuLi. On the one hand, the acidic proton at C2 can be replaced by Li^+ as expected **(a)** or on the other hand, the a 1,2-addition reaction of the metalorganyl to the C=P double bond (**(b)** and **(c)**) can take place due to the nucleophilicity of the *t*Bu anion (see Scheme 2-46).[138]

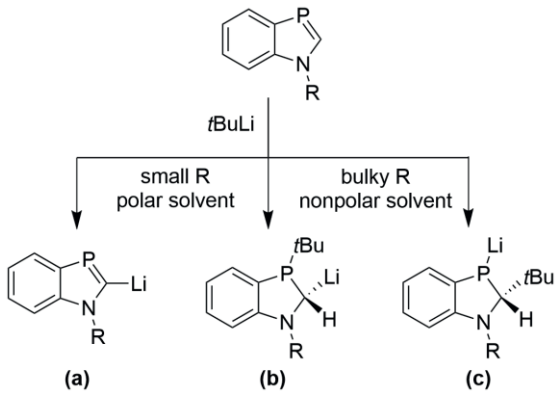

Scheme 2-46: Possible reactions of *N*-substituted benzazaphosphole with *t*BuLi dependent on the steric bulk of the residues.[138a]

By adjusting the size of the amine residue and the polarity of the used solvent, the reaction with the electron rich phosphole can be forced either to the C2-lithiation or to the 1,2-addition product. If the residue R stands for a rather small moiety like methyl or ethyl and the reaction is carried out in diethyl ether or THF, the lithiated species **(a)** is the main

product. The addition product **(b)** can only be detected in traces.[138a, 138b] The top picture of Figure 2-64 shows the crystal structure of the lithiated *N*-methylated benzazaphosphole, which is a dimeric species in the solid state with the two deprotonated C2 atoms bridging between the lithium cations. The 2-lithio-1,3-benzazaphospholes show a preferred reactivity towards electrophiles at the carbanionic centre, for example with chlorophosphanes, disulfides, CO_2 or trimethylsilyl chloride.[138b] The two latter ones were additionally used as quenching/trapping reagents for the lithiated species to confirm the intermediate structure. Going to bulkier substituents like neopentyl (Figure 2-63 *right*), 1-adamantyl or Dipp, the major product is shifted towards species **(b)** (see Scheme 2-46).[135, 138a] The neopentyl derivative is a special example for controlling the reaction selectivity: when the lithiation is carried out in pentane, the products **(b)** and **(c)** are obtained in a molar ratio of 3:1. In contrast, the use of THF as solvent and the presence of KO*t*Bu leads preferentially to the CH lithiation **(a)**. In the case of the bulkier 1-adamantyl group, the addition reaction of the *t*Bu carbanion (see species **(c)**) does not take place.[138a]

There is a quite small amount of compounds investigated so far, in which these heterocycles are involved in the coordination of transition metals.[139] Most of them are limited to the corresponding transition metal carbonyl complexes. Exemplary, different W(0) and W(II) complexes were synthesized and structurally characterized, where the coordination of one or two tungsten centres, respectively, is accomplished by the endocyclic phosphorus donor.[139c]

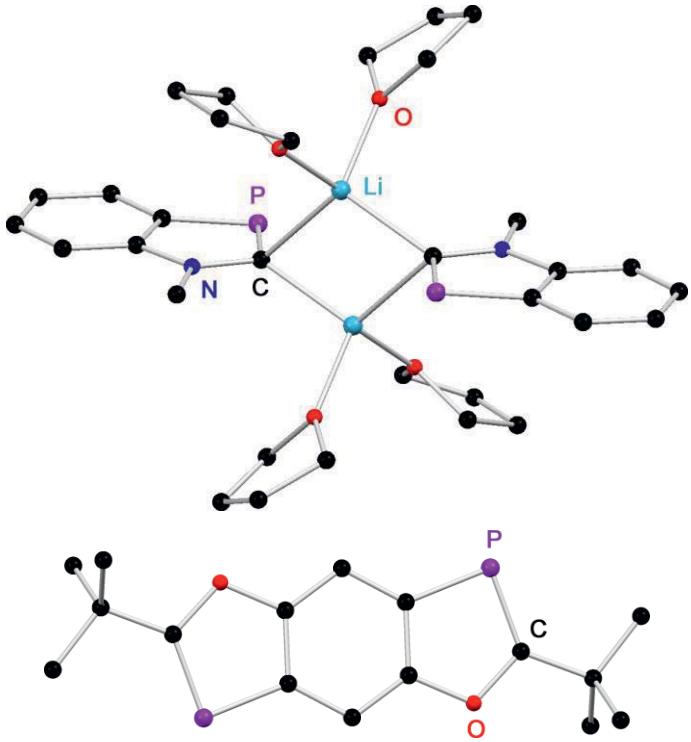

Figure 2-64: Crystal structures without anisotropic displacement parameters for a lithiated dimeric benzazaphosphole[138b] (*top*) and a benzbisoxaphosphole[140] (*bottom*).

Apart from the nitrogen and phosphorus containing benzazaphospholes, other benzannulated five-membered ring systems were part of intense research due to their photophysical properties: the replacement of the nitrogen atom by a chalcogen atom like oxygen or sulfur leads to the related class of benzoxaphospholes[140, 141a, 141b, 141c] and benzothiaphospholes.[142] In both cases, the synthesis is accomplished by a cyclocondensation reaction of the corresponding *ortho*-phosphino substituted phenol or thiophenol[143] derivative with a suitable C1 building block. For the oxygen containing phosphole, *N*-aryl imidoylchlorides or acyl chlorides were used to achieve a successful cyclization.[141b] For the higher congener benzothiaphosphole, acyl chlorides or *N*,*N*-dimethyl formamide dimethyl acetal can be used efficiently for the ring closure.[142] Furthermore, the associated arsenic containing benzazarsoles[144] and benzoxarsoles[145] were investigated several decades ago.

2.7.2 Synthesis of the Precursors

Starting with the synthesis of the benzoxaphosphole **55**, analogue to that one of the nitrogen containing ligand **4**, the *ortho* PH_2 substituted phenol derivative **51** has to be generated. This precursor is accessible in a quite good overall yield (34 %) via a three-step synthesis shown in Scheme 2-47. The first step involves the deprotonation of phenol and a subsequent reaction with diethyl phosphite to achieve a transesterification by means of the phosphate derivative **49**.[146] Afterwards, a rearrangement of the phosphonate moiety took place to obtain **50**. By using LDA as a non-nucleophilic base, a directed *ortho*-metallation of **49** could be realized, so that the requirements for the following rearrangement reaction are fulfilled.[147] The last step of this procedure was carried out by reduction of the phosphonate compound with $LiAlH_4$ in an etheral suspension to get 2-phosphinophenol **51** as precursor for the following coupling attempts (*vide infra*).[148]

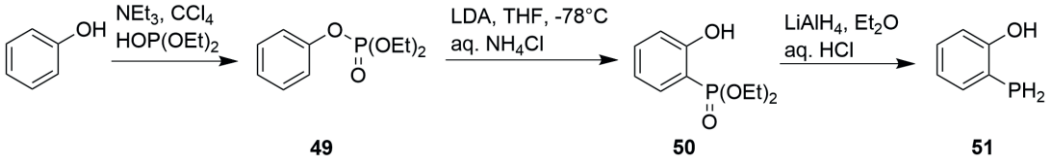

49 **50** **51**

Scheme 2-47: Synthesis route for the primary phosphane **51**.

The recorded ^{31}P-NMR spectra of those compounds are shown in Spectrum 2-20. It is obvious that the chemical shift of the phosphorus atom changes from −6.32 ppm in the phosphate **49** to 22.36 ppm in the corresponding phosphonate **50** after rearrangement. The successful synthesis of the primary phosphane **51** can be proven by the bottom spectrum, in which a proton coupled ^{31}P-NMR spectrum is measured. The phosphorus signal is significantly shifted towards higher field by means of −147.65 ppm and the coupling to the adjacent protons of the PH_2 moiety is observable as the signal's triplet structure ($^1J_{PH}$ = 199.9 Hz). Due to the high sensitivity of ^{31}P-NMR spectra, even small amounts of slight contaminations can be seen readily. But in this case no further phosphorus contain-

ing compounds were detected in solution for all three stages, underlining the high degree of purity supported by the obtained results for elemental analyses.

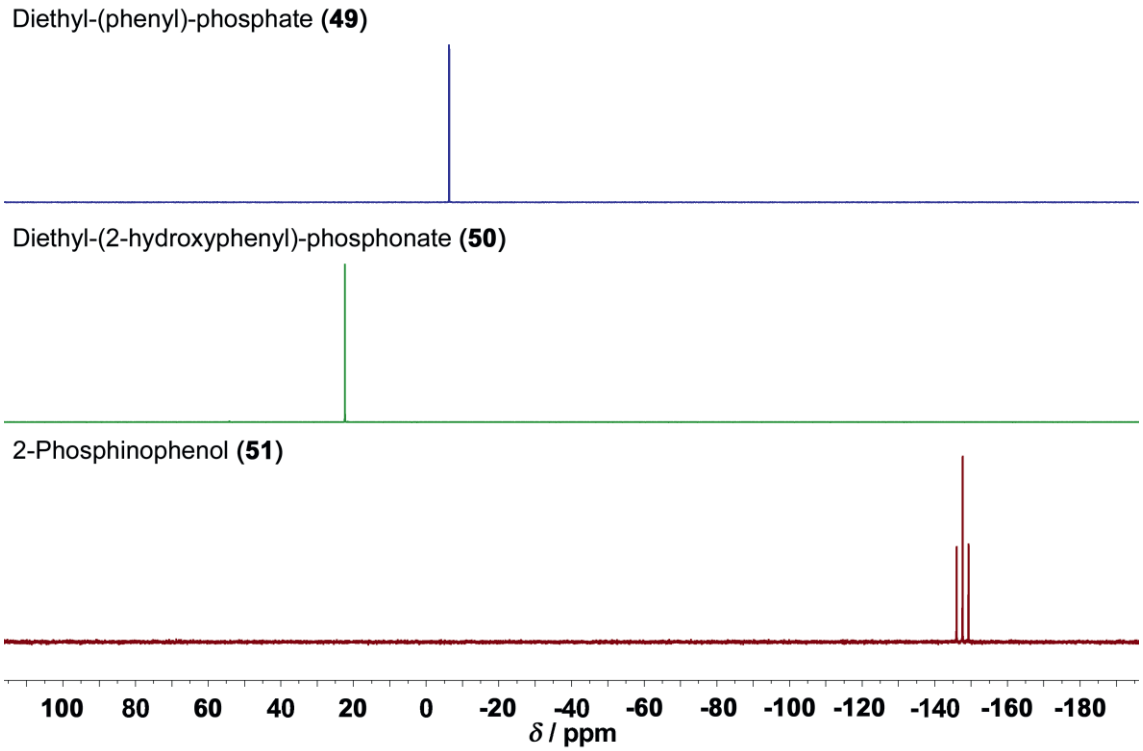

Spectrum 2-20: Overlay of the ^{31}P-NMR spectra (rt) of the precursors **49**, **50** and **51**; the upper and middle proton decoupled spectra are measured in $CDCl_3$, the bottom proton coupled spectrum is measured in THF-d_8.

According to the procedure described in Scheme 2-47, the *ortho* PH_2 substituted aniline derivative **54** has to be synthesized in advance to achieve an expected cyclocondensation reaction as in the case of the previously discussed imidazole and oxazole containing ligand systems (see Chapters 2.1 and 2.2). As depicted in Scheme 2-48, a three-step approach for the synthesis of **54** was utilized. But in contrast to the synthetic route of **51**, in this case 2-bromoaniline was used as starting material. The first step was the selective mono-methylation of the primary amine functionality by using *n*BuLi as deprotonating agent and subsequent reaction with methyl iodide. The selective mono-methylation was obtained by using two equivalents of the starting material and just one equivalent of the base and the methylation reagent at low temperature. In the next step, the bromo substituent in **52** should be replaced by the corresponding phosphonate, using a Palladium catalyzed coupling reaction with triethylphosphite.[135] Analogue to the phenol derivative **51**, the last step covers the reduction of the phosphonate **53** with $LiAlH_4$ to achieve 2-phosphino-*N*-methylaniline **54**.[135] Compared to the synthesis pathway of **51**, this route towards **54** was more challenging, so that the overall yield and the amount of the isolated final precursor **54** was quite low.

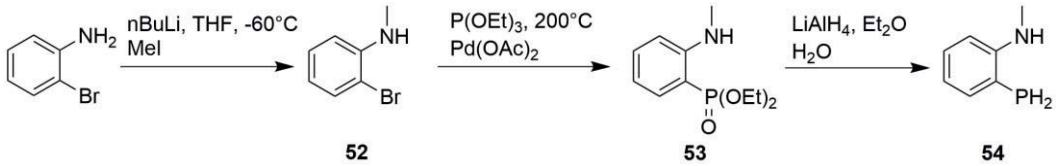

Scheme 2-48: Synthesis route for the primary phosphane **54**.

The reaction product **53** obtained after successful Palladium catalyzed coupling shows a typical chemical shift for a phosphonate (21.96 ppm). Due to the fact, that more than 100 % yield were obtained for this reaction step because of contaminations with side products and the starting material, the whole amount of the crude isolated phosphane **54** was used for the coupling attempts (*vide infra*) without running further spectroscopic investigations.

2.7.3 Coupling Attempts

Subsequently to the successful syntheses of the precursors **51** and **54**, these compounds were used as starting material with the intention to discover the new phosphorus containing ligand systems **55** and **56** as new promising ligands with different coordination behaviour. For achieving this goal, the same conditions and coupling reagents were used as in the case of the benzoxazole or benzothiazole containing methane derivatives described in Chapter 2.1.1. This means, that the *ortho*-substituted phosphino phenyl derivatives **51** and **54** were treated with different linker types like malonic dinitrile, malonyl dichloride or the activated bisimidate **3** in methanol or diethylether as appropriate organic solvent under inert gas atmosphere (see Scheme 2-49).

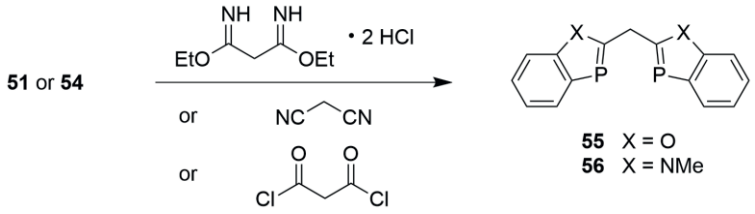

Scheme 2-49: Coupling attempts for the synthesis of **55** and **56**.

Unfortunately, each synthesis attempt failed, even if the reaction time and temperature were adjusted from several hours up to ten days, and room temperature until refluxing conditions of the used solvent. As indicator for the failed coupling and for reaction control, ^{31}P-NMR spectra of the crude reaction mixtures were recorded and evaluated. In each case, nearly no reaction took place based on the recorded ^{31}P-NMR spectrum, indicating that the major fraction of the crude product consists of the used starting material, the primary phosphane. As an example for this result, the reaction NMR for the synthesis of **55** is depicted in Spectrum 2-21. The main signal belongs to the precursor **51** and there

are a few other signals arising, which are demonstrating that many other phosphorus containing side products are formed in the course of the reaction procedure.

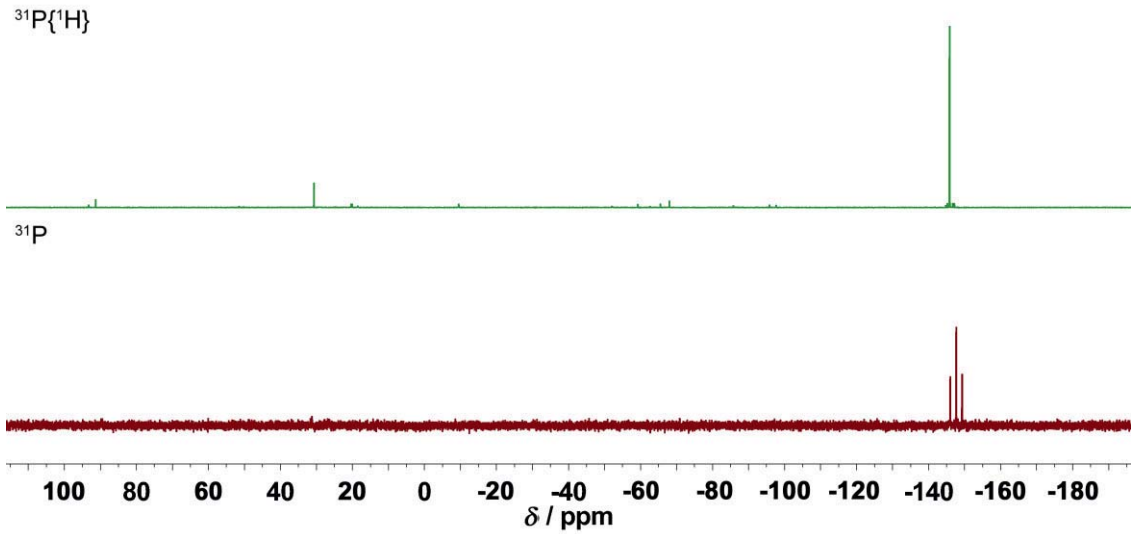

Spectrum 2-21: ^{31}P-NMR spectra (THF-d_8, rt) for the crude reaction product of the precursor **51** and **3**.

It is known, that the phosphorus resonance signal of a benzaza- or benzoxaphosphole is in a range from 70 to 85 ppm.[130, 131, 132, 133, 138b, 141b] Because in this region of the recorded NMR spectra no signal occurs, it can be concluded that no cyclic phosphole was successfully synthesized in any approach.

3 Summary and Outlook

To conclude the results of this thesis, five promising and new bisheterocyclo methane ligand systems (**4**, **5**, **19**, **32** and **34**) as well as four bisheterocyclo amine platforms (**40**, **41**, **42** and **43**) have been synthesized successfully (see Scheme 3-1). Furthermore, the derived lithiated species and group 13 metal complexes thereof (containing $AlMe_2$, AlMeCl, AlMeI, AlEtI, $GaMe_2$ or $InMe_2$ as metal fragment) were also accessible via treatment of the respective parent ligand systems with the suitable metalorganic reagent. Following this reaction procedure, it was possible to successfully synthesize 23 metal complexes bearing the monoanionic bisheterocyclo methanide ligand (**6** – **11**, **13**, **14**, **17**, **18**, **21** – **26**, **29**, **30**, **35** – **39**) and five metallated species carrying the different amine bridged ligand systems (**44** – **48**). Each compound was structurally characterized in solution by application of appropriate NMR spectroscopic techniques and performing mass spectrometry as well as elemental analyses as supporting characterization methods. Additionally, SCXRD experiments were applied for the majority of the synthesized molecules, which yielded suitable single crystals, to enable a structural elucidation and comparison of the investigated ligands and complexes in the solid state. Due to the remarkable fluorescence properties of the bisheterocyclo methanide containing complexes, fluorescence spectroscopic investigations were performed on some selected compounds to elucidate their performance as the core component of metal ion sensors.

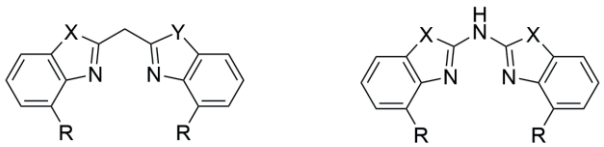

4 X = Y = O; R = H
5 X = Y = S; R = H
19 X = Y = O; R = Me
32 X = S; Y = O; R = H
34 X = S; Y = NMe; R = H

40 X = O; R = H
41 X = S; R = H
42 X = S; R = Me
43 X = S; R = OMe

Scheme 3-1: Overview of the synthesized ligand systems.

A comparison of the crystal structures of the group 13 metal complexes bearing the different homo disubstituted bisheterocyclo methanides reveals, that in each case the ligand system adopts the *trans-trans* arrangement upon deprotonation and metallation. Hence, the corresponding metal fragment is coordinated exclusively by the endocyclic nitrogen donors in a chelating fashion to form a six-membered metalla heterocycle. The other heteroatoms within the heterocyclic side arms are not involved in any significant coordination interactions. It was also shown by 2D-NMR experiments, that the chelating coordination motif observed in the solid state is also adopted in solution.

The lone pair at the bridging CH moiety, resulting from deprotonation, is delocalized over the whole ligand framework due to the mesomeric stabilization, which is also observed in the case of the nacnac ligand. This delocalization causes the ligand to adopt a nearly planar arrangement with just slight folding angles between the heteroaromatic planes, de-

pending on the coordinated metal cation. As a reason for this, the change of the bridging carbon atom's C1' hybridization can be stated: in the parent neutral ligands, C1' is assumed to be sp^3-hybridized due to the distorted tetrahedral coordination geometry by four adjacent atoms. However, after deprotonation C1' is coordinated by three neighbouring atoms in a trigonal planar geometry, suggesting that the carbon atom's hybridization changed to a more pronounced sp^2 character. The observed angles in the ligand's backbone are widened to approximately 120 deg in the metallated methanide species, whereas the angles for the parent ligands are slightly bigger than the ideal tetrahedral angle of 109.5 deg (see Figure 3-1). As a result of the delocalization, the experimentally determined bond lengths within the six-membered metalla heterocycle are half way between distinct C(sp^2)–C(sp^2) and C(sp^2)–N(sp^2) single or double bonds, respectively.

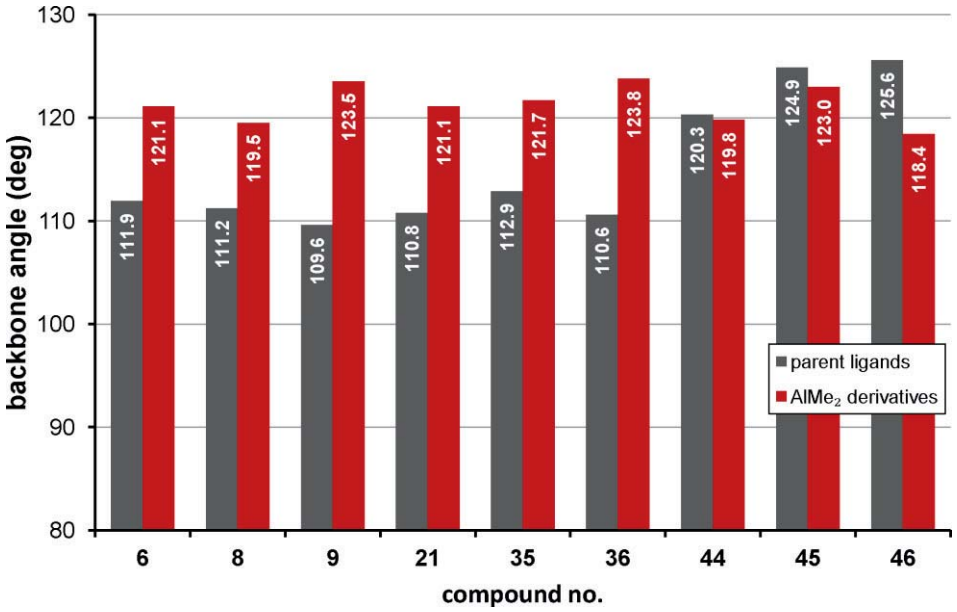

Figure 3-1: Metallation induced influence on the backbone angle in the case of the $AlMe_2$ derivatives (*red columns*) compared to their parent ligand systems (*grey columns*).

In the most cases, the metal cation is displaced out of the chelating C_3N_2 plane, which is also dependent on the used ligand platform and the coordinated metal fragment. For example, the experimentally determined folding angles and M···plane distances show for the $AlMe_2$ species **8** (9.12 deg and 29.57 pm) and **9** (1.36 deg and 13.79 pm), that the benzothiazole containing ligand fits more properly for the coordination of the Al(III) cation. In contrast to this, for the $GaMe_2$ complexes **13** (3.62 deg and 14.34 pm) and **14** (8.90 deg and 20.61 pm) the inverted preference is observed. Interestingly, the implementation of two methyl groups at the annulated benzene moieties in the case of the parent ligand **19** led to a significant change of the former stated parameters for the corresponding complexes **21** (3.72 deg and 0.54 pm) and **22** (3.80 deg and 0.68 pm). In both compounds an almost planar C_3N_2M metalla heterocycle is formed, whose high degree of planarity could not be found in other related bisheterocyclo methanides (see Figure 3-2).

For further investigations on the $AlMe_2$ or $GaMe_2$ methanide complexes, low-temperature NMR experiments should be accomplished to investigate, if the two methyl groups attached to the metal centre lead to two different signals in the ^{1}H- or ^{13}C-NMR spectra. Although in the solid state those methyl groups are not equivalent due to the ligand's folding and the out-of-plane arrangement of the metal fragment, at room temperature no splitting for those protons can be detected indicating either a different conformation in solution or fast interchange with regard to the NMR timescale. Based on the results of accompanied $^{1}H,^{15}N$-HMBC NMR correlations, the chelate complex maintains in solution, so that in theory also in solution at low temperatures a signal splitting for the two magnetically not equivalent methyl groups is expected.

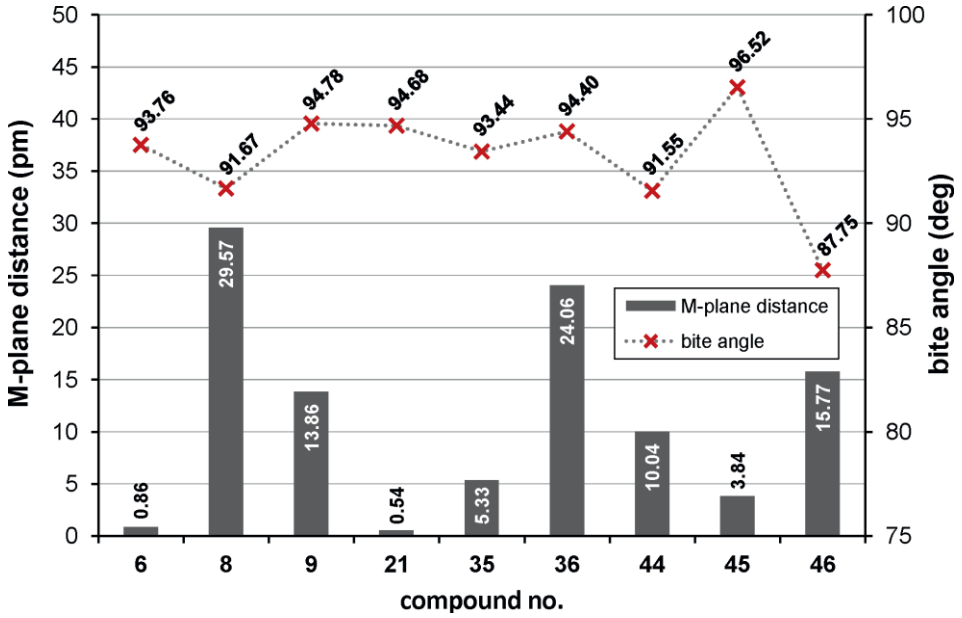

Figure 3-2: Ligand system dependent deviations from the chelating C_3N_2 or C_2N_3 plane (*grey columns*) and N–Al–N bite angles (*red crosses*) for the $AlMe_2$ compounds.

Due to the planarity within the metallated species derived from **19**, this ligand system was chosen for the synthesis attempts of the corresponding low-valent metallylene. In this planar arrangement the enhanced orbital overlap of the coordinating nitrogen atoms and the future Al(I) cation should be beneficial for the stabilization of the carbenoid structure. Therefore, several synthesis routes were tested for the generation of the corresponding intermediate $[I_2Al\{(4\text{-}MeNCOC_6H_3)_2CH\}]$, which should be reduced to the metallylene afterwards. Unfortunately, the synthesis of the AlI_2 derivative and the reduction attempts of partially halogenated aluminium complexes just led to the formation of unexpected side products. From a synthetic point of view and due to the observed formation of the hydroxido bridged metal complex **29**, it should also be feasible to yield in a corresponding terminal hydroxido complex. This controlled hydrolysis can be achieved presumably by treating the $AlMe_2$, AlMeCl or AlEtI compound directly with one equivalent of water to form a monomeric alumoxane.

Regarding to the future synthesis of a metallylene carrying $[(4\text{-}MeNCOC_6H_3)_2CH]^-$ as ligand, following aspects can be taken into account to gain deeper knowledge of the reactivity of the corresponding complexes: on the one hand, cyclovoltammetric investigations of selected aluminium containing species like **21**, **24** or **26** should be performed. The results of these measurements can reveal, if the aluminium compounds are stable at different oxidation states and if the ligand exhibits non-innocent redox behaviour. Furthermore, it can be shown, if the redox process is reversible and how the structure is affected upon the change of the metal's oxidation state.

Theoretical calculations for the stability of the desired low-valent $[Al\{(4\text{-}MeNCOC_6H_3)_2CH\}]$ should also be performed. This can support the above-mentioned assumption, that the orbital overlap within the planar ligand system stabilizes the metal centre, which bears nucleophilic as well as electrophilic reaction behaviour. By calculating the formal charge of the aluminium cation, e.g. in the case of the $AlMe_2$ derivatives **8** and **21**, it seems also to be possible to observe a correlation between that charge and the deviation of the metal centre from the metalla heterocycle.

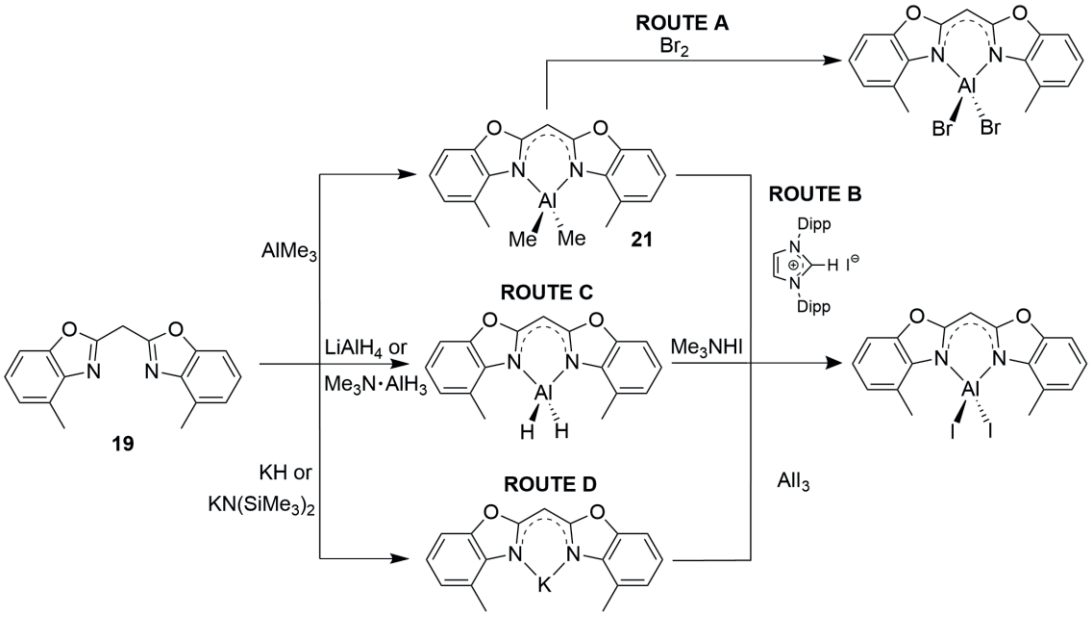

Scheme 3-2: Alternative synthesis pathways for $[X_2Al\{(4\text{-}MeNCOC_6H_3)_2CH\}]$ (X = Br, I).

Despite of the already utilized synthesis procedures for the formation of the carbenoid species, which failed so far, following alternative pathways should be considered for further synthesis attempts of the AlX_2 species (see Scheme 3-2). In route **A** the synthesis of the $AlBr_2$ containing methanide derivative is depicted. In analogy to the previously stated substitution reaction with elemental iodine, in this case bromine should be applied for substitution at the dimethyl aluminium complex **21**. Presumably, the reaction procedure using bromine leads to a better conversion. Route **B** also starts from **21** and for this approach the HI adduct of the Dipp-substituted NHC should be used the formation of $[I_2Al\{(4\text{-}MeNCOC_6H_3)_2CH\}]$. As the side products of this reaction, the free NHC and

gaseous methane are generated. In route **C** a procedure, which is already known for nacnac derivatives, is described. $LiAlH_4$ or the Lewis acid-base adduct trimethylamine and aluminium hydride can be added to the parent ligand system **19** to yield in the corresponding AlH_2 complex.[14h, 23] In a next step, this compound can be treated with trimethyl ammonium iodide, which should give the desired AlI_2 intermediate under release of H_2 and NMe_3.[14f] The last described synthesis pathway **D** deals with the fact, that another transmetallation reaction should be carried out by using the potassium complex instead of the lithiated species. This route should work better, because upon transmetallation the formed potassium iodide is more stable compared to LiI referring to the HSAB principle. The deprotonation should be feasible via usage of KH or potassium hexamethyl disilazane.

Furthermore, the conversion of the easy accessible $AlMe_2$ derivative **21** into a corresponding aluminium alkoxide by reaction with suitable alcohols seems to be a promising idea. Presumably, the resulting alkoxy residues at the aluminium act as are better leaving groups and therefore the substitution can take place more simply. The reaction with elemental iodine should also be repeated, because this starting material was not dried before usage. Thus, the iodine should be sublimed and dried over P_2O_5 prior to use, in order to get rid of residual water. Also the reduction attempts, which were performed with elemental potassium, can be optimized by using molten potassium instead of just solid pieces. This procedure enhances the reactivity of the alkali metal, because the surface area is increased and the former inert surface layer, which is covered by oxidation products, will be eliminated.

As a further outlook, also the synthesis of the derived scorpionate ligands should be attempted due to the enhanced CH-acidity of the investigated methylene bridged ligand systems. This mainly tridentate ligand class is distinguished by its facial coordination geometry in metal complexation, wherein two similar donor sites coordinate the metal centre in a chelating fashion and the remaining, different donor approaches the cation from the back. By reaction of e.g. salicylaldehyde or 2-pyridine carboxaldehyde with the parent ligands, the third donor site can be attached to the bridging moiety in a Knoevenagel condensation (see Scheme 3-3).[98a, 98b] The reduction of the resulting double bond should also lead to more flexibility in the backbone of the tripodal ligand and therefore a coordination motif as in the case of scorpionate ligands is should be achieved.

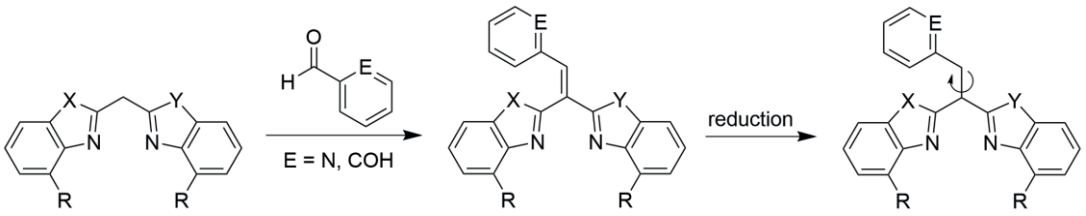

Scheme 3-3: Possible synthesis of scorpionate ligands derived from the bisheterocyclo methanes.

Additionally to the structural comparison in the solid state, the hetero or asymmetrically disubstituted bisheterocyclo methanes, which combine the features of two different benzannulated 1,3-azoles, were also comprehensively investigated by NMR spectroscopy. The complex peak pattern observed in the recorded ^{1}H- and ^{13}C-NMR spectra of the metallated derivatives could be assigned perfectly to the corresponding hydrogen and carbon atoms due to the reasonable resolution of the spectra and by applying 2D-NMR experiments. Furthermore, the different lithiated methanides were part of NMR spectroscopic investigations, so that a structural characterization thereof was ensured.

The parent ligands of the amine bridged derivatives show an interesting aggregation behaviour in the solid state depending on the substituent at the benzene perimeter, which is caused by the formation of intermolecular hydrogen bonds. In contrast to the related methane derivatives, the neutral amine ligands prefer a planar *cis-trans* arrangement in the solid state. The coordination geometry of the central nitrogen atom is trigonal planar instead of distorted tetrahedral as in the case of the bisheterocyclo methanes (see Figure 3-1). Due to those facts, in the case of **41** a vital NH tautomerism is present, wherein the proton can either be bond at the bridging or at the endocyclic nitrogen atom. Again, the metallation with $AlMe_3$ led to the formation of the *trans-trans* aligned monoanionic ligand system, in which the metal fragment is chelated by the two endocyclic imine nitrogen donors also observed for the methanides. For compound **46** it should be highlighted, that the bridging nitrogen atom is also involved in metal coordination of a second equivalent of $AlMe_3$. Within the series of herein investigated methanides and amides, this coordination via the bridging moiety is unique. Furthermore, the solid state structure of the lithiated compound **48** showed an unique feature: in absence of Lewis-donating solvent, a tetrameric species is formed, in which the ligand adopts the *cis-cis* conformation and the endocyclic as well as the bridging nitrogen atoms are involved in coordination.

4 Experimental Information

4.1 General Working Procedure

Air and moisture sensitive reactions were carried out under Schlenk conditions[149] in dried nitrogen or argon atmosphere and resulting sensitive substances were stored in an argon glovebox. The glassware was dried at 115 °C, assembled hot and cooled down under high vacuum. The used solvents were purchased in high quality and all solvents used for metallation reactions were distilled from Na or K prior to use. The starting materials were received from the companies *ABCR*, *Acros Organics*, *Sigma Aldrich*, *Deutero* and *VWR*.

4.2 Applied Analytical Methods

4.2.1 Mass Spectrometry

EI-MS:[150] Instrument *Finnigan MAT 95* (70 eV); ESI-MS:[151] Instrument *HCT Ultra*. The mass to charge ratios of the molecular ions and the fragment ions are based on the isotopes bearing the highest natural abundances (^{1}H, ^{7}Li, ^{12}C, ^{14}N, ^{16}O, ^{27}Al, ^{32}S, ^{31}P, ^{69}Ga, ^{79}Br/^{81}Br).

4.2.2 Elemental Analyses

The elemental analyses for the determination of the mass fraction of C, H, N and S were carried out on an *Elementar Vario EL3* at the Mikroanalytisches Labor, Institut für Anorganische Chemie, University of Göttingen. Several compounds are containing lattice solvent confirmed by X-ray diffraction, because the crystals were grown from the toluene mother liquor. As a result of drying these samples, not the whole amount of incorporated lattice solvent could be removed, so that no complete solvent free compounds were yielded. The remaining solvent leads to slightly enhanced values in the elemental analyses for C and H.

4.2.3 NMR Spectroscopy

The ^{1}H, ^{7}Li, ^{13}C, ^{15}N, ^{27}Al and ^{31}P-NMR spectroscopic data were recorded on a *Bruker Avance III 300 MHz*, *Bruker Avance III 400 MHz* or on a *Bruker Avance III 500 MHz* instrument. The measurements were carried out at room temperature in 1–10 % solutions of deuterated solvents. The chemical shifts δ are given in ppm and the coupling constants *J* in Hz. The residual proton signals of the deuterated solvents (mostly THF-d_8 for comparison reasons) were chosen as internal standards for ^{1}H-NMR spectra. For ^{13}C spectra, the carbon resonances of the solvents were used for calibration, too.[128, 152] In both cases the most highfield shifted signal of the deuterated THF (^{1}H-NMR: 1.73 ppm; ^{13}C-NMR: 25.37 ppm) was picked for the correct calibration. The assignment of the peaks was ac-

complished by applying two dimensional NMR techniques (^{1}H,^{1}H-COSY,[153] ^{1}H,^{13}C-HSQC,[154] ^{1}H,^{13}C-HMBC[155]). The observed multiplicities are abbreviated as follows: s = singlet, d = doublet, t = triplet, q = quartet, m = multiplet. Combined abbreviations are derived from their components (e.g. dd = doublet of doublets).

4.2.4 Fluorescence Analyses

For fluorescence analysis, a *FluoroMax-4* of the company *HORIBA Jobin Yvon* was used. The implemented xenon arc-lamp is applied as a continuous light source with a power of 150 W. The excitation and emission monochromators are based on the Czerny-Turner all-reflective optics. The excitation beam is focused to the sample compartment and about 8 % of the excitation light is split off to the reference photodiode. A photon-counting detector monitors the observed signal. It consists of a photomultiplier tube with a spectral range of 180 – 850 nm. The linear range of photon counting is up to two million cps. The entrance and exit slit widths of each monochromator can be adjusted to vary the amount of passing light. The wider the slits are, the more intense the monitored spectrum is but due to loss of resolution. Furthermore, the overflow of the detector by measurements of strong emitting samples can be prevented by decreasing the slit widths. At the host computer the software *FluorEssence* v3.0 was applied to record fluorescence spectra as well as analyze the received data graphically.

4.2.5 X-Ray Diffraction

Choice and Application of Crystals

Air sensitive crystals were extracted from Schlenk flasks under a counterflow of argon covered with perfluorinated polyether oil on a microscope slide, which was cooled with a nitrogen gas flow using the X-TEMP2 device.[156] An appropriate single crystal was chosen with the help of a polarizing microscope and mounted, inside a droplet of oil, on the tip of a MiTeGen© MicroMount loop. The loop was moved immediately to the diffractometer and fixed to a goniometer head, where the droplet was frozen due to the nitrogen flow with a temperature of 100(2) K surrounding the crystal. The oil solidified in a glass-like manner and fixed the crystal during the data collection.

Data Collection, Structure Solution and Refinement

The majority of data sets of the parent organic ligand systems or the aluminium complexes were recorded at an *Incoatec* Mo Microsource[157] and a *Bruker* TXS-Mo rotating anode, each equipped with mirror optics and an APEX II detector with a D8 goniometer. Mostly the data of the gallium and indium containing complexes were measured on an *Incoatec* Ag Microsource[158] with mirror optics and APEX II detector with a D8 goniometer. All diffractometers were equipped with a low-temperature device and used either MoK_{α} radiation of λ = 0.71073 Å or AgK_{α} radiation of λ = 0.56086 Å. The reflexes

were detected by combined ω-and φ-scans with a step width of 0.3 deg or 0.5 deg in the respective directions.

The last used version of all used programs is listed below, although different versions of them were applied over the last four years. The determination and refinement of the unit cells were accomplished by usage of APEX2 v2012/2.[159] The data were integrated with Saint v8.30C[160] and a semi-empirical absorption correction with the help of SADABS v2014/1[158, 161] was applied. In the case of non-merohedral twinned structures, the program TWINABS v2012/2[162] was used instead. After space group determination with XPREP v2014/2,[163] the structures were solved by direct methods using the program SHELXT v2014/1[164] and refined by full-matrix least-squares methods against F^2 (SHELXL v2013/4)[165] in the graphical user interface shelXle v2013/6.[166] All non-hydrogen-atoms were refined with anisotropic displacement parameters. The hydrogen atoms were refined isotropically on calculated positions using riding models[167] with their U_{iso} values constrained to equal to 1.5 times the U_{eq} of their pivot atoms for terminal sp^3 carbon atoms and 1.2 times for all other carbon atoms. Hydrogen atoms attached to heteroatoms (oxygen or nitrogen) have been found in the Fourier-density-difference map. Disordered moieties were refined using bond lengths restraints and isotropic displacement parameter restraints.

4.3 Synthesis and Characterization

4.3.1 Ethylbisimidate dihydrochloride (3)

To a solution of malonic dinitrile (3.30 g, 50.0 mmol, 1.00 eq.) in 1,4-dioxane (20 mL) ethanol (11.7 mL, 9.21 g, 200 mmol, 4.00 eq.) and hydrogen chloride (4 M in 1,4-dioxane, 50 mL, 200 mmol, 4.00 eq.) was added at once. The reaction mixture was stirred for additional 48 h at rt. Afterwards, the crude product was filtered off, washed twice with Et_2O (2 x 20 mL) and the residual solvent was removed under reduced pressure yielding the linker unit **3** (7.46 g, 32.0 mmol, 64 %) in the form of a colourless powder.

The resulting powder was used for the following cyclization reactions without further purification and spectroscopic characterization.

Molecular formula: $C_7H_{16}Cl_2N_2O_2$
Molecular weight: 231.12 g mol^{-1}
Yield: 7.460 g, 32.0 mmol, 64 %

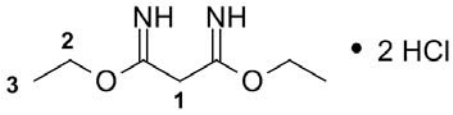

^{1}H-NMR
(300 MHz, THF-d_8): δ / ppm = 8.37 (s_{br}, 4 H, NH), 4.56 – 4.40 (m, 2 H, H1), 4.28 – 4.10 (m, 4 H, H2), 1.29 (t, J_{HH} = 7.1 Hz, 6 H, H3).

4.3.2 Bis-(benzoxazol-2-yl)-methane (4)

Method 1:

2-Aminophenol (1.99 g, 18.0 mmol, 2.0 eq.) and **3** (2.11 g, 9.1 mmol, 1.0 eq.) were dissolved in methanol (50 mL). Subsequently the reaction mixture was heated to reflux for 3 h and after cooling to rt stored at −32 °C in a refrigerator. The resulting crystalline material was filtered off, washed with sat. aq. $NaHCO_3$ solution (2 x 50 mL) and water (2 x 50 mL) and dried under reduced pressure. Crystals suitable for X-ray diffraction experiments could be obtained upon recrystallisation from ethanol. Pale yellow crystals were obtained in a yield of 1.29 g (5.1 mmol, 56 %).

Method 2:

A mixture of 2-aminophenol (8.73 g, 80.0 mmol, 2.00 eq.) and malonic acid (4.16 g, 40.0 mmol, 1.00 eq.) was suspended in polyphosphoric acid (100 mL) with the use of a sealed precision glass (KPG) stirrer. Under vigorous stirring, the reaction mixture was heated up to 150 °C and the resulting dark blue viscous solution was kept stirring at this elevated temperature over night. Then the solution was allowed to cool off to about 90 °C and was poured over ice. The formed brown solid was filtered off, washed several times with sat. aq. $NaHCO_3$ solution (6 x 50 mL) and distilled water (10 x 50 mL) until the pH neutrality. The crude product was again dissolved in acetone (60 mL) and by further filtration insoluble side products were detached. After removal of the solvent under reduced pressure, the remaining solid was recrystallized from toluene (75 mL) and stored over

night at −32 °C. The brown crystalline material was filtered off and washed with hexane (8 x 20 mL). The filtrate was concentrated to the half of the former volume, stored again at −32 °C over night, the solid was filtrated and washed with cooled pentane (4 x 20 mL). Remaining solvent of both fractions was evaporated in vacuo to give an overall yield of **4** of 3.23 g (12.9 mmol, 32 %) as pale brown powder.

Molecular formula: $C_{15}H_{10}N_2O_2$
Molecular weight: 250.25 g mol^{-1}
Yield (method 1): 1.29 g, 5.1 mmol, 56 %
Yield (method 2): 3.23 g, 12.9 mmol, 32 %

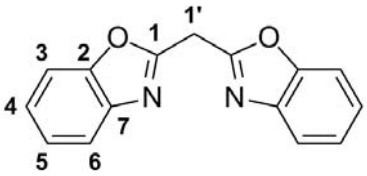

^{1}H-NMR
(300 MHz, THF-d_8): δ / ppm = 7.70 – 7.62 (m, 2 H, H6), 7.59 – 7.50 (m, 2 H, H3), 7.37 – 7.27 (m, 4 H, H4 + H5), 4.70 (s, 2 H, H1').

^{13}C{^{1}H}-NMR
(75 MHz, THF-d_8): δ / ppm = 161.46 (s, 2 C, C1), 152.35 (s, 2 C, C2), 142.66 (s, 2 C, C7), 125.89 (s, 2 C, C4), 125.17 (s, 2 C, C5), 120.83 (s, 2 C, C6), 111.30 (s, 2 C, C3), 29.58 (s, 1 C, C1').

^{15}N{^{1}H}-NMR
(30 MHz, THF-d_8): δ / ppm = −133.56 (s).

elemental analysis
in % (calculated): C, 71.86 (71.99); H, 4.03 (4.03); N, 11.12 (11.19).

EI-MS
m/*z* (%): 250 (100) $[M]^+$, 132 (25) $[M - NCOC_6H_4]^+$.

4.3.3 Bis-(benzothiazol-2-yl)-methane (5)

2-Aminothiophenol (8.55 mL, 10.0 g, 80.0 mmol, 2.0 eq.) and malononitrile (2.64 g, 40.0 mmol, 1.0 eq.) were dissolved in ethanol (40 mL). Subsequently, the reaction mixture was heated to reflux for 6 h and after cooling to rt stored at −32 °C in a fridge. The resulting yellow precipitate was filtered off, washed with hexane (2 x 50 mL) and dried under reduced pressure. Crystals suitable for X-ray diffraction experiments could be obtained upon recrystallisation from ethanol. Yellow powder was obtained in a yield of 8.36 g (30.0 mmol, 74 %).

Molecular formula: $C_{15}H_{10}N_2S_2$
Molecular weight: 282.37 g mol^{-1}
Yield: 8.36 g, 29.6 mmol, 74 %

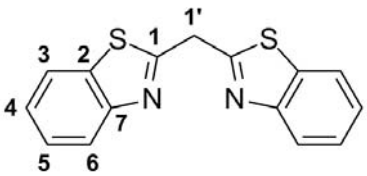

^{1}H-NMR
(300 MHz, THF-d_8): δ / ppm = 7.97 (ddd, J_{HH} = 8.2, 1.2, 0.6 Hz, 2 H, H6), 7.92 (ddd, J_{HH} = 7.9, 1.3, 0.6 Hz, 2 H, H3), 7.45 (ddd, J_{HH} = 7.9, 7.3, 1.3 Hz, 2 H, H5), 7.36 (ddd, J_{HH} = 8.1, 7.3, 1.3 Hz, 2 H, H4), 4.97 (s, 2 H, H1').

$^{13}C\{^1H\}$-NMR
(75 MHz, THF-d_8): δ / ppm = 166.68 (s, 2 C, C1), 154.47 (s, 2 C, C7), 137.04 (s, 2 C, C2), 126.79 (s, 2 C, C5), 125.94 (s, 2 C, C4), 123.88 (s, 2 C, C6), 122.49 (s, 2 C, C3), 39.19 (s, 1 C, C1').

$^{15}N\{^1H\}$-NMR
(30 MHz, THF-d_8): δ / ppm = −65.02 (s).

elemental analysis
in % (calculated): C, 63.80 (63.80); H, 3.52 (3.57); N, 9.90 (9.92); S, 22.63 (22.71).

EI-MS
m/*z* (%): 282 (100) $[M]^+$, 148 (10) $[M - NCSC_6H_4]^+$.

4.3.4 Bis-(4-methylbenzoxazol-2-yl)-methane (19)

Analogue to the synthesis of **4**

Method 1:

2-Amino-3-methylphenol (11.28 g, 91.2 mmol, 2.00 eq.) and **3** (10.54 g, 45.6 mmol, 1.00 eq.) were dissolved in methanol (170 mL). Subsequently, the reaction mixture was heated to reflux for 5 h and after cooling to rt stored at −32 °C in a refrigerator. The resulting crystalline material was filtered off, washed with sat. aq. $NaHCO_3$ solution (3 x 50 mL) and water (6 x 50 mL) and dried under reduced pressure. 4.05 g of the crude impure product were isolated and 500 mg thereof were purified via column chromatography (silica, PE/EtOAc = 5:1, 1st fraction, R_f = 0.26) to obtain compound **19** as brown powder (406 mg, 1.46 mmol, 26 % based on the applied amount of crude product). The 2nd fraction in the column chromatographic separation was isolated by using pure EtOAc as eluent, since the 1st fraction was completely collected. This side product could be identified as **20** (88 mg, 0.46 mmol, 8 %), which is a representative for the not completely proceeded cyclization reaction. Crystals of **20** suitable for X-ray diffraction experiments could be obtained upon recrystallisation from toluene.

Method 2:

In this case a smaller batch was chosen, where 2-amino-3-methylphenol (2.91 g, 23.6 mmol, 2.00 eq.) and **3** (2.73 g, 11.8 mmol, 1.00 eq.) were dissolved in methanol (55 mL). The heating time of the reaction mixture was extended for reflux over night and after cooling to rt stored at −32 °C in a refrigerator. The resulting crystalline material was filtered off, washed with sat. aq. $NaHCO_3$ solution (3 x 50 mL) and water (3 x 50 mL) and dried under reduced pressure. Crystals suitable for X-ray diffraction experiments could be obtained upon recrystallisation from toluene. Pale brown crystals were obtained in a yield of 1.43 g (5.15 mmol, 44 %).

Method 3:

A mixture of 2-amino-3-methylphenol (9.85 g, 80.0 mmol, 2.00 eq.) and malonic acid (4.16 g, 40.0 mmol, 1.00 eq.) was suspended in polyphosphoric acid (100 mL) with the use of a sealed precision glass (KPG) stirrer. Under vigorous stirring, the reaction mixture was heated up to 150 °C and the resulting dark blue viscous solution was kept stirring at this elevated temperature for 5 h. Then the solution was allowed to cool off to about 90 °C and was poured over ice. The formed grey solid was filtered off, washed several times with sat. aq. $NaHCO_3$ solution (9 x 50 mL) and distilled water (10 x 50 mL) until the pH neutrality. Remaining solvent was evaporated in vacuo to obtain **19** (6.26 g, 22.5 mmol, 56 %) as pale grey powder.

Molecular formula: $C_{17}H_{14}N_2O_2$
Molecular weight: 278.31 g mol^{-1}
Yield (method 1): 406 mg, 1.46 mmol, 26 %
Yield (method 2): 1.43 g, 5.15 mmol, 44 %
Yield (method 3): 6.26 g, 22.5 mmol, 56 %

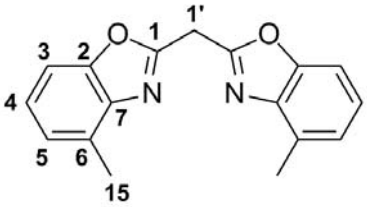

^{1}H-NMR
(300 MHz, THF-d_8): δ / ppm = 7.33 (d, $^3J_{HH}$ = 8.1 Hz, 2 H, H3,), 7.20 (t, $^3J_{HH}$ = 7.8 Hz, 2 H, H4), 7.11 (d, $^3J_{HH}$ = 7.5 Hz, 2 H, H5), 4.68 (s, 2 H, H1'), 2.55 (s, 6 H, H15).

^{13}C{^{1}H}-NMR
(75 MHz, THF-d_8): δ / ppm = 160.62 (s, 2 C, C1), 152.05 (s, 2 C, C2), 141.74 (s, 2 C, C7), 131.32 (s, 2 C, C6), 125.62 (s, 2 C, C4), 125.58 (s, 2 C, C5) 108.58 (s, 2 C, C3), 29.69 (s, 1 C, C1'), 16.41 (s, 2 C, C15).

^{15}N{^{1}H}-NMR
(30 MHz, THF-d_8): δ / ppm = −135.87 (s).

elemental analysis
in % (calculated): C, 72.90 (73.37); H, 5.14 (5.07); N, 9.90 (10.07).

EI-MS
m/*z* (%): 278 (100) $[M]^+$, 146 (10) $[M - NCOC_7H_6]^+$.

Side Product
Molecular formula: $C_{10}H_{10}N_2O_2$
Molecular weight: 190.20 g mol^{-1}
Yield: 88 mg, 0.46 mmol, 8 %

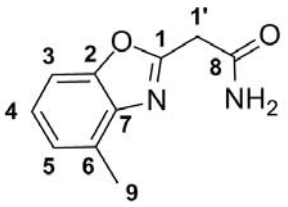

^{1}H-NMR
(300 MHz, THF-d_8): δ / ppm = 7.32 (d, $^3J_{HH}$ = 7.7 Hz, 1 H, H3), 7.17 (t, $^3J_{HH}$ = 7.8 Hz, 1 H, H4), 7.08 (d, $^3J_{HH}$ = 7.5 Hz, 1 H, H5), 7.10 – 6.90 (s_{br}, 1 H, NH_2), 6.70 – 6.45 (s_{br}, 1 H, NH_2), 3.80 (s, 2 H, H1'), 2.54 (s, 3 H, H9).

$^{13}C\{^1H\}$-NMR
(75 MHz, THF-d_8): δ / ppm = 167.60 (s, 1 C, C8), 162.07 (s, 1 C, C1), 151.85 (s, 1 C, C2), 141.77 (s, 1 C, C7), 130.88 (s, 1 C, C6), 125.37 (s, 1 C, C4), 125.18 (s, 1 C, C5), 108.42 (s, 1 C, C3), 36.89 (s, 1 C, C1'), 16.41 (s, 1 C, C9).

$^{15}N\{^1H\}$-NMR
(30 MHz, THF-d_8): δ / ppm = −279.92 (s, N2), −136.33 (s, N1).

elemental analysis
in % (calculated) C, 63.28 (63.15); H, 5.45 (5.30); N, 14.40 (14.73).

EI-MS
m/*z* (%): 190 (35) $[M]^+$, 147 (100) $[M - C(O)NH_2]^+$.

Metallation Reactions of the Bisheterocyclo Methanes:

To a solution of the corresponding ligand **1**, **2**, **4, 5, 19, 32** or **34** (1.0 eq.), dissolved in toluene, a slight excess of the organometallic reactant $AlMe_3$, $AlMe_2Cl$, $GaMe_3$ or $InMe_3$ (1.1 eq.) or a solution of *n*BuLi (3.93 M in hexane, 1.1 eq.) was slowly added at 0 °C. The reaction mixture was stirred over night and allowed to warm to rt. In the case of the lithiated species **17**, **18**, **30** and the AlMeCl complexes **10**, **11** and **24** the resulting precipitate was filtered off. The reaction mixture of the other metallated MMe_2 species **6 - 9**, **13**, **14**, **22** and **35 - 37** afforded a clear solution. Afterwards the volume of the (filtrated) solution was reduced to a few mL and the resulting concentrated solution stored at −32 °C in a refrigerator. Overnight in the most cases crystals suitable for X-ray diffraction experiments could be obtained. The crystals thus formed were filtered, washed twice with precooled toluene or hexane (0 °C) and finally dried in vacuum. The given yields below are just based on the received crystals unless stated otherwise. No further improvement of the yields was attempted because the solutions might have contained impurities upon repeated precipitation.

4.3.5 Dimethylaluminium-bis-(*N*-methylimidazol-2-yl)-methanide (6)

Big block-shaped, colourless crystals were isolated in a yield of 92 mg (0.40 mmol, 20 %; not optimized).

Molecular formula: $C_{11}H_{17}AlN_4$
Molecular weight: 232.27 g mol^{-1}
Yield: 92 mg, 0.40 mmol, 20%

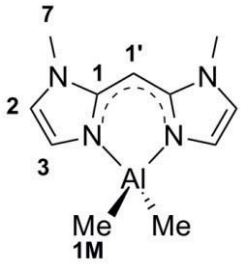

^{1}H-NMR

(400 MHz, THF-d_8): δ / ppm = 6.54 (m, 2 H, H2), 6.52 (m, 2 H, H3), 4.06 (s, 1 H, H1'), 3.28 (s, 6 H, H7), −0.85 (s, 6 H, H1M).

^{13}C{^{1}H}-NMR

(75 MHz, THF-d_8): δ / ppm = 153.92 (s, 2 C, C1), 118.32 (s, 2 C, C3), 117.45 (s, 2 C, C2), 50.46 (s, 1 C, C1'), 32.07 (s, 2 C, C7), −9.59 (s, 2 C, C1M).

^{15}N{^{1}H}-NMR

(40 MHz, THF-d_8): δ / ppm = −222.08 (s, N2), −255.73 (s, N1).

^{27}Al{^{1}H}-NMR

(78 MHz, THF-d_8): δ / ppm = 149 (s).

elemental analysis

in % (calculated): C, 56.52 (56.88); H, 7.76 (7.38); N, 24.36 (24.12).

EI-MS

m/*z* (%): 176 (100) $[M - AlMe_2]^+$, 95 (77) $[M - AlMe_2 - C_4H_5N_2]^+$, 81 (18) $[C_4H_5N_2]^+$.

4.3.6 Dimethylaluminium-bis-(*N*-methylbenzimidazol-2-yl)-methanide (7)

Colourless needle-shaped crystals in an amount of 72 mg (0.22 mmol, 44 %; not optimized) were obtained. Due to the crystals sensitivity towards air and moisture, no SCXRD could be applied for further structural investigations.

Molecular formula: $C_{19}H_{12}AlN_4$

Molecular weight: 332.39 g mol^{-1}

Yield: 72 mg, 0.22 mmol, 44 %

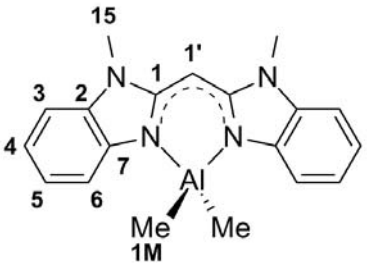

^{1}H-NMR

(300 MHz, THF-d_8): δ / ppm = 7.35 – 7.28 (m, 2 H, H6), 7.18 – 7.11 (m, 2 H, H3), 7.10 – 7.02 (m, 4 H, H4 + H5), 4.72 (s, 1 H, H1'), 3.57 (s, 6 H, H15), −0.57 (s, 6 H, H1M).

^{13}C{^{1}H}-NMR

(75 MHz, THF-d_8): δ / ppm = 156.98 (s, 2 C, C1), 139.32 (s, 2 C, C7), 135.98 (s, 2 C, C2), 122.33 (s, 2 C, C5), 121.47 (s, 2 C, C4), 112.58 (s, 2 C, C6), 108.07 (s, 2 C, C3), 55.41 (s, 1 C, C1'), 29.09 (s, 2 C, C15), −9.85 (s, 2 C, C1M).

4.3.7 Dimethylaluminium-bis-(benzoxazol-2-yl)-methanide (8)

Colourless crystals were obtained in a yield of 46 mg (0.15 mmol, 8 %; not optimized).

Molecular formula: $C_{17}H_{15}AlN_2O_2$
Molecular weight: 306.29 g mol^{-1}
Yield: 46 mg, 0.14 mmol, 8 %

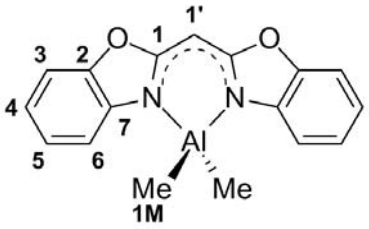

^{1}H-NMR
(300 MHz, THF-d_8): δ / ppm = 7.42 (ddd, J_{HH} = 7.8, 1.2, 0.6 Hz, 4 H, H3 + H6), 7.29 (td, J_{HH} = 7.7, 1.2 Hz, 2 H, H5), 7.19 (dd, J_{HH} = 7.7, 1.4 Hz, 2 H, H4), 5.41 (s, 1 H, H1'), −0.48 (s, 6 H, H1M).

^{13}C{^{1}H}-NMR
(75 MHz, THF-d_8): δ / ppm = 169.42 (s, 2 C, C1), 149.39 (s, 2 C, C2), 137.31 (s, 2 C, C7), 125.81 (s, 2 C, C5), 123.86 (s, 2 C, C4), 113.58 (s, 2 C, C6), 110.67 (s, 2 C, C3), 60.48 (s, 1 C, C1'), −10.22 (s, 2 C, C1M).

^{15}N{^{1}H}-NMR
(30 MHz, THF-d_8): δ / ppm = −231.31 (s).

^{27}Al{^{1}H}-NMR
(78 MHz, THF-d_8): δ / ppm = 155 (s).

elemental analysis
in % (calculated): C, 66.65 (66.66); H, 5.08 (4.94); N, 9.19 (9.15).

EI-MS
m/*z* (%): 306 (9) $[M]^+$, 291 (100) $[M - Me]^+$, 276 (10) $[M - 2\,Me]^+$, 145.5 (10) $[M - Me]^{2+}$.

4.3.8 Dimethylaluminium-bis-(benzothiazol-2-yl)-methanide (9)

Orange crystals were obtained in a yield of 450 mg (1.3 mmol, 7 %; not optimized).

Molecular formula: $C_{17}H_{15}AlN_2S_2$
Molecular weight: 338.41 g mol^{-1}
Yield: 450 mg, 1.3 mmol, 7 %

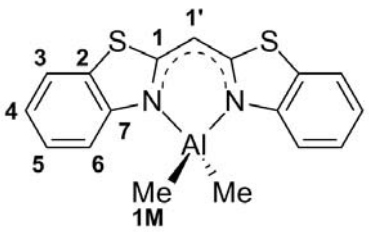

^{1}H-NMR
(500 MHz, THF-d_8): δ / ppm = 7.68 (ddd, J_{HH} = 7.9, 1.2, 0.5 Hz, 2 H, H3), 7.59 (ddd, J_{HH} = 8.2, 1.0, 0.6 Hz, 2 H, H6), 7.39 (ddd, J_{HH} = 8.2, 7.4, 1.3 Hz, 2 H, H5), 7.20 (ddd, J_{HH} = 7.9, 7.4, 1.0 Hz, 2 H, H4), 6.05 (s, 1 H, H1'), −0.43 (s, 6 H, H1M).

$^{13}C\{^{1}H\}$-NMR

(125 MHz, THF-d_8): δ / ppm = 167.22 (s, 2 C, C1), 149.25 (s, 2 C, C7), 129.48 (s, 2 C, C2), 127.52 (s, 2 C, C5), 124.01 (s, 2 C, C4), 122.56 (s, 2 C, C3), 116.09 (s, 2 C, C6), 82.56 (s, 1 C, C1'), −9.54(s, 2 C, C1M).

$^{15}N\{^{1}H\}$-NMR

(30 MHz, THF-d_8): δ / ppm = −201.16 (s).

$^{27}Al\{^{1}H\}$-NMR

(130 MHz, THF-d_8): δ / ppm = 151 (s).

elemental analysis

in % (calculated): C, 60.66 (60.33); H, 4.52 (4.47); N, 8.26 (8.28); S, 18.72 (18.95).

EI-MS

m/z (%): 338 (11) $[M]^+$, 323 (100) $[M - Me]^+$, 308 (5) $[M - 2\,Me]^+$, 161.5 (14) $[M - Me]^{2+}$.

4.3.9 Dimethylaluminium-bis-(4-methylbenzoxazol-2-yl)-methanide (21)

After the first filtration of the formed crystalline material, the filtrate was concentrated two more times, was again stored at −32 °C for further crystallization and this additional precipitate was filtered off again. So **21** can be obtained in an overall yield of 3.79 g (11.3 mmol, 68 %) in the form of yellow crystals.

Molecular formula: $C_{19}H_{19}AlN_2O_2$
Molecular weight: 334.35 g mol^{-1}
Yield: 3.79 g, 11.3 mmol, 68 %

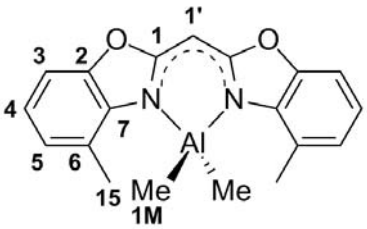

^{1}H-NMR

(500 MHz, THF-d_8): δ / ppm = 7.26 – 7.22 (m, 2 H, H3), 7.11 – 7.06 (m, 4 H, H4 + H5), 5.33 (s, 1 H, H1'), 2.66 (s, 6 H, H15), −0.38 (s, 6 H, H1M).

$^{13}C\{^{1}H\}$-NMR

(125 MHz, THF-d_8): δ / ppm = 168.70 (s, 2 C, C1), 149.29 (s, 2 C, C2), 136.98 (s, 2 C, C7), 127.63 (s, 2 C, C5), 124.33 (s, 2 C, C6), 123.81 (s, 2 C, C4), 108.01 (s, 2 C, C3), 59.95 (s, 1 C, C1'), 19.51 (s, 2 C, C15), −3.86 (s, 2 C, C1M).

$^{15}N\{^{1}H\}$-NMR

(50 MHz, THF-d_8): δ / ppm = −230.50 (s).

$^{27}Al\{^{1}H\}$-NMR

(130 MHz, THF-d_8): δ / ppm = 153 (s).

elemental analysis

in % (calculated): C, 68.21 (68.25); H, 6.18 (5.73); N, 8.30 (8.38).

EI-MS

m/*z* (%): 334.1 (10) $[M]^+$, 319.1 (64) $[M - Me]^+$, 303.1 (5) $[M - 2\ Me]^+$, 278.1 (100) $[M - AlMe_2]^+$.

4.3.10 Chloromethylaluminium-bis-(benzoxazol-2-yl)-methanide (10)

A colourless powder was obtained in a yield of 1.21 g (3.7 mmol, 74 %).

Molecular formula: $C_{16}H_{12}AlClN_2O_2$
Molecular weight: 326.72 g mol^{-1}
Yield: 1.21 g, 3.7 mmol, 74 %

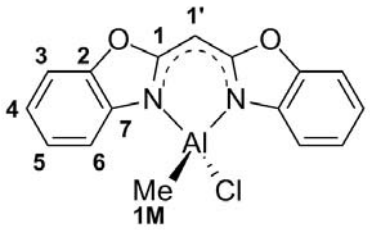

^{1}H-NMR

(500 MHz, THF-d_8): δ / ppm = 7.51 (dddd, J_{HH} = 17.1, 8.0, 1.1, 0.6 Hz, 4 H, H3 + H6), 7.35 (dd, J_{HH} = 7.7, 1.2 Hz, 2 H, H5), 7.28 – 7.24 (m, 2 H, H4), 5.62 (s, 1 H, H1'), −0.18 (s, 3 H, H1M).

^{13}C{^{1}H}-NMR

(125 MHz, THF-d_8): δ / ppm = 169.31 (s, 2 C, C1), 149.22 (s, 2 C, C2), 136.57 (s, 2 C, C7), 126.12 (s, 2 C, C5), 124.60 (s, 2 C, C4), 114.08 (s, 2 C, C6), 110.98 (s, 2 C, C3), 61.79 (s, 1 C, C1'), −10.18 (s, 1 C, C1M).

^{15}N{^{1}H}-NMR

(50 MHz, THF-d_8): δ / ppm = −231.52 (s).

^{27}Al{^{1}H}-NMR

(78 MHz, THF-d_8): δ / ppm = 133 (s).

elemental analysis

in % (calculated): C, 60.13 (58.82); H, 4.04 (3.70); N, 8.25 (8.57) (deviation due to remaining toluene).

EI-MS

m/*z* (%): 326 (26) $[M]^+$, 311 (100) $[M - Me]^+$, 291 (4) $[M - Cl]^+$, 155.5 (10) $[M - Me]^{2+}$.

4.3.11 Chloromethylaluminium-bis-(benzothiazol-2-yl)-methanide (11)

A yellow powder was obtained in a yield of 3.33 g (9.3 mmol, 93 %).

Molecular formula: $C_{16}H_{12}AlClN_2S_2$
Molecular weight: 358.84 g mol^{-1}
Yield: 3.33 g, 9.3 mmol, 93 %

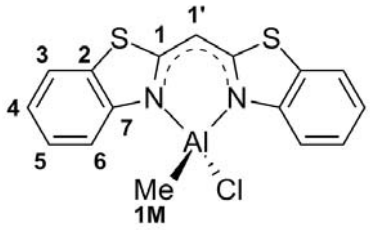

^{1}H-NMR
(500 MHz, THF-d_8): δ / ppm = 7.77 (ddd, J_{HH} = 8.2, 1.0, 0.6 Hz, 2 H, H3), 7.72 (ddd, J_{HH} = 7.9, 1.2, 0.6 Hz, 2 H, H6), 7.47 – 7.40 (m, 2 H, H5), 7.26 (ddd, J_{HH} = 7.9, 7.4, 1.0 Hz, 2 H, H4), 6.26 (s, 1 H, H1'), −0.18 (s, 3 H, H1M).

^{13}C{^{1}H}-NMR
(125 MHz, THF-d_8): δ / ppm = 167.55 (s, 2 C, C1), 148.29 (s, 2 C, C7), 129.12 (s, 2 C, C2), 127.80 (s, 2 C, C5), 124.68 (s, 2 C, C4), 122.75 (s, 2 C, C3), 116.69 (s, 2 C, C6), 83.55 (s, 1 C, C1'), −9.27 (s, 1 C, C1M).

^{15}N{^{1}H}-NMR
(50 MHz, THF-d_8): δ / ppm = −204.41 (s).

^{27}Al{^{1}H}-NMR
(78 MHz, THF-d_8): δ / ppm = 128 (s).

elemental analysis
in % (calculated): C, 53.09 (53.56); H, 3.32 (3.37); N, 7.92 (7.81); S, 17.40 (17.87).

EI-MS
m/*z* (%): 358 (28) $[M]^+$, 343 (100) $[M - Me]^+$, 323 (4) $[M - Cl]^+$, 171.5 (18) $[M - Me]^{2+}$.

4.3.12 Chloromethylaluminium-bis-(4-methylbenzoxazol-2-yl)-methanide (24)

A pale yellow powder was obtained in a yield of 1.37 g (3.9 mmol, 77 %).

Molecular formula: $C_{18}H_{16}AlClN_2O_2$
Molecular weight: 354.77 g mol^{-1}
Yield: 1.37 g, 3.9 mmol, 77 %

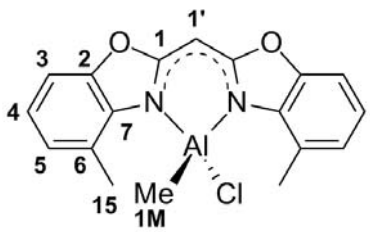

^{1}H-NMR

(400 MHz, THF-d_8): δ / ppm = 7.33 – 7.27 (m, 2 H, H3), 7.17 – 7.11 (m, 4 H, H4 + H5), 5.55 (s, 1 H, H1'), 2.78 (s, 6 H, H15), −0.14 (s, 3 H, H1M).

^{13}C{^{1}H}-NMR

(125 MHz, THF-d_8): δ / ppm = 168.67 (s, 2 C, C1), 149.14 (s, 2 C, C2), 136.07 (s, 2 C, C7), 128.02 (s, 2 C, C5), 125.05 (s, 2 C, C6), 124.54 (s, 2 C, C4), 108.24 (s, 2 C, C3), 61.18 (s, 1 C, C1'), 19.93 (s, 2 C, C15), −3.68 (s, 1 C, C1M).

^{15}N{^{1}H}-NMR

(50 MHz, THF-d_8): δ / ppm = −246.89 (s).

^{27}Al{^{1}H}-NMR

(78 MHz, THF-d_8): δ / ppm = 128 (s).

elemental analysis

in % (calculated): C, 60.99 (60.94); H, 4.57 (4.55); N, 8.17 (7.90).

EI-MS

m/*z* (%): 278 (100) $[M - AlMeCl]^+$, 146 (45) $[M - AlMeCl - NCOC_7H_6]^+$, 132 (8) $[NCOC_7H_6]^+$.

4.3.13 Trimethylgallium (12)

Under argon atmosphere a 100 mL two-necked flask, whose middle neck was equipped with a distillation bridge and a preceding Vigreux column and the second neck with a pressure-equalizing dropping funnel, was charged with $GaCl_3$ (14.9 g, 84.6 mmol, 1.00 eq.). The dropping funnel was filled with pure $AlMe_3$ (24.5 mL, 18.36 g, 254.7 mmol, 3.00 eq.) and, under ice-cooling and stirring, $AlMe_3$ was added dropwisely to the $GaCl_3$, whereby temporarily a sticky grey suspension is formed. After complete addition of $AlMe_3$, a colourless liquid could be obtained and the reaction mixture was stirred for additional 30 min at rt. Then the crude product was distilled to separate the two major fractions: 1st fraction (boiling point 55 °C, colourless liquid, $GaMe_3$), 2nd fraction (boiling point 120 °C, colourless liquid, $AlMe_2Cl$). Please note, that each glass connection has to be sealed airtight by using special PTFE grease, because all reagents are very pyrophoric in contact with air and are prone for reacting with silicon grease. Referring to the first fraction, compound **12** could be isolated as a colourless liquid (7.77 mL, 8.80 g, 76.6 mmol, 91 %). The isolated 1st fraction was used for following metallation reactions without further purification and spectroscopic characterization.

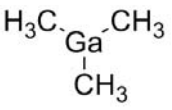

Molecular formula: C_3H_9Ga

Molecular weight: 114.83 g mol^{-1}

Yield: 7.77 mL, 8.80 g, 76.6 mmol, 91 %

boiling points

1st fraction 55 °C (literature for $GaMe_3$: 55.7 °C)[168]

2nd fraction 120 °C (literature for $AlMe_2Cl$: 126-127 °C)[103a]

4.3.14 Dimethylgallium-bis-(benzoxazol-2-yl)-methanide (13)

Pale yellow crystals were obtained in a yield of 0.583 g (1.54 mmol, 31 %; not optimized).

Molecular formula: $C_{17}H_{15}GaN_2O_2$
Molecular weight: 349.04 g mol^{-1}
Yield: 0.583 g, 1.54 mmol, 31 %

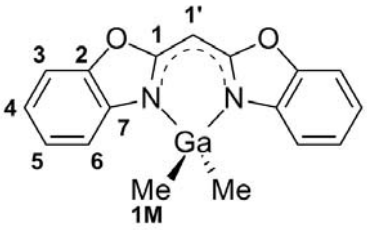

^{1}H-NMR
(500 MHz, THF-d_8): δ / ppm = 7.38 (ddd, J_{HH} = 8.0, 1.1, 0.6 Hz, 2 H, H3), 7.29 – 7.21 (m, 4 H, H5 + H6), 7.14 (ddd, J_{HH} = 8.0, 7.2, 1.5 Hz, 2 H, H4), 5.25 (s, 1 H, H1'), −0.06 (s, 6 H, H1M).

^{13}C{^{1}H}-NMR
(75 MHz, THF-d_8): δ / ppm = 168.63 (s, 2 C, C1), 149.35 (s, 2 C, C2), 138.41 (s, 2 C, C7), 125.53 (s, 2 C, C5), 123.21 (s, 2 C, C4), 112.95 (s, 2 C, C6), 110.40 (s, 2 C, C3), 59.23 (s, 1 C, C1'), −7.39 (s, 2 C, C1M).

^{15}N{^{1}H}-NMR
(50 MHz, THF-d_8): δ / ppm = −229.86 (s).

elemental analysis
in % (calculated): C, 58.45 (58.50); H, 4.35 (4.33); N, 8.21 (8.03).

EI-MS
m/*z* (%): 348 (11) $[M]^+$, 333 (100) $[M - Me]^+$, 318 (17) $[M - 2\ Me]^+$, 166.5 (10) $[M - Me]^{2+}$, 69 (11) Ga^+.

4.3.15 Dimethylgallium-bis-(benzothiazol-2-yl)-methanide (14)

Yellow crystals were obtained in a yield of 138 mg (0.36 mmol, 36 %; not optimized).

Molecular formula: $C_{17}H_{15}GaN_2S_2$
Molecular weight: 381.16 g mol^{-1}
Yield: 138 mg, 0.36 mmol, 36 %

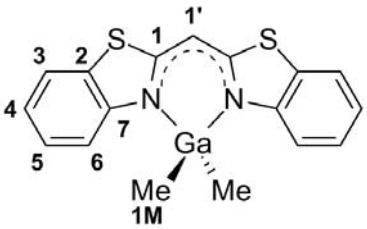

^{1}H-NMR
(500 MHz, THF-d_8): δ / ppm = 7.64 (ddd, J_{HH} = 7.8, 1.2, 0.6 Hz, 2 H, H3), 7.40 (ddd, J_{HH} = 8.1, 1.1, 0.6 Hz, 2 H, H6), 7.36 – 7.32 (m, 2 H, H5), 7.14 (ddd, J_{HH} = 7.9, 7.3, 1.2 Hz, 2 H, H4), 5.87 (s, 1 H, H1'), −0.02 (s, 6 H, H1M).

$^{13}C\{^1H\}$-NMR
(75 MHz, THF-d_8): δ / ppm = 165.82 (s, 2 C, C1), 149.77 (s, 2 C, C7), 129.57 (s, 2 C, C2), 127.35 (s, 2 C, C5), 123.48 (s, 2 C, C4), 122.40 (s, 2 C, C3), 115.44 (s, 2 C, C6), 81.28 (s, 1 C, C1'), −6.71 (s, 2 C, C1M).

$^{15}N\{^1H\}$-NMR
(50 MHz, THF-d_8): δ / ppm = −199.22 (s).

elemental analysis
in % (calculated): C, 58.45 (58.50); H, 4.35 (4.33); N, 8.21 (8.03).

EI-MS
m/*z* (%): 380 (13) $[M]^+$, 365 (100) $[M - Me]^+$, 350 (21) $[M - 2\,Me]^+$, 182.5 (9) $[M - Me]^{2+}$, 69 (14) Ga^+.

4.3.16 Dimethylgallium-bis-(4-methylbenzoxazol-2-yl)-methanide (22)

Yellow brownish crystals were obtained in a yield of 308 mg (0.82 mmol, 17 %; not optimized).

Molecular formula: $C_{19}H_{19}GaN_2O_2$
Molecular weight: 377.10 g mol^{-1}
Yield: 308 mg, 0.82 mmol, 17 %

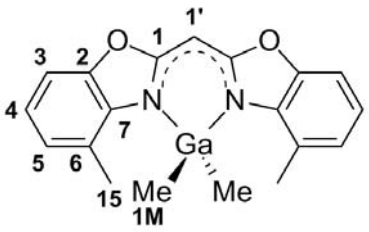

^1H-NMR
(400 MHz, THF-d_8): δ / ppm = 7.22 – 7.13 (m, 2 H, H3), 7.07 – 6.99 (m, 4 H, H4 + H5), 5.18 (s, 1 H, H1'), 2.57 (s, 6 H, H15), 0.06 (s, 6 H, H1M).

$^{13}C\{^1H\}$-NMR
(75 MHz, THF-d_8): δ / ppm = 167.84 (s, 2 C, C1), 149.20 (s, 2 C, C2), 137.57 (s, 2 C, C7), 127.27 (s, 2 C, C5), 123.60 (s, 2 C, C6), 123.15 (s, 2 C, C4), 107.85 (s, 2 C, C3), 58.83 (s, 1 C, C1'), 19.01 (s, 2 C, C15), −0.95 (s, 2 C, C1M).

$^{15}N\{^1H\}$-NMR
(40 MHz, THF-d_8): δ / ppm = −229.69 (s).

elemental analysis
in % (calculated) C, 60.84 (60.52); H, 5.24 (5.08); N, 7.45 (7.43).

EI-MS
m/*z* (%): 376.1 (17) $[M]^+$, 361.0 (100) $[M - Me]^+$, 346.0 (20) $[M - 2\,Me]^+$, 277.1 (12) $[M - GaMe_2]^+$, 68.9 (41) Ga^+.

4.3.17 Dimethylindium-bis-(4-methylbenzoxazol-2-yl)-methanide (23)

Orange crystals were obtained in a yield of 78 mg (0.18 mmol, not optimized). In this particular case the added amount of $InMe_3$ could not be determined correctly due to following facts: Under ambient temperature and pressure, pure $InMe_3$ should normally be solid, but in the used flask a liquid was present. As a consequence, this has to be a solution of $InMe_3$ in an unknown solvent with an unknown concentration, because nothing of those properties was given at the flask. So 0.3 mL of this solution was added to the dissolved ligand. Because of not knowing the added equivalents of $InMe_3$, no percental yield of the resulting crystals can be stated.

Molecular formula: $C_{19}H_{19}InN_2O_2$
Molecular weight: 422.18 g mol^{-1}
Yield: 78 mg, 0.18 mmol

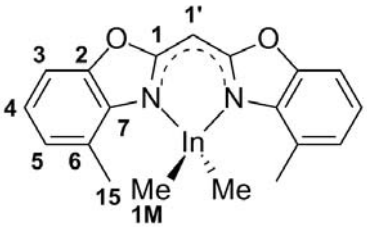

^{1}H-NMR
(500 MHz, THF-d_8): δ / ppm = 7.18 – 7.13 (m, 2 H, H3), 7.00 – 6.95 (m, 4 H, H4 + H5), 5.12 (s, 1 H, H1'), 2.54 (s, 6 H, H15), 0.13 (s, 6 H, H1M).

^{13}C{^{1}H}-NMR
(125 MHz, THF-d_8): δ / ppm = 168.36 (s, 2 C, C1), 148.95 (s, 2 C, C2), 139.27 (s, 2 C, C7), 126.58 (s, 2 C, C5), 122.94 (s, 2 C, C6), 122.66 (s, 2 C, C4), 107.81 (s, 2 C, C3), 59.07 (s, 1 C, C1'), 18.59 (s, 2 C, C15), −2.91 (s, 2 C, C1M).

^{15}N{^{1}H}-NMR
(50 MHz, THF-d_8): δ / ppm = −226.16 (s).

elemental analysis
in % (calculated): C, 54.52 (54.05); H, 4.92 (4.54); N, 6.70 (6.64).

4.3.18 Lithium-bis-(benzoxazol-2-yl)-methanide (17)

To a solution of **4** (1.0 mmol, 1.0 eq.), dissolved in toluene (20 mL), dropwisely *n*-BuLi (3.93 M in hexane, 0.51 mL, 2.0 mmol, 2.0 eq.) was added under ice-cooling. After warming up to rt, the resulting slurry was stirred over night. The remaining solvent was evaporated under reduced pressure to give the lithiated species as a powder.

A pale yellow powder was yielded in an amount of 210 mg (0.81 mmol, 81 %).

Molecular formula: $C_{15}H_{12}LiN_2O_2$
Molecular weight: 259.21 g mol^{-1}
Yield: 210 mg, 0.81 mmol, 81 %

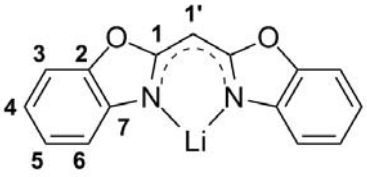

^{1}H-NMR

(400 MHz, THF-d_8): δ / ppm = 7.12 (d, J_{HH} = 7.7 Hz, 2 H, H3), 7.08 (d, J_{HH} = 7.7 Hz, 2 H, H6), 6.98 (t, J_{HH} = 7.5 Hz, 2 H, H5), 6.82 (t, J_{HH} = 7.6 Hz, 2 H, H4), 4.80 (s, 1 H, H1').

^{13}C{^{1}H}-NMR

(75 MHz, THF-d_8): δ / ppm = 171.16 (s, 2 C, C1), 150.35 (s, 2 C, C2), 145.48 (s, 2 C, C7), 123.53 (s, 2 C, C5), 119.67 (s, 2 C, C4), 113.39 (s, 2 C, C6), 108.54 (s, 2 C, C3), 57.37 (s, 1 C, C1').

^{7}Li{^{1}H}-NMR

(117 MHz, THF-d_8): δ / ppm = 1.89 (s).

^{15}N{^{1}H}-NMR

(50 MHz, THF-d_8): δ / ppm = −201.42 (s).

EI-MS

m/*z* (%): 250 (100) $[M - Li]^+$, 132 (45) $[M - NCOC_6H_4]^+$, 43 (51) $[NCO]^+$.

4.3.19 Lithium-bis-(benzothiazol-2-yl)-methanide (18)

An orange powder was isolated in an amount of 256 mg (0.88 mmol, 88 %).

Molecular formula: $C_{15}H_{12}LiN_2S_2$
Molecular weight: 291.34 g mol^{-1}
Yield: 256 mg, 0.88 mmol, 88 %

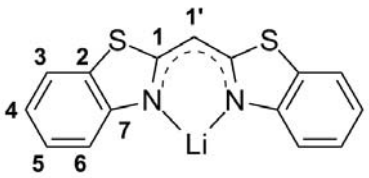

^{1}H-NMR

(300 MHz, THF-d_8): δ / ppm = 7.43 (ddd, J_{HH} = 7.7, 1.3, 0.6 Hz, 2 H, H3), 7.23 (ddd, J_{HH} = 8.0, 1.2, 0.5 Hz, 2 H, H6), 7.09 (ddd, J_{HH} = 8.0, 7.3, 1.3 Hz, 2 H, H5), 6.83 (ddd, J_{HH} = 7.7, 7.3, 1.2 Hz, 2 H, H4), 5.38 (s, 1 H, H1').

^{13}C{^{1}H}-NMR

(75 MHz, THF-d_8): δ / ppm = 167.05 (s, 2 C, C1), 156.88 (s, 2 C, C7), 131.90 (s, 2 C, C2), 125.76 (s, 2 C, C5), 121.08 (s, 2 C, C4), 120.34 (s, 2 C, C3), 116.01 (s, 2 C, C6), 80.12 (s, 1 C, C1').

^{7}Li{^{1}H}-NMR

(117 MHz, THF-d_8): δ / ppm = 2.26 (s).

^{15}N{^{1}H}-NMR

(50 MHz, THF-d_8): δ / ppm = −157.14 (s).

elemental analysis

in % (calculated): C, 60.43 (62.49); H, 3.24 (3.15); N, 9.01 (9.72); S, 20.12 (22.24).

EI-MS

m/*z* (%): 282 (100) $[M - Li]^+$, 148 (16) $[M - NCSC_6H_4]^+$, 134 (5) $[NCSC_6H_4]^+$.

4.3.20 Lithium-bis-(4-methylbenzoxazol-2-yl)-methanide (30)

A colourless powder was yielded in an amount of 69 mg (0.24 mmol, 24 %; not optimized).

Molecular formula: $C_{17}H_{16}LiN_2O_2$
Molecular weight: 287.26 g mol^{-1}
Yield: 69 mg, 0.24 mmol, 24 %

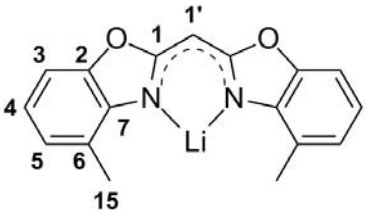

^{1}H-NMR
(400 MHz, THF-d_8): δ / ppm = 6.94 (ddd, J_{HH} = 7.7, 1.1, 0.5 Hz, 2 H, H3), 6.79 (d, $^{3}J_{HH}$ = 7.6 Hz, 2 H, H5), 6.71 (t, $^{3}J_{HH}$ = 7.6 Hz, 2 H, H4), 4.79 (s, 1 H, H1'), 2.45 (s, 6 H, H15).

^{13}C{^{1}H}-NMR
(75 MHz, THF-d_8): δ / ppm = 170.55 (s, 2 C, C1), 149.88 (s, 2 C, C2), 144.33 (s, 2 C, C7), 124.59 (s, 2 C, C5), 123.26 (s, 2 C, C6), 119.43 (s, 2 C, C4), 105.99 (s, 2 C, C3), 57.17 (s, 1 C, C1'), 17.12 (s, 2 C, C15).

^{7}Li{^{1}H}-NMR
(117 MHz, THF-d_8): δ / ppm = 2.03 (s).

^{15}N{^{1}H}-NMR
(40 MHz, THF-d_8): δ / ppm = −203.71 (s).

EI-MS
m/*z* (%): 278 (100) $[M - Li]^+$, 146 (37) $[M - Li - NCOC_7H_6]^+$, 132 (7) $[NCOC_7H_6]^+$.

4.3.21 Benzothiazol-2-yl-acetonitrile (31)

2-Aminothiophenol (10.02 g, 8.56 mL, 80.0 mmol, 1.00 eq.) and malonic dinitrile (5.29 g, 80.0 mmol, 1.00 eq.) were dissolved in ethanol (60 mL) under addition of glacial acetic acid (4.81 g, 4.58 mL, 80.0 mmol, 1.00 eq.) and stirred over night at rt. After about 1 h, a yellow crystalline precipitate was formed. This crude product was then filtered off, washed twice with pre-cooled ethanol (2 x 50 mL) and remaining solvent was removed under reduced pressure to afford **31** as bright yellow crystals in a yield of 9.73 g (55.8 mmol, 70 %).

Molecular formula: $C_9H_6N_2S$
Molecular weight: 174.22 g mol^{-1}
Yield: 9.73 g, 55.8 mmol, 70 %

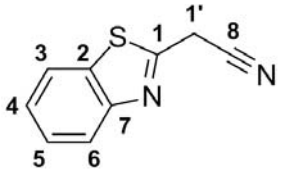

^{1}H-NMR

(300 MHz, DMSO-d_6): δ / ppm = 8.13 (d, $^{3}J_{HH}$ = 7.8 Hz, 1 H, H6), 8.04 (d, $^{3}J_{HH}$ = 7.8 Hz, 1 H, H3), 7.55 (td, J_{HH} = 7.3, 1.4 Hz, 1 H, H5), 7.48 (td, J_{HH} = 7.6, 1.3 Hz, 1 H, H4), 4.76 (s, 2 H, H1').

^{13}C{^{1}H}-NMR

(75 MHz, DMSO-d_6): δ / ppm = 160.60 (s, 1 C, C1), 152.26 (s, 1 C, C7), 135.09 (s, 1 C, C2), 126.57 (s, 1 C, C5), 125.64 (s, 1 C, C4), 122.64 (s, 1 C, C6), 122.39 (s, 1 C, C3), 116.59 (s, 1 C, C8), 22.39 (s, 1 C, C1').

^{15}N{^{1}H}-NMR

(40 MHz, THF-d_8): δ / ppm = −126.48 (s, N2), −63.78 (s, N1).

elemental analysis

in % (calculated): C, 62.13 (62.05); H, 3.46 (3.47); N, 15.99 (16.08); S, 18.42 (18.40).

EI-MS

m/*z* (%): 174 (100) $[M]^{+}$.

4.3.22 (Benzothiazol-2-yl)-(benzoxazol-2'-yl)-methane (32)

Method 1:

31 (4.86 g, 28.0 mmol, 1.00 eq.) and 2-aminophenol (3.03 g, 28.0 mmol, 1.00 eq.) were milled in a mortar before being transferred in a two-necked flask, then polyphosphoric acid (80 %, ca. 40 mL) was added. Under inert gas atmosphere, the reaction mixture was heated up to 185 °C while being vigorously stirred with a sealed precision glass (KPG) stirrer. After 3 h the dark green viscous reaction mixture was allowed to cool down to approximately 80 °C, was then poured over ice and kept stirring over night. The resulting brown solid was filtrated, washed several times with distilled water (6 x 100 mL) and sat. aq. $NaHCO_3$ solution (3 x 30 mL) until pH neutrality. After purification by column chromatography (silica, hexane/EtOAc = 5:1, 1st fraction, R_f = 0.20) and recrystallisation from toluene, compound **32** could be obtained as yellow powder (2.09 g, 7.8 mmol, 28 %). The 2nd fraction in the column chromatographic separation was isolated by using an eluent mixture of hexane/EtOAc = 1:1, since the 1st fraction was completely collected. This side product could be identified as **33** (1.00 g, 3.5 mmol, 13 %), which is a representative for the not completely proceeded cyclization reaction. Crystals of compounds **32** and **33** suitable for X-ray diffraction experiments could be obtained upon recrystallisation from toluene.

Method 2:

31 (12.86 g, 74.0 mmol, 1.00 eq.) and 2-aminophenol (8.08 g, 74.0 mmol, 1.00 eq.) were milled in a mortar before being transferred in a two-necked flask, then polyphosphoric acid (80 %, ca. 250 mL) was added. Under inert gas atmosphere the reaction mixture was heated up to 185 °C while being vigorously stirred with a sealed precision glass (KPG) stirrer. In contrast to method 1 the heating time of the dark green viscous reaction mixture

was increased to 7 h to complete the cyclization reaction. Afterwards it was allowed to cool down to approximately 80 °C, then poured over ice and kept stirring over night. The resulting brown solid was filtrated, washed several times with distilled water (6 x 100 mL) and saturated aqueous $NaHCO_3$ solution (3 x 30 mL) until pH neutrality. The desired product **32** was obtained as brown powder (17.5 g, 65.7 mmol, 89 %).

Molecular formula: $C_{15}H_{10}N_2OS$
Molecular weight: 266.32 g mol^{-1}
Yield (method 1): 2.09 g, 7.8 mmol, 28 %
Yield (method 2): 17.5 g, 65.7 mmol, 89 %

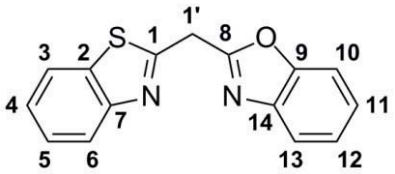

^{1}H-NMR
(300 MHz, THF-d_8): δ / ppm = 7.99 – 7.90 (m, 2 H, H3 + H6), 7.73 – 7.65 (m, 1 H, H13), 7.59 – 7.51 (m, 1 H, H10), 7.49 – 7.41 (m, 1 H, H5), 7.40 – 7.28 (m, 3 H, H4 + H11 + H12), 4.85 (s, 2 H, H1').

^{13}C{^{1}H}-NMR
(75 MHz, THF-d_8): δ / ppm = 164.62 (s, 1 C, C1), 163.00 (s, 1 C, C8), 154.37 (s, 1 C, C7), 152.27 (s, 1 C, C9), 142.69 (s, 1 C, C14), 137.06 (s, 1 C, C2), 126.82 (s, 1 C, C5), 126.00 (s, 1 C, C4), 125.86 (s, 1 C, C11), 125.15 (s, 1 C, C12), 123.93 (s, 1 C, C6), 122.47 (s, 1 C, C3), 120.83 (s, 1 C, C13), 111.29 (s, 1 C, C10), 34.38 (s, 1 C, C1').

^{15}N{^{1}H}-NMR
(30 MHz, THF-d_8): δ / ppm = −64.40 (s, N1), −132.37 (s, N2).

elemental analysis
in % (calculated): C, 67.42 (67.65); H, 3.78 (3.78); N, 10.39 (10.52); S, 12.29 (12.04).

EI-MS
m/*z* (%): 266 (100) $[M]^+$, 148 (15) $[M - NCOC_6H_4]^+$.

Side Product
Molecular formula: $C_{15}H_{13}N_3OS$
Molecular weight: 284.33 g mol^{-1}
Yield: 1.00 g, 3.5 mmol, 13 %

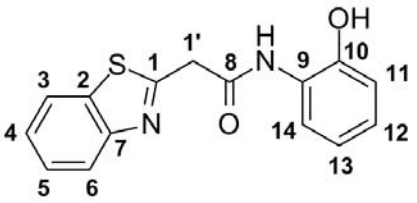

^{1}H-NMR
(300 MHz, DMSO-d_6): δ / ppm = 9.85 (s, 1 H, OH), 9.72 (s, 1 H, NH), 8.08 (d, $^3J_{HH}$ = 7.2 Hz, 1 H, H6), 7.97 (d, $^3J_{HH}$ = 7.8 Hz, 1 H, H3), 7.84 (d, $^3J_{HH}$ = 7.8 Hz, 1 H, H14), 7.50 (td, J_{HH} = 7.7, 1.3 Hz, 1 H, H5), 7.42 (td, J_{HH} = 7.7, 1.2 Hz, 1 H, H4), 6.99 – 6.84 (m, 2 H, H11 + H12), 6.77 (t, J_{HH} = 7.6 Hz, 1 H, H13), 4.40 (s, 2 H, H1').

$^{13}C\{^{1}H\}$-NMR

(75 MHz, DMSO-d_6): δ / ppm = 176.76 (s, 1 C, C8), 166.17 (s, 1 C, C1), 165.36 (s, 1 C, C10), 152.23 (s, 1 C, C7), 147.87 (s, 1 C, C9), 135.20 (s, 1 C, C2), 126.00 (s, 1 C, C5), 125.85 (s, 1 C, C4), 124.94 (s, 1 C, C12), 124.79 (s, 1 C, C13), 122.20 (s, 1 C, C6), 122.00 (s, 1 C, C3), 118.87 (s, 1 C, C14), 115.30 (s, 1 C, C11), 41.20 (s, 1 C, C1').

elemental analysis

in % (calculated): C, 62.84 (63.36); H, 4.33 (4.25); N, 9.64 (9.85); S, 11.11 (11.28).

EI-MS

m/*z* (%): 284 (22) $[M]^+$, 266 (16) $[M - H_2O]^+$, 176 (74) $[M - HNC_6H_4OH]^+$, 149 (100) $[M - C(O)NHC_6H_4OH]^+$.

4.3.23 (Benzothiazol-2-yl)-(*N*-methylbenzimidazol-2'-yl)-methane (34)

31 (2.82 g, 17.6 mmol, 1.00 eq.) and *N*-methyl-*ortho*-phenylendiamine (2.0 mL, 2.16 g, 17.6 mmol, 1.00 eq.) were mixed with polyphosphoric acid (80 %, ca. 40 mL). Under inert gas atmosphere, the green reaction mixture was heated up to 185 °C while being vigorously stirred with a sealed precision glass (KPG) stirrer over night. Afterwards, it was allowed to cool down to approximately 80 °C, then poured over ice and kept stirring for 1 h. The resulting green solid was filtrated, washed twice with distilled water (2 x 50 mL) and sat. aq. $NaHCO_3$ solution (3 x 50 mL) until pH neutrality. Crystals suitable for X-ray diffraction experiments could be obtained upon recrystallisation from ethanol. The desired product **32** was obtained as green grey powder (2.35 g, 8.4 mmol, 48 %).

Molecular formula: $C_{16}H_{13}N_3S$

Molecular weight: 279.36 g mol^{-1}

Yield: 2.35 g, 8.4 mmol, 48 %

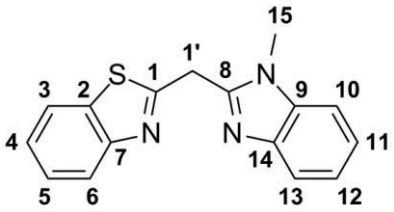

^{1}H-NMR

(300 MHz, THF-d_8): δ / ppm = 7.92 (d, $^3J_{HH}$ = 8.1 Hz, 2 H, H6), 7.88 (d, $^3J_{HH}$ = 7.9 Hz, 2 H, H3), 7.64 – 7.56 (m, 1 H, H13), 7.45 – 7.29 (m, 3 H, H4 + H5 + H10), 7.22 – 7.11 (m, 2 H, H11 + H12), 4.80 (s, 2 H, H1'), 3.83 (s, 3 H, H15).

$^{13}C\{^{1}H\}$-NMR

(75 MHz, THF-d_8): δ / ppm = 167.44 (s, 1 C, C1), 154.39 (s, 1 C, C7), 151.16 (s, 1 C, C8), 144.17 (s, 1 C, C14), 137.41 (s, 1 C, C9), 137.07 (s, 1 C, C2), 126.64 (s, 1 C, C5), 125.80 (s, 1 C, C4), 123.69 (s, 1 C, C6), 122.88 (s, 1 C, C3), 122.45 (s, 1 C, C11), 122.25 (s,

1 C, C12), 120.33 (s, 1 C, C13), 110.10 (s, 1 C, C10), 33.76 (s, 1 C, C1'), 30.33 (s, 1 C, C15).

$^{15}N\{^1H\}$-NMR

(30 MHz, THF-d_8): δ / ppm = −67.71 (s, N1), −132.50 (s, N3), −240.63 (s, N2).

elemental analysis

in % (calculated): C, 67.23 (68.79); H, 4.76 (4.69); N, 14.72 (15.04); S, 11.71 (11.48).

EI-MS

m/*z* (%): 279 (100) $[M]^+$, 149 (11) $[M - H_3CNCNC_6H_4]^+$, 131 (36) $[H_3CNCNC_6H_4]^+$.

4.3.24 Dimethylaluminium-(benzothiazol-2-yl)-(benzoxazol-2'-yl)-methanide (35)

Orange crystals suitable for X-ray diffraction experiments were obtained upon recrystallisation from toluene in a yield of 455 mg (1.41 mmol, 71 %; not optimized).

Molecular formula: $C_{17}H_{15}AlN_2OS$
Molecular weight: 322.36 g mol^{-1}
Yield: 455 mg, 1.41 mmol, 71 %

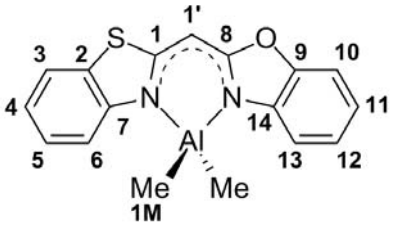

^1H-NMR

(500 MHz, THF-d_8): δ / ppm = 7.69 (ddd, J_{HH} = 7.9, 1.3, 0.6 Hz, 1 H, H3), 7.58 (ddd, J_{HH} = 8.2, 1.0, 0.6 Hz, 1 H, H6), 7.42 (ddd, J_{HH} = 8.0, 1.1, 0.6 Hz, 1 H, H10), 7.42 (ddd, J_{HH} = 7.9, 1.2, 0.6 Hz, 1 H, H13), 7.39 (ddd, J_{HH} = 8.2, 7.3, 1.3 Hz, 1 H, H5), 7.29 (td, J_{HH} = 7.7, 1.1 Hz, 1 H, H12), 7.20 (ddd, J_{HH} = 7.9, 7.6, 1.2 Hz, 1 H, H11), 7.19 (ddd, J_{HH} = 7.9, 7.4, 1.0 Hz, 1 H, H4), 5.76 (s, 1 H, H1'), −0.45 (s, 6 H, H1M).

$^{13}C\{^1H\}$-NMR

(75 MHz, THF-d_8): δ / ppm = 170.57 (s, 1 C, C8), 166.62 (s, 1 C, C1), 149.08 (s, 1 C, C9), 149.05 (s, 1 C, C7), 137.74 (s, 1 C, C14), 129.55 (s, 1 C, C2), 127.55 (s, 1 C, C5), 125.79 (s, 1 C, C12), 124.07 (s, 1 C, C4 / C11), 123.87 (s, 1 C, C4 / C11), 122.52 (s, 1 C, C3), 115.93 (s, 1 C, C6), 113.70 (s, 1 C, C13), 110.74 (s, 1 C, C10), 71.35 (s, 1 C, C1'), −9.78 (s, 2 C, C1M).

$^{15}N\{^1H\}$-NMR

(50 MHz, THF-d_8): δ / ppm = −202.16 (s, N1), −228.74 (s, N2).

$^{27}Al\{^1H\}$-NMR

(78 MHz, THF-d_8): δ / ppm = 151 (s).

elemental analysis

in % (calculated): C, 63.26 (63.34); H, 4.78 (4.69); N, 8.54 (8.69); S, 9.77 (9.95).

EI-MS

m/*z* (%): 266 (100) $[M - AlMe_2]^+$, 148 (24) $[M - AlMe_2 - NCOC_6H_4]^+$.

4.3.25 Dimethylaluminium-(benzothiazol-2-yl)-(*N*-methylbenzimidazol-2'-yl)-methane (36)

Yellow greenish crystals suitable for X-ray diffraction experiments were obtained upon recrystallisation from toluene in a yield of 49 mg (0.15 mmol, 30 %; not optimized).

Molecular formula: $C_{18}H_{18}AlN_3S$
Molecular weight: 335.40 g mol^{-1}
Yield: 49 mg, 0.15 mmol, 30 %

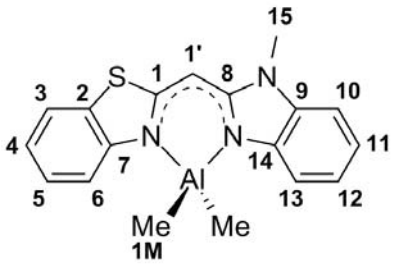

^{1}H-NMR

(400 MHz, THF-d_8): δ / ppm = 7.52 (ddd, J_{HH} = 7.8, 1.3, 0.6 Hz, 1 H, H3), 7.49 – 7.44 (m, 1 H, H13), 7.43 (ddd, J_{HH} = 8.1, 1.1, 0.6 Hz, 1 H, H6), 7.33 – 7.30 (m, 1 H, H10), 7.27 (ddd, J_{HH} = 8.1, 7.4, 1.3 Hz, 1 H, H5), 7.23 – 7.16 (m, 2 H, H11 + H12), 7.05 (ddd, J_{HH} = 7.8, 7.4, 1.1 Hz, 1 H, H4), 5.57 (s, 1 H, H1'), 3.63 (s, 3 H, H15), −0.50 (s, 6 H, H1M).

^{13}C{^{1}H}-NMR

(75 MHz, THF-d_8): δ / ppm = 166.65 (s, 1 C, C1), 154.42 (s, 1 C, C8), 149.90 (s, 1 C, C7), 138.64 (s, 1 C, C14), 135.42 (s, 1 C, C9), 128.98 (s, 1 C, C2), 127.00 (s, 1 C, C5), 123.28 (s, 1 C, C12), 122.83 (s, 1 C, C11), 122.57 (s, 1 C, C4), 121.90 (s, 1 C, C3), 114.87 (s, 1 C, C6), 113.67 (s, 1 C, C13), 109.44 (s, 1 C, C10), 70.71 (s, 1 C, C1'), 29.35 (s, 1 C, C15), −9.58 (s, 2 C, C1M).

^{15}N{^{1}H}-NMR

(40 MHz, THF-d_8): δ / ppm = −223.12 (s, N1), −226.41 (s, N3), −257.67 (s, N2).

^{27}Al{^{1}H}-NMR

(78 MHz, THF-d_8): δ / ppm = 150 (s).

elemental analysis

in % (calculated): C, 62.68 (64.46); H, 5.41 (5.41); N, 11.92 (12.53); S, 9.07 (9.56).

EI-MS

m/*z* (%): 335.1 (11) $[M]^+$, 320.1 (100) $[M - Me]^+$, 305.1 (19) $[M - 2\ Me]^+$, 160.0 (12) $[M - Me]^{2+}$.

4.3.26 Dimethylgallium-(benzothiazol-2-yl)-(benzoxazol-2'-yl)-methanide (37)

Orange crystals suitable for X-ray diffraction experiments were obtained upon recrystallisation from toluene in a yield of 184 mg (0.50 mmol, 50 %; not optimized).

Molecular formula: $C_{17}H_{15}GaN_2OS$
Molecular weight: 365.10 g mol^{-1}
Yield: 184 mg, 0.50 mmol, 50 %

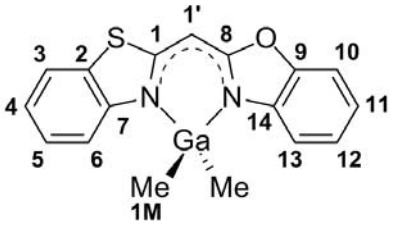

^{1}H-NMR
(400 MHz, THF-d_8): δ / ppm = 7.65 (ddd, J_{HH} = 7.9, 1.2, 0.6 Hz, 1 H, H3), 7.39 (ddd, J_{HH} = 8.2, 1.4, 0.6 Hz, 1 H, H6), 7.38 (ddd, J_{HH} = 8.0, 1.1, 0.6 Hz, 1 H, H10), 7.34 (ddd, J_{HH} = 8.2, 7.1, 1.2 Hz, 1 H, H5), 7.29 (ddd, J_{HH} = 7.8, 1.4, 0.6 Hz, 1 H, H13), 7.24 (ddd, J_{HH} = 7.8, 7.4, 1.1 Hz, 1 H, H12), 7.15 (ddd, J_{HH} = 8.0, 7.4, 1.4 Hz, 1 H, H11), 7.13 (ddd, J_{HH} = 7.9, 7.1, 1.4 Hz, 1 H, H4), 5.58 (s, 1 H, H1'), −0.03 (s, 6 H, H1M).

^{13}C{^{1}H}-NMR
(75 MHz, THF-d_8): δ / ppm = 169.13 (s, 1 C, C8), 165.71 (s, 1 C, C1), 149.62 (s, 1 C, C7), 148.93 (s, 1 C, C9), 138.46 (s, 1 C, C14), 129.64 (s, 1 C, C2), 127.37 (s, 1 C, C5), 125.51 (s, 1 C, C12), 123.44 (s, 1 C, C4 / C11), 123.30 (s, 1 C, C4 / C11), 122.35 (s, 1 C, C3), 115.41 (s, 1 C, C6), 112.99 (s, 1 C, C13), 110.48 (s, 1 C, C10), 70.09 (s, 1 C, C1'), −6.97 (s, 2 C, C1M).

^{15}N{^{1}H}-NMR
(40 MHz, THF-d_8): δ / ppm = −200.07 (s, N1), −228.48 (s, N2).

elemental analysis
in % (calculated): C, 55.35 (55.92); H, 4.27 (4.14); N, 7.49 (7.67); S, 8.61 (8.78).

EI-MS
m/*z* (%): 364.0 (13) $[M]^+$, 349.0 (100) $[M - Me]^+$, 334.0 (27) $[M - 2\ Me]^+$, 265.1 (9) $[M - GaMe_2]^+$, 68.9 (58) Ga^+.

4.3.27 Lithium-(benzothiazol-2-yl)-(benzoxazol-2'-yl)-methanide (38)

A dark orange powder could be isolated in a yield of 211 mg (0.78 mmol, 78 %; not optimized).

Molecular formula: $C_{15}H_9LiN_2OS$
Molecular weight: 272.25 g mol^{-1}
Yield: 211 mg, 0.78 mmol, 78 %

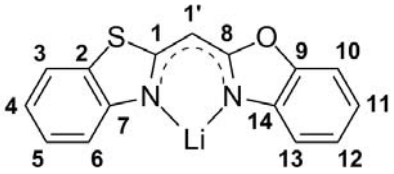

^{1}H-NMR
(400 MHz, THF-d_8): δ / ppm = 7.42 (ddd, J_{HH} = 7.7, 1.3, 0.5 Hz, 1 H, H3), 7.22 (ddd, J_{HH} = 8.0, 1.1, 0.5 Hz, 1 H, H6), 7.12 (ddd, J_{HH} = 7.8, 1.1, 0.6 Hz, 1 H, H10), 7.08 overlap (ddd, J_{HH} = 7.7, 1.3, 0.6 Hz, 1 H, H13), 7.08 overlap (ddd, J_{HH} = 8.0, 7.3, 1.3 Hz, 1 H, H5), 6.99 (td, J_{HH} = 7.6, 1.1 Hz, 1 H, H12), 6.87 – 6.79 (m, 2 H, H4 + H11), 5.11 (s, 1 H, H1').

^{13}C{^{1}H}-NMR
(75 MHz, THF-d_8): δ / ppm = 169.28 (s, 1 C, C8), 169.01 (s, 1 C, C1), 156.73 (s, 1 C, C7), 150.01 (s, 1 C, C9), 145.46 (s, 1 C, C14), 131.93 (s, 1 C, C2), 125.71 (s, 1 C, C5), 123.55 (s, 1 C, C12), 120.97 (s, 1 C, C3), 120.04 (s, 2 C, C4 / C11), 115.79 (s, 1 C, C6), 113.53 (s, 1 C, C13), 108.71 (s, 1 C, C10), 68.73 (s, 1 C, C1').

^{7}Li{^{1}H}-NMR
(117 MHz, THF-d_8): δ / ppm = 0.35 (s).

^{15}N{^{1}H}-NMR
(40 MHz, THF-d_8): δ / ppm = −159.98 (s, N1), −198.68 (s, N2).

4.3.28 Lithium-(benzothiazol-2-yl)-(*N*-methylbenzimidazol-2'-yl)-methanide (39)

To a suspension of **34** (140 mg, 0.5 mmol, 1.00 eq.) in 1,4-dioxane (15 mL) slowly *n*BuLi (2.93 M in hexane, 0.17 mL, 0.5 mmol, 1.00 eq.) was added at rt. The resulting yellow brown suspension was stirred over night at rt and filtrated to obtain a brown solution. This solution was concentrated to a few millilitres and stored at rt for crystallisation. After a week, crystals suitable for X-ray diffraction could be isolated as yellow needles (145 mg, 0.39 mmol, 78 %).

Molecular formula: $C_{20}H_{20}LiN_3O_2S$
Molecular weight: 373.40 g mol^{-1}
Yield: 145 mg, 0.39 mmol, 78 %

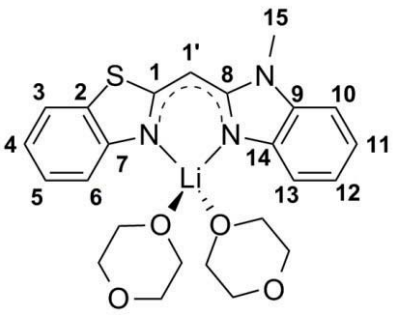

^{1}H-NMR
(400 MHz, THF-d_8): δ / ppm = 7.30 (ddd, J_{HH} = 7.6, 1.3, 0.5 Hz, 1 H, H3), 7.12 (ddd, J_{HH} = 7.6, 1.3, 0.6 Hz, 1 H, H13), 7.09 (ddd, J_{HH} = 8.0, 1.2, 0.5 Hz, 1 H, H6), 7.01 – 6.96 (m, 2 H, H5 + H10), 6.89 (td,

J_{HH} = 7.5, 1.4 Hz, 1 H, H12), 6.83 (td, J_{HH} = 7.5, 1.3 Hz, 1 H, H11), 6.68 (ddd, J_{HH} = 7.6, 7.3, 1.2 Hz, 1 H, H4), 4.95 (s, 1 H, H1'), 3.48 (s, 3 H, H15).

^{13}C{^{1}H}-NMR

(75 MHz, THF-d_8): δ / ppm = 167.44 (s, 1 C, C1), 157.78 (s, 1 C, C7 / C8), 157.64 (s, 1 C, C7 / C8), 145.45 (s, 1 C, C14), 136.62 (s, 1 C, C9), 131.78 (s, 1 C, C2), 125.42 (s, 1 C, C5), 120.68 (s, 1 C, C12), 120.46 (s, 1 C, C3), 118.74 (s, 1 C, C4 / C11), 118.73 (s, 1 C, C4 / C11), 114.75 (s, 1 C, C6), 113.60 (s, 1 C, C13), 107.01 (s, 1 C, C10), 68.46 (s, 1 C, C1'), 28.98 (s, 1 C, C15).

^{7}Li{^{1}H}-NMR

(117 MHz, THF-d_8): δ / ppm = 2.37 (s).

^{15}N{^{1}H}-NMR

(40 MHz, THF-d_8): δ / ppm = −168.43 (s, N1), −190.35 (s, N3), −261.53 (s, N2).

elemental analysis

in % (calculated): C, 60.33 (64.33); H, 6.50 (5.40); N, 7.95 (11.25); S, 6.64 (8.59) (deviations due to remaining lattice solvent).

EI-MS

m/*z* (%): 293 (13) $[M + Li]^+$, 279 (100) $[M - Li]^+$, 149 (18) $[M - Li - NCNC_7H_7]^+$, 131 (57) $[NCNC_7H_7]^+$.

4.3.29 Iodomethylaluminium-bis-(4-methylbenzoxazol-2-yl)-methanide (25)

To a solution of **21** (334 mg, 1.00 mmol, 1.00 eq.), dissolved in toluene (20 mL), trimethylsilyl iodide (0.31 mL, 440 mg, 2.20 mmol, 2.20 eq.) was added. The reaction mixture was heated until refluxing temperature was reached and stirred for additional 3.5 d at reflux. The formed precipitate was filtered off and residual solvent was removed under reduced pressure. The mono iodide substituted derivative **25** could be isolated as a brown powder (111 mg, 0.25 mmol, 25 %). After recrystallisation from toluene also crystals suitable for SXCRD were obtained.

Molecular formula: $C_{18}H_{16}AlIN_2O_2$
Molecular weight: 446.22 g mol^{-1}
Yield: 111 mg, 0.25 mmol, 25 %

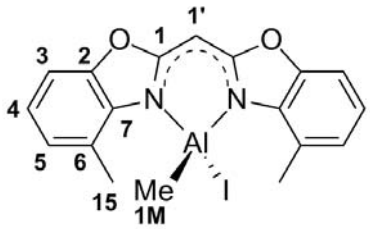

^{1}H-NMR

(300 MHz, THF-d_8): δ / ppm = 7.29 – 7.25 (m, 2 H, H3), 7.14 – 7.10 (m, 4 H, H4 + H5), 5.47 (s, 1 H, H1'), 2.77 (s, 6 H, H15), −0.47 (s, 3 H, H1M).

$^{13}C\{^1H\}$-NMR

(125 MHz, THF-d_8): δ / ppm = 168.90 (s, 2 C, C1), 149.13 (s, 2 C, C2), 136.66 (s, 2 C, C7), 127.72 (s, 2 C, C5), 125.12 (s, 2 C, C6), 124.11 (s, 2 C, C4), 108.05 (s, 2 C, C3), 60.58 (s, 1 C, C1'), 18.88 (s, 2 C, C15), −6.83 (s, 1 C, C1M).

$^{15}N\{^1H\}$-NMR

(50 MHz, THF-d_8): δ / ppm = −230.77 (s).

elemental analysis

in % (calculated): C, 45.53 (48.45); H, 3.32 (3.61); N, 6.07 (6.28) (deviation due to slight contamination with the AlI_2 derivative).

EI-MS

m/*z* (%): 278 (100) $[M - AlMeI]^+$, 146 (37) $[M - AlMeI - NCOC_7H_6]^+$, 132 (9) $[NCOC_7H_6]^+$.

4.3.30 Iodoethylaluminium-bis-(4-methylbenzoxazol-2-yl)-methanide (26)

To a solution of **19** (1.39 g, 5.00 mmol, 1.00 eq.), dissolved in toluene (80 mL), diethyl aluminium iodide (0.73 mL, 1.17 g, 5.50 mmol, 1.10 eq.) was added under ice cooling. The resulting reaction suspension was allowed to warm up to rt and was stirred over night at that temperature. Overnight a clear orange solution was formed. The volume of this solution was reduced to a few mL and the resulting concentrated solution was stored at rt. Overnight crystals suitable for X-ray diffraction experiments could be obtained. The crystals thus formed were filtered, washed twice with pre-cooled toluene and finally dried in vacuum. The above-called compound **26** could be isolated as orange crystals (1.160 g, 2.52 mmol, 50 %).

Molecular formula: $C_{19}H_{18}AlIN_2O_2$

Molecular weight: 460.24 g mol^{-1}

Yield: 1.160 g, 2.52 mmol, 50 %

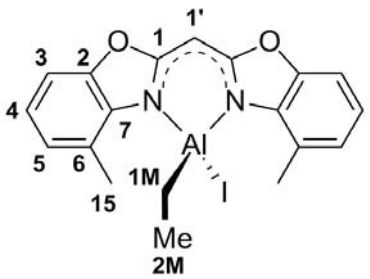

^1H-NMR

(400 MHz, THF-d_8): δ / ppm = 7.29 – 7.24 (m, 2 H, H3), 7.14 – 7.11 (m, 4 H, H4 + H5), 5.46 (s, 1 H, H1'), 2.79 (s, 6 H, H15), 0.85 (t, $^3J_{HH}$ = 8.2 Hz, 3 H, H2M), 0.21 (q, $^3J_{HH}$ = 8.2 Hz, 2 H, H1M).

$^{13}C\{^1H\}$-NMR

(75 MHz, THF-d_8): δ / ppm = 169.09 (s, 2 C, C1), 149.12 (s, 2 C, C2), 136.72 (s, 2 C, C7), 127.73 (s, 2 C, C5), 125.15 (s, 2 C, C6), 124.10 (s, 2 C, C4), 108.05 (s, 2 C, C3), 60.52 (s, 1 C, C1'), 18.74 (s, 2 C, C15), 8.66 (s, 1 C, C2M), 3.13 (s, 1 C, C1M).

$^{15}N\{^{1}H\}$-NMR
(40 MHz, THF-d_8): δ / ppm = −232.32 (s).
elemental analysis
in % (calculated): C, 49.35 (49.58); H, 4.02 (3.94); N, 6.09 (6.09).
EI-MS
m/*z* (%): 278 (100) $[M - AlEtI]^+$, 146 (41) $[M - AlEtI - NCOC_7H_6]^+$, 132 (7) $[NCOC_7H_6]^+$.

4.3.31 μ-Hydroxido-di-(ethylaluminium-bis-(4-methylbenzoxazol-2-yl)-methanide) iodide (29)

Method 1:

To a mixture of **26** (100 mg, 0.22 mmol, 1.00 eq.) and KC_8 (30 mg, 0.22 mmol, 1.00 eq.) toluene (20 mL) was added to give an orange brown suspension. The reaction mixture was stirred at rt for 2 d and afterwards the suspension was filtered off over cellite and a P4 glass frit to get rid of the remaining KC_8 and the formed graphite. This led to a clear light orange solution, whose volume was reduced to a few mL under vacuum. After storage at 4 °C in the refrigerator, overnight a small amount of crystalline material was formed, which was examined for SCXRD under the microscope to find suitable crystals. Due to the mostly powder-like appearance of the pale yellow solid barely a crystal suitable for the X-ray diffraction experiment could be mounted. Just the hydrolysis product **29** could be structurally characterized and due to the small amounts limited to some crystals no further spectroscopic investigations were performed.

Molecular formula: $C_{38}H_{37}Al_2IN_4O_5$
Molecular weight: 810.59 g mol^{-1}
Yield: some crystals

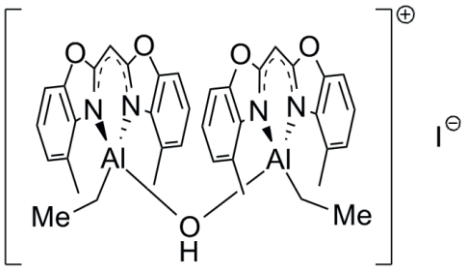

Method 2:

According to method 1, a second attempt on larger scale was executed to overcome the possible hydrolysis and gain better accuracy of the weighed starting material. Again to a mixture of **26** (1.16 g, 2.52 mmol, 1.00 eq.) and KC_8 (341 mg2.52 mmol, 1.00 eq.) toluene (40 mL) was added to give an orange brown suspension. The reaction mixture was then heated to reflux and stirred at that temperature for one additional day. Afterwards the suspension was filtered off over cellite and a P4 glass frit to get rid of the remaining KC_8 and the formed graphite. This led to a clear light orange solution, whose volume was reduced to a few mL under vacuum. After storage at 4 °C in the refrigerator overnight crystals suitable for SCXRD could be achieved. In this case just another polymorphic structure of the starting material **26** could be experimentally determined.

4.3.32 (4-Methylbenzoxazol-2-yl)-(4'-methylbenzoxazolium-2'-yl)-methane triiodide(27)

To **21** (334 mg, 1.00 mmol, 1.00 eq.), dissolved in toluene (20 mL), a solution of elemental iodine (508 mg, 2.00 mmol, 2.00 eq.) in toluene (7 mL) was added. The reaction mixture was heated until reflux temperature was reached and stirred for additional 3.5 d at reflux. Afterwards the solution was concentrated and stored in the refrigerator at −32 °C over night. The resulting precipitate was filtered off and residual solvent was removed under reduced pressure. The protonated ligand **27** could be isolated as dark brown powder (130 mg, 0.20 mmol, 20 %). Due to its sensitivity towards air and moisture no specific NMR-spectroscopic data could be collected, just the parent ligand **19** was detected in the recorded spectra. The few crystals were enough to determine the molecular structure of **27** by applying SCXRD.

Molecular formula: $C_{17}H_{15}I_3N_2O_2$
Molecular weight: 660.03 g mol^{-1}
Yield: 130 mg, 0.20 mmol, 20 %

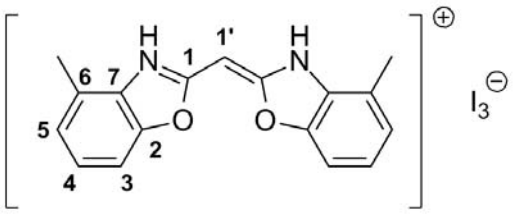

elemental analysis
in % (calculated): C, 38.84 (30.94); H, 2.80 (2.29); N, 5.42 (4.24) (deviations due to partial loss of I_2).

4.3.33 1,1,2,2-Tetrakis-(4-methylbenzoxazol-2-yl)-ethane (28)

19 (278 mg, 1.00 mmol, 1.0 eq.) was dissolved in THF (30 mL). Under ice cooling, *n*BuLi (3.8 M in hexane, 0.28 mL, 1.10 mmol, 1.10 eq.) was syringed slowly to the parent solution and the reaction mixture was allowed to heat up to rt, where it was kept stirring for additional 1.5 h. Then aluminium triiodide (408 mg, 1.00 mmol, 1.00 eq.) in THF (70 mL) was added slowly and the resulting solution was stirred for 3 d at rt. Afterwards, the solution was concentrated and stored in the refrigerator at −32 °C over night. The few crystals were enough to determine the molecular structure of the dimerized ligand **28** by applying SCXRD.

Molecular formula: $C_{34}H_{26}N_4O_4$
Molecular weight: 554.20 g mol^{-1}
Yield: 29 mg, 0.05 mmol, 10 %

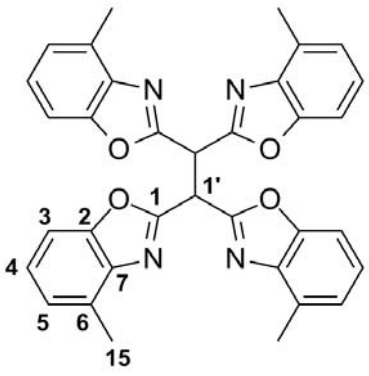

^{1}H-NMR

(300 MHz, Tol-d_8): δ / ppm = 6.89 (ddd, J_{HH} = 8.2, 1.1, 0.6 Hz, 4 H, H3), 6.76 (t, $^{3}J_{HH}$ = 7.8 Hz, 4 H, H4), 6.70 (s, 2 H, H1'), 6.68 – 6.63 (m, 4 H, H5), 2.23 (s, 12 H, H15).

^{13}C{^{1}H}-NMR

(75 MHz, Tol-d_8): δ / ppm = 160.67 (s, 4 C, C1), 151.37 (s, 4 C, C2), 140.39 (s, 4 C, C7), 131.23 (s, 2 C, C6), 125.19 (overlap with toluene signal) (s, 8 C, C4 + C5), 108.10 (s, 2 C, C3), 42.09 (s, 2 C, C1'), 16.12 (s, 4 C, C15).

EI-MS

m/*z* (%): 554 (24) $[M]^+$, 420 (3) $[M - NCOC_7H_6]^+$, 277 (100) $[M]^{2+}$.

4.3.34 Bis-(benzoxazol-2-yl)-amine (40)

A mixture of 2-aminobenzoxazole (5.11 g, 38.1 mmol, 2.0 eq.) and phenol (2.51 g, 26.7 mmol, 1.4 eq.) was heated to 50 °C until a homogenous solution upon melting phenol was formed. Subsequently, the reaction mixture was heated to reflux for 24 h, after cooling to rt ethanol (9.5 mL) was added in one portion to the solidified reaction mixture und was boiled to reflux for an additional hour. The resulting pale grey slurry was again cooled to rt, stirred over night, filtered off, washed with ethanol (2 x 5 mL) and dried under reduced pressure. A pale grey powder was obtained in a yield of 152 mg (0.60 mmol, 3 %; not optimized). No crystals suitable for X-ray diffraction experiments could be obtained upon recrystallisation from neither ethanol, acetone nor THF.

Molecular formula: $C_{14}H_9N_3O_2$
Molecular weight: 251.25 g mol^{-1}
Yield: 152 mg, 0.06 mmol, 3 %

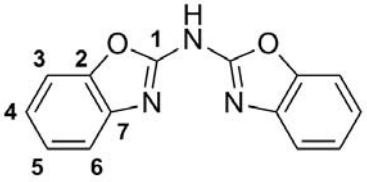

^{1}H-NMR

(300 MHz, DMSO-d_6): δ / ppm = 7.29 (d, $^{3}J_{HH}$ = 4.5 Hz, 2 H, H3), 7.27 (d, $^{3}J_{HH}$ = 5.1 Hz, 2 H, H6), 7.07 (t, $^{3}J_{HH}$ = 7.6 Hz, 2 H, H5), 6.95 (t, $^{3}J_{HH}$ = 7.7 Hz, 2 H, H4), NH not detected because of fast exchange with remaining water.

^{13}C{^{1}H}-NMR

(75 MHz, DMSO-d_6): δ / ppm = 163.04 (s, 2 C, C1), 147.14 (s, 2 C, C2), 141.62 (s, 2 C, C7), 123.06 (s, 2 C, C5), 120.54 (s, 2 C, C4), 114.52 (s, 2 C, C6), 108.45 (s, 2 C, C3).

elemental analysis

in % (calculated): C, 66.44 (66.93); H, 3.56 (3.61); N, 16.73 (16.73).

EI-MS

m/*z* (%): 251 (100) $[M]^+$.

4.3.35 Bis-(benzothiazol-2-yl)-amine (41)

A mixture of 2-aminobenzothiazole (7.51 g, 50.0 mmol, 2.0 eq.) and phenol (3.13 g, 33.0 mmol, 1.4 eq.) was heated to 50 °C until a homogenous solution upon melting phenol was formed. Subsequently, the reaction mixture was heated to reflux for 24 h, after cooling to rt ethanol (12.8 mL) was added in one portion to the solidified reaction mixture und was boiled to reflux for an additional hour. The resulting dark blue slurry was again cooled to rt, stirred over night, filtered off, washed with ethanol (2 x 5 mL) and dried under reduced pressure. A dark blue powder was obtained in a yield of 2.58 g (9.10 mmol, 36 %). Crystals suitable for X-ray diffraction experiments could be obtained upon recrystallisation from toluene.

Molecular formula: $C_{14}H_9N_3S_2$
Molecular weight: 283.37 g mol^{-1}
Yield: 2.58 g, 9.10 mmol, 36 %

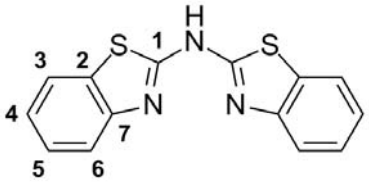

^{1}H-NMR
(300 MHz, THF-d_8): δ / ppm = 11.60 (s, 1 H, NH), 7.75 (d, $^3J_{HH}$ = 7.8 Hz, 2 H, H3), 7.62 (d, $^3J_{HH}$ = 8.0 Hz, 2 H, H6), 7.35 (t, $^3J_{HH}$ = 7.7 Hz, 2 H, H5), 7.19 (t, $^3J_{HH}$ = 7.6 Hz, 2 H, H4).

^{13}C{^{1}H}-NMR
(75 MHz, THF-d_8): δ / ppm = 163.70 (s, 2 C, C1), 148.71 (s, 2 C, C7), 132.13 (s, 2 C, C2), 126.86 (s, 2 C, C5), 123.69 (s, 2 C, C4), 122.25 (s, 2 C, C3), 119.14 (s, 2 C, C6).

elemental analysis
in % (calculated): C, 59.50 (59.34); H, 3.38 (3.20); N, 14.27 (14.83); S, 21.70 (22.63).

EI-MS
m/*z* (%): 283 (100) $[M]^+$.

4.3.36 Bis-(4-methylbenzothiazol-2-yl)-amine (42)

A mixture of 2-amino-4-methylbenzothiazole (8.21 g, 50.0 mmol, 2.0 eq.) and phenol (3.13 g, 33.0 mmol, 1.4 eq.) was heated to 50 °C until a homogenous solution upon melting phenol was formed. Subsequently, the reaction mixture was heated to reflux for 24 h, after cooling to rt ethanol (12.8 mL) was added in one portion to the solidified reaction mixture und was boiled to reflux for an additional hour. The resulting grey slurry was again cooled to rt, stirred over night, filtered off, washed with ethanol (2 x 5 mL) and dried under reduced pressure. A grey powder was obtained in a yield of 2.98 g (9.56 mmol, 38 %). Crystals suitable for X-ray diffraction experiments could be obtained upon recrystallisation from toluene.

Molecular formula: $C_{16}H_{13}N_3S_2$
Molecular weight: 311.42 g mol^{-1}
Yield: 2.98 g, 9.56 mmol, 38 %

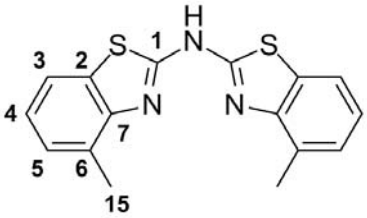

^{1}H-NMR
(300 MHz, THF-d_8): δ / ppm = 11.51 (s, 1 H, NH), 7.59 (d, $^3J_{HH}$ = 7.7 Hz, 2 H, H3), 7.18 (d, $^3J_{HH}$ = 7.3 Hz, 2 H, H5), 7.10 (t, $^3J_{HH}$ = 7.6 Hz, 2 H, H4), 2.64 (s, 6 H, H15).

^{13}C{^{1}H}-NMR
(75 MHz, THF-d_8): δ / ppm = 161.77 (s, 2 C, C1), 148.71 (s, 2 C, C7), 132.04 (s, 2 C, C2), 129.52 (s, 2 C, C6), 127.50 (s, 2 C, C5), 123.67 (s, 2 C, C4), 119.53 (s, 2 C, C3), 18.38 (s, 2 C, C15).

elemental analysis
in % (calculated): C, 63.61 (61.71); H, 4.33 (4.21); N, 12.51 (13.49); S, 19.04 (20.59) (deviation due to remaining toluene).

EI-MS
m/*z* (%): 311 (100) $[M]^+$.

4.3.37 Bis-(4-methoxybenzothiazol-2-yl)-amine (43)

A mixture of 2-amino-4-methoxybenzothiazole (5.38 g, 29.9 mmol, 2.0 eq.) and phenol (1.97g, 20.9 mmol, 1.4 eq.) was heated to 50 °C until a homogenous solution upon melting phenol was formed. Subsequently, the reaction mixture was heated to reflux for 24 h, after cooling to rt ethanol (11.4 mL) was added in one portion to the solidified reaction mixture und was boiled to reflux for an additional hour. The resulting brown slurry was again cooled to rt, stirred over night, filtered off, washed with ethanol (2 x 5 mL) and dried under reduced pressure. A brown powder was obtained in a yield of 693 mg (2.02 mmol, 13 %; not optimized). Crystals suitable for X-ray diffraction experiments could be obtained upon recrystallisation from toluene.

Molecular formula: $C_{16}H_{13}N_3O_2S_2$
Molecular weight: 343.42 g mol^{-1}
Yield: 693 g, 2.02 mmol, 13 %

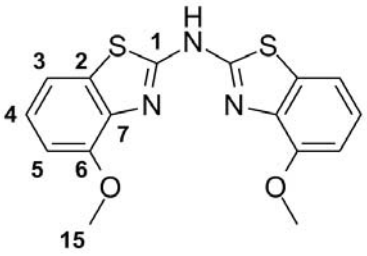

^{1}H-NMR
(300 MHz, THF-d_8): δ / ppm = 11.69 (s, 1 H, NH), 7.30 (d, $^3J_{HH}$ = 7.8 Hz, 2 H, H5), 7.11 (d, $^3J_{HH}$ = 7.9 Hz, 2 H, H4), 6.92 (d, $^3J_{HH}$ = 7.9 Hz, 2 H, H3), 4.02 (s, 6 H, H15).

$^{13}C\{^{1}H\}$-NMR

(75 MHz, THF-d_8): δ / ppm = 164.28 (s, 2 C, C1), 150.80 (s, 2 C, C6), 136.82 (s, 2 C, C7), 132.82 (s, 2 C, C2), 124.15 (s, 2 C, C4), 114.58 (s, 2 C, C5), 109.43 (s, 2 C, C3), 56.74 (s, 2 C, C15).

elemental analysis

in % (calculated): C, 57.58 (55.96); H, 4.08 (3.82); N, 11.24 (12.24) (deviation due to remaining toluene).

EI-MS

m/*z* (%): 343 (100) $[M]^+$.

Metallation reactions of the amines:

To a solution of the corresponding ligand **41**, **42** or **43** (1.0 eq.), dissolved in toluene, a slight excess of the organometallic reactant $AlMe_3$ or *n*BuLi (1.1 eq.) was slowly added at 0 °C. The reaction mixture was stirred over night and allowed to warm to rt. Afterwards, the volume of the solution was reduced to a few mL and the resulting concentrated solution was stored at −32 °C in a refrigerator. Overnight crystals suitable for X-ray diffraction experiments could be obtained. The crystals thus formed were filtered, washed twice with pre-cooled toluene or hexane (0 °C) and finally dried in vacuum. The given yields below are just based on the received crystals unless stated otherwise. No further improvement of the yields was attempted, because the solutions might have contained impurities upon repeated precipitation.

4.3.38 Dimethylaluminium-bis-(benzothiazol-2-yl)-amide (44)

Pale green crystals were obtained in a yield of 80 mg (0.24 mmol, 24 %; not optimized).

Molecular formula: $C_{16}H_{14}AlN_3S_2$
Molecular weight: 339.41 g mol^{-1}
Yield: 80 mg, 0.24 mmol, 24 %

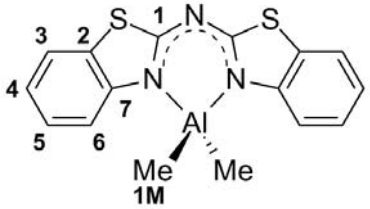

^{1}H-NMR

(300 MHz, THF-d_8): δ / ppm = 7.78 (d, $^3J_{HH}$ = 7.9 Hz, 2 H, H3), 7.66 (d, $^3J_{HH}$ = 7.7 Hz, 2 H, H6), 7.47 (t, $^3J_{HH}$ = 7.8 Hz, 2 H, H5), 7.32 (t, $^3J_{HH}$ = 7.7 Hz, 2 H, H4), −0.42 (s, 6 H, H1M).

$^{13}C\{^{1}H\}$-NMR

(75 MHz, THF-d_8): δ / ppm = 174.27 (s, 2 C, C1), 146.48 (s, 2 C, C7), 129.39 (s, 2 C, C2), 127.81 (s, 2 C, C5), 125.26 (s, 2 C, C4), 123.10 (s, 2 C, C3), 117.00 (s, 2 C, C6), −9.64 (s, 2 C, C1M).

$^{15}N\{^{1}H\}$-NMR

(50 MHz, THF-d_8): δ / ppm = −196.33 (s, N1) (no second signal detected).

^{27}Al{^{1}H}-NMR
(130 MHz, THF-d_8): δ / ppm = 153 (s).
elemental analysis
in % (calculated): C, 56.53 (56.62); H, 4.40 (4.16); N, 14.44 (14.38); S, 19.03 (18.89).
EI-MS
m/*z* (%): 339 (3) $[M]^+$, 324 (41) $[M - Me]^+$, 309 (3) $[M - 2\ Me]^+$, 283 (100) $[M - AlMe_2]^+$.

4.3.39 Dimethylaluminium-bis-(4-methylbenzothiazol-2-yl)-amide (45)

Colourless crystals were obtained in a yield of 203 mg (0.55 mmol, 55 %, not optimized)

Molecular formula: $C_{18}H_{18}AlN_3S_2$
Molecular weight: 367.47 g mol^{-1}
Yield: 203 mg, 0.55 mmol, 55 %

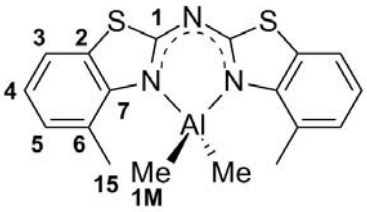

^{1}H-NMR
(500 MHz, THF-d_8): δ / ppm = 7.58 − 7.54 (m, 2 H, H3), 7.10 (d, $^{3}J_{HH}$ = 7.3 Hz, 2 H, H5), 7.03 (t, $^{3}J_{HH}$ = 7.6 Hz, 2 H, H4), 2.51 (s, 6 H, H15), −0.52 (s, 6 H, H1M).
^{13}C{^{1}H}-NMR
(125 MHz, THF-d_8): δ / ppm = 173.07 (s, 2 C, C1), 148.79 (s, 2 C, C7), 132.55 (s, 2 C, C2), 127.83 (s, 2 C, C5), 127.12 (s, 2 C, C6), 123.15 (s, 2 C, C4), 119.90 (s, 2 C, C3), 18.85 (s, 2 C, C15), −8.06 (s, 2 C, C1M).
^{15}N{^{1}H}-NMR
(40 MHz, THF-d_8): δ / ppm = −135.65 (s, N1'), −194.65 (s, N1).
^{27}Al{^{1}H}-NMR
(130 MHz, THF-d_8): δ / ppm = 182 (s).
elemental analysis
in % (calculated): C, 58.40 (58.51); H, 5.26 (5.46); N, 11.30 (11.37); S, 17.41 (17.36).
EI-MS
m/*z* (%): 367 (3) $[M]^+$, 352 (100) $[M - Me]^+$, 336 (9) $[M - 2\ Me]^+$, 311 (54) $[M - AlMe_2]^+$.

4.3.40 Dimethylaluminium-bis-(4-methoxybenzothiazol-2-yl)-amide trimethylaluminium (46)

A pale brown powder was obtained in a yield of 119 mg (0.25 mmol, 25 %; not optimized).

Molecular formula: $C_{21}H_{27}Al_2N_3O_2S_2$
Molecular weight: 471.55 g mol^{-1}
Yield: 119 mg, 0.25 mmol, 25 %

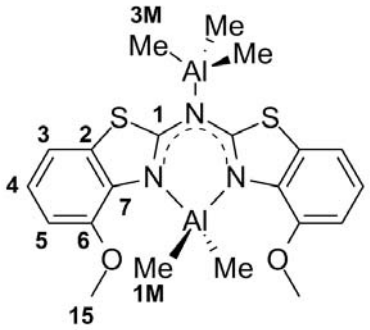

^{1}H-NMR
(400 MHz, THF-d_8): δ / ppm = 7.26 (dd, $^3J_{HH}$ = 8.0, 1.2 Hz, 2 H, H3), 7.20 (t, $^3J_{HH}$ = 7.9 Hz, 2 H, H4), 6.98 (dd, $^3J_{HH}$ = 8.0, 1.1 Hz, 2 H, H5), 3.98 (s, 6 H, H15), −0.64 (s, 6 H, H1M), −0.95 (s, 6 H, H3M).

^{13}C{^{1}H}-NMR
(125 MHz, THF-d_8): δ / ppm = 173.16 (s, 2 C, C1), 149.29 (s, 2 C, C6), 137.75 (s, 2 C, C7), 129.91 (s, 2 C, C2), 125.55 (s, 2 C, C4), 114.56 (s, 2 C, C3), 108.32 (s, 2 C, C5), 55.32 (s, 2 C, C15), −5.96 (s, 3 C, C1M), −9.13 (s, 2 C, C3M).

^{15}N{^{1}H}-NMR
(40 MHz, THF-d_8): δ / ppm = −193.32 (s, N1, N1') (no second signal detected due to the quite similar chemical environment of both positions).

^{27}Al{^{1}H}-NMR
(130 MHz, THF-d_8): δ / ppm = 183 (s).

elemental analysis
in % (calculated): C, 52.52 (53.49); H, 4.36 (5.77); N, 10.37 (8.91); S, 15.49 (13.60) (deviations due to partial loss of $AlMe_3$).

EI-MS
m/*z* (%): 384 (100) $[M - AlMe_4]^+$, 354 (64) $[M - AlMe_4 - OMe]^+$, 339 (72) $[M - AlMe_4 - OMe - Me]^+$.

4.3.41 Lithium-bis-(benzothiazol-2-yl)-amide (47)

A colourless powder was obtained in a yield of 149 mg (0.51 mmol, 51 %).

Molecular formula: $C_{14}H_8LiN_3S_2$
Molecular weight: 289.30 g mol^{-1}
Yield: 149 mg, 0.51 mmol, 51 %

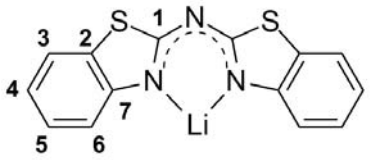

^{1}H-NMR

(500 MHz, THF-d_8): δ / ppm = 7.52 (d, $^{3}J_{HH}$ = 7.6 Hz, 2 H, H3), 7.33 (d, $^{3}J_{HH}$ = 7.9 Hz, 2 H, H6), 7.16 (t, $^{3}J_{HH}$ = 7.3 Hz, 2 H, H5), 6.98 (t, $^{3}J_{HH}$ = 7.3 Hz, 2 H, H4).

^{13}C{^{1}H}-NMR

(125 MHz, THF-d_8): δ / ppm = 173.61 (s, 2 C, C1), 153.83 (s, 2 C, C7), 132.35 (s, 2 C, C2), 125.65 (s, 2 C, C5), 121.77 (s, 2 C, C4), 121.51 (s, 2 C, C3), 117.37 (s, 2 C, C6).

^{7}Li{^{1}H}-NMR

(117 MHz, THF-d_8): δ / ppm = 2.09 (s).

^{15}N{^{1}H}-NMR

(50 MHz, THF-d_8): δ / ppm = −155.42 (s, N1, N1') (no second signal detected due to fast exchange of the Li at both positions).

elemental analysis

in % (calculated): C, 57.62 (58.12); H, 2.42 (2.79); N, 14.06 (14.52); S, 20.69 (22.17).

EI-MS

m/*z* (%): 289 (59) $[M]^+$, 283 (100) $[M - Li]^+$.

4.3.42 Lithium-bis-(4-methylbenzothiazol-2-yl)-amide (48)

Colourless crystals were obtained in a yield of 122 mg (0.38 mmol, 38 %).

Molecular formula: $C_{16}H_{12}LiN_3S_2$
Molecular weight: 317.36 g mol^{-1}
Yield: 122 mg, 0.38 mmol, 38 %

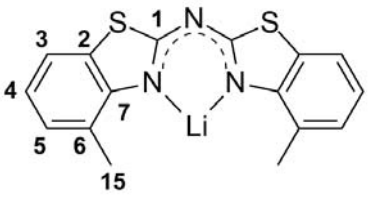

^{1}H-NMR

(300 MHz, THF-d_8): δ / ppm = 7.41 (ddd, $^{3}J_{HH}$ = 7.7, 1.2, 0.6 Hz, 2 H, H3), 7.01 (ddd, $^{3}J_{HH}$ = 7.3, 1.3, 0.8 Hz, 2 H, H5), 6.86 (t, $^{3}J_{HH}$ = 7.5 Hz, 2 H, H4), 2.58 (s, 6 H, H15).

^{13}C{^{1}H}-NMR

(75 MHz, THF-d_8): δ / ppm = 170.87 (s, 2 C, C1), 151.70 (s, 2 C, C7), 132.95 (s, 2 C, C2), 127.61 (s, 2 C, C6), 126.31 (s, 2 C, C5), 120.84 (s, 2 C, C4), 118.83 (s, 2 C, C3), 18.78 (s, 2 C, C15).

^{7}Li{^{1}H}-NMR

(117 MHz, THF-d_8): δ / ppm = −0.68 (s).

^{15}N{^{1}H}-NMR

(40 MHz, THF-d_8): δ / ppm = −144.80 (s, N1, N1') (no second signal detected due to fast exchange of the Li at both positions).

elemental analysis

in % (calculated): C, 61.97 (60.55); H, 4.05 (3.81); N, 12.27 (13.24) (deviation due to remaining toluene).

EI-MS
m/*z* (%): 317 (5) $[M]^+$, 311 (100) $[M - Li]^+$.

4.3.43 Diethyl-(phenyl)-phosphate (49)[146]

Triethylamine (14.3 mL, 10.1 g, 0.10 mol, 1.00 eq.) was poured slowly under vigorous stirring into an ice-cooled solution of phenol (9.41 g, 0.10 mol, 1.00 eq.) and diethyl-phosphite (13.4 mL, 13.8 g, 0.10 mol, 1.00 eq.) in tetrachloro methane (30 mL). After addition of triethylamine, triethylammonium chloride started precipitating as colourless solid. The reaction mixture was stirred over night and afterwards combined with water (80 mL). The organic layer was separated and washed once with aq. HCl solution (2 M, 80 mL), four times with aq. NaOH solution (2 M, 4 x 80 mL) and once again with water (80 mL). After drying over $MgSO_4$ the remaining solvent was removed by applying vacuum und the pale yellow residue was distilled under reduced pressure. A colourless liquid could be obtained in a yield of 16.21 g (70.4 mmol, 70 %).

Molecular formula: $C_{10}H_{15}O_4P$
Molecular weight: 230.20 g mol^{-1}
Yield: 16.21 g, 70.4 mmol, 70 %

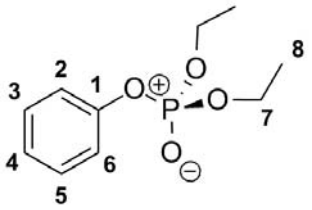

^{1}H-NMR
(300 MHz, $CDCl_3$): δ / ppm = 7.37 − 7.27 (m, 2 H, H3 + H5), 7.24 − 7.11 (m, 3 H, H2 + H4 + H6), 4.27 – 4.13 (m, 4 H, H7), 1.33 (tt, J_{HH} = 7.1, 1.3 Hz, 6 H, H8).

^{13}C{^{1}H}-NMR
(75 MHz, $CDCl_3$): δ / ppm = 150.88 (d, $^2J_{CP}$ = 6.8 Hz, 1 C, C1), 129.76 (s, 2 C, C3 + C5), 125.02 (d, $^5J_{CP}$ = 0.9 Hz, 1 C, C4), 120.06 (d, $^5J_{CP}$ = 4.9 Hz, 2 C, C2 + C6), 64.64 (d, $^2J_{CP}$ = 6.1 Hz, 2 C, C7), 16.16 (d, $^3J_{CP}$ = 6.7 Hz, 2 C, C8).

^{31}P{^{1}H}-NMR
(121 MHz, $CDCl_3$): δ / ppm = −6.32 (s).

EI-MS
m/*z* (%): 230.1 (63) $[M]^+$, 202.0 (18) $[M - C_2H_5]^+$.

4.3.44 Diethyl-(2-hydroxyphenyl)-phosphonate (50)[147]

Diisopropyl amine (21.8 mL, 15.7 g, 155 mmol, 2.20 eq.) was dissolved under inert gas atmosphere in THF (70 mL) and the solution was cooled to −78 °C. Afterwards *n*-BuLi (53.0 mL, 2.93 M in hexane, 155 mmol, 2.20 eq.) was added slowly and the resulting orange solution was stirred for 30 min at −78 °C. In a next step, **49** (16.2 g, 70.4 mmol, 1.00 eq.) dissolved in THF (50 mL) was added and the reaction mixture was stirred for additional 1.5 h at −78 °C. The solution was poured under vigorous stirring into a mixture of Et_2O (210 mL) and saturated NH_4Cl solution (210 mL). A colourless solid was formed

temporarily, which again disappears upon warming to rt. The pale orange organic phase was separated, the aqueous phase was extracted twice with Et_2O (2 x 40 mL). The combined organic layers were dried over $MgSO_4$ and remaining solvent was removed under reduced pressure. After distillation under reduced pressure of the crude product a colourless liquid could be isolated in a yield of 12.8 g (55.6 mmol, 79 %). Over night the purest fraction solidified.

Molecular formula: $C_{10}H_{15}O_4P$
Molecular weight: 230.20 g mol^{-1}
Yield: 12.8 g, 55.6 mmol, 79 %

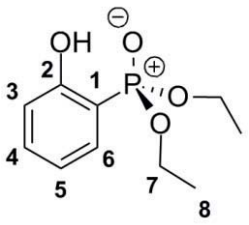

^{1}H-NMR
(300 MHz, $CDCl_3$): δ / ppm = 10.19 (s_{br}, 1 H, OH), 7.46 − 7.29 (m, 2 H, H4 + H6), 6.98 – 6.85 (m, 2 H, H3 + H5), 4.22 – 3.94 (m, 4 H, H7), 1.30 (td, J_{HH} = 7.1, 0.5 Hz, 6 H, H8).

^{13}C{^{1}H}-NMR
(75 MHz, $CDCl_3$): δ / ppm = 162.12 (d, $^2J_{CP}$ = 7.3 Hz, 1 C, C2), 135.25 (d, $^4J_{CP}$ = 2.4 Hz, 1 C, C4), 131.63 (d, 1 C, $^2J_{CP}$ = 6.1 Hz, C6), 119.66 (d, $^3J_{CP}$ = 13.7 Hz, 1 C, C5), 117.70 (d, $^3J_{CP}$ = 12.0 Hz, 1 C, C3), 108.86 (d, $^1J_{CP}$ = 180.0 Hz, 1 C, C1), 62.76 (d, $^2J_{CP}$ = 4.8 Hz, 2 C, C7), 16.22 (d, $^3J_{CP}$ = 6.7 Hz, 2 C, C8).

^{31}P{^{1}H}-NMR
(121 MHz, $CDCl_3$): δ / ppm = 22.36 (s).

elemental analysis
in % (calculated): C, 52.08 (52.18); H, 6.54 (6.57).

EI-MS
m/*z* (%): 230.0 (54) $[M]^+$, 202.0 (19) $[M - C_2H_5]^+$, 174.0 (92) $[M - 2\ C_2H_5]^+$.

4.3.45 2-Phosphinophenol (51)[148a]

Under inert gas atmosphere, to an ice-cooled slurry of $LiAlH_4$ (1.03 g, 27.1 mmol, 3.00 eq.) in Et_2O (25 mL) a solution of **50** (2.05 g, 8.92 mmol, 1.00 eq.) in Et_2O (20 mL) was syringed slowly. The grey suspension was allowed to warm up to rt and was kept stirring for additional 2 d. Then degassed aq. HCl solution (2 M, 50 mL) was added under ice-cooling to the reaction mixture until no more gas evolution was detected and the formed grey solid was suspended in the aqueous phase. The etheral phase was decanted via syringe into a flask with $MgSO_4$, the aqueous layer was extracted three times with Et_2O (3 x 20 mL) and the combined organic phases were dried over $MgSO_4$. After removal of the solvent under reduced pressure and purification by sublimation, the primary phosphane **51** could be yielded as colourless solid (687 mg, 5.45 mmol, 61 %).

Molecular formula: C_6H_7OP
Molecular weight: 126.09 g mol^{-1}
Yield: 678 mg, 5.45 mmol, 61 %

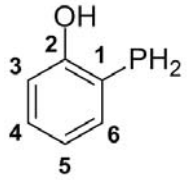

^{1}H-NMR
(300 MHz, THF-d_8): δ / ppm = 8.67 (s_{br}, 1 H, OH), 7.32 (t, $^3J_{HH}$ = 7.7 Hz, 1 H, H6), 7.09 (t, $^3J_{HH}$ = 7.7 Hz, 1 H, H4), 6.78 – 6.64 (m, 2 H, H3 + H5), 3.72 (d, $^1J_{HP}$ = 199.8 Hz, 2 H, PH_2).

^{13}C{^{1}H}-NMR
(75 MHz, THF-d_8): δ / ppm = 160.03 (d, $^2J_{CP}$ = 6.2 Hz, 1 C, C2), 136.52 (d, $^3J_{CP}$ = 14.6 Hz, 1 C, C6), 130.58 (s, 1 C, C4), 120.34 (d, $^3J_{CP}$ = 5.3 Hz, 1 C, C5), 116.10 (s, 1 C, C1), 115.07 (s, 1 C, C3).

^{31}P{^{1}H}-NMR
(121 MHz, THF-d_8): δ / ppm = −145.78 (s).

^{31}P-NMR
(121 MHz, THF-d_8): δ / ppm = −147.65 (td, J_{PH} = 199.9, 6.7 Hz).

EI-MS
m/*z* (%): 126.0 (100) $[M]^+$, 107.0 (26) $[M - OH]^+$, 94.0 (36) $[M - PH_2]^+$, 77.0 (38) $[M - OH - PH_2]^+$.

4.3.46 2-Bromo-*N*-methylaniline (52)

Method 1:

2-Bromoaniline (7.50 g, 43.6 mmol, 2.00 eq.), dissolved in THF (45 mL), was cooled to −40 °C under nitrogen atmosphere. A solution of *n*-BuLi (7.40 mL, 2.93 M in hexane, 21.8 mmol, 1.00 eq.) was added slowly and the resulting pale yellow mixture kept stirring for 30 min at −40 °C. After cooling to −60 °C methyl iodide (1.40 mL, 3.09 g, 21.8 mmol, 1.00 eq.) was added dropwise, the reaction mixture was allowed to warm up to rt and stirred for additional 18 h at rt. The reaction was quenched by adding water (30 mL) and the organic phase was separated. The aqueous phase was extracted three times with EtOAc (3 x 40 mL), the combined organic phases were washed once with sat. aq. $NaHCO_3$ solution (40 mL), dried over $MgSO_4$ and remaining solvent was evaporated under reduced pressure. After purification by column chromatography (silica, pentane/EtOAc = 50:1, R_f = 0.34), compound **52** could be obtained as a pale yellow liquid (3.45 g, 18.6 mmol, 85 % based on MeI).

Method 2:

2-Bromoaniline (7.50 g, 43.6 mmol, 1.00 eq.) dissolved in THF (45 mL) was added dropwise under nitrogen atmosphere into an ice-cooled suspension of NaH (1.05 g, 43.6 mmol, 1.00 eq.) in THF (25 mL). The resulting slurry was allowed to warm up to rt and stirred over night at rt, to complete the amine's deprotonation. Then methyl iodide

(2.80 mL, 6.19 g, 43.6 mmol, 1.00 eq.) was added slowly to the ice-cooled greenish-brown suspension. The reaction mixture was allowed to slowly warm up to rt and stirred for additional 24 h at rt. Water (30 mL) was poured into the yellow suspension and the organic layer was separated. The aqueous layer was extracted twice with EtOAc (2 x 50 mL), the combined organic phases were washed once with saturated $NaHCO_3$ solution (50 mL) and dried over $MgSO_4$. The yellow solution was concentrated under reduced pressure to give a light brown liquid. After purification by column chromatography (silica, pentane/EtOAc = 50:1) compound **52** could be obtained as a pale yellow liquid (3.88 g, 20.8 mmol, 48 % based on MeI).

Molecular formula: C_7H_8BrN
Molecular weight: 186.05 g mol^{-1}
Yield (method 1): 3.45 g, 18.6 mmol, 85 %
Yield (method 2): 3.88 g, 20.8 mmol, 48 %

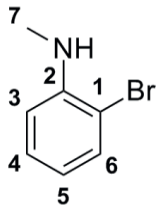

^{1}H-NMR
(300 MHz, $CDCl_3$): δ / ppm = 7.43 (dd, J_{HH} = 7.9, 1.5 Hz, 1 H, H6), 7.22 (ddd, J_{HH} = 8.1, 7.4, 1.5 Hz, 1 H, H4), 6.66 (dd, J_{HH} = 8.1, 1.2 Hz, 1 H, H3), 6.59 (td, J_{HH} = 7.8, 1.5 Hz, 1 H, H5), 4.55 (s_{br}, 1 H, NH), 2.91 (s, 3 H, H7).

^{13}C{^{1}H}-NMR
(75 MHz, $CDCl_3$): δ / ppm = 145.94 (s, 1 C, C2), 132.36 (s, 1 C, C6), 128.64 (s, 1 C, C4), 117.80 (s, 1 C, C5), 110.96 (s, 1 C, C3), 109.76 (s, 1 C, C1), 29.80 (s, 1 C, C7).

^{15}N{^{1}H}-NMR
(40 MHz, THF-d_8): δ / ppm = −324.21 (s).

elemental analysis
in % (calculated): C, 45.04 (45.19); H, 4.33 (4.33); N, 7.55 (7.53).

EI-MS
m/*z* (%): 185.0 (100) $[M]^+$, 105.0 (16) $[M - HBr]^+$, 77 (26) $[C_6H_5]^+$.

4.3.47 Diethyl-(2-methylaminophenyl)-phosphonate (53)[135]

Method 1:

52 (1.00 g, 5.38 mmol, 1.00 eq.) was dissolved under nitrogen-atmosphere in toluene (50 mL). Then successively $Pd_2(dba)_3$ (0.10 g, 0.11 mmol, 2.00 mol%), 1,1′-bis-(diphenylphosphino)-ferrocene (DPPF) (0.09 g, 0.16 mmol, 3.00 mol%), diethylphosphite (0.76 mL, 5.92 mmol, 1.10 eq.) and NaO*t*Bu (0.72 g, 7.53 mmol, 1.40 eq.) were added and the resulting brown reaction mixture was heated at 120 °C for 12 h. Insoluble material was filtered off over cellite and the residual yellow solution was concentrated under reduced pressure to give the crude product as orange oil. After purification by column chromatography (silica, pentane/EtOAc = 95:5 (2 L), R_f = 0.05; then 1:1 (2 L)) compound **53** could be obtained as light brown liquid (559 mg, 2.3 mmol, 43 %).

Molecular formula: $C_{11}H_{18}NO_3P$
Molecular weight: 243.24 g mol^{-1}
Yield: 559 mg, 2.3 mmol, 43 %

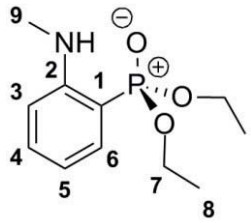

^{1}H-NMR
(300 MHz, $CDCl_3$): δ / ppm = 7.48 – 7.31 (m, 2 H, H4 + H6), 6.69 – 6.58 (m, 2 H, H3 + H5), 5.28 (s, 1 H, NH), 4.18 – 3.92 (m, 4 H, H7), 2.83 (s, 3 H, H9), 1.30 (t, $^3J_{HH}$ = 7.1 Hz, 6 H, H8).

^{13}C{^{1}H}-NMR
(75 MHz, $CDCl_3$): δ / ppm = 152.83 (d, $^2J_{CP}$ = 9.2 Hz, 1 C, C2), 134.36 (d, $^4J_{CP}$ = 2.2 Hz, 1 C, C4), 133.50 (d, 1 C, $^2J_{CP}$ = 7.0 Hz, C6), 115.42 (d, $^3J_{CP}$ = 14.2 Hz, 1 C, C5), 110.60 (d, $^3J_{CP}$ = 12.2 Hz, 1 C, C3), 107.55 (d, $^1J_{CP}$ = 182.7 Hz, 1 C, C1), 62.10 (d, $^2J_{CP}$ = 4.9 Hz, 2 C, C7), 30.18 (s, 1 C, C9), 16.33 (d, $^3J_{CP}$ = 6.7 Hz, 2 C, C8).

^{31}P{^{1}H}-NMR
(121 MHz, THF-d_8): δ / ppm = 21.96 (s).

EI-MS
m/*z* (%): 243.1 (100) $[M]^+$, 215.0 (15) $[M - C_2H_5]^+$, 186.0 (17) $[M - 2\ C_2H_5]^+$.

4.3.48 *N*-Methyl-2-phosphinoaniline (54)[135]

Under inert gas atmosphere to an ice-cooled slurry of $LiAlH_4$ (250 g, 6.9 mmol, 3.00 eq.) in Et_2O (15 mL) a solution of **53** (559 mg, 2.3 mmol, 1.00 eq.) in Et_2O (5 mL) was added slowly via syringe. The suspension was allowed to warm up to rt and was kept stirring for additional 2 d. Then degassed aq. HCl solution (2 M, 30 mL) was added under ice-cooling to the reaction mixture and stirring was continued for 30 min. The formed colourless solid was filtered off and washed twice with Et_2O (2 x 20 mL). The organic phase was decanted via syringe into a flask with $MgSO_4$, the aqueous layer was extracted three times with Et_2O (3 x 10 mL) and the combined organic phases were dried over $MgSO_4$. After removal of the solvent under reduced pressure the primary phosphane **54** could be obtained as light brown liquid (446 mg, 3.21 mmol, 139 % due to impurities). The whole isolated amount of phosphane was used for cyclization attempts without further spectroscopic investigations.

Molecular formula: $C_7H_{10}NP$
Molecular weight: 139.13 g mol^{-1}
Yield (method 1): 446 mg, 3.21 mmol,
139 % due to impurities

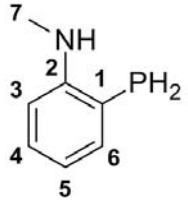

5 Supplement

5.1 Crystallographic information

5.1.1 Bis-(benzoxazol-2-yl)-methane (4)

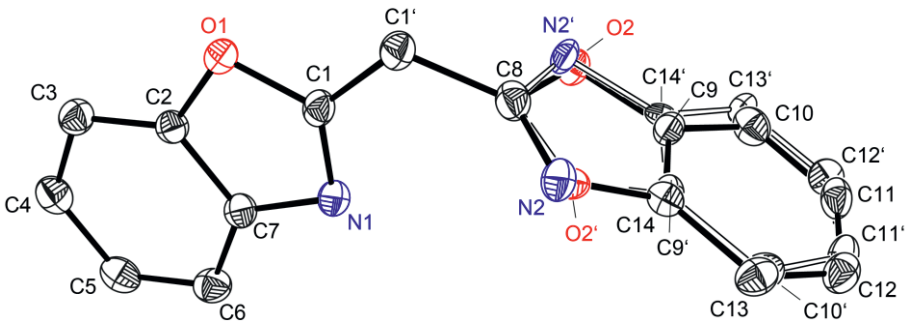

Figure 5-1: Asymmetric unit of **4**. Anisotropic displacement parameters are displayed at the 50 % probability level. Hydrogen atoms are omitted for clarity and disordered moieties (sof: 0.790(10)) are depicted in faded colour.

Table 5-1: Crystallographic information of $(NCOC_6H_4)_2CH_2$ (**4**).

CCDC no.	995110	μ [mm^{-1}]	0.096
Structure code	box2CH2	F(000)	520
Empirical formula	$C_{15}H_{10}N_2O_2$	Crystal size [mm^3]	0.200 x 0.200 x 0.080
Formula weight [g mol^{-1}]	250.25	θ range [deg]	2.318 to 29.687
Temperature [K]	100(2)	Reflections collected	18686
Wavelength [Å]	0.71073	Independent reflections	3321
Crystal system	monoclinic	R_{int}	0.0290
Space group	$P2_1/c$	Completeness to θ_{max}	99.2 %
Unit cell dimensions	a = 9.066(2) Å	Restraints / parameters	478 / 245
	b = 9.457(2) Å	Goodness-of-fit on F^2	1.043
	c = 14.172(3) Å	$R1$ [I>2σ(I)]	0.0387
	α = 90 deg	w$R2$ (all data)	0.1008
	β = 104.23(2) deg	$g1$ / $g2$	0.0453 / 0.4674
	γ = 90 deg	max. diff. peak / hole [e Å^{-3}]	0.365 / −0.255
Volume [Å^3]	1177.8(4)	max. / min. transmission	0.7459 / 0.6953
Z	4	Absolute structure param.[169]	–
ρ_{calc} [Mg m^{-3}]	1.411	Extinction coefficient	–

5.1.2 Bis-(benzothiazol-2-yl)-methane (5)

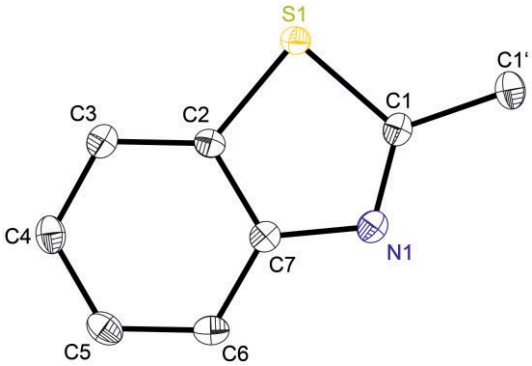

Figure 5-2: Asymmetric unit of **5**. Anisotropic displacement parameters are displayed at the 50 % probability level. Hydrogen atoms are omitted for clarity. The remaining part of the molecule is generated by symmetry.

Table 5-2: Crystallographic information of $(NCSC_6H_4)_2CH_2$ (**5**).

CCDC no.	995111	μ [mm^{-1}]	0.409
Structure code	bth2CH2	F(000)	584
Empirical formula	$C_{15}H_{10}N_2S_2$	Crystal size [mm^3]	0.120 x 0.100 x 0.100
Formula weight [g mol^{-1}]	282.37	θ range [deg]	1.643 to 27.097
Temperature [K]	100(2)	Reflections collected	24628
Wavelength [Å]	0.71073	Independent reflections	1379
Crystal system	monoclinic	R_{int}	0.0234
Space group	$C2/c$	Completeness to θ_{max}	99.6 %
Unit cell dimensions	a = 25.412(3) Å	Restraints / parameters	0 / 87
	b = 4.536(1) Å	Goodness-of-fit on F^2	1.091
	c = 11.165(2) Å	$R1$ [I>2σ(I)]	0.0245
	α = 90 deg	w$R2$ (all data)	0.0634
	β = 102.76(2) deg	$g1$ / $g2$	0.0267 / 1.6801
	γ = 90 deg	max. diff. peak / hole [e Å^{-3}]	0.343 / −0.163
Volume [Å^3]	1255.2(4)	max. / min. transmission	0.7461 / 0.7084
Z	4	Absolute structure param.[169]	–
ρ_{calc} [Mg m^{-3}]	1.494	Extinction coefficient	–

5.1.3 Bis-(4-methylbenzoxazol-2-yl)-methane (19)

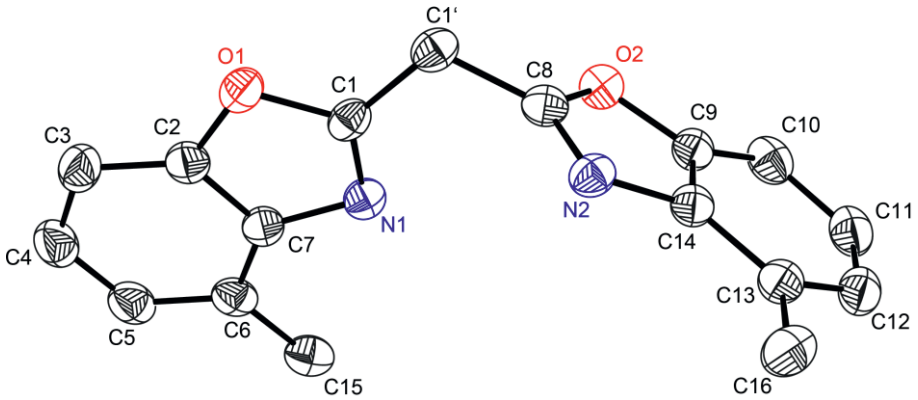

Figure 5-3: Asymmetric unit of **19**. Anisotropic displacement parameters are displayed at the 50 % probability level. Hydrogen atoms are omitted for clarity.

Table 5-3: Crystallographic information of $(4\text{-MeNCOC}_6H_3)_2CH_2$ (**19**).

CCDC no.	1429338	μ [mm^{-1}]	0.090
Structure code	DD_LW008	F(000)	292
Empirical formula	$C_{17}H_{14}N_2O_2$	Crystal size [mm^3]	0.178 x 0.115 x 0.046
Formula weight [g mol^{-1}]	278.30	θ range [deg]	1.586 to 25.347
Temperature [K]	100(2)	Reflections collected	23615
Wavelength [Å]	0.71073	Independent reflections	2495
Crystal system	triclinic	R_{int}	0.0369
Space group	$P\bar{1}$	Completeness to θ_{max}	99.8 %
Unit cell dimensions	a = 4.741(2) Å	Restraints / parameters	0 / 193
	b = 11.471(3) Å	Goodness-of-fit on F^2	1.057
	c = 13.084(3) Å	R1 [I>2σ(I)]	0.0364
	α = 79.15(2) deg	wR2 (all data)	0.0938
	β = 85.84(2) deg	g1 / g2	0.0385 / 0.2479
	γ = 78.19(2) deg	max. diff. peak / hole [e Å^{-3}]	0.170 / −0.162
Volume [Å^3]	683.6(4)	max. / min. transmission	0.9705 / 0.8714
Z	2	Absolute structure param.[169]	–
ρ_{calc} [Mg m^{-3}]	1.352	Extinction coefficient	0.016(3)

5.1.4 4-Methylbenzoxazol-2-yl-carboxamide (20)

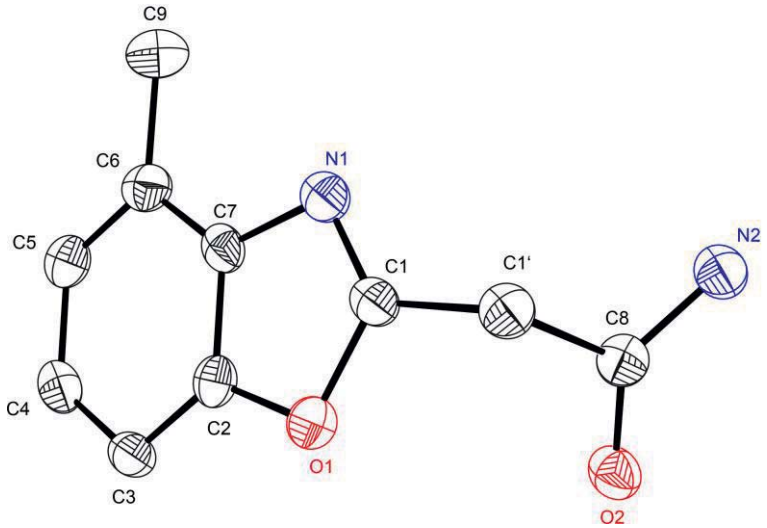

Figure 5-4: Asymmetric unit of **20**. Anisotropic displacement parameters are displayed at the 50 % probability level. Hydrogen atoms are omitted for clarity.

Table 5-4: Crystallographic information of 4-Methylbenzoxazol-2-yl-carboxamide (**20**).

CCDC no.	1429356	μ [mm^{-1}]	0.099
Structure code	mbox2CH2_Fraktion2	F(000)	200
Empirical formula	$C_{10}H_{10}N_2O_2$	Crystal size [mm^3]	0.100 x 0.050 x 0.050
Formula weight [g mol^{-1}]	190.20	θ range [deg]	2.621 to 25.503
Temperature [K]	100(2)	Reflections collected	7223
Wavelength [Å]	0.71073	Independent reflections	1691
Crystal system	triclinic	R_{int}	0.0406
Space group	$P\bar{1}$	Completeness to θ_{max}	99.9 %
Unit cell dimensions	a = 7.790(2) Å	Restraints / parameters	198 / 137
	b = 7.974(2) Å	Goodness-of-fit on F^2	1.088
	c = 8.279(3) Å	$R1$ [I>2σ(I)]	0.0496
	α = 93.24(2) deg	w$R2$ (all data)	0.1345
	β = 115.09(3) deg	$g1$ / $g2$	0.0606 / 0.2790
	γ = 99.95(2) deg	max. diff. peak / hole [e Å^{-3}]	0.408 / −0.228
Volume [Å^3]	453.9(3)	max. / min. transmission	0.7452 / 0.6823
Z	2	Absolute structure param.[169]	–
ρ_{calc} [Mg m^{-3}]	1.392	Extinction coefficient	–

5.1.5 Dimethylaluminium-bis-(*N*-methylimidazol-2-yl)-methanide (6)

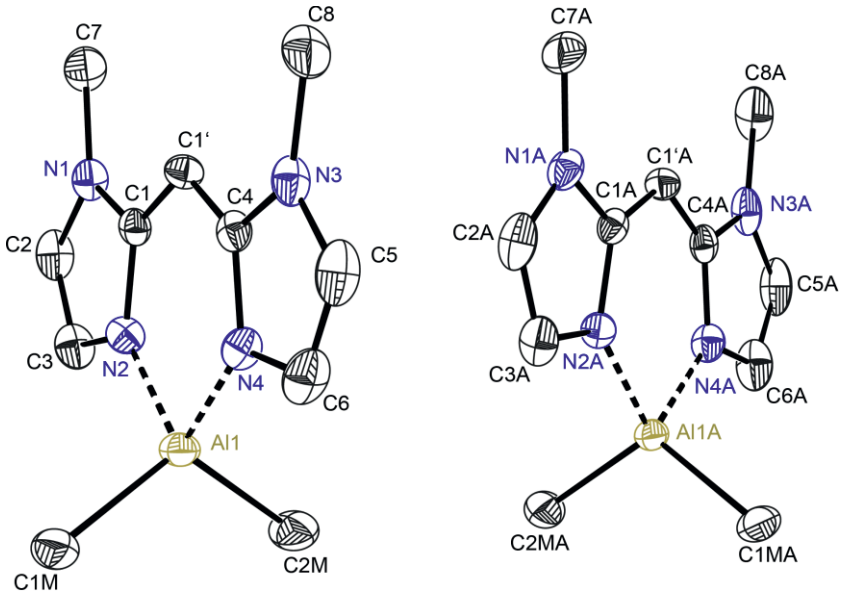

Figure 5-5: Asymmetric unit of **6**. Anisotropic displacement parameters are displayed at the 50 % probability level. Hydrogen atoms are omitted for clarity.

Table 5-5: Crystallographic information of $[Me_2Al\{(1\text{-}MeNCNC_2H_2)_2CH\}]$ (**6**).

CCDC no.	–	μ [mm^{-1}]	0.140
Structure code	mim2CHAlMe2	F(000)	992
Empirical formula	$C_{11}H_{17}AlN_4$	Crystal size [mm^3]	0.158 x 0.148 x 0.074
Formula weight [g mol^{-1}]	232.26	θ range [deg]	1.188 to 25.496
Temperature [K]	100(2)	Reflections collected	39058
Wavelength [Å]	0.71073	Independent reflections	4697
Crystal system	monoclinic	R_{int} / BASF (pseudo-mero.)	0.0930 / 0.0442 TWIN -1 0 -1 0 -1 0 0 0 1
Space group	$P2_1/c$	Completeness to θ_{max}	99.7 %
Unit cell dimensions	a = 13.500(3) Å	Restraints / parameters	0 / 300
	b = 17.133(4) Å	Goodness-of-fit on F^2	1.045
	c = 12.370(3) Å	$R1$ [I>2σ(I)]	0.0484
	α = 90 deg	w$R2$ (all data)	0.1414
	β = 117.14(2) deg	$g1$ / $g2$	0.0672 / 1.2704
	γ = 90 deg	max. diff. peak / hole [e Å^{-3}]	0.419 / −0.311
Volume [Å^3]	2546.1(11)	max. / min. transmission	0.7136 / 0.6100
Z	8	Absolute structure param.[169]	–
ρ_{calc} [Mg m^{-3}]	1.212	Extinction coefficient	0.0020(5)

5.1.6 Dimethylaluminium-bis-(benzoxazol-2-yl)-methanide (8)

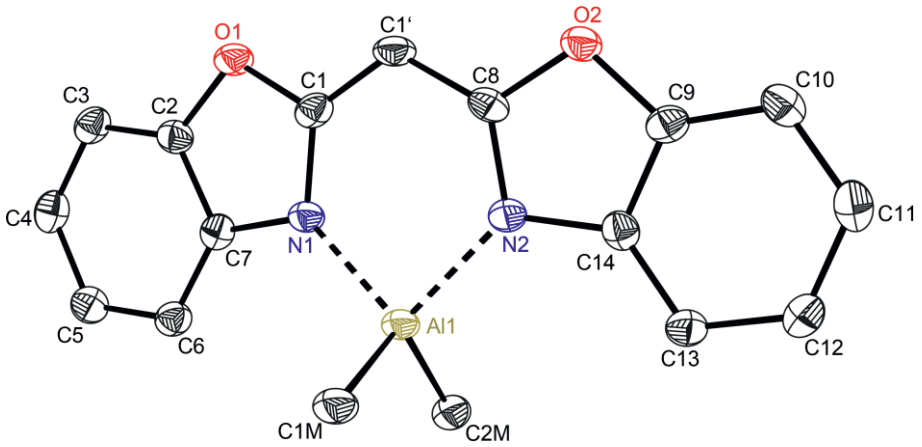

Figure 5-6: Asymmetric unit of **8**. Anisotropic displacement parameters are displayed at the 50 % probability level. Hydrogen atoms are omitted for clarity.

Table 5-6: Crystallographic information of $[Me_2Al\{(NCOC_6H_4)_2CH\}]$ (**8**).

CCDC no.	995112	μ [mm^{-1}]	0.144
Structure code	box2CHAlMe2	F(000)	320
Empirical formula	$C_{17}H_{15}AlN_2O_2$	Crystal size [mm^3]	0.120 x 0.080 x 0.080
Formula weight [g mol^{-1}]	306.29	θ range [deg]	1.605 to 25.415
Temperature [K]	100(2)	Reflections collected	12679
Wavelength [Å]	0.71073	Independent reflections	2745
Crystal system	triclinic	R_{int}	0.0496
Space group	$P\bar{1}$	Completeness to θ_{max}	99.9 %
Unit cell dimensions	a = 7.998(2) Å	Restraints / parameters	24 / 201
	b = 8.336(2) Å	Goodness-of-fit on F^2	1.057
	c = 13.294(3) Å	$R1$ [I>2σ(I)]	0.0447
	α = 93.54(2) deg	w$R2$ (all data)	0.1181
	β = 103.31(2) deg	$g1$ / $g2$	0.0610 / 0.3249
	γ = 117.86(3) deg	max. diff. peak / hole [e Å^{-3}]	0.412 / −0.368
Volume [Å^3]	747.6(4)	max. / min. transmission	0.9705 / 0.8155
Z	2	Absolute structure param.[169]	–
ρ_{calc} [Mg m^{-3}]	1.361	Extinction coefficient	–

5.1.7 Dimethylaluminium-bis-(benzothiazol-2-yl)-methanide (9)

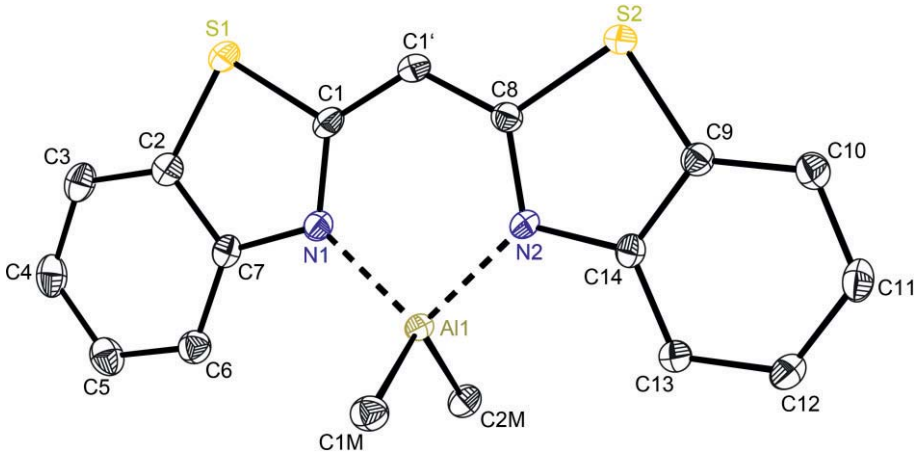

Figure 5-7: Asymmetric unit of **9**. Anisotropic displacement parameters are displayed at the 50 % probability level. Hydrogen atoms are omitted for clarity.

Table 5-7: Crystallographic information of $[Me_2Al\{(NCSC_6H_4)_2CH\}]$ (**9**).

CCDC no.	995113	μ [mm^{-1}]	0.382
Structure code	bth2CHAlMe2	F(000)	352
Empirical formula	$C_{17}H_{15}AlN_2S_2$	Crystal size [mm^3]	0.120 x 0.100 x 0.100
Formula weight [g mol^{-1}]	338.41	θ range [deg]	1.385 to 26.471
Temperature [K]	100(2)	Reflections collected	34844
Wavelength [Å]	0.71073	Independent reflections	3313
Crystal system	triclinic	R_{int} / BASF (non-mero.)	0.0421 / 0.5300
Space group	$P\bar{1}$	Completeness to θ_{max}	99.9 %
Unit cell dimensions	a = 7.126(2) Å	Restraints / parameters	30 / 202
	b = 7.696(2) Å	Goodness-of-fit on F^2	1.035
	c = 14.730(3) Å	R1 [I>2σ(I)]	0.0305
	α = 90.50(2) deg	wR2 (all data)	0.0850
	β = 93.12(2) deg	g1 / g2	0.0490 / 0.1837
	γ = 93.44(2) deg	max. diff. peak / hole [e Å^{-3}]	0.432 / −0.262
Volume [Å^3]	805.1(3)	max. / min. transmission	0.7454 / 0.6837
Z	2	Absolute structure param.[169]	–
ρ_{calc} [Mg m^{-3}]	1.396	Extinction coefficient	–

5.1.8 Dimethylaluminium-bis-(4-methylbenzoxazol-2-yl)-methanide (21)

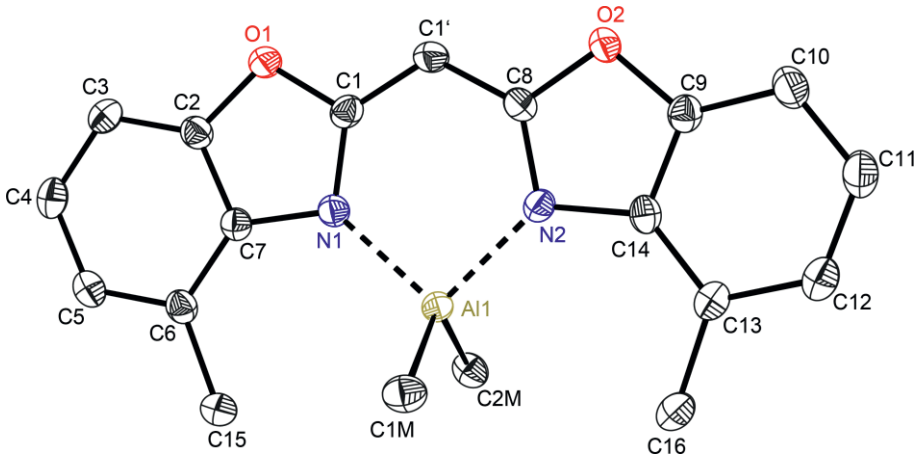

Figure 5-8: Asymmetric unit of **21**. Anisotropic displacement parameters are displayed at the 50 % probability level. Hydrogen atoms are omitted for clarity.

Table 5-8: Crystallographic information of $[Me_2Al\{(4\text{-}MeNCOC_6H_3)_2CH\}]$ (**21**).

CCDC no.	1429357	μ [mm^{-1}]	0.135
Structure code	DD_LW009	F(000)	704
Empirical formula	$C_{19}H_{19}AlN_2O_2$	Crystal size [mm^3]	0.249 x 0.150 x 0.104
Formula weight [g mol^{-1}]	334.34	θ range [deg]	1.378 to 25.351
Temperature [K]	100(2)	Reflections collected	57930
Wavelength [Å]	0.71073	Independent reflections	3060
Crystal system	monoclinic	R_{int} / BASF (pseudo-mero.)	0.0384 / 0.3569 TWIN -1 0 0 0 -1 0 0 0 1
Space group	$P2_1/c$	Completeness to θ_{max}	100.0 %
Unit cell dimensions	a = 8.029(2) Å	Restraints / parameters	32 / 223
	b = 14.773(3) Å	Goodness-of-fit on F^2	1.072
	c = 14.072(3) Å	$R1$ [I>2σ(I)]	0.0306
	α = 90 deg	w$R2$ (all data)	0.0868
	β = 90.03(2) deg	$g1$ / $g2$	0.0526 / 0.4560
	γ = 90 deg	max. diff. peak / hole [e Å^{-3}]	0.222 / −0.323
Volume [Å^3]	1669.1(6)	max. / min. transmission	0.7452 / 0.7119
Z	4	Absolute structure param.[169]	–
ρ_{calc} [Mg m^{-3}]	1.330	Extinction coefficient	0.0025(5)

5.1.9 Chloromethylaluminium-bis-(benzoxazol-2-yl)-methanide (10)

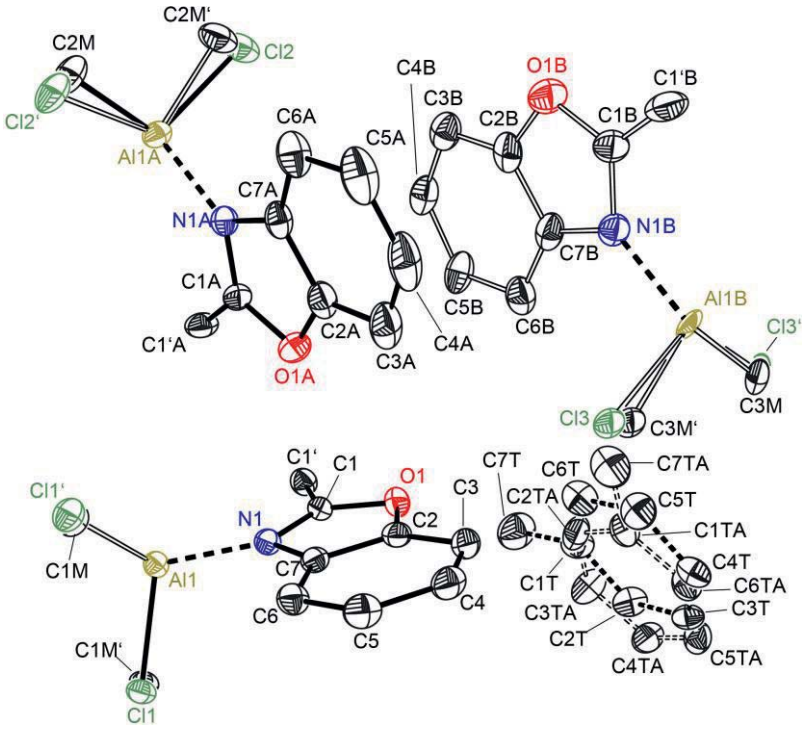

Figure 5-9: Asymmetric unit of **10** · 0.4 tol. Anisotropic displacement parameters are displayed at the 50 % probability level. Hydrogen atoms are omitted for clarity and disordered moieties (*sofs*: 0.411(2), 0402(2), 0.203(2)) are depicted in faded colour. Molecule _B and toluene are located on a special position. The remaining part of the molecules is generated by symmetry.

Table 5-9: Crystallographic information of [ClMeAl{$(NCOC_6H_4)_2CH$}] (**10**) · 0.4 tol.

CCDC no.	995114	μ [mm^{-1}]	0.287
Structure code	box2CHAlMeCl	F(000)	1880
Empirical formula	$C_{16}H_{12}AlClN_2O_2 \cdot 0.4\ C_7H_8$	Crystal size [mm^3]	0.241 x 0.192 x 0.086
Formula weight [g mol^{-1}]	363.56	θ range [deg]	1.559 to 26.368
Temperature [K]	100(2)	Reflections collected	49655
Wavelength [Å]	0.71073	Independent reflections	4564
Crystal system	monoclinic	R_{int}	0.0424
Space group	$C2/m$	Completeness to θ_{max}	99.8 %
Unit cell dimensions	a = 21.226(3) Å	Restraints / parameters	729 / 449
	b = 15.558(2) Å	Goodness-of-fit on F^2	1.118
	c = 14.163(2) Å	$R1$ [I>2σ(I)]	0.0414
	α = 90 deg	w$R2$ (all data)	0.1025
	β = 112.76(2) deg	$g1$ / $g2$	0.0262 / 10.6027
	γ = 90 deg	max. diff. peak / hole [e Å^{-3}]	0.384 / −0.230
Volume [Å^3]	4312.9(12)	max. / min. transmission	0.7454 / 0.7066
Z	10	Absolute structure param.[169]	–
ρ_{calc} [Mg m^{-3}]	1.400	Extinction coefficient	0.00031(7)

5.1.10 Chloromethylaluminium-bis-(benzothiazol-2-yl)-methanide (11)

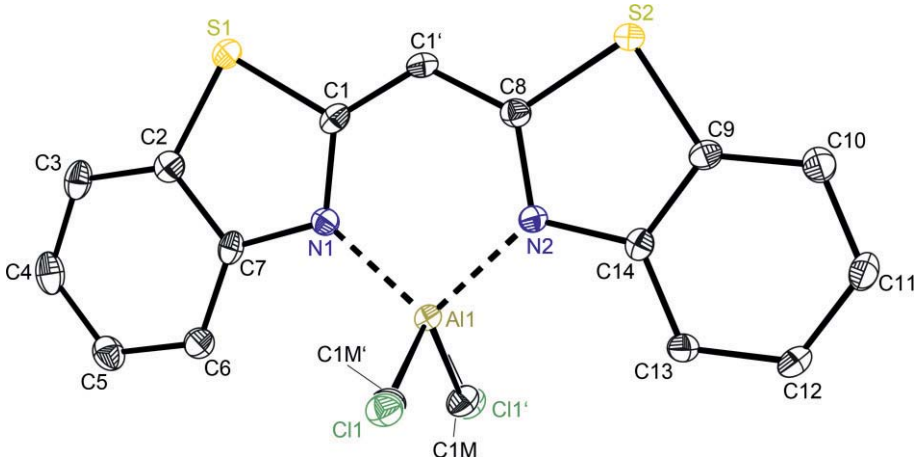

Figure 5-10: Asymmetric unit of **11**. Anisotropic displacement parameters are displayed at the 50 % probability level. Hydrogen atoms are omitted for clarity and the chloro methyl disorder (*sof*: 0.705(3)) is depicted in faded colour.

Table 5-10: Crystallographic information of [ClMeAl{$(NCSC_6H_4)_2CH$}] (**11**).

CCDC no.	995115	μ [mm^{-1}]	0.555
Structure code	bth2CHAlMeCl	F(000)	368
Empirical formula	$C_{16}H_{12}AlClN_2S_2$	Crystal size [mm^3]	0.110 x 0.110 x 0.080
Formula weight [g mol^{-1}]	358.83	θ range [deg]	1.393 to 25.376
Temperature [K]	100(2)	Reflections collected	21727
Wavelength [Å]	0.71073	Independent reflections	2882
Crystal system	triclinic	R_{int} / BASF (non-mero.)	0.0476 / 0.1174
Space group	$P\bar{1}$	Completeness to θ_{max}	99.5 %
Unit cell dimensions	a = 7.074(2) Å	Restraints / parameters	32 / 209
	b = 7.694(2) Å	Goodness-of-fit on F^2	1.054
	c = 14.664(3) Å	$R1$ [I>2σ(I)]	0.0348
	α = 89.97(2) deg	w$R2$ (all data)	0.0801
	β = 85.29(2) deg	$g1$ / $g2$	0.0326 / 0.6194
	γ = 85.89(2) deg	max. diff. peak / hole [e Å^{-3}]	0.309 / −0.340
Volume [Å^3]	793.4(3)	max. / min. transmission	0.9143 / 0.7544
Z	2	Absolute structure param.[169]	–
ρ_{calc} [Mg m^{-3}]	1.502	Extinction coefficient	–

5.1.11 Chloromethylaluminium-bis-(4-methylbenzoxazol-2-yl)-methanide (24)

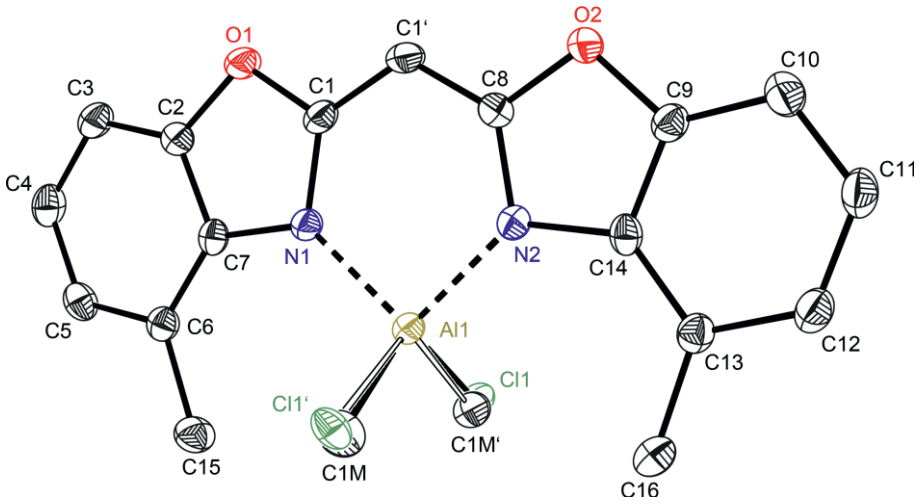

Figure 5-11: Asymmetric unit of **24**. Anisotropic displacement parameters are displayed at the 50 % probability level. Hydrogen atoms are omitted for clarity and the chloro methyl disorder (*sofs*: 0.552(11), 0.554(11), 0.452(5), 0.441(5)) is depicted in faded colour.

Table 5-11: Crystallographic information of [ClMeAl{(4-MeNCOC$_6$H$_3$)$_2$CH}] (**24**).

CCDC no.	1429341	μ [mm^{-1}]	0.153
Structure code	mbox2CHAlMeCl	F(000)	733
Empirical formula	$C_{18.1}H_{16.3}AlCl_{0.9}N_2O_2$	Crystal size [mm^3]	0.232 x 0.107 x 0.074
Formula weight [g mol^{-1}]	352.59	θ range [deg]	1.591 to 19.579
Temperature [K]	100(2)	Reflections collected	20579
Wavelength [Å]	0.56086	Independent reflections	2904
Crystal system	monoclinic	R_{int}	0.0370
Space group	$P2_1/c$	Completeness to θ_{max}	98.4 %
Unit cell dimensions	a = 7.982(2) Å	Restraints / parameters	290 / 243
	b = 14.727(3) Å	Goodness-of-fit on F^2	1.066
	c = 13.890(3) Å	R1 [I>2σ(I)]	0.0322
	α = 90 deg	wR2 (all data)	0.0885
	β = 91.73(2) deg	g1 / g2	0.0480 / 0.4255
	γ = 90 deg	max. diff. peak / hole [e Å^{-3}]	0.206 / −0.314
Volume [Å^3]	1632.0(6)	max. / min. transmission	0.7444 / 0.7112
Z	4	Absolute structure param.[169]	–
ρ_{calc} [Mg m^{-3}]	1.435	Extinction coefficient	–

5.1.12 Dimethylgallium-bis-(benzoxazol-2-yl)-methanide (13)

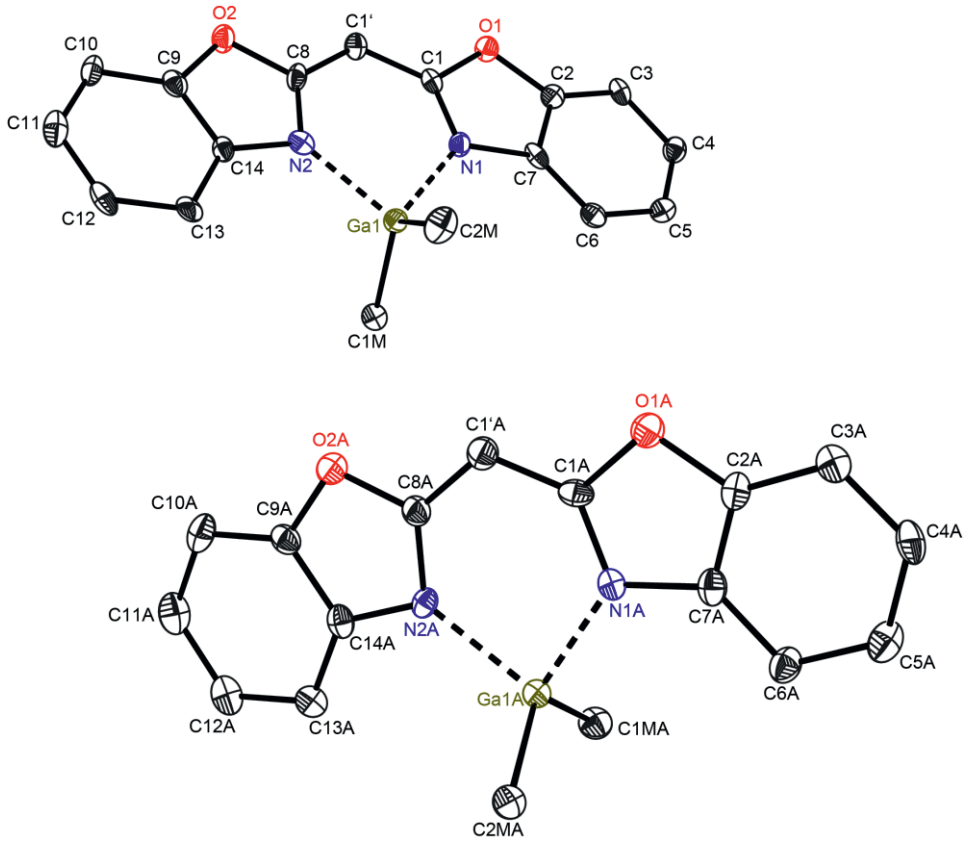

Figure 5-12: Asymmetric unit of **13**. Anisotropic displacement parameters are displayed at the 50 % probability level. Hydrogen atoms are omitted for clarity.

Table 5-12: Crystallographic information of $[Me_2Ga\{(NCOC_6H_4)_2CH\}]$ (**13**).

CCDC no.	995116	μ [mm^{-1}]	1.792
Structure code	box2CHGaMe2	F(000)	712
Empirical formula	$C_{17}H_{15}GaN_2O_2$	Crystal size [mm^3]	0.089 x 0.073 x 0.070
Formula weight [g mol^{-1}]	349.03	θ range [deg]	1.460 to 28.321
Temperature [K]	100(2)	Reflections collected	46102
Wavelength [Å]	0.71073	Independent reflections	7674
Crystal system	monoclinic	R_{int} / BASF (pseudo-mero.)	0.0451 / 0.45355 TWIN -1 0 0 0 -1 0 1 0 1
Space group	$P2_1$	Completeness to θ_{max}	99.9 %
Unit cell dimensions	a = 8.386(2) Å	Restraints / parameters	176 / 402
	b = 13.944(3) Å	Goodness-of-fit on F^2	1.026
	c = 13.838(3) Å	$R1$ [I>2σ(I)]	0.0339
	α = 90 deg	w$R2$ (all data)	0.0790
	β = 107.60(2) deg	$g1$ / $g2$	0.0369 / 2.0037
	γ = 90 deg	max. diff. peak / hole [e Å^{-3}]	1.298 / −0.517
Volume [Å^3]	1542.4(6)	max. / min. transmission	0.7457 / 0.7031
Z	4	Absolute structure param.[169]	−0.551(6)
ρ_{calc} [Mg m^{-3}]	1.503	Extinction coefficient	–

5.1.13 Dimethylgallium-bis-(benzothiazol-2-yl)-methanide (14)

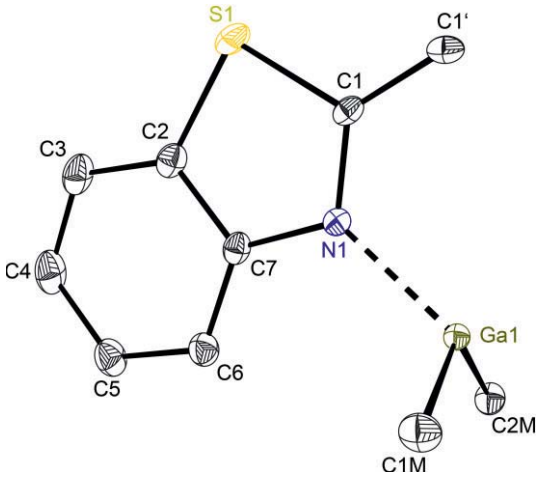

Figure 5-13: Asymmetric unit of **14**. Anisotropic displacement parameters are displayed at the 50 % probability level. Hydrogen atoms are omitted for clarity. The remaining part of the molecule is generated by symmetry.

Table 5-13: Crystallographic information of $[Me_2Ga\{(NCSC_6H_4)_2CH\}]$ (**14**).

CCDC no.	995117	μ [mm^{-1}]	1.023
Structure code	bth2CHGaMe2	F(000)	776
Empirical formula	$C_{17}H_{15}GaN_2S_2$	Crystal size [mm^3]	0.420 x 0.266 x 0.260
Formula weight [g mol^{-1}]	381.15	θ range [deg]	2.081 to 23.681
Temperature [K]	100(2)	Reflections collected	40129
Wavelength [Å]	0.56086	Independent reflections	2580
Crystal system	orthorhombic	R_{int}	0.0338
Space group	*Pnma*	Completeness to θ_{max}	99.9 %
Unit cell dimensions	a = 15.446(3) Å	Restraints / parameters	1 / 108
	b = 15.177(3) Å	Goodness-of-fit on F^2	1.267
	c = 6.929(2) Å	$R1$ [I>2σ(I)]	0.0251
	α = 90 deg	w$R2$ (all data)	0.0602
	β = 90 deg	$g1$ / $g2$	0.0070 / 2.2382
	γ = 90 deg	max. diff. peak / hole [e Å^{-3}]	0.491 / −0.518
Volume [Å^3]	1624.3(6)	max. / min. transmission	0.7449 / 0.6769
Z	4	Absolute structure param.[169]	–
ρ_{calc} [Mg m^{-3}]	1.559	Extinction coefficient	–

5.1.14 Dimethylgallium-bis-(4-methylbenzoxazol-2-yl)-methanide (22)

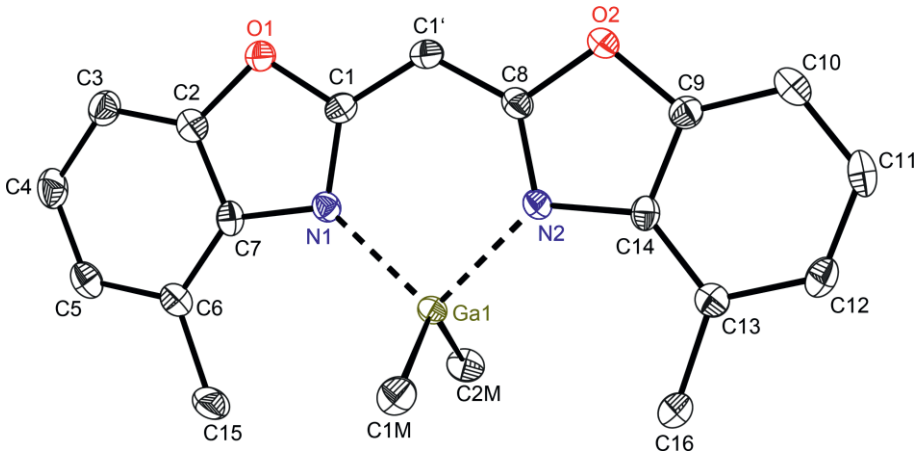

Figure 5-14: Asymmetric unit of **22**. Anisotropic displacement parameters are displayed at the 50 % probability level. Hydrogen atoms are omitted for clarity.

Table 5-14: Crystallographic information of $[Me_2Ga\{(4\text{-}MeNCOC_6H_3)_2CH\}]$ (**22**).

CCDC no.	1429403	μ [mm^{-1}]	0.879
Structure code	mbox2CHGaMe2	F(000)	776
Empirical formula	$C_{19}H_{19}GaN_2O_2$	Crystal size [mm^3]	0.142 x 0.098 x 0.065
Formula weight [g mol^{-1}]	377.08	θ range [deg]	1.572 to 19.770
Temperature [K]	100(2)	Reflections collected	45271
Wavelength [Å]	0.56086	Independent reflections	3069
Crystal system	monoclinic	R_{int}	0.0445
Space group	$P2_1/c$	Completeness to θ_{max}	99.9 %
Unit cell dimensions	a = 7.986(2) Å	Restraints / parameters	0 / 221
	b = 14.852(3) Å	Goodness-of-fit on F^2	1.049
	c = 14.087(3) Å	$R1$ [I>2σ(I)]	0.0248
	α = 90 deg	w$R2$ (all data)	0.0672
	β = 90.18(2) deg	$g1$ / $g2$	0.0353 / 1.1047
	γ = 90 deg	max. diff. peak / hole [e Å^{-3}]	0.386 / −0.372
Volume [Å^3]	1670.81(9)	max. / min. transmission	0.7444 / 0.7051
Z	4	Absolute structure param.[169]	–
ρ_{calc} [Mg m^{-3}]	1.499	Extinction coefficient	–

5.1.15 Dimethylindium-bis-(4-methylbenzoxazol-2-yl)-methanide (23)

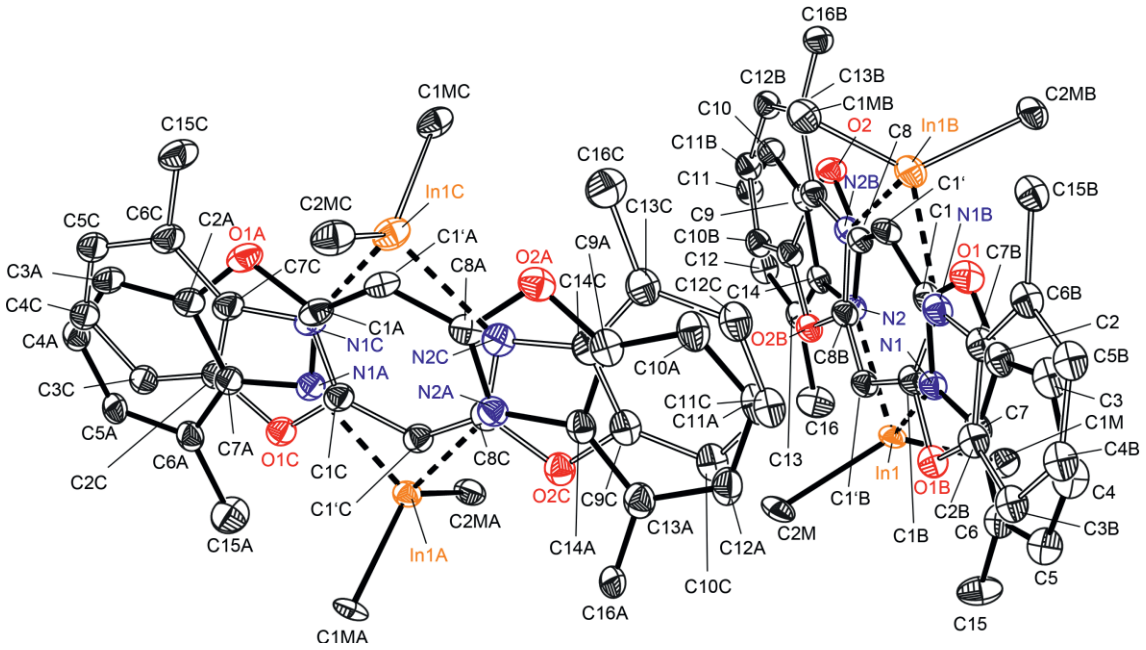

Figure 5-15: Asymmetric unit of **23**. Anisotropic displacement parameters are displayed at the 50 % probability level. Hydrogen atoms are omitted for clarity reasons and disordered moieties (*sofs*: 0.971(3), 0.938(3)) are depicted in faded colour.

Table 5-15: Crystallographic information of $[Me_2In\{(4\text{-}MeNCOC_6H_3)_2CH\}]$ (**23**).

CCDC no.	1429339	μ [mm^{-1}]	0.741
Structure code	mbox2CHInMe2	F(000)	848
Empirical formula	$C_{19}H_{19}InN_2O_2$	Crystal size [mm^3]	0.109 x 0.104 x 0.081
Formula weight [g mol^{-1}]	422.18	θ range [deg]	1.154 to 21.987
Temperature [K]	106(2)	Reflections collected	49033
Wavelength [Å]	0.56086	Independent reflections	8534
Crystal system	monoclinic	R_{int} / BASF (pseudo-mero.)	0.0481 / 0.4558 TWIN 0 0 1 0 -1 0 1 0 0
Space group	*Pn*	Completeness to θ_{max}	100.0 %
Unit cell dimensions	a = 15.629(3) Å	Restraints / parameters	3149 / 744
	b = 7.894(2) Å	Goodness-of-fit on F^2	1.030
	c = 15.631(3) Å	R1 [I>2σ(I)]	0.0248
	α = 90 deg	wR2 (all data)	0.0546
	β = 117.04(2) deg	g1 / g2	0.0261 / 0.1318
	γ = 90 deg	max. diff. peak / hole [e Å^{-3}]	0.334 / −0.463
Volume [Å^3]	1717.7(7)	max. / min. transmission	0.7447 / 0.6620
Z	4	Absolute structure param.[169]	–
ρ_{calc} [Mg m^{-3}]	1.633	Extinction coefficient	–

5.1.16 Benzothiazol-2-yl-benzoxazol-2'-yl-methane (32)

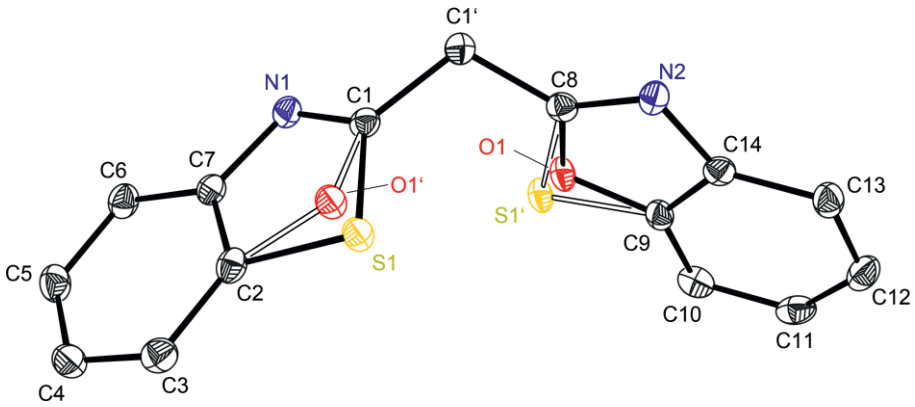

Figure 5-16: Asymmetric unit of **32**. Anisotropic displacement parameters are displayed at the 50 % probability level. Hydrogen atoms are omitted for clarity and disordered moieties (*sof*: 0.946(2)) are depicted in faded colour.

Table 5-16: Crystallographic information of $(NCSC_6H_4)CH_2(NCOC_6H_4)$ (**32**).

CCDC no.	–	μ [mm^{-1}]	0.258
Structure code	bthCH2box	F(000)	276
Empirical formula	$C_{15}H_{10}N_2OS$	Crystal size [mm^3]	0.132 x 0.105 x 0.097
Formula weight [g mol^{-1}]	266.31	θ range [deg]	1.926 to 26.730
Temperature [K]	100(2)	Reflections collected	20040
Wavelength [Å]	0.71073	Independent reflections	2588
Crystal system	triclinic	R_{int}	0.0221
Space group	$P\bar{1}$	Completeness to θ_{max}	99.7 %
Unit cell dimensions	a = 5.908(2) Å	Restraints / parameters	227 / 179
	b = 9.841(2) Å	Goodness-of-fit on F^2	1.032
	c = 10.682(3) Å	$R1$ [I>2σ(I)]	0.0297
	α = 81.96(2) deg	w$R2$ (all data)	0.0755
	β = 87.52(3) deg	$g1$ / $g2$	0.0312 / 0.4370
	γ = 81.07(2) deg	max. diff. peak / hole [e Å^{-3}]	0.348 / −0.342
Volume [Å^3]	607.4(3)	max. / min. transmission	0.7454 / 0.7219
Z	2	Absolute structure param.[169]	–
ρ_{calc} [Mg m^{-3}]	1.456	Extinction coefficient	–

5.1.17 2-(Benzothiazol-2-yl)-*N*-(2'-hydroxyphenyl)-acetamide (33)

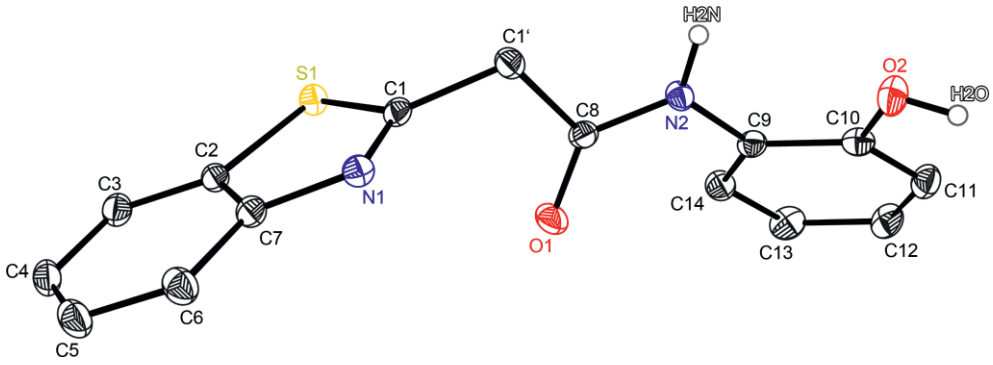

Figure 5-17: Asymmetric unit of **33**. Anisotropic displacement parameters are displayed at the 50 % probability level. Hydrogen atoms are omitted for clarity except the freely refined ones.

Table 5-17: Crystallographic information of 2-(benzothiazol-2'-yl)-*N*-(2''-hydroxyphenyl)-acetamide (**33**).

CCDC no.	–	μ [mm^{-1}]	0.250
Structure code	bthCH2boxFraktion2	F(000)	592
Empirical formula	$C_{15}H_{12}N_2O_2S$	Crystal size [mm^3]	0.190 x 0.148 x 0.082
Formula weight [g mol^{-1}]	284.33	θ range [deg]	1.843 to 27.104
Temperature [K]	100(2)	Reflections collected	16106
Wavelength [Å]	0.71073	Independent reflections	2850
Crystal system	orthorhombic	R_{int}	0.0318
Space group	$Pna2_1$	Completeness to θ_{max}	99.8 %
Unit cell dimensions	a = 22.105(4) Å	Restraints / parameters	1 / 190
	b = 4.696(2) Å	Goodness-of-fit on F^2	1.034
	c = 12.590(3) Å	$R1$ [I>2σ(I)]	0.0254
	α = 90 deg	w$R2$ (all data)	0.0651
	β = 90 deg	$g1$ / $g2$	0.0341 / 0.3624
	γ = 90 deg	max. diff. peak / hole [e Å^{-3}]	0.275 / −0.176
Volume [Å^3]	1306.9(7)	max. / min. transmission	0.7455 / 0.7203
Z	4	Absolute structure param.[169]	0.04(3)
ρ_{calc} [Mg m^{-3}]	1.445	Extinction coefficient	–

5.1.18 Benzothiazol-2-yl-*N*-methylbenzimidazol-2'-yl-methane (34)

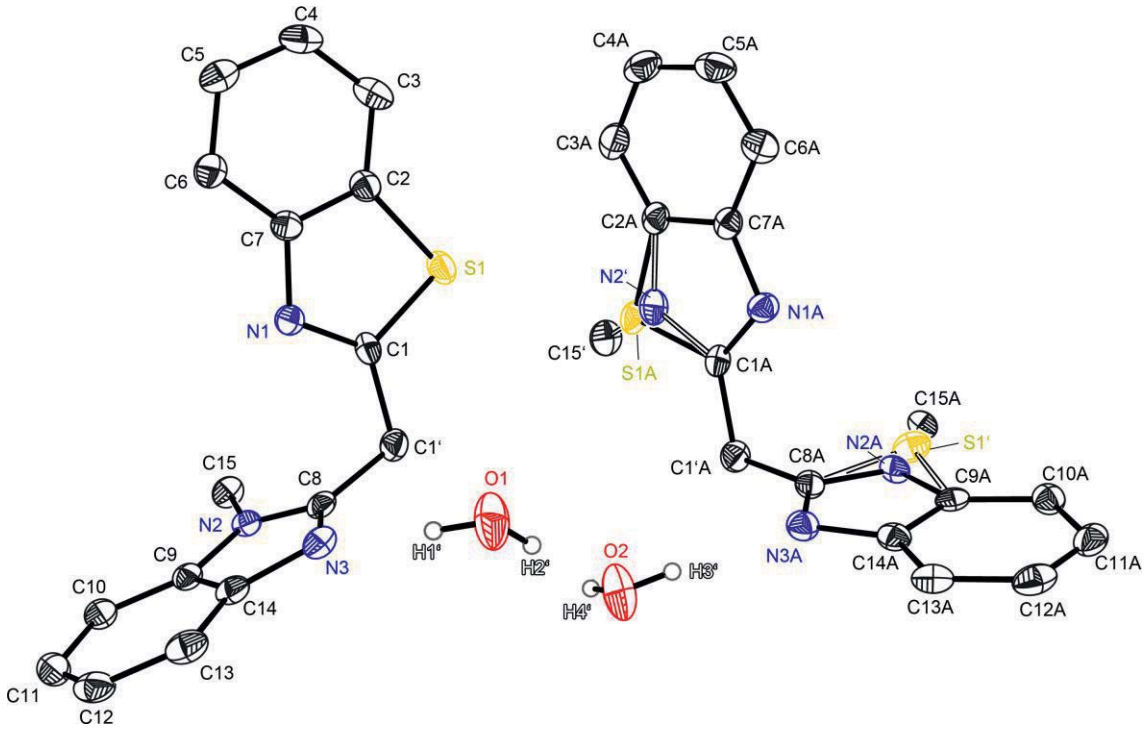

Figure 5-18: Asymmetric unit of **34** · H_2O. Anisotropic displacement parameters are displayed at the 50 % probability level. Hydrogen atoms are omitted for clarity and disordered moieties (*sof*: 0.942(3)) are depicted in faded colour.

Table 5-18: Crystallographic information of $(NCSC_6H_4)CH_2(1\text{-}MeNCNC_6H_4)$ (**34**) · H_2O.

CCDC no.	–	μ [mm^{-1}]	0.226
Structure code	bthCH2mbim	F(000)	624
Empirical formula	$C_{16}H_{13}N_3S$	Crystal size [mm^3]	0.219 x 0.189 x 0.072
Formula weight [g mol^{-1}]	297.37	θ range [deg]	1.426 to 26.717
Temperature [K]	100(2)	Reflections collected	24144
Wavelength [Å]	0.71073	Independent reflections	6106
Crystal system	monoclinic	R_{int}	0.0294
Space group	$P2_1$	Completeness to θ_{max}	99.9 %
Unit cell dimensions	a = 4.790(2) Å	Restraints / parameters	584 / 426
	b = 28.552(4) Å	Goodness-of-fit on F^2	1.032
	c = 10.749(3) Å	$R1$ [I>2σ(I)]	0.0305
	α = 90 deg	w$R2$ (all data)	0.0723
	β = 99.92(2) deg	$g1$ / $g2$	0.0333 / 0.3589
	γ = 90 deg	max. diff. peak / hole [e Å^{-3}]	0.242 / −0.226
Volume [Å^3]	1448.1(8)	max. / min. transmission	0.7454 / 0.7011
Z	4	Absolute structure param.[169]	0.209(69)
ρ_{calc} [Mg m^{-3}]	1.364	Extinction coefficient	–

5.1.19 Dimethylaluminium-benzothiazol-2-yl-benzoxazol-2'-yl-methanide (35)

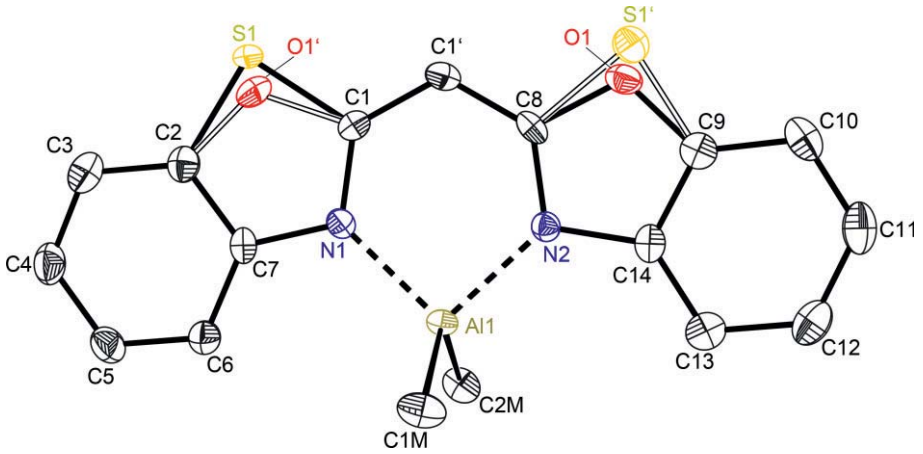

Figure 5-19: Asymmetric unit of **35**. Anisotropic displacement parameters are displayed at the 50 % probability level. Hydrogen atoms are omitted for clarity reasons and disordered moieties (*sof*: 0.842(1)) are depicted in faded colour.

Table 5-19: Crystallographic information of $[Me_2Al\{(NCSC_6H_4)CH(NCOC_6H_4)\}]$ (**35**).

CCDC no.	–	μ [mm^{-1}]	0.263
Structure code	bthCHboxAlMe2	F(000)	672
Empirical formula	$C_{17}H_{15}AlN_2OS$	Crystal size [mm^3]	0.230 x 0.120 x 0.050
Formula weight [g mol^{-1}]	322.35	θ range [deg]	1.398 to 25.364
Temperature [K]	101(2)	Reflections collected	31166
Wavelength [Å]	0.71073	Independent reflections	2916
Crystal system	monoclinic	R_{int} / BASF (non-mero.)	0.0543 / 0.3514
Space group	$P2_1/c$	Completeness to θ_{max}	100.0 %
Unit cell dimensions	a = 14.594(3) Å	Restraints / parameters	287 / 221
	b = 7.086(2) Å	Goodness-of-fit on F^2	1.149
	c = 15.288(3) Å	R1 [I>2σ(I)]	0.0396
	α = 90 deg	wR2 (all data)	0.1039
	β = 93.35(2) deg	g1 / g2	0.0434 / 1.1317
	γ = 90 deg	max. diff. peak / hole [e Å^{-3}]	0.343 / −0.286
Volume [Å^3]	1578.3(6)	max. / min. transmission	0.7452 / 0.6415
Z	4	Absolute structure param.[169]	–
ρ_{calc} [Mg m^{-3}]	1.357	Extinction coefficient	–

5.1.20 Dimethylaluminium-benzothiazol-2-yl-*N*-methylbenz-imidazol-2'-yl-methanide (36)

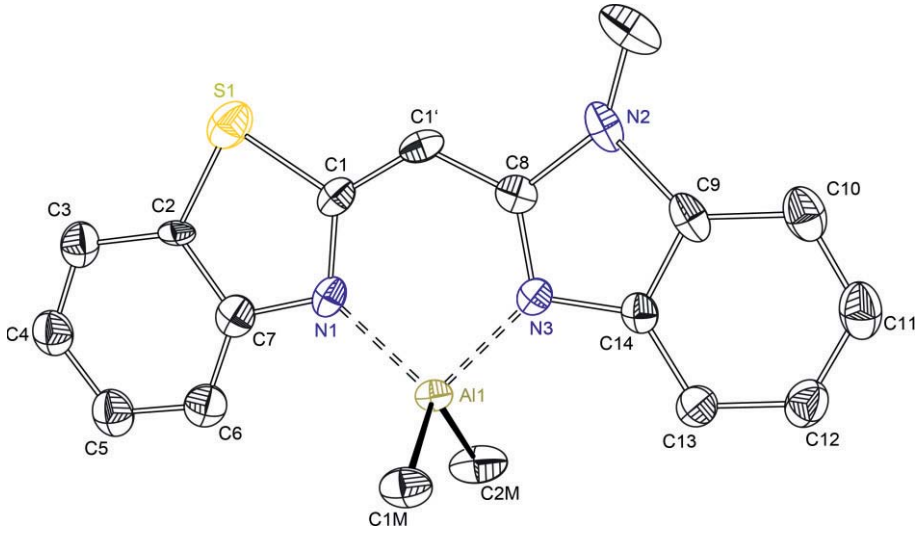

Figure 5-20: Asymmetric unit of **36**. Anisotropic displacement parameters are displayed at the 50 % probability level. Hydrogen atoms are omitted for clarity reasons and the disordered ligand framework (on special position) is depicted in faded colour.

Table 5-20: Crystallographic information of $[Me_2Al\{(NCSC_6H_4)CH(1\text{-}MeNCNC_6H_4)\}]$ (**36**).

CCDC no.	–	μ [mm^{-1}]	0.251
Structure code	bthCHmbimAlMe2	F(000)	352
Empirical formula	$C_{18}H_{18}AlN_3S$	Crystal size [mm^3]	0.146 x 0.120 x 0.077
Formula weight [g mol^{-1}]	335.39	θ range [deg]	2.647 to 28.688
Temperature [K]	100(2)	Reflections collected	9160
Wavelength [Å]	0.71073	Independent reflections	2210
Crystal system	monoclinic	R_{int}	0.0310
Space group	$P2_1/m$	Completeness to θ_{max}	99.6 %
Unit cell dimensions	a = 7.230(3) Å	Restraints / parameters	398 / 201
	b = 14.864(4) Å	Goodness-of-fit on F^2	1.075
	c = 8.340(3) Å	$R1$ [I>2σ(I)]	0.0705
	α = 90 deg	w$R2$ (all data)	0.2025
	β = 112.67(2) deg	$g1$ / $g2$	0.0894 / 1.4166
	γ = 90 deg	max. diff. peak / hole [e Å^{-3}]	0.782 / −0.948
Volume [Å^3]	827.0(5)	max. / min. transmission	0.7458 / 0.6993
Z	2	Absolute structure param.[169]	–
ρ_{calc} [Mg m^{-3}]	1.347	Extinction coefficient	–

5.1.21 Dimethylgallium-benzothiazol-2-yl-benzoxazol-2'-yl-methanide (37)

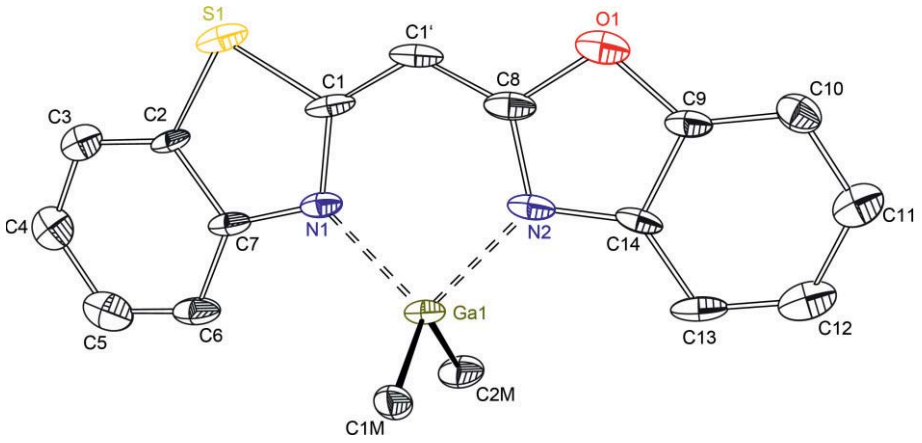

Figure 5-21: Asymmetric unit of **37**. Anisotropic displacement parameters are displayed at the 50 % probability level. Hydrogen atoms are omitted for clarity reasons and the disordered ligand framework (on special position) is depicted in faded colour.

Table 5-21: Crystallographic information of $[Me_2Ga\{(NCSC_6H_4)CH(NCOC_6H_4)\}]$ (**37**).

CCDC no.	–	μ [mm^{-1}]	1.002
Structure code	bthCHboxGaMe2	F(000)	744
Empirical formula	$C_{17}H_{15}AlN_2OS$	Crystal size [mm^3]	0.350 x 0.279 x 0.236
Formula weight [g mol^{-1}]	365.09	θ range [deg]	1.708 to 23.637
Temperature [K]	100(2)	Reflections collected	37294
Wavelength [Å]	0.56086	Independent reflections	2464
Crystal system	orthorhombic	R_{int}	0.0346
Space group	*Pnma*	Completeness to θ_{max}	100.0 %
Unit cell dimensions	a = 8.262(2) Å	Restraints / parameters	382 / 192
	b = 16.440(4) Å	Goodness-of-fit on F^2	1.526
	c = 11.473(3) Å	$R1$ [I>2σ(I)]	0.0494
	α = 90 deg	w$R2$ (all data)	0.1143
	β = 90 deg	$g1$ / $g2$	0.0000 / 4.6698
	γ = 90 deg	max. diff. peak / hole [e Å^{-3}]	0.751 / −0.884
Volume [Å^3]	1558.3(7)	max. / min. transmission	0.7449 / 0.6547
Z	4	Absolute structure param.[169]	–
ρ_{calc} [Mg m^{-3}]	1.556	Extinction coefficient	–

5.1.22 Lithium-benzothiazol-2-yl-*N*-methylbenzimidazol-2'-yl-methanide (39)

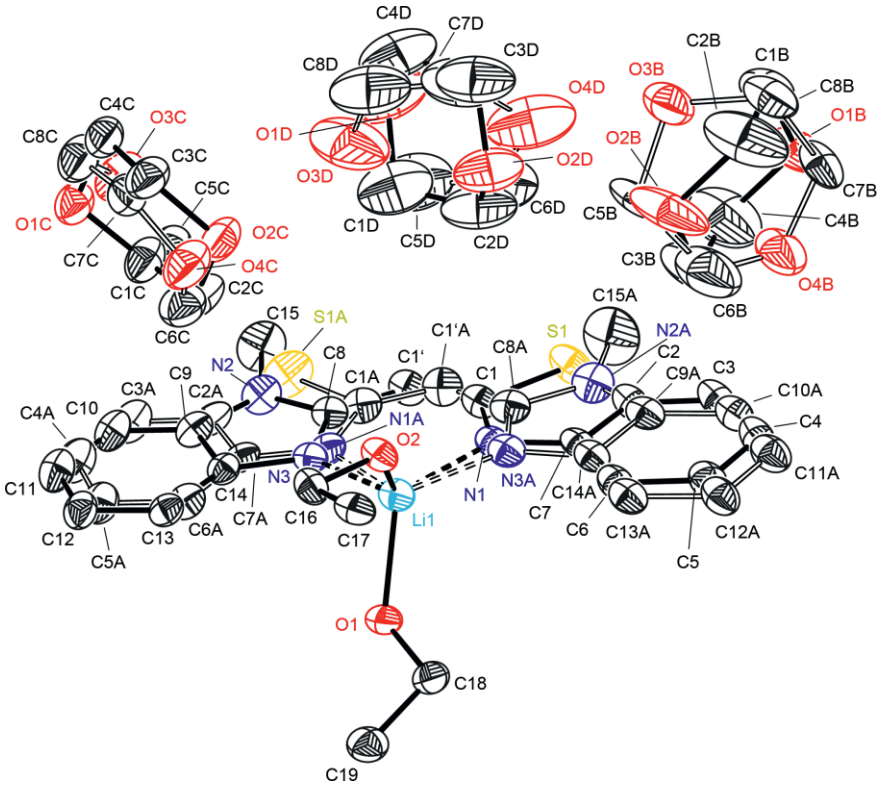

Figure 5-22: Asymmetric unit of **39** · 3 diox. Anisotropic displacement parameters are displayed at the 50 % probability level. Hydrogen atoms are omitted for clarity reasons and disordered moieties (*sofs*: 0.758(4), 0.779(13), 0.541(8), 0.694(7)) are depicted in faded colour.

Table 5-22: Crystallographic information of $[(diox)_2Li\{(NCSC_6H_4)CH(1\text{-}MeNCNC_6H_4)\}]$ (**39**) · 3 diox.

CCDC no.	–	μ [mm^{-1}]	0.153
Structure code	bthCHmbimLidiox2	F(000)	1360
Empirical formula	$C_{32}H_{44}LiN_3O_8S$	Crystal size [mm^3]	0.200 x 0.050 x 0.050
Formula weight [g mol^{-1}]	637.70	θ range [deg]	1.544 to 27.548
Temperature [K]	100(2)	Reflections collected	51453
Wavelength [Å]	0.71073	Independent reflections	7527
Crystal system	monoclinic	R_{int}	0.0583
Space group	$P2_1/c$	Completeness to θ_{max}	100.0 %
Unit cell dimensions	a = 9.609(2) Å	Restraints / parameters	2373 / 756
	b = 12.915(3) Å	Goodness-of-fit on F^2	1.061
	c = 26.515(4) Å	$R1$ [I>2σ(I)]	0.0962
	α = 90 deg	w$R2$ (all data)	0.2306
	β = 95.94(3) deg	$g1$ / $g2$	0.0557 / 9.7167
	γ = 90 deg	max. diff. peak / hole [e Å^{-3}]	0.890 / −0.541
Volume [Å^3]	3272.8(11)	max. / min. transmission	0.7456 / 0.6828
Z	4	Absolute structure param.[169]	–
ρ_{calc} [Mg m^{-3}]	1.294	Extinction coefficient	0.0027(6)

5.1.23 Iodomethylaluminium-bis-(4-methylbenzoxazol-2-yl)-methanide (25)

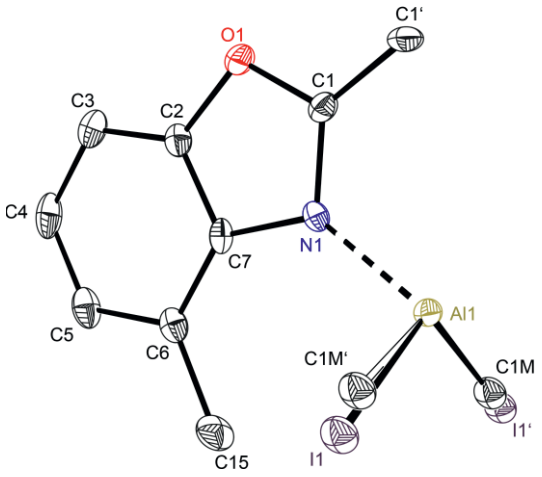

Figure 5-23: Asymmetric unit of **25**. Anisotropic displacement parameters are displayed at the 50 % probability level. Hydrogen atoms are omitted for clarity reasons and disordered moieties (*sof*: 0.514(1)) are depicted in faded colour. The remaining part of the molecule is generated by symmetry.

Table 5-23: Crystallographic information of [IMeAl{(4-MeNCOC$_6$H$_3$)$_2$CH}] (**25**).

CCDC no.	1429342	μ [mm^{-1}]	1.019
Structure code	mbox2CHAlMeI	F(000)	880
Empirical formula	$C_{18}H_{16}AlIN_2O_2$	Crystal size [mm^3]	0.159 x 0.108 x 0.069
Formula weight [g mol^{-1}]	446.21	θ range [deg]	2.005 to 20.793
Temperature [K]	100(2)	Reflections collected	25400
Wavelength [Å]	0.56086	Independent reflections	1915
Crystal system	orthorhombic	R_{int}	0.0431
Space group	*Pbcm*	Completeness to θ_{max}	100.0 %
Unit cell dimensions	a = 8.015(2) Å	Restraints / parameters	5 / 118
	b = 13.868(2) Å	Goodness-of-fit on F^2	1.081
	c = 15.566(3) Å	R1 [I>2σ(I)]	0.0222
	α = 90 deg	wR2 (all data)	0.0542
	β = 90 deg	g1 / g2	0.0241 / 2.0659
	γ = 90 deg	max. diff. peak / hole [e Å^{-3}]	0.502 / −0.894
Volume [Å^3]	1730.2(6)	max. / min. transmission	0.7445 / 0.6987
Z	4	Absolute structure param.[169]	–
ρ_{calc} [Mg m^{-3}]	1.713	Extinction coefficient	–

5.1.24 Iodoethylaluminium-bis-(4-methylbenzoxazol-2-yl)-methanide (26)

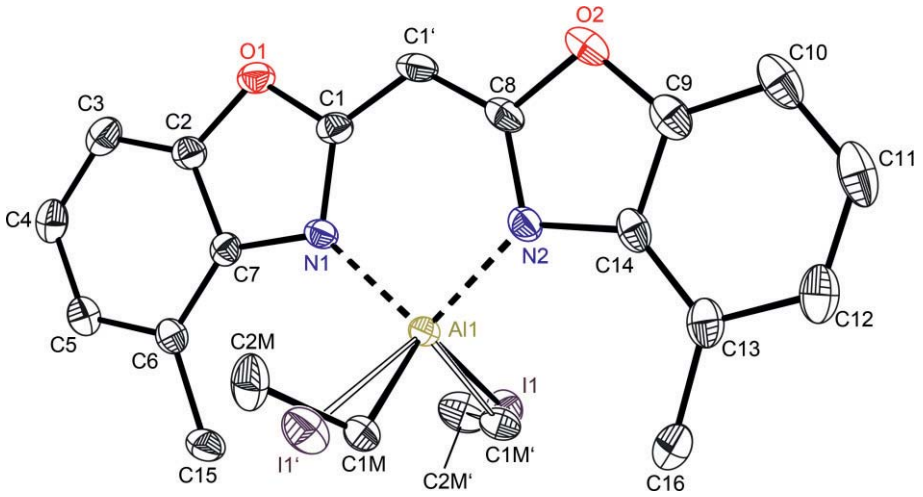

Figure 5-24: Asymmetric unit of **26**. Anisotropic displacement parameters are displayed at the 50 % probability level. Hydrogen atoms are omitted for clarity reasons and disordered moieties (*sof*: 0.923(1)) are depicted in faded colour.

Table 5-24: Crystallographic information of [IEtAl{(4-MeNCOC$_6$H$_3$)$_2$CH}] (**26**).

CCDC no.	1429343	μ [mm^{-1}]	1.796
Structure code	mbox2CHAlEtI	F(000)	912
Empirical formula	$C_{19}H_{18}AlIN_2O_2$	Crystal size [mm^3]	0.152 x 0.096 x 0.090
Formula weight [g mol^{-1}]	460.23	θ range [deg]	1.535 to 27.884
Temperature [K]	100(2)	Reflections collected	38660
Wavelength [Å]	0.71073	Independent reflections	4398
Crystal system	monoclinic	R_{int}	0.0231
Space group	$P2_1/c$	Completeness to θ_{max}	99.9 %
Unit cell dimensions	a = 9.102(3) Å	Restraints / parameters	349 / 257
	b = 7.647(2) Å	Goodness-of-fit on F^2	1.065
	c = 26.711(4) Å	$R1$ [I>2σ(I)]	0.0210
	α = 90 deg	w$R2$ (all data)	0.0534
	β = 96.59(2) deg	$g1$ / $g2$	0.0255 / 1.2530
	γ = 90 deg	max. diff. peak / hole [e Å^{-3}]	0.730 / −0.406
Volume [Å^3]	1846.9(8)	max. / min. transmission	0.7456 / 0.6996
Z	4	Absolute structure param.[169]	–
ρ_{calc} [Mg m^{-3}]	1.655	Extinction coefficient	–

5.1.25 μ-Hydroxido-di-(ethylaluminium-bis-(4-methylbenzoxazol-2-yl)-methanide) iodide (29)

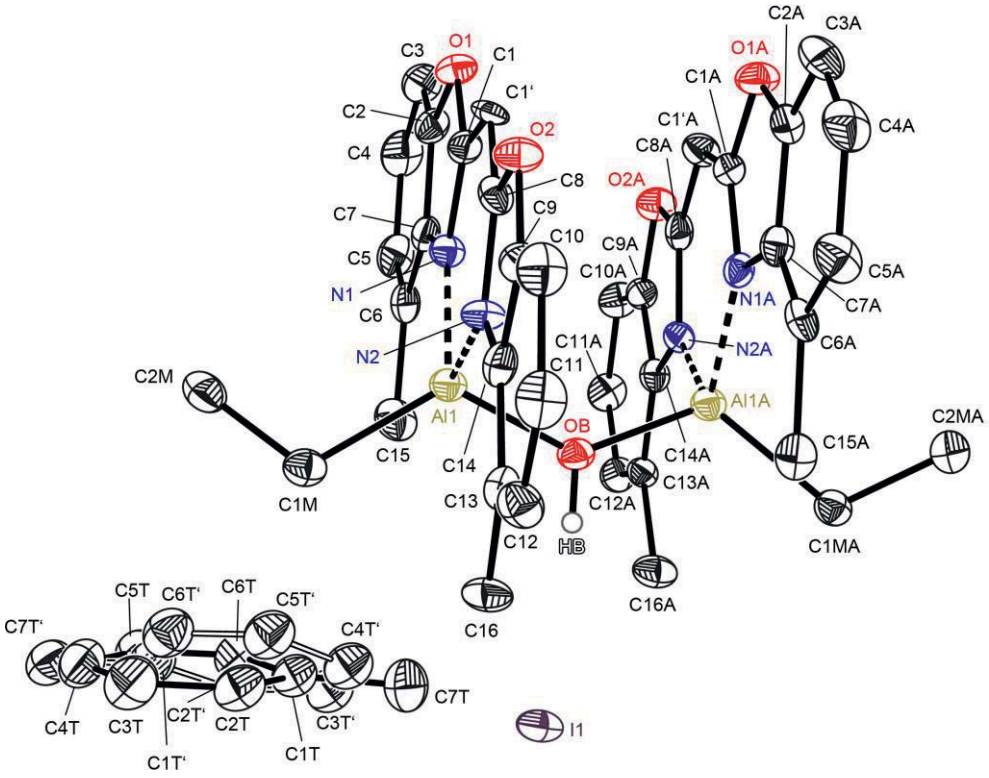

Figure 5-25: Asymmetric unit of **29** · 1 tol. Anisotropic displacement parameters are displayed at the 50 % probability level. Hydrogen atoms are omitted for clarity reasons and disordered moieties (*sof*: 0.965(5)) are depicted in faded colour.

Table 5-25: Crystallographic information of [(μ-OH){EtAl((4-MeNCOC$_6$H$_3$)$_2$CH)}$_2$]I (**29**) · 1 tol.

CCDC no.	–	μ [mm^{-1}]	0.869
Structure code	(mbox2CHAlEt)2OHI	F(000)	1848
Empirical formula	$C_{38}H_{37}Al_2IN_4O_5 \cdot C_7H_8$	Crystal size [mm^3]	0.116 x 0.048 x 0.038
Formula weight [g mol^{-1}]	902.71	θ range [deg]	1.256 to 25.418
Temperature [K]	100(2)	Reflections collected	73523
Wavelength [Å]	0.71073	Independent reflections	7596
Crystal system	monoclinic	R_{int} / BASF (pseudo-mero.)	0.0886 / 0.4217 TWIN -1 0 0 0 -1 0 0 0 1
Space group	$P2_1/c$	Completeness to θ_{max}	100.0 %
Unit cell dimensions	a = 16.213(3) Å	Restraints / parameters	889 / 591
	b = 11.368(2) Å	Goodness-of-fit on F^2	0.918
	c = 22.415(4) Å	$R1$ [I>2σ(I)]	0.0376
	α = 90 deg	w$R2$ (all data)	0.0615
	β = 90.14(2) deg	$g1$ / $g2$	0.0162 / 0.0000
	γ = 90 deg	max. diff. peak / hole [e Å^{-3}]	0.710 / −0.604
Volume [Å^3]	4131.3(13)	max. / min. transmission	0.7452 / 0.6412
Z	4	Absolute structure param.[169]	–
ρ_{calc} [Mg m^{-3}]	1.451	Extinction coefficient	–

5.1.26 (*Z*)-2-(4'-methylbenzoxazol-2'-(3'*H*)-ylidene)-4-methyl-benzoxazolium triiodide (27)

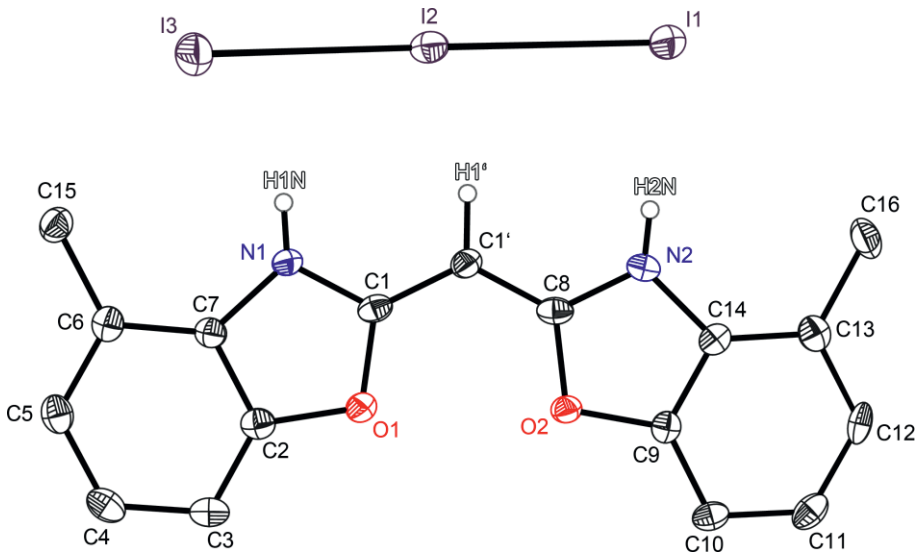

Figure 5-26: Asymmetric unit of **27**. Anisotropic displacement parameters are displayed at the 50 % probability level. Hydrogen atoms are omitted for clarity except the freely refined ones and H1'.

Table 5-26: Crystallographic information of $[(4\text{-MeNHCOC}_6H_3)_2CH]I_3$ (**27**).

CCDC no.	–	μ [mm^{-1}]	4.721
Structure code	mf21_mbox2CH3I3	F(000)	612
Empirical formula	$C_{17}H_{15}I_3N_2O_2$	Crystal size [mm^3]	0.120 x 0.079 x 0.057
Formula weight [g mol^{-1}]	660.01	θ range [deg]	1.827 to 27.273
Temperature [K]	100(2)	Reflections collected	11911
Wavelength [Å]	0.71073	Independent reflections	4451
Crystal system	triclinic	R_{int}	0.0213
Space group	$P\bar{1}$	Completeness to θ_{max}	100.0%
Unit cell dimensions	a = 8.506(2) Å	Restraints / parameters	0 / 227
	b = 11.098(3) Å	Goodness-of-fit on F^2	1.038
	c = 11.972(3) Å	$R1$ [I>2σ(I)]	0.0258
	α = 69.04(2) deg	w$R2$ (all data)	0.0609
	β = 87.41(3) deg	$g1$ / $g2$	0.0249 / 1.3790
	γ = 71.13(2) deg	max. diff. peak / hole [e Å^{-3}]	1.849 / −0.590
Volume [Å^3]	995.5(5)	max. / min. transmission	0.4302 / 0.3653
Z	2	Absolute structure param.[169]	–
ρ_{calc} [Mg m^{-3}]	2.202	Extinction coefficient	–

5.1.27 1,1,2,2-Tetrakis-(4'-methylbenzoxazol-2'-yl)-ethane (28)

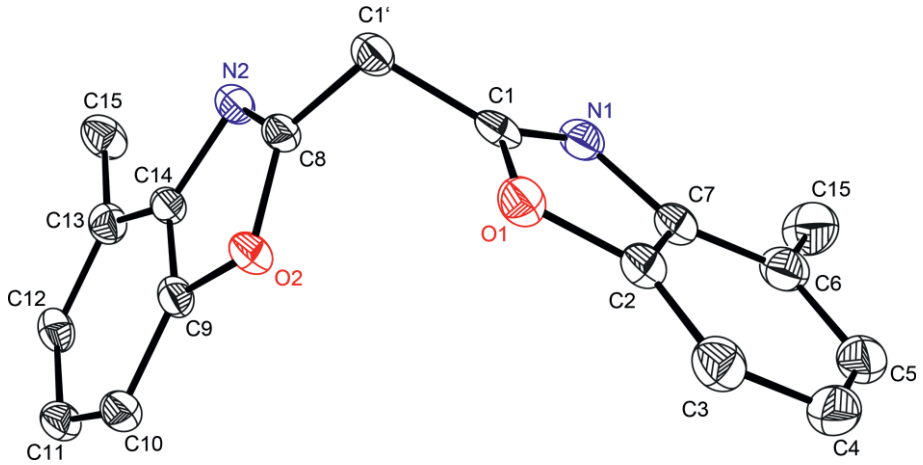

Figure 5-27: Asymmetric unit of **28**. Anisotropic displacement parameters are displayed at the 50 % probability level. Hydrogen atoms are omitted for clarity reasons. The remaining part of the molecule is generated by symmetry.

Table 5-27: Crystallographic information of $[(4\text{-MeNCOC}_6H_3)_2CH]_2$ (**28**).

CCDC no.	–	μ [mm^{-1}]	0.090
Structure code	mf22_mbox2CHdimer	F(000)	580
Empirical formula	$C_{34}H_{26}N_4O_4$	Crystal size [mm^3]	0.119 x 0.065 x 0.048
Formula weight [g mol^{-1}]	554.59	θ range [deg]	2.106 to 25.349
Temperature [K]	101(2)	Reflections collected	14710
Wavelength [Å]	0.71073	Independent reflections	2508
Crystal system	monoclinic	R_{int}	0.0641
Space group	$P2_1/n$	Completeness to θ_{max}	100.0 %
Unit cell dimensions	a = 7.866(2) Å	Restraints / parameters	0 / 192
	b = 8.994(3) Å	Goodness-of-fit on F^2	1.014
	c = 19.518(4) Å	$R1$ [I>2σ(I)]	0.0436
	α = 90 deg	w$R2$ (all data)	0.0998
	β = 97.74(2) deg	$g1$ / $g2$	0.0405 / 0.5552
	γ = 90 deg	max. diff. peak / hole [e Å^{-3}]	0.266 / −0.203
Volume [Å^3]	1368.3(6)	max. / min. transmission	0.7452 / 0.5954
Z	2	Absolute structure param.[169]	–
ρ_{calc} [Mg m^{-3}]	1.346	Extinction coefficient	–

5.1.28 Bis-(benzothiazol-2-yl)-amine (41)

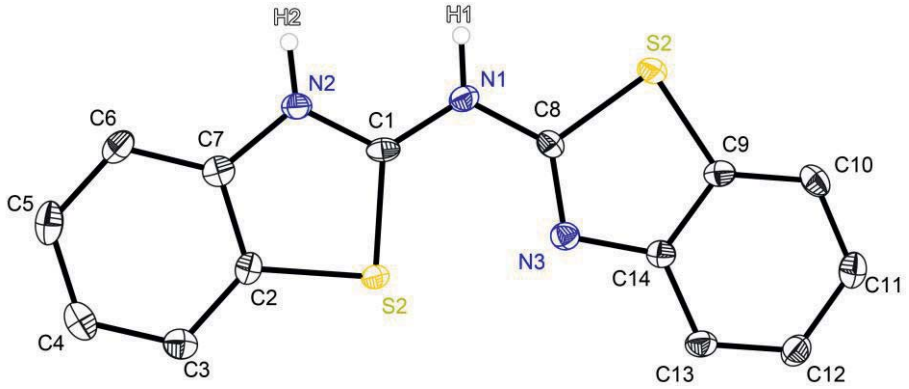

Figure 5-28: Asymmetric unit of **41**. Anisotropic displacement parameters are displayed at the 50 % probability level. Hydrogen atoms are omitted for clarity except the disordered amine moieties (*sof*: 0.675(50)).

Table 5-28: Crystallographic information of $(NCSC_6H_4)_2NH$ (**41**).

CCDC no.	1042655	μ [mm^{-1}]	0.415
Structure code	mf11_bth2NH	F(000)	292
Empirical formula	$C_{14}H_9N_3S_2$	Crystal size [mm^3]	0.171 x 0.080 x 0.037
Formula weight [g mol^{-1}]	283.37	θ range [deg]	1.631 to 27.313
Temperature [K]	100(2)	Reflections collected	14858
Wavelength [Å]	0.71073	Independent reflections	2785
Crystal system	monoclinic	R_{int}	0.0240
Space group	$P2_1$	Completeness to θ_{max}	99.9 %
Unit cell dimensions	a = 10.853(3) Å	Restraints / parameters	3 / 179
	b = 4.587(2) Å	Goodness-of-fit on F^2	1.188
	c = 12.513(4) Å	$R1$ [I>2σ(I)]	0.0309
	α = 90 deg	w$R2$ (all data)	0.0801
	β = 93.90(2) deg	$g1$ / $g2$	0.0379 / 0.3188
	γ = 90 deg	max. diff. peak / hole [e Å^{-3}]	0.365 / −0.281
Volume [Å^3]	621.5(4)	max. / min. transmission	0.7455 / 0.7037
Z	2	Absolute structure param.[169]	0.02(2)
ρ_{calc} [Mg m^{-3}]	1.514	Extinction coefficient	–

5.1.29 Bis-(4-methylbenzothiazol-2-yl)-amine (42)

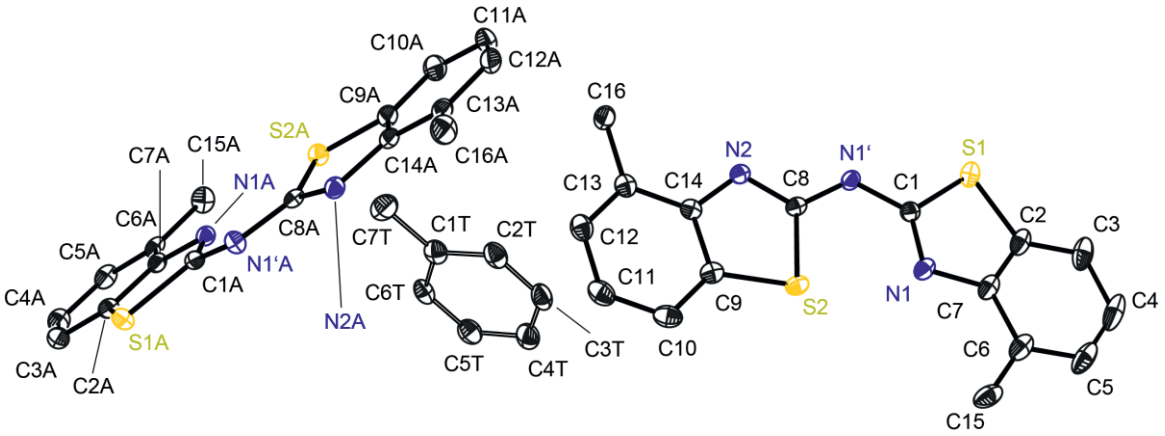

Figure 5-29: Asymmetric unit of **42** · 0.25 tol. Anisotropic displacement parameters are displayed at the 50 % probability level. Hydrogen atoms are omitted for clarity and the toluene molecule is disordered due to its location on an inversion centre.

Table 5-29: Crystallographic information of (4-MeNCSC$_6$H$_3$)$_2$NH (**42**) · 0.25 tol.

CCDC no.	1042656	μ [mm^{-1}]	0.340
Structure code	mf04_mbth2NH	F(000)	698
Empirical formula	$C_{16}H_{13}N_3S_2 \cdot 0.25\ C_7H_8$	Crystal size [mm^3]	0.132 x 0.088 x 0.072
Formula weight [g mol^{-1}]	334.45	θ range [deg]	1.292 to 27.398
Temperature [K]	100(2)	Reflections collected	25733
Wavelength [Å]	0.71073	Independent reflections	7109
Crystal system	triclinic	R_{int}	0.0358
Space group	$P\bar{1}$	Completeness to θ_{max}	99.8 %
Unit cell dimensions	a = 8.317(2) Å	Restraints / parameters	49 / 453
	b = 12.009(3) Å	Goodness-of-fit on F^2	1.030
	c = 16.306(4) Å	$R1$ [I>2σ(I)]	0.0344
	α = 85.55(2) deg	w$R2$ (all data)	0.0871
	β = 75.83(2) deg	$g1$ / $g2$	0.0350 / 0.9254
	γ = 89.23(3) deg	max. diff. peak / hole [e Å^{-3}]	0.366 / −0.340
Volume [Å^3]	1574.3(7)	max. / min. transmission	0.7456 / 0.7106
Z	4	Absolute structure param.[169]	–
ρ_{calc} [Mg m^{-3}]	1.411	Extinction coefficient	–

5.1.30 Bis-(4-methoxybenzothiazol-2-yl)-amine (43)

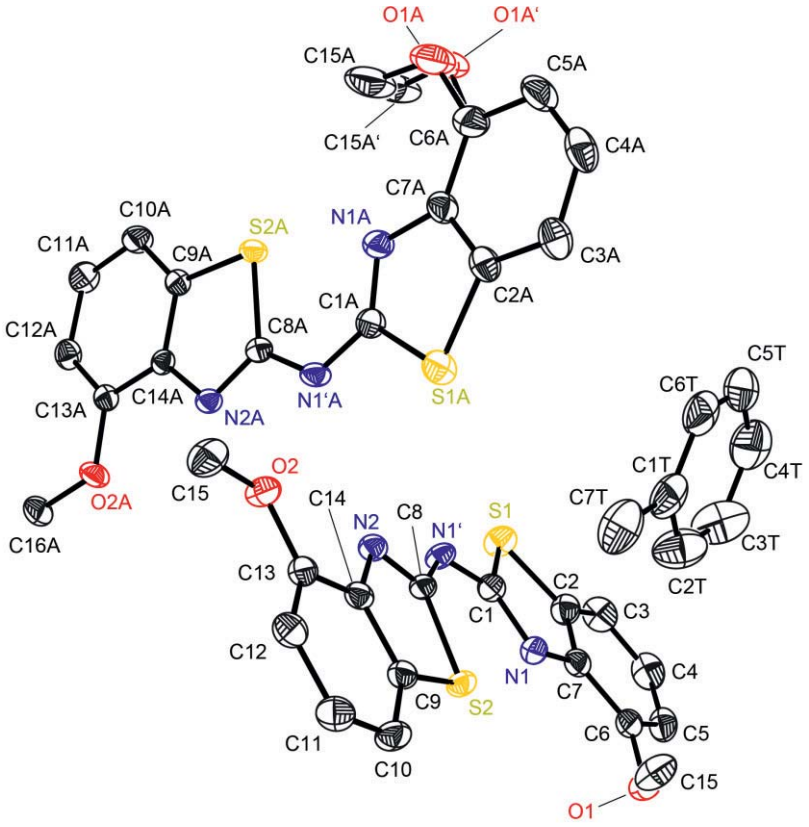

Figure 5-30: Asymmetric unit of **43** · 0.5 tol. Anisotropic displacement parameters are displayed at the 50 % probability level. Hydrogen atoms are omitted for clarity and one methoxy group is disordered (*sof*: 0.546(47)).

Table 5-30: Crystallographic information of (4-OMeNCSC$_6$H$_3$)$_2$NH (**43**) · 0.5 tol.

CCDC no.	1042657	μ [mm^{-1}]	0.318
Structure code	mf18_OMebth2NH	F(000)	3248
Empirical formula	$C_{16}H_{13}N_3O_2S_2 \cdot 0.5\ C_7H_8$	Crystal size [mm^3]	0.15 x 0.10 x 0.10
Formula weight [g mol^{-1}]	389.48	θ range [deg]	1.573 to 27.364
Temperature [K]	100(2)	Reflections collected	58842
Wavelength [Å]	0.71073	Independent reflections	8090
Crystal system	monoclinic	R_{int}	0.0592
Space group	*C*2/*c*	Completeness to θ_{max}	100.0 %
Unit cell dimensions	a = 28.107(4) Å	Restraints / parameters	30 / 511
	b = 12.581(2) Å	Goodness-of-fit on F^2	1.039
	c = 21.980(3) Å	$R1$ [I>2σ(I)]	0.0400
	α = 90 deg	w$R2$ (all data)	0.1027
	β = 112.93(3) deg	$g1$ / $g2$	0.0432 / 8.3423
	γ = 90 deg	max. diff. peak / hole [e Å^{-3}]	0.428 / −0.397
Volume [Å^3]	7158(2)	max. / min. transmission	0.7455 / 0.6712
Z	16	Absolute structure param.[169]	–
ρ_{calc} [Mg m^{-3}]	1.446	Extinction coefficient	–

5.1.31 Dimethylaluminium-bis-(benzothiazol-2-yl)-amide (44)

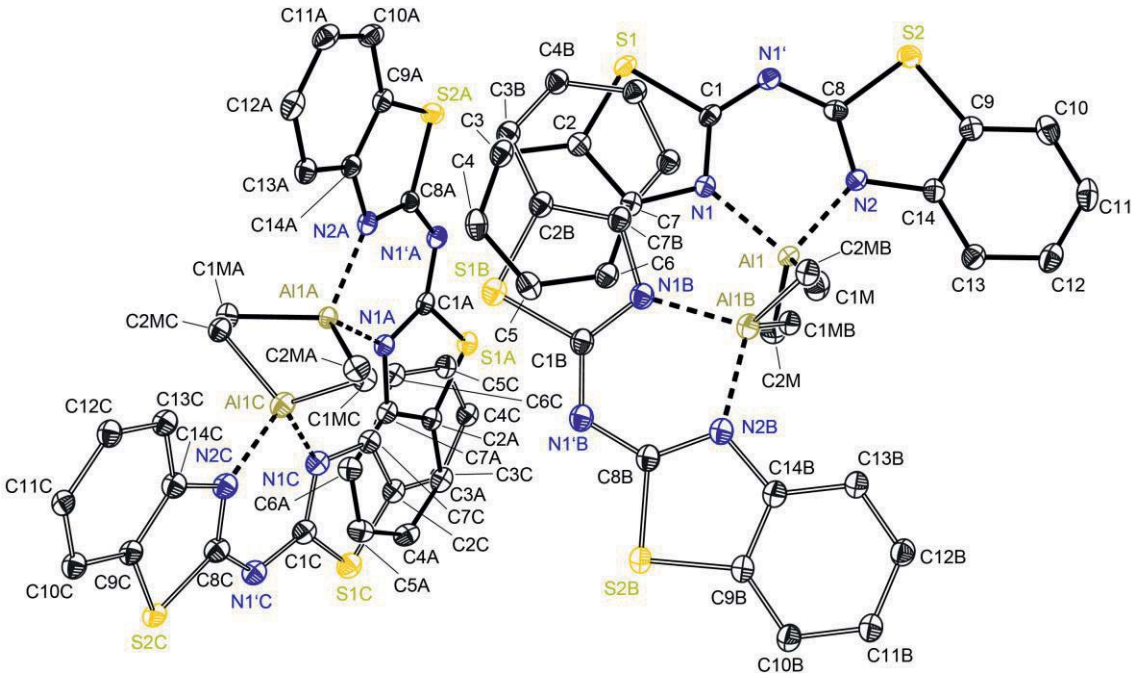

Figure 5-31: Asymmetric unit of **44**. Anisotropic displacement parameters are displayed at the 50 % probability level. Hydrogen atoms are omitted for clarity and disordered molecules are depicted (*sofs*: 0.960(1); 0.976(1)) in faded colour.

Table 5-31: Crystallographic information of $[Me_2Al\{(NCSC_6H_4)_2N\}]$ (**44**).

CCDC no.	1042658	μ [mm^{-1}]	0.204
Structure code	mf17_bth2NAlMe2	F(000)	704
Empirical formula	$C_{16}H_{14}AlN_3S_2$	Crystal size [mm^3]	0.286 x 0.131 x 0.103
Formula weight [g mol^{-1}]	339.40	θ range [deg]	1.223 to 21.117
Temperature [K]	100(2)	Reflections collected	38457
Wavelength [Å]	0.56086	Independent reflections	7063
Crystal system	triclinic	R_{int}	0.0280
Space group	$P\bar{1}$	Completeness to θ_{max}	100.0 %
Unit cell dimensions	a = 8.678(2) Å	Restraints / parameters	5846 / 799
	b = 14.569(3) Å	Goodness-of-fit on F^2	1.132
	c = 14.732(3) Å	R1 [I>2σ(I)]	0.0349
	α = 63.90(2) deg	wR2 (all data)	0.0800
	β = 88.93(3) deg	g1 / g2	0.0204 / 1.6597
	γ = 74.02(2) deg	max. diff. peak / hole [e Å^{-3}]	0.381 / −0.234
Volume [Å^3]	1596.6(7)	max. / min. transmission	0.7446 / 0.7172
Z	4	Absolute structure param.[169]	–
ρ_{calc} [Mg m^{-3}]	1.412	Extinction coefficient	–

5.1.32 Dimethylaluminium-bis-(4-methylbenzothiazol-2-yl)-amide (45)

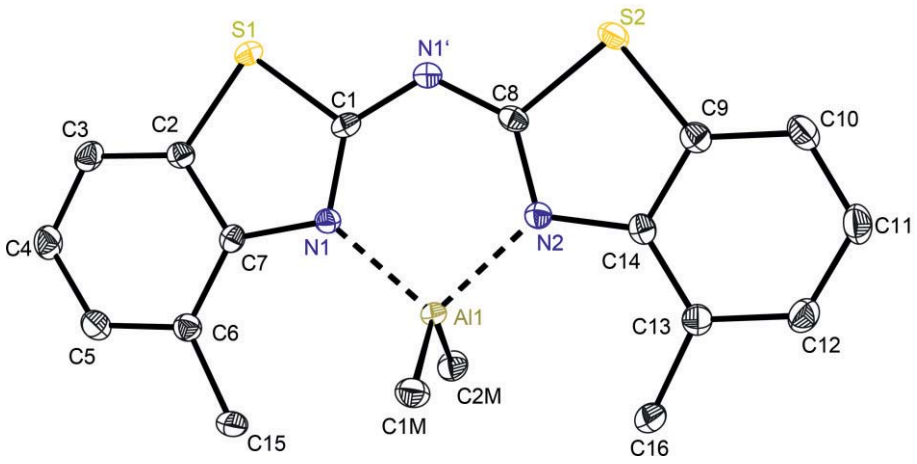

Figure 5-32: Asymmetric unit of **45**. Anisotropic displacement parameters are displayed at the 50 % probability level. Hydrogen atoms are omitted for clarity.

Table 5-32: Crystallographic information of $[Me_2Al\{(4\text{-}MeNCSC_6H_3)_2N\}]$ (**45**).

CCDC no.	1042659	μ [mm^{-1}]	0.191
Structure code	mf15_mbth2NAlMe2	F(000)	1536
Empirical formula	$C_{18}H_{18}AlN_3S_2$	Crystal size [mm^3]	0.212 x 0.189 x 0.137
Formula weight [g mol^{-1}]	367.47	θ range [deg]	1.898 to 20.584
Temperature [K]	100(2)	Reflections collected	100934
Wavelength [Å]	0.56086	Independent reflections	3588
Crystal system	orthorhombic	R_{int}	0.0346
Space group	*Pccn*	Completeness to θ_{max}	99.9 %
Unit cell dimensions	a = 16.013(3) Å	Restraints / parameters	0 / 221
	b = 16.930(3) Å	Goodness-of-fit on F^2	1.073
	c = 12.855(2) Å	$R1$ [I>2σ(I)]	0.0267
	α = 90 deg	w$R2$ (all data)	0.0725
	β = 90 deg	$g1$ / $g2$	0.0322 / 2.6182
	γ = 90 deg	max. diff. peak / hole [e Å^{-3}]	0.370 / −0.210
Volume [Å^3]	3485.0(10)	max. / min. transmission	0.7445 / 0.7314
Z	8	Absolute structure param.[169]	–
ρ_{calc} [Mg m^{-3}]	1.401	Extinction coefficient	–

5.1.33 Trimethylaluminium dimethylaluminium-bis-(4-methoxybenzothiazol-2-yl)-amide (46)

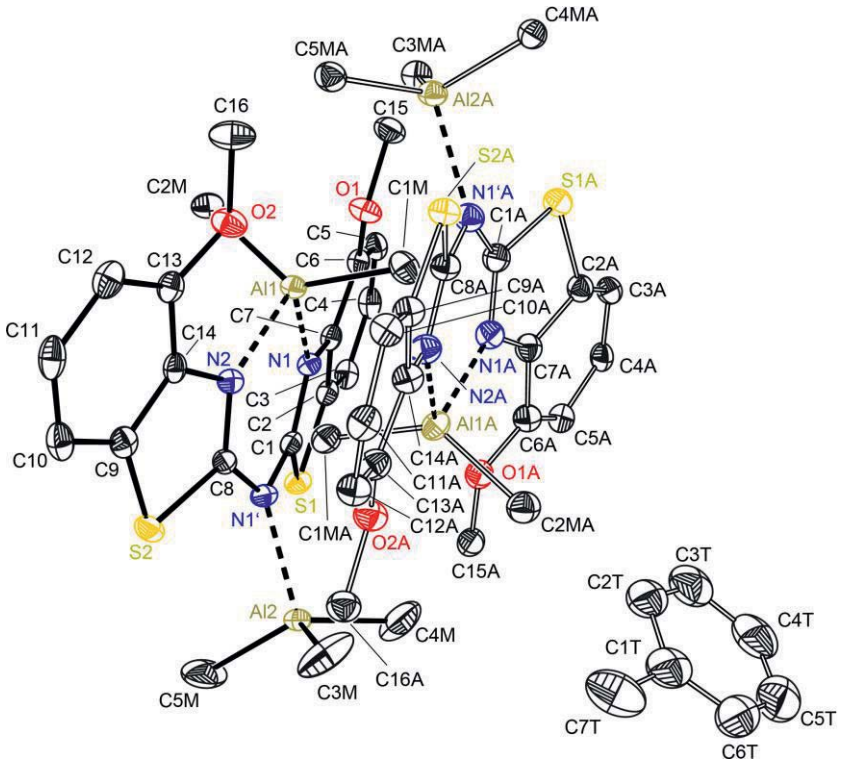

Figure 5-33: Asymmetric unit of **46** · 0.42 tol. Anisotropic displacement parameters are displayed at the 50 % probability level. Hydrogen atoms are omitted for clarity and disordered molecules (*sofs*: 0.941(1); 0.417(3)) are depicted in faded colour.

Table 5-33: Crystallographic information of $[Me_2Al\{(4\text{-}OMeNCSC_6H_3)_2N\}]$ (**46**) · 0.42 tol.

CCDC no.	1042660	μ [mm^{-1}]	0.286
Structure code	mf19_OMebth2NAlMe2	F(000)	1075
Empirical formula	$C_{21}H_{27}Al_2N_3O_2S_2 \cdot 0.42\ C_7H_8$	Crystal size [mm^3]	0.132 x 0.128 x 0.086
Formula weight [g mol^{-1}]	509.92	θ range [deg]	1.839 to 26.499
Temperature [K]	100(2)	Reflections collected	23794
Wavelength [Å]	0.71073	Independent reflections	5593
Crystal system	monoclinic	R_{int}	0.0351
Space group	$P2_1/c$	Completeness to θ_{max}	99.9 %
Unit cell dimensions	a = 11.136(2) Å	Restraints / parameters	5376 / 614
	b = 17.335(3) Å	Goodness-of-fit on F^2	1.041
	c = 14.122(2) Å	$R1$ [I>2σ(I)]	0.0432
	α = 90 deg	w$R2$ (all data)	0.1351
	β = 95.96(2) deg	$g1$ / $g2$	0.0761 / 1.7063
	γ = 90 deg	max. diff. peak / hole [e Å^{-3}]	0.730 / −0.666
Volume [Å^3]	2711.4(8)	max. / min. transmission	0.7454 / 0.6604
Z	4	Absolute structure param.[169]	-
ρ_{calc} [Mg m^{-3}]	1.249	Extinction coefficient	-

5.1.34 Lithium-bis-(4-methylbenzothiazol-2-yl)-amide (48)

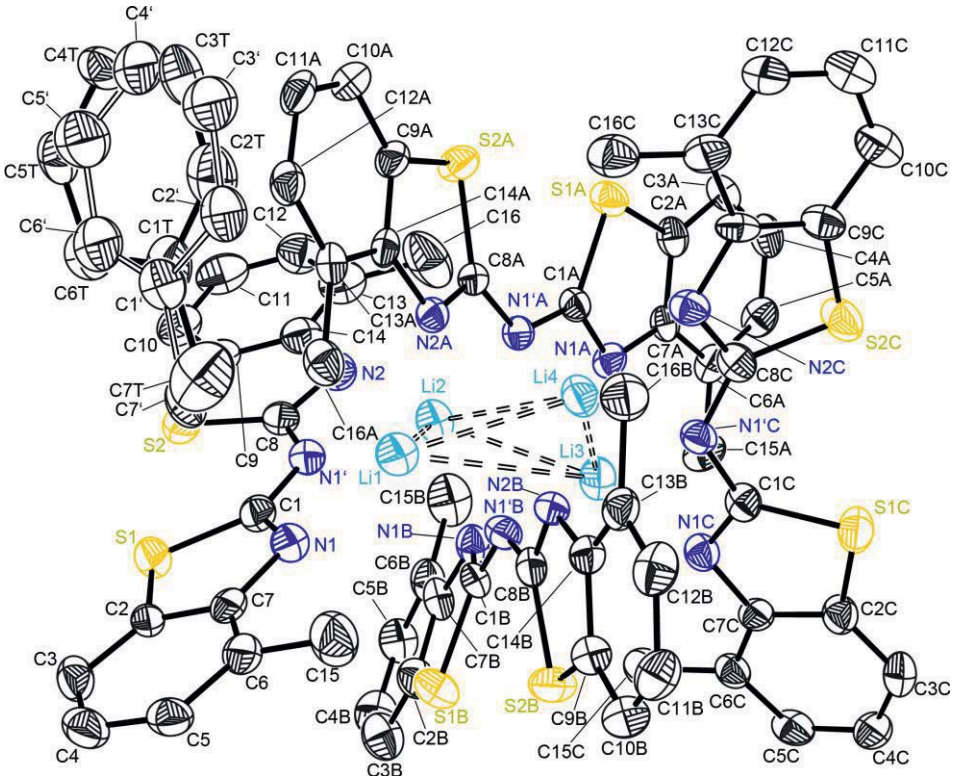

Figure 5-34: Asymmetric unit of **48** · 0.25 tol. Anisotropic displacement parameters are displayed at the 50 % probability level. Hydrogen atoms are omitted for clarity and disordered molecules (*sof*: 0.658(24)) are depicted in faded colour.

Table 5-34: Crystallographic information of $[Li\{(4\text{-}MeNCSC_6H_3)_2N\}]_4$ (**48**) · 0.25 tol.

CCDC no.	1042661	μ [mm^{-1}]	0.325
Structure code	mf14_(mbth2NLi)4	F(000)	1412
Empirical formula	$C_{16}H_{12}LiN_3S_2 \cdot 0.25\ C_7H_8$	Crystal size [mm^3]	0.098 x 0.052 x 0.052
Formula weight [g mol^{-1}]	340.38	θ range [deg]	1.314 to 23.289
Temperature [K]	100(2)	Reflections collected	38560
Wavelength [Å]	0.71073	Independent reflections	9464
Crystal system	triclinic	R_{int}	0.0862
Space group	$P\bar{1}$	Completeness to θ_{max}	79.5 %
Unit cell dimensions	a = 14.094(2) Å	Restraints / parameters	345 / 930
	b = 16.125(3) Å	Goodness-of-fit on F^2	1.017
	c = 16.706(3) Å	$R1$ [I>2σ(I)]	0.0571
	α = 71.00(3) deg	w$R2$ (all data)	0.1491
	β = 73.41(3) deg	$g1$ / $g2$	0.0635 / 2.2084
	γ = 69.20(2) deg	max. diff. peak / hole [e Å^{-3}]	0.323 / −0.317
Volume [Å^3]	3293.3(13)	max. / min. transmission	0.7449 / 0.6937
Z	8	Absolute structure param.[169]	–
ρ_{calc} [Mg m^{-3}]	1.373	Extinction coefficient	–

6 References

[1] R. C. Mehrotra, R. Bohra, D. P. Gaur, *Metal ß-Diketonates and Allied Derivatives*, Academic Press, New York, **1978**.

[2] **a)** M. Calligaris, L. Randaccio, *Comprehensive Coordination Chemistry, Vol. 2*, chapter 20.21, Pergamon, Oxford, U.K., **1987**; **b)** J. E. Parks, R. H. Holm, *Inorg. Chem.* **1968**, *7*, 1408-1416.

[3] N. F. Curtis, *Comprehensive Coordination Chemistry, Vol. 2*, chapter 21.22, Pergamon, Oxford, U.K., **1987**.

[4] **a)** A. D. Phillips, *Organomet. Chem.* **2014**, *39*, 72-147; **b)** P. L. Holland, *Acc. Chem. Res.* **2008**, *41*, 905-914; **c)** C. J. Cramer, W. B. Tolman, *Acc. Chem. Res.* **2007**, *40*, 601-608; **d)** D. J. Mindiola, *Acc. Chem. Res.* **2006**, *39*, 813-821; **e)** H. W. Roesky, S. Singh, V. Jancik, V. Chandrasekhar, *Acc. Chem. Res.* **2004**, *37*, 969-981; **f)** W. E. Piers, D. J. H. Emslie, *Coord. Chem. Rev.* **2002**, *233–234*, 131-155.

[5] H. Meerwein, G. Hinz, P. Hofmann, E. Kroning, E. Pfeil, *J. Prakt. Chem.* **1937**, *147*, 257-285.

[6] S. G. McGeachin, *Can. J. Chem.* **1968**, *46*, 1903-1912.

[7] L. C. Dorman, *Tetrahedron Lett.* **1966**, *7*, 459-464.

[8] W. J. Barry, I. L. Finar, E. F. Mooney, *Spectrochim. Acta* **1965**, *21*, 1095-1099.

[9] J. Feldman, S. J. McLain, A. Parthasarathy, W. J. Marshall, J. C. Calabrese, S. D. Arthur, *Organometallics* **1997**, *16*, 1514-1516.

[10] **a)** M. Cheng, D. R. Moore, J. J. Reczek, B. M. Chamberlain, E. B. Lobkovsky, G. W. Coates, *J. Am. Chem. Soc.* **2001**, *123*, 8738-8749; **b)** M. Stender, R. J. Wright, B. E. Eichler, J. Prust, M. M. Olmstead, H. W. Roesky, P. P. Power, *J. Chem. Soc., Dalton Trans.* **2001**, 3465-3469.

[11] P. H. M. Budzelaar, A. B. van Oort, A. G. Orpen, *Eur. J. Inorg. Chem.* **1998**, *1998*, 1485-1494.

[12] A. L. Kenward, J. A. Ross, W. E. Piers, M. Parvez, *Organometallics* **2009**, *28*, 3625-3628.

[13] R. Bonnett, D. C. Bradley, K. J. Fisher, *Chem. Commun.* **1968**, 886-887.

[14] **a)** A. Jana, H. W. Roesky, C. Schulzke, A. Döring, T. Beck, A. Pal, R. Herbst-Irmer, *Inorg. Chem.* **2008**, *48*, 193-197; **b)** S. Nagendran, H. W. Roesky, *Organometallics* **2008**, *27*, 457-492; **c)** Y. Cheng, D. J. Doyle, P. B. Hitchcock, M. F. Lappert, *Dalton Trans.* **2006**, 4449-4460; **d)** S. Singh, H.-J. Ahn, A. Stasch, V. Jancik, H. W. Roesky, A. Pal, M. Biadene, R. Herbst-Irmer, M. Noltemeyer, H.-G. Schmidt, *Inorg. Chem.* **2006**, *45*, 1853-1860; **e)** Z. Yang, H. Zhu, X. Ma, J. Chai, H. W. Roesky, C. He, J. Magull, H.-G. Schmidt, M. Noltemeyer, *Inorg. Chem.* **2006**, *45*, 1823-1827; **f)** N. Kuhn, S. Fuchs, M. Steimann, *Z. Anorg. Allg. Chem.* **2002**, *628*, 458-462; **g)** Y. Ding, H. W. Roesky, M. Noltemeyer, H.-G. Schmidt, P. P. Power, *Organometallics* **2001**, *20*, 1190-1194; **h)** N. Kuhn, S. Fuchs, M. Steimann, *Eur. J. Inorg. Chem.* **2001**, *2001*, 359-361; **i)** M. Stender, B. E. Eichler, N. J. Hardman, P. P. Power, J. Prust, M. Noltemeyer, H. W. Roesky, *Inorg. Chem.* **2001**, *40*, 2794-2799; **j)** N. Kuhn, J. Fahl, S. Fuchs, M. Steimann, G.

Henkel, A. H. Maulitz, *Z. Anorg. Allg. Chem.* **1999**, *625*, 2108-2114; **k)** C. E. Radzewich, I. A. Guzei, R. F. Jordan, *J. Am. Chem. Soc.* **1999**, *121*, 8673-8674; **l)** B. Qian, D. L. Ward, M. R. Smith, *Organometallics* **1998**, *17*, 3070-3076.

[15] D. Li, Y. Peng, C. Geng, K. Liu, D. Kong, *Dalton Trans.* **2013**, *42*, 11295-11303.

[16] **a)** Y.-C. Tsai, *Coord. Chem. Rev.* **2012**, *256*, 722-758; **b)** L. Bourget-Merle, M. F. Lappert, J. R. Severn, *Chem. Rev.* **2002**, *102*, 3031-3066.

[17] **a)** P. B. Hitchcock, M. F. Lappert, S. Tian, *J. Chem. Soc., Dalton Trans.* **1997**, 1945-1952; **b)** M. F. Lappert, D.-S. Liu, *J. Organomet. Chem.* **1995**, *500*, 203-217; **c)** P. B. Hitchcock, M. F. Lappert, D.-S. Liu, *J. Chem. Soc., Chem. Commun.* **1994**, 2637-2638.

[18] **a)** B.-J. Deelman, M. F. Lappert, H.-K. Lee, T. C. W. Mak, W.-P. Leung, P.-R. Wei, *Organometallics* **1997**, *16*, 1247-1252; **b)** P. B. Hitchcock, M. F. Lappert, D.-S. Liu, *J. Chem. Soc., Chem. Commun.* **1994**, 1699-1700.

[19] W. Clegg, S. J. Coles, E. K. Cope, F. S. Mair, *Angew. Chem. Int. Ed.* **1998**, *37*, 796-798.

[20] B. Räke, F. Zülch, Y. Ding, J. Prust, H. W. Roesky, M. Noltemeyer, H.-G. Schmidt, *Z. Anorg. Allg. Chem.* **2001**, *627*, 836-840.

[21] C. Chen, S. M. Bellows, P. L. Holland, *Dalton Trans.* **2015**, *44*, 16654-16670.

[22] N. Kuhn, A. Kuhn, J. Lewandowski, M. Speis, *Chem. Ber.* **1991**, *124*, 2197-2201.

[23] Y. Yang, H. Li, C. Wang, H. W. Roesky, *Inorg. Chem.* **2012**, *51*, 2204-2211.

[24] N. Kuhn, S. Fuchs, M. Steimann, *Z. Anorg. Allg. Chem.* **2000**, *626*, 1387-1392.

[25] **a)** Z. Yang, M. Zhong, X. Ma, S. De, C. Anusha, P. Parameswaran, H. W. Roesky, *Angew. Chem. Int. Ed.* **2015**, *54*, 10225-10229; **b)** C. Cui, H. W. Roesky, H. Hao, H. G. Schmidt, M. Noltemeyer, *Angew. Chem. Int. Ed.* **2000**, *39*, 1815-1817.

[26] C. E. Radzewich, M. P. Coles, R. F. Jordan, *J. Am. Chem. Soc.* **1998**, *120*, 9384-9385.

[27] G. Bai, S. Singh, H. W. Roesky, M. Noltemeyer, H.-G. Schmidt, *J. Am. Chem. Soc.* **2005**, *127*, 3449-3455.

[28] X. Li, X. Cheng, H. Song, C. Cui, *Organometallics* **2007**, *26*, 1039-1043.

[29] **a)** N. Burford, M. D'Eon, P. J. Ragogna, R. McDonald, M. J. Ferguson, *Inorg. Chem.* **2003**, *43*, 734-738; **b)** P. J. Ragogna, N. Burford, M. D'Eon, R. McDonald, *Chem. Commun.* **2003**, 1052-1053.

[30] **a)** W. W. Schoeller, *Inorg. Chem.* **2011**, *50*, 2629-2633; **b)** C.-H. Chen, M.-L. Tsai, M.-D. Su, *Organometallics* **2006**, *25*, 2766-2773.

[31] **a)** P. Hao, Z. Yang, W. Li, X. Ma, H. W. Roesky, Y. Yang, J. Li, *Organometallics* **2015**, *34*, 105-108; **b)** Y. Yang, T. Schulz, M. John, Z. Yang, V. M. Jiménez-Pérez, H. W. Roesky, P. M. Gurubasavaraj, D. Stalke, H. Ye, *Organometallics* **2008**, *27*, 769-777; **c)** G. Bai, Y. Peng, H. W. Roesky, J. Li, H. G. Schmidt, M. Noltemeyer, *Angew. Chem. Int. Ed.* **2003**, *42*, 1132-1135; **d)** G. Bai, H. W. Roesky, J. Li, M. Noltemeyer, H. G. Schmidt, *Angew. Chem. Int. Ed.* **2003**, *42*, 5502-5506; **e)** D. Neculai, H. W. Roesky, A. M. Neculai, J. Magull, B. Walfort, D. Stalke, *Angew. Chem.* **2002**, *114*, 4470-4472.

[32] **a)** L. L. Böhm, *Angew. Chem.* **2003**, *115*, 5162-5183; **b)** E. Y.-X. Chen, T. J. Marks, *Chem. Rev.* **2000**, *100*, 1391-1434; **c)** A. Andresen, H. G. Cordes, J. Her-

wig, W. Kaminsky, A. Merck, R. Mottweiler, J. Pein, H. Sinn, H. J. Vollmer, *Angew. Chem.* **1976**, *88*, 689-690; **d)** G. Natta, *Angew. Chem.* **1964**, *76*, 553-566; **e)** K. Ziegler, E. Holzkamp, H. Breil, H. Martin, *Angew. Chem.* **1955**, *67*, 541-547.

[33] **a)** J. Storre, A. Klemp, H. W. Roesky, R. Fleischer, D. Stalke, *Organometallics* **1997**, *16*, 3074-3076; **b)** J. Storre, C. Schnitter, H. W. Roesky, H.-G. Schmidt, M. Noltemeyer, R. Fleischer, D. Stalke, *J. Am. Chem. Soc.* **1997**, *119*, 7505-7513; **c)** J. Storre, A. Klemp, H. W. Roesky, H.-G. Schmidt, M. Noltemeyer, R. Fleischer, D. Stalke, *J. Am. Chem. Soc.* **1996**, *118*, 1380-1386; **d)** J. Storre, T. Belgardt, D. Stalke, H. W. Roesky, *Angew. Chem.* **1994**, *106*, 1365-1366.

[34] **a)** M. S. Hill, P. B. Hitchcock, R. Pongtavornpinyo, *Dalton Trans.* **2005**, 273-277; **b)** M. S. Hill, P. B. Hitchcock, *Chem. Commun.* **2004**, 1818-1819; **c)** C. Cui, H. W. Roesky, H.-G. Schmidt, M. Noltemeyer, H. Hao, F. Cimpoesu, *Angew. Chem. Int. Ed.* **2000**, *39*, 4274-4276; **d)** N. J. Hardman, B. E. Eichler, P. P. Power, *Chem. Commun.* **2000**, 1991-1992.

[35] **a)** M. Asay, C. Jones, M. Driess, *Chem. Rev.* **2011**, *111*, 354-396; **b)** Y. Mizuhata, T. Sasamori, N. Tokitoh, *Chem. Rev.* **2009**, *109*, 3479-3511.

[36] M. N. Sudheendra Rao, H. W. Roesky, G. Anantharaman, *J. Organomet. Chem.* **2002**, *646*, 4-14.

[37] A. F. Holleman, N. Wiberg, E. Wiberg, *Lehrbuch der Anorganischen Chemie*, 102th ed., Walter de Gruyter, Berlin, New York, **2007**.

[38] **a)** M. L. H. Green, P. Mountford, G. J. Smout, S. R. Speel, *Polyhedron* **1990**, *9*, 2763-2765; **b)** M. Wilkinson, I. J. Worrall, *J. Organomet. Chem.* **1975**, *93*, 39-42.

[39] **a)** M. S. Hill, P. B. Hitchcock, R. Pongtavornpinyo, *Dalton Trans.* **2007**, 731-733; **b)** M. S. Hill, P. B. Hitchcock, R. Pongtavornpinyo, *Angew. Chem. Int. Ed.* **2005**, *44*, 4231-4235.

[40] Z. Yang, X. Ma, R. B. Oswald, H. W. Roesky, H. Zhu, C. Schulzke, K. Starke, M. Baldus, H. G. Schmidt, M. Noltemeyer, *Angew. Chem.* **2005**, *117*, 7234-7236.

[41] H. Zhu, J. Chai, H. Fan, H. W. Roesky, C. He, V. Jancik, H. G. Schmidt, M. Noltemeyer, W. A. Merrill, P. P. Power, *Angew. Chem. Int. Ed.* **2005**, *44*, 5090-5093.

[42] Z. Yang, X. Ma, R. B. Oswald, H. W. Roesky, M. Noltemeyer, *J. Am. Chem. Soc.* **2006**, *128*, 12406-12407.

[43] C. Cui, S. Köpke, R. Herbst-Irmer, H. W. Roesky, M. Noltemeyer, H.-G. Schmidt, B. Wrackmeyer, *J. Am. Chem. Soc.* **2001**, *123*, 9091-9098.

[44] C. Cui, H. W. Roesky, H. G. Schmidt, M. Noltemeyer, *Angew. Chem. Int. Ed.* **2000**, *39*, 4531-4533.

[45] H. Zhu, J. Chai, H. Fan, H. W. Roesky, U. N. Nehete, H. G. Schmidt, M. Noltemeyer, *Eur. J. Inorg. Chem.* **2005**, *2005*, 2147-2150.

[46] Y. Peng, H. Fan, H. Zhu, H. W. Roesky, J. Magull, C. E. Hughes, *Angew. Chem. Int. Ed.* **2004**, *43*, 3443-3445.

[47] V. Jancik, Monica M. M. Cabrera, Herbert W. Roesky, R. Herbst-Irmer, D. Neculai, Ana M. Neculai, M. Noltemeyer, H. G. Schmidt, *Eur. J. Inorg. Chem.* **2004**, *2004*, 3508-3512.

[48] Y. Peng, H. Fan, V. Jancik, H. W. Roesky, R. Herbst-Irmer, *Angew. Chem. Int. Ed.* **2004**, *43*, 6190-6192.

[49] H. Zhu, J. Chai, V. Jancik, H. W. Roesky, W. A. Merrill, P. P. Power, *J. Am. Chem. Soc.* **2005**, *127*, 10170-10171.

[50] **a)** W. A. Herrmann, *Angew. Chem. Int. Ed.* **2002**, *41*, 1290-1309; **b)** W. A. Herrmann, C. Köcher, *Angew. Chem. Int. Ed. Engl.* **1997**, *36*, 2162-2187.

[51] P. P. Power, *Nature* **2010**, *463*, 171-177.

[52] **a)** D. W. Stephan, *Org. Biomol. Chem.* **2008**, *6*, 1535-1539; **b)** W. Tochtermann, *Angew. Chem. Int. Ed. Engl.* **1966**, *5*, 351-371; **c)** G. Wittig, E. Benz, *Chem. Ber.* **1959**, *92*, 1999-2013.

[53] **a)** D. W. Stephan, G. Erker, *Angew. Chem. Int. Ed.* **2010**, *49*, 46-76; **b)** P. Spies, G. Kehr, K. Bergander, B. Wibbeling, R. Fröhlich, G. Erker, *Dalton Trans.* **2009**, 1534-1541; **c)** G. C. Welch, R. R. S. Juan, J. D. Masuda, D. W. Stephan, *Science* **2006**, *314*, 1124-1126.

[54] G. C. Welch, J. D. Masuda, D. W. Stephan, *Inorg. Chem.* **2006**, *45*, 478-480.

[55] C. Appelt, J. C. Slootweg, K. Lammertsma, W. Uhl, *Angew. Chem. Int. Ed.* **2013**, *52*, 4256-4259.

[56] Y. Zhang, G. M. Miyake, E. Y. X. Chen, *Angew. Chem. Int. Ed.* **2010**, *49*, 10158-10162.

[57] **a)** G. Ménard, D. W. Stephan, *Angew. Chem. Int. Ed.* **2011**, *50*, 8396-8399; **b)** G. Ménard, D. W. Stephan, *J. Am. Chem. Soc.* **2010**, *132*, 1796-1797.

[58] **a)** A. Stasch, C. Jones, *Dalton Trans.* **2011**, *40*, 5659-5672; **b)** J. Overgaard, C. Jones, A. Stasch, B. B. Iversen, *J. Am. Chem. Soc.* **2009**, *131*, 4208-4209; **c)** M. Westerhausen, *Angew. Chem. Int. Ed.* **2008**, *47*, 2185-2187; **d)** S. P. Green, C. Jones, A. Stasch, *Science* **2007**, *318*, 1754-1757.

[59] **a)** C. Ruspic, S. Harder, *Inorg. Chem.* **2007**, *46*, 10426-10433; **b)** S. Harder, *Organometallics* **2002**, *21*, 3782-3787.

[60] D. F. J. Piesik, S. Range, S. Harder, *Organometallics* **2008**, *27*, 6178-6187.

[61] J. Spielmann, F. Buch, S. Harder, *Angew. Chem. Int. Ed.* **2008**, *47*, 9434-9438.

[62] H. W. Roesky, S. S. Kumar, *Chem. Commun.* **2005**, 4027-4038.

[63] B. Li, C. Zhang, Y. Yang, H. Zhu, H. W. Roesky, *Inorg. Chem.* **2015**, *54*, 6641-6646.

[64] **a)** Z. Zhu, X. Wang, Y. Peng, H. Lei, J. C. Fettinger, E. Rivard, P. P. Power, *Angew. Chem. Int. Ed.* **2009**, *48*, 2031-2034; **b)** R. J. Wright, M. Brynda, P. P. Power, *Angew. Chem. Int. Ed.* **2006**, *45*, 5953-5956; **c)** R. J. Wright, A. D. Phillips, S. Hino, P. P. Power, *J. Am. Chem. Soc.* **2005**, *127*, 4794-4799; **d)** N. J. Hardman, R. J. Wright, A. D. Phillips, P. P. Power, *Angew. Chem. Int. Ed.* **2002**, *41*, 2842-2844; **e)** J. Su, X.-W. Li, R. C. Crittendon, G. H. Robinson, *J. Am. Chem. Soc.* **1997**, *119*, 5471-5472.

[65] **a)** A. Kempter, C. Gemel, R. A. Fischer, *Chem. Eur. J.* **2007**, *13*, 2990-3000; **b)** A. Kempter, C. Gemel, R. A. Fischer, *Chem. Commun.* **2006**, 1551-1553.

[66] R. Jackstell, M. G. Andreu, A. Frisch, K. Selvakumar, A. Zapf, H. Klein, A. Spannenberg, D. Röttger, O. Briel, R. Karch, M. Beller, *Angew. Chem. Int. Ed.* **2002**, *41*, 986-989.

[67] N. J. Hardman, R. J. Wright, A. D. Phillips, P. P. Power, *J. Am. Chem. Soc.* **2003**, *125*, 2667-2679.

[68] A. Kempter, C. Gemel, N. J. Hardman, R. A. Fischer, *Inorg. Chem.* **2006**, *45*, 3133-3138.

[69] A. Kempter, C. Gemel, T. Cadenbach, R. A. Fischer, *Organometallics* **2007**, *26*, 4257-4264.

[70] **a)** E. J. Corey, N. Imai, H. Y. Zhang, *J. Am. Chem. Soc.* **1991**, *113*, 728-729; **b)** D. A. Evans, K. A. Woerpel, M. M. Hinman, M. M. Faul, *J. Am. Chem. Soc.* **1991**, *113*, 726-728; **c)** J. Hall, J.-M. Lehn, A. DeCian, J. Fischer, *Helv. Chim. Acta* **1991**, *74*, 1-6; **d)** D. Müller, G. Umbricht, B. Weber, A. Pfaltz, *Helv. Chim. Acta* **1991**, *74*, 232-240; **e)** R. E. Lowenthal, A. Abiko, S. Masamune, *Tetrahedron Lett.* **1990**, *31*, 6005-6008.

[71] **a)** B. D. Ward, L. H. Gade, *Chem. Commun.* **2012**, *48*, 10587-10599; **b)** G. Desimoni, G. Faita, K. A. Jørgensen, *Chem. Rev.* **2011**, *111*, 284-437.

[72] **a)** R. Rasappan, D. Laventine, O. Reiser, *Coord. Chem. Rev.* **2008**, *252*, 702-714; **b)** J. S. Johnson, D. A. Evans, *Acc. Chem. Res.* **2000**, *33*, 325-335; **c)** M. Gómez, G. Muller, M. Rocamora, *Coord. Chem. Rev.* **1999**, *193–195*, 769-835; **d)** K. A. Jørgensen, M. Johannsen, S. Yao, H. Audrain, J. Thorhauge, *Acc. Chem. Res.* **1999**, *32*, 605-613.

[73] S. Dagorne, S. Bellemin-Laponnaz, A. Maisse-François, *Eur. J. Inorg. Chem.* **2007**, *2007*, 913-925.

[74] **a)** N. Schneider, M. Kruck, S. Bellemin-Laponnaz, H. Wadepohl, L. H. Gade, *Eur. J. Inorg. Chem.* **2009**, *2009*, 493-500; **b)** S. Nanchen, A. Pfaltz, *Chem. Eur. J.* **2006**, *12*, 4550-4558.

[75] M. Schönleber, R. Hilgraf, A. Pfaltz, *Adv. Synth. Catal.* **2008**, *350*, 2033-2038.

[76] H. Werner, R. Vicha, A. Gissibl, O. Reiser, *J. Org. Chem.* **2003**, *68*, 10166-10168.

[77] U. Leutenegger, G. Umbricht, C. Fahrni, P. von Matt, A. Pfaltz, *Tetrahedron* **1992**, *48*, 2143-2156.

[78] **a)** D. C. Sauer, R. L. Melen, M. Kruck, L. H. Gade, *Eur. J. Inorg. Chem.* **2014**, *2014*, 4715-4725; **b)** D. C. Sauer, H. Wadepohl, L. H. Gade, *Inorg. Chem.* **2012**, *51*, 12948-12958; **c)** B. K. Langlotz, H. Wadepohl, L. H. Gade, *Angew. Chem.* **2008**, *120*, 4748-4752.

[79] B. Ramalingam, M. Neuburger, A. Pfaltz, *Synthesis* **2007**, *2007*, 572-582.

[80] S. Michlik, R. Kempe, *Nat. Chem.* **2013**, *5*, 140-144.

[81] **a)** S. Michlik, R. Kempe, *Chem. Eur. J.* **2010**, *16*, 13193-13198; **b)** B. Blank, S. Michlik, R. Kempe, *Chem. Eur. J.* **2009**, *15*, 3790-3799; **c)** B. Blank, S. Michlik, R. Kempe, *Adv. Synth. Catal.* **2009**, *351*, 2903-2911.

[82] H. Schödel, C. Näther, H. Bock, F. Butenschön, *Acta Crystallogr., Sect. B* **1996**, *52*, 842-853.

[83] **a)** H. Gornitzka, C. Hemmert, G. Bertrand, M. Pfeiffer, D. Stalke, *Organometallics* **2000**, *19*, 112-114; **b)** T. Kottke, D. Stalke, *Chem. Ber.* **1997**, *130*, 1365-1374; **c)** H. Gornitzka, D. Stalke, *Angew. Chem. Int. Ed. Engl.* **1994**, *33*, 693-695; **d)** H. Gornitzka, D. Stalke, *Organometallics* **1994**, *13*, 4398-4405.

[84] L. Mahalakshmi, D. Stalke, in *Group 13 Chemistry I, Vol. 103* (Eds.: H. W. Roesky, D. A. Atwood), Springer Berlin Heidelberg, **2002**, pp. 85-115.

[85] **a)** M. Pfeiffer, A. Murso, L. Mahalakshmi, D. Moigno, W. Kiefer, D. Stalke, *Eur. J. Inorg. Chem.* **2002**, *2002*, 3222-3234; **b)** M. Pfeiffer, F. Baier, T. Stey, D. Leusser, D. Stalke, B. Engels, D. Moigno, W. Kiefer, *J. Mol. Model.* **2000**, *6*, 299-311; **c)** H. Gornitzka, D. Stalke, *Eur. J. Inorg. Chem.* **1998**, *1998*, 311-317.

[86] **a)** J. Henn, K. Meindl, A. Oechsner, G. Schwab, T. Koritsanszky, D. Stalke, *Angew. Chem. Int. Ed.* **2010**, *49*, 2422-2426; **b)** F. Baier, Z. Fei, H. Gornitzka, A. Murso, S. Neufeld, M. Pfeiffer, I. Rüdenauer, A. Steiner, T. Stey, D. Stalke, *J. Organomet. Chem.* **2002**, *661*, 111-127; **c)** M. Pfeiffer, T. Stey, H. Jehle, B. Klupfel, W. Malisch, V. Chandrasekhar, D. Stalke, *Chem. Commun.* **2001**, 337-338; **d)** A. Steiner, D. Stalke, *Angew. Chem.* **1995**, *107*, 1908-1910; **e)** A. Steiner, D. Stalke, *J. Chem. Soc., Chem. Commun.* **1993**, 444-446.

[87] A. Steiner, D. Stalke, *Organometallics* **1995**, *14*, 2422-2429.

[88] T. Stey, J. Henn, D. Stalke, *Chem. Commun.* **2007**, 413-415.

[89] **a)** S. Aduldecha, B. Hathaway, *J. Chem. Soc., Dalton Trans.* **1991**, 993-998; **b)** L. A. Oro, M. A. Ciriano, F. Viguri, C. Foces-Foces, F. H. Cano, *Inorg. Chim. Acta* **1986**, *115*, 65-73; **c)** T. J. Hurley, M. A. Robinson, *Inorg. Chem.* **1968**, *7*, 33-38.

[90] R. G. Pearson, *J. Am. Chem. Soc.* **1985**, *107*, 6801-6806.

[91] **a)** C. Kling, D. Leusser, T. Stey, D. Stalke, *Organometallics* **2011**, *30*, 2461-2463; **b)** M. M. Meinholz, S. K. Pandey, S. M. Deuerlein, D. Stalke, *Dalton Trans.* **2011**, *40*, 1662-1671; **c)** M. M. Meinholz, D. Stalke, *Eur. J. Inorg. Chem.* **2011**, *2011*, 4578-4584; **d)** I. Objartel, N. A. Pott, M. John, D. Stalke, *Organometallics* **2010**, *29*, 5670-5675; **e)** T. Stey, M. Pfeiffer, J. Henn, S. K. Pandey, D. Stalke, *Chem. Eur. J.* **2007**, *13*, 3636-3642; **f)** T. Stey, D. Stalke, *Z. Anorg. Allg. Chem.* **2005**, *631*, 2931-2936.

[92] R. G. Parr, R. G. Pearson, *J. Am. Chem. Soc.* **1983**, *105*, 7512-7516.

[93] Janus coin, https://commons.wikimedia.org/wiki/File:Janus_coin.png, 1st July 2016.

[94] J. Hey, D. Leusser, D. Kratzert, H. Fliegl, J. M. Dieterich, R. A. Mata, D. Stalke, *Phys. Chem. Chem. Phys.* **2013**, *15*, 20600-20610.

[95] D.-R. Dauer, D. Stalke, *Dalton Trans.* **2014**, *43*, 14432-14439.

[96] **a)** C. Rai, J. B. Braunwarth, *J. Org. Chem.* **1961**, *26*, 3434-3436; **b)** W. H. Mills, *J. Chem. Soc., Trans.* **1922**, *121*, 455-466.

[97] **a)** C. Avendaño, M. T. Ramos, J. Elguero, M. L. Jimeno, J. Bellanato, F. Florencio, *Can. J. Chem.* **1988**, *66*, 1467-1473; **b)** T. Ramos, C. Avendaño, J. Elguero, *J. Heterocycl. Chem.* **1987**, *24*, 247-249.

[98] **a)** A. Abbotto, S. Bradamante, A. Facchetti, G. A. Pagani, *J. Org. Chem.* **2002**, *67*, 5753-5772; **b)** A. Abbotto, S. Bradamante, N. Capri, H. Rzepa, D. J. Williams, A. White, *J. Org. Chem.* **1996**, *61*, 1770-1778; **c)** A. Abbotto, S. Bradamante, G. A. Pagani, *J. Org. Chem.* **1996**, *61*, 1761-1769.

[99] **a)** A. Abbotto, A. Facchetti, S. Bradamante, G. A. Pagani, *J. Org. Chem.* **1998**, *63*, 436-444; **b)** F. Ragaini, M. Pizzotti, S. Cenini, A. Abbotto, G. A. Pagani, F. Demartin, *J. Organomet. Chem.* **1995**, *489*, 107-112; **c)** A. Abbotto, S.

Bradamante, G. A. Pagani, *J. Org. Chem.* **1993**, *58*, 444-448; **d)** C. Gatti, A. Ponti, A. Gamba, G. Pagani, *J. Am. Chem. Soc.* **1992**, *114*, 8634-8644; **e)** A. Abbotto, V. Alanzo, S. Bradamante, G. A. Pagani, *J. Chem. Soc., Perkin Trans. 2* **1991**, 481-488; **f)** S. Bradamante, G. A. Pagani, *J. Chem. Soc., Perkin Trans. 2* **1986**, 1035-1046; **g)** S. Bradamante, G. A. Pagani, *J. Org. Chem.* **1984**, *49*, 2863-2870.

[100] H. Ben Ammar, J. Le Nôtre, M. Salem, M. T. Kaddachi, P. H. Dixneuf, *J. Organomet. Chem.* **2002**, *662*, 63-69.

[101] **a)** D.-R. Dauer, Master of Science thesis, Georg-August-University (Göttingen), **2011**; **b)** F. d. S. Miranda, F. G. Menezes, J. Vicente, A. J. Bortoluzzi, C. Zucco, A. Neves, N. S. Gonçalves, *J. Mol. Struct.* **2009**, *938*, 1-9; **c)** C. T. Burns, R. F. Jordan, *Organometallics* **2007**, *26*, 6737-6749; **d)** H.-C. Yao, M.-M. Li, G.-S. Yang, Z.-J. Li, Y. Zhu, *Inorg. Chim. Acta* **2007**, *360*, 3959-3964; **e)** N. Braussaud, T. Rüther, K. J. Cavell, B. W. Skelton, A. H. White, *Synthesis* **2001**, *2001*, 626-632; **f)** S. Elgafi, L. D. Field, B. A. Messerle, P. Turner, T. W. Hambley, *J. Organomet. Chem.* **1999**, *588*, 69-77.

[102] F. G. Bordwell, *Acc. Chem. Res.* **1988**, *21*, 456-463.

[103] **a)** D. C. Bradley, H. C. Chudzynska, I. S. Harding, K. S. Brewer, D. Rosenblum, O. T. Beachley, *Inorg. Synth.*, **2007**, 67-74; **b)** D. F. Gaines, J. Borlin, E. P. Fody, *Inorg. Synth.* **1974**, *15*, 203-207.

[104] **a)** D. F. Foster, D. J. Cole-Hamilton, R. A. Jones, *Inorg. Synth.* **1997**, *31*, 29-51; **b)** D. F. Foster, S. A. Rushworth, D. J. Cole-Hamilton, R. Cafferty, J. Harrison, P. Parkes, *J. Chem. Soc., Dalton Trans.* **1988**, 7-11.

[105] J. J. McKinnon, M. A. Spackman, A. S. Mitchell, *Acta Crystallogr., Sect. B* **2004**, *60*, 627-668.

[106] **a)** S. K. Wolff, D. J. Grimwood, J. J. McKinnon, M. J. Turner, D. Jayatilaka, M. A. Spackman, in *CrystalExplorer (Version 3.1)*, University of Western Australia, **2012**; **b)** M. A. Spackman, D. Jayatilaka, *CrystEngComm* **2009**, *11*, 19-32.

[107] M. A. Spackman, J. J. McKinnon, *CrystEngComm* **2002**, *4*, 378-392.

[108] **a)** P. Müller, R. Herbst-Irmer, A. L. Spek, T. R. Schneider, M. R. Sawaya, *Crystal Structure Refinement A Crystallographer's Guide to SHELXL*, 1st ed., Oxford University Press, New York, **2006**; **b)** P. Rademacher, *Strukturen organischer Moleküle, Vol. 2*, 1st ed., VCH, Weinheim, **1987**.

[109] **a)** Z. Dauter, *Acta Crystallogr., Sect. D* **2003**, *59*, 2004-2016; **b)** S. Parsons, *Acta Crystallogr., Sect. D* **2003**, *59*, 1995-2003.

[110] D. R. Lide, *CRC Handbook of Chemistry and Physics : a ready-reference book of chemical and physical data*, CRC Press, Boca Raton, **2006**.

[111] K. E. Horner, P. B. Karadakov, *J. Org. Chem.* **2015**, *80*, 7150-7157.

[112] **a)** E. Barchiesi, S. Bradamante, *J. Phys. Org. Chem.* **1990**, *3*, 139-142; **b)** S. Bradamante, G. A. Pagani, *J. Chem. Soc., Perkin Trans. 2* **1986**, 1055-1061.

[113] **a)** J. C. Huffman, W. E. Streib, *J. Chem. Soc. D* **1971**, 911-912; **b)** S. K. Byram, J. K. Fawcett, S. C. Nyburg, R. J. O'Brien, *J. Chem. Soc. D* **1970**, 16-17; **c)** R. G. Vranka, E. L. Amma, *J. Am. Chem. Soc.* **1967**, *89*, 3121-3126.

[114] R. Boese, A. J. Downs, T. M. Greene, A. W. Hall, C. A. Morrison, S. Parsons, *Organometallics* **2003**, *22*, 2450-2457.

[115] D.-R. Dauer, M. Flügge, R. Herbst-Irmer, D. Stalke, *Dalton Trans.* **2016**, *45*, 6149-6158.

[116] D.-R. Dauer, M. Flügge, R. Herbst-Irmer, D. Stalke, *Dalton Trans.* **2016**, *45*, 6136-6148.

[117] **a)** G. R. Newkome, Y. J. Joo, D. W. Evans, F. R. Fronczek, G. R. Baker, *J. Org. Chem.* **1990**, *55*, 5714-5719; **b)** E. Klemm, D. Klemm, H. H. Hörhold, *Synthesis* **1977**, *1977*, 342-343.

[118] H. Gornitzka, D. Stalke, *Angew. Chem.* **1994**, *106*, 695-698.

[119] I. Langmuir, *J. Am. Chem. Soc.* **1919**, *41*, 1543-1559.

[120] A. Walli, S. Dechert, F. Meyer, *Eur. J. Org. Chem.* **2013**, *2013*, 7044-7049.

[121] G. R. Desiraju, *J. Am. Chem. Soc.* **2013**, *135*, 9952-9967.

[122] E. S. Wallis, F. H. Adams, *J. Am. Chem. Soc.* **1933**, *55*, 3838-3851.

[123] **a)** D. Stalke, E. Carl, in *Lithium Compounds in Organic Synthesis* (Eds.: R. Luisi, V. Capriati), Wiley-VCH, Weinheim, **2014**, pp. 1-32; **b)** H. J. Reich, *Chem. Rev.* **2013**, *113*, 7130-7178; **c)** V. H. Gessner, C. Däschlein, C. Strohmann, *Chem. Eur. J.* **2009**, *15*, 3320-3334; **d)** D. B. Collum, A. J. McNeil, A. Ramirez, *Angew. Chem. Int. Ed.* **2007**, *46*, 3002-3017; **e)** T. Stey, D. Stalke, in *The Chemistry of Organolithium Compounds*, Wiley, Chichester, **2004**, pp. 47-120; **f)** M. C. Whisler, S. MacNeil, V. Snieckus, P. Beak, *Angew. Chem.* **2004**, *116*, 2256-2276; **g)** B. L. Lucht, D. B. Collum, *Acc. Chem. Res.* **1999**, *32*, 1035-1042.

[124] H. Dietrich, *J. Organomet. Chem.* **1981**, *205*, 291-299.

[125] E. Weiss, T. Lambertsen, B. Schubert, J. K. Cockeroft, A. Wiedenmann, *Chem. Ber.* **1990**, *123*, 79-81.

[126] T. Kottke, D. Stalke, *Angew. Chem. Int. Ed. Engl.* **1993**, *32*, 580-582.

[127] **a)** R. E. Mulvey, *Chem. Soc. Rev.* **1998**, *27*, 339-346; **b)** K. Gregory, P. v. R. Schleyer, R. Snaith, *Adv. Inorg. Chem.* **1991**, *37*, 47-142; **c)** R. E. Mulvey, *Chem. Soc. Rev.* **1991**, *20*, 167-209; **d)** D. R. Armstrong, D. Barr, R. Snaith, W. Clegg, R. E. Mulvey, K. Wade, D. Reed, *J. Chem. Soc., Dalton Trans.* **1987**, 1071-1081.

[128] G. R. Fulmer, A. J. M. Miller, N. H. Sherden, H. E. Gottlieb, A. Nudelman, B. M. Stoltz, J. E. Bercaw, K. I. Goldberg, *Organometallics* **2010**, *29*, 2176–2179.

[129] J. R. Lakowicz, *Principles of Fluorescence Spectroscopy* 3rd ed., Springer, New York, **2006**.

[130] K. Issleib, R. Vollmer, H. Oehme, H. Meyer, *Tetrahedron Lett.* **1978**, *19*, 441-444.

[131] K. Issleib, R. Vollmer, *Z. Anorg. Allg. Chem.* **1981**, *481*, 22-32.

[132] **a)** B. R. Aluri, B. Niaz, M. K. Kindermann, P. G. Jones, J. Heinicke, *Dalton Trans.* **2011**, *40*, 211-224; **b)** J. Heinicke, N. Gupta, A. Surana, N. Peulecke, B. Witt, K. Steinhauser, R. K. Bansal, P. G. Jones, *Tetrahedron* **2001**, *57*, 9963-9972.

[133] R. K. Bansal, N. Gupta, J. Heinicke, G. N. Nikonov, F. Saguitova, D. C. Sharma, *Synthesis* **1999**, *1999*, 264-269.

[134] M. S. S. Adam, P. G. Jones, J. W. Heinicke, *Eur. J. Inorg. Chem.* **2010**, *2010*, 3307-3316.

[135] B. R. Aluri, M. K. Kindermann, P. G. Jones, I. Dix, J. Heinicke, *Inorg. Chem.* **2008**, *47*, 6900-6912.

[136] **a)** C. Hilf, F. Bosold, K. Harms, M. Marsch, G. Boche, *Chem. Ber.* **1997**, *130*, 1213-1221; **b)** C. Hill, F. Bosold, K. Harms, J. C. W. Lohrenz, M. Marsch, M. Schmieczek, G. Boche, *Chem. Ber.* **1997**, *130*, 1201-1212; **c)** G. Boche, C. Hilf, K. Harms, M. Marsch, J. C. W. Lohrenz, *Angew. Chem. Int. Ed. Engl.* **1995**, *34*, 487-489; **d)** P. Jutzi, U. Gilge, *J. Organomet. Chem.* **1983**, *246*, 159-162.

[137] R. Roussel, M. Oteyza de Guerrero, J. C. Galin, *Macromolecules* **1986**, *19*, 291-299.

[138] **a)** B. R. Aluri, M. K. Kindermann, P. G. Jones, J. Heinicke, *Chem. Eur. J.* **2008**, *14*, 4328-4335; **b)** J. Heinicke, K. Steinhauser, N. Peulecke, A. Spannenberg, P. Mayer, K. Karaghiosoff, *Organometallics* **2002**, *21*, 912-919; **c)** J. Heinicke, A. Tzschach, *Tetrahedron Lett.* **1982**, *23*, 3643-3646.

[139] **a)** A. Surana, S. Singh, R. K. Bansal, N. Peulecke, A. Spannenberg, J. Heinicke, *J. Organomet. Chem.* **2002**, *646*, 113-124; **b)** R. K. Bansal, J. Heinicke, *Chem. Rev.* **2001**, *101*, 3549-3578; **c)** J. Heinicke, A. Surana, N. Peulecke, Raj K. Bansal, A. Murso, D. Stalke, *Eur. J. Inorg. Chem.* **2001**, *2001*, 2563-2567.

[140] M. P. Washington, V. B. Gudimetla, F. L. Laughlin, N. Deligonul, S. He, J. L. Payton, M. C. Simpson, J. D. Protasiewicz, *J. Am. Chem. Soc.* **2010**, *132*, 4566-4567.

[141] **a)** M. P. Washington, J. L. Payton, M. C. Simpson, J. D. Protasiewicz, *Organometallics* **2011**, *30*, 1975-1983; **b)** J. Heinicke, A. Tzschach, *Phosphorus Sulfur Relat. Elem.* **1985**, *25*, 345-356; **c)** J. Heinicke, A. Tzschach, *Z. Chem.* **1980**, *20*, 342-343.

[142] **a)** J. C. Worch, D. N. Chirdon, A. B. Maurer, Y. Qiu, S. J. Geib, S. Bernhard, K. J. T. Noonan, *J. Org. Chem.* **2013**, *78*, 7462-7469; **b)** K. Issleib, R. Vollmer, *Tetrahedron Lett.* **1980**, *21*, 3483-3484.

[143] S. Masson, J.-F. Saint-Clair, M. Saquet, *Synthesis* **1993**, *1993*, 485-486.

[144] J. Heinicke, A. Tzschach, *J. Organomet. Chem.* **1978**, *154*, 1-12.

[145] J. Heinicke, B. Raap, A. Tzschach, *J. Organomet. Chem.* **1980**, *186*, 39-50.

[146] G. W. Kenner, N. R. Williams, *J. Chem. Soc.* **1955**, 522-525.

[147] B. Dhawan, D. Redmore, *J. Org. Chem.* **1984**, *49*, 4018-4021.

[148] **a)** X. Couillens, M. Gressier, Y. Coulais, M. Dartiguenave, *Inorg. Chim. Acta* **2004**, *357*, 195-201; **b)** J. Heinicke, I. Böhle, A. Tzschach, *J. Organomet. Chem.* **1986**, *317*, 11-21.

[149] **a)** T. T. Tidwell, *Angew. Chem. Int. Ed.* **2001**, *40*, 331-337; **b)** W. Schlenk, A. Thal, *Chem. Ber.* **1913**, *46*, 2840-2854; **c)** Georg-August-Universität Göttingen, Virtuelles Labor, http://www.stalke.chemie.uni-goettingen.de/virtuelles_labor/advanced/13_de.html, 1st July 2016.

[150] H. J. Svec, *Int. J. Mass Spectrom. Ion Processes* **1985**, *66*, 3-29.

[151] J. F. d. l. Mora, G. J. V. Berkel, C. G. Enke, R. B. Cole, M. Martinez-Sanchez, J. B. Fenn, *J. Mass Spectrom.* **2000**, *35*, 939-952.

[152] Georg-August-Universität Göttingen, Virtuelles Labor, http://www.stalke.chemie.uni-goettingen.de/virtuelles_labor/nmr/de.html, 1st July 2016.

[153] W. P. Aue, E. Bartholdi, R. R. Ernst, *J. Chem. Phys.* **1976**, *64*, 2229-2246.

[154] G. Bodenhausen, D. J. Ruben, *Chem. Phys. Lett.* **1980**, *69*, 185-189.

[155] A. Bax, M. F. Summers, *J. Am. Chem. Soc.* **1986**, *108*, 2093-2094.

[156] **a)** D. Stalke, *Chem. Soc. Rev.* **1998**, *27*, 171-178; **b)** T. Kottke, R. J. Lagow, D. Stalke, *J. Appl. Crystallogr.* **1996**, *29*, 465-468; **c)** T. Kottke, D. Stalke, *J. Appl. Crystallogr.* **1993**, *26*, 615-619; **d)** H. Hope, *Acta Crystallogr., Sect. B* **1988**, *44*, 22-26; **e)** Georg-August-Universität Göttingen, Virtuelles Labor, http://www.stalke.chemie.uni-goettingen.de/virtuelles_labor/special/22_de.html,

[157] T. Schulz, K. Meindl, D. Leusser, D. Stern, J. Graf, C. Michaelsen, M. Ruf, G. M. Sheldrick, D. Stalke, *J. Appl. Crystallogr.* **2009**, *42*, 885-891.

[158] L. Krause, R. Herbst-Irmer, G. M. Sheldrick, D. Stalke, *J. Appl. Crystallogr.* **2015**, *48*, 3-10.

[159] Bruker AXS Inc., in *APEX2* (Ed.: Bruker AXS Inst. Inc.), WI, USA, Madison, **2012**.

[160] Bruker AXS Inc., in *Bruker Apex CCD, SAINT v8.30C* (Ed.: Bruker AXS Inst. Inc.), WI, USA, Madison, **2013**.

[161] G. M. Sheldrick, Göttingen, **2014**.

[162] G. M. Sheldrick, in *TWINABS 2012/1*, Göttingen, **2012**.

[163] G. M. Sheldrick, in *XPREP in SHELXTL 2014/2* (Ed.: Bruker AXS Inst. Inc.), WI, USA, Madison, **2014**.

[164] G. Sheldrick, *Acta Crystallogr., Sect. A* **2015**, *71*, 3-8.

[165] **a)** G. Sheldrick, *Acta Crystallogr., Sect. C* **2015**, *71*, 3-8; **b)** G. M. Sheldrick, *Acta Crystallogr., Sect. A* **2014**, *70*, C1437; **c)** G. M. Sheldrick, *Acta Crystallogr., Sect. A* **2008**, *64*, 112-122.

[166] **a)** C. B. Huebschle, G. M. Sheldrick, B. Dittrich, *J. Appl. Crystallogr.* **2011**, *44*, 1281-1284; **b)** C. B. Huebschle, G. M. Sheldrick, B. Dittrich, *Acta Crystallogr., Sect. A* **2011**, *67*, C592.

[167] R. Srinivasan, N. R. Jagannathan, *Acta Crystallogr., Sect. B* **1982**, *38*, 2093-2095.

[168] B. B. Snider, in *Encyclopedia of Reagents for Organic Synthesis*, John Wiley & Sons, Ltd, **2001**.

[169] S. Parsons, H. D. Flack, T. Wagner, *Acta Crystallogr., Sect. B* **2013**, *69*, 249-259.

7 Curriculum Vitae

Personal Data

Name:	David-Raphael Dauer
Date of birth:	07.02.1987
Place of birth:	Northeim
Citizenship:	German

Scientific Career

01/2016 − today	**R&D Scientist** at Continental Reifen Deutschland GmbH, Hannover
12/2011 − 10/2016	**Ph.D. thesis** "*Studies of Group 13 Metal Complexes Bearing nacnac-Mimetic Bisheterocyclo Methanides and Amides* " in charge of Prof. Dr. Stalke at the Institute of Inorganic Chemistry Georg-August-University Göttingen, within the Ph.D. program Georg-August-University School of Science (GAUSS)
10/2009 − 09/2011	**Graduate studies** in Chemistry at the Georg-August-University Göttingen; degree: Master of Science with honours, grade: 1.2
03/2011 − 09/2011	Master's thesis "*Synthese und Charakterisierung chelatisierender Heteroaromaten als Vorstufe zu höheren Homologen der Carbene*" in charge of Prof. Dr. Stalke, grade: 1.0
10/2006 − 08/2009	**Undergraduate studies** in Chemistry at the Georg-August-University Göttingen; degree: Bachelor of Science, grade: 1.8
04/2009 − 08/2009	Bachelor's thesis "*Gekoppelte Organyldiimidosulfinate*" in charge of Prof. Dr. Stalke, grade: 1.3
09/1999 − 07/2006	**Allgemeine Hochschulreife** at Gymnasium Paul-Gerhardt-Schule, Dassel, degree: Abitur (equivalent to A-level), grade: 1.4

Awards

06/2014	Award for the best non-independent teaching at the Institute for Inorganic Chemistry (winter term 2013/14)
09/2011	Master of Science with honours
07/2006	GDCh award for the valedictorian high school graduate in the subject Chemistry

Skills

Radiation protection	Qualification: S1.1, S1.2, S1.3, S2.1, S.2.2, S5, S6.1 (StrSchV) and R2.1 (RöV)
Expertise	According to §5 Chemikalienverbotsordnung
Safety representative	Participation in "Grundlagenseminar für neu bestellte Sicherheitsbeauftragte"

Scientific Contributions

- Gordon Research Conference on Organometallic Chemistry, 06. − 11.07.2014 in Newport, RI, USA (poster presentation: *Synthetic Approaches and Characterization of Novel Bisheterocyclomethanide/-amide Containing Group 13 Metallylene Precursors*)
- Hot Topics in Contemporary Crystallography 2014, 10. − 15.05.2014 in Šibenik, Croatia (computational workshop)
- 8th Workshop of Center for Materials Crystallography, 27.03.2014 in Göttingen, Germany (oral presentation: *Higher Homologues of NHCs Derived from Chelating Heteroaromates*)
- Midterm Review Center for Materials Crystallography, 27. − 28.06.2013 in Aarhus, Denmark (poster presentation: *New (A-)symmetric Bisheterocyclomethanes and ChelatingGroup-13-Complexes Thereof*)
- 6th Chemie-Forum, Jungchemiker-Forum, 05.06.2013 in Göttingen, Germany (poster presentation: *New (A-)symmetric Bisheterocyclomethanes and Chelating Group-13-Complexes Thereof*)
- 16th Lecture Meeting of the Wöhler-Vereinigung, 26. − 28.09.2012 in Göttingen, Germany (poster presentation: *On the Brink to New Metallylenes*)
- 5th Workshop of Center for Materials Crystallography, 13. − 14.08.2012 in Aarhus, Denmark (oral presentation: *On the Brink to Metallo Carbenes*)
- 5th Chemie-Forum, Jungchemiker-Forum, 11.07.2012 in Göttingen, Germany (poster presentation: *Synthesis and Characterization of Chelating Heteroaromates as Precursors for Higher Homologues of N-Heterocyclic Carbenes*)

Scientific Publications

- David-Raphael Dauer, Melchior Flügge, Regine Herbst-Irmer, Dietmar Stalke, Group 13 metal complexes containing the bis-(4-methyl-benzoxazol-2-yl)-methanide ligand, *Dalton Trans.* **2016**, *45*, 6149-6158.
- David-Raphael Dauer, Melchior Flügge, Regine Herbst-Irmer, Dietmar Stalke, Bis-(benzothiazol-2-yl)-amines and their metal amides: a structural comparison in the solid state, *Dalton Trans.* **2016**, *45*, 6136-6148.
- David-Raphael Dauer, Dietmar Stalke, Heterocyclic substituted methanides as promising alternatives to the ubiquitous nacnac ligand, *Dalton Trans.* **2014**, *43*, 14432-14439.
- Thomas Schulz, David-Raphael Dauer, Dietmar Stalke, π-Spacer-coupled Diimidosulfinates, *Z. Naturforsch.* **2010**, *65b*, 711-718.